frontiers | Research Topics

Diagnosis and treatment of bone metastases

Edited by
Feifei Pu, Zhidao Xia, Akshara Raghavendra and Wenwen Zhang

Published in
Frontiers in Oncology

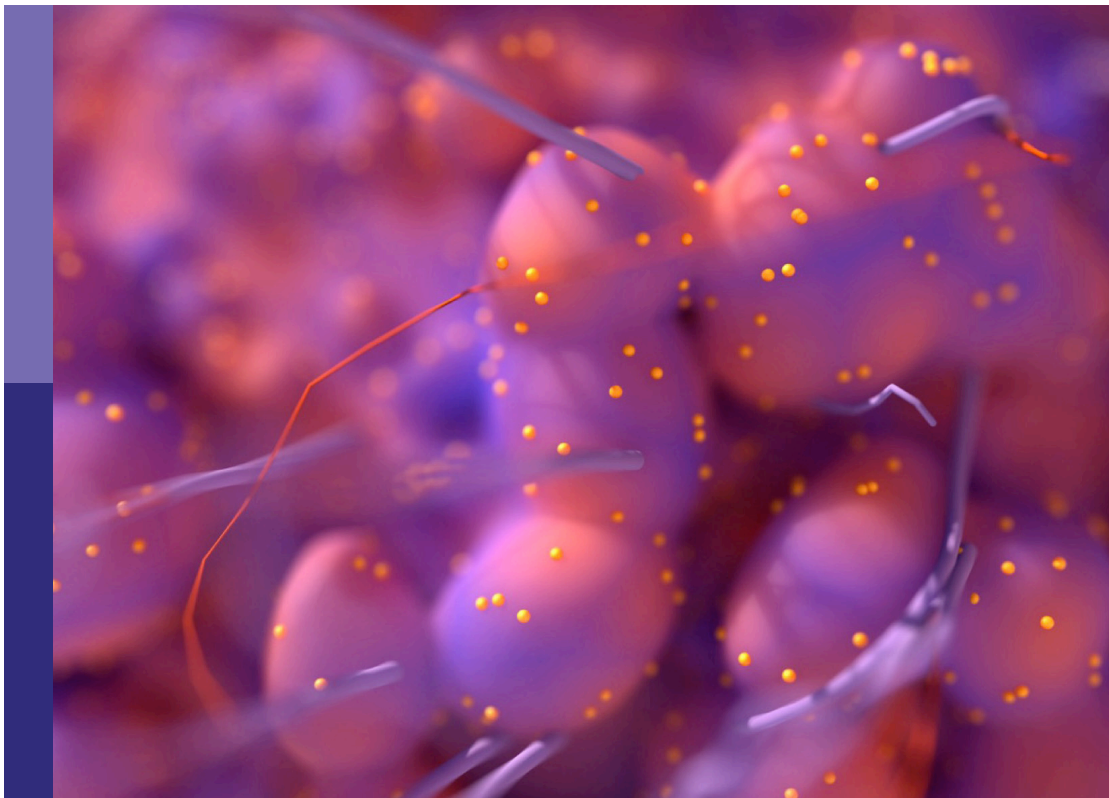

ISSN 1664-8714
ISBN 978-2-8325-3382-6
DOI 10.3389/978-2-8325-3382-6

About Frontiers

Frontiers is more than just an open access publisher of scholarly articles: it is a pioneering approach to the world of academia, radically improving the way scholarly research is managed. The grand vision of Frontiers is a world where all people have an equal opportunity to seek, share and generate knowledge. Frontiers provides immediate and permanent online open access to all its publications, but this alone is not enough to realize our grand goals.

Frontiers journal series

The Frontiers journal series is a multi-tier and interdisciplinary set of open-access, online journals, promising a paradigm shift from the current review, selection and dissemination processes in academic publishing. All Frontiers journals are driven by researchers for researchers; therefore, they constitute a service to the scholarly community. At the same time, the *Frontiers journal series* operates on a revolutionary invention, the tiered publishing system, initially addressing specific communities of scholars, and gradually climbing up to broader public understanding, thus serving the interests of the lay society, too.

Dedication to quality

Each Frontiers article is a landmark of the highest quality, thanks to genuinely collaborative interactions between authors and review editors, who include some of the world's best academicians. Research must be certified by peers before entering a stream of knowledge that may eventually reach the public - and shape society; therefore, Frontiers only applies the most rigorous and unbiased reviews. Frontiers revolutionizes research publishing by freely delivering the most outstanding research, evaluated with no bias from both the academic and social point of view. By applying the most advanced information technologies, Frontiers is catapulting scholarly publishing into a new generation.

What are Frontiers Research Topics?

Frontiers Research Topics are very popular trademarks of the *Frontiers journals series*: they are collections of at least ten articles, all centered on a particular subject. With their unique mix of varied contributions from Original Research to Review Articles, Frontiers Research Topics unify the most influential researchers, the latest key findings and historical advances in a hot research area.

Find out more on how to host your own Frontiers Research Topic or contribute to one as an author by contacting the Frontiers editorial office: frontiersin.org/about/contact

Diagnosis and treatment of bone metastases

Topic editors

Feifei Pu — Huazhong University of Science and Technology, China
Zhidao Xia — Swansea University, United Kingdom
Akshara Raghavendra — University of Texas MD Anderson Cancer Center, United States
Wenwen Zhang — Nanjing Medical University, China

Citation

Pu, F., Xia, Z., Raghavendra, A., Zhang, W., eds. (2023). *Diagnosis and treatment of bone metastases*. Lausanne: Frontiers Media SA. doi: 10.3389/978-2-8325-3382-6

Table of contents

frontiers | Frontiers in Oncology

TYPE Editorial
PUBLISHED 15 August 2023
DOI 10.3389/fonc.2023.1247231

OPEN ACCESS

EDITED AND REVIEWED BY
Francesco Giovinazzo,
Agostino Gemelli University Polyclinic (IRCCS), Italy

*CORRESPONDENCE
Ping Xia
xiapingfm@163.com
Zhidao Xia
z.xia@swansea.ac.uk

RECEIVED 25 June 2023
ACCEPTED 21 July 2023
PUBLISHED 15 August 2023

CITATION
Pu F, Hu Z, Yang Y, Xia P and Xia Z (2023) Editorial: Diagnosis and treatment of bone metastases. *Front. Oncol.* 13:1247231. doi: 10.3389/fonc.2023.1247231

Editorial: Diagnosis and treatment of bone metastases

Feifei Pu[1,2], Zuowei Hu[3], Yanping Yang[4], Ping Xia[5]* and Zhidao Xia[6]*

[1]Department of Orthopedics, Traditional Chinese and Western Medicine Hospital of Wuhan, Tongji Medical College, Huazhong University of Science and Technology, Wuhan, China, [2]Department of Orthopedics, Wuhan No.1 Hospital, Wuhan, China, [3]Department of Oncology, Traditional Chinese and Western Medicine Hospital of Wuhan, Wuhan, China, [4]Spine Institute, Shanghai University of Traditional Chinese Medicine, Shanghai, China, [5]Department of Orthopedics, Wuhan Fourth Hospital (Puai Hospital), Wuhan, China, [6]Institute of Life Science, Swansea University Medical School, Swansea, United Kingdom

KEYWORDS

bone metastases, diagnosis, minimally invasive operation, radiotherapy, targeted therapy

Editorial on the Research Topic
Diagnosis and treatment of bone metastases

Bone metastasis is one of the common complications of malignant tumors. Patients often present with bone pain and fracture, which not only seriously affect patients' quality of life, but also imply poor prognosis (1, 2). In recent years, with the deepening of the understanding of the mechanism of bone metastases and the relevant regulatory network between tumor cells and bone microenvironment, the development and application of many new drugs have made great progress in the treatment of bone metastases (3). It is particularly important to find effective, economical, small adverse reactions and effective treatment methods to improve the quality of life of cancer patients. However, bone metastasis is often in the terminal stage of tumor development, the prognosis of patients is poor, and the treatment plan is difficult to be unified (4). Bone related biomarkers can reflect bone metabolism and bone turnover, and are associated with bone metastasis of malignant tumors (5). The development of diagnostic radiology is helpful to early identification of high-risk groups of pathological fractures, which is conducive to early intervention and improving the quality of life of patients (6). The incidence of bone metastasis is high, and an individualized comprehensive treatment plan should be developed according to the specific condition. The main treatment means include antitumor therapy, bone modifying drug therapy, surgery, radiation therapy, analgesia and supportive therapy (6–10).

In this Research Topic, 16 articles has been published which focusing on recent advances in the treatments for patients with bone metastases. Current published papers cover the following research areas: pathogenesis, establishment of animal models, pain management, imaging diagnosis, minimally invasive surgery and chemoradiotherapy of bone metastases.

Bone metastasis is a multi-step, continuous and extremely complex process involving both tumor and host factors. Yang W. et al. explained the epidemiology, clinical features, pathogenesis and clinical treatment strategies of bone metastasis in detail. They believed that with a better understanding of how bone metastases occur, there will be more new

drugs and new technologies in the future, which will benefit more patients. Choosing the right animal model is an important bridge between basic research and applied research (11). Yu et al. summarized the current articles on the preparations and studies of animal models of bone metastases, including solid tumors such as lung cancer, breast cancer, and prostate cancer. This review is conducive to promoting the development of preclinical models and improving the translation of drugs and technologies for the treatment of bone metastases.

Early detection and treatment of bone metastases are of great significance to improve the prognosis of patients. Yang et al. reviewed the biomarkers related to bone metastasis, hoping to provide guidance for the early diagnosis of bone metastasis. Biomarkers can effectively reflect the occurrence, progression, tumor treatment monitoring, recurrence detection and so on. Brouns et al. found that the expression of nuclear factor κB ligand receptor activator (RANKL) gene and the increased ratio of RANKL: osteoprotegerin (OPG) were associated with the presence of bone metastases. The study also showed that an increased proportion of the RANKL: OPG gene was associated with a higher incidence of bone metastasis. The study suggested that research into the mechanism of bone metastases may facilitate the development of new drugs and may change the entire treatment strategy.

In recent years, deep learning based on big data is developing rapidly, and the biological behavior of tumors can be reflected by the texture features of lesion areas that are difficult to be recognized by the naked eye through imaging omics (12). The algorithm extracts abstract features of tumor regions through multi-layer network structure (13). Long et al. developed an ensemble machine-learning model for predicting early mortality among patients with bone metastases of hepatocellular carcinoma, Huo et al. developed a deep learning-based algorithm in lung cancer bone metastases detection on computed tomography, and Cui et al. developed a web-based calculator to predict three-month mortality among patients with bone metastases from cancer of unknown primary. Surveillance, Epidemiology, and End Results (SEER) database provides good data support for clinical research, Nomogram has been widely used in cancer and other medical research because of its intuitive and convenient characteristics (14). Yin et al. constructed a novel web-based nomogram for lung cancer patients with bone metastasis, they found the prediction models may be helpful for doctors to make accurate judgment and guidance on the treatment plan and clinical prognosis of patients.

Bone pain is the main clinical symptom of patients with bone metastatic cancer, and also the main reason for the decline of patients' quality of life. Therefore, lasting and effective pain relief is the focus of clinical treatment. Jing et al. reviewed the management of pain in patients with bone metastases, which has important guiding significance for the majority of clinicians. Denosumab (the RANKL neutralizing antibody) can not only relieve pain symptoms in patients with bone metastases, but also prevent the occurrence of bone-related adverse events (15). Lu et al. reviewed current comprehensive understanding the pharmacological action and clinical trial results of denosumab in the treatment of bone metastases.

At present, clinicians are increasingly recognizing the importance and scientific nature of multiple disciplinary team (MDT) in the diagnosis and treatment of bone metastases. As an important means of treatment, surgery can be divided into different surgical methods according to different therapeutic purposes. The surgical goals of bone metastases in the extremities are to prevent and treat pathological fractures and to control the tumor locally (16). Pu et al. found that total removal of bone metastases and implantation of personalized modular prostheses can reduce pain and improve limb function and quality of life in patients with femoral shaft metastasis. Wu et al. preserved rectus femoris after total femoral prosthesis replacement following resection of femoral malignant tumors, this could improve limb function.

Treatment strategies for metastatic tumors of the extremities and spine differ. Surgical goals for metastatic tumors of the spine are local tumor control, pain relief, spinal stability, relief of spinal cord neurologic compression, and improved quality of life (16). Positive vitreous pressure (PVP) and percutaneous kyphoplasty (PKP) can effectively relieve the pain degree of spinal metastasis patients, with the advantages of small trauma, low risk, short operation time and quick analgesic effect (17). Wang et al. Pulmonary cement embolism is a rare, Wang et al. investigated risk factors for pulmonary cement embolism after PVP and radiofrequency ablation for spinal metastases. But underestimated complication of vertebroplasty, Zhang C. et al. specifieded the direct and indirect damage zone of radiofrequency ablation in porcine lumbar vertebra by conducting animal experiments, this will improve the guidance for improving the safety of the operation. According to literature reports, about 60% of spinal metastases are tumors with abundant blood flow. Arterial embolization can not only be used as an auxiliary means before surgery to reduce hemorrhage in the hand and improve the safety of surgical operation, but also as palliative treatment. Vascular embolization can cause tumor ischemic necrosis and relieve patients' pain and tumor compression and other symptoms (18). Zhang B. et al. found that preoperative embolization is an effective and safe method to control bleeding in patients with metastatic epidural spinal cord compression. Spinal metastasis of malignant adrenal tumor (SMMAT) are rare malignant neoplasms originating from the adrenal glands. Liu et al. reported six cases of SMMAT, and they elucidated the clinical characteristics and discussed surgical management and outcomes of SMMAT.

At present, the treatment concept and technology of bone metastases have developed rapidly, and there are still many clinical problems to be solved. After the occurrence of bone metastasis in a certain pathological type of cancer, the specific selection of radiotherapy, surgery, systemic therapy, targeted drugs, immunotherapy, its sequence and the details of the basis of combination are one of the important clinical issues at present, which still need clinical research and practice verification. According to the practical experience of MDT for cancer bone metastasis, it is one of the important directions of clinical research to evaluate the classification of different cancers and select treatment strategies in the future.

Author contributions

All authors listed have made a substantial, direct and intellectual contribution to the work, and approved it for publication.

Funding

This work was supported in part by the National Natural Science Foundation of China (No. 82274559), Hubei Provincial Key Research and Development Program (No. 2021BCA105), and National Clinical Research Center for Orthopedics and Sports Medicine & Rehabilitation Program (No. 2021-NCRC-CXJJ-ZH-15).

Conflict of interest

The authors declare that the research was conducted in the absence of any commercial or financial relationships that could be construed as a potential conflict of interest.

Publisher's note

References

1. Fornetti J, Welm AL, Stewart SA. Understanding the bone in cancer metastasis. *J Bone Miner Res* (2018) 33(12):2099–113. doi: 10.1002/jbmr.3618

2. Riffel RM, Göbel A, Rachner TD. Bone Metastases: From mechanisms to treatment. *Semin Oncol Nurs* (2022) 38(2):151277. doi: 10.1016/j.soncn.2022.151277

3. Hiraga T. Bone metastasis: Interaction between cancer cells and bone microenvironment. *J Oral Biosci* (2019) 61(2):95–8. doi: 10.1016/j.job.2019.02.002

4. Coleman RE, Croucher PI, Padhani AR, Clézardin P, Chow E, Fallon M, et al. Bone metastases. *Nat Rev Dis Primers* (2020) 6(1):83. doi: 10.1038/s41572-020-00216-3

5. Clézardin P, Coleman R, Puppo M, Ottewell P, Bonnelye E, Paycha F, et al. Bone metastasis: mechanisms, therapies, and biomarkers. *Physiol Rev* (2021) 101(3):797–855. doi: 10.1152/physrev.00012.2019

6. Errani C, Bazzocchi A, Spinnato P, Facchini G, Campanacci L, Rossi G, et al. What's new in management of bone metastases? *Eur J Orthop Surg Traumatol* (2019) 29(7):1367–75. doi: 10.1007/s00590-019-02446-y

7. Chen F, Pu F. Safety of denosumab versus zoledronic acid in patients with bone metastases: ameta-analysis of randomized controlled trials. *Oncol Res Treat* (2016) 39 (7-8):453–9. doi: 10.1159/000447372

8. Siegel GW, Biermann JS, Calinescu AA, Spratt DE, Szerlip NJ. Surgical approach to bone metastases. *Curr Osteoporos Rep* (2018) 16(4):512–8. doi: 10.1007/s11914-018-0463-7

9. Pu F, Zhang Z, Wang B, Liu J, Shao Z. En bloc resection and intercalary prosthesis implantation for the treatment of humeral diaphyseal bone metastases. *Int Orthop* (2021) 45(1):281–8. doi: 10.1007/s00264-020-04845-x

10. Pu F, Liu J, Zhang Z, Shi D, Huang X, Zhang J, et al. Reconstruction with 3D-printed prostheses after sacroiliac joint tumor resection: a retrospective case-control study. *Front Oncol* (2022) 11:764938. doi: 10.3389/fonc.2021.764938

11. Wang Q. The cornerstone of translational research - selection of appropriate animal models. *Biomater Transl* (2021) 2(2):87–8. doi: 10.12336/biomatertransl.2021.02.001

12. She Y, He B, Wang F, Zhong Y, Wang T, Liu Z, et al. Deep learning for predicting major pathological response to neoadjuvant chemoimmunotherapy in non-small cell lung cancer: A multicentre study. *EBioMedicine* (2022) 86:104364. doi: 10.1016/j.ebiom.2022.104364

13. Din NMU, Dar RA, Rasool M, Assad A. Breast cancer detection using deep learning: Datasets, methods, and challenges ahead. *Comput Biol Med* (2022) 149:106073. doi: 10.1016/j.compbiomed.2022.106073

14. Zhang W, Ji L, Wang X, Zhu S, Luo J, Zhang Y, et al. Nomogram predicts risk and prognostic factors for bone metastasis of pancreatic cancer: a population-based analysis. *Front Endocrinol* (2022) 12:752176. doi: 10.3389/fendo.2021.752176

15. Zhang Z, Pu F, Shao Z. The skeletal-related events of denosumab versus zoledronic acid in patients with bone metastases: a meta-analysis of randomized controlled trials. *J Bone Oncol* (2017) 9:21–4. doi: 10.1016/j.jbo.2017.09.003

16. Hayashi K, Tsuchiya H. The role of surgery in the treatment of metastatic bone tumor. *Int J Clin Oncol* (2022) 27(8):1238–46. doi: 10.1007/s10147-022-02144-6

17. Zhang JX, Song ZR, Zou J, Ge J, Yang HL. Balloon kyphoplasty as palliative care for painful pathological spinal fracture followed by lung cancer metastasis: A cohort study. *Front Surg* (2023) 9:1081823. doi: 10.3389/fsurg.2022.1081823

18. Huang YC, Tsuang FY, Lee CW, Lin YH. Efficacy of preoperative embolization for metastatic spinal tumor surgery using angiographic vascularity assessment. *Eur Radiol* (2023) 33(4):2638–46. doi: 10.1007/s00330-022-09276-3

frontiers | Frontiers in Oncology

TYPE Original Research
PUBLISHED 07 December 2022
DOI 10.3389/fonc.2022.1095059

OPEN ACCESS

EDITED BY
Feifei Pu,
Huazhong University of Science and Technology, China

REVIEWED BY
Doudou Jing,
Second Hospital of Shanxi Medical University, China
Zhicai Zhang,
Huazhong University of Science and Technology, China

*CORRESPONDENCE
Xuedong Shi
xuedongs@hotmail.com
Mingxing Lei
leimingxing2@sina.com
Bailin Wang
wangbailin301@163.com

†These authors have contributed equally to this work

SPECIALTY SECTION
This article was submitted to Surgical Oncology, a section of the journal Frontiers in Oncology

RECEIVED 10 November 2022
ACCEPTED 25 November 2022
PUBLISHED 07 December 2022

CITATION
Cui Y, Wang Q, Shi X, Ye Q, Lei M and Wang B (2022) Development of a web-based calculator to predict three-month mortality among patients with bone metastases from cancer of unknown primary: An internally and externally validated study using machine-learning techniques. *Front. Oncol.* 12:1095059. doi: 10.3389/fonc.2022.1095059

Development of a web-based calculator to predict three-month mortality among patients with bone metastases from cancer of unknown primary: An internally and externally validated study using machine-learning techniques

Yunpeng Cui[1†], Qiwei Wang[1†], Xuedong Shi[1*], Qianwen Ye[2], Mingxing Lei[3,4*] and Bailin Wang[5*]

[1]Department of Orthopedic Surgery, Peking University First Hospital, Beijing, China, [2]Department of Oncology, Hainan Hospital of PLA General Hospital, Sanya, China, [3]Department of Orthopedic Surgery, Hainan Hospital of PLA General Hospital, Sanya, China, [4]Chinese PLA Medical School, Beijing, China, [5]Department of Thoracic Surgery, Hainan Hospital of PLA General Hospital, Sanya, China

Background: Individualized therapeutic strategies can be carried out under the guidance of expected lifespan, hence survival prediction is important. Nonetheless, reliable survival estimation in individuals with bone metastases from cancer of unknown primary (CUP) is still scarce. The objective of the study is to construct a model as well as a web-based calculator to predict three-month mortality among bone metastasis patients with CUP using machine learning-based techniques.

Methods: This study enrolled 1010 patients from a large oncological database, the Surveillance, Epidemiology, and End Results (SEER) database, in the United States between 2010 and 2018. The entire patient population was classified into two cohorts at random: a training cohort (n=600, 60%) and a validation cohort (410, 40%). Patients from the validation cohort were used to validate models after they had been developed using the four machine learning approaches of random forest, gradient boosting machine, decision tree, and eXGBoosting machine on patients from the training cohort. In addition, 101 patients from two large teaching hospital were served as an external validation cohort. To evaluate each model's ability to predict the outcome, prediction measures such as area under the receiver operating characteristic (AUROC) curves, accuracy, and Youden index were generated. The study's risk stratification was done using the best cut-off value. The Streamlit software was used to establish a web-based calculator.

Results: The three-month mortality was 72.38% (731/1010) in the entire cohort. The multivariate analysis revealed that older age (P=0.031), lung metastasis (P=0.012), and liver metastasis (P=0.008) were risk contributors for three-month mortality, while radiation (P=0.002) and chemotherapy (P<0.001) were protective factors. The random forest model showed the highest area under curve (AUC) value (0.796, 95% CI: 0.746-0.847), the second-highest precision (0.876) and accuracy (0.778), and the highest Youden index (1.486), in comparison to the other three machine learning approaches. The AUC value was 0.748 (95% CI: 0.653-0.843) and the accuracy was 0.745, according to the external validation cohort. Based on the random forest model, a web calculator was established: https://starxueshu-codeok-main-8jv2ws.streamlitapp.com/. When compared to patients in the low-risk groups, patients in the high-risk groups had a 1.99 times higher chance of dying within three months in the internal validation cohort and a 2.37 times higher chance in the external validation cohort (Both P<0.001).

Conclusions: The random forest model has promising performance with favorable discrimination and calibration. This study suggests a web-based calculator based on the random forest model to estimate the three-month mortality among bone metastases from CUP, and it may be a helpful tool to direct clinical decision-making, inform patients about their prognosis, and facilitate therapeutic communication between patients and physicians.

KEYWORDS

bone metastasis, cancer of unknown primary, survival estimation, machine learning, risk stratification

Introduction

Cancers of unknown primary (CUP) are metastatic malignancies with verified histology, whereas routine assessments and imaging techniques are unable to identify the primary cancer site (1). According to estimates, CUP occurs in 1% to 5% of all malignant neoplasms (2, 3), hence it is not exceptionally rare. CUP is featured by early and aggressive metastasis (4), such as bone metastases, and up to 30% bone metastases had unknown origin at the time of diagnosis although thorough physical examinations, laboratory tests, and contemporary radiological images were conducted (5).

CUP is still a cancer group of very dismal outcome (6), and CUP patient's prognoses regrettably obtained minimal improvement for recent decades, despite the emergence of precision oncology which is able to identify the putative origin of the CUP (6). Currently, the appropriate treatments for CUP required evaluation of prognosis. In general, patients with a favorable outcome (20% of CUP patients) were advised to receive locoregional treatment or systemic chemotherapy, while those with an unfavorable outcome (80% of CUP patients) were treated with empirical chemotherapy, and locoregional therapy such as surgical remove of bone metastasis should not be performed in this circumstance (2). Thus, estimating the prognosis is crucial for those patients.

To elaborate, accurate and individualized prediction of survival is vital to making clinical decision for the treatment of CUP patients with bone metastases. Surgery shouldn't be performed on patients who have a low chance of survival since it could cause more harm than good. In particular, palliative therapies should be used to treat patients with a survival time of fewer than three months (7–9). It should be noted that early appropriate prognostic discussions with patients could lead to better medical education of therapeutic goals and life expectancy (10). Although a multitude of studies proposed individual prognostic scoring systems to predict survival prognosis, survival classification models among CUP patients with bone metastases were really limited (11). Besides, oncologists did not frequently encounter CUP patients, which restricted physician's experience and intuitions that they could depend on for prognostic discussion.

Therefore, this study attempted to propose and validate an accurate model to predict three-month mortality among CUP patients with bone metastases. Because of individualized

prognostic evaluation and favorable predictive performance, machine learning approaches were widely used among oncologists to predict the survival prognosis of cancer patients (12, 13). Additionally, to encourage clinical implementation, the model will be presented as the format of a web-based calculator that is user-friendly for doctors to use. The study's hypothesis was that the model could be developed after choosing relevant risk factors as model parameters, utilizing machine learning to achieve the excellent accuracy of models, and establishing web calculator to increase utility.

Patients and methods

Patient selection

In the Surveillance, Epidemiology and End Results (SEER) database, 61036 individuals with bone metastases between 2010 and 2018 were examined for this investigation. The SEER database is a project of the National Cancer Institute and, in an effort to lessen the burden of cancer, it provides an authoritative source of information on cancer incidence and survival rate of 28.0% of the population in the United States. The SEER program is supported by the Surveillance Research Program in NCI's Division of Cancer Control and Population Sciences (http://seer.cancer.gov). SEER gathers data on cancer cases from a variety of locations and sources in the whole United States. The SEER*Stat Version 8.4.0.1 program was used in this investigation to retrieve information about individuals with bone metastases from the SEER database (2010–2018). CUP Patients were included in analysis. Patients were disqualified if they met the following criteria (1): 18 years old or less (2), death due to missing or unknown cause (3), having missing values in needed variable, and (4) having a follow-up of 3 months or less (Figure 1). Based on the above inclusive and exclusive criteria, 1010 patients were enrolled, and a 6:4 split of the entire patient population was randomly assigned to a training group (n=600) and a validation cohort (n=410). Patients from the validation cohort were used to validate the model, which had been developed with patients from the training cohort. A series of 106 CUP patients with bone metastases underwent external validation. Between December 2013 and June 2022, these patients were gathered from the Peking University First Hospital and the Hainan hospital of Chinese PLA General Hospital. The study protocol was approved by the Ethics Committee of the Peking University First Hospital and the Hainan hospital of Chinese PLA General Hospital, and written informed consent was waived due to retrospective data in nature.

Variables and the outcome

The study extracted the following variables: age (years), race (black or other or unknown or white), sex (female or male), brain metastasis (no or unknown or yes), liver metastasis (no or unknown or yes), lung metastasis (no or unknown or yes), radiation (no/unknown or yes), and chemotherapy (no/unknown or yes). Based on the Extent of Disease classification and the American Joint Committee on Cancer, the tumor stage and node stage were recoded. Three-month mortality was defined as patients had a survival outcome of three or less months according to the data in the SEER database.

Machine-learning models and evaluation of models

This study used four machine learning approaches including random forest (14), gradient boosting machine (15), decision tree (16), and eXGBoosting machine (17) to establish models in the training cohort. Leo Breiman in 2001 introduced random forest, and, using the bagging method (Bootstrap AGGregatING), random forest takes use of a series of decision trees with low reciprocal correlation and randomly selected attributes (14). Gradient boosting machine, introduced by Microsoft, is regarded as an ensemble algorithm, and it is able to provide an efficient use of the gradient boosting algorithm with the primary benefit of dramatic acceleration of the training algorithms (15). Decision tree is a data mining method for classification data, and it is presented as a tree-like structure, and in this structure each internal node indicates a test of a feature and each leaf node indicates a classification (16). eXGBoosting machine is a supervised machine learning model, and it utilizes an improved generalized gradient boosting technique to quickly determine the value of all input features (17).

Prior to modelling, significant variables should be identified by multivariate analysis in the training cohort. In the validation cohort, the nine prediction measures, including area under the receiver operating characteristic (AUROC) curves, discrimination slope, calibration slope, intercept-in-large, sensitivity, specificity, precision, Youden index, and accuracy, were used to evaluate predictive performance of the models. Among the nine metrics, AUROC, calibration, sensitivity, specificity, and accuracy are commonly used to evaluate model's effectiveness. The optimal model is the one with the most favorable discrimination and calibration.

AUROC was plotted using "pROC" package. Accuracy is better when the area under the curve (AUC) is higher. In details, an AUC value of 0.5 denotes chance, whereas an AUC value of 1.0 denotes complete compliance. Calibration curve was plotted using the "val.prob.ci" function, and the curve was plotted with the predicted probability against actual probability. Decision curve was plotted using the "ggDCA" package, and the curve was used to evaluate the clinical benefit of the model by quantifying the net benefit under different threshold probabilities. In this curve, two reference lines were placed to show the highest clinical cost (treat-for-all plan) and no clinical benefit (treat-for-none plan).

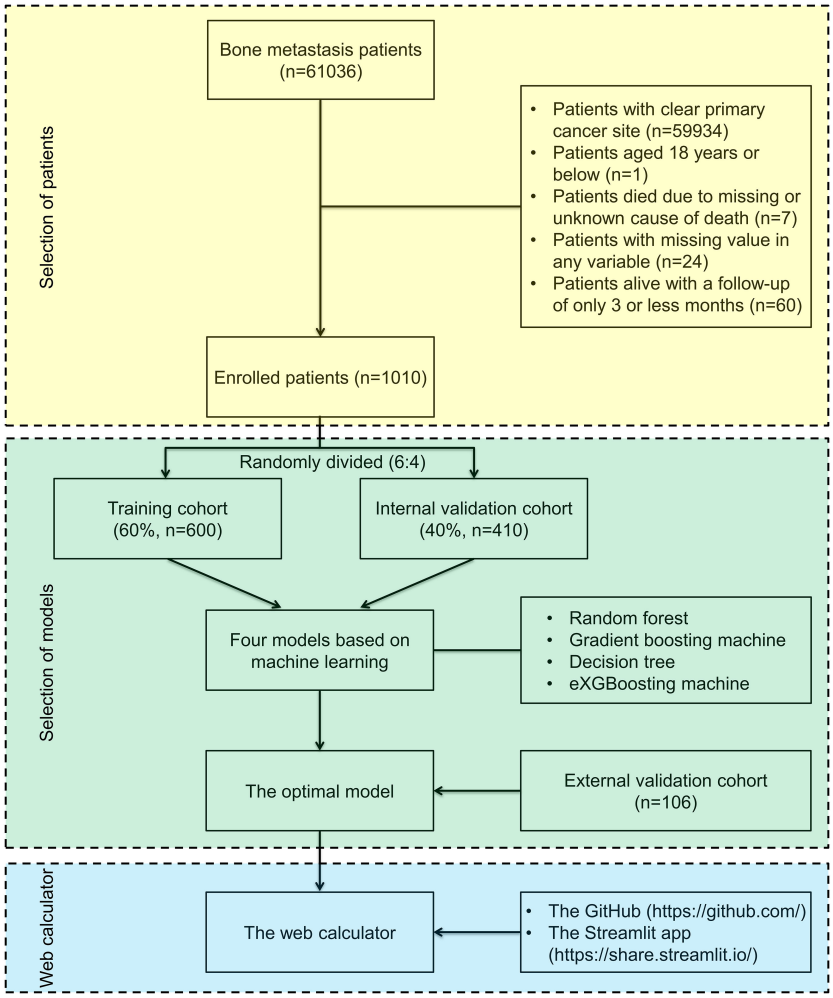

FIGURE 1
Flow diagram outlining patients and methods. The yellow area indicates selection of patients, the green area indicates selection of the optimal machine-learning model in the study, and the blue area indicates establishment of a web-based calculator.

Establishment of web-based calculator

The optimal machine-learning model was used to construct the web-based calculator. Firstly, the optimal model was saved as the format of PKL document *via* Python software (version 3.9.7). Secondly, the optimal model and corresponding Python code were both uploaded to the GitHub (https://github.com/) website. Lastly, a web calculator can be subsequently deployed after interlinking the Streamlit app (https://share.streamlit.io/) into the GitHub. In the calculator, this study designed a panel of feature selection, an introduction of the web calculator, a submit bottom, and results showing probability of three-month mortality and risk group classification.

Statistical analysis

All continuous data from the entire study were shown as mean and standard deviation (SD), while all categorical data were shown as proportions. To check for comparability, data from patients in the training and validation cohorts were compared. In the training cohort, a subgroup analysis was done between individuals who experienced three-month mortality and those who did not. Additionally, risk stratification was carried out in the study based on the ideal cut-off value (threshold), and a comparison between low-risk and high-risk groups using Chi-square test. R programming language (version 4.1.2) was used for data visualization and

statistical analysis, while Python (version 3.9.7) was used for machine learning operations. A P value of less than 0.05 was regarded as statistically significant, and all P values were two-tailed.

Results

Patient's basic clinical characteristics

A total of 1010 bone metastasis patients were enlisted for analysis based on the inclusive and exclusive criteria. Age was 71.41 years (SD: 13.43 years) on average. The majority patients were white (79.5%) and male (54.3%) (Table 1). Only a small fraction of patients suffered from brain metastasis (9.7%), but up to 46.4% of patients had liver metastasis, and 35.0% of patients diagnosed with lung metastasis, indicating that the burden due to metastatic diseases was relatively high. The therapeutic interventions were not so commonly performed since only 26.8% of patients underwent radiation and 20.7% treated with chemotherapy possibly. This could be because the primary origin of cancers was not known, making it difficult to undertake the proper interventions. The median survival time was 1.0 months (95% CI: 0.83-1.17 months) in the entire cohort. In addition, Table 1 also demonstrated that the baseline characteristics were comparable between the training and validation cohorts (All P>0.05).

Analyses of three-month mortality

Of all enrolled patients, up to 72.38% patients passed away at or within three months. Patients with bone metastases from CUP saw relatively steady three-month mortality from 2010 to 2018 (Figure 2A). The three-month mortality increased significantly with age (Figure 2B). When compared to patients

TABLE 1 Patient's demographics and clinical characteristics.

Characteristics	Overall	Cohorts		P-values [a]
		Training	Validation	
n	1010	600	410	
Age (mean (SD))	71.41 (13.43)	71.17 (14.04)	71.77 (12.50)	0.487
Race (%)				0.619
Black	135 (13.4)	75 (12.5)	60 (14.6)	
White	803 (79.5)	482 (80.3)	321 (78.3)	
Others	72 (7.1)	43 (7.2)	29 (7.1)	
Sex (%)				0.793
Female	462 (45.7)	277 (46.2)	185 (45.1)	
Male	548 (54.3)	323 (53.8)	225 (54.9)	
Brain metastasis (%)				0.553
No	747 (74.0)	440 (73.3)	307 (74.9)	
Unknown	165 (16.3)	104 (17.3)	61 (14.9)	
Yes	98 (9.7)	56 (9.3)	42 (10.2)	
Liver metastasis (%)				0.289
No	431 (42.7)	253 (42.2)	178 (43.4)	
Unknown	110 (10.9)	73 (12.2)	37 (9.0)	
Yes	469 (46.4)	274 (45.7)	195 (47.6)	
Lung metastasis (%)				0.276
No	502 (49.7)	299 (49.8)	203 (49.5)	
Unknown	155 (15.3)	100 (16.7)	55 (13.4)	
Yes	353 (35.0)	201 (33.5)	152 (37.1)	
Radiation (%)				0.277
No/unknown	739 (73.2)	431 (71.8)	308 (75.1)	
Yes	271 (26.8)	169 (28.2)	102 (24.9)	
Chemotherapy (%)				0.832
No/unknown	801 (79.3)	474 (79.0)	327 (79.8)	
Yes	209 (20.7)	126 (21.0)	83 (20.2)	

SD, Standard deviation.
[a]indicates the continuity adjusted Chi-square test.

without three-month mortality, patients with three-month mortality had significantly a higher age (73.21 years vs. 66.12 years, P<0.001, Table 2) and a higher proportion of white people (82.0% vs. 76.3%, P=0.029). Besides, three-month mortality group had a significantly greater rate of liver metastasis (47.8% vs. 40.5%, P=0.031) and lung metastasis (36.3% vs. 26.6%, P=0.035) and a significant lower rate of receiving radiation (21.1% vs. 45.7%, P<0.001) and chemotherapy (9.4% vs. 49.7%, P<0.001) versus no three-month mortality group.

Selection of features for web calculator

Univariate analysis revealed that age (P<0.001), other race (P=0.044), liver metastasis (P=0.027), lung metastasis (P=0.011), radiation (P<0.001), and chemotherapy (P<0.001) were significantly associated with three-month mortality (Table 3). Based on the multivariate analysis, age (P=0.031), liver metastasis (P=0.008), lung metastasis (P=0.012), radiation (P=0.002), and chemotherapy (P<0.001) were significantly relevant to three-month mortality. To be more specific, older age, lung metastasis, and liver metastasis were risk contributors, while radiation and chemotherapy both were protective features. Depending on the multivariate analysis, features for the model was determined. Thus, the four machine learning approaches were used to train and optimize models using the aforementioned five factors.

Selection of model for web calculator

Model construction

The super-parameters were obtained after randomized search with cross validation in each machine learning model, and the full super-parameters were shown in the Supplementary Table 1. Supplementary Figure 1 shows the learning curves of the random forest and gradient boosting machine, and Supplementary Figure 2 shows the learning curves of the decision tree and eXGBoosting machine. All of these learning curves suggested that underfitting and overfitting were largely avoided after randomized search for appropriate super-parameters.

Internal validation

The area under curve (AUC) values were 0.796 (95% CI: 0.746-0.847, Figure 3A) in the random forest model, 0.784 (95% CI: 0.732-0.837, Figure 3B) in the gradient boosting machine model, 0.755 (95% CI: 0.701-0.810, Figure 3C) in the decision tree model, 0.786 (95% CI: 0.734-0.838, Figure 3D) in the eXGBoosting machine model. Figure 4 shows probability curve of each machine learning model, and it demonstrated that all the four models had favorable discrimination since the two groups were largely separated. The discrimination slope was 0.196 in the random forest (Figure 5A), 0.237 in the gradient boosting machine (Figure 5B), 0.215 in the decision tree (Figure 5C), 0.208 in the eXGBoosting machine approach (Figure 5D). The corresponding calibration slopes were 1.36 (Supplementary Figure 3A), 0.97 (Supplementary Figure 3B), 0.83 (Supplementary Figure 3C), and 1.13 (Supplementary Figure 3D) respectively. Figure 6 shows decision curve analysis of all models, and it denoted favorable clinical usefulness of each approach. Table 4 shows predictive performance of each approach, and it demonstrated that the random forest not only had the highest AUC value, but also the highest Youden index and the second-highest accuracy and precision. Therefore, the random forest model was used as the optimal model in the study. Accordingly, external validation, risk stratification, and the development of a web calculator were conducted using the random forest model.

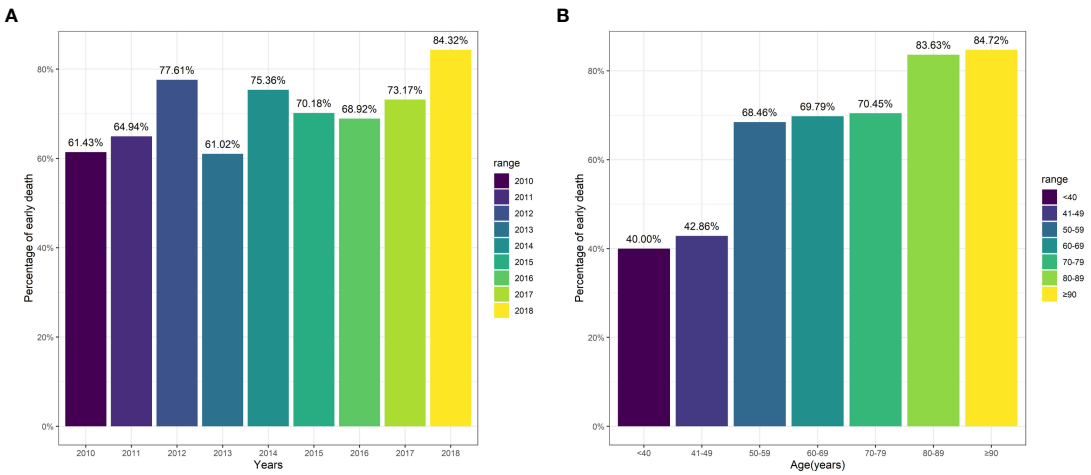

FIGURE 2
Three-month mortality among patients stratified by variables. **(A)** Year of diagnosis; **(B)** Age.

TABLE 2 Subgroup analysis between patients according to three-month mortality in the training cohort.

Characteristics	Overall	Three-month mortality		P-values [a]
		No	Yes	
n	600	173	427	
Age (mean (SD))	71.17 (14.04)	66.12 (15.59)	73.21 (12.83)	<0.001
Race (%)				0.029
Black	75 (12.5)	21 (12.1)	54 (12.6)	
White	482 (80.3)	132 (76.3)	350 (82.0)	
Other	43 (7.2)	20 (11.6)	23 (5.4)	
Sex (%)				0.669
Female	277 (46.2)	77 (44.5)	200 (46.8)	
Male	323 (53.8)	96 (55.5)	227 (53.2)	
Brain metastasis (%)				0.785
No	440 (73.3)	127 (73.4)	313 (73.3)	
Unknown	104 (17.3)	28 (16.2)	76 (17.8)	
Yes	56 (9.3)	18 (10.4)	38 (8.9)	
Liver metastasis (%)				0.031
No	253 (42.2)	87 (50.3)	166 (38.9)	
Unknown	73 (12.2)	16 (9.2)	57 (13.3)	
Yes	274 (45.7)	70 (40.5)	204 (47.8)	
Lung metastasis (%)				0.035
No	299 (49.8)	100 (57.8)	199 (46.6)	
Unknown	100 (16.7)	27 (15.6)	73 (17.1)	
Yes	201 (33.5)	46 (26.6)	155 (36.3)	
Radiation (%)				<0.001
No/unknown	431 (71.8)	94 (54.3)	337 (78.9)	
Yes	169 (28.2)	79 (45.7)	90 (21.1)	
Chemotherapy (%)				<0.001
No/unknown	474 (79.0)	87 (50.3)	387 (90.6)	
Yes	126 (21.0)	86 (49.7)	40 (9.4)	

SD, standard deviation.
[a]indicates the continuity adjusted Chi-square test.

External validation

A series of 106 bone metastasis patients with CUP underwent external validation. The basic clinical characteristics are summarized in Supplementary Table 2. The AUC value was 0.748 (95% CI: 0.653-0.843, Supplementary Figure 4). The probability curve is depicted in Supplementary Figure 5, with discrimination slope being 0.113 (Supplementary Figure 6) and the calibration slope being 1.250 (Supplementary Figure 7). Supplementary Figure 8 shows model's decision curve analysis in the external validation cohort. The above results indicated that the optimal model also exhibited good discrimination and calibration in the external validation cohort.

Establishment of web calculator

A web calculator was constructed according the optimal model (the random forest model) in the study. Visiting https://starxueshu-codeok-main-8jv2ws.streamlitapp.com/, users is able to access to the online calculator. If the online calculator has gone to sleep (shut down), users are able to access to it *via* clicking "Yes, get this app back up!". After about 30 seconds, the web-based calculator would be accessible. Users can choose features according to their conditions in the panel of selecting parameters, and then probability of three-month mortality could be obtained by submitting all parameters. In addition, related therapy recommendation was displayed in accordance with the risk stratification. The risk stratification was achieved based on the best cut-off value (71.10%) in the random forest model: Patients in the high-risk group were 1.99 times more likely to suffer from three-month mortality than patients in the low-risk group (P<0.001, Table 5) in the internal validation cohort. External validation showed the similar trend (Table 6): patients in the high-risk group had 2.37-time odds of three-month mortality than patient in the low-risk group (P<0.001).

TABLE 3 Univariate and multivariate analysis of potential risk factors for predicting three-month mortality among bone metastasis from CUP in the training cohort.

Characteristics	Univariate analysis		Multivariate analysis	
	OR (95%CI)	P-value	OR (95%CI)	P-value
n				
Age (mean (SD))	1.04 (1.02-1.05)	<0.001	1.02 (1.00-1.03)	0.031
Race (%)				
Black	Reference		Reference	
White	1.03 (0.60-1.77)	0.912	1.39 (0.73-2.65)	0.311
Other	0.45 (0.20-0.98)	0.044	0.56 (0.23-1.37)	0.204
Sex (%)				
Female	Reference		Reference	
Male	0.91 (0.64-1.30)	0.604	1.06 (0.70-1.61)	0.780
Brain metastasis (%)				
No	Reference		Reference	
Unknown	1.10 (0.68-1.78)	0.693	0.51 (0.22-1.18)	0.117
Yes	0.86 (0.47-1.56)	0.612	1.05 (0.49-2.23)	0.902
Liver metastasis (%)				
No	Reference		Reference	
Unknown	1.87 (1.01-3.44)	0.046	1.85 (0.66-5.20)	0.241
Yes	1.53 (1.05-2.22)	0.027	1.90 (1.18-3.04)	0.008
Lung metastasis (%)				
No	Reference		Reference	
Unknown	1.36 (0.82-2.25)	0.232	1.43 (0.58-3.52)	0.437
Yes	1.69 (1.13-2.54)	0.011	1.93 (1.16-3.22)	0.012
Radiation				
No/unknown (%)	Reference		Reference	
Yes (%)	0.32 (0.22-0.46)	<0.001	0.49 (0.31-0.76)	0.002
Chemotherapy				
No/unknown (%)	Reference		Reference	
Yes (%)	0.10 (0.07-0.16)	<0.001	0.11 (0.07-0.18)	<0.001

OR, odds ratio; CI: confident interval; CUP, cancer of unknown primary; SD, standard deviation.

Additionally, introduction of the model was shown at the end of the interface. Supplementary Figure 9 shows a screenshot of the web calculator. In the screenshot, a specific example was presented: a 57-year-old patient without liver and lung metastasis did not receive radiation and chemotherapy, and the three-month mortality was up to 72.30%.

Discussion

Main findings

This study found that older age, lung metastasis, and liver metastasis were significant contributors for three-month mortality, with radiation and chemotherapy being protective factors for survival. Furthermore, using machine learning, the study developed an accurate model that was able to predict survival among bone metastases patients from CUP, and its predictive performance showed good discriminative and calibrating ability. The model was incorporated into a web-based calculator to encourage clinical reference and research use. This model might be a useful tool to facilitate personalized survival estimation and do some help to guide clinical decision-making.

Survival prognosis

In the entire cohort of patients, up to 72.38% patients passed away at or within three months, and this incidence was significantly higher as compared to that among patients with other cancers. It was reported that 33.7% of bone metastasis patients with common cancers suffered from three-month mortality (18) and 44.4% of lung cancer patients with synchronous brain metastasis had early death

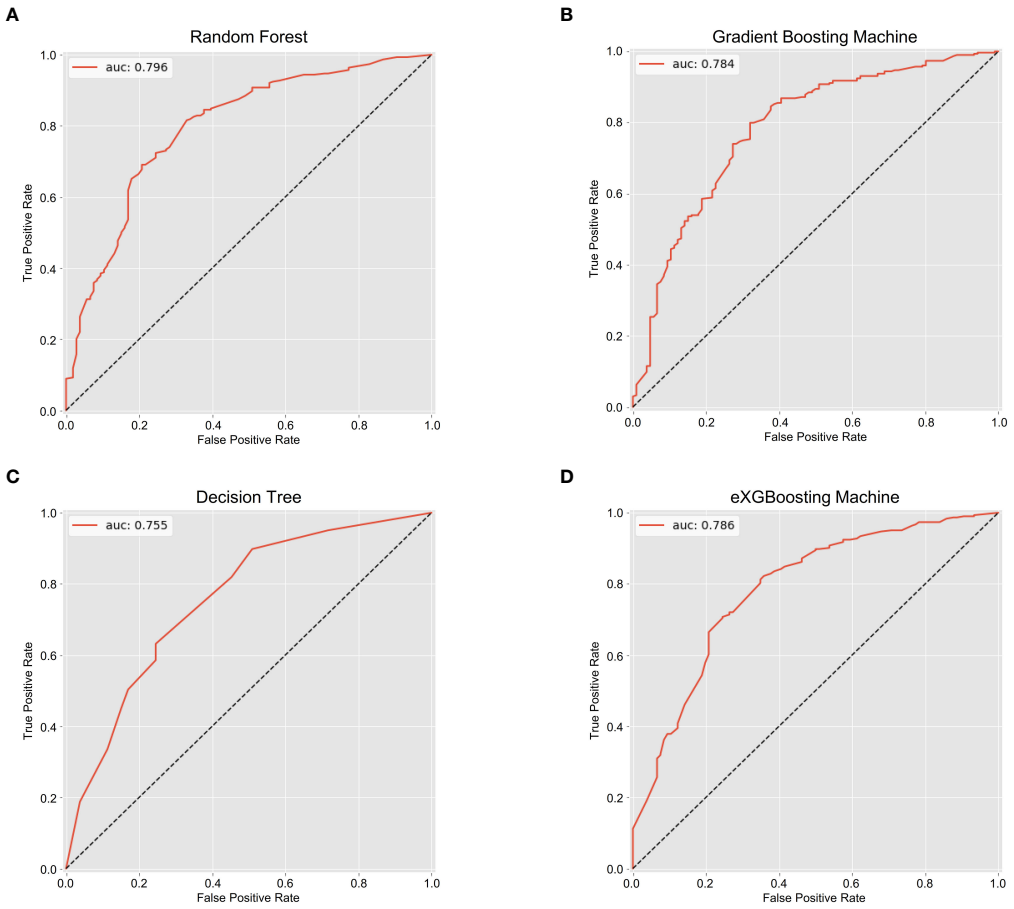

FIGURE 3
The area under the receiver operating characteristic curves for each approach. **(A)** Random Forest; **(B)** Gradient Boosting Machine; **(C)** Decision Tree; **(D)** eXGBoosting Machine.

(a survival outcome of three or less months) (19). Raghav et al. (20) showed that the median survival time of CUP patients was 14.7 months in a retrospective study. Jin et al. (21) found that the median overall survival time of CUP patients was 6.0 months among patients from the SEER database. Chambard et al. (22) reported that bone metastasis patients with lung cancer had a median survival of 7.0 months. Another large retrospective study found that the median survival time of bone metastasis patients with common cancers was 6.0 months (18). As for the cohort of patients in the present study, the median survival time was only 1.0 months. This short survival time could be explained by the evidence that bone metastasis and CUP were all contributors to negatively affecting survival outcome. What's more, the majority of CUP (80%) had unfavorable prognosis (2). Additionally, this study found that the three-month mortality increased significantly with age, and Shen et al. (19) found the similar trend among lung cancer patients with synchronous brain metastasis.

Model features

The model features in the study contained five variables: age, lung metastasis, liver metastasis, radiation, and chemotherapy. These variables were also proved to be associated with survival outcome among CUP patients in other studies (20, 23). Furthermore, a recent study showed that gender, Eastern Cooperative Oncology Group performance status, histology, number of metastatic sites, and neutrophil-lymphocyte ratio were independent prognostic factors for survival among CUP patients (20). Huey et al. (24) demonstrated that high neutrophil-to-lymphocyte ratio were associated with worse overall survival among CUP with bone-predominant or lymph node-only disease. Consequently, some measures to improve empirical chemotherapy or radiation, performance status, and neutrophil-lymphocyte ratio would be beneficial to survival prognosis among CUP patients.

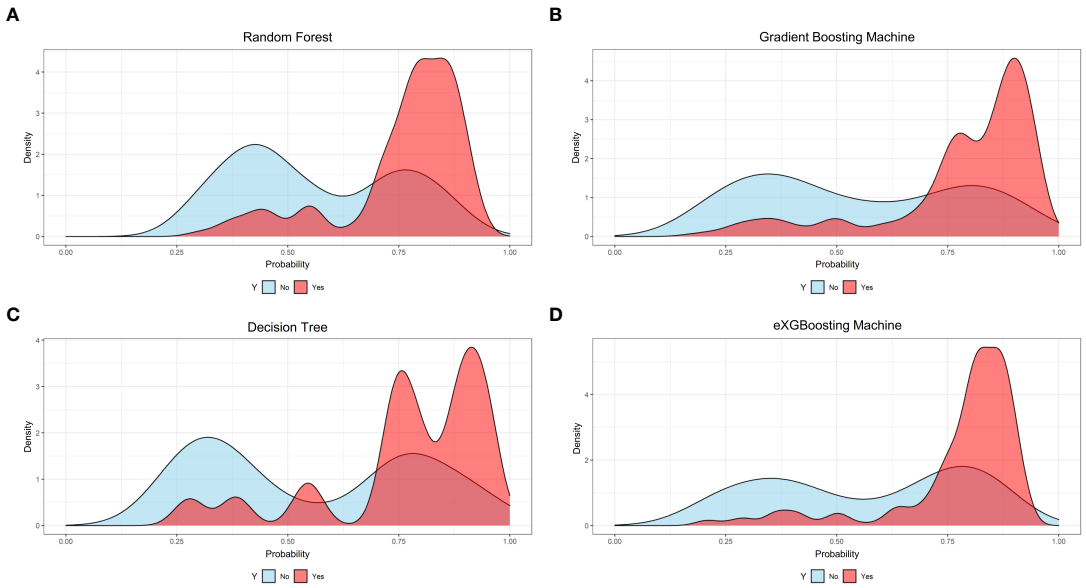

FIGURE 4
Probability curves for each approach. **(A)** Random Forest; **(B)** Gradient Boosting Machine; **(C)** Decision Tree; **(D)** eXGBoosting Machine.

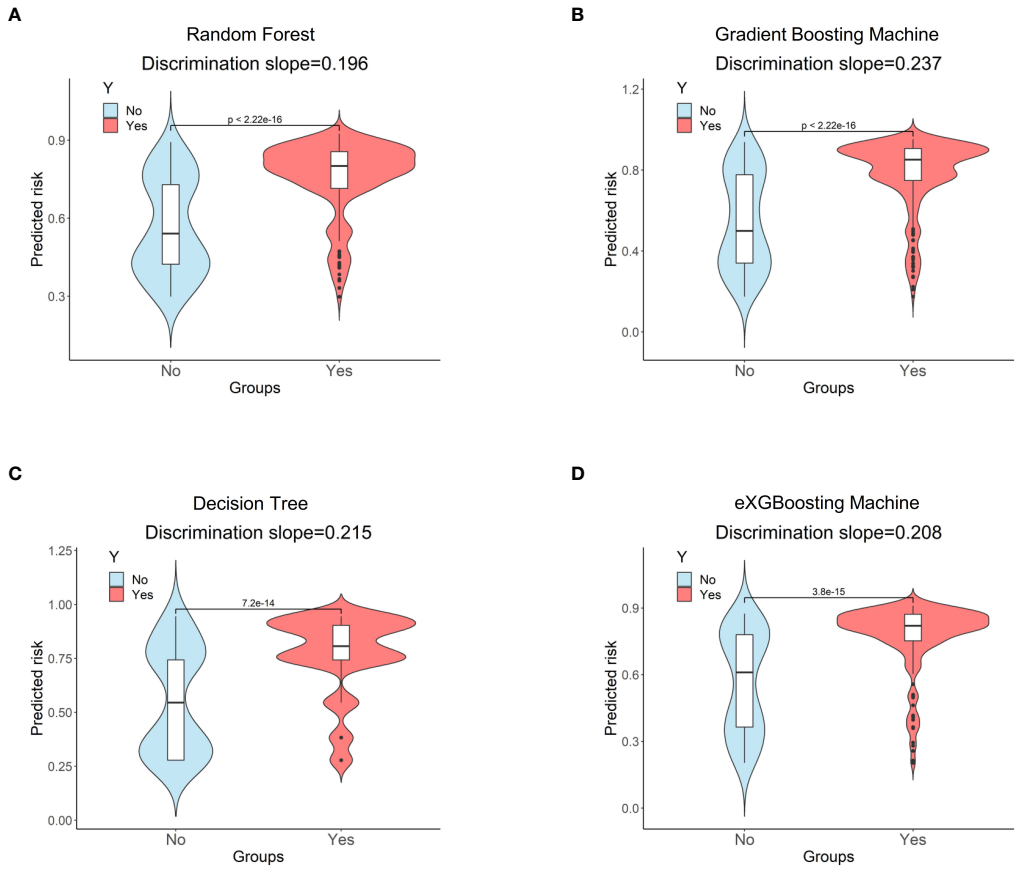

FIGURE 5
Discrimination slopes for each approach. **(A)** Random Forest; **(B)** Gradient Boosting Machine; **(C)** Decision Tree; **(D)** eXGBoosting Machine.

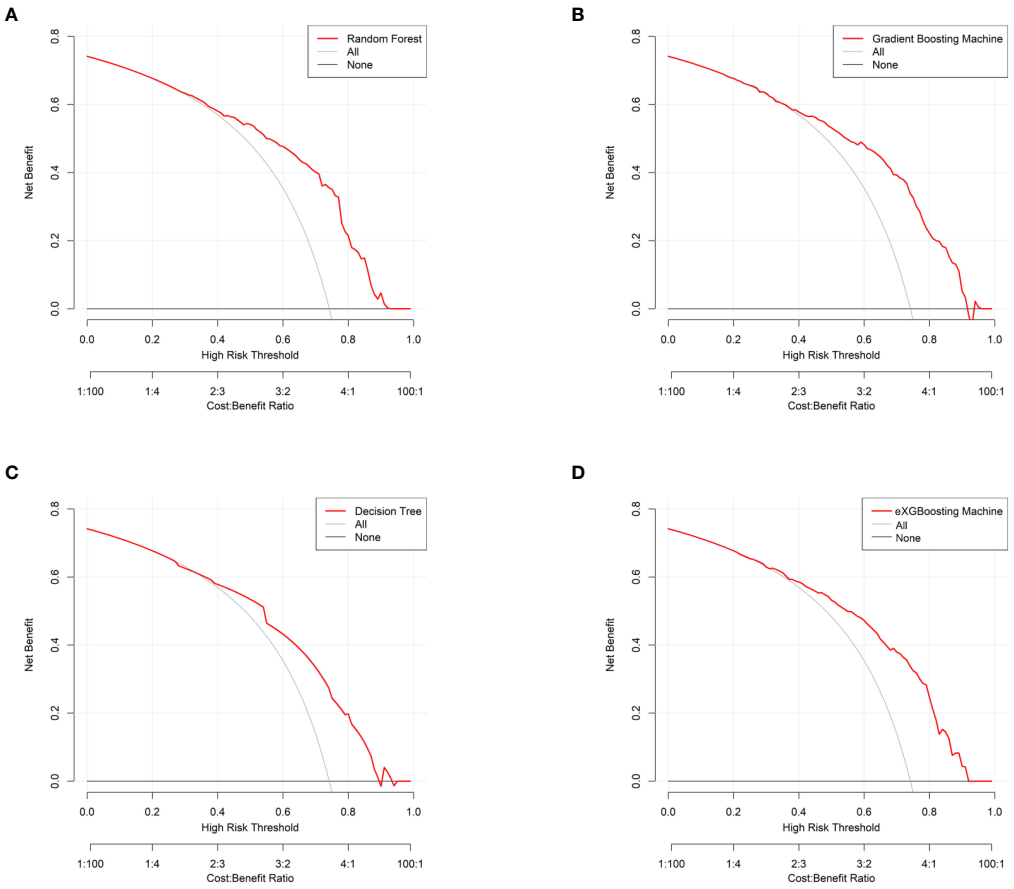

FIGURE 6
Decision curve analysis for each approach. **(A)** Random Forest; **(B)** Gradient Boosting Machine; **(C)** Decision Tree; **(D)** eXGBoosting Machine.

TABLE 4 Prediction performance of machine learning approaches for predicting three-month mortality among bone metastatic patients from CUP.

Measures	Internal validation cohort				External validation cohort
	Random forest	Gradient boosting machine	Decision tree	eXGBoosting machine	
Intercept-in-large	0.20	0.14	0.18	0.12	-0.95
Calibration slope	1.36	0.97	0.83	1.13	1.25
AUC (95%CI)	0.796 (0.746-0.847)	0.784 (0.732-0.837)	0.755 (0.701-0.810)	0.786 (0.734-0.838)	0.748 (0.653-0.843)
Discrimination slope	0.196	0.237	0.215	0.208	0.113
Specificity	0.670	0.679	0.491	0.642	0.772
Sensitivity	0.816	0.799	0.898	0.822	0.714
Precision	0.876	0.877	0.835	0.868	0.729
Youden	1.486	1.479	1.389	1.464	1.486
Accuracy	0.778	0.768	0.793	0.776	0.745
Threshold	0.711	0.724	0.464	0.723	0.718

AUC, Area under the curve; CI, Confident interval; CUP, cancer of unknown primary; eXGBoosting machine, eXtreme gradient boosting machine.

TABLE 5 Risk stratification among patients in the internal validation cohort.

Risk groups	Patients (n = 410)	Probability		P-value [a]
		Predicted	Actual	
Low-risk (≦71.10%)	127	47.25%	44.09% (56/127)	<0.001
High-risk (> 71.10%)	283	81.32%	87.63% (248/283)	

[a]indicates P-value was obtained from the Chi-square test.

Survival prediction

A number of survival scoring systems had already proposed to predict survival outcome among bone metastasis patients (25), spine metastasis patients (9), and various cancer patients (26–28). As for CUP, in the year of 2021, Raghav et al. (20) developed a model to predict survival prognosis among CUP in a series of 521 patients and validated the model in two cohorts (n=103 and 302). Five independent prognostic factors were included in the model and the model had a C-index of 0.71. In the same year, Jin et al. (21) proposed a model for predicting survival among CUP. A total of 3347 patients were divided into a training cohort and a validation cohort. The C-index of the model was 0.705 in the training cohort and 0.727 in the validation cohort. More recently, in 2022, Yang et al. (29) created a model including six independent prognostic factors (pathology, visceral metastases, Frankel score, weight loss, hemoglobin, and serum tumor markers) to predict survival outcome among spinal metastasis from CUP in a retrospective derivation cohort of 268 patients and this model was validated in a prospective validation cohort of 105 patients. The C-index was 0.775 in the derivation group and 0.771 in the validation cohort. The above prediction models were designed for CUP and might not be applicable in particular bone metastasis patients with CUP. In the present study, the C-index was up to 0.796 based on the random forest model, and the number was the highest as compared to the above studies. Internal and external validation both confirmed that the model had favorable discriminative and calibrating ability.

Individualized therapeutic strategies

Risk classification of patients was accomplished in the study, and patients could be split into two risk categories based on the ideal threshold, allowing for the personalized execution of therapeutic strategies. Patients in the high-risk categories had a roughly two-fold greater chance than those in the low-risk groups of dying within three months.

For palliative pain relief, patients in the high-risk group may benefit from the best supportive care, short-term radiation, or even minimally invasive procedures like cementoplasty (7). The study's proposed model, which dose not ask for any additional staff training, can be used clinically to forecast the survival benefit of patients with bone metastases and raise the performance of oncologists and radiologists who aren't professionals to that of experts.

Limitations

Although this study was well designed, there were still several drawbacks. To begin with, some variables, such as comorbidity and laboratory data, were not available due to the limitation of the SEER database, and clinically the detailed information on cancer were also unavailable because of the unclear primary cancer site. Incorporating those variables might further improve prediction performance of the model, but the AUC values demonstrated that the model was useful enough to predict three-month mortality. Furthermore, our study aimed at proposing a model with routine clinical data that were widely available and easily accessible. Under such circumstances, it would be more practical for oncologists to apply the model in these situations. In addition, external validation was only performed in a small study, thus the generalization of the model needs further validation. Therefore, although the model was validated and embraced favorable prediction performance, it warrants further extensive revision and validation.

Conclusions

The random forest model has promising performance with favorable discrimination and calibration. This study suggests a web-

TABLE 6 Risk stratification among patients in the external validation cohort.

Risk groups	Patients (n = 106)	Probability		P-value [a]
		Predicted	Actual	
Low-risk (≦71.10%)	37	48.43%	24.32% (9/37)	<0.001
High-risk (> 71.10%)	69	76.73%	57.97% (40/69)	

[a]indicates P-value was obtained from the Chi-square test.

based calculator based on the random forest model to estimate the three-month mortality among bone metastases from CUP, and it may be a helpful tool to direct clinical decision-making, inform patients about their prognosis, and facilitate therapeutic communication between patients and physicians. Patients in the high-risk group may better be treated with best supportive care due to very limited survival expectancy.

Data availability statement

Publicly available datasets were analyzed in this study. This data can be found here: SEER program is supported by the Surveillance Research Program in NCI's Division of Cancer Control and Population Sciences (http://seer.cancer.gov).

Ethics statement

The studies involving human participants were reviewed and approved by The study protocol was approved by the Ethics Committee of Peking University First Hospital and Hainan hospital of Chinese PLA General Hospital. Written informed consent for participation was not required for this study in accordance with the national legislation and the institutional requirements.

Author contributions

All authors conceived and designed the analysis, XS and QW oversaw data collection, YC, QY, and ML performed the analysis and all authors provided clinical interpretation of the findings. XS and ML drafted the manuscript. All authors reviewed, edited and confirmed their acceptance of the final submitted version.

Conflict of interest

The authors declare that the research was conducted in the absence of any commercial or financial relationships that could be construed as a potential conflict of interest.

Publisher's note

Supplementary material

The Supplementary Material for this article can be found online at: https://www.frontiersin.org/articles/10.3389/fonc.2022.1095059/full#supplementary-material

SUPPLEMENTARY FIGURE 1
Learning curves. A. Random Forest; B. Gradient Boosting Machine.

SUPPLEMENTARY FIGURE 2
Learning curves. C. Decision Tree; D. eXGBoosting Machine.

SUPPLEMENTARY FIGURE 3
Calibration curves for each approach. **(A)** Random Forest; **(B)** Gradient Boosting Machine; **(C)** Decision Tree; **(D)** eXGBoosting Machine.

SUPPLEMENTARY FIGURE 4
The area under the receiver operating characteristic curve in the external validation cohort.

SUPPLEMENTARY FIGURE 5
Probability curve in the external validation cohort.

SUPPLEMENTARY FIGURE 6
Discrimination slope in the external validation cohort.

SUPPLEMENTARY FIGURE 7
Calibration curve in the external validation cohort.

SUPPLEMENTARY FIGURE 8
Decision curve analysis in the external validation cohort.

SUPPLEMENTARY FIGURE 9
The web calculator.

References

1. Lee MS, Sanoff HK. Cancer of unknown primary. *BMJ* (2020) 371:m4050. doi: 10.1136/bmj.m4050

2. Pavlidis N, Pentheroudakis G. Cancer of unknown primary site. *Lancet* (2012) 379:1428–35. doi: 10.1016/S0140-6736(11)61178-1

3. Rassy E, Parent P, Lefort F, Boussios S, Baciarello G, Pavlidis N. New rising entities in cancer of unknown primary: Is there a real therapeutic benefit? *Crit Rev Oncol Hematol* (2020) 147:102882. doi: 10.1016/j.critrevonc.2020.102882

4. Rassy E, Assi T, Pavlidis N. Exploring the biological hallmarks of cancer of unknown primary: where do we stand today? *Br J Cancer* (2020) 122:1124–32. doi: 10.1038/s41416-019-0723-z

5. Piccioli A, Maccauro G, Spinelli MS, Biagini R, Rossi B. Bone metastases of unknown origin: epidemiology and principles of management. *J Orthop Traumatol* (2015) 16:81–6. doi: 10.1007/s10195-015-0344-0

6. Olivier T, Fernandez E, Labidi-Galy I, Dietrich PY, Rodriguez-Bravo V, Baciarello G, et al. Redefining cancer of unknown primary: Is precision medicine really shifting the paradigm? *Cancer Treat Rev* (2021) 97:102204. doi: 10.1016/j.ctrv.2021.102204

7. Cui YP, Shi XD, Wang SJ, Qin Y, Wang BL, Che XT, et al. Machine learning approaches for prediction of early death among lung cancer patients with bone metastases using routine clinical characteristics: An analysis of 19,887 patients. *Front Public Health* (2022) 10:1019168. doi: 10.3389/fpubh.2022.1019168

8. Cui Y, Lei M, Pan Y, Lin Y, Shi X. Scoring algorithms for predicting survival prognosis in patients with metastatic spinal disease: The current status and future directions. *Clin Spine Surg* (2020) 33:296–306. doi: 10.1097/BSD.0000000000001031

9. Lei M, Li J, Liu Y, Jiang W, Liu S, Zhou S. Who are the best candidates for decompressive surgery and spine stabilization in patients with metastatic spinal

cord compression? A new scoring system. *Spine (Phila Pa 1976)* (2016) 41:1469–76, 41. doi: 10.1097/BRS.0000000000001538

10. Liu PH, Landrum MB, Weeks JC, Huskamp HA, Kahn KL, He YL, et al. Physicians' propensity to discuss prognosis is associated with patients' awareness of prognosis for metastatic cancers. *J Palliat Med* (2014) 17:673–U49. doi: 10.1089/jpm.2013.0460

11. Culine S. Prognostic factors in unknown primary cancer. *Semin Oncol* (2009) 36:60–4. doi: 10.1053/j.seminoncol.2008.10.004

12. Ngiam KY, Khor IW. Big data and machine learning algorithms for health-care delivery. *Lancet Oncol* (2019) 20:e262–73. doi: 10.1016/S1470-2045(19)30149-4

13. Tahmassebi A, Wengert GJ, Helbich TH, Bago-Horvath Z, Alaei S, Bartsch R, et al. Impact of machine learning with multiparametric magnetic resonance imaging of the breast for early prediction of response to neoadjuvant chemotherapy and survival outcomes in breast cancer patients. *Invest Radiol* (2019) 54:110–7. doi: 10.1097/RLI.0000000000000518

14. Strobl C, Malley J, Tutz G. An introduction to recursive partitioning: rationale, application, and characteristics of classification and regression trees, bagging, and random forests. *Psychol Methods* (2009) 14:323–48. doi: 10.1037/a0016973

15. Ke GL, Meng Q, Finley T, Wang TF, Chen W, Ma WD, et al. *Lightgbm: A highly efficient gradient boosting decision tree. in advances in neural information processing systems 30 (NIP 2017)* (2017). Available at: https://proceedings.neurips.cc/paper/2017/hash/6449f44a102fde848669bdd9eb6b76fa-Abstract.html (Accessed 22 November 2022).

16. Che DS, Liu Q, Rasheed K, Tao XP. Decision tree and ensemble learning algorithms with their applications in bioinformatics. *Software Tools Algorithms Biol Syst* (2011) 696:191–9. doi: 10.1007/978-1-4419-7046-6_19

17. Alim M, Ye GH, Guan P, Huang DS, Zhou BS, Wu W. Comparison of ARIMA model and XGBoost model for prediction of human brucellosis in mainland China: a time-series study. *BMJ Open* (2020) 10:e039676. doi: 10.1136/bmjopen-2020-039676

18. Phanphaisarn A, Patumanond J, Settakorn J, Chaiyawat P, Klangjorhor J, Pruksakorn D. Prevalence and survival patterns of patients with bone metastasis from common cancers in Thailand. *Asian Pac J Cancer Prev* (2016) 17:4335–40. Available at: http://journal.waocp.org/?sid=Entrez:PubMed&id=pmid:27797240&key=2016.17.9.4335.

19. Shen H, Deng G, Chen Q, Qian J. The incidence, risk factors and predictive nomograms for early death of lung cancer with synchronous brain metastasis: a retrospective study in the SEER database. *BMC Cancer* (2021) 21:825. doi: 10.1186/s12885-021-08490-4

20. Raghav K, Hwang H, Jacome AA, Bhang E, Willett A, Huey RW, et al. Development and validation of a novel nomogram for individualized prediction of survival in cancer of unknown primary. *Clin Cancer Res* (2021) 27:3414–21. doi: 10.1158/1078-0432.CCR-20-4117

21. Jin YZ, Lin MX, Luo ZG, Hu XC, Zhang J. Development and validation of a nomogram for predicting overall survival of patients with cancer of unknown primary: a real-world data analysis. *Ann Transl Med* (2021) 9:198. doi: 10.21037/atm-20-4826

22. Chambard L, Girard N, Ollier E, Rousseau JC, Duboeuf F, Carlier MC, et al. Bone, muscle, and metabolic parameters predict survival in patients with synchronous bone metastases from lung cancers. *Bone* (2018) 108:202–9. doi: 10.1016/j.bone.2018.01.004

23. Li X, Shao Y, Sheng L, Zhu J, Wang Z, Guo K, et al. Risk factors and predictors for tumor site origin in metastatic adenocarcinoma of unknown primary site. *Cancer Med* (2021) 10:974–88. doi: 10.1002/cam4.3684

24. Huey RW, Smaglo BG, Estrella JS, Matamoros A, Overman MJ, Varadhachary GR, et al. Cancer of unknown primary presenting as bone-predominant or lymph node-only disease: A clinicopathologic portrait. *Oncologist* (2021) 26:E650–7. doi: 10.1002/onco.13700

25. Katagiri H, Okada R, Takagi T, Takahashi M, Murata H, Harada H, et al. New prognostic factors and scoring system for patients with skeletal metastasis. *Cancer Med* (2014) 3:1359–67. doi: 10.1002/cam4.292

26. Chi C, Fan Z, Yang B, Sun H, Zheng Z. The clinical characteristics and prognostic nomogram for head and neck cancer patients with bone metastasis. *J Oncol* (2021) 2021:5859757. doi: 10.1155/2021/5859757

27. Jia Y, Zhang W, You S, Li M, Lei L, Chen L. A nomogram for predicting depression in patients with hepatocellular carcinoma: an observational cross-sectional study. *Int J Psychiatry Clin Pract* (2019) 23:273–80. doi: 10.1080/13651501.2019.1619777

28. Wu J, Zhang H, Li L, Hu M, Chen L, Xu B, et al. A nomogram for predicting overall survival in patients with low-grade endometrial stromal sarcoma: A population-based analysis. *Cancer Commun* (2020) 40:301–12. doi: 10.1002/cac2.12067

29. Yang M, Ma X, Wang P, Yang J, Zhong N, Liu Y, et al. Prediction of survival prognosis for spinal metastasis from cancer of unknown primary: Derivation and validation of a nomogram model. *Global Spine J* (2022) 21925682221103833. doi: 10.1177/21925682221103833

frontiers | Frontiers in Oncology

TYPE Original Research
PUBLISHED 09 December 2022
DOI 10.3389/fonc.2022.1075217

OPEN ACCESS

EDITED BY
Feifei Pu,
Huazhong University of Science and Technology, China

REVIEWED BY
Shisheng He,
Tongji University, China
Guoqing Tan,
Affiliated Hospital of Shandong University of Traditional Chinese Medicine, China

*CORRESPONDENCE
Jianru Xiao
jianruxiao83@smmu.edu.cn
Wen Mo
mw2218@126.com

†These authors contributed equally to this work and share first authorship

SPECIALTY SECTION
This article was submitted to Surgical Oncology, a section of the journal Frontiers in Oncology

RECEIVED 27 October 2022
ACCEPTED 15 November 2022
PUBLISHED 09 December 2022

CITATION
Yin M, Guan S, Ding X, Zhuang R, Sun Z, Wang T, Zheng J, Li L, Gao X, Wei H, Ma J, Huang Q, Xiao J and Mo W (2022) Construction and validation of a novel web-based nomogram for patients with lung cancer with bone metastasis: A real-world analysis based on the SEER database.
Front. Oncol. 12:1075217.
doi: 10.3389/fonc.2022.1075217

Construction and validation of a novel web-based nomogram for patients with lung cancer with bone metastasis: A real-world analysis based on the SEER database

Mengchen Yin[1,2†], Sisi Guan[1†], Xing Ding[1†], Ruoyu Zhuang[1†], Zhengwang Sun[3], Tao Wang[4], Jiale Zheng[1], Lin Li[2], Xin Gao[2], Haifeng Wei[2], Junming Ma[1], Quan Huang[2], Jianru Xiao[2*] and Wen Mo[1*]

[1]Longhua Hospital, Shanghai University of Traditional Chinese Medicine, Shanghai, China, [2]Changzheng Hospital, Second Affiliated Hospital of Naval Medical University, Shanghai, China, [3]Department of Musculoskeletal Surgery, Shanghai Cancer Center, Fudan University, Shanghai, China, [4]Department of Orthopaedics, The Second Hospital of Anhui Medical University, Anhui, China

Purpose: Patients with lung cancer with bone metastasis (LCBM) often have a very poor prognosis. The purpose of this study is to characterize the prevalence and associated factors and to develop a prognostic nomogram to predict the overall survival (OS) and cancer-specific survival (CSS) for patients with LCBM using multicenter population-based data.

Methods: Patients with LCBM at the time of diagnosis were identified using the Surveillance, Epidemiology, and End Results (SEER) Program database of the National Cancer Institute (NCI) from 2010 to 2015. Multivariable and univariate logistic regression analyses were performed to identify factors associated with all-cause mortality and lung cancer (LC)–specific mortality. The performance of the nomograms was evaluated with the calibration curves, area under the curve (AUC), and decision curve analysis (DCA). Kaplan–Meier analysis and log-rank tests were used to estimate the survival times of patients with LCBM.

Results: We finally identified 26,367 patients with LCBM who were selected for survival analysis. Multivariate analysis demonstrated age, sex, T stage, N stage, grade, histology, radiation therapy, chemotherapy, primary site, primary surgery, liver metastasis, and brain metastasis as independent predictors for LCBM. The AUC values of the nomogram for the OS prediction were 0.755, 0.746, and 0.775 in the training cohort; 0.757, 0.763, and 0.765 in the internal validation cohort; and 0.769, 0.781, and 0.867 in the external validation cohort. For CSS, the values were 0.753, 0.753, and 0.757 in the training cohort; 0.753,

0.753, and 0.757 in the internal validation cohort; and 0.767, 0.774, and 0.872 in the external validation cohort.

Conclusions: Our study constructs a new prognostic model and clearly presents the clinicopathological features and survival analysis of patients with LCBM. The result indicated that the nomograms had favorable discrimination, good consistency, and clinical benefits in patients. In addition, our constructed nomogram prediction models may assist physicians in evaluating individualized prognosis and deciding on treatment for patients.

KEYWORDS

lung cancer, bone metastases, SEER, overall survival, cancer-specific survival

Introduction

As the most lethal cancer worldwide, there are approximately 1.8 million new patients with lung cancer (LC) diagnosed each year (1, 2). Bone is the most common and the earliest site of metastases from LC, and 30%–40% of patients with LC already have bone metastases (BMs) upon initial diagnosis, which is usually associated with a poor prognosis (3–5). The therapy for patients with lung cancer with bone metastasis (LCBM) is diverse, including primary tumor resection, metastatic surgery, chemotherapy, and radiotherapy. However, in many cases, the survival of patients with LCBM could not be accurately assessed, and individualized therapeutic scheme could not be provided, which leads to additional distress and poorer prognosis of patients.

In LCBM, tumor cells release cytokines and chemical mediators to stimulate the periosteum and bone, combined with the mechanical stress caused by tumor tissue in the osteolytic lesions, causing serious bone pain. Moreover, it increases the risk of complications referred to as skeletal-related events (SREs), including pathologic fracture, spinal cord compression, and hypercalcemia of malignancy. The main therapeutic options for treating LCBM are chemotherapy and radiotherapy. The therapy for BM from solid tumors has been revolutionized over the last few decades. Since the 1990s, bisphosphonates were introduced to treat BM and became a mainstay of the management of BM. Until around the year 2000, the appearance of denosumab challenged this dominance. Based on existing studies, denosumab was found to be more effective in reducing SREs. However, aforementioned treatment development in BM was mainly dedicated to reducing SREs and bone pain, and the increase of overall survival (OS) was still limited. Data are still limited on the epidemiology, signatures, and prognostic factors of LCBM in general (6–8).

For data visualization, nomograms can increase the accuracy of prognostic prediction in cancer, using the tumor size. The chart integration predicts the probability of events. In previous studies, nomograms have demonstrated its superior predictive ability to the TNM staging system (9–12). As far as we know, the current study is the first that developed nomograms based on a large-size number of patients, which was verified by internal and external validation sets to guarantee the reliability of the results.

The Surveillance, Epidemiology, and End Results (SEER) Program's registry is maintained by the National Cancer Institute (NCI), which collects a large number of cancer-related survival data from 1973 based on the US population. The cancer-related data in the SEER Program were obtained from 18 population-based registries, covering approximately 26% of the US population. Compared with any single institution, the SEER database encompasses much more population-level cancer data based on the largest sample size worldwide (13–16).

In this study, we analyzed the data extracted from the SEER database to identify risk factors associated with prognosis. Then, we subsequently created nomograms as a comprehensive prognostic assessment system. Both internal and external validation cohorts were employed to ensure the nomogram's accuracy and reliability.

Abbreviations: LC, lung cancer; LCBM, lung cancer with bone metastasis; SEER, Surveillance, Epidemiology and End Results; CSS, cancer-specific survival; OS, overall survival; ROC, receiver operating characteristic; AUC, area under the curves; DCA, decision curve analysis.

Materials and methods

Patient population

Patient data were extracted from the updated SEER database (https://seer.cancer.gov). We used the SEER Stat software

version 8.3.9 published by SEER to identify eligible patients in this study. In addition, the data of eligible patients with LCBM in the external validation cohort treated in these institutions were acquired. The inclusion and exclusion criteria were the same as those for the training cohort from the SEER database. Eventually, we identified the prognostic factors of LCBM through the included patients. For each cohort, patients were randomly divided into the training set (70%) and the internal validation set (30%). Prognostic factors identified from patients in the training set were used to construct the nomogram that was validated by the internal validation set. The inclusion criteria are as follows: diagnosis with BM in 2010–2015 of all ages and patients with complete information recorded. To identify patients with metastatic LC to the bone, we selected cases with LCBM at the first diagnosis, for further research. In addition, patients who died during the study period were excluded. The independent external validation cohort was derived from patients with LCBM treated in four medical institutions (Longhua Hospital, Changzheng Hospital, Shanghai Cancer Center, and The Second Hospital of Anhui Medical University). The inclusion criteria are as follows: definite diagnosis of LCBM, 18 years of age and above, and complete follow-up information. Figure 1 demonstrates the flowchart of the procedure. Analysis of the data from the SEER Program was exempted from medical ethics review, and no informed consent was required. The studies involving human participants were reviewed and approved by the Ethical Committee and Institutional Review Board. The patients/participants provided their written informed consent to participate in this study, and all procedures followed the Declaration of Helsinki.

Data collection

The collected clinicopathological factors included the following: age, sex, histology/behavior, malignant, histrionic, radiation recode, chemotherapy recode, brain, liver, survival months, vital status recode, the SEER data on cause-specific death classification, the TNM stage, and pathological nodal grade. In accordance with the seventh edition of the American Joint Committee on Cancer staging system, we classified various clinicopathological factors, and the histological type of CRC patients was determined following the International Classification of Diseases for Oncology, third edition (ICD-O-3). The endpoints in our study were cancer-specific survival (CSS) and OS.

Construction and validation of the prognostic scoring system

Univariable and multivariable Cox regression analyses were used to calculate the effects of variables on CSS and OS in the training, testing, and external validation cohorts. We formulated the nomogram based on the independent prognostic factors identified by the Cox multivariate analysis by employing R (version 4.0.1) with the rms package (available at http://CRAN.R-project.org/package=rms). The overall points for each patient in the training, testing, and external validation cohorts were calculated using the established nomogram, after which a Cox regression analysis of the entire cohort was carried out using the overall points as a parameter.

The Hosmer–Lemeshow test was used to evaluate the calibration of the nomogram and displayed in the form of the calibration curve. Both 1-, 3-, and 5-year CSS and OS can be estimated by the developed nomogram, respectively. Receiver operating characteristic (ROC) curve analyses were performed to test the performance evaluation of constructed nomograms by the areas under the ROC curves (AUCs), and Harrell's concordance index (C-index) was applied to evaluate the predictive value of the constructed nomogram. At the same time, decision curve analysis (DCA) was applied to assess the nomogram in the current research that was a novel strategy for evaluating prognostic scoring system methods and has advantages over AUROC in clinical value evaluation.

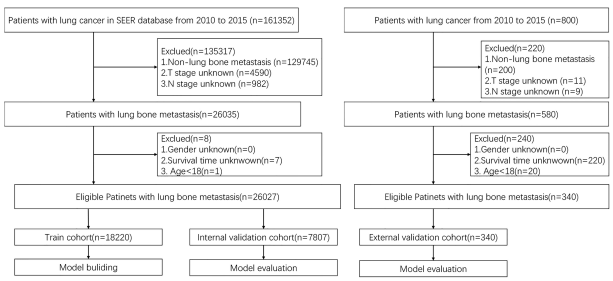

FIGURE 1
Flow chart of the study.

Statistical analysis

Statistical analysis was performed by SPSS v22.0 (IBM, Armonk, NY, USA) and R for Windows v4.0.5 (https://www.r-project.org). Chi-squared test was employed to analyze the categorical variables. The survival analysis was completed through the Kaplan–Meier method and log-rank test. The measure of the effect of each variable on CSS and OS is presented as the hazard ratio (HR) and was used to identify independent risk factors. HR greater than 1 indicated that the prognostic factor is unfavorable for survival, whereas HR smaller than 1 indicated that the prognostic factor is favorable for survival compared with the reference. A value of 1 revealed that there was no significant relationship between them. To minimize the influence of missing data, a backward stepwise method was used to further sort out prognostic factors selected in the multivariate Cox regression. The R statistical packages "rms", "survival", "Hmisc", "MASS", and "time ROC" were used to build a nomogram, plot calibration, and time-dependent ROC curves, whereas "rmda" was used to draw the DCA curves. All tests were two-sided, and $P < 0.05$ was considered statistically significant (17–19).

Result

Characteristics of the study population

A total of 26,027 patients with LCBM were included in our research. Meanwhile, 18,220 patients were enrolled into the training set, and the remaining 7,807 patients were enrolled into the internal validation set. The external validation set was composed by 340 eligible patients with LCBM. Table 1 provides the characteristics of the 26,367 patients.

Most of the patients with LCBM from the SEER dataset were men (57.49%) and older than 65 years (56.77%). The most common histological type was adenocarcinoma (51.52%), and the most common primary site was the upper lobe (51.67%). Compared with living patients, those deceased were more likely to have had poor tumor histological type, poor tumor stage, poor tumor grade, and higher rates of liver metastasis. In terms of treatment, only 6.07% patients underwent metastatic surgeries, 59.15% patients have received chemotherapy, and 52.82% patients have received radiation therapy.

Independent prognostic features in patients with lung cancer with bone metastasis

On univariable logistic regression analysis in the training cohort, there were 12 factors associated with OS that showed statistical significance ($P < 0.05$). These are age, sex, T stage, N stage, grade, radiation, chemotherapy, histology, primary site, primary surgery, brain metastasis (mets-brain), and liver metastasis (mets-liver). Then, the multivariate logistic regression analysis showed that age, sex, T stage, N stage, grade, radiation, chemotherapy, histology, primary site, primary surgery, mets-brain, and mets-liver were the independent predictors for the OS of patients with LCBM (Tables 2 and 3) Figure 2 shows that all the above variables were significant in relation to OS.

On univariable logistic regression analysis in the training cohort, there were 13 factors associated with CSS that showed statistical significance ($P < 0.05$). These were age, sex, T stage, N stage, grade, radiation, chemotherapy, histology, primary site, primary surgery, metastatic surgery, mets-brain, and mets-liver. Then, the multivariate logistic regression analysis showed that age, sex, T stage, N stage, grade, radiation, chemotherapy, histology, primary site, primary surgery, metastatic surgery, mets-brain, and mets-liver were the independent predictors predicting the CSS for patients with LCBM (Tables 4 and 5). Figure 3 shows that all the above variables were significant in relation to CSS.

Construction of the nomogram

To predict 1-, 3-, and 5-year OS and CSS of patients with LCBM, we built a nomogram in accordance with the major prognostic factors identified by the multivariable Cox regression analysis. Total points can be calculated by adding up the values for each variable corresponding to nomogram points. Subsequently, the value of total points corresponds vertically to survival chances at multiple time points (Figure 4).

Comparison of the values of area under the curves of the nomogram with TNM stage

We conducted the time-dependent ROC analyses at 1, 3, and 5 years in the training, internal validation, and external validation cohorts. In the training cohort, the AUC values of the nomogram for the prediction of OS (AUCOS) were 0.755, 0.746, and 0.775, compared with 0.558, 0.583, and 0.616 for the AUC values of TNM stage (AUCTNM), respectively. In the internal validation cohort, AUCOS were 0.757, 0.763, and 0.765, compared with 0.542, 0.578, and 0.587 for the AUCTNM, respectively. In the external validation cohort, AUCOS were 0.769, 0.781, and 0.867, compared with 0.566, 0.606, and 0.628 for the AUCTNM, respectively (Figure 5).

Likewise, in the training cohort, the AUC values of the nomogram for the prediction of CSS (AUCCSS) were 0.753,

TABLE 1 Demographic and clinicopathological characteristics of patients in the training, internal validation, and external validation cohorts (N, %).

Variables	Level	SEER database						Patient database		
		Training set			Internal validation set			External validation set		
		Overall 18,220	Alive 557	Dead 17,663	Overall 7,807	Alive 244	Dead 7,563	Overall 340	Alive 11	Dead 329
Age (%)	<65	7,857 (43.1)	338 (60.7)	7,519 (42.6)	3,394 (43.5)	144 (59.0)	3,250 (43.0)	136 (40.0)	7 (63.6)	129 (39.2)
	≥65	10,363 (56.9)	219 (39.3)	10,144 (57.4)	4,413 (56.5)	100 (41.0)	4313 (57.0)	204 (60.0)	4 (36.4)	200 (60.8)
Sex (%)	Male	10,479 (57.5)	266 (47.8)	10,213 (57.8)	4,483 (57.4)	126 (51.6)	4,357 (57.6)	201 (59.1)	5 (45.5)	196 (59.6)
	Female	7,741 (42.5)	291 (52.2)	7,450 (42.2)	3,324 (42.6)	118 (48.4)	3,206 (42.4)	139 (40.9)	6 (54.5)	133 (40.4)
Histology (%)	Squamous cell	2,617 (14.4)	47 (8.4)	2,570 (14.6)	1,165 (14.9)	23 (9.4)	1,142 (15.1)	53 (15.6)	2 (18.2)	51 (15.5)
	Adenocarcinoma	9,363 (51.4)	397 (71.3)	8,966 (50.8)	4,047 (51.8)	182 (74.6)	3,865 (51.1)	174 (51.2)	7 (63.6)	167 (50.8)
	Small cell	4,460 (24.5)	64 (11.5)	4,396 (24.9)	1,845 (23.6)	20 (8.2)	1,825 (24.1)	78 (22.9)	2 (18.2)	76 (23.1)
	Large cell	317 (1.7)	4 (0.7)	313 (1.8)	122 (1.6)	2 (0.8)	120 (1.6)	4 (1.2)	0 (0.0)	4 (1.2)
	Other	1,463 (8.0)	45 (8.1)	1,418 (8.0)	628 (8.0)	17 (7.0)	611 (8.1)	31 (9.1)	0 (0.0)	31 (9.4)
T (%)	T1	2,003 (11.0)	92 (16.5)	1,911 (10.8)	853 (10.9)	42 (17.2)	811 (10.7)	42 (12.4)	2 (18.2)	40 (12.2)
	T2	4,813 (26.4)	145 (26.0)	4,668 (26.4)	2,047 (26.2)	66 (27.0)	1,981 (26.2)	90 (26.5)	3 (27.3)	87 (26.4)
	T3	4,771 (26.2)	143 (25.7)	4,628 (26.2)	2,085 (26.7)	73 (29.9)	2,012 (26.6)	90 (26.5)	2 (18.2)	88 (26.7)
	T4	6,633 (36.4)	177 (31.8)	6,456 (36.6)	2,822 (36.1)	63 (25.8)	2,759 (36.5)	118 (34.7)	4 (36.4)	114 (34.7)
N (%)	N0	3,523 (19.3)	167 (30.0)	3,356 (19.0)	1,501 (19.2)	69 (28.3)	1,432 (18.9)	73 (21.5)	4 (36.4)	69 (21.0)
	N1	1,487 (8.2)	60 (10.8)	1,427 (8.1)	633 (8.1)	19 (7.8)	614 (8.1)	27 (7.9)	1 (9.1)	26 (7.9)
	N2	8,936 (49.0)	222 (39.9)	8,714 (49.3)	3,924 (50.3)	99 (40.6)	3,825 (50.6)	160 (47.1)	3 (27.3)	157 (47.7)
	N3	4,274 (23.5)	108 (19.4)	4,166 (23.6)	1,749 (22.4)	57 (23.4)	1,692 (22.4)	80 (23.5)	3 (27.3)	77 (23.4)
M (%)	M1a	465 (2.6)	16 (2.9)	449 (2.5)	216 (2.8)	10 (4.1)	206 (2.7)	7 (2.1)	0 (0.0)	7 (2.1)
	M1b	17,484 (96.0)	532 (95.5)	16,952 (96.0)	7,462 (95.6)	229 (93.9)	7,233 (95.6)	331 (97.4)	11 (100.0)	320 (97.3)
	M1NOS	271 (1.5)	9 (1.6)	262 (1.5)	129 (1.7)	5 (2.0)	124 (1.6)	2 (0.6)	0 (0.0)	2 (0.6)
Primary site (%)	Main bronchus	1,068 (5.9)	22 (3.9)	1,046 (5.9)	466 (6.0)	9 (3.7)	457 (6.0)	26 (7.6)	1 (9.1)	25 (7.6)
	Upper lobe	9,453 (51.9)	304 (54.6)	9,149 (51.8)	3,995 (51.2)	138 (56.6)	3,857 (51.0)	166 (48.8)	8 (72.7)	158 (48.0)
	Middle lobe	740 (4.1)	24 (4.3)	716 (4.1)	329 (4.2)	15 (6.1)	314 (4.2)	12 (3.5)	0 (0.0)	12 (3.6)
	Lower lobe	4,694 (25.8)	153 (27.5)	4,541 (25.7)	2,006 (25.7)	65 (26.6)	1,941 (25.7)	80 (23.5)	2 (18.2)	78 (23.7)
	Overlapping lesion of lung	187 (1.0)	5 (0.9)	182 (1.0)	91 (1.2)	2 (0.8)	89 (1.2)	7 (2.1)	0 (0.0)	7 (2.1)
	Lung, NOS	2,078 (11.4)	49 (8.8)	2,029 (11.5)	920 (11.8)	15 (6.1)	905 (12.0)	49 (14.4)	0 (0.0)	49 (14.9)
Grade (%)	I	291 (1.6)	16 (2.9)	275 (1.6)	144 (1.8)	6 (2.5)	138 (1.8)	7 (2.1)	0 (0.0)	7 (2.1)
	II	1,820 (10.0)	81 (14.5)	1,739 (9.8)	745 (9.5)	41 (16.8)	704 (9.3)	30 (8.8)	2 (18.2)	28 (8.5)
	III	4,346 (23.9)	140 (25.1)	4,206 (23.8)	1,876 (24.0)	54 (22.1)	1,822 (24.1)	82 (24.1)	1 (9.1)	81 (24.6)
	IV	608 (3.3)	6 (1.1)	602 (3.4)	262 (3.4)	3 (1.2)	259 (3.4)	12 (3.5)	0 (0.0)	12 (3.6)

(Continued)

TABLE 1 Continued

Variables	Level	SEER database						Patient database		
		Training set			Internal validation set			External validation set		
		Overall 18,220	Alive 557	Dead 17,663	Overall 7,807	Alive 244	Dead 7,563	Overall 340	Alive 11	Dead 329
	Unknown	11,155 (61.2)	314 (56.4)	10,841 (61.4)	4,780 (61.2)	140 (57.4)	4,640 (61.4)	209 (61.5)	8 (72.7)	201 (61.1)
Primary surgery (%)	Yes	331 (1.8)	37 (6.6)	294 (1.7)	125 (1.6)	21 (8.6)	104 (1.4)	9 (2.6)	3 (27.3)	6 (1.8)
	No	17,889 (98.2)	520 (93.4)	17,369 (98.3)	7,682 (98.4)	223 (91.4)	7,459 (98.6)	331 (97.4)	8 (72.7)	323 (98.2)
Metastatic surgery (%)	Yes	1,100 (6.0)	33 (5.9)	1,067 (6.0)	480 (6.1)	25 (10.2)	455 (6.0)	19 (5.6)	0 (0.0)	19 (5.8)
	No	17,120 (94.0)	524 (94.1)	16,596 (94.0)	7,327 (93.9)	219 (89.8)	7,108 (94.0)	321 (94.4)	11 (100.0)	310 (94.2)
Radiation (%)	Yes	9,653 (53.0)	296 (53.1)	9,357 (53.0)	4,095 (52.5)	137 (56.1)	3,958 (52.3)	170 (50.0)	2 (18.2)	168 (51.1)
	No	8,567 (47.0)	261 (46.9)	8,306 (47.0)	3,712 (47.5)	107 (43.9)	3,605 (47.7)	170 (50.0)	9 (81.8)	161 (48.9)
Chemotherapy (%)	Yes	10,778 (59.2)	450 (80.8)	10,328 (58.5)	4,618 (59.2)	203 (83.2)	4,415 (58.4)	189 (55.6)	10 (90.9)	179 (54.4)
	No	7,442 (40.8)	107 (19.2)	7,335 (41.5)	3,189 (40.8)	41 (16.8)	3,148 (41.6)	151 (44.4)	1 (9.1)	150 (45.6)
Brain metastasis (%)	Yes	4,380 (24.0)	116 (20.8)	4,264 (24.1)	1,813 (23.2)	58 (23.8)	1,755 (23.2)	90 (26.5)	1 (9.1)	89 (27.1)
	No	13,840 (76.0)	441 (79.2)	13,399 (75.9)	5,994 (76.8)	186 (76.2)	5,808 (76.8)	250 (73.5)	10 (90.9)	240 (72.9)
Liver metastasis (%)	Yes	5,649 (31.0)	83 (14.9)	5,566 (31.5)	2,473 (31.7)	33 (13.5)	2,440 (32.3)	105 (30.9)	3 (27.3)	102 (31.0)
	No	12,571 (69.0)	474 (85.1)	12,097 (68.5)	5,334 (68.3)	211 (86.5)	5,123 (67.7)	235 (69.1)	8 (72.7)	227 (69.0)

0.753, and 0.757, compared with 0.558, 0.579, and 0.611 for the AUCTNM stage, respectively. In the internal validation cohort, AUCCSS were 0.753, 0.753, and 0.757, compared with 0.544, 0.579, and 0.595 for the AUCTNM, respectively. In the external validation cohort, AUCCSS were 0.767, 0.774, and 0.872, compared with 0.561, 0.578, and 0.604 for the AUCTNM, respectively (Figure 6). The results showed that the novel prognostic scoring system had better efficacy in predicting the prognosis of patients with LCBM than TNM stage.

Evaluation and validation of the overall survival and cancer-specific survival prediction nomograms using receiver operating characteristic curves

We also used time-dependent ROC curves and the AUC to validate the discrimination ability of nomograms. In the training cohort, the 1-, 3-, and 5-year AUC values of nomograms predicting OS were 0.755, 0.746, and 0.775, respectively. In the internal validation cohort, the AUC values for OS were 0.757, 0.763, and 0.765, respectively. In the external validation cohort, the AUC values for OS were 0.769, 0.781, and 0.867, respectively.

Likewise, in the training cohorts, the 1-, 3-, and 5-year AUC values of nomograms predicting for CSS were 0.751, 0.739, and 0.763, respectively. In the internal validation cohorts, the AUC values for CSS were 0.753, 0.753, and 0.757, respectively. In the external validation cohorts, the AUC values for CSS were 0.767, 0.774, and 0.872, respectively. The results showed that the novel prognostic scoring system had a favorable predictive sensitivity (Figure 7).

C-index values for the prediction of OS and CSS were also used to evaluate the discriminatory power of the nomogram. The C-index values for OS were 0.717 (95% CI, 0.715–0.719), 0.721 (95% CI, 0.718–0.725), and 0.731 (95% CI, 0.716–0.746) in the training, internal validation, and external validation cohorts, respectively. Likewise, the C-index values for CSS were 0.716 (95% CI, 0.714–0.718), 0.720 (95% CI, 0.716–0.723), and 0.731 (95% CI, 0.715–0.746) in the training, internal validation, and external validation cohorts. The result indicated that the nomogram had favorable discrimination in patients with LCBM.

10.3389/fonc.2022.1075217

TABLE 2 Univariate Cox regression model in the training, internal validation, and external validation cohorts of overall survival (OS) (N, %).

Variables	Level	SEER database				Patient database	
		Training cohort		Internal validation cohort		External validation cohort	
		HR (95% CI)	P	HR (95% CI)	P	HR (95% CI)	P
Age	<65						
	≥65	1.27 (1.23–1.31)	<0.001	1.3 (1.24–1.36)	<0.001	1.18 (0.95–1.48)	0.135
Sex	Male						
	Female	0.82 (0.79–0.84)	<0.001	0.84 (0.8–0.88)	<0.001	0.77 (0.61–0.96)	0.018
T	T1						
	T2	1.17 (1.11–1.24)	<0.001	1.18 (1.08–1.28)	<0.001	1.16 (0.8–1.69)	0.44
	T3	1.26 (1.2–1.33)	<0.001	1.32 (1.21–1.43)	<0.001	1.52 (1.04–2.21)	0.03
	T4	1.31 (1.24–1.38)	<0.001	1.33 (1.23–1.43)	<0.001	1.38 (0.96–1.98)	0.083
N	N0						
	N1	1.05 (0.99–1.12)	0.131	1.07 (0.97–1.17)	0.179	1.08 (0.69–1.7)	0.737
	N2	1.2 (1.16–1.25)	<0.001	1.16 (1.09–1.23)	0	1.2 (0.9–1.6)	0.207
	N3	1.15 (1.1–1.2)	<0.001	1.09 (1.01–1.17)	0.018	1.01 (0.73–1.4)	0.944
M	M1a						
	M1b	1.03 (0.94–1.13)	0.576	1.08 (0.94–1.24)	0.267	0.71 (0.34–1.51)	0.379
	M1NOS	0.99 (0.85–1.15)	0.861	0.95 (0.76–1.19)	0.65	0.69 (0.14–3.33)	0.644
Grade	I						
	II	1.04 (0.92–1.18)	0.534	1.12 (0.93–1.34)	0.232	1.19 (0.52–2.73)	0.68
	III	1.4 (1.24–1.59)	<0.001	1.5 (1.27–1.79)	<0.001	1.88 (0.86–4.07)	0.112
	IV	1.55 (1.35–1.79)	<0.001	1.59 (1.29–1.95)	<0.001	2.71 (1.06–6.93)	0.037
	Unknown	1.35 (1.2–1.52)	<0.001	1.4 (1.18–1.66)	<0.001	1.64 (0.77–3.49)	0.2
Radiation	Yes						
	No	1.21 (1.18–1.25)	<0.001	1.2 (1.15–1.26)	<0.001	1.1 (0.88–1.37)	0.394
Chemotherapy	Yes						
	No	3.04 (2.95–3.14)	<0.001	3.19 (3.04–3.35)	<0.001	3.23 (2.57–4.06)	<0.001
Histology	Squamous cell						
	Adenocarcinoma	0.69 (0.66–0.72)	<0.001	0.65 (0.61–0.69)	<0.001	0.74 (0.54–1.01)	0.06
	Small cell	1.03 (0.91–1.16)	0.637	1.07 (0.89–1.3)	0.456	1.64 (0.59–4.55)	0.343
	Large cell	0.88 (0.83–0.94)	<0.001	0.89 (0.81–0.98)	0.021	1.31 (0.83–2.05)	0.246
	Other	0.89 (0.85–0.93)	<0.001	0.85 (0.79–0.92)	<0.001	0.99 (0.69–1.42)	0.953
Primary site	Main bronchus						
	Upper lobe	0.85 (0.8–0.91)	<0.001	0.81 (0.73–0.89)	<0.001	0.63 (0.41–0.97)	0.037
	Middle lobe	0.8 (0.73–0.88)	<0.001	0.78 (0.67–0.9)	0.001	0.78 (0.39–1.56)	0.484
	Lower lobe	0.87 (0.81–0.93)	<0.001	0.78 (0.71–0.87)	<0.001	0.69 (0.44–1.08)	0.107
	Overlapping lesion of lung	1.03 (0.88–1.21)	0.714	0.82 (0.65–1.02)	0.079	0.81 (0.35–1.89)	0.631
	Lung, NOS	1.01 (0.94–1.09)	0.7	1.05 (0.94–1.17)	0.401	1.02 (0.63–1.66)	0.922
Primary surgery	Yes						
	No	1.79 (1.59–2.01)	<0.001	1.85 (1.52–2.25)	<0.001	3.17 (1.41–7.13)	0.005
Metastatic surgery	Yes						
	No	1.07 (1–1.13)	0.041	1.2 (1.09–1.32)	<0.001	0.87 (0.55–1.39)	0.564
Brain metastasis	Yes						
	No	0.94 (0.91–0.98)	0.001	0.94 (0.89–0.99)	0.014	0.73 (0.57–0.93)	0.011
Liver metastasis	Yes						
	No	0.73 (0.71–0.75)	<0.001	0.7 (0.66–0.73)	<0.001	0.73 (0.58–0.93)	0.009

HR, hazard ratio.

10.3389/fonc.2022.1075217

TABLE 3 Multivariate Cox regression model in the training, internal validation, and external validation cohorts of overall survival (OS) (N, %).

Variables	Levels	SEER database				Patient database	
		Training cohort		Internal validation cohort		External validation cohort	
		HR (95% CI)	P	HR (95% CI)	P	HR (95% CI)	P
Age	<65						
	≥65	1.18 (1.14–1.21)	<0.001	1.15 (1.1–1.21)	<0.001	NA	NA
Sex	Male						
	Female	0.84 (0.81–0.86)	<0.001	0.87 (0.83–0.91)	<0.001	0.75 (0.59–0.94)	0.0118
T	T1						
	T2	1.13 (1.07–1.19)	<0.001	1.15 (1.05–1.24)	0.0013	1.05 (0.72–1.56)	0.7873
	T3	1.21 (1.15–1.28)	<0.001	1.24 (1.15–1.35)	<0.001	1.27 (0.86–1.88)	0.2215
	T4	1.23 (1.17–1.3)	<0.001	1.22 (1.12–1.32)	<0.001	1.07 (0.73–1.57)	0.7204
N	N0						
	N1	1.15 (1.08–1.22)	<0.001	1.04 (0.95–1.15)	0.3712	NA	NA
	N2	1.26 (1.21–1.31)	<0.001	1.25 (1.17–1.33)	<0.001	NA	NA
	N3	1.28 (1.22–1.34)	<0.001	1.21 (1.13–1.3)	<0.001	NA	NA
M	M1a						
	M1b	NA	NA	NA	NA	NA	NA
	M1NOS	NA	NA	NA	NA	NA	NA
Grade	I						
	II	1.06 (0.94–1.21)	0.3446	1.2 (1–1.44)	0.0526	2.55 (1.08–6.04)	0.0333
	III	1.35 (1.19–1.52)	<0.001	1.51 (1.27–1.79)	<0.001	3.13 (1.39–7.05)	0.006
	IV	1.38 (1.19–1.59)	<0.001	1.55 (1.25–1.91)	<0.001	4.04 (1.49–10.99)	0.0062
	Unknown	1.29 (1.15–1.46)	<0.001	1.43 (1.2–1.69)	<0.001	2.71 (1.22–5.99)	0.0139
Radiation	Yes						
	No	1.12 (1.08–1.15)	<0.001	1.09 (1.04–1.14)	<0.001	NA	NA
Chemotherapy	Yes						
	No	3.24 (3.13–3.34)	<0.001	3.37 (3.2–3.54)	<0.001	3.97 (3.09–5.11)	<0.001
Histology	Squamous cell						
	Adenocarcinoma	0.78 (0.74–0.81)	<0.001	0.78 (0.73–0.83)	<0.001	NA	NA
	Small cell	1.05 (0.94–1.19)	0.3786	1.13 (0.94–1.37)	0.1938	NA	NA
	Large cell	0.89 (0.83–0.95)	<0.001	0.89 (0.81–0.99)	0.0286	NA	NA
	Other	0.97 (0.92–1.02)	0.299	0.95 (0.88–1.03)	0.2403	NA	NA
Primary site	Main bronchus						
	Upper lobe	0.89 (0.83–0.95)	<0.001	0.9 (0.82–0.99)	0.0359	0.63 (0.4–0.97)	0.038
	Middle lobe	0.79 (0.71–0.87)	<0.001	0.84 (0.73–0.97)	0.02	0.76 (0.37–1.55)	0.4503
	Lower lobe	0.9 (0.84–0.96)	0.0027	0.87 (0.78–0.96)	0.0067	0.6 (0.37–0.97)	0.0373
	Overlapping lesion of lung	1.04 (0.89–1.21)	0.6493	0.84 (0.67–1.05)	0.1334	0.79 (0.33–1.88)	0.6003
	Lung, NOS	0.98 (0.91–1.06)	0.6851	1.13 (1.01–1.27)	0.034	0.97 (0.59–1.6)	0.9153
Primary surgery	Yes						
	No	1.72 (1.53–1.94)	<0.001	1.79 (1.47–2.18)	<0.001	2.25 (0.98–5.17)	0.0562
Metastatic surgery	Yes						
	No	1.06 (0.99–1.13)	0.0728	1.07 (0.98–1.18)	0.1481	NA	NA
Brain metastasis	Yes						
	No	0.85 (0.82–0.88)	<0.001	0.83 (0.79–0.88)	<0.001	0.78 (0.61–1.01)	0.0621
Liver metastasis	Yes						
	No	0.74 (0.72–0.77)	<0.001	0.71 (0.67–0.74)	<0.001	0.67 (0.52–0.86)	0.0022

N/A, Not Applicable.

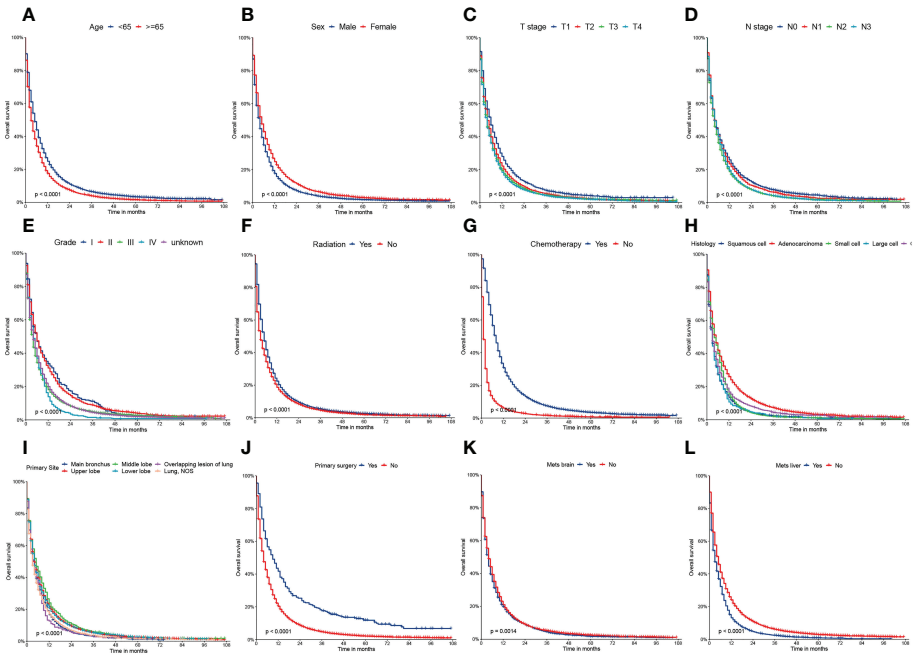

FIGURE 2
Kaplan–Meier curves of the overall survival (OS) factors: **(A)** age, **(B)** sex, **(C)** T stage, **(D)** N stage, **(E)** grade, **(F)** radiation, **(G)** chemotherapy, **(H)** histology, **(I)** primary site, **(J)** primary surgery, **(K)** mets-brain, and **(L)** mets-liver.

The result of calibration curves for the nomogram showed no obvious deviations from the reference line, indicating a high degree of credibility (Figure 8). In addition, DCA of the nomogram and TNM stage for the OS and CSS prediction of patients was used to evaluate the clinical value. The result of DCA indicated that the nomogram had better clinical outcome values compared with the TNM staging system with higher net benefits (Figure 9).

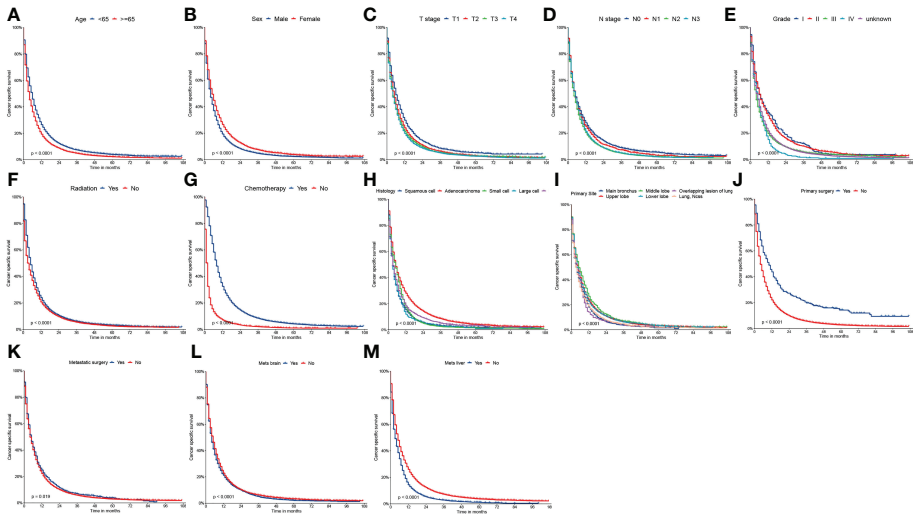

FIGURE 3
Kaplan-Meier curves of CSS **(A)** age, **(B)** sex, **(C)** T stage, **(D)** N stage, **(E)** grade, **(F)** radiation, **(G)** chemotherapy, **(H)** histology, **(I)** primary site, **(J)** primary surgery, **(K)** metastatic surgery, **(L)** mets-brain and **(M)** mets-liver.

10.3389/fonc.2022.1075217

TABLE 4 Univariate Cox regression model in the training, internal validation, and external validation cohorts of cancer-specific survival (CSS) (N, %).

Variables	Level	SEER database				Patient database	
		Training cohort		Internal validation cohort		External validation cohort	
		HR (95% CI)	P	HR (95% CI)	P	HR (95% CI)	P
Age	<65						
	≥65	1.25 (1.21–1.29)	<0.001	1.28 (1.22–1.34)	<0.001	1.11 (0.89–1.4)	0.36
Sex	Male						
	Female	0.82 (0.8–0.85)	<0.001	0.85 (0.81–0.89)	<0.001	0.72 (0.58–0.91)	0.006
T	T1						
	T2	1.18 (1.12–1.24)	<0.001	1.2 (1.11–1.31)	<0.001	1.11 (0.76–1.64)	0.58
	T3	1.27 (1.2–1.34)	<0.001	1.32 (1.22–1.44)	<0.001	1.43 (0.98–2.11)	0.066
	T4	1.32 (1.25–1.39)	<0.001	1.36 (1.25–1.47)	<0.001	1.31 (0.91–1.9)	0.147
N	N0						
	N1	1.06 (0.99–1.13)	0.092	1.08 (0.98–1.19)	0.139	1.07 (0.67–1.69)	0.783
	N2	1.21 (1.17–1.27)	<0.001	1.17 (1.1–1.25)	<0.001	1.13 (0.84–1.52)	0.406
	N3	1.16 (1.1–1.21)	<0.001	1.11 (1.03–1.19)	0.006	0.98 (0.7–1.37)	0.911
M	M1a						
	M1b	1.07 (0.97–1.17)	0.204	1.09 (0.95–1.26)	0.229	0.67 (0.32–1.43)	0.301
	M1NOS	1.02 (0.87–1.19)	0.808	0.93 (0.74–1.17)	0.517	0.7 (0.14–3.35)	0.65
Grade	I						
	II	1.05 (0.92–1.2)	0.471	1.14 (0.94–1.37)	0.179	1.6 (0.62–4.17)	0.332
	III	1.42 (1.25–1.61)	<0.001	1.54 (1.29–1.84)	<0.001	2.58 (1.04–6.39)	0.04
	IV	1.57 (1.36–1.82)	<0.001	1.64 (1.33–2.03)	<0.001	3.77 (1.32–10.76)	0.013
	Unknown	1.37 (1.21–1.55)	<0.001	1.41 (1.19–1.69)	<0.001	2.1 (0.86–5.13)	0.101
Radiation	Yes						
	No	1.19 (1.16–1.23)	<0.001	1.17 (1.12–1.23)	<0.001	1.08 (0.86–1.34)	0.525
Chemotherapy	Yes						
	No	3.02 (2.92–3.12)	<0.001	3.15 (3–3.31)	<0.001	3.19 (2.52–4.04)	<0.001
Histology	Squamous cell						
	Adenocarcinoma	0.69 (0.66–0.73)	<0.001	0.64 (0.6–0.69)	<0.001	0.77 (0.55–1.07)	0.114
	Small cell	1.04 (0.92–1.17)	0.515	1.08 (0.89–1.31)	0.425	1.78 (0.64–4.97)	0.268
	Large cell	0.9 (0.84–0.96)	0.001	0.88 (0.8–0.98)	0.016	1.29 (0.8–2.07)	0.296
	Other	0.9 (0.85–0.94)	<0.001	0.85 (0.79–0.92)	<0.001	1.04 (0.72–1.51)	0.83
Primary site	Main bronchus						
	Upper lobe	0.84 (0.79–0.9)	<0.001	0.82 (0.74–0.9)	<0.001	0.6 (0.39–0.92)	0.019
	Middle lobe	0.78 (0.71–0.86)	<0.001	0.79 (0.68–0.92)	0.002	0.71 (0.35–1.45)	0.352
	Lower lobe	0.85 (0.79–0.91)	<0.001	0.79 (0.71–0.87)	<0.001	0.66 (0.42–1.04)	0.072
	Overlapping lesion of lung	1.01 (0.86–1.19)	0.895	0.87 (0.69–1.09)	0.23	0.82 (0.35–1.9)	0.641
	Lung, NOS	1 (0.93–1.08)	0.904	1.05 (0.94–1.18)	0.392	0.94 (0.57–1.53)	0.797
Primary surgery	Yes						
	No	1.82 (1.61–2.05)	<0.001	1.9 (1.55–2.33)	<0.001	2.96 (1.31–6.66)	0.009
Metastatic surgery	Yes						
	No	1.08 (1.01–1.15)	0.018	1.19 (1.08–1.31)	<0.001	0.81 (0.51–1.3)	0.385
Brain metastasis	Yes						
	No	0.93 (0.9–0.96)	<0.001	0.92 (0.87–0.97)	0.003	0.7 (0.55–0.9)	0.006
Liver metastasis	Yes						
	No	0.72 (0.7–0.74)	<0.001	0.69 (0.65–0.72)	<0.001	0.7 (0.55–0.89)	0.004

10.3389/fonc.2022.1075217

TABLE 5 Multivariate Cox regression model in the training, internal validation, and external validation cohorts of cancer-specific survival (CSS) (N, %).

Variables	Levels	SEER database				Patient database	
		Training cohort		Internal validation cohort		External validation cohort	
		HR (95% CI)	P	HR (95% CI)	P	HR (95% CI)	P
Age	<65						
	≥65	1.16 (1.13–1.2)	<0.001	1.14 (1.08–1.19)	<0.001	NA	NA
Sex	Male						
	Female	0.84 (0.82–0.87)	<0.001	0.88 (0.84–0.92)	<0.001	0.69 (0.54–0.87)	0.0019
T	T1						
	T2	1.14 (1.07–1.2)	<0.001	1.17 (1.07–1.27)	<0.001	NA	NA
	T3	1.21 (1.15–1.28)	<0.001	1.25 (1.14–1.36)	<0.001	NA	NA
	T4	1.24 (1.17–1.31)	<0.001	1.24 (1.14–1.35)	<0.001	NA	NA
N	N0						
	N1	1.15 (1.08–1.23)	<0.001	1.05 (0.95–1.16)	0.309	NA	NA
	N2	1.26 (1.21–1.32)	<0.001	1.25 (1.17–1.33)	<0.001	NA	NA
	N3	1.28 (1.22–1.35)	<0.001	1.22 (1.14–1.32)	<0.001	NA	NA
M	M1a						
	M1b	NA	NA	NA	NA	NA	NA
	M1NOS	NA	NA	NA	NA	NA	NA
Grade	I						
	II	1.07 (0.94–1.22)	0.2936	1.21 (1–1.47)	0.0449	3.48 (1.3–9.29)	0.0128
	III	1.36 (1.2–1.54)	<0.001	1.53 (1.27–1.83)	<0.001	4.41 (1.74–11.19)	0.0018
	IV	1.39 (1.2–1.62)	<0.001	1.57 (1.26–1.96)	<0.001	5.68 (1.89–17.08)	0.002
	Unknown	1.3 (1.15–1.48)	<0.001	1.42 (1.19–1.7)	<0.001	3.57 (1.42–8.96)	0.0068
Radiation	Yes						
	No	1.1 (1.06–1.13)	<0.001	1.07 (1.02–1.12)	0.0108	NA	NA
Chemotherapy	Yes						
	No	3.23 (3.12–3.34)	<0.001	3.35 (3.18–3.52)	<0.001	4.06 (3.13–5.27)	<0.001
Histology	Squamous cell						
	Adenocarcinoma	0.79 (0.75–0.82)	<0.001	0.77 (0.72–0.83)	<0.001	NA	NA
	Small cell	1.06 (0.94–1.2)	0.315	1.13 (0.93–1.37)	0.2294	NA	NA
	Large cell	0.9 (0.84–0.97)	0.0031	0.89 (0.8–0.98)	0.0226	NA	NA
	Other	0.98 (0.93–1.03)	0.4556	0.95 (0.88–1.03)	0.221	NA	NA
Primary site	Main bronchus						
	Upper lobe	0.88 (0.82–0.94)	<0.001	0.92 (0.83–1.01)	0.0901	0.6 (0.39–0.94)	0.025
	Middle lobe	0.77 (0.7–0.85)	<0.001	0.87 (0.75–1)	0.0567	0.71 (0.34–1.48)	0.36
	Lower lobe	0.89 (0.83–0.95)	<0.001	0.88 (0.79–0.98)	0.0162	0.59 (0.37–0.96)	0.0329
	Overlapping lesion of lung	1.02 (0.87–1.2)	0.8241	0.9 (0.72–1.14)	0.3853	0.86 (0.36–2.04)	0.7357
	Lung, NOS	0.98 (0.9–1.05)	0.5287	1.14 (1.02–1.28)	0.0262	0.93 (0.56–1.54)	0.7666
Primary surgery	Yes						
	No	1.74 (1.55–1.97)	<0.001	1.86 (1.51–2.28)	<0.001	2.1 (0.91–4.81)	0.0802
Metastatic surgery	Yes						
	No	1.08 (1.01–1.15)	0.0255	1.07 (0.97–1.18)	0.1971	NA	NA
Brain metastasis	Yes						
	No	0.85 (0.82–0.88)	<0.001	0.83 (0.78–0.88)	<0.001	0.75 (0.57–0.97)	0.0274
Liver metastasis	Yes						
	No	0.73 (0.71–0.76)	<0.001	0.7 (0.66–0.73)	<0.001	0.65 (0.5–0.85)	0.0013

N/A, Not Applicable.

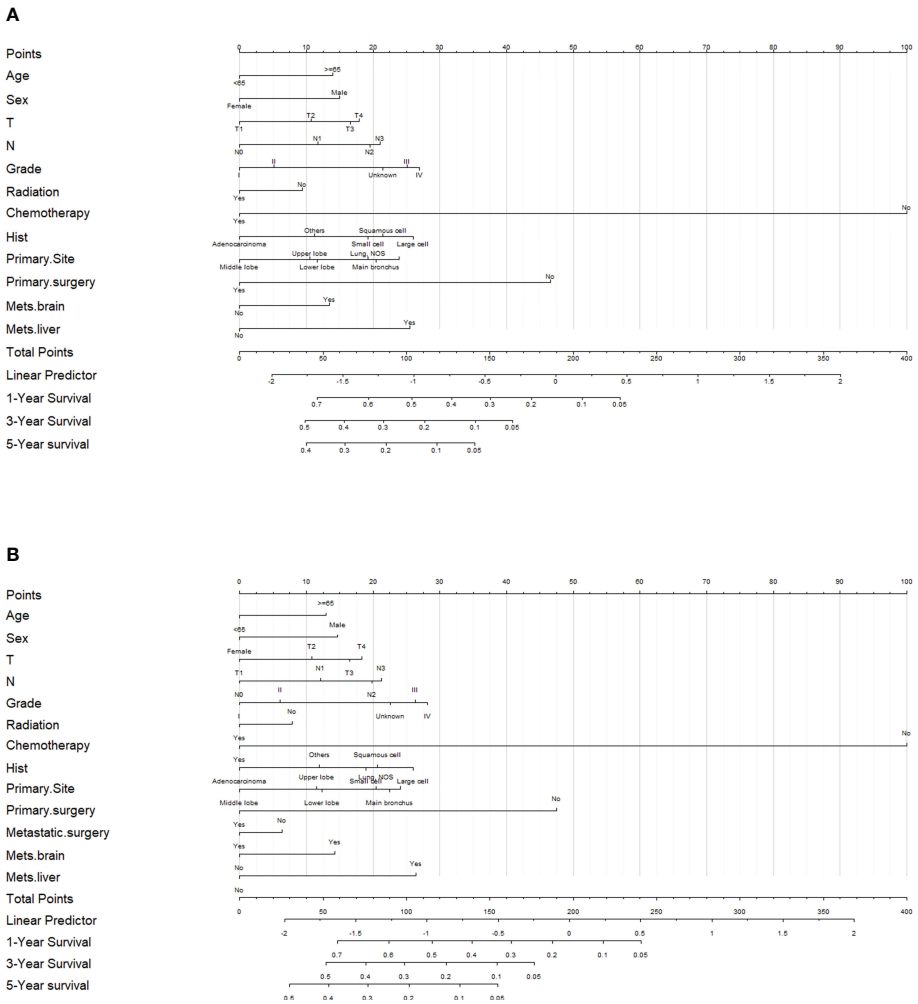

FIGURE 4
Evaluation of the overall survival (OS)- and cancer-specific survival (CSS)-associated nomograms for patients with lung cancer with bone metastasis (LCBM). **(A)** OS nomogram integrating age, sex, T stage, N stage, grade, radiation, chemotherapy, histology, primary site, primary surgery, mets-brain, and mets-liver for predicting 1-, 3-, and 5-year OS rates. **(B)** CSS nomogram integrating age, sex, T stage, N stage, grade, radiation, chemotherapy, histology, primary site, primary surgery, metastatic surgery, mets-brain, and mets-liver for predicting 1-, 3-, and 5-year CSS rates.

Web-based nomogram

A freely available, web-based calculator was deployed for predicting the postoperative OS and CSS of patients with LCBM (https://yiinmengchen.shinyapps.io/DynNom_os/ and https://yiinmengchen.shinyapps.io/DynNom_css/). With the use of the web-based nomogram, we can individually assess the OS and CSS of patients based on the input clinical factors. As an example of calculating OS, we included a 60-year-old male patient with LCBM with mets-brain and mets-liver. TNM stage was T3N2. Pathological grade was I. Histology was small cell. He received chemotherapy and radiation. As shown in Figure 10, the probability of OS for this patient was estimated to be 19.5% and 3.1% at 1 and 3 years, respectively. As shown in Figure 11, the probability of CSS for this patient was estimated to be 24.5% and 5.1% at 1 and 3 years, respectively.

Discussion

Commonly, the symptoms associated with patients with LCBM are pain, occasional fractures, or interference with daily activities (20). BM accounts for approximately 350,000 deaths in the United States every year and nearly three times this number if patients in the European countries and Japan are also included (21). In the retrospective analysis of Swedish national inpatient

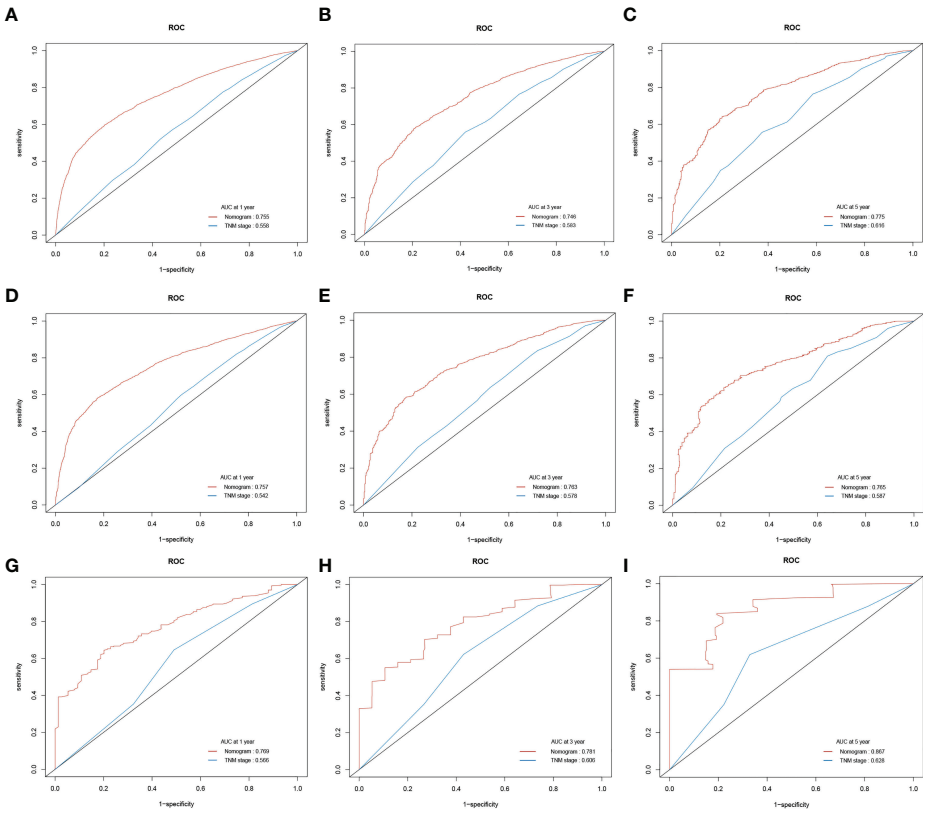

FIGURE 5
The receiver operating characteristic (ROC) curve of the TNM stage and the overall survival (OS) nomogram. **(A–C)** The area under the curve (AUC) values of ROC predicted 1-, 3-, and 5-year OS rates of the nomogram and TNM stage in the training cohort. **(D–F)** AUC values of ROC predicted 1-, 3-, and 5-year OS rates of the nomogram and TNM stage in the internal validation cohort. **(G–I)** AUC values of ROC predicted 1-, 3-, and 5-year OS rates of the nomogram and TNM stage in the external validation cohort.

data involving 21,169 patients with LC, by Riihimaki et al., BM conferred the worst prognosis compared with other frequent metastatic sites, which was one of the most frequent metastatic sites as well (22). In another study based on the nationwide Korean health insurance database, SREs most commonly occurred in patients with LC among the 1,849 patients with BM (23). The condition of patients with LCBM can rapidly progress to an advanced stage after initial diagnosis and display metastasis, which often renders the treatment difficult. Therefore, there is an urgent need for the development of more clinically applied risk predictors as well as novel tools for prediction of survival of patients with LCBM in the clinic. Based on the data extracted from the SEER database, we analyzed the survival of patients with LCBM. The prognostic factors associated with OS and CSS were also identified to accurately predict the prognosis of patients. As far as we know, this was the first multicenter population-based study that includes internal and external validation.

Our study found that some prognostic factors of LCBM were in accordance with previously published reports, including a male predominance, older age, and a propensity for high-grade tumors and more patients who were diagnosed with advanced stage III/IV disease (20, 24, 25). In addition to this, T, N, and M stages were correlated with shortened survival time. The effect of primary location of LC on prognosis after BM could not be defined, in accordance with our findings; the primary site was a factor associated with survival. We found that patients with main bronchial neoplasm had worse prognosis compared with other locations. Although there has been a previous study that confirmed that T3 centrally located early non–small cell LC (NSCLC) has a better survival than other types, more research studies obtained similar results with the present study (26, 27). This conclusion could be explained as the technical limitations of tumor resection involved in the main bronchus due to its anatomy. On the other hand, the main bronchus neoplasm had a high rate of lymph node metastasis, which was associated with worse outcomes (28).

As one of the most common metastatic sites, the bone is a unique microenvironment that appears to promote tumor

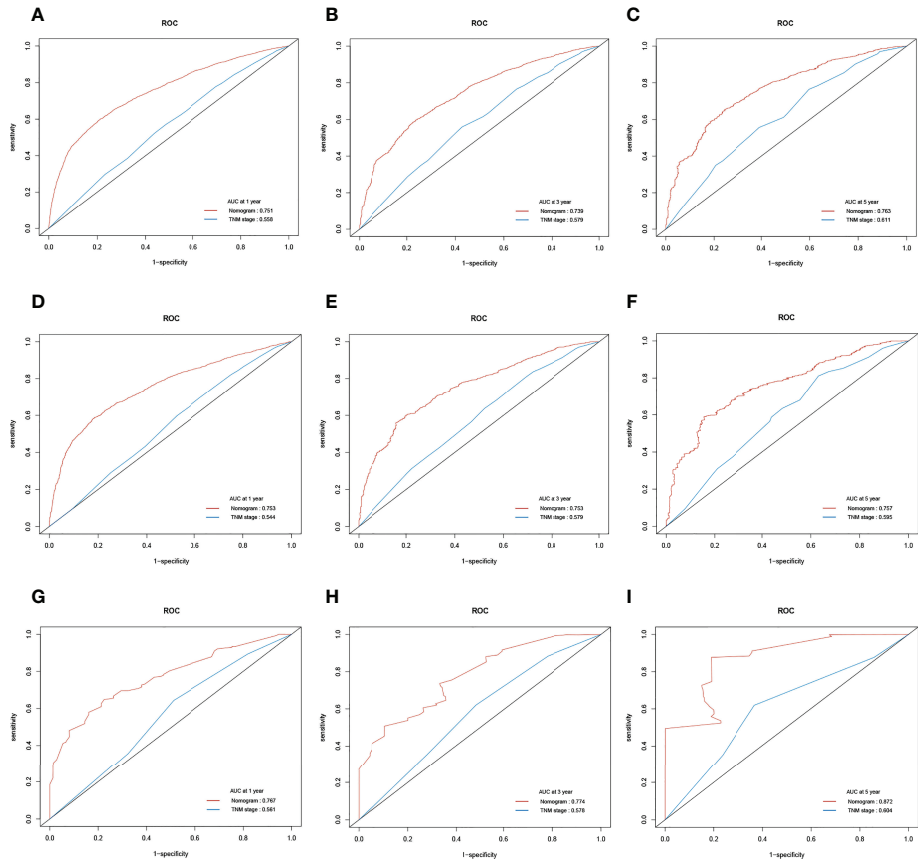

FIGURE 6
The receiver operating characteristic (ROC) curve of the TNM stage and the cancer-specific survival (CSS) nomogram. **(A–C)** The area under the curve (AUC) values of ROC predicted 1-, 3-, and 5-year CSS rates of the nomogram and TNM stage in the training cohort. **(D–F)** AUC values of ROC predicted 1-, 3-, and 5-year CSS rates of the nomogram and TNM stage in the internal validation cohort. **(G–I)** AUC values of ROC predicted 1-, 3-, and 5-year CSS rates of the nomogram and TNM stage in the external validation cohort.

growth. Our results revealed that liver and brain metastases were independent predictors of survival in LCBM. According to the theory of "seed and soil hypothesis," metastatic cancer cells can dynamically interact with particular organ microenvironment and lead to different patterns of metastatic spread. Several studies found that the site of metastasis did not significantly influence patients' survivals. However, our findings were supported by other researchers (20, 29). Tamura et al. reported a 1.55-fold increase in mortality in patients with liver metastasis compared with those with other metastasis (30). Most patients with LC with liver metastasis had multiple nodules morphologically and biliary tract obstruction may have been caused by LC metastatic to the lymph nodes in the porta hepatis or the hepatic parenchyma lesion. Patients would be jaundiced and would have a progressive divergence of hepatic synthetic and coagulation function. Meanwhile, the activation or metabolism of several cytotoxic drugs commonly used in various procedures for chemotherapy could be affected, in turn, leading to the limitation of chemotherapy's administration. There were several cases reporting that patients with liver metastases could not receive conventional chemotherapy for liver dysfunction (31, 32). As one of the most common sites of metastasis in patients with LC, brain metastasis was regarded as one of the unfavorable prognostic factors in previous research studies. In one study, based on the SEER database, the cancer-specific case fatality was 91.01% after a median follow-up of 52 months in 5,974 patients with LC and with brain metastasis (33, 34). This study also revealed that patients with additional sites of metastasis (like BM) were related to worse survival. Thus, patients with LCBM combined with brain metastasis tend to exhibit poor prognosis. In the case of brain metastasis, the daily living activities of patients could be limited significantly and they could develop severe neurological symptoms, which may lead to reduced willingness of patients

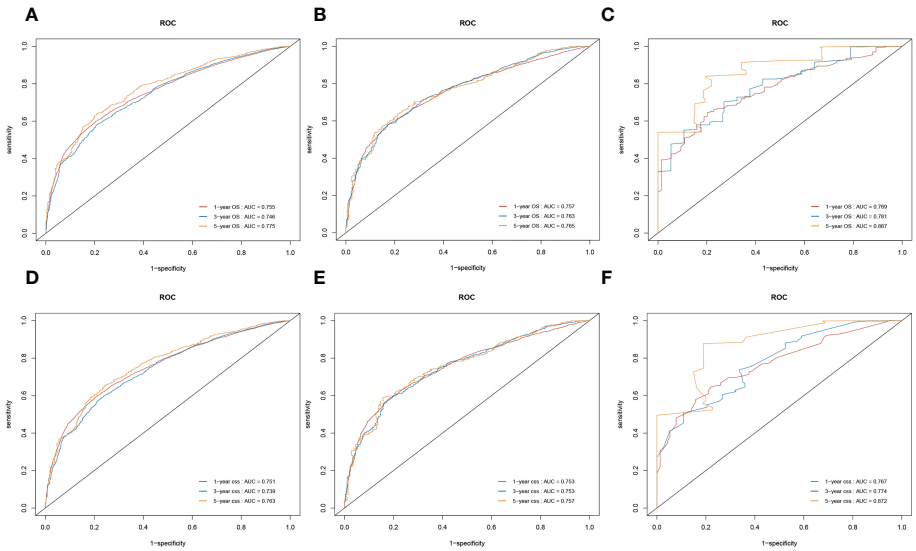

FIGURE 7
Nomograms of time-dependent receiver operating characteristic (ROC) curves for the overall survival (OS) and cancer-specific survival (CSS) prediction of patients with lung cancer with bone metastasis (LCBM). **(A–C)** The training, internal validation, and external validation cohorts for the OS. **(D–F)** The training, internal validation, and external validation cohorts for the CSS.

and doctors to pursue aggressive therapy. In addition, the use of chemotherapy for brain metastasis patients could be limited by poor efficacy and high toxicity. In the case of LCBM with brain metastasis, surgical treatment is not recommended because it has no significant impact on the long-term prognosis (32). In comparison, intracranial tumor biopsy is the gold standard for the diagnosis, which can determine not only the nature of intracranial lesions but also their source.

We found that radiotherapy, chemotherapy, and surgery of primary lesions were of prognostic significance in LCBM. Among them, chemotherapy contributed most significantly to prognosis in accordance with the nomogram. As is well known,

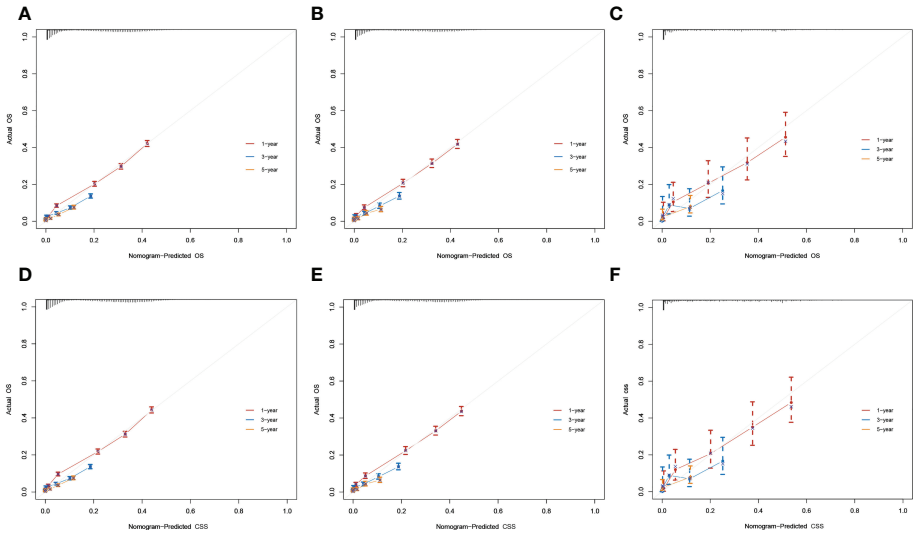

FIGURE 8
Calibration curves for 1-, 3-, and 5-year overall survival (OS) and cancer-specific survival (CSS) rates of the nomogram predictions. **(A–C)** The training, internal validation, and external validation cohorts for the OS. **(D–F)** The training, internal validation, and external validation cohorts for the CSS.

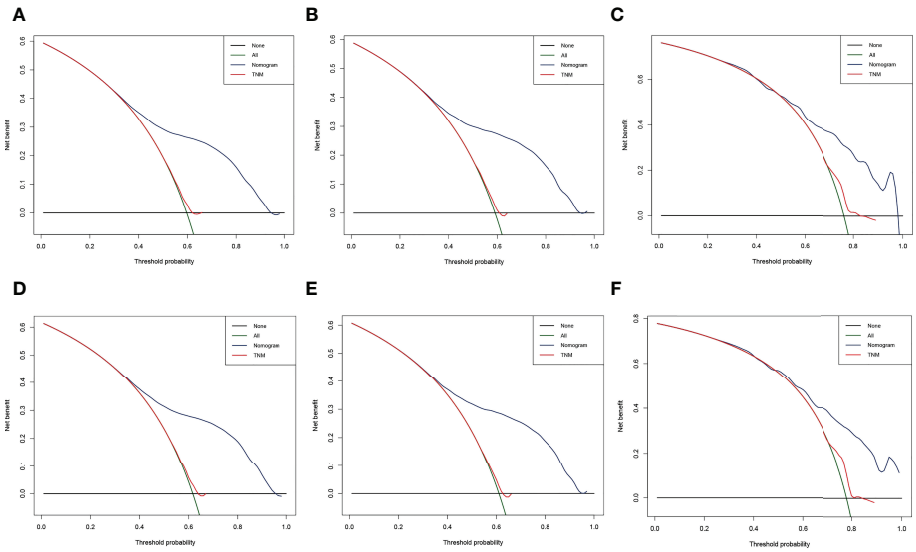

FIGURE 9
Decision curve analysis (DCA) of the nomogram and TNM stage for the overall survival (OS) and cancer-specific survival (CSS) prediction of patients with lung cancer with bone metastasis (LCBM). **(A)** The training, **(B)** internal validation, and **(C)** external validation cohorts for the OS. **(D)** The training, **(E)** internal validation, and **(F)** external validation cohorts for the CSS.

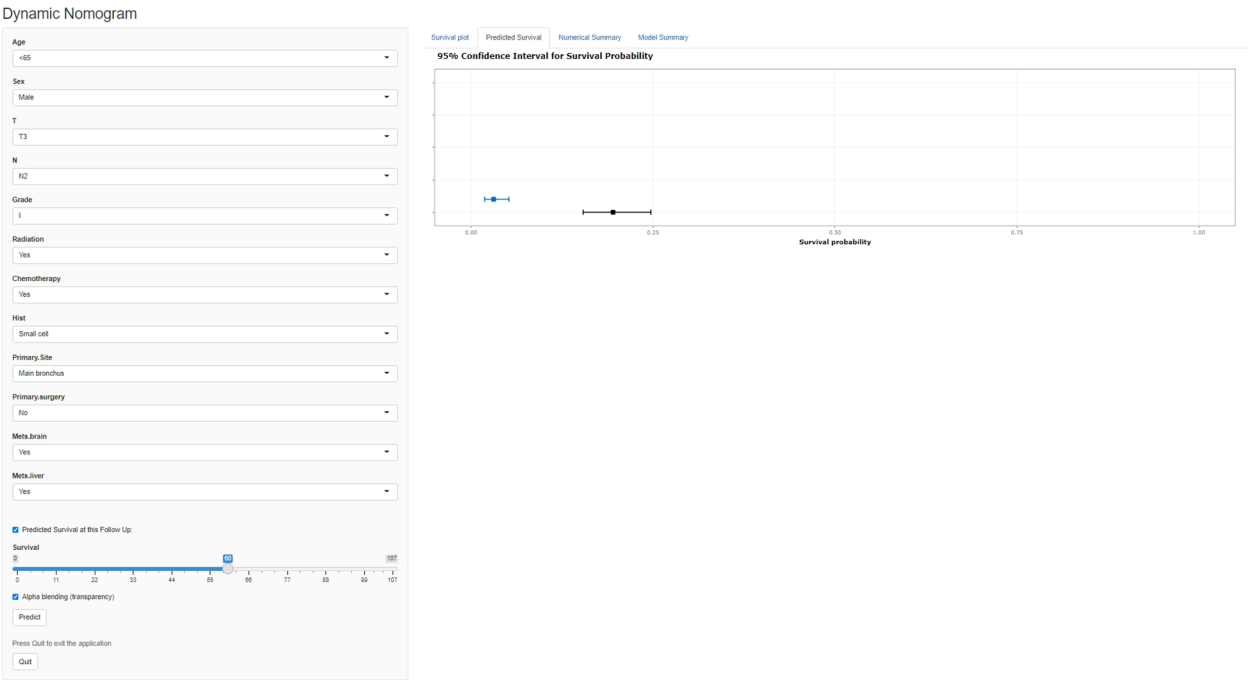

FIGURE 10
A web-based nomogram for predicting postoperative overall survival (OS). The line segments of the graphical summary show the approximate range of overall survival rates.

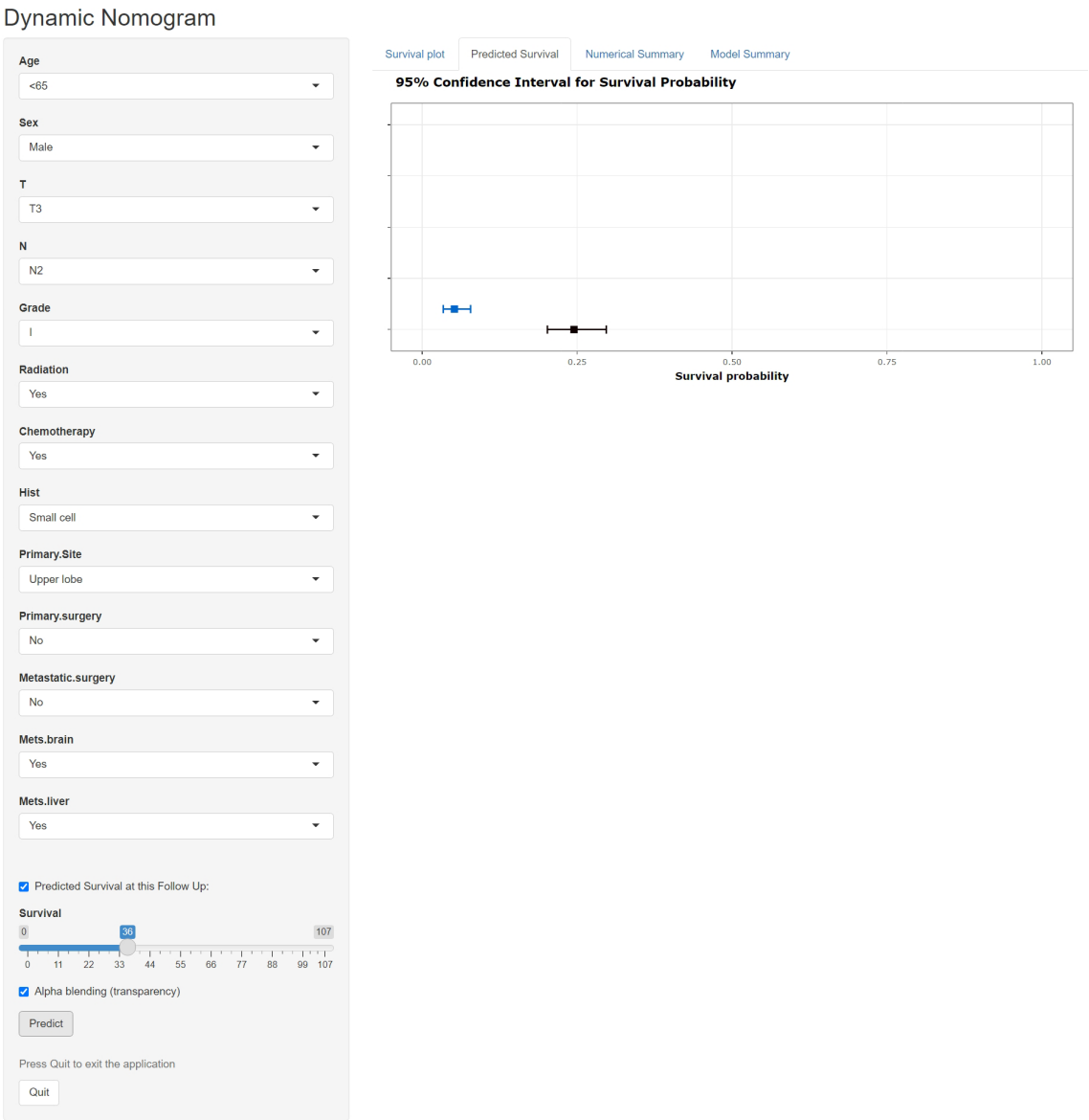

FIGURE 11
A web-based nomogram for predicting postoperative cancer-specific survival (CSS). The line segments of the graphical summary show the approximate range of overall survival rates.

chemotherapy remains the cornerstone of therapy in the management of advanced LC. First-line chemotherapy, maintenance chemotherapy, and second-line therapy were considered as regular therapeutic regimen to advanced NSCLC for many years (35, 36). Platinum-based doublets were used for the standard first-line chemotherapy, which could achieve symptoms remission and increased median survival by 1.5 months and the 1-year survival rate by 9%. Radiotherapy could relieve pain at the site of skeletal metastasis, reduce the incident of SRE, and could be used as an alternative treatment option for medically inoperable LC with high local control rates and with low toxicity (37). The technology of stereotactic body radiotherapy (SBRT) improved the accuracy and safety of radiotherapy for patients with LCBM, especially for those with spinal metastasis, which optimized radiation dose delivery to the BM while sparing the spinal cord.

We found that surgery of primary lesions was beneficial for prolonging both the OS and CSS of patients with LCBM. Although it is the standard treatment for patients with advanced LC, surgeons have performed curative resection in those who present with oligometastases. In the retrospective study by Takahashi et al., patients with NSCLC and synchronous isolated BMs achieved longer survival rates following primary lung tumor resection (38). However, other studies had different opinions. Patrini et al. suggested that there was no case in which BM was considered as an oligometastatic for the infaust prognosis (39). Considering quite the low number of patients who underwent surgery of the primary site, we speculated that they received surgery for oligometastases. The role of surgery in LCBM has not been effectively identified yet, especially for those with polymetastasis.

In addition to the previously mentioned treatments, bone-targeted pharmacological treatments including bisphosphonates and denosumab were widely used clinically to reduce pain and avoid SREs. In the last 30 years, bisphosphonate has been considered a key player in the therapy of BM from various cancers. Among bisphosphonates, zoledronic acid's clinical effectiveness was validated in multiple studies (40). Compared with bisphosphonates, denosumab was found to be associated with delayed first and subsequent SREs and lower incidence of renal toxicity but higher incidence of hypocalcemia in several meta-analyses. However, we failed to consider the bone-targeted pharmacological treatments as the information in this regard was not provided by the SEER data center. In recent years, the application of next-generation sequencing technology has been widely used in the auxiliary diagnosis and target therapy of cancers (40). Epidermal growth factor receptor (EGFR) is the most widely used driving gene for the targeted treatment of LC and responds well to EGFR tyrosine kinase inhibitors (41). Previous studies have shown that microRNA, Dickkopf1, and insulin-like growth factor binding protein 3 are potential therapeutic targets for LCBM (40). Mukai et al. reported a high expression of mesenchymal-to-epithelial transition (MET) in both the primary metastasis and BM of patients with LC and suggested that drugs targeted at MET amplification, such as crizotinib and cabotinib, would have a certain effect on patients with LCBM (42). Recently, the study by Huang et al. found a high consistency of mutation patterns between primary LC lesions and matched BM, which indicated that the effective treatment of primary LC may also be suitable for matched LCBM, such as the EGFR-TKI treatment for LCBM with sensitive EGFR mutations (43). Unfortunately, the data of molecular alterations were not available in the SEER database, and our nomogram failed to include relevant factors.

Our study also has significant advantages. Compared with the previous studies, we identified the risk factors for BM in patients with LC and the prognostic factors of patients with LCBM. Meanwhile, we created a nomogram containing identified independent factors as a convenient and intuitive visual tool for prognostic prediction, which was verified by internal and external validation sets to guarantee the reliability of the results. As a retrospective cohort analysis with a large sample size, we point out that the validated results of current study can provide guidance to clinicians in daily routine practice and decision-making. However, some limitations are present. First, this was a retrospective study in which selection bias existed inevitably. Our study was limited by the data available in the SEER database. Second, in the process of patient screening, many failed to be enrolled to the SEER database for lack of detailed information like insurance and details on treatment. Missing data of these patients may mildly affect the accuracy of the research result. Third, the SEER database is based on the US population. The nomograms that we constructed may be limited by geographic constraints and may only be considered as a reference in the Chinese LCBM population. In the future, large multicenter studies should be performed in Chinese patients to develop a model to demonstrate its clinical validity for the Chinese population.

Conclusion

In conclusion, the findings of this study based on a population level identified several factors that affect the OS and CSS of patients with LCBM, namely, age, sex, T stage, N stage, grade, histology, radiation therapy, chemotherapy, primary site, primary surgery, liver metastasis, and brain metastasis. We also found that metastatic surgery was beneficial for prolonging the CSS of patients with LCBM. Moreover, nomograms were developed to objectively predict 1-, 3, and 5-year OS and CSS of patients with this devastating disease. The result indicated that the nomogram had favorable discrimination, good consistency, and clinical benefits in patients with LCBM. For LCBM's extremely poor prognosis, the development of the prediction models was important for patients and meant a lot to them. We point out that nomograms could help oncologists to make better clinical decisions and provide personalized treatment plans for patients.

Data availability statement

The original contributions presented in the study are included in the article/supplementary material. Further inquiries can be directed to the corresponding authors.

Author contributions

All authors were responsible for the study concept and design. MY, SG, XD, and RZ are co-first authors. JX and WM are co-response authors. All authors contributed to the article and approved the submitted version.

Funding

The authors declare that they have received funding support from Shanghai University of Traditional Chinese Medicine combines medical care with high-level scientific innovation project: 602072D and 602064D, Shanghai Health and Family Planning Commission: 20224Y0165, and National Natural Science Foundation of China: 82205145.

Acknowledgments

We would like to thank the reviewers for their thorough review of our manuscript, especially under the severe circumstance of the COVID-19 pandemic, and we wish that everybody pulls through safe and sound. Many thanks to all authors who provided the cases.

Conflict of interest

The authors declare that the research was conducted in the absence of any commercial or financial relationships that could be construed as a potential conflict of interest.

Publisher's note

All claims expressed in this article are solely those of the authors and do not necessarily represent those of their affiliated organizations, or those of the publisher, the editors and the reviewers. Any product that may be evaluated in this article, or claim that may be made by its manufacturer, is not guaranteed or endorsed by the publisher.

References

1. Zaman A, Bivona TG. Emerging application of genomics-guided therapeutics in personalized lung cancer treatment. *Ann Transl Med* (2018) 6:160. doi: 10.21037/atm.2018.05.02

2. Yu K, Chen Y, Tian Y, Kang H, Song K, Dong Y, et al. Characteristics, incidence, and risk factors for death from fatal pneumonia among patients with primary malignant bone tumors: a SEER-based observational study. *Transl Cancer Res* (2021) 10:3659–70. doi: 10.21037/tcr-21-306

3. Allemani C, Weir HK, Carreira H, Harewood R, Spika D, Wang XS, et al. Global surveillance of cancer survival 1995-2009: analysis of individual data for 25,676,887 patients from 279 population-based registries in 67 countries (CONCORD-2). *Lancet* (2015) 385:977–1010. doi: 10.1016/S0140-6736(14)62038-9

4. Jarry U, Bostoen M, Pineau R, Chaillot L, Mennessier V, Montagne P, et al. Orthotopic model of lung cancer: isolation of bone micro-metastases after tumor escape from osimertinib treatment. *BMC Cancer* (2021) 21:530. doi: 10.1186/s12885-021-08205-9

5. Tam AH, Schepers AJ, Qin A, Nachar VR. Impact of extended-interval versus standard dosing of zoledronic acid on skeletal events in non-Small-Cell lung cancer and small-cell lung cancer patients with bone metastases. *Ann Pharmacother* (2021) 55:697–704. doi: 10.1177/1060028020967629

6. Boudou-Rouquette P, Arrondeau J, Gervais C, Durand JP, Fabre E, De Percin S, et al. Development and validation of a host-dependent, PDL1-independent, biomarker to predict 6-month progression-free survival in metastatic non-small cell lung cancer (mNSCLC) patients treated with anti-PD1 immune checkpoint inhibitors (ICI) in the CERTIM cohort: The ELY study. *EBioMedicine* (2021) 73:103630. doi: 10.1016/j.ebiom.2021.103630

7. Cao Y, Afzal MZ, Shirai K. Does denosumab offer survival benefits? -our experience with denosumab in metastatic non-small cell lung cancer patients treated with immune-checkpoint inhibitors. *J Thorac Dis* (2021) 13:4668–77. doi: 10.21037/jtd-21-150

8. Qin A, Zhao S, Miah A, Wei L, Patel S, Johns A, et al. Bone metastases, skeletal-related events, and survival in patients with metastatic non-small cell lung cancer treated with immune checkpoint inhibitors. *J Natl Compr Canc Netw* (2021) 19:915–21. doi: 10.6004/jnccn.2020.7668

9. Li Q, Chen Q, Chen J, Wang Z, Wang P, Zhao H, et al. Prognostic nomogram for predicting long-term survival in bronchopulmonary carcinoid tumor patients receiving resection. *Ann Transl Med* (2021) 9:1402. doi: 10.21037/atm-21-1929

10. He Y, Zhao F, Han Q, Zhou Y, Zhao S. Prognostic nomogram for predicting long-term cancer-specific survival in patients with lung carcinoid tumors. *BMC Cancer* (2021) 21:141. doi: 10.1186/s12885-021-07832-6

11. Huang CY, Li MY, Liu W, Li XX, Xu Y, Li JY, et al. Performance of prognostic nomogram in predicting long-term survival outcomes for osteosarcoma. *J Biol Regul Homeost Agents* (2020) 34:1819–24. doi: 10.23812/20-105-L

12. Heng Y, Zhu X, Zhou L, Zhang M, Li J, Tao L, et al. A prognostic nomogram for predicting the long-term survival outcome of hypopharyngeal squamous cell carcinoma patients after tumour resection to assist the decision-making of postoperative adjuvant treatment. *Eur J Surg Oncol* (2020) 46:245–51. doi: 10.1016/j.ejso.2019.09.005

13. Tian S, Li Q, Li R, Chen X, Tao Z, Gong H, et al. Development and validation of a prognostic nomogram for hypopharyngeal carcinoma. *Front Oncol* (2021) 11:696952. doi: 10.3389/fonc.2021.696952

14. Wang YQ, Liu XD, Bai WL, Li SQ. Identification of resectable N2 in NSCLC: A single center experience and review of the SEER database. *Front Oncol* (2021) 11:647546. doi: 10.3389/fonc.2021.647546

15. Duan F, Li J, Huang J, Hua X, Song C, Wang L, et al. Establishment and validation of prognostic nomograms based on serum copper level for patients with early-stage triple-negative breast cancer. *Front Cell Dev Biol* (2021) 9:770115. doi: 10.3389/fcell.2021.770115

16. Yang QK, Lai QY, Wang Y, Wang Y, Yao ZX, Zhang XJ, et al. Establishment and validation of prognostic nomograms to predict overall survival and cancer-specific survival for patients with osteosarcoma. *Neoplasma* (2021) 68:434–46. doi: 10.4149/neo_2020_200617N639

17. Ranstam J, Cook JA. Kaplan-Meier Curve. *Br J Surg* (2017) 104:442. doi: 10.1002/bjs.10238

18. Heagerty PJ, Lumley T, Pepe MS. Time-dependent ROC curves for censored survival data and a diagnostic marker. *Biometrics* (2000) 56:337–44. doi: 10.1111/j.0006-341x.2000.00337.x

19. Vickers AJ, Elkin EB. Decision curve analysis: a novel method for evaluating prediction models. *Med Decis Making* (2006) 26:565–74. doi: 10.1177/0272989X06295361

20. Shi S, Wang H, Liu X, Xiao J. Prediction of overall survival of non-small cell lung cancer with bone metastasis: an analysis of the surveillance, epidemiology and end results (SEER) database. *Transl Cancer Res* (2021) 10:5191–203. doi: 10.21037/tcr-21-1507

21. Mundy GR. Metastasis to bone: causes, consequences and therapeutic opportunities. *Nat Rev Cancer* (2002) 2:584–93. doi: 10.1038/nrc867

22. Riihimaki M, Hemminki A, Fallah M, Thomsen H, Sundquist K, Sundquist J, et al. Metastatic sites and survival in lung cancer. *Lung Cancer* (2014) 86(1):78–84. doi: 10.1016/j.lungcan.2014.07.020(2014

23. Hong S, Youk T, Lee SJ, Kim KM, Vajdic CM, et al. Bone metastasis and skeletal-related events in patients with solid cancer: A Korean nationwide health insurance database study. *PloS One* (2020) 15(7):e0234927. doi: 10.1371/journal.pone.0234927

24. Popper HH. Progression and metastasis of lung cancer. *Cancer Metastasis Rev* (2016) 35:75–91. doi: 10.1007/s10555-016-9618-0

25. Zhang L, Gong Z. Clinical characteristics and prognostic factors in bone metastases from lung cancer. *Med Sci Monit* (2017) 23:4087–94. doi: 10.12659/msm.902971

26. Song L, Zhu Z, Mao L, Li X, Han W, Du H, et al. Clinical, conventional CT and radiomic feature-based machine learning models for predicting ALK rearrangement status in lung adenocarcinoma patients. *Front Oncol* (2020) 10:369. doi: 10.3389/fonc.2020.00369

27. Li C, Liu J, Lin J, Li Z, Shang X, Wang H. Poor survival of non-small-cell lung cancer patients with main bronchus tumor: a large population-based study. *Future Oncol* (2019) 5(24):2819–27. doi: 10.2217/fon-2019-0098

28. Yang L, Wang S, Gerber DE, Zhou Y, Xu F, Liu J, et al. Main bronchus location is a predictor for metastasis and prognosis in lung adenocarcinoma: A large cohort analysis. *Lung Cancer* (2018) 120:22–6. doi: 10.1016/j.lungcan.2018.03.011

29. Bilen MA, Shabto JM, Martini DJ, Liu Y, Lewis C, Collins H, et al. Sites of metastasis and association with clinical outcome in advanced stage cancer patients treated with immunotherapy. *BMC Cancer* (2019) 19:857. doi: 10.1186/s12885-019-6073-7

30. Tamura T, Kurishima K, Nakazawa K, Kagohashi K, Ishikawa H, Satoh H, et al. Specific organ metastases and survival in metastatic non-small-cell lung cancer. *Mol Clin Oncol* (2015) 3(1):217–21. doi: 10.3892/mco.2014.410(2015

31. Cho S, Yum S, Kim K, Jheon S. Prognostic factors for post-recurrence survival in patients with completely resected stage III (N2) non-small-cell lung cancer. *Eur J Cardiothorac Surg* (2018) 54:554–9. doi: 10.1093/ejcts/ezy063

32. Song IH, Yeom SW, Heo S, Choi WS, Yang HC, Jheon S, et al. Prognostic factors for post-recurrence survival in patients with completely resected stage I non-small-cell lung cancer. *Eur J Cardiothorac Surg* (2014) 45:262–7. doi: 10.1093/ejcts/ezt333

33. Achrol AS, Rennert RC, Anders C, Soffietti R, Ahluwalia MS, Nayak L, et al. Brain metastases. *Nat Rev Dis Primers* (2019) 5:5. doi: 10.1038/s41572-018-0055-y

34. Xing P, Mu Y, Hao X, Wang Y, Li J. Data from real world to evaluate the efficacy of osimertinib in non-small cell lung cancer patients with central nervous system metastasis. *Clin Transl Oncol* (2019) 21:1424–31. doi: 10.1007/s12094-019-02071-5

35. Pirker R. Chemotherapy remains a cornerstone in the treatment of nonsmall cell lung cancer. *Curr Opin Oncol* (2020) 32:63–7. doi: 10.1097/CCO.0000000000000592

36. Hanna N, Johnson D, Temin S, Masters G. Systemic therapy for stage IV non-Small-Cell lung cancer: American society of clinical oncology clinical practice guideline update summary. *J Oncol Pract* (2017) 13:832–7. doi: 10.1200/JOP.2017.026716

37. Yu XJ, Dai WR, Xu Y. Survival outcome after stereotactic body radiation therapy and surgery for early stage non-small cell lung cancer: A meta-analysis. *J Invest Surg* (2017) 1–8. doi: 10.1080/08941939.2017.1341573

38. Takahashi Y, Adachi H, Mizukami Y, Yokouchi H, Oizumi S, Watanabe A. Patient outcomes post-pulmonary resection for synchronous bone-metastatic non-small cell lung cancer. *J Thorac Dis* (2019) 11(9):3836–45. doi: 10.21037/jtd.2019.09.17(2019

39. Patrini D, Panagiotopoulos N, Bedetti B, Mitsos S, Crisci R, Solli P, et al. Surgical approach in oligometastatic non-small cell lung cancer. *Ann Transl Med* (2018) 6(5):93. doi: 10.21037/atm.2018.02.16(2018

40. Mei M, Xiang Z, Yang J, Xiang R. Efficacy of zoledronic acid for prevention of bone loss in early-stage breast cancer patients receiving adjuvant therapy: A meta-analysis of 13 randomized controlled trials. *Curr Probl Cancer* (2020) 44 (2):100507. doi: 10.1016/j.currproblcancer.2019.100507

41. Pang H, Ma N, Jiao M, Shen W, Xin B, Wang T, et al. The biological effects of Dickkopf1 on small cell lung cancer cells and bone metastasis. *Oncol Res* (2017) 25:35–42. doi: 10.3727/096504016X14719078133249

42. Mukai S, Yorita K, Kawagoe Y, Nakahara K, Kamibeppu T, Sugie S, et al. Matriptase and MET are prominently expressed at the site of bone metastasis in renal cell carcinoma: immunohistochemical analysis. *Hum Cell* (2015) 28(1):44–50. doi: 10.1007/s13577-014-0101-3

43. Huang X, Shi X, Huang D, Li B, Lin N, Pan W, et al. Mutational characteristics of bone metastasis of lung cancer. *Ann Palliat Med* (2021) 10:8818–26. doi: 10.21037/apm-21-1595

frontiers | Frontiers in Oncology

TYPE Original Research
PUBLISHED 15 December 2022
DOI 10.3389/fonc.2022.1098182

OPEN ACCESS

EDITED BY
Feifei Pu,
Huazhong University of Science and Technology, China

REVIEWED BY
Tianhua Rong,
Beijing Tiantan Hospital, Capital Medical University, China
Yining Gong,
Xi'an Jiaotong University, China

*CORRESPONDENCE
Yaosheng Liu
15810069346@qq.com;
632763246@qq.com
Zheng Wang
wangzheng301@163.com
Xiaolin Shi
xlshi-2002@163.com

†These authors share first authorship

SPECIALTY SECTION
This article was submitted to Surgical Oncology, a section of the journal Frontiers in Oncology

RECEIVED 14 November 2022
ACCEPTED 29 November 2022
PUBLISHED 15 December 2022

CITATION
Zhang B, Yu H, Zhao X, Cao X, Cao Y, Shi X, Wang Z and Liu Y (2022) Preoperative embolization in the treatment of patients with metastatic epidural spinal cord compression: A retrospective analysis.
Front. Oncol. 12:1098182.
doi: 10.3389/fonc.2022.1098182

Preoperative embolization in the treatment of patients with metastatic epidural spinal cord compression: A retrospective analysis

Bin Zhang[1,2†], Haikuan Yu[1,3†], Xiongwei Zhao[4,5†], Xuyong Cao[1,4], Yuncen Cao[1,4], Xiaolin Shi[6*], Zheng Wang[1*] and Yaosheng Liu[1,2,5*]

[1]Senior Department of Orthopedics, The Fourth Medical Center of PLA General Hospital, Beijing, China, [2]Department of Orthopedic Surgery, National Clinical Research Center for Orthopedics, Sports Medicine & Rehabilitation, Chinese PLA General Hospital, Beijing, China, [3]Chinese PLA Medical School, Beijing, China, [4]Department of Orthopedic Surgery, The Fifth Clinical Medical College of Anhui Medical University, Beijing, China, [5]Department of Orthopedic Surgery, The Fifth Medical Center of PLA General Hospital, Beijing, China, [6]Department of Orthopedic Surgery, The Second Affiliated Hospital of Zhejiang Chinese Medical University, Hangzhou, China

Purpose: The purpose of the study was to assess the effectiveness and safety of preoperative embolization in the treatment of patients with metastatic epidural spinal cord compression (MESCC).

Methods: A retrospective analysis of 138 MESCC patients who underwent decompressive surgery and spine stabilization was performed in a large teaching hospital. Among all enrolled patients, 46 patients were treated with preoperative embolization (the embolization group), whereas 92 patients did not (the control group). Patient's baseline clinical characteristics, surgery-related characteristics, and postoperative neurological status, complications, and survival prognoses were collected and analyzed. Subgroup analysis was performed according to the degree of tumor vascularity between patients with and without preoperative embolization.

Results: Patients with severe hypervascularity experienced more mean blood loss in the control group than in the embolization group, and this difference was statistically significant (P=0.02). The number of transfused packed red cells (PRC) showed a similar trend (P=0.01). However, for patients with mild and moderate hypervascularity, both blood loss and the number of PRC transfusion were comparable across the two groups. Regarding decompressive techniques, the embolization group (64.29%, 9/14) had a higher proportion of circumferential decompression in comparison to the control group (30.00%, 9/30) among patients with severe hypervascularity (P=0.03), whereas the rates were similar among patients with mild (P=0.45) and moderate (P=0.54) hypervascularity. In addition, no subgroup analysis revealed any statistically significant differences in operation time, postoperative functional recovery,

postoperative complications, or survival outcome. Multivariate analysis showed that higher tumor vascularity (OR[odds ratio]=3.69, 95% CI [confident interval]: 1.30-10.43, P=0.01) and smaller extent of embolization (OR=4.16, 95% CI: 1.10-15.74, P=0.04) were significantly associated with more blood loss.

Conclusions: Preoperative embolization is an effective and safe method in treating MESCC patients with severe hypervascular tumors in terms of intra-operative blood loss and surgical removal of metastatic tumors. Preoperative tumor vascularity and extent of embolization are independent risk factors for blood loss during surgery. This study implies that MESCC patients with severe hypervascular tumors should be advised to undergo preoperative embolization.

KEYWORDS

decompressive surgery, metastatic epidural spinal cord compression, blood loss, prognosis, preoperative embolization

Introduction

Metastatic epidural spinal cord compression (MESCC) is the secondary compression of the spinal cord due to cancer metastases to the spine or epidural space, and it can reduce the quality of life because of cancer-associated back and leg pain, neurological deficit, and loss of bladder and bowel continence (1, 2). The morbidity of this disease is about 5%–10% among patients with malignant tumors (1), and approximately one out of ten spine metastases patients will develop MESCC (3). Therapeutic standards for MESCC patients are not yet accessible. Decompressive surgery followed by postoperative irradiation is typically recommended among individuals who have progressive neurologic deficit, a generally healthy level of physical activity, and an anticipated survival period of longer than three months (4).

Nevertheless, intra-operative blood loss poses a great significant problem for MESCC patients undergoing decompressive surgery. Several publications have noted that that surgically treated patients with metastatic spinal illness experienced blood loss of 1,630 to 3,640 ml (5) and sometimes up to 10,000 ml of significant bleeding (6), and a meta-analysis revealed that the pooled mean blood loss was above 2100 ml (7). Allogeneic blood transfusion was necessary for those patients under these circumstances, but it has been shown to be linked to an increased risk of postoperative infection, delirium, venous thromboembolism, and even mortality (8, 9). Thus, it is an intriguing topic to discuss ways to assist patients and surgeons in minimizing blood loss and transfusion.

Preoperative embolization is a technique that was developed to lessen intra-operative blood loss, simplify the process of spine surgery, and make operation safer (10–12). This method was first made available in 1974 to treat spine tumors and lessen intra-operative blood loss (13). Nowadays, it is widely used in the treatment of a variety of spinal tumors (10–12). However, several investigations showed that intra-operative blood loss during the surgical excision of spinal tumors was not significantly affected by preoperative embolization (11, 14, 15). This might be the case since the amount of blood loss varied greatly according to histology and surgical methods (16). In particular, highly vascularized cancers such as renal and live carcinoma were relevant to a high risk of blood bleeding, and more invasive procedures like corpectomy resulted in a significantly high volume of blood loss in comparison to laminectomy (16). More recently, a number of studies with a small size sample reported that preoperative embolization for patients with hypervascular metastatic tumors was able to decrease intra-operative blood loss (17, 18), but inconsistent results still existed (19, 20). In addition, patients with non-hypervascular lesions did not experience the benefit of lowering blood loss (16). Additionally, these findings still require further verification (21).

Therefore, this study aimed to assess the effectiveness and safety of preoperative embolization in the treatment of MESCC patients. Intra-operative features such as blood loss, number of packed red cells (PRC), and surgical methods and postoperative outcome including complication, functional recovery, and survival outcome were thoroughly collected and compared in the study to evaluate the role of preoperative embolization in MESCC patients. This study speculated that preoperative embolization might be an efficient and safe method to reduce

blood loss during surgery, which would make it easier to remove metastases.

Patients and methods

Inclusion criteria and exclusion criteria

This study retrospectively examined 138 MESCC patients underwent decompressive surgery and spine stabilization between January 2012 and December 2018. Patients were considered for analysis if they met the following criteria: (1) patients were diagnosed with metastatic spinal cord compression, (2) patients were treated with decompression and spine stabilization combined with or without preoperative embolization, and (3) patients presented at least one of symptoms listed below as a result of MESCC: a. severe back pain; b. sensory dysfunction; c. motor dysfunction; d. sphincter dysfunction. Patients were excluded for the analysis if they met any of the following criteria: (1) age less than 18 years, (2) MESCC due to primary spinal malignant tumor or intramedullary metastases, (3) prior spinal surgery treatment, (4) poor health precluding surgery (an expected lifespan of less than three months), or (5) uncorrectable coagulopathy or renal impairment. Patient's flowchart is outlined in Supplementary Figure 1.

Patients included in the analysis were classified according to the presence of preoperative embolization, and there were the embolization group and the control group. Patients in the embolization group were treated with preoperative embolization, whereas patients in the control group did not receive preoperative embolization. The Ethics Committee Board of the Fourth Medical Center of PLA General Hospital and waived the informed consent from patients since all data were retrospective in nature, and the study was conducted in accordance with the Declaration of Helsinki.

Procedure and techniques

The indication for surgery was neurological deficit, mechanical back pain, and a predicted survival time of more than three months. The main indication of preoperative embolization was to reduce intra-operative bleeding (22), and the aim of embolization was to block the cephalad and caudal segmental arteries. Selection of patients for preoperative embolization was mainly based on the two criteria: (1) preoperative radiography represented hypervascularity; (2) radical surgery was planned. In our institution, preoperative embolization of metastatic spinal tumors was routinely recommended for eligible patients, particularly those with hypervascular tumors, but such surgeries are typically performed in emergencies and limited by the availability of interventional radiologists. In addition, embolization was not done if there was an evidence of major Adamkiewicz artery linked to the tumor vascularization, and Adamkiewicz artery provided blood supply to the spinal cord (23), because embolization of this artery may lead to serious complications, including paralysis, anesthesia, incontinence, and sexual dysfunction. In some cases, embolization was performed partially to preserve the blood supply to the anterior spinal artery. In regional anesthesia, patients received standard endovascular techniques through arterial access to one femoral artery. Selective catheterization and digital subtraction angiography of spinal segmental arteries were performed. Routinely, a 5 F catheter (Cordis) was selectively inserted into thoracic aorta and the corresponding intercostal artery, followed by a 2.6 F catheter (Stride, Japan) being selectively inserted into the branch of intercostal artery. Particles were injected to prevent blood reflux. The interventional radiologist chose the optional embolization material. Polyvinyl alcohol embolization microspheres (500–700 um, Heng Rui, China), gelatin sponge (1000 um, Alicon, China), and microcoils (Cook, Inc, Bloomington, Indiana) were used during embolization. Decompressive surgery was generally conducted within 48 hours after preoperative embolization to avoid the revascularization of the tumor (24). Decompressive surgery was performed by wide laminectomy using the posterior approach, and intralesional excision was conducted as soon as possible in order to prevent massive blood loss. Besides, circumferential decompression was completed as fast as possible, if applicable. Tamponade of the cavity was done using absorbable hemostatic gauze to achieve hemostasis after the removal of tumor tissue. A case report is depicted in Figure 1. Intensity-modulated radiotherapy was routinely performed after surgical wound healing among the two groups.

Baseline characteristics and definitions

A series of patient's characteristics, including age, gender, location of MESCC, primary cancer types, preoperative neurological status, spinal instability neoplastic score (SINS), tumor vascularity, preoperative hemoglobin, preoperative international normalized ratio (INR), and preoperative thrombocytes, were collected from the two groups. The preoperative neurological statue was evaluated using ambulatory status (25), and patients with Frankel A, B, and C are unable to walk, while patients with Frankel D and E are ambulatory. The spine instability was evaluated using SINS (26). Before embolization, spinal angiography was used to assess the tumor vascularity in the embolization group by visual evaluation of the intensity of tumor blush (14, 22): mild hypervascularity was defined as no or slightly more prominent than the normal vertebral body blush, moderate hypervascularity was defined as medium tumor blush without early arteriovenous shunting, and

10.3389/fonc.2022.1098182

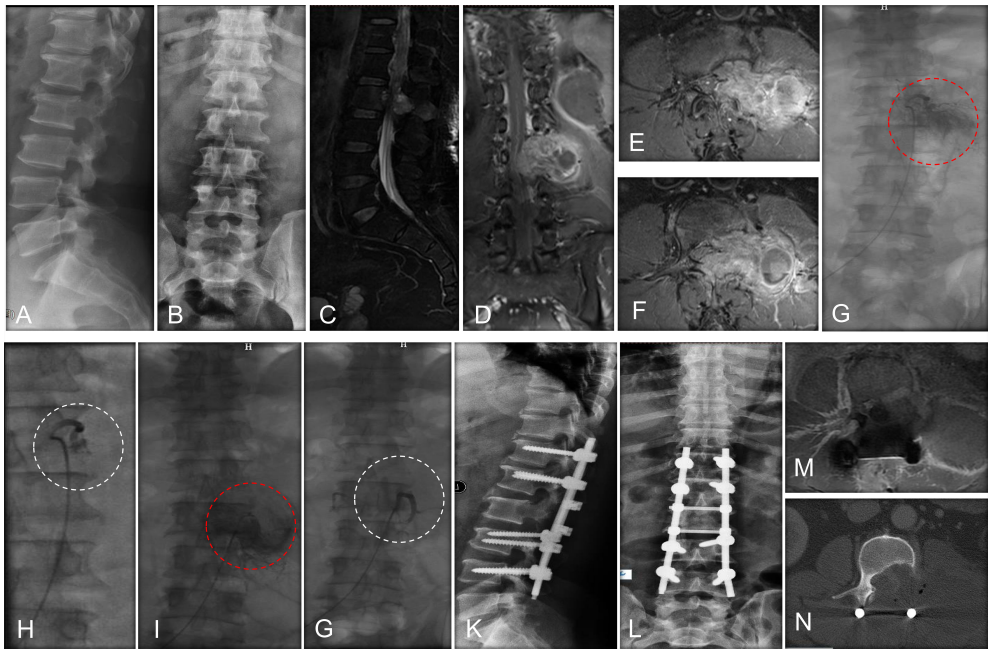

FIGURE 1
A case report of a MESCC patient who was a 50-year-old man with a histology of renal cancer and treated with preoperative embolization. **(A)** Perioperative lateral X-ray of MESCC; **(B)** Perioperative anteroposterior X-ray showed that pedicle of the vertebral arch disappeared in the left side of L2; **(C)** Preoperative T2-weighted sagittal MRI showing cord compression at L7; **(D)** Preoperative T2-weighted coronal enhanced MRI showing metastatic cancer; **(E)** Preoperative T2-weighted cross enhanced MRI showing metastatic cancer at L1; **(F)** Preoperative T2-weighted cross enhanced MRI showing metastatic cancer at L2; **(G)** Preoperative angiography showed extensive tumor blush from first lumbar artery at left; **(H)** The extensive tumor blush was successfully embolized; **(I)** Preoperative angiography showed extensive tumor blush from the second lumbar artery at left; **(J)** The extensive tumor blush was successfully embolized; **(K)** Lateral radiograph at 1 week after surgery; **(L)** Anteroposterior radiograph at 1 week after surgery; **(M)** MRI of metastatic tumor site at 3 months after surgery, indicating no further tumor progress; **(N)** CT image of metastatic tumor site at 3 months after surgery. Red dotted circle indicates preoperative blush and white dotted circle indicates postoperative blush.

severe hypervascularity was defined as intense tumor blush with early arteriovenous shunting. Examples of the degree of vascularity are provided in Figure 2. In the control group, hypervascularity was evaluated using tumor histology in terms of previous studies (27). To elaborate, severe hypervascular tumors included hepatocellular cancer, renal cell carcinoma, and thyroid carcinoma (27), moderate hypervascularity included lung cancer, breast cancer, prostate cancer, colon

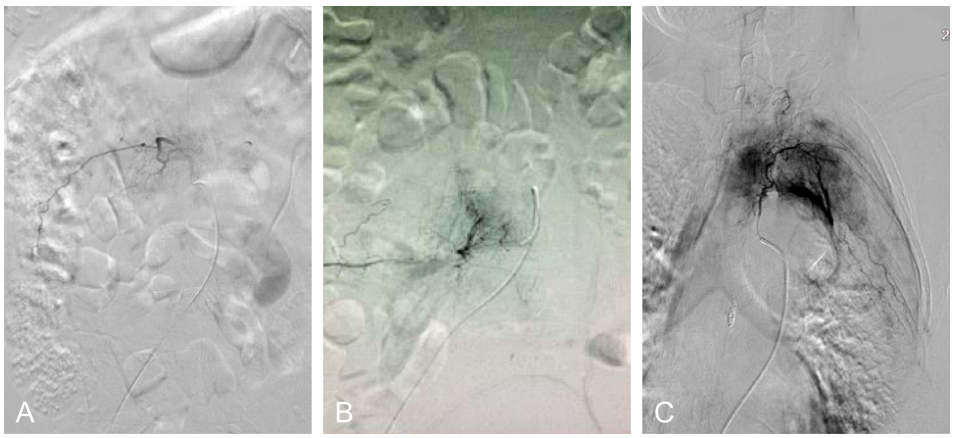

FIGURE 2
The evaluation of hypervascularity. **(A)** Mild hypervascularity; **(B)** Moderate hypervascularity; **(C)** Severe hypervascularity.

cancer, and nasopharyngeal cancer (27), and mild hypervascularity included others. In addition, subgroup analysis was further performed among patients stratified by severe vs. moderate vs. mild hypervascularity.

Surgery-related characteristics and definitions

Characteristics evaluated between the two groups included operation time (min), blood loss (ml), number of transfused PRC, and decompressive methods. Operation time was calculated from skin incision to closure, blood loss was determined according to anesthesiologists' records, and the degree of transfusion was estimated based on the number of used packed red blood cells (RBC). Decompressive methods included circumferential decompression and simple posterior decompression. Circumferential decompression for MESCC was defined as the metastatic tumor being successfully removed around the spinal cord and the complete decompression being achieved. Circumferential decompressive surgery referred to posterolateral transpedicular decompression and tumor resection combined with internal transpedicular screws and rods fixation in the study. Simple posterior decompression was defined as the metastatic tumor being not successfully removed in the anterior spinal cord, and thus the decompression of MESCC was not completely achieved. During surgery, decompression cannot be completely removed mainly due to massive intra-operative blood loss, and thus simple posterior decompression in the study mainly referred to laminectomy and internal transpedicular screws and rods fixation.

Postoperative outcomes

Postoperative characteristics analyzed in the study included postoperative complication, postoperative neurological status, and postoperative survival outcome. Postoperative neurological status was evaluated ambulatory status one week after surgery (25). The postoperative complications included local and systematic complications due to surgery: local complications included hematoma, infection, or wound dehiscence, and systematic complications included pneumonia, cardiac problem, bedsore or sudden death. Survival time was defined as the overall survival time interval between the operation date and death/or last follow-up.

Identification of risk factors for affecting blood loss

Identification of risk factors for predicting blood loss were performed in the embolization group after analyze eleven preoperative characteristics, and these characteristics included age, gender (female vs. male), location of MESCC (thoracic spine vs. lumbar spine), ambulatory status (yes vs. no), SINS, tumor vascularity (mild vs. moderate vs. severe), preoperative hemoglobin (mmol/L), preoperative INR, preoperative thrombocytes ($\times 10^9$/L), extent of embolization (partial vs. subtotal vs. total), and time interval of embolization (0–24 h vs. 25–48 h). The extent of embolization was classified into three groups according to the technical success of embolization which was evaluated by visual estimation of tumor blush intensity reduction: partial (<70%), subtotal (70%–90%), and total (>90%) (28).

Statistical methods

Observational data are reported as mean ± standard deviation (SD). The *t* test, Wilcoxon rank test, and Chi-square test were performed to analyze and compared the patient's baseline characteristics between two groups. The *t* test, supplied with the Wilcoxon rank test, was used to compare operation time, blood loss, and the number of PRC transfusion. The Chi-square, adjusted continuous Chi-square, and fisher exact test were used to compare postoperative neurological status, complications, and decompressive methods. The log-rank test was used to compare the survival time and Kaplan-Meier method was used to generate the survival curve. Simple and multiple logistic regression models were used to analyze potential characteristics for blood loss. Discrimination of the significant features was evaluated by calculating the area under the receiver operating characteristic curve (AUROC). Calibration was assessed by using the Hosmer-Lemeshow goodness-of-fit test with a P-value of more than 0.05 indicating that there is no evidence of a lack of fit in the selected model. A P value of 0.05 or less was considered statistically significant. Statistical analysis was performed using SAS software (version 9.2), and data visualization was conducted using R programming software (version 4.0)

Results

Baseline clinical characteristics

The 138 MESCC patients had a median follow-up of 14.33 months (range: 3.2 to 25.31 months). The mean age at surgery was 58.00 ± 7.43 years in the embolization group and 59.95 ± 8.99 years in the control group (P=0.21). The most common location of MESCC was thoracic vertebra (28/46, 60.9%), followed by lumbar vertebra (18/46, 39.1%) in the embolization group. Similar trend was also observed in the control group for the most common location of MESCC. In the embolization group, 23.9% (11/46) of patients had mild hypervascularity, with 45.7% (21/46) being

moderate hypervascularity and 30.4% (14/46) being severe hypervascularity, based on the angiography. The corresponding proportions in the control group were 17.4% (16/92), 50.0% (46/92), and 32.6% (30/92), respectively, in terms of cancer histology. Table 1 shows more details on baseline clinical characteristics, and it demonstrated that there was no significant difference in the distribution of these clinical characteristics between the two groups.

Subgroup analysis of intra-operative characteristics among patients stratified by tumor vascularity

Subgroup analysis indicated that mean blood loss was greater in the control group (1852.93 ± 749.31 mL) than in the embolization group especially among patients with severe hypervascularity (1372.14 ± 469.49 mL, Figure 3A), and the difference was significant (P=0.02, Table 2). However, the blood loss was similar between two groups among patients with mild (P=0.75) and moderate (P=0.67) hypervascularity. In addition, patients with severe hypervascularity in the embolization group also had a significantly lower mean number of transfused PRC as compared with patients in the control group (6.14 ± 2.10 vs. 8.23 ± 2.63 units, P=0.01, Figure 3B). However, this trend was also not observed among patients in the mild (P=0.29) and moderate (P=0.96) hypervascularity. With regards to decompressive methods, the embolization group (64.29%, 9/14) had a higher rate of circumferential decompression in comparison to the control group (30.00%, 9/30) among patients with severe hypervascularity (P=0.03), but the rates were similar among patients with mild (P=0.45) and moderate (P=0.54) hypervascularity. Additionally, no subgroup analysis revealed a significant difference in operation time.

Subgroup analysis of postoperative characteristics among patients stratified by tumor vascularity

This study assessed postoperative ambulatory status, complications, and survival prognoses in relation to postoperative outcomes. Subgroup analysis demonstrated that the influence of preoperative embolization on postoperative ambulatory status was insignificant, although the embolization group had better

TABLE 1 Baseline clinical characteristics of the embolization and control groups.

Characteristics	Embolization group (n=46)	Control group (n=92)	P
Age (means ± SD, year)	58.00 ± 7.43	59.95 ± 8.99	0.21
Gender			
Male	21	49	0.40
Female	25	43	
Location of MESCC			
Thoracic spine	28	51	0.54
Lumbar spine	18	41	
Primary cancer types			
Lung cancer	10	20	0.92
Renal cancer	7	17	
Breast cancer	8	18	
Others	21	37	
Preoperative ambulatory status			
No	27	52	0.81
Yes	19	40	
SINS (means ± SD)	7.96 ± 1.86	8.52 ± 2.41	0.17
Tumor vascularity [a]			
Mild hypervascularity	11	16	0.66
Moderate hypervascularity	21	46	
Severe hypervascularity	14	30	
Preoperative hemoglobin (means ± SD, mmol/L)	7.80 ± 1.01	8.13 ± 1.27	0.12
Preoperative INR (means ± SD)	1.06 ± 0.11	1.04 ± 0.09	0.37
Preoperative thrombocytes (means ± SD, $\times 10^9$/L)	318.34 ± 72.02	338.27 ± 108.32	0.28

MESCC, metastatic epidural spinal cord compression; SINS, spinal instability neoplastic score; INR, international normalized ratio.
[a]indicates the tumor vascularity in the control group was evaluated using tumor histology.

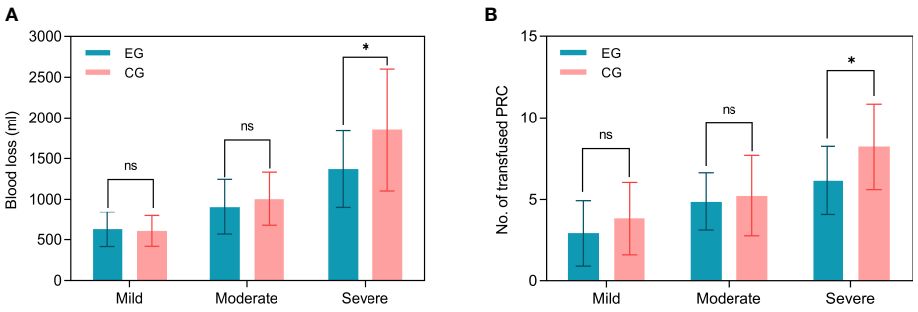

FIGURE 3
Subgroup analyses of blood loss and number of PRC transfusion among MESCC patients stratified by the degree of hypervascularity. **(A)** Intra-operative blood loss; **(B)** Number of PRC transfusion. EG indicates the embolization group; CG indicating the control group. "ns" indicates no significance, and "*" indicates P<0.05.

postoperative functional recovery in comparison to the control group (85.71% (12/14) vs. 63.33% (19/30), P=0.25), in particular among patients with severe hypervascularity (Table 2). Regardless of vascularity, the proportions of postoperative complication were similarly distributed between patients with and without preoperative complication (All P≧0.75). Survival outcome was compared between the embolization and control groups, and it showed no significance, with the median survival time of the embolization group being 9.77 (95% CI: 8.43-10.53) months and the control group being 8.50 (95% CI: 7.70-8.93) months (P=0.11, log-rank test, Figure 4A). In addition, subgroup analysis of survival outcome was performed in terms of mild (P=0.16, log-rank test, Figure 4B), moderate (P=0.40 log-rank test, Figure 4C), and severe (P=0.55 log-rank test, Figure 4D) hypervascularity, and no significant difference was obtained neither.

Risk analysis of preoperative clinical characteristics for predicting blood loss

In the univariate analysis of characteristics for blood loss among patients treated with preoperative embolization,

TABLE 2 Subgroup analysis of intra-operative and postoperative characteristics among patients stratified by tumor vascularity.

Characteristics	Mild hypervascularity			Moderate hypervascularity			Severe hypervascularity		
	Embolization group(N=11)	Control group (N=16)	P	Embolization group(N=21)	Control group (N=46)	P	Embolization group(N=14)	Control group (N=30)	P
Blood loss (means ± SD, ml)	628.55 ± 213.46	606.81 ± 188.39	0.75	907.00 ± 338.21	1004.63 ± 328.64	0.67	1372.14 ± 469.49	1852.93 ± 749.31	0.02
Number of transfused PRC (means ± SD, unit)	2.91 ± 2.02	3.81 ± 2.23	0.29	4.86 ± 1.77	5.22 ± 2.47	0.96	6.14 ± 2.10	8.23 ± 2.63	0.01
Decompressive methods									
Circumferential decompression	8	9	0.45	8	14	0.54	9	9	0.03
Simple posterior decompression	3	7		13	32		5	21	
Operation time (means ± SD, min)	215.18 ± 49.84	208.42 ± 55.10	0.75	218.24 ± 66.08	223.20 ± 73.15	0.79	229.79 ± 61.53	242.87 ± 72.63	0.71
Ambulatory status									
No	1	3	0.62	3	11	0.57	2	11	0.25
Yes	10	13		18	35		12	19	
Postoperative complication									
Yes	2	2	1.00	4	9	0.96	4	10	0.75
No	9	14		17	37		10	20	

PRC, packed red blood cells; SD, standard deviation.

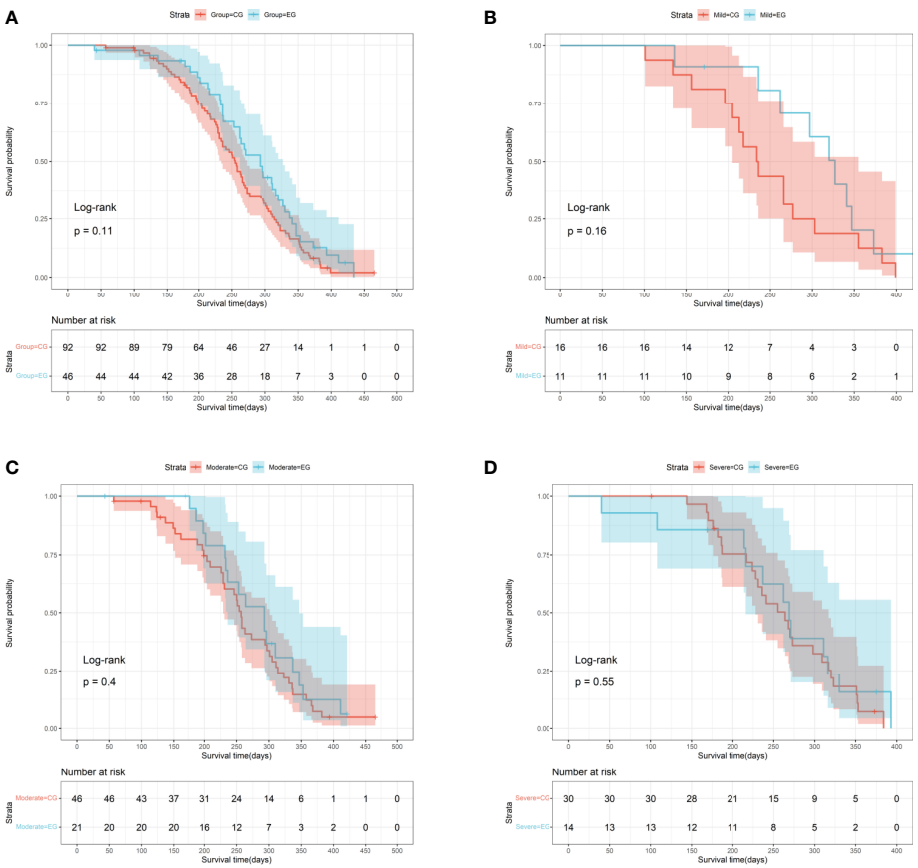

FIGURE 4
Survival curves for MESCC patients stratified by the presence of preoperative embolization. **(A)** The entire cohort (P=0.11, log-rank test); **(B)** Patients with mild hypervascularity (P=0.16, log-rank test); **(C)** Patients with moderate hypervascularity (P=0.40, log-rank test); **(D)** Patients with severe hypervascularity (P=0.55, log-rank test). EG indicates the embolization group; CG indicating the control group.

significance was found for tumor vascularity (OR=2.98, 95%CI: 1.17-7.57, P=0.02, Table 3) and extent of embolization (OR=2.83, 95%CI: 1.00-8.02, P=0.05), whereas no significance was observed for other characteristics (All P>0.05). In the multiply analysis of the risk factors, statistical significance was also observed for tumor vascularity (OR=3.69, 95%CI: 1.30-10.43, P=0.01) and extent of embolization (OR=4.16, 95%CI: 1.10-15.74, P=0.04).

Evaluation of the two significant factors was conducted using discrimination and calibration. AUROC of the tumor vascularity alone was 0.692 (95% CI: 0.552-0.833) (Figure 5A), AUROC of the extent of embolization alone was 0.668 (95% CI: 0.524-0.812) (Figure 5B), and AUROC of the tumor vascularity combined with the extent of embolization was 0.812 (95% CI: 0.668-0.957) (Figure 5C). In addition, calibration was assessed by using the Hosmer-Lemeshow goodness-of-fit test, and the P-value was 0.32 when the model included tumor vascularity alone, 0.48 when the model included the extent of embolization alone, and 0.06 when the model included the two features.

Additionally, no significant complication was noted in relation to the safety of preoperative embolization. Only four patients suffered from myalgia and one patient had fever because of preoperative embolization, and the symptoms subsided within three days.

Discussion

Patients with MESCC commonly had decompressive surgical surgery along with postoperative radiotherapy for rapid decompression and local tumor management (4). However, decompressive open surgery may cause significant perioperative blood loss and unfavorable postoperative consequences (5–7). Thus, preoperative embolization has been claimed to reduce intra-operative blood loss among spine metastases patients, particularly those with hypervascular tumors (17, 18), whereas some recent studies have suggested that the blood loss was not different when preoperative

TABLE 3 Univariate and multivariate analysis of characteristics for predicting blood loss among patients treated with preoperative embolization.

Characteristics	Patients (n=46)	Simple logistic regression		Multiple logistic regression	
		OR (95% CI)	P	OR (95% CI)	P
Age (year)	58.00 ± 7.43	1.08 (0.99-1.18)	0.07	Insignificance	
Gender					
Male	21	1.08 (0.33-3.56)	0.90	Insignificance	
Female	25				
Location of MESCC					
Thoracic spine	28	3.12 (0.91-10.79)	0.07	Insignificance	
Lumbar spine	18				
Preoperative ambulatory status					
No	27	1.18 (0.35-3. 94)	0.79	Insignificance	
Yes	19				
SINS	7.96 ± 1.86	1.17 (0.84-1.63)	0.35	Insignificance	
Tumor vascularity					
Mild hypervascularity	11				
Moderate hypervascularity	21	2.98 (1.17-7.57)	0.02	3.69 (1.30-10.43)	0.01
Severe hypervascularity	14				
Preoperative hemoglobin (means ± SD, mmol/L)	7.80 ± 1.01	0.66 (0.36-1.23)	0.19	Insignificance	
Preoperative INR (means ± SD)	1.06 ± 0.11	0.17 (0.10-39.01)	0.52	Insignificance	
Preoperative thrombocytes (means ± SD, 10^9/L)	318.34 ± 72.02	1.01 (0.99-1.01)	0.30	Insignificance	
Extent of embolization					
Partial	5				
Subtotal	17	2.83 (1.00-8.02)	0.05	4.16 (1.10-15.74)	0.04
Total	24				
Time interval of embolization					
0-24 h	41	7.71 (0.79-75.75)	0.08	Insignificance	
25-48 h	5				

MESCC, metastatic epidural spinal cord compression; SINS, spinal instability neoplastic score; SD, standard deviation; INR, international normalized ratio.

embolization was performed among those patients (19, 20). This study examined MESCC patients in great detail using vascularity-based stratification.

In the present study, it demonstrated that patients with severe hypervascular tumor had significant lower blood loss, less number of PRC transfusion, and a higher rate of circumferential decompression, but these effects were not observed among patients with moderate and mild vascular cancers, indicating that preoperative embolization might be an effective therapeutic strategy particularly for MESCC patients with severe hypervascularity. Similar findings were reported in a previous study conducted by Hong et al. (29) and it elucidated that intra-operative blood loss was greater in the non-embolization patients (1988 mL, n=34) than in the embolization patients (1095 ml, n=18) with hypervascular tumor. In a single-blind, randomized controlled clinical study, Clausen et al. (14) also showed that a small reduction of intra-operative blood loss was shown in hypervascular metastases. As for patients with non-hypervascular metastatic spinal tumors, Yoo et al. (16) found that there were no significant differences in intra-operative blood loss, perioperative blood loss, and total blood transfusion between the patients treated with and without preoperative embolization, and the result was consistent with our study.

Furthermore, our study newly proved that patients with severe hypervascular tumor had a significantly higher proportion of circumferential decompression. The reason might be because less intra-operative blood loss provided better surgical views for surgeons, which would definitely facilitate the removal of metastatic tumors. In addition, no significant differences were found in terms of operation time, postoperative ambulatory status, postoperative complication, and survival outcome. The complication rates between the embolization and control groups were similar, which was consistent with other studies (5, 30–32), and the incidence ranged from 15.0% to 35.5%. In a meta-analysis, Gao et al. (32) also found that preoperative embolization had no influence

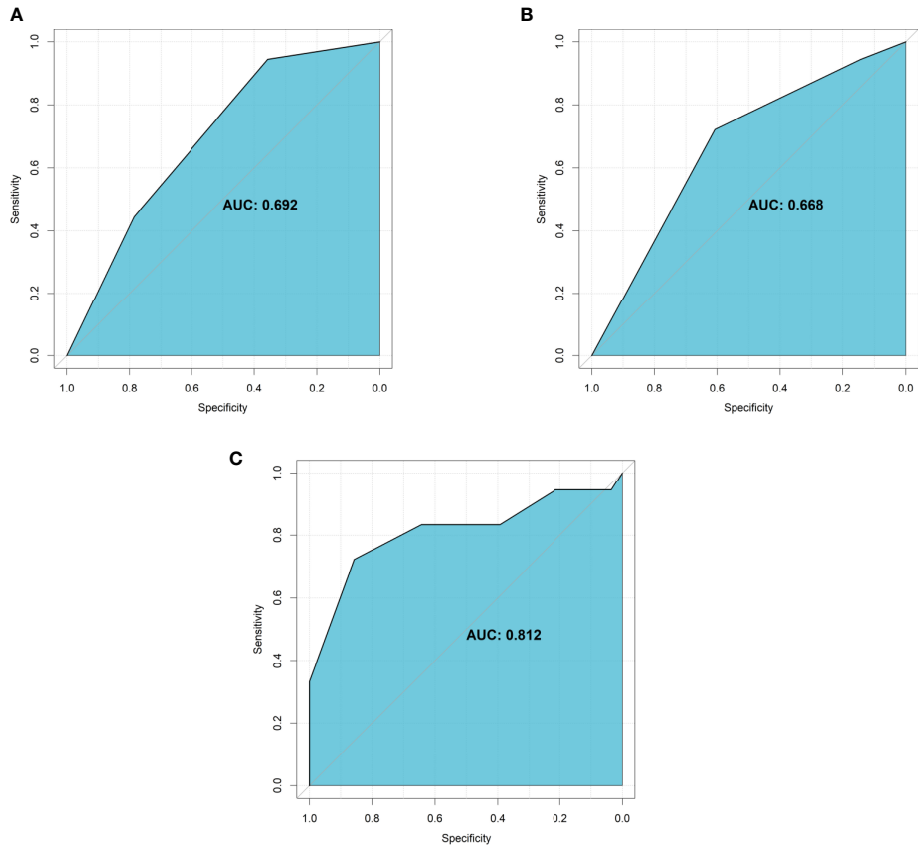

FIGURE 5
The AUROC of significant characteristics for predicting intra-operative blood loss. **(A)** Tumor vascularity alone; **(B)** Extent of embolization alone; **(C)** The combination of tumor vascularity and extent of embolization.

on survival prognosis among spine metastases patients. Regarding the safety of preoperative embolization, some studies has shown that it had the potential risk of hematoma or pseudoaneurysm at the puncture site, arteriovenous fistula, and post-embolization syndrome. The post-embolization syndrome was normally characterized by pain, fever, nausea, myalgia, and general weakness, all of which were possibly originated from tissue infarction due to release of inflammatory mediators and vasoactive substances (14). The symptoms were usually relieved within about 3 days. The frequency of these complications was relatively low, and the number was only 0% to 8.5% (14). In this study, four patients suffer from myalgia and one patient had fever because of preoperative embolization, and the symptoms subsided within 3 days, indicating that preoperative embolization was considered a relatively safe therapeutic approach to treat MESCC patients.

In addition, eleven risk factors were analyzed for intra-operative blood loss among MESCC patients treated with preoperative embolization. Significance was found for tumor vascularity and extent of embolization, while other features showed no significance as risk factors. It indicated the tumor vascularity and the extent of embolization were independent risk factors for predicting blood loss. Other studies showed that more blood loss was found in patients with incomplete embolization (17, 27) and hypervascularity tumor (29). Previous studies also indicated that the location of MESCC and the time interval of embolization both were correlated with intra-operative blood loss. In detail, a decrease in blood loss was related to lumbar localization and the short interval (19, 27). However, other authors found that there was no correlation between the time interval and intra-operative blood loss (33). Thus, this parameter needs further investigation. Evaluation of the two significant features was conducted with the help of discrimination and calibration. It indicated that the tumor vascularity and extent of embolization combined together or alone were useful features for evaluating intra-operative blood loss among MESCC patients.

Limitations

The study has some constraints. First, it was determined that the study's bias existed because it was a retrospective analysis

and not random. Additionally, some cancer kinds that were thought to have high hypervascularity, like neuroendocrine tumors and hemangiopericytoma instances, were uncommon at our institution. Additionally, several MESCC patients who were paralyzed while admitting the hospital were chosen for urgent surgery without embolization. Although there were some limitations, this study brought great supplements to current literature that preoperative embolization was able to reduce intra-operative blood loss and facilitate surgical removal of metastatic tumors among MESCC patients with severe hypervascularity. Nevertheless, a large prospective study is still warranted.

Conclusions

Preoperative embolization is an effective and safe method in treating MESCC patients with severe hypervascular tumors in terms of intra-operative blood loss and surgical removal of metastatic tumors. Preoperative tumor vascularity and extent of embolization are independent risk factors for blood loss during surgery. This study implies that MESCC patients with severe hypervascular tumors should be advised to undergo preoperative embolization.

Data availability statement

The original contributions presented in the study are included in the article/Supplementary material. Further inquiries can be directed to the corresponding authors.

Ethics statement

The studies involving human participants were reviewed and approved by The Ethics Committee Board of the Fourth Medical Center of PLA General Hospital and waived the informed consent from patients since all data were retrospective in nature, and the study was conducted to be in line with the Declaration of Helsinki. Written informed consent for participation was not required for this study in accordance with the national legislation and the institutional requirements.

Author contributions

BZ, HY, and XZ conceived and designed this study together. BZ, XC, YC, and XS undertook the data analysis, results interpretation and manuscript preparation. XS, ZW, and YL performed supervision. All authors contributed to the article and approved the submitted version.

Funding

The work was supported by Beijing Municipal Science and Technology Commission (grant number Z171100001017176).

Conflict of interest

The authors declare that the research was conducted in the absence of any commercial or financial relationships that could be construed as a potential conflict of interest.

Publisher's note

Supplementary material

The Supplementary Material for this article can be found online at: https://www.frontiersin.org/articles/10.3389/fonc.2022.1098182/full#supplementary-material

References

1. Cole JS, Patchell RA. Metastatic epidural spinal cord compression. *Lancet Neurol* (2008) 7:459–66. doi: 10.1016/S1474-4422(08)70089-9

2. Vellayappan BA, Kumar N, Chang EL, Sahgal A, Sloan AE, Lo SS. Novel multidisciplinary approaches in the management of metastatic epidural spinal cord compression. *Future Oncol* (2018) 14:1665–8. doi: 10.2217/fon-2018-0133

3. Van den Brande R, Cornips EM, Peeters M, Ost P, Billiet C, Van de Kelft E. Epidemiology of spinal metastases, metastatic epidural spinal cord compression and pathologic vertebral compression fractures in patients with solid tumors: A systematic review. *J Bone Oncol* (2022) 35:100446. doi: 10.1016/j.jbo.2022.100446

4. Lei M, Li J, Liu Y, Jiang W, Liu S, Zhou S. Who are the best candidates for decompressive surgery and spine stabilization in patients with metastatic spinal cord compression?: A new scoring system. *Spine (Phila Pa 1976)* (2016) 41:1469–76. doi: 10.1097/BRS.0000000000001538

5. Tateiwa D, Oshima K, Nakai T, Imura Y, Tanaka T, Outani H, et al. Clinical outcomes and significant factors in the survival rate after decompression surgery

for patients who were non-ambulatory due to spinal metastases. *J Orthop Sci* (2019) 24:347–52. doi: 10.1016/j.jos.2018.10.003

6. Westbroek EM, Pennington Z, Ahmed AK, Xia Y, Boone C, Gailloud P, et al. Comparison of complete and near-complete endovascular embolization of hypervascular spine tumors with partial embolization. *J Neurosurg Spine* (2020) 3:1–7. doi: 10.3171/2020.1.SPINE191337

7. Chen Y, Tai BC, Nayak D, Kumar N, Chua KH, Lim JW, et al. Blood loss in spinal tumour surgery and surgery for metastatic spinal disease: A meta-analysis. *Bone Joint J* (2013) 95-B:683–8. doi: 10.1302/0301-620X.95B5.31270

8. Aoude A, Aldebeyan S, Fortin M, Nooh A, Jarzem P, Ouellet JA, et al. Prevalence and complications of postoperative transfusion for cervical fusion procedures in spine surgery: An analysis of 11,588 patients from the American college of surgeons national surgical quality improvement program database. *Asian Spine J* (2017) 11:880–91. doi: 10.4184/asj.2017.11.6.880

9. Pennington Z, Ehresman J, Feghali J, Schilling A, Hersh A, Hung B, et al. A clinical calculator for predicting intraoperative blood loss and transfusion risk in spine tumor patients. *Spine J* (2021) 21:302–11. doi: 10.1016/j.spinee.2020.09.011

10. Stylianos P, Eyal I, Yair B, Amir H, Leon K, Moshe G, et al. Preoperative embolization of hypervascular spinal tumors: Current practice and center experience. *Neurol Res* (2014) 36:502–9. doi: 10.1179/1743132814Y.0000000361

11. Thiex R, Harris MB, Sides C, Bono CM, Frerichs KU. The role of preoperative transarterial embolization in spinal tumors. A large single-center experience. *Spine J* (2013) 13:141–9. doi: 10.1016/j.spinee.2012.10.031

12. Zaborovskii N, Ptashnikov D, Mikaylov D, Masevnin S, Smekalenkov O. Preoperative embolization and local hemostatic agents in palliative decompression surgery for spinal metastases of renal cell carcinoma. *Eur J Orthop Surg Traumatol* (2018) 28:1047–52. doi: 10.1007/s00590-018-2162-6

13. Benati A, Ore GD, Pian RD, Bricolo A, Perini S. Transfemoral selective embolisation in the treatment of some cranial and vertebro-spinal vascular malformations and tumours. preliminary results. *J Neurosurg Sci* (1974) 18:233–8.

14. Clausen C, Dahl B, Frevert SC, Hansen LV, Nielsen MB, Lönn L. Preoperative embolization in surgical treatment of spinal metastases: Single-blind, randomized controlled clinical trial of efficacy in decreasing intraoperative blood loss. *J Vasc Interv Radiol* (2015) 26:402–12.e1. doi: 10.1016/j.jvir.2014.11.014

15. Zhihong Q, Jia N, He Q. Does preoperative transarterial embolization decrease blood loss during spine tumor surgery? *Interv Neuroradiol* (2015) 21:129–35. doi: 10.15274/inr-2014-10091

16. Yoo SL, Kim YH, Park HY, Kim SI, Ha KY, Min HK, et al. Clinical significance of preoperative embolization for non-hypervascular metastatic spine tumors. *J Korean Neurosurg Soc* (2019) 62:106–13. doi: 10.3340/jkns.2018.0073

17. Wilson MA, Cooke DL, Ghodke B, Mirza SK. Retrospective analysis of preoperative embolization of spinal tumors. *AJNR Am J Neuroradiol* (2010) 31:656–60. doi: 10.3174/ajnr.A1899

18. Robial N, Charles YP, Bogorin I, Godet J, Beaujeux R, Boujan F, et al. Is preoperative embolization a prerequisite for spinal metastases surgical management? *Orthop Traumatol Surg Res* (2012) 98:536–42. doi: 10.1016/j.otsr.2012.03.008

19. Reitz M, Mende KC, Cramer C, Krätzig T, Nagy Z, Vettorazzi E, et al. Surgical treatment of spinal metastases from renal cell carcinoma–effects of preoperative embolization on intraoperative blood loss. *Neurosurg Rev* (2018) 41:861–7. doi: 10.1007/s10143-017-0935-8

20. Thirunavu VM, Roumeliotis A, Shlobin NA, Kandula V, Shah P, Larkin C, et al. The role of preoperative embolization in the treatment of spinal metastases from renal cell carcinoma. *Clin Neurol Neurosurg* (2022) 215:107181. doi: 10.1016/j.clineuro.2022.107181

21. Groot OQ, van Steijn NJ, Ogink PT, Pierik RJ, Bongers MER, Zijlstra H, et al. Preoperative embolization in surgical treatment of spinal metastases originating from non-hypervascular primary tumors: A propensity score matched study using 495 patients. *Spine J* (2022) 22:1334–44. doi: 10.1016/j.spinee.2022.03.001

22. Ozkan E, Gupta S. Embolization of spinal tumors: vascular anatomy, indications, and technique. *Tech Vasc Interv Radiol* (2011) 14:129–40. doi: 10.1053/j.tvir.2011.02.005

23. Ma J, Tullius T, Van Ha TG. Update on preoperative embolization of bone metastases. *Semin Intervent Radiol* (2019) 36:241–8. doi: 10.1055/s-0039-1693120

24. Berkefeld J, Scale D, Kirchner J, Heinrich T, Kollath J. Hypervascular spinal tumors: influence of the embolization technique on perioperative hemorrhage. *AJNR Am J Neuroradiol* (1999) 20:757–63. Available at: http://www.ajnr.org/content/20/5/757.long.

25. Patchell RA, Tibbs PA, Regine WF, Payne R, Saris S, Kryscio RJ, et al. Direct decompressive surgical resection in the treatment of spinal cord compression caused by metastatic cancer: A randomised trial. *Lancet* (2005) 366:643–8. doi: 10.1016/S0140-6736(05)66954-1

26. Fourney DR, Frangou EM, Ryken TC, Dipaola CP, Shaffrey CI, Berven SH, et al. Spinal instability neoplastic score: An analysis of reliability and validity from the spine oncology study group. *J Clin Oncol* (2011) 29:3072–7. doi: 10.1200/JCO.2010.34.3897

27. Kumar N, Tan B, Zaw AS, Khine HE, Maharajan K, Lau LL, et al. The role of preoperative vascular embolization in surgery for metastatic spinal tumours. *Eur Spine J* (2016) 25:3962–70. doi: 10.1007/s00586-016-4494-4

28. Shi HB, Suh DC, Lee HK, Lim SM, Kim DH, Choi CG, et al. Preoperative transarterial embolization of spinal tumor: embolization techniques and results. *AJNR Am J Neuroradiol* (1999) 20:2009–15. Available at: http://www.ajnr.org/content/20/10/2009.long.

29. Hong CG, Cho JH, Suh DC, Hwang CJ, Lee DH, Lee CS. Preoperative embolization in patients with metastatic spinal cord compression: mandatory or optional? *World J Surg Oncol* (2017) 15:45. doi: 10.1186/s12957-017-1118-3

30. Paulino Pereira NR, Ogink PT, Groot OQ, Ferrone ML, Hornicek FJ, van Dijk CN, et al. Complications and reoperations after surgery for 647 patients with spine metastatic disease. *Spine J* (2019) 19:144–56. doi: 10.1016/j.spinee.2018.05.037

31. Schuss P, Guresir A, Schneider M, Velten M, Vatter H, Guresir E. Factors influencing early postoperative complications following surgery for symptomatic spinal metastasis: A single-center series and multivariate analysis. *Neurosurg Rev* (2020) 43:211–6. doi: 10.1007/s10143-018-1032-3

32. Gao ZY, Zhang T, Zhang H, Pang CG, Xia Q. Effectiveness of preoperative embolization in patients with spinal metastases: A systematic review and meta-analysis. *World Neurosurg* (2021) 152:e745–57. doi: 10.1016/j.wneu.2021.06.062

33. Kato S, Murakami H, Minami T, Demura S, Yoshioka K, Matsui O, et al. Preoperative embolization significantly decreases intraoperative blood loss during palliative surgery for spinal metastasis. *Orthopedics* (2012) 35:e1389–95. doi: 10.3928/01477447-20120822-27

frontiers | Frontiers in Oncology

TYPE Review
PUBLISHED 25 January 2023
DOI 10.3389/fonc.2022.1105745

OPEN ACCESS

EDITED BY
Wenwen Zhang,
Nanjing Medical University, China

REVIEWED BY
Duoyi Zhao,
Fourth Affiliated Hospital of China Medical University, China
Zhi-Li Liu,
The First Affiliated Hospital of Nanchang University, China

*CORRESPONDENCE
Hongzhi Hu
13720105746@qq.com
Zengwu Shao
szwpro@163.com

†These authors have contributed equally to this work and share first authorship

SPECIALTY SECTION
This article was submitted to Surgical Oncology, a section of the journal Frontiers in Oncology

RECEIVED 23 November 2022
ACCEPTED 21 December 2022
PUBLISHED 25 January 2023

CITATION
Yang W, Pan Q, Huang F, Hu H and Shao Z (2023) Research progress of bone metastases: From disease recognition to clinical practice. *Front. Oncol.* 12:1105745. doi: 10.3389/fonc.2022.1105745

Research progress of bone metastases: From disease recognition to clinical practice

Wenbo Yang†, Qing Pan†, Fuhua Huang†, Hongzhi Hu* and Zengwu Shao*

Department of Orthopaedics, Union Hospital, Tongji Medical College, Huazhong University of Science and Technology, Wuhan, China

Bone metastases, as one of the common types of metastatic tumors, have a great impact on the survival period and quality of life of patients. Bone metastases are usually characterized by bone destruction. Skeletal related events caused by bone destruction often lead to pain, pathological fractures and even paralysis. In this review, we provide a detailed explanation of bone metastases from the epidemiology, clinical features, pathogenesis, and recently developed clinical treatment viewpoints. We concluded that the incidence of bone metastases is increasing gradually, with serious clinical symptoms, complex pathogenesis and diverse clinical treatment. Tumor cells, immune cells, osteoblasts/osteoclasts and other cells as well as cytokines and enzymes all play a key role in the pathogenesis of bone metastases. We believe that the future treatment of bone metastases will be diversified and comprehensive. Some advanced technologies, such as nanomedicine, could be used for treatment, but this depends on understanding how disease occurs. With the development of treatment, the survival time and quality of life of patients will be improved.

KEYWORDS

bone metastases, disease recognition, clinical practice, review, scope

1 Introduction

Bone metastases are malignant tumors that colonize bone through such as hematogenous metastases to form bone lesions (1). They are a common complication of many malignant tumors and may lead to poor prognosis (2). As a kind of disease, the epidemiological and pathological features of bone metastases are more complex than those of other malignant tumors. With the development of comprehensive tumor therapy, the survival time of tumor patients has been extended, and the occurrence probability of bone metastases has also shown an increasing trend (3). Once a patient is diagnosed with bone metastasis of malignant tumor, the prognosis will be significantly

worse and the quality of life will be significantly decreased. Related complications will significantly increase the financial burden of patients and families (4). Therefore, bone metastases of malignant tumors have gradually attracted extensive attention from clinicians and clinical researchers. With the development of relevant scientific experiments and clinical studies, clinicians' views on the treatment of bone metastases are constantly being updated, from the previous negative conservative treatment and analgesic treatment to the current personalized comprehensive treatment such as surgery, radiotherapy, chemotherapy and targeted therapy, which improves the quality and survival time of patients (5). Multidisciplinary cooperation has also helped improve the quality of life of patients with bone metastases. A variety of medical concomitant symptoms and drug side effects can be diagnosed and treated in time. In addition, based on the development of scientific research in related fields, some newer fields, such as the diagnosis and treatment of bone metastases with nanomaterials, are developing rapidly. In view of the important role of bone metastases in bone and soft tissue tumors, we reviewed the epidemiology, pathogenesis and clinical treatment of bone metastases in order to provide necessary guidance for the development of related disciplines.

2 Epidemiological, pathological and clinical features of bone metastases

According to the existing epidemiological data, bone metastases can appear in many types of malignant tumors, especially breast cancer, lung cancer, prostate cancer, kidney cancer and thyroid cancer (6). Bone metastases have been reported in 40% of non-small cell lung cancer (7). More than 70-85% of patients with advanced prostate cancer develop bone metastases (8). The incidence of bone metastases in differentiated thyroid carcinoma(DTC) ranges from 1% to 20%. About 44% of metastatic DTC patients have lesion that has spread to bone (9). About 75% of patients with advanced breast cancer develop bone metastases (10). Bone metastases have been reported in 30% of patients with renal cell carcinoma (RCC) (11). Some reports concluded that bone is the second most common site of RCC metastasis (12, 13). About 35-40% of patients with RCC metastases are bone related (12). In addition, cancers such as bronchial carcinoma often cause bone metastases (14). The incidence of bone metastases in gastrointestinal cancer is relatively low (14). According to current clinical observation, it is rare for gastrointestinal tumors to develop bone metastases without liver and lung metastases. The relevant data is described in Table 1. Clarifying the relevant epidemiological data of bone metastases has important clinical significance, which can help clinicians to make a comprehensive assessment of patients with related malignant tumors and develop appropriate follow-up protocols.

The pathological features of bone metastases are also varied. For common bone metastases, some bones show a higher incidence, such as the spine, pelvis, femur, humerus and so on (15). Studies have indicated that spinal metastases are common in patients with advanced malignancies, with a reported incidence of 30-50% (16, 17). The prevalence of spinal metastases in some malignancies may even be as high as 70%, with most metastases occurring in the thoracic spine (70%), followed by the lumbar spine (20%) and the cervical and sacral vertebrae (10%) (18, 19). Some long bones such as humerus and femur may also exhibit bone metastasis. Guzik noted in his study that about 10% of patients with primary malignant tumors develop proximal femur metastases (20). In metastatic tumors of the femur, 50% of the lesions occurred in the neck of the femur, 30% occurred in the subtrochanteric site, and 20% occurred in the intertrochanteric site, which may be related to the local developed blood supply (20). Wedin et al. mentioned in their study that the humerus is the second most common site of bone metastases in long bones (21). The common metastatic sites showed more cancellous bone and more abundant blood circulation. In addition, different bone metastases have different forms of bone damage. According to the changes of bone content in the lesion, bone metastases are mainly divided into osteoblastic lesions and osteolytic lesions (22). However, in some patients with bone metastases, both lesions may be present (23). Osteoblastic bone metastases are more common in prostate cancer (24, 25). On the contrary, most of the bone metastases of breast cancer, kidney cancer and other malignant tumors are

TABLE 1 A summary of the types of bone destruction, occurrence probability and common sites of bone metastasis.

Type of primary tumor	Main type of bone destruction	Proportion of metastasis	Common site of metastasis
Lung cancer	Osteolytic destruction	40%	Spinal metastases: ——thoracic vertebra (70%) ——lumbar vertebra (20%) ——Cervical and sacral vertebrae (10%) Pelvis; Femur: ——Neck of the femur (50%) ——Subtrochanteric site (30%) ——Intertrochanteric site (20%); Other parts of long bones.
Prostatic cancer	Osteogenic destruction	>70-85%	
Breast cancer	Osteolytic destruction	75%	
Thyroid cancer	Osteolytic destruction	1~ 20%	
Renal carcinoma	Osteolytic destruction	30%	

The concluded data presented in the table are reported in partial typical literature. Relevant references are reflected in the preceding paragraphs.

often presented as osteolytic lesions (26–29). Bone metastases of lung cancer and thyroid cancer are also often presented as osteolytic lesions (30, 31). It is important to identify the relevant pathological mechanism for subsequent treatment. The clinician can give appropriate clinical examination and symptomatic treatment according to the type and location of lesions that may occur. At the same time, the specific mechanism of the lesion is also the key basis for the design of the treatment of bone metastases.

Once bone metastases occur in malignant tumors, they often present complicated symptoms, and the prognosis of patients is often significantly worse. For example, bone metastasis is the main cause of death in prostate cancer patients, and there is no good treatment plan at present (32, 33). When bone metastases occur in patients with DTC, the survival rate may be reduced by more than 60% (34). Patients with bone metastases often experience pain, spinal cord compression, pathological fractures, and bone radiation; these symptoms are known as skeletal-related events (SREs) (35, 36). SREs occurs in a large number of patients with metastatic bone tumors, and brings great difficulties to the treatment. For example, it has been reported that 30-40% of patients with advanced lung cancer develop bone metastases that lead to SREs, which causing hypercalcemia, pathological fractures, spinal compression, and bone pain, leading to a poor prognosis (14, 37). SREs associated with bone metastases in prostate cancer have also been reported (38). Although bone metastases of prostate cancer are mainly osteoblasts, pathological fractures are still common (39). This may be due to the fact that the mechanical properties and structure of the diseased area are abnormal despite the "bone formation". Liu et al. mentioned in their study that more than 70-85% of patients with advanced prostate cancer develop bone metastases, which are characterized by severe pain and an increased possibility of fracture (8). Bone metastases with SREs have been reported to induce lower survival rates (40). After metastatic renal carcinoma metastases to the spine, pelvis and proximal femur, SREs such as pain, pathological fracture, hypercalcemia and spinal cord compression may occur, seriously affecting the quality and survival time of patients (12). Particularly severe SREs include pathological fractures, spinal cord compression and hypercalcemia requiring dialysis, which can incapacitate the patient in a relatively short period of time, and can quickly become life-threatening. In addition, due to the comprehensive impact of SREs on patients with bone metastases, the overall health of patients may deteriorate rapidly in a short time, making it difficult for them to withstand radiotherapy and chemotherapy with greater side effects. Therefore, clinicians should detect, diagnose and treat patients with bone metastases as early as possible, and take necessary preventive measures for possible serious complications. Laboratory and imaging tests such as X-ray, CT, MRI, bone scans, and tumor markers should be considered and used if necessary to achieve early and accurate diagnosis.

3 Advances in the pathogenesis of bone metastases

At present, studies on the pathogenesis of bone metastases are increasing, including the formation mechanism of bone metastases and the pathogenesis of local bone destruction. These scientific studies provide an important reference for clarifying the pathophysiology and clinical treatment of diseases. From the perspective of pathophysiology, bone metastases are a comprehensive disease. Tumor cells, osteoblasts/osteoclasts, immune cells and other components all play an important role in the pathogenic process. The relevant contents are shown in Figure 1. The pathogenesis and development of bone metastases will be discussed from the perspectives of tumor cells, osteoblasts/osteoclasts, immune cells, cytokines and other possible aspects.

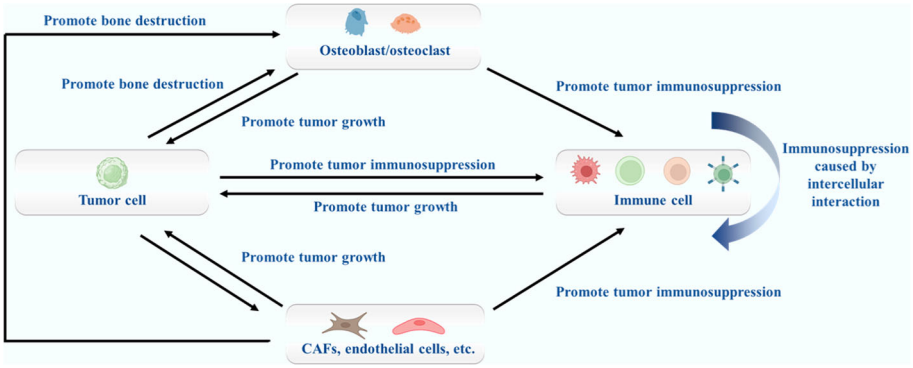

FIGURE 1
The role of different cell types in bone metastases.

3.1 The role of tumor cells in the pathogenesis of bone metastases

Metastatic tumor cells are one of the major players in bone metastases. In essence, the occurrence of bone metastases is a coordinated process in which malignant tumor cells leave the primary site to spread to bone and survive in the bone microenvironment (41). The metastases of malignant tumors generally include tumor cells leaving the primary site, entering the blood circulation and ectopic colonization. In particular, for bone metastases, circulating tumor cells reside and become dormant in the normal vascular of the bone marrow long before clinically detectable metastases develop. Over time they proliferate and regulate the function of bone resorption (osteoclasts) and bone formation (osteoblasts) cells, leading to the development of bone metastases (42). Tumor cells show a tendency to metastasize more easily under certain conditions. For example, the tumor has gene mutation, epithelial-mesenchymal transformation, and metabolic changes. The gene mutation of malignant tumor cells plays a key role in bone metastasis. In a study by Huang et al. on the mechanism of bone metastasis in lung cancer, 425 and 422 genomic alterations were detected in primary and metastatic lesions respectively (43). There were significant differences in tumor mutational burden between primary lung adenocarcinoma and matched bone metastases (43). This indicates that tumor mutational burden may play a role in bone metastasis of lung cancer. Arnold et al. mentioned in their study that the number of somatic mutations in the site of bone metastasis was statistically significantly higher than that in the site of primary or soft tissue metastasis (44). Bartels et al. concluded through their study that mutations in ESR1 are associated with estrogen receptor expression as well as high proliferative activity, and affect bone metastases in a part of estrogen receptor positive breast cancers (45). However, the current researches on the influence of gene mutation on the occurrence of bone metastases are mostly reflected in the research level of epidemiological data statistics, and there are few in-depth researches on the mechanism. In the future, related research needs to be further in-depth. In addition to some reported gene mutations, epithelial mesenchymal transformation (EMT) in tumor cells may also be an important factor promoting the occurrence of bone metastases. EMT refers to the differentiation and transformation process of epithelial cells into mesenchymal cells, which is believed to be related to tumor progression including tumor metastasis (46, 47). Several studies have been published on the pathogenesis of the relationship between epithelial mesenchymal transformation and bone metastases. Liu et al. pointed out in their study that Notch3 was associated with EMT and overexpressed in bone metastases of NSCLC, and inhibition of Notch3 expression could reduce the invasion ability of NSCLC cells *in vitro* (48). Epithelial mesenchymal transformation may also be associated with metastasis of malignant tumors such as breast cancer and prostate cancer. Horas et al. confirmed that the deficiency of vitamin D receptor (VDR) in human breast cancer cells can promote can promote EMT and the spread of cancer cells (49). In the study of the pathogenesis of bone metastases, EMT is often mentioned (50, 51). Therefore, EMT can be used as a key breakthrough in future research on the treatment of bone metastases. In addition, metabolic changes of tumor cells are also considered to be a key factor in the development of tumor metastasis (52). Studies have shown that different tumor stem cells adapt to unique metabolic characteristics for organ metastasis (53). Thysell et al. analyzed the metabolism of bone metastasis in prostate cancer and identified metabolites such as cholesterol that might be associated with prostate cancer metastasis (54). In addition to the mechanisms mentioned above, cancer stem cells (CSCs), a new concept proposed in recent years, are also believed to be closely related to bone metastasis of tumors (55). Based on existing studies, we believe that in bone metastases of malignant tumors, the tumor cells should usually be changed compared to the primary site. Such changes may be at the genetic level, at the metabolic level, or at the cellular phenotype level. However, the specific changes of bone metastases in different malignancies may be different, so specific studies are needed. At present, there is still a relative lack of research on mutant genes or altered metabolic functions. After the relevant epidemiological data are revealed, more mechanism studies should be conducted to identify the target of bone metastasis and design corresponding interventions.

3.2 The role of osteoblasts/osteoclasts in the pathogenesis of bone metastases

The role of osteoblasts/osteoclasts in bone metastases has been studied for a long time, and many drugs are gradually being completed in clinical trials. During the occurrence and development of bone metastases, many pathological changes are related to abnormal regulation of osteoblasts and osteoclasts. Inhibition of osteoblasts and abnormal activation of osteoclasts are often the key mechanisms of osteolytic metastases. Osteoblasts and osteoclasts are the direct “executors” of bone destruction in bone metastases, and their regulation may be related to a variety of cells and factors, such as tumor cells, immune cells and inflammatory factors (56–58). For osteoblasts and osteoclasts themselves, Wnt/β-catenin pathway, RANK-RANKL pathway and other pathways closely related to osteogenesis/osteoclast process are the focus of research (59, 60). Wnt signaling pathway may play an important role in bone metastasis of malignant tumors (61). The Wnt pathway and the role of osteoblasts have attracted much attention since bone metastases of prostate cancer are often manifested as osteoblastic

lesions. Dai et al. showed in their study that prostate cancer can promote osteoblast differentiation through classical and non-classical Wnt signaling pathways and stimulate BMP-dependent and BMP-independent osteoblast differentiation (62). However, there are some different studies. Aufderklamm et al. have shown that DKK-1, an inhibitor of the Wnt pathway, mediated osteoblast inhibition contributes to prostate cancer progression (63). The RANK/RANKL signaling pathway has also received attention in bone metastases. This pathway mainly affects the function of osteoclasts in the local microenvironment of bone metastases. It has been suggested that the RANK/RANKL signaling pathway is involved in the castration-insensitive prostate cancer (64). SREs can be prevented with the RANKL inhibitor Denosumab (65). Interestingly, RANKL connects bone to the immune system, while RANK-RANKL is a regulator of osteoclast development, lymph node development, bone metabolism, and T cell/dendritic cell communication (66). This suggests that the regulation of the RANK/RANKL signaling pathway does not only affect osteoclasts. Not only the above common pathways, but also the effects of other factors on osteoblasts/osteoclasts have been extensively studied. For example, osteoblasts may be negatively regulated by cancer cells and appear apoptosis (67). The main mechanisms of interaction and regulation of osteoblasts/osteoclasts with tumor cells in osteolytic bone metastases are summarized in Figure 2. In the future, some more detailed cell interactions on osteoblasts/osteoclasts in bone metastases should be further investigated, for example, the regulation of osteoblasts/osteoclasts by exosomes produced by bone metastatic tumor cells. RANK/RANKL and Wnt/β-catenin pathways are both downstream signaling pathways. In bone metastatic cancer, which signaling pathway changes may trigger the changes of the above downstream pathways is a more valuable research direction.

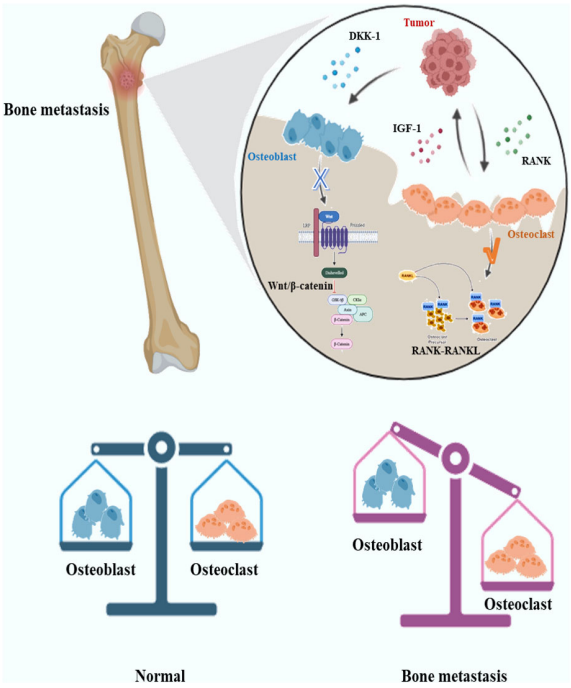

FIGURE 2
Schematic diagram of the interaction between tumor cells and osteoblasts/osteoclasts in osteolytic bone metastases. In osteolytic lesions, tumor cells may secrete molecules such as DKK-1 to inhibit osteoblast Wnt signaling pathway and promote osteoclast function through RANK-RANKL signaling pathway. Osteoclasts may secrete IGF-1 and other molecules to promote tumor growth.DKK-1, Dickkopf-1; IFG-1, Insulin-like growth factor 1; RANK, Receptor Activator of NF-κB.

3.3 The regulatory role of cytokines other key proteins (enzymes)

Different from cells, cytokines are a class of small molecules that regulate cell function with a wide range of effects. Common cytokines include interleukin(IL), tumor necrosis factor(TNF), and so on (68). In the past few decades, cytokines and cytokine receptors have been extensively studied as targets for cancer treatment (69). In the pathogenesis of metastatic tumor, cytokines may be secreted by tumor cells and immune cells, and the target may include tumor cells, immune cells, osteoblasts/osteoclasts, etc. There are many types of interleukin, which is closely related to inflammation and tumor growth, etc. At present, certain studies have been conducted in bone metastases. Claudia et al. reported in their review that IL-1B is important in the inflammatory process, and influences the growth of bone metastases in breast cancer, including angiogenesis, etc. (10). IL-6 overexpression is also associated with bone metastases (70). Interleukin is also produced by osteoclasts to regulate tumor cells. The study of He et al. showed that lung cancer cells induced osteoclasts to secrete IL-19 to act on IL20RB on the surface of lung cancer cells, thus promoting the proliferation and bone metastasis of lung cancer cells (71). Tumor necrosis factor also plays an important role in the development of bone metastases. Hamaguchi et al. found that inhibition of TNF-α has a novel role in reducing or preventing bone metastasis in breast cancer models (72). Interferon has been less studied in bone metastases. Chemokines are a class of cytokines secreted by cells, which can induce the directed migration of nearby cells (73). Chemokines play an important role in metastatic tumors because they have an important effect on cell migration, colonization and other processes. Chemokine/chemokine receptor CXCL12/CXCR4 pathway and CCR3/CCL7 pathway can be used as mediators in the process of bone metastasis and may affect the colonization of tumor cells in bone (74, 75). According to current studies, the interleukin family and chemokine family related pathways may be relatively important in the influence of bone metastases. The design of

relevant targeted drugs for these two pathways may be an important idea to delay the progression of bone metastases or prevent the appearance of bone metastases.

In addition to common cytokines some enzymes can also promote the disease progression of bone metastases by influencing immunity and bone formation. Matrix metalloproteinases (MMPs) is a type of enzyme containing zinc, which can decompose extracellular matrix (76). Since MMPs is closely related to the synthesis of bone matrix and the regulation of osteoblasts/osteoclasts, it is believed that MMPs may promote the onset of bone metastases. Pego et al. mentioned in their review that MMPs, especially MMP-9, played an important role in bone metastasis of prostate cancer (77). MMP-9 is also significant in the occurrence and development of other bone metastases, such as breast cancer bone metastases, and may be a therapeutic target for bone metastases (78). In addition, MMPs such as MMP-13 also play a role in promoting bone metastasis of malignant tumors (79). In addition to MMPs, the role of Cyclooxygenase-2 (COX-2) in bone metastases is also attracting increasing attention. COX-2 is a key rate-limiting enzyme in the synthesis of prostaglandin E2 (PGE2), which is closely related to inflammation, tumor growth, angiogenesis and other aspects (80). Studies have shown that COX-2 can increase the proportion of osteoclast and is one of the key genes in breast cancer bone metastasis (81). Karavitis et al. mentioned that COX-2 and PGE2 can regulate bone metastasis by influencing immunity (82). In addition, enzymes such as Indoleamine 2, 3-dioxygenase 1 (IDO1) have also been found to be associated with bone metastases (83). In the future, more enzymes with the potential function of promoting tumor bone metastasis can be identified through RNA sequencing and proteomics. As a special catalyst, enzymes often correspond to certain characteristics of substrates and products, as well as related chemical reactions, which may provide conditions for targeted therapy of bone metastases.

3.4 The role of immune cells in the pathogenesis of bone metastases

The immune cells in the body include specific immune cells and non-specific immune cells. The specific immune cells include T cells, B cells and so on, and their mechanism of action is often highly specific. Non-specific immune cells include monocytes/macrophages, dendritic cells, etc., which usually exhibit low specificity and are responsible for assisting specific immune cells in some cases. In cancer patients, it is generally believed that local immunity plays a potential role in promoting the occurrence, development and metastasis of tumors. The relevant immune cells may “migrate” to the tumor tissue and “protect” it instead. Interestingly, bone is actually an important immune organ in the body, because bone marrow is an important site of white blood cell production (84). So there has to be a special environment for immune activation to be suppressed. The relationship between bone marrow and metastatic tumors began to be studied earlier, and many cells were found to be related to immunosuppression, such as myeloid-derived suppressor cells (MDSCs) and Mesenchymal stem cells (MSCs) (85, 86). However, the mechanisms related to immune microenvironment are. For example, regarding the Irf7 pathway, existing studies have shown that its role in bone metastasis of breast cancer and prostate cancer seems to be suppressive (87, 88). The immunosuppressive mechanism of bone metastases with different primary lesions should be studied independently. Regulatory T cells (Tregs) play an important role in specific immunity (89). CD4+CD25+ Tregs are an important group of T cells in bone marrow and may be highly related to immunosuppression (90). The study of Tan et al. indicated that the RANKL-RANK pathway may affect the content of Tregs, thus affecting local immunity (91). Tregs can secrete anti-inflammatory cytokines such as IL-10, TGF-β and IL-35, and act on such as CD8+T cells to achieve immune suppression (92, 93). These related cytokines may play a key role in circulating tumor cell dormancy in bone metastases or in tumor cell proliferation in metastatic sites. CD8+T cells are also regulated by immature myeloid cells and osteoblasts (94). In non-specific immunity, macrophages, especially tumor-associated macrophages(TAMs), have a great influence on the pathogenesis of metastatic tumors (95). The role of macrophages is diverse, and under different circumstances they will polarize into different subtypes, mainly including M1 type and M2 type (96). Their main effects on tumor cells are almost opposite, with M1-type macrophages often showing killing effect on tumor, while M2-type macrophages often showing promoting effect on tumor (97). TAMs in malignant tumor usually exhibit an M2-like appearance (98). Macrophages are often regulated by cytokines and other factors, which may promote the occurrence of bone metastases (99). According to the results of current studies, the representative role of different types of immune cells in bone metastases is shown in Figure 3. In future studies, we believe that in terms of the immune regulation of bone metastases, how to correctly find the immune cells that promote tumor bone metastases and make them defunction, apoptosis or transform into normal immune cells is the key to the research.

3.5 Other mechanisms related to the pathogenesis of bone metastases

It can be seen from the above description that the pathogenesis of bone metastases is very complex. As the main function of bone metastases, different types of cells are widely affected by immune, metabolic and tumor microenvironments. In recent years, the role of some connective tissue cells in bone metastases, such as fibroblasts and endothelial cells, in bone

metastases has received increasing attention. Similar to macrophages, fibroblasts in malignant tumor tissues are known as cancer-associated fibroblasts (CAFs) and they often show potential tumor-promoting effects (100). CAFs may promote tumor metastasis (101). Li et al. mentioned in their study that CAFs played a key role in bone metastasis of breast cancer cells by influencing tumor microenvironment and other aspects (102). Mukaida et al. fully described the possible effects of CAFs on tumor bone metastasis, including the function of tumor cells and immune cells through the secretion of cytokines by CAFs (103). The relevant content is illustrated in Figure 4. In addition to CAFs, the role of endothelial cells in metastases has also been emphasized. Zhang et al. indicated that bone-derived endothelial cells (BDECs) may be involved in pathologic bone lysis in the pathogenesis of bone metastases (104). Wang et al. proposed that tumor cell-vertebral bone marrow endothelial cell interactions promote spinal metastasis in NSCLC (105). In fact, whether in the primary lesion of malignant tumor or the metastasis of bone metastases, tumor cells are only part of the tumor, and the influence of non-tumor cells on the occurrence and development of bone metastases should be paid more attention. Regulation of these cells may have a positive significance in reducing the incidence of bone metastases, delaying the occurrence time of bone metastases, and alleviating the symptoms of bone metastases.

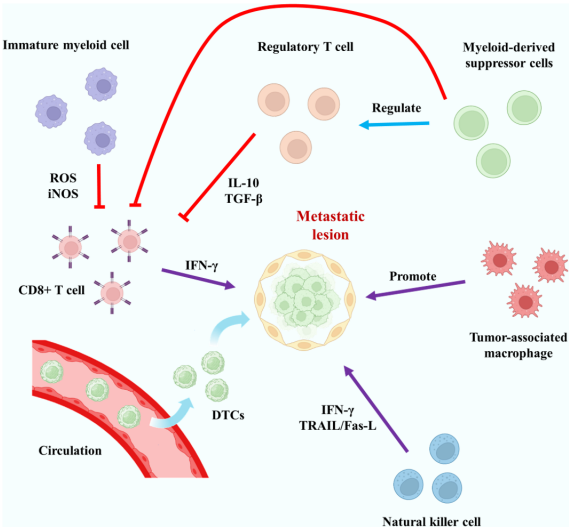

FIGURE 3
Typical mechanisms of action of key specific and non-specific immune cells in bone metastases. The red lines represent inhibitory effects.

4 Clinical treatment prospects of bone metastases

With the deepening of the research on the pathogenesis of bone metastases, clinicians' understanding of bone metastases is also constantly innovating. In the past, the general consensus reached in clinical practice was that the occurrence of bone metastases in malignant tumors meant that the survival time of patients was shorter, and the treatment should be mainly palliative therapy such as analgesia rather than surgery. However, with the development of scientific progress and clinical research, clinicians gradually found the positive significance of various surgical procedures, especially when there was only a single bone metastasis. With the further study of pathogenesis, some therapies targeting specific cell types are being developed, including advanced nanotechnology therapy. Based on the above scientific research basis, we introduce a series of cutting-edge clinical treatment viewpoints of bone metastases and emerging treatment methods under development.

4.1 Progress and prospect of surgical treatment and chemotherapy

The surgical treatment of bone metastases has been paid more attention due to the progress of epidemiological research. In recent years, more emphasis has been placed on the surgical treatment of bone metastases. Surgical treatment of bone metastases often includes pain relief, quality of life improvement and SREs treatment, and may also be used as a means to create conditions for radiotherapy. Because of the complex local pathology, excision may have some positive significance. However, it is important to note that not all patients are candidates for surgery. Whether or not a patient should be treated surgically depends on a number of factors, including systemic conditions, primary tumor status, number and location of metastases, expected survival time, and financial status of the patient. Prior to surgical treatment of bone metastases, it is important to conduct examinations. Some patient-specific scores are important in assessing whether a patient with bone metastases is ready for surgery. For example, for patients with spinal metastases, the Tokuhashi score is a commonly used method to determine whether a patient should be operated on (106). At the same time, the New England Spinal Metastasis Score (NESMS) score had relatively good clinical accuracy in predicting complications after spinal metastasis surgery (107). For patients with limb metastases, Katagiri score might be important references (108, 109). With the development of treatment methods, the surgical methods of spinal metastasis and limb metastasis are gradually diversified. Both open surgery and minimally invasive surgery are used in bone metastases (Table 2), and their adaptations have been recognized based on

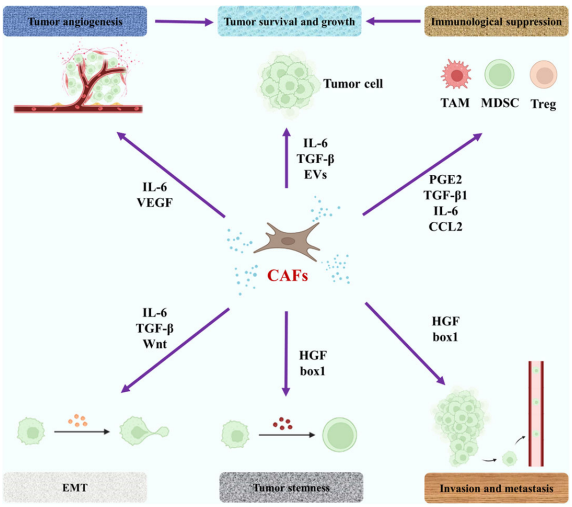

FIGURE 4
The role of CAFs in the pathogenesis of bone metastases. The purple arrow represents an influence. EMT, epithelial-mesenchymal transition; PGE2, prostaglandin E2; EVs, extracellular vesicles; HGF, hepatocyte growth factor; VEGF, vascular endothelial growth factor.

epidemiological studies (115). In particular, the development of new techniques has led to advances in bone metastases surgery. For example, the application of 3D printing technology in joint prostheses enables patients to achieve better motor function and improve the quality of life of patients (116). However, it should be noted that there are potential complications, including intraoperative and postoperative complications, such as spinal cord and vascular injury, failure of internal fixation, local tumor recurrence and so on, no matter what kind of surgery. Bone metastatic tumor surgery has been used as an important treatment method for many patients, but it is different from general orthopaedic trauma surgery, orthopaedic joint surgery and other conventional operations, it is often difficult to operate, high risk, and so far there is a lack of appropriate procedure standards. Therefore, surgery for bone metastases needs to be conducted by an experienced orthopaedic surgeon who carefully evaluates each patient and follows the principle of "personalization." More epidemiological studies should be carried out.

The deepening of scientific research also has a certain impact on the concept of chemotherapy for bone metastases. Surgical treatment of bone metastases usually has limited effects. As mentioned earlier, circulating tumor cells may metastasize before they are detected. Subsequently, these circulating tumor cells may form micrometastases, which are the main cause of tumor recurrence and a major factor affecting survival. Therefore, it is necessary to supplement the corresponding medical treatment. The specific chemotherapy regimen for different bone metastases is different, which is related to the pathological type of the primary lesion.

4.2 Targeted therapy—more advanced and promising systemic therapy for bone metastases

With the progress of research on the pathogenesis of bone metastases and primary bone tumors, the concept of "precision therapy" has been gradually formed. Some malignancies may be hormone-related, so some hormone-targeted therapies have been developed, such as Tamoxifen (estrogen inhibitor), Darolutamide (androgen receptor inhibitor), etc. (117, 118) A more widely known type of targeted therapy is targeting specific proteins or signaling pathways, such as Bevacizumab (VEGF inhibitor) (119), Trastuzumab (HER2 inhibitor) (120), Imatinib (tyrosine kinase inhibitor) (121), Olaparib (PARP inhibitor) (122), etc. Other organ-specific drugs such as I^{131} also act as targeted therapies (123). The basic principle of tumor targeted therapy is to design drugs or antibodies for molecules that may be abnormally expressed or have abnormal functions in certain malignant tumors according to epidemiological and pathogenesis studies, so as to interfere with tumor growth and promote tumor killing. Targeted therapy drugs usually cause less damage to normal human tissue than conventional chemotherapy drugs. The combination of targeted therapy with conventional chemotherapy often produces better effects (124). Now, targeted therapy is starting to be used in bone metastases. Tokito et al. showed that bevacizumab may enhance the antitumor activity of chemotherapy against bone metastases and reduce the incidence of SREs (125). A HER2-overexpressed Salivary carcinoma reported by Bergamini et al. developed bone

TABLE 2 Comparison of characteristics of minimally invasive surgery and traditional open surgery.

	Minimally invasive surgery	Traditional open surgery
Type	PVP/PKP (110, 111), RFA (112)	Total vertebrae excision, separation surgery (113, 114)
Complication	Relatively rare	More common, such as wound infection
Blood loss and transfusion rate	The blood loss is small and the transfusion rate is low	Often associated with greater blood loss and higher transfusion rate
Hospital stays	Short	Long

metastases and the treatment plan included trastuzumab (126). It is worth noting that bone-targeting drugs are more widely used in bone metastases. In patients with bone metastases, targeted drugs targeting the primary tumor are often used as a means of comprehensive therapy. In addition to targeting the primary tumor, the more commonly used targeted therapy for bone metastases is "bone-modulatory drugs" for bone lesions, which can be regarded as a type of bone targeting. As mentioned in the previous part, osteoclasts and osteoblasts play an important role in the occurrence of bone metastases. Although the therapeutic effect on tumor is limited, bone targeting drugs can regulate osteoblasts/osteoclasts to inhibit bone destruction and delay the occurrence of SREs, which will greatly improve the quality of life of patients. Some commonly used bone-targeting drugs such as bisphosphonates (BPs) can promote osteoclast apoptosis (127). Denosumab inhibits osteoclast differentiation and activity as a RANK/RANKL inhibitor to delay bone metastasis (128). Some common bone-regulating drugs that inhibit bone destruction in bone metastases are shown in Table 3. The positive effect of bone-targeting drugs in bone metastases confirms the necessary for their use in patients.

However, in practice, targeted drugs are not targeted to tumor cells, which may limit the efficiency of their application to some extent. In recent years, combined with published pathogenesis and clinical studies, more targeted therapies are being developed. Among them, nanotechnology as an emerging means of targeted therapy has attracted wide attention. Nanomaterials can be targeted by a variety of relevant chemical modifications, and properly designed nanomaterials often show high safety and degradability (139). It is a common idea to combine nanotechnology with traditional bone targeting drugs to prepare nanoparticles for the treatment of bone metastases. For example, He et al. have designed a nanoparticle DSP-Zn@PEG-ALN targeted to focal bone *via* the alendronate molecule, which has great potential for improving the efficacy of chemotherapy for bone metastatic breast cancer (140). Qiao et al. highlighted the importance of therapeutic nanomedicine and osteocyte-targeted therapy in the treatment of early bone metastases (141). More representative studies related to nanomaterials with bone targeting drugs for the treatment of bone metastases are presented in Table 4. Also, Tamura et al. mentioned in their review that extracellular vesicles may play an important role in tumor bone metastasis, especially in influencing the local tumor microenvironment (148). Ge et al. designed a multifunctional scaffold called CePO4/CS/GO scaffold that promotes bone formation while killing tumors for the treatment of breast cancer with bone metastases (149). These studies are closely related to the pathogenesis of bone metastases. The relevant signaling pathways here have been mentioned in related pathogenesis studies. In future studies, targeting immune cells, osteoblasts or other stromal cells may be an important direction for the innovation of targeted therapy for bone metastases. Until now, the main methods to target nanomaterials to cells have been through specific ligands on the cell surface, through essential substances for cell metabolism, or through the preparation of

TABLE 3 Common types of bone regulatory drugs, representative drugs, related mechanisms and typical applications.

Drug class	Representative drug	Mechanism of action	Partial relevant BM treatment	Typical relevant reference
BP	Alendronate, Zoledronate, Risedronate	Inhibits osteoclast activity and promotes osteoclast apoptosis	Pain control/delayed occurrence of SREs in cancer patients with bone metastasis	(129–131)
RANK-L mAb	Denosumab	Inhibits osteoclast differentiation and activity by inhibiting the RANK-RANKL pathway	To reduce the skeletal complications of cancer	(132, 133)
mTOR inhibitor	Everolimus	Inhibition of osteoclast differentiation and activation; Promotion of osteoclast apoptosis	Everolimus plays a bone-protective role in bone metastasis of breast cancer	(134)
Proteasome inhibitor	Bortezomib, Carfilzomib	Inhibits osteoclast formation and promotes osteoblast differentiation	Improves bone destruction in breast cancer	(135)
CYP17 inhibitor	Abiraterone	Inhibits the generation and activity of osteoclasts and promotes the differentiation of osteoblasts	Combined with other BRIs for the treatment of bone metastases from prostate cancer	(136)
Tyrosine kinase inhibitor	Cabozantinib	TKI; Inhibition of VEGF/VEGFR pathway; Regulation of osteoblast activity	Bone metastasis of advanced renal cell carcinoma	(137)
ET-1 antagonist	Bosentan	Regulation of angiogenesis, etc.	–	(138)
DKK-1 inhibitor	–	Promote Wnt pathway and osteoblast differentiation	–	–

TABLE 4 Representative studies related to nanomaterials with bone targeting drugs for the treatment of bone metastases.

Components of bone targeting	The main components of nanomaterials	Loaded components with therapeutic effects	Related disease/ models	Reference
Alendronate	PLGA	Curcumin and bortezomib	Breast cancer bone metastasis	(142)
Alendronate	Liposome	Doxorubicin	Breast cancer bone metastasis	(143)
Zoledronic acid	Au@mesoporous silica nanoparticles	Gold nanorods and zoledronic acid	Breast cancer bone metastasis	(144)
cRGD	Complex	Bortezomib	Bone metastasis	(145)
RNA aptamer targeting PSMA	Atelocollagen	miR-15a and miR-16-1	Prostate cancer bone metastasis	(146)
Alendronate and hyaluronic acid	Complex	Doxorubicin	Breast cancer bone metastasis	(147)

biomimetic nanoparticles (nanoparticles coated with natural cell membranes, etc.). These methods can be used as reference for the design of nanomaterials for the treatment of bone metastases. The development of new targeted therapies must be strictly dependent on the pathogenesis of bone metastases. Therefore, the development of clinical diagnosis and treatment and the study of pathogenesis are complementary.

5 Summary and scope

In summary, we summarized the development status of bone metastases from the aspects of epidemiology, clinical features, pathogenesis and clinical practice. So far, compared with kinds of primary tumors, there are still relatively few researches on bone metastases either in pathogenesis or clinical trials. As the most common malignant tumor of bone, bone metastases should receive more attention in the future. In the future, research on the pathogenesis of bone metastases should focus on the cellular level interaction mechanism. The establishment of animal models of bone metastases is also a very important direction, because successful animal model preparation is the basis of *in vivo* experiments. There should be more studies and reviews on the establishment of *in vivo* models of bone metastases, such as Peng et al. 's review of *in vivo* experimental design for intervertebral disc disease (150). Clinical research requires researchers to develop a wide range of new drugs. Nanomaterials are an emerging approach to targeted therapy because they can be multi-functional through modified design. However, its development must rely on the study of pathogenesis, including the discovery of new and effective local targets, how to kill tumors while promoting osteogenesis and tissue recovery, etc. In the future, the comprehensive treatments of bone metastases need to be further improved. The clinician should ensure that the patient has the best quality of life while fully considering the patient's survival, disease status, and financial status.

Author contributions

ZS and HH designed the review topic and revised the manuscript. WY and QP conducted data collation and manuscript writing. WY and FH collected data and drew figures. All authors contributed to the article and approved the submitted version.

Acknowledgments

Thanks to all authors for their contributions to this study.

Conflict of interest

The authors declare that the research was conducted in the absence of any commercial or financial relationships that could be construed as a potential conflict of interest.

Publisher's note

References

1. Coleman RE, Croucher PI, Padhani AR, Clézardin P, Chow E, Fallon M, et al. Bone metastases. *Nat Rev Dis primers* (2020) 6(1):83. doi: 10.1016/B978-0-323-47674-4.00056-6

2. Ban J, Fock V, Aryee DNT, Kovar H. Mechanisms, diagnosis and treatment of bone metastases. *Cells* (2021) 10(11):2944. doi: 10.3390/cells10112944

3. Migliorini F, Maffulli N, Trivellas A, Eschweiler J, Tingart M, Driessen A. Bone metastases: a comprehensive review of the literature. *Mol Biol Rep* (2020) 47 (8):6337–45. doi: 10.1007/s11033-020-05684-0

4. Cadieux B, Coleman R, Jafarinasabian P, Lipton A, Orlowski RZ, Saad F, et al. Experience with denosumab (XGEVA®) for prevention of skeletal-related events in the 10 years after approval. *J Bone Oncol* (2022) 33:100416. doi: 10.1016/j.jbo.2022.100416

5. Isogai N, Yagi M, Nishimura S, Nishida M, Mima Y, Hosogane N, et al. Risk predictors of perioperative complications for the palliative surgical treatment of spinal metastasis. *J orthopaedic Sci Off J Japanese Orthopaedic Assoc* (2021) 26 (6):1107–12. doi: 10.1016/j.jos.2020.09.005

6. Li C, Wu Q, Chang D, Liang H, Ding X, Lao C, et al. State-of-the-art of minimally invasive treatments of bone metastases. *J Bone Oncol* (2022) 34:100425. doi: 10.1016/j.jbo.2022.100425

7. Yang XY, Liao JJ, Xue WR. FMNL1 down-regulation suppresses bone metastasis through reducing TGF-β1 expression in non-small cell lung cancer (NSCLC). *Biomedicine pharmacotherapy = Biomedecine pharmacotherapie* (2019) 117:109126. doi: 10.1016/j.biopha.2019.109126

8. Liu Z, Murphy SF, Huang J, Zhao L, Hall CC, Schaeffer AJ, et al. A novel immunocompetent model of metastatic prostate cancer-induced bone pain. *Prostate* (2020) 80(10):782–94. doi: 10.1002/pros.23993

9. Kondraciuk JD, Rice SL, Zhou X, Gharzeddine K, Knezevic A, Spratt DE, et al. Thyroid cancer bone metastasis: Survival and genomic characteristics of a Large tertiary care cohort. *Clin Nucl Med* (2019) 44(8):e465–e71. doi: 10.1097/RLU.0000000000002626

10. Tulotta C, Ottewell P. The role of IL-1B in breast cancer bone metastasis. *Endocrine-related Cancer* (2018) 25(7):R421–r34. doi: 10.1530/ERC-17-0309

11. Haber T, Jöckel E, Roos FC, Junker K, Prawitt D, Hampel C, et al. Bone metastasis in renal cell carcinoma is preprogrammed in the primary tumor and caused by AKT and integrin α5 signaling. *J urology* (2015) 194(2):539–46. doi: 10.1016/j.juro.2015.01.079

12. [Expert consensus on renal cell carcinoma with bone metastasis (2020 edition)]. *Zhonghua zhong liu za zhi [Chinese J oncology]* (2020) 42(7):537–42. doi: 10.3760/cma.j.cn112152-20200401-00292

13. Wong ECL, Kapoor A. Does bone-targeted therapy benefit patients with metastatic renal cell carcinoma? *Trans Oncol* (2020) 13(2):241–4. doi: 10.1016/j.tranon.2019.10.009

14. Coleman RE. Clinical features of metastatic bone disease and risk of skeletal morbidity. *Clin Cancer Res an Off J Am Assoc Cancer Res* (2006) 12(20 Pt 2):6243s–9s. doi: 10.1158/1078-0432.CCR-06-0931

15. Rath B, Tingart M, Migliorini F, Eschweiler J, Zureik R, Hardes J. [Differentiated treatment strategies for bone metastases of the extremities]. *Der Orthopade* (2019) 48(9):752–9. doi: 10.1007/s00132-019-03791-w

16. Harel R, Angelov L. Spine metastases: current treatments and future directions. *Eur J Cancer (Oxford Engl 1990)* (2010) 46(15):2696–707. doi: 10.1016/j.ejca.2010.04.025

17. McCabe FJ, Jadaan MM, Byrne F, Devitt AT, McCabe JP. Spinal metastasis: The rise of minimally invasive surgery. *surgeon J R Colleges Surgeons Edinburgh Ireland* (2022) 20(5):328–33. doi: 10.1016/j.surge.2021.08.007

18. Scutellari PN, Antinolfi G, Galeotti R, Giganti M. [Metastatic bone disease. *Strategies imaging] Minerva medica* (2003) 94(2):77–90.

19. Yildizhan S, Boyaci MG, Rakip U, Aslan A, Canbek I. Role of radiofrequency ablation and cement injection for pain control in patients with spinal metastasis. *BMC musculoskeletal Disord* (2021) 22(1):912. doi: 10.1186/s12891-021-04799-0

20. Guzik G. Oncological and functional results after surgical treatment of bone metastases at the proximal femur. *BMC surgery* (2018) 18(1):5. doi: 10.1186/s12893-018-0336-0

21. Wedin R, Hansen BH, Laitinen M, Trovik C, Zaikova O, Bergh P, et al. Complications and survival after surgical treatment of 214 metastatic lesions of the humerus. *J shoulder elbow surgery* (2012) 21(8):1049–55. doi: 10.1016/j.jse.2011.06.019

22. Hashimoto K, Ochi H, Sunamura S, Kosaka N, Mabuchi Y, Fukuda T, et al. Cancer-secreted hsa-miR-940 induces an osteoblastic phenotype in the bone metastatic microenvironment *via* targeting ARHGAP1 and FAM134A. *Proc Natl Acad Sci United States America* (2018) 115(9):2204–9. doi: 10.1073/pnas.1717363115

23. Lipton A, Uzzo R, Amato RJ, Ellis GK, Hakimian B, Roodman GD, et al. The science and practice of bone health in oncology: managing bone loss and metastasis in patients with solid tumors. *J Natl Compr Cancer Network JNCCN* (2009) 7 Suppl 7(Suppl 7):S1–29. doi: 10.6004/jnccn.2009.0080

24. LeRoy BE, Thudi NK, Nadella MV, Toribio RE, Tannehill-Gregg SH, van Bokhoven A, et al. New bone formation and osteolysis by a metastatic, highly invasive canine prostate carcinoma xenograft. *Prostate* (2006) 66(11):1213–22. doi: 10.1002/pros.20408

25. LeRoy BE, Sellers RS, Rosol TJ. Canine prostate stimulates osteoblast function using the endothelin receptors. *Prostate* (2004) 59(2):148–56. doi: 10.1002/pros.10370

26. Wang J, Rouse C, Jasper JS, Pendergast AM. ABL kinases promote breast cancer osteolytic metastasis by modulating tumor-bone interactions through TAZ and STAT5 signaling. *Sci Signaling* (2016) 9(413):ra12. doi: 10.1126/scisignal.aad3210

27. Quattrocchi CC, Piciucchi S, Sammarra M, Santini D, Vincenzi B, Tonini G, et al. Bone metastases in breast cancer: Higher prevalence of osteosclerotic lesions. *La Radiologia medica* (2007) 112(7):1049–59. doi: 10.1007/s11547-007-0205-x

28. Pan T, Lin SC, Yu KJ, Yu G, Song JH, Lewis VO, et al. BIGH3 promotes osteolytic lesions in renal cell carcinoma bone metastasis by inhibiting osteoblast differentiation. *Neoplasia (New York NY)* (2018) 20(1):32–43. doi: 10.1016/j.neo.2017.11.002

29. Haider MT, Ridlmaier N, Smit DJ, Taipaleenmäki H. Interleukins as mediators of the tumor cell-bone cell crosstalk during the initiation of breast cancer bone metastasis. *Int J Mol Sci* (2021) 22(6):2898. doi: 10.3390/ijms22062898

30. Otsuka S, Hanibuchi M, Ikuta K, Yano S, Goto H, Ogino H, et al. A bone metastasis model with osteolytic and osteoblastic properties of human lung cancer ACC-LC-319/bone2 in natural killer cell-depleted severe combined immunodeficient mice. *Oncol Res* (2009) 17(11-12):581–91. doi: 10.3727/096504009789745511

31. Song HJ, Wu CG, Xue YL, Xu YH, Qiu ZL, Luo QY. Percutaneous osteoplasty combined with radioiodine therapy as a treatment for bone metastasis developing after differentiated thyroid carcinoma. *Clin Nucl Med* (2012) 37(6):e129–33. doi: 10.1097/RLU.0b013e31824786d0

32. Zhang X. Interactions between cancer cells and bone microenvironment promote bone metastasis in prostate cancer. *Cancer Commun (London England)* (2019) 39(1):76. doi: 10.1186/s40880-019-0425-1

33. Xi X, Hu Z, Wu Q, Hu K, Cao Z, Zhou J, et al. High expression of small nucleolar RNA host gene 3 predicts poor prognosis and promotes bone metastasis in prostate cancer by activating transforming growth factor-beta signaling. *Bioengineered* (2022) 13(1):1895–907. doi: 10.1080/21655979.2021.2020393

34. Osorio M, Moubayed SP, Su H, Urken ML. Systematic review of site distribution of bone metastases in differentiated thyroid cancer. *Head neck* (2017) 39(4):812–8. doi: 10.1002/hed.24655

35. Leung AK. Optimizing skeletal-related events prevention in patients with advanced prostate cancer. *Asia-Pacific J Clin Oncol* (2020) 16 Suppl 3:4–6. doi: 10.1111/ajco.13315

36. Bhowmik D, Song X, Intorcia M, Gray S, Shi N. Examination of burden of skeletal-related events in patients naive to denosumab and intravenous bisphosphonate therapy in bone metastases from solid tumors population. *Curr Med Res opinion* (2019) 35(3):513–23. doi: 10.1080/03007995.2018.1532884

37. Cao PP, Chen WJ, Pang HL, Shen WW, Xue P, Duan L, et al. Effect of CUL4A on the metastatic potential of lung adenocarcinoma to the bone. *Oncol Rep* (2020) 43(2):662–70. doi: 10.3892/or.2019.7448

38. Miyashita H, Cruz C, Patel V. Risk factors of skeletal-related events in patients with bone metastatic castration-resistant prostate cancer undergoing treatment with zoledronate. *Supportive Care Cancer Off J Multinational Assoc Supportive Care Cancer* (2022) 30(2):981–4. doi: 10.1007/s00520-021-06340-4

39. Yu L, Sui B, Fan w, Lei L, Zhou L, Yang L, et al. Exosomes derived from osteogenic tumor activate osteoclast differentiation and concurrently inhibit osteogenesis by transferring COL1A1-targeting miRNA-92a-1-5p. *J Extracell Vesicles.* (2021) 10(3):e12056. doi: 10.1002/jev2.12056

40. Navarro-Gonzalez E. Use of multikinase inhibitors/lenvatinib concomitant with antiresorptive therapy for bone metastases from radioiodine-resistant differentiated thyroid cancer. *Cancer Med* (2022) 11 Suppl 1(Suppl 1):54–8. doi: 10.1002/cam4.4983

41. Valastyan S, Weinberg RA. Tumor metastasis: Molecular insights and evolving paradigms. *Cell* (2011) 147(2):275–92. doi: 10.1016/j.cell.2011.09.024

42. Clézardin P, Coleman R, Puppo M, Ottewell P, Bonnelye E, Paycha F, et al. Bone Metastasis: mechanisms, therapies, and biomarkers. *Physiol Rev* (2021) 101 (3):797–855. doi: 10.1152/physrev.00012.2019

43. Huang X, Shi X, Huang D, Li B, Lin N, Pan W, et al. Mutational characteristics of bone metastasis of lung cancer. *Ann palliative Med* (2021) 10 (8):8818–26. doi: 10.21037/apm-21-1595

44. Arnold RS, Fedewa SA, Goodman M, Osunkoya AO, Kissick HT, Morrissey C, et al. Bone metastasis in prostate cancer: Recurring mitochondrial DNA mutation reveals selective pressure exerted by the bone microenvironment. *Bone* (2015) 78:81–6. doi: 10.1016/j.bone.2015.04.046

45. Bartels S, Christgen M, Luft A, Persing S, Jödecke K, Lehmann U, et al. Estrogen receptor (ESR1) mutation in bone metastases from breast cancer. *Modern Pathol an Off J United States Can Acad Pathology Inc* (2018) 31(1):56–61. doi: 10.1038/modpathol.2017.95

46. Yilmaz M, Christofori G. EMT, the cytoskeleton, and cancer cell invasion. *Cancer metastasis Rev* (2009) 28(1-2):15–33. doi: 10.1007/s10555-008-9169-0

47. Lamouille S, Xu J, Derynck R. Molecular mechanisms of epithelial-mesenchymal transition. *Nat Rev Mol Cell Biol* (2014) 15(3):178–96. doi: 10.1038/nrm3758

48. Liu L, Chen X, Wang Y, Qu Z, Lu Q, Zhao J, et al. Notch3 is important for TGF-β-induced epithelial-mesenchymal transition in non-small cell lung cancer bone metastasis by regulating ZEB-1. *Cancer Gene Ther* (2014) 21(9):364–72. doi: 10.1038/cgt.2014.39

49. Horas K, Zheng Y, Fong-Yee C, Macfarlane E, Manibo J, Chen Y, et al. Loss of the vitamin d receptor in human breast cancer cells promotes epithelial to mesenchymal cell transition and skeletal colonization. *J Bone mineral Res Off J Am Soc Bone Mineral Res* (2019) 34(9):1721–32. doi: 10.1002/jbmr.3744

50. Huang S, Wa Q, Pan J, Peng X, Ren D, Huang Y, et al. Downregulation of miR-141-3p promotes bone metastasis *via* activating NF-κB signaling in prostate cancer. *J Exp Clin Cancer Res CR* (2017) 36(1):173. doi: 10.1186/s13046-017-0645-7

51. Ren D, Yang Q, Dai Y, Guo W, Du H, Song L, et al. Oncogenic miR-210-3p promotes prostate cancer cell EMT and bone metastasis *via* NF-κB signaling pathway. *Mol cancer* (2017) 16(1):117 doi: 10.1186/s12943-017-0688-6.

52. Bergers G, Fendt SM. The metabolism of cancer cells during metastasis. *Nat Rev Cancer* (2021) 21(3):162–80. doi: 10.1038/s41568-020-00320-2

53. Nimmakayala RK, Leon F, Rachagani S, Rauth S, Nallasamy P, Marimuthu S, et al. Metabolic programming of distinct cancer stem cells promotes metastasis of pancreatic ductal adenocarcinoma. *Oncogene* (2021) 40(1):215–31. doi: 10.1038/s41388-020-01518-2

54. Thysell E, Surowiec I, Hörnberg E, Crnalic S, Widmark A, Johansson AI, et al. Metabolomic characterization of human prostate cancer bone metastases reveals increased levels of cholesterol. *PloS One* (2010) 5(12):e14175. doi: 10.1371/journal.pone.0014175

55. Luo A, Xu Y, Li S, Bao J, Lü J, Ding N, et al. Cancer stem cell property and gene signature in bone-metastatic breast cancer cells. *Int J Biol Sci* (2020) 16 (14):2580–94. doi: 10.7150/ijbs.45693

56. Huang J, Freyhult E, Buckland R, Josefsson A, Damber JE, Welén K. Osteoclasts directly influence castration-resistant prostate cancer cells. *Clin Exp metastasis* (2022) 39(5):801–14. doi: 10.1007/s10585-022-10179-2

57. Yang H, Yu Z, Ji S, Huo Q, Yan J, Gao Y, et al. Targeting bone microenvironments for treatment and early detection of cancer bone metastatic niches. *J Controlled release Off J Controlled Release Society* (2022) 341:443–56. doi: 10.1016/j.jconrel.2021.11.005

58. Kähkönen TE, Halleen JM, Bernoulli J. Osteoimmuno-oncology: Therapeutic opportunities for targeting immune cells in bone metastasis. *Cells* (2021) 10(6):1529. doi: 10.3390/cells10061529

59. Liu SC, Sun QZ, Qiao XF, Li XG, Yang JH, Wang TQ, et al. LncRNA TUG1 influences osteoblast proliferation and differentiation through the wnt/β-catenin signaling pathway. *Eur Rev Med Pharmacol Sci* (2019) 23(11):4584–90. doi: 10.26355/eurrev_201906_18035

60. Udagawa N, Koide M, Nakamura M, Nakamichi Y, Yamashita T, Uehara S, et al. Osteoclast differentiation by RANKL and OPG signaling pathways. *J Bone mineral Metab* (2021) 39(1):19–26. doi: 10.1007/s00774-020-01162-6

61. Liu XH, Kirschenbaum A, Weinstein BM, Zaidi M, Yao S, Levine AC. Prostaglandin E2 modulates components of the wnt signaling system in bone and prostate cancer cells. *Biochem Biophys Res Commun* (2010) 394(3):715–20. doi: 10.1016/j.bbrc.2010.03.057

62. Dai J, Hall CL, Escara-Wilke J, Mizokami A, Keller JM, Keller ET. Prostate cancer induces bone metastasis through wnt-induced bone morphogenetic protein-dependent and independent mechanisms. *Cancer Res* (2008) 68(14):5785–94. doi: 10.1158/0008-5472.CAN-07-6541

63. Aufderklamm S, Hennenlotter J, Leidenberger P, Rausch S, Hohneder A, Kühs U, et al. Systemic alterations of wnt inhibitors in patients with prostate cancer and bone metastases. *Dis markers* (2018) 2018:1874598. doi: 10.1155/2018/1874598

64. Takayama K, Inoue T, Narita S, Maita S, Huang M, Numakura K, et al. Inhibition of the RANK/RANKL signaling with osteoprotegerin prevents castration-induced acceleration of bone metastasis in castration-insensitive prostate cancer. *Cancer letters* (2017) 397:103–10. doi: 10.1016/j.canlet.2017.03.034

65. Kopper L. Denosumab–a powerful RANKL inhibitor to stop lytic metastases and other bone loss actions by osteoclasts. *Pathol Oncol Res POR* (2012) 18(4):743–7. doi: 10.1007/s12253-012-9538-4

66. Li B, Wang P, Jiao J, Wei H, Xu W, Zhou P. Roles of the RANKL-RANK axis in immunity-implications for pathogenesis and treatment of bone metastasis. *Front Immunol* (2022) 13:824117. doi: 10.3389/fimmu.2022.824117

67. Chen YC, Sosnoski DM, Mastro AM. Breast cancer metastasis to the bone: Mechanisms of bone loss. *Breast Cancer Res BCR* (2010) 12(6):215. doi: 10.1186/bcr2781

68. Chauhan P, Nair A, Patidar A, Dandapat J, Sarkar A. Saha b. *A primer cytokines Cytokine* (2021) 145:155458. doi: 10.1016/j.cyto.2021.155458

69. Propper DJ, Balkwill FR. Harnessing cytokines and chemokines for cancer therapy. *Nat Rev Clin Oncol* (2022) 19(4):237–53. doi: 10.1038/s41571-021-00588-9

70. Harmer D, Falank C, Reagan MR. Interleukin-6 interweaves the bone marrow microenvironment, bone loss, and multiple myeloma. *Front endocrinology* (2018) 9:788. doi: 10.3389/fendo.2018.00788

71. He Y, Luo W, Liu Y, Wang Y, Ma C, Wu Q, et al. IL-20RB mediates tumoral response to osteoclastic niches and promotes bone metastasis of lung cancer. *J Clin Invest* (2022) 132(20):e157917. doi: 10.1172/JCI157917

72. Hamaguchi T, Wakabayashi H, Matsumine A, Sudo A, Uchida A. TNF inhibitor suppresses bone metastasis in a breast cancer cell line. *Biochem Biophys Res Commun* (2011) 407(3):525–30. doi: 10.1016/j.bbrc.2011.03.051

73. Lee JS, Lee JB, Cha JK, Choi EY, Park SY, Cho KS, et al. Chemokine in inflamed periodontal tissues activates healthy periodontal-ligament stem cell migration. *J Clin periodontology* (2017) 44(5):530–9. doi: 10.1111/jcpe.12710

74. Weidle UH, Birzele F, Kollmorgen G, Rüger R. Molecular mechanisms of bone metastasis. *Cancer Genomics proteomics* (2016) 13(1):1–12.

75. Guérard A, Laurent V, Fromont G, Estève D, Gilhodes J, Bonnelye E, et al. The chemokine receptor CCR3 is potentially involved in the homing of prostate cancer cells to bone: Implication of bone-marrow adipocytes. *Int J Mol Sci* (2021) 22(4):1994. doi: 10.3390/ijms22041994

76. Zitka O, Kukacka J, Krizkova S, Huska D, Adam V, Masarik M, et al. Matrix metalloproteinases. *Curr medicinal Chem* (2010) 17(31):3751–68. doi: 10.2174/092986710793213724

77. Pego ER, Fernández I, Núñez MJ. Molecular basis of the effect of MMP-9 on the prostate bone metastasis: A review. *Urologic Oncol* (2018) 36(6):272–82. doi: 10.1016/j.urolonc.2018.03.009

78. Zhang X, Yu X, Zhao Z, Yuan Z, Ma P, Ye Z, et al. MicroRNA-429 inhibits bone metastasis in breast cancer by regulating CrkL and MMP-9. *Bone* (2020) 130:115139. doi: 10.1016/j.bone.2019.115139

79. Morrison C, Mancini S, Cipollone J, Kappelhoff R, Roskelley C, Overall C. Microarray and proteomic analysis of breast cancer cell and osteoblast co-cultures: role of osteoblast matrix metalloproteinase (MMP)-13 in bone metastasis. *J Biol Chem* (2011) 286(39):34271–85. doi: 10.1074/jbc.M111.222513

80. Frejborg E, Salo T, Salem A. Role of cyclooxygenase-2 in head and neck tumorigenesis. *Int J Mol Sci* (2020) 21(23):9246. doi: 10.3390/ijms21239246

81. Li Z, Schem C, Shi YH, Medina D, Zhang M. Increased COX2 expression enhances tumor-induced osteoclastic lesions in breast cancer bone metastasis. *Clin Exp metastasis* (2008) 25(4):389–400. doi: 10.1007/s10585-007-9117-3

82. Karavitis J, Zhang M. COX2 regulation of breast cancer bone metastasis. *Oncoimmunology* (2013) 2(3):e23129. doi: 10.4161/onci.23129

83. Zhang J, Pang Y, Xie T, Zhu L. CXCR4 antagonism in combination with IDO1 inhibition weakens immune suppression and inhibits tumor growth in mouse breast cancer bone metastases. *OncoTargets Ther* (2019) 12:4985–92. doi: 10.2147/OTT.S200643

84. Okamoto K, Takayanagi H. Osteoimmunology. *Cold Spring Harbor Perspect Med* (2019) 9(1):a031245. doi: 10.1101/cshperspect.a031245

85. Fernández Vallone VB, Hofer EL, Choi H, Bordenave RH, Batagelj E, Feldman L, et al. Behaviour of mesenchymal stem cells from bone marrow of untreated advanced breast and lung cancer patients without bone osteolytic metastasis. *Clin Exp metastasis* (2013) 30(3):317–32. doi: 10.1007/s10585-012-9539-4

86. Wu MY, Li CJ, Yiang GT, Cheng YL, Tsai AP, Hou YT, et al. Molecular regulation of bone metastasis pathogenesis. *Cell Physiol Biochem Int J Exp Cell physiology biochemistry Pharmacol* (2018) 46(4):1423–38. doi: 10.1159/000489184

87. Zhao Y, Chen W, Zhu W, Meng H, Chen J, Zhang J. Overexpression of interferon regulatory factor 7 (IRF7) reduces bone metastasis of prostate cancer cells in mice. *Oncol Res* (2017) 25(4):511–22. doi: 10.3727/096504016X14756226781802

88. Bidwell BN, Slaney CY, Withana NP, Forster S, Cao Y, Loi S, et al. Silencing of Irf7 pathways in breast cancer cells promotes bone metastasis through immune escape. *Nat Med* (2012) 18(8):1224–31. doi: 10.1038/nm.2830

89. Zou W. Regulatory T cells, tumour immunity and immunotherapy. *Nat Rev Immunol* (2006) 6(4):295–307. doi: 10.1038/nri1806

90. Zou L, Barnett B, Safah H, Larussa VF, Evdemon-Hogan M, Mottram P, et al. Bone marrow is a reservoir for CD4+CD25+ regulatory T cells that traffic through CXCL12/CXCR4 signals. *Cancer Res* (2004) 64(22):8451–5. doi: 10.1158/0008-5472.CAN-04-1987

91. Tan W, Zhang W, Strasner A, Grivennikov S, Cheng JQ, Hoffman RM, et al. Tumour-infiltrating regulatory T cells stimulate mammary cancer metastasis through RANKL-RANK signalling. *Nature* (2011) 470(7335):548–53. doi: 10.1038/nature09707

92. Jarnicki AG, Lysaght J, Todryk S, Mills KH. Suppression of antitumor Immunity by IL-10 and TGF-beta-producing T cells infiltrating the growing tumor: influence of tumor environment on the induction of CD4+ and CD8+ regulatory T cells. *J Immunol (Baltimore Md 1950)* (2006) 177(2):896–904. doi: 10.4049/jimmunol.177.2.896

93. Collison LW, Workman CJ, Kuo TT, Boyd K, Wang Y, Vignali KM, et al. The inhibitory cytokine IL-35 contributes to regulatory T-cell function. *Nature* (2007) 450(7169):566–9. doi: 10.1038/nature06306

94. Muscarella AM, Aguirre S, Hao X, Waldvogel SM, Zhang XH. Exploiting bone niches: progression of disseminated tumor cells to metastasis. *J Clin Invest* (2021) 131(6):e143764. doi: 10.1172/JCI143764

95. Consonni FM, Bleve A, Totaro MG, Storto M, Kunderfranco P, Termanini A, et al. Heme catabolism by tumor-associated macrophages controls metastasis formation. *Nat Immunol* (2021) 22(5):595–606. doi: 10.1038/s41590-021-00921-5

96. Ye Y, Xu Y, Lai Y, He W, Li Y, Wang R, et al. Long non-coding RNA cox-2 prevents immune evasion and metastasis of hepatocellular carcinoma by altering M1/M2 macrophage polarization. *J Cell Biochem* (2018) 119(3):2951–63. doi: 10.1002/jcb.26509

97. Zhao CC, Han QJ, Ying HY, Gu XX, Yang N, Li LY, et al. TNFSF15 facilitates differentiation and polarization of macrophages toward M1 phenotype to inhibit tumor growth. *Oncoimmunology* (2022) 11(1):2032918. doi: 10.1080/2162402X.2022.2032918

98. Tariq M, Zhang JQ, Liang GK, He QJ, Ding L, Yang B. Gefitinib inhibits M2-like polarization of tumor-associated macrophages in Lewis lung cancer by targeting the STAT6 signaling pathway. *Acta pharmacologica Sinica* (2017) 38 (11):1501–11. doi: 10.1038/aps.2017.124

99. Ma RY, Zhang H, Li XF, Zhang CB, Selli C, Tagliavini G, et al. Monocyte-derived macrophages promote breast cancer bone metastasis outgrowth. . *J Exp Med* (2020) 217(11):e20191820. doi: 10.1084/jem.20191820

100. Lin Y, Cai Q, Chen Y, Shi T, Liu W, Mao L, et al. CAFs shape myeloid-derived suppressor cells to promote stemness of intrahepatic cholangiocarcinoma through 5-lipoxygenase. *Hepatol (Baltimore Md)* (2022) 75(1):28–42. doi: 10.1002/hep.32099

101. Paauwe M, Schoonderwoerd MJA, Helderman R, Harryvan TJ, Groenewoud A, van Pelt GW, et al. Endoglin expression on cancer-associated fibroblasts regulates invasion and stimulates colorectal cancer metastasis. *Clin Cancer Res an Off J Am Assoc Cancer Res* (2018) 24(24):6331–44. doi: 10.1158/1078-0432.CCR-18-0329

102. Li H, Lin X, Yang D, Chen Z, Wang X, Re F, et al. Cancer-associated fibroblasts support bone tropic metastasis by acting as coordinators between the tumor microenvironment and bone matrix in breast cancer. *Neoplasma* (2021) 68 (1):10–22. doi: 10.4149/neo_2020_200905N951

103. Mukaida N, Zhang D, Sasaki SI. Emergence of cancer-associated fibroblasts as an indispensable cellular player in bone metastasis process. *Cancers* (2020) 12 (10):2896. doi: 10.3390/cancers12102896

104. Zhang Y, Fujita N, Oh-hara T, Morinaga Y, Nakagawa T, Yamada M, et al. Production of interleukin-11 in bone-derived endothelial cells and its role in the formation of osteolytic bone metastasis. *Oncogene* (1998) 16(6):693–703. doi: 10.1038/sj.onc.1201581

105. Wang K, Jiang L, Hu A, Sun C, Zhou L, Huang Y, et al. Vertebral-specific activation of the CX3CL1/ICAM-1 signaling network mediates non-small-cell lung cancer spinal metastasis by engaging tumor cell-vertebral bone marrow endothelial cell interactions. *Theranostics* (2021) 11(10):4770–89. doi: 10.7150/thno.54235

106. Eap C, Tardieux E, Goasgen O, Bennis S, Mireau E, Delalande B, et al. Tokuhashi score and other prognostic factors in 260 patients with surgery for vertebral metastases. *Orthopaedics traumatology Surg Res OTSR* (2015) 101 (4):483–8. doi: 10.1016/j.otsr.2015.03.007

107. De la Garza Ramos R, Naidu I, Choi JH, Pennington Z, Goodwin CR, Sciubba DM, et al. Comparison of three predictive scoring systems for morbidity in oncological spine surgery. *J Clin Neurosci Off J Neurosurgical Soc Australasia* (2021) 94:13–7. doi: 10.1016/j.jocn.2021.09.031

108. Tanaka A, Katagiri H, Murata H, Wasa J, Miyagi M, Honda Y, et al. Surgery for femoral metastases. *Bone Joint J* (2020) 102-b(3):285–92. doi: 10.1302/0301-620X.102B3.BJJ-2019-0976.R1

109. Hoban H, Soejima T, Sulaiman NS, Sekii S, Matsumoto Y, Ota Y, et al. Predicting the survival of patients with bone metastases treated with radiation therapy: A validation study of the Katagiri scoring system? *Radiat Oncol.* (2019) 14 (1):13. doi: 10.1186/s13014-019-1218-z

110. Sun G, Li L, Jin P, Liu XW, Li M. Percutaneous vertebroplasty for painful spinal metastasis with epidural encroachment. *J Surg Oncol* (2014) 110(2):123–8. doi: 10.1002/jso.23608

111. Chen F, Xia YH, Cao WZ, Shan W, Gao Y, Feng BO, et al. Percutaneous kyphoplasty for the treatment of spinal metastases. *Oncol letters* (2016) 11(3):1799–806. doi: 10.3892/ol.2016.4121

112. Sayed D, Jacobs D, Sowder T, Haines D, Orr W. Spinal radiofrequency ablation combined with cement augmentation for painful spinal vertebral metastasis: A single-center prospective study. *Pain physician* (2019) 22(5):E441–e9. doi: 10.36076/ppj/2019.22.E441

113. Li RF, Qiao RQ, Xu MY, Ma RX, Hu YC. Separation surgery in the treatment of spinal metastasis. *Technol Cancer Res Treat* (2022) 21:15330338221107208. doi: 10.1177/15330338221107208

114. Liu DD, Leary OP, Camara-Quintana JQ, Galgano MA. Two-Level Separation Surgery for Thoracic Epidural Metastatic Disease: An Operative Video Demonstration. *World Neurosurg.* (2021) 147::160. doi: 10.1016/j.wneu.2020.12.022

115. Pranata R, Lim MA, Vania R, Bagus Mahadewa TG. Minimal invasive surgery instrumented fusion versus conventional open surgical instrumented fusion for the treatment of spinal metastases: A systematic review and meta-analysis. *World neurosurgery* (2021) 148:e264–e74. doi: 10.1016/j.wneu.2020.12.130

116. Fang X, Lei S, Luo Y, Zhou Y, Min L, Zhang W, et al. Research on three-dimensional printing technology based on three-dimensional multimodality imaging to assist the operation of malignant bone tumors of limbs. *Zhongguo xiu fu chong jian wai ke za zhi = Zhongguo xiufu chongjian waike zazhi = Chin J reparative reconstructive surgery* (2022) 36(7):804–10. doi: 10.7507/1002-1892.202202060

117. Osborne CK. Tamoxifen in the treatment of breast cancer. *New Engl J Med* (1998) 339(22):1609–18. doi: 10.1056/NEJM199811263392207

118. Smith MR, Hussain M, Saad F, Fizazi K, Sternberg CN, Crawford ED, et al. Darolutamide and survival in metastatic, hormone-sensitive prostate cancer. *New Engl J Med* (2022) 386(12):1132–42. doi: 10.1056/NEJMoa2119115

119. Garcia J, Hurwitz HI, Sandler AB, Miles D, Coleman RL, Deurloo R, et al. Bevacizumab (Avastin®) in cancer treatment: A review of 15 years of clinical experience and future outlook. *Cancer Treat Rev* (2020) 86:102017. doi: 10.1016/j.ctrv.2020.102017

120. Watanabe S, Yonesaka K, Tanizaki J, Nonagase Y, Takegawa N, Haratani k, et al. Targeting of the HER2/HER3 signaling axis overcomes ligand-mediated resistance to trastuzumab in HER2-positive breast cancer. *Cancer Med.* (2019) 8 (3):1258–1268. doi: 10.1002/cam4.1995

121. Kang J, Lee JY, Park JH, Chang DJ. Synthesis of imatinib, a tyrosine kinase inhibitor, labeled with carbon-14. *J labelled compounds radiopharmaceuticals* (2020) 63(4):174–82. doi: 10.1002/jlcr.3830

122. de Bono J, Mateo J, Fizazi K, Saad F, Shore N, Sandhu S, et al. Olaparib for metastatic castration-resistant prostate cancer. *New Engl J Med* (2020) 382 (22):2091–102. doi: 10.1056/NEJMoa1911440

123. Chung JK, Cheon GJ. Radioiodine therapy in differentiated thyroid cancer: the first targeted therapy in oncology. *Endocrinol Metab (Seoul).* (2014) 29(3):233–9. doi: 10.3803/EnM.2014.29.3.233

124. Rodler ET, Kurland BF, Griffin M, Gralow JR, Porter P, Yeh RF, et al. Phase I study of veliparib (ABT-888) combined with cisplatin and vinorelbine in advanced triple-negative breast cancer and/or BRCA mutation-associated breast cancer. *Clin Cancer Res an Off J Am Assoc Cancer Res* (2016) 22(12):2855–64. doi: 10.1158/1078-0432.CCR-15-2137

125. Tokito T, Shukuya T, Akamatsu H, Taira T, Ono A, Kenmotsu H, et al. Efficacy of bevacizumab-containing chemotherapy for non-squamous non-small cell lung cancer with bone metastases. *Cancer chemotherapy Pharmacol* (2013) 71 (6):1493–8. doi: 10.1007/s00280-013-2148-3

126. Bergamini C, Cavalieri S, Sanguineti G, Farneti A, Licitra L. Treatment of HER2+ metastatic salivary ductal carcinoma in a pregnant woman: a case report. *Oxford Med Case Rep* (2019) 2019(10):omz102. doi: 10.1093/omcr/omz102

127. Singh T, Kaur V, Kumar M, Kaur P, Murthy RS, Rawal RK. The critical role of bisphosphonates to target bone cancer metastasis: an overview. *J Drug targeting* (2015) 23(1):1–15. doi: 10.3109/1061186X.2014.950668

128. Smith MR, Saad F, Coleman R, Shore N, Fizazi K, Tombal B, et al. Denosumab and bone-metastasis-free survival in men with castration-resistant prostate cancer: results of a phase 3, randomised, placebo-controlled trial. *Lancet (London England)* (9810) 2012:39–46:379. doi: 10.1016/S0140-6736(11)61226-9

129. Goldvaser H, Amir E. Role of bisphosphonates in breast cancer therapy. *Curr Treat options Oncol* (2019) 20(4):26. doi: 10.1007/s11864-019-0623-8

130. Hosaka S, Katagiri H, Niwakawa M, Harada H, Wasa J, Murata H, et al. Radiotherapy combined with zoledronate can reduce skeletal-related events in renal cell carcinoma patients with bone metastasis. *Int J Clin Oncol* (2018) 23 (6):1127–33. doi: 10.1007/s10147-018-1310-7

131. Wei Z, Pan B, Jia D, Yu Y. Long-term safety and efficacy of bisphosphonate therapy in advanced lung cancer with bone metastasis. *Future Oncol (London England)* (2022) 18(18):2257–67. doi: 10.2217/fon-2022-0098

132. Chen SC, Kuo PL. Bone metastasis from renal cell carcinoma. *Int J Mol Sci* (2016) 17(6):987. doi: 10.3390/ijms17060987

133. Irelli A, Sirufo MM, D'Ugo C, Ginaldi L, De Martinis M. Real-life use of denosumab 120 mg every 12 weeks in prolonged treatment over 2 years of patients with breast cancer bone metastases. *J BUON Off J Balkan Union Oncol* (2020) 25 (4):1799–804.

134. Browne AJ, Kubasch ML, Göbel A, Hadji P, Chen D, Rauner M, et al. Concurrent antitumor and bone-protective effects of everolimus in osteotropic breast cancer. *Breast Cancer Res BCR* (2017) 19(1):92. doi: 10.1186/s13058-017-0885-7

135. Jones MD, Liu JC, Barthel TK, Hussain S, Lovria E, Cheng D, et al. A proteasome inhibitor, bortezomib, inhibits breast cancer growth and reduces osteolysis by downregulating metastatic genes. *Clin Cancer Res an Off J Am Assoc Cancer Res* (2010) 16(20):4978–89. doi: 10.1158/1078-0432.CCR-09-3293

136. Francini E, Montagnani F, Nuzzo PV, Gonzalez-Velez M, Alimohamed NS, Rosellini P, et al. Association of concomitant bone resorption inhibitors with overall survival among patients with metastatic castration-resistant prostate cancer and bone metastases receiving abiraterone acetate with prednisone as first-line therapy. *JAMA network Open* (2021) 4(7):e2116536. doi: 10.1001/jamanetworkopen.2021.16536

137. Escudier B, Powles T, Motzer RJ, Olencki T, Arén Frontera O, Oudard S, et al. Cabozantinib, a new standard of care for patients with advanced renal cell carcinoma and bone metastases? subgroup analysis of the METEOR trial. *J Clin Oncol Off J Am Soc Clin Oncol* (2018) 36(8):765–72. doi: 10.1200/JCO.2017.74.7352

138. Dréau D, Karaa A, Culberson C, Wyan H, McKillop IH, Clemens MG. Bosentan inhibits tumor vascularization and bone metastasis in an immunocompetent skin-fold chamber model of breast carcinoma cell metastasis. *Clin Exp metastasis* (2006) 23(1):41–53. doi: 10.1007/s10585-006-9016-z

139. Tan R, Wan Y, Yang X. Hydroxyethyl starch and its derivatives as nanocarriers for delivery of diagnostic and therapeutic agents towards cancers. *Biomaterials translational* (2020) 1(1):46–57. doi: 10.3877/cma.j.issn.2096-112X.2020.01.005

140. He Y, Huang Y, Huang Z, Jiang Y, Sun X, Shen Y, et al. Bisphosphonate-functionalized coordination polymer nanoparticles for the treatment of bone metastatic breast cancer. *J Controlled release Off J Controlled Release Society* (2017) 264:76–88. doi: 10.1016/j.jconrel.2017.08.024

141. Qiao H, Cui Z, Yang S, Ji D, Wang Y, Yang Y, et al. Targeting osteocytes to attenuate early breast cancer bone metastasis by theranostic upconversion nanoparticles with responsive plumbagin release. *ACS nano* (2017) 11(7):7259–73. doi: 10.1021/acsnano.7b03197

142. Thamake SI, Raut SL, Gryczynski Z, Ranjan AP, Vishwanatha JK. Alendronate coated poly-lactic-co-glycolic acid (PLGA) nanoparticles for active targeting of metastatic breast cancer. *Biomaterials* (2012) 33(29):7164–73. doi: 10.1016/j.biomaterials.2012.06.026

143. Dos Santos Ferreira D, Jesus de Oliveira Pinto BL, Kumar V, Cardoso VN, Fernandes SO, Souza CM, et al. Evaluation of antitumor activity and cardiac toxicity of a bone-targeted ph-sensitive liposomal formulation in a bone metastasis tumor model in mice. *Nanomedicine nanotechnology biology Med* (2017) 13 (5):1693–701. doi: 10.1016/j.nano.2017.03.005

144. Sun W, Ge K, Jin Y, Han Y, Zhang H, Zhou G, et al. Bone-targeted nanoplatform combining zoledronate and photothermal therapy to treat breast cancer bone metastasis. *ACS nano* (2019) 13(7):7556–67. doi: 10.1021/acsnano.9b00097

145. Wang M, Cai X, Yang J, Wang C, Tong L, Xiao J, et al. A targeted and pH-responsive bortezomib nanomedicine in the treatment of metastatic bone tumors. *ACS Appl materials interfaces* (2018) 10(48):41003–11. doi: 10.1021/acsami.8b07527

146. Hao Z, Fan W, Hao J, Wu X, Zeng GQ, Zhang LJ, et al. Efficient delivery of micro RNA to bone-metastatic prostate tumors by using aptamer-conjugated atelocollagen *in vitro* and in vivo. *Drug delivery* (2016) 23(3):874–81. doi: 10.3109/10717544.2014.9200597

147. Zhao YP, Ye WL, Liu DZ, Cui H, Cheng Y, Liu M, et al. Redox and pH dual sensitive bone targeting nanoparticles to treat breast cancer bone metastases and inhibit bone resorption. *Nanoscale* (2017) 9(19):6264–77. doi: 10.1039/C7NR00962C

148. Tamura T, Yoshioka Y, Sakamoto S, Ichikawa T, Ochiya T. Extracellular vesicles in bone metastasis: Key players in the tumor microenvironment and promising therapeutic targets. *Int J Mol Sci* (2020) 21(18):6680. doi: 10.3390/ijms21186680

149. Ge YW, Liu XL, Yu DG, Zhu ZA, Ke QF, Mao YQ, et al. Graphene-modified CePO4 nanorods effectively treat breast cancer-induced bone metastases and regulate macrophage polarization to improve osteo-inductive ability. *J nanobiotechnology* (2021) 19(1):11. doi: 10.1186/s12951-020-00753-9

150. Peng Y, Qing X, Shu H, Tian S, Yang W, Chen S, et al. Proper animal experimental designs for preclinical research of biomaterials for intervertebral disc regeneration. *Biomaterials translational* (2021) 2(2):91–142. doi: 10.12336/biomatertransl.2021.02.003

frontiers | Frontiers in Oncology

TYPE Original Research
PUBLISHED 26 January 2023
DOI 10.3389/fonc.2023.1110045

OPEN ACCESS

EDITED BY
Feifei Pu,
Huazhong University of Science and Technology, China

REVIEWED BY
Mirza Pojskic,
University Hospital of Giessen and Marburg, Germany
Zhibo Zheng,
Peking Union Medical College Hospital (CAMS), China
Wangjun Yan,
Fudan University, China
Alessandro Gasbarrini,
Rizzoli Orthopedic Institute (IRCCS), Italy

*CORRESPONDENCE
Tielong Liu
liutielongvip@163.com
Jianru Xiao
xiaojianruvvip@163.com
Xin Gao
czyygaoxin@smmu.edu.cn

†These authors have contributed equally to this work and share first authorship

SPECIALTY SECTION
This article was submitted to Surgical Oncology, a section of the journal Frontiers in Oncology

RECEIVED 28 November 2022
ACCEPTED 09 January 2023
PUBLISHED 26 January 2023

CITATION
Ni X, Wang J, Cao J, Zhang K, Hou S, Huang X, Song Y, Gao X, Xiao J and Liu T (2023) Surgical management and outcomes of spinal metastasis of malignant adrenal tumor: A retrospective study of six cases and literature review.
Front. Oncol. 13:1110045.
doi: 10.3389/fonc.2023.1110045

Surgical management and outcomes of spinal metastasis of malignant adrenal tumor: A retrospective study of six cases and literature review

Xiangzhi Ni[1†], Jing Wang[1†], Jiashi Cao[2†], Kun Zhang[1†], Shuming Hou[1], Xing Huang[1], Yuanjin Song[3], Xin Gao[1*], Jianru Xiao[1*] and Tielong Liu[1*]

[1]Department of Orthopaedic Oncology, Changzheng Hospital of the Navy Medical University, Shanghai, China, [2]Department of Orthopedics, No. 455 Hospital of Chinese People's Liberation Army, The Navy Medical University, Shanghai, China, [3]Department of Orthopaedics, The 80th Group Army Hospital, Weifang, Shandong, China

Purpose: Spinal metastasis of malignant adrenal tumor (SMMAT) is an extremely rare and poorly understood malignant tumor originating from the adrenal gland. The objective of this study is to elucidate the clinical characteristics and discuss surgical management and outcomes of SMMAT.

Methods: Included in this study were six SMMAT patients who received surgical treatment in our center between February 2013 and May 2022. Their clinical data and outcomes were retrospectively analyzed to gain a better understanding of SMMAT. In addition, ten cases from the literature focusing on SMMAT were also reviewed.

Results: Surgery was performed successfully, and the associated symptoms were relieved significantly in all patients postoperatively. The mean follow-up duration was 26.2 (range 3-55) months. Two patients died of tumor recurrence 12 and 48 months after operation respectively. The other four patients were alive at the last follow-up.

Conclusions: The prognosis of SMMAT is usually poor. Preoperative embolization and early surgical radical resection can offer satisfactory clinical outcomes. The patient's health status, preoperative neurological function, tumor location and the resection mode are potential prognostic factors of SMMAT.

KEYWORDS

adrenal tumor, spinal metastasis, adrenocortical carcinoma, malignant phaeochromocytoma, surgery, adjuvant therapy

Introduction

Adrenal tumor is a common disease seriously threatening people's health, with the prevalence ranging from 1.0% to 8.7% with a mean of about 2% (1, 2). About 1-12% patients with adrenal tumors are diagnosed with malignancy, mainly including adrenocortical carcinoma (ACC) from the adrenal cortex and malignant phaeochromocytoma (MP) from the adrenal medulla (3, 4).

Bone metastasis is an uncommon occurrence in adrenal tumor patients but may cause poor survival prognosis. Bone metastasis accounts for about 7% in ACC patients, portending a limited survival perspective (median, 11 months) and the 5-year survival rate of MP patients is only about 40% (5–7). Especially, spinal metastasis can cause severe pain, spinal cord compression and pathological fracture, leading to poor quality of life and reduced survival (5–8).

The presence of spinal metastasis symbolizes the advanced stage of the disease in most cases. Patients in this stage are usually considered incurable and can only receive supportive care. In recent years, the important role of surgery in the treatment of spinal metastatic tumors has gradually been recognized and widely accepted (9). However, due to the rarity of spinal metastasis of malignant adrenal tumor (SMMAT) with only a few sporadic cases reported (10–15), the role and prognostic outcome of surgery for SMMAT are poorly understood. In this study, we reviewed six consecutive patients with SMMAT to present our empirical understanding about the clinical characteristics, surgical treatment, potential contributing factors for spinal metastasis, as well as prognostic factors affecting spinal overall survival of patients with this intractable malignant tumor.

Materials and methods

This retrospective study included six patients who were pathologically confirmed as having SMMAT and received surgical treatment in our institution between February 2013 and May 2022. Hospitalization records, progress notes, surgical information, radiological presentations and pathological reports of all patients were all collected and recorded for analysis. Follow-up observation ended at the date of patient death or in May 2022. Informed consent was obtained from all participating patients before initiation of the study. The study procedures were conducted according to the principles of the Declaration of Helsinki and approved by the ethics committee of Changzheng Hospital (Shanghai, China).

All patients underwent X-ray, CT and MRI scans of the spine after admission. Positron emission tomography–computed tomography (PET–CT) was performed to detect possible metastatic sites. Tumors were further classified according to the Enneking staging system for all patients and Weinstein-BorianiBiagini (WBB) classification system for mobile spine based on radiological findings. Frankel grade and Eastern Cooperative Oncology Group performance score (ECOG-PS) were used to evaluate the neurological status and performance status, respectively. All patients had a history of adrenal tumor, and the diagnosis of metastatic adrenal tumor was confirmed by imageology. Although we emphasized the significance of percutaneous needle biopsy, some patients with serious neurological symptoms refused to have a needle biopsy for fear of aggravation of the existing condition.

Surgery was performed in all six patients successfully. Individualized adjuvant therapy was designed and implemented in each patient. X-ray and/or MRI examination was performed during the follow-up period. The last status of the patients was obtained through telephone interviews.

Studies related to SMMAT were searched by using PubMed as the searching engine, and 10 case reports were selected. Data from our own patients and those from literature research were compared and analyzed.

Results

Epidemiology and clinical presentation

The clinical data of the six patients in our series are listed in Table 1. They included of four men and two women, ranging in age from 13 to 71 years at diagnosis, with a mean of 42.2 years and a median of 41 years. The most common symptoms were radiating pain and movement disorder. Of them, two patients presented with paraplegia, and the remaining four patients had varying degrees of pain and decreased muscle strength. Four patients with pheochromocytoma had uncontrolled hypertension. The mean time from adrenal tumor resection to diagnosis of spinal metastasis was 77.5 (rang 9-216) months. The mean duration of the symptoms was 3.3 (range 1-12) months. The adrenal tumors (two cases of ACC and four cases of MP) in these patients were mainly located in the lumbar vertebrae in three cases, the thoracic vertebrae in two cases, and the sacral vertebra in one case. The Frankel scores are as follows: Grade B, Grade C and D each were documented in two patients.

Imaging assessment

All patients underwent MRI and CT scans. Imageologically, SMMAT presented low signals on T1-weighted imaging and moderate signal on T2-weighted imaging on MR imaging, and on CT imaging, the diseased vertebral body presented osteolytic changes with obvious enhancement at the edge of the lesion.

Treatment

The treatment process of all patients was implemented in a multi-disciplinary team (MDT) mode. The surgical indications are as follows: 1) patients with a life expectancy of more than 3 months; and 2) patients with intractable pain, spinal cord compression, and impending pathological fractures. All surgical procedures were performed by the same surgical team. The whole operation process comprised tumor excision, decompression of the spinal cord, reconstruction, and stabilization of the spine *via* a posterior approach. The surgical modality included total en-bloc resection in one patient (Case 6), subtotal resection in one patient (Case2), and total piecemeal resection

10.3389/fonc.2023.1110045

TABLE 1 Clinical data of patients with SMMAT.

NO	Age/ Sex	DOS (months)	Pathology	Location	Time of spinal metastasis	Tumor Size (cm)	WBB	F-S pre	ECOG pre	Operation	F-S post	Complication	Follow-up (months)	Adjunctive therapy	LR/ meta	Last status
1	29/F	1	ACC	L1	120	16.8	10-12 A-E	D	1	TPR	D	None	3	Radiotherapy	None	Alive
2	71/F	1	ACC	L1-L2	9	3.7	5-10 A-D	D	2	SR	D	None	12	Radiotherapy	SM	Dead
3	13/M	1	MP	T3	24	4.6	1-4 A-D	B	3	TPR	E	None	32	None	SM	Alive
4	58/M	3	MP	S1-S3	24	1.0	1-12 A-D	C	1	TPR	E	Infection	55	None	None	Alive
5	40/M	12	MP	T3	216	5.2	5-12 A-D	C	3	TPR	D	None	48	Radiotherapy	SM	Dead
6	42/M	2	MP	L1-L2	72	0.7	1-7 A-D	B	3	TER	E	None	7	Radiotherapy	None	Alive

SMMAT, spinal metastasis of malignant adrenal tumor; DOS, duration of symptom; WBB, Weinstein-BorianiBiagini; F-S pre, preoperative Frankel scores; ECOG pre, preoperative Eastern Cooperative Oncology Group; F-S post, postoperative Frankel scores; LR/meta, local recurrence/metastasis; M, male; F, female; ACC, adrenocortical cancer; MP, malignant pheochromocytoma; TER, Total en-bloc resection; TPR, Total piecemeal resection; SR, Subtotal resection; SM, systemic metastasis.

in the other four patients. The vertebral defects were repaired by the titanium filled with the bone allograft in Case 3, and the titanium filled with the bone cement in Case 5. Vertebral bone cement fixation was applied in Case 1 and 2. Pedicle screws were applied in Case 4 and Case 6 (Figure 1). Intraoperative blood loss ranged from 500 to 4000 (mean 2050) ml. The mean duration of surgery was 312.5 (range: 200-490) min. All patients recovered well without significant surgical complications except one patient (Case 4) who developed infection, which was cured after antibiotic therapy. Pain was relieved and muscle strength was improved postoperatively in all patients. After multidisciplinary evaluation, individualized treatment plans were performed in each patient. Four patients (Case 1, 2, 5 and 6) received adjuvant radiotherapy, and the other two patients refused adjuvant radiotherapy for financial reasons.

Follow-up observation

The mean follow-up duration was 26.2 (range: 3-55) months. Pain and numbness of the lower limbs were significantly relieved in all patients after operation. Two patients (Case 3 and 6) who were unable to ambulate (Frankel grade B) preoperatively became ambulatory postoperatively. Three patients (Case 2, 3 and 5) experienced systemic tumor recurrence. Two patients (Case 2 and 5) died at the last follow-up of 12 and 48 months after operation, respectively. The others were still alive at the last follow-up. The result of survival curve for all 6 patients are shown in Figure 2. The median survival of the six patients was 48 months.

Cases illustration

Case 1

A 29-year-old woman presented with decreased muscle strength in the right leg in February 2022. Imaging demonstrated lesions in L1 (Figure 3). The patient's preoperative Frankle score was D. An operation was subsequently performed to prevent further deterioration of the disease. Postoperative pathology confirmed adrenocortical carcinoma. The patient's postoperative Frankle score was D. Patients received radiotherapy in other hospitals after surgery. The patient underwent adrenal tumor resection at local hospital in 2012.

Case 2

A 71-year-old woman presented with low-back pain in November 2018. Imaging demonstrated lesions in L1-L2 (Supplementary Figure 1). The patient's preoperative Frankle score was D. Postoperative pathology confirmed adrenocortical carcinoma. The patient's postoperative Frankle score was D. Patients received radiotherapy in other hospitals after surgery. And the patient underwent adrenal tumor resection at local hospital in February 2012.

Case 3

A 13-year-old boy received pheochromocytoma resection in 2017. The patient came to our hospital for lower limb mobility disorder in September 2019. Imaging demonstrated lesions in T3 (Supplementary Figure 2).

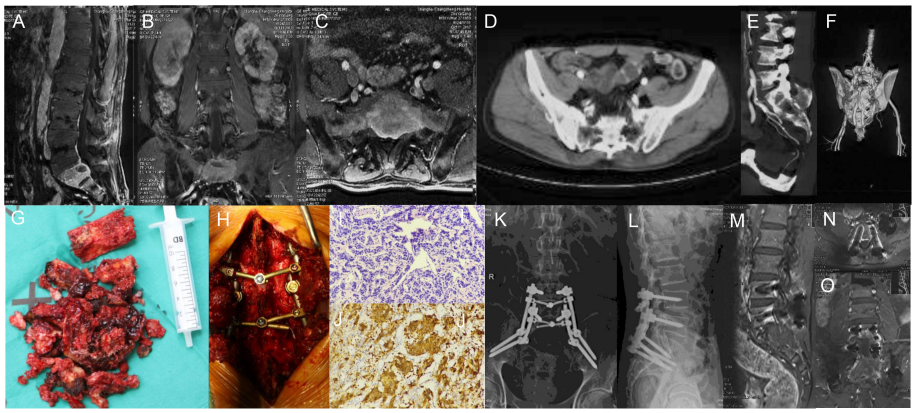

FIGURE 1
(A–C) Preoperative sagittal, coronal, and transverse MRI images of S1-2 vertebral body tumors; **(D–F)** Preoperative transverse and sagittal 3D CT images of S1-2 vertebral body tumors; **(G, H)** He had a history of adrenal tumor (4 points). Visceral metastases were not detectable (0 point). Bone metastases were isolated (1 point). His total prognostic score was 5 points. So, we chose the surgical strategy of total piecemeal resection. The tumor was excised by total piecemeal resection, pedicle screws, iliac screws and titanium rods were used to reconstruct the stability; **(I)** Hematoxylin-eosin (H&E) staining of pheochromocytoma; **(J)** Immunohistochemical staining for NSE; **(K, L)** Postoperative X-ray; **(M–O)** Postoperative sagittal, transverse, and coronal MRI.

Thepatient's preoperative Frankle score was B. Postoperative pathology confirmed pheochromocytoma. The patient's postoperative Frankle score was E. And he didn't receive other adjunctive therapy.

Case 4

A 58-year-old man received pheochromocytoma resection in 2015. He came to hospital for sacrococcygeal pain. Imaging demonstrated lesions in S1-S2 (Figure 1). The patient's preoperative Frankle score was C. Postoperative pathology confirmed pheochromocytoma. And pain was significantly relieved after operation. The patient's postoperative Frankle score was E. He didn't receive other adjunctive therapy.

Case 5

A 40-year-old man received pheochromocytoma resection in 1995. He came to our hospital for lower limb mobility disorder in February 2013. Imaging demonstrated lesions in T3. The patient's preoperative Frankle score was C. Postoperative pathology confirmed pheochromocytoma. The patient's postoperative Frankle score was D. He received radiotherapy in other hospitals after surgery.

Case 6

A 42-year-old man received pheochromocytoma resection in 2002. He was diagnosed with spinal metastasis of malignant adrenal tumor in 2008 and underwent surgical resection. He came to our hospital for lower limb mobility disorder in September 2021. Imaging demonstrated lesions in L1-L2 (Supplementary Figure 3). The patient's preoperative Frankle score was B. The patient's postoperative Frankle score was E. He received radiotherapy in other hospitals after surgery.

Discussion

Clinical features

Spinal metastasis of malignant adrenal tumor is a malignant tumor originating from the adrenal gland. As reported in many

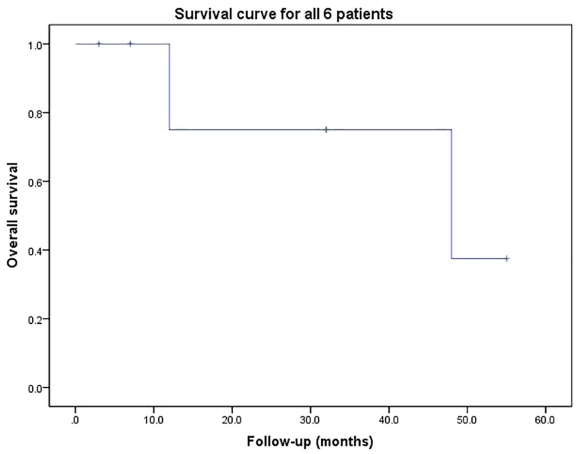

FIGURE 2
Survival curve for all 6 patients. The median survival of the six patients was 48 months.

10.3389/fonc.2023.1110045

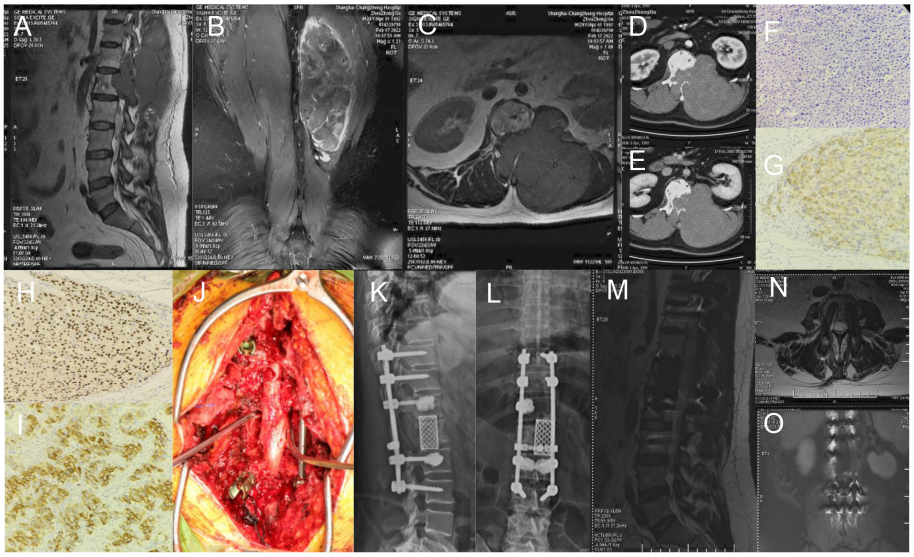

FIGURE 3
(A–C) Preoperative sagittal, coronal, and transverse MRI images of L1 vertebral body tumors; **(D, E)** Preoperative transverse CT scan showed L1 vertebral body tumors; **(F)** H&E staining of adrenocortical carcinoma; **(G–I)** Immunohistochemical stainings for Inhibin a, SF-1 and Syn; **(J)** She had a history of adrenal tumor (4 points). Visceral metastases were not detectable (0 point). Bone metastases were isolated (1 point). Her total prognostic score was 5 points. So, we chose the surgical strategy of total piecemeal resection. The tumor was excised by total piecemeal resection, pedicle screws, titanium mesh and titanium rods were used to reconstruct the stability; **(K, L)** Postoperative X-ray; **(M–O)** Postoperative sagittal, transverse, and coronal MRI.

studies (6, 7, 16), SMMAT has a man predominance, mainly affecting individuals aged 40-60 years. ACC bone metastasis has a woman predominance with a female to male ratio of 2:1, whereas MP bone metastasis has a male predominance. The overall ratio of SMMAT is roughly the same. As ACC spinal metastasis is much rarer than MP spinal metastasis, the number of cases and reports is variable. Similar results were obtained in our center, with a man age of 42.2 years and a male to female ratio of 4:2. Most metastases of malignant adrenal tumors are more likely to occur in the thoracic vertebrae, probably due to the proximity of the adrenal gland to the thoracic vertebrae (7, 17). Due to the extremely low incidence of SMMAT, there is a lack of alertness and understanding of the disease. It is our hope that our experience, together with the patients reported in the literature, could help better understand the clinical characteristics, diagnosis and treatment of the disease.

There are no data available on the specific time from adrenal tumor resection to spinal metastasis. In our center, the mean time from adrenal tumor resection to diagnosis of spinal metastasis is 77.5 (range: 9-216) months. As the time span from adrenal tumor resection to spinal metastasis is wide and varied, it is still necessary to be alert to the occurrence of bone metastasis after adrenal tumor resection, especially spinal metastasis.

The diagnosis of patients with SMMAT represents one of the most complex and difficult problems facing clinicians. The diagnosis is usually based on pathology. In most cases of SMMAT, the clinical symptoms are caused by spinal cord compression characterized by radiating pain and varying degrees of decline in muscle strength (18, 19). Notably, two of our four MP patients with MP developed hypertension, which did not seem to be well responsive to conventional antihypertensive drug treatment. Like other spinal metastases, SMMAT is not radiographically specific (20, 21). In our case series, SMMAT presented low signals on T1-weighted imaging and moderate signals on T2-weighted MRI. On CT imaging, the diseased vertebral body showed osteolytic changes, with obvious enhancement in the edge of the lesion. All the patients in our series had a history of adrenal tumor resection. Therefore, the diagnosis of SMMAT should be considered in patients with spinal tumors who have a history of adrenal tumor resection. We recommend needle biopsy for such patients to confirm the diagnosis. Although we emphasize the importance of percutaneous needle biopsy, patients with severe neurological symptoms caused by spinal cord compression often refused to receive needle biopsy for fear of causing dissemination of cancer cells or delaying treatment.

In our center, the time from symptom onset to various degrees of muscle loss and paraplegia averaged 3.3 months for SMMAT. Compared with the 3.8-month duration of symptoms in liver cancer spinal metastasis (22), and the 4.4-month duration in clear cell renal cell carcinoma (ccRCC) (23), the progression of SMMAT seems more rapid and the degree of malignancy is relatively higher. Therefore, SMMAT is more likely to cause spinal cord compression leading to paralysis. Meanwhile, surgery for spinal metastasis is gaining acceptance, which is an effective treatment for spinal metastasis (9). In our center, all patients achieved different degrees of neurological function improvement and better mobility after surgery. Notably, thanks to rapid and timely surgical treatment, two patients (Cases 3 and 6) in our series recovered from being unable to ambulate (Frankel grade B) before operation to being able to ambulate after operation. We advocate giving patients surgery as early as possible if they are well prepared.

Surgical strategies

In recent years, the understanding of surgery for spinal metastasis has changed. It is generally accepted that surgery could be considered when a patient has a life expectancy of more than 3 months (24). More recent evidence has shown that MDT can undoubtedly bring about better outcomes as compared with radiotherapy or chemotherapy alone, as represented by the improved quality of life after surgery (25, 26). Indications for surgery include intractable pain, spinal cord compression, and the need for stabilization of impending pathological fractures (27). The six patients in our series had definite spinal cord compression by imaging analysis and cancer pain that was difficult to be controlled by drugs. However, there are controversies over the surgical modality for spinal metastasis. In our series, total en-bloc resection was performed in one patient (Case 6), subtotal resection in one patient (Case2), and total piecemeal resection in the other four patients. Compared with patients who received subtotal resection and laminectomy (Table 2), patients who received total resection had a better prognosis in terms of neurological function and survival. In addition, one patient who received total en-bloc resection had better performance in local tumor recurrence control, indicating that local tumor control is important in SMMAT. For patients with a solitary lesion and surgical indications, en-bloc resection is suggested, though this tentative idea needs to be verified by more studies due to the limited number of patients in our series.

Relevant studies present (28–30) that adrenal tumor is a hypervascular tumor with highly variable blood pressure, especially in MP. MP commonly produces one or more catecholamines, and the excess secretion of catecholamines may cause a wide array of clinical features, including hypertension (30). However, in the SMMAT patients of our series, intraoperative blood pressure did not fluctuate significantly. In addition, comparison of the surgical information of the six patients showed that the intraoperative blood loss of patients and time of surgery with preoperative embolization were lower than those of patients without embolization. Moreover, the risk factors of hemodynamic instability during the perioperative period were greatly reduced. It was reported (29, 31, 32) that preoperative embolization of spinal metastasis was safe and effective in reducing intraoperative blood loss, which also could simplify the surgical procedures. Therefore, we recommend preoperative embolization for all patients with SMMAT to ensure perioperative safety.

Adjunctive therapy

For the adjuvant treatment of SMMAT, the team consulted about the therapeutic schedule of primary adrenal tumors. The effectiveness of radiotherapy on adrenal carcinoma has been recognized. Gonias et al. (33) affirmed the efficacy of high-dose [131I] MIBG in metastatic malignant pheochromocytoma. It was also reported that (3) adjuvant radiotherapy reduced the risk of local recurrence in ACC. However, there are controversies over the efficacy of chemotherapy for adrenal spinal metastasis. Some researchers believed (34, 35) that chemotherapy had beneficial effects on local tumor control and prolongation of survival, while others (33, 36) argued that it lacked support from large clinical trials; in addition, these trials were mostly retrospective so they could not provide direct evidence. We highlight the pros and cons of adjuvant therapy and insist that patients should have the right to choose the treatment independently. Finally, four of our six patients received radiotherapy, of whom two died of

TABLE 2 Literature review for SMMAT.

No.	Author [ref.]	Age, sex	Adjunctive therapy	Time of spinal metastasis	Location	Pathology	Operation	LR/ meta	Last status
1	Daniel Lee et al. (10)	55/M	Radiotherapy	5	T12	ACC	TER	None	NA
2	Drane WE et al. (11)	69/F	None	NA	L1	ACC	laminectomy	SM	Dead at 1 years
3	Ishida K et al. (12)	48/F	Chemotherapy	NA	S	ACC	None	SM	Dead at 1 years
4	Kheir E. et al. (13)	69/F	Radiotherapy	12	C6-C7	MP	SR	NA	NA
5	Yurt A et al. (14)	47/M	None	NA	T8-T9	MP	laminectomy	None	NA
6	Kaloostian PE et al. (15)	28/M	Chemotherapy	21	L3-L4	MP	SR	None	Alive
7	Kaloostian PE et al. (15)	41/M	None	36	T5-T7	MP	SR	SM	NA
8	Kaloostian PE et al. (15)	62/F	None	54	L1	MP	SR	None	Dead at 1 years
9	Kaloostian PE et al. (15)	23/M	Chemotherapy+ Radiotherapy	144	T10	MP	TER	None	NA
10	Kaloostian PE et al. (15)	21/F	Chemotherapy	NA	C7-T2,T4-T7	MP	SR + laminectomy	SM	Dead at 3 years

SMMAT, spinal metastasis of malignant adrenal tumor; LR/meta, local recurrence/metastasis; NA, not available; F, female; M, male; ACC, adrenocortical cancer; MP, malignant pheochromocytoma; TER, Total en-bloc resection; TPR, Total piecemeal resection; SR, Subtotal resection; SM, systemic metastasis.

recurrence and the other two were still alive at the last follow-up. We are reluctant to make a conclusion whether or not the adjuvant therapy is effective in SMMAT due to the limited number of the patients in our series. Despite this, radiotherapy and chemotherapy remain the preferred option for advanced SMMAT at present.

Prognosis

Although different types of adrenal tumor have the same origin, their prognoses may vary substantially. ACC seems to have the poorest prognosis, with a 5-year survival rate of 30% *vs.* 40% for MP (28, 37). Survival for spinal metastasis of ACC and MP is about 11 months (6) and 24 months (7) respectively. The median OS of the six patients in our series is 26.2 months, including the two patients who died of recurrence, which is relatively long as compared with other reports, though further statistical validation is required. On the one hand, we followed the standards of preoperative preparation strictly, and on the other hand, surgeons in the surgical team have rich experience. Compared with other carcinomas metastasized to the spine reported by our center, SMMAT showed a better prognosis than kidney cancer patients (17 months) and a poorer prognosis than liver (26.3 months) and prostate (44 months) cancer patients (22, 23, 38).

Comparison of the data between the disease-free patients (Case 1, 4 and 6) and the patients who developed recurrence or died (Cases 2, 3 and 5) showed that patients with smaller tumor sizes, a better state of health, the pathological type of MP, and better preoperative neurological function had better prognoses, suggesting that tumor size, pathological type, preoperative neurological function and the state of health may prove to be potential prognostic factors of SMMAT. However, we feel reluctant to draw a conclusion with statistical significance due to the limited number of the patients and the relatively short follow-up period. Larger-sample studies with longer follow-up periods are required to verify our findings and suggestions.

Limitation

Our study has several limitations. First, the retrospective nature is the main limitation. Second, due to the rarity of spinal metastasis of malignant adrenal tumor, the number of cases is too small. Moreover, our study lacked a control group without surgery.

Conclusion

SMMAT is a rare tumor with poor prognosis. The disease onset mainly presents as an osteolytic destruction. Spinal lesions can result in neurological dysfunction which seriously affecting the quality of life of the patients. The diagnosis of SMMAT is usually based on the pathology. And preoperative embolization, early surgical treatment, and total resection are usually associated with satisfactory clinical outcomes. The patient's health status, preoperative neurological function, tumor location and the resection mode are potential prognostic factors of spinal metastasis of malignant adrenal tumor. Larger-sample, multicenter and prospective studies are required to gain deeper insights into pathogenesis, diagnosis and management of the disease.

Data availability statement

The original contributions presented in the study are included in the article/Supplementary Material. Further inquiries can be directed to the corresponding authors.

Ethics statement

Written informed consent was obtained from the individual(s), and minor(s)' legal guardian/next of kin, for the publication of any potentially identifiable images or data included in this article.

Author contributions

TL: Conceptualization, Supervision, Methodology. JX: Supervision, Writing- Reviewing and Editing. XG: Visualization, Investigation. XN: Formal analysis, Investigation, Writing- Original draft preparation. JC: Data curation, Writing- Reviewing and Editing. JW: Data curation, Investigation. KZ: Data curation, Investigation. SH: Investigation. XH: Investigation. YS: Investigation. All authors contributed to the article and approved the submitted version.

Funding

This work was supported by the National Natural Science Foundation of China (82172779 and 81972506). There is no relevant financial activity outside the submitted work.

Conflict of interest

The authors declare that the research was conducted in the absence of any commercial or financial relationships that could be construed as a potential conflict of interest.

Publisher's note

Supplementary material

The Supplementary Material for this article can be found online at: https://www.frontiersin.org/articles/10.3389/fonc.2023.1110045/full#supplementary-material

SUPPLEMENTARY FIGURE 1
(A–C) Preoperative sagittal and transverse MRI images of L1-L2 vertebral body tumors; **(D, E)** Preoperative transverse CT scan showed L1-L2 vertebral body tumors; **(F, G)** She had a history of adrenal tumor (4 points). Visceral metastases were detectable (2 points). Bone metastases were multiple (2 points). Her total prognostic score was 8 points. So, we chose the surgical strategy of subtotal resection. The tumor was excised by subtotal resection, pedicle screws, bone cement and titanium rods were used to reconstruct the stability; **(H, I)** Postoperative X-ray.

SUPPLEMENTARY FIGURE 2
(A–C) Preoperative sagittal, coronal, and transverse MRI images of T3 vertebral body tumors; **(D)** Preoperative transverse CT scan showed T3 vertebral body tumors; **(E, F)** He had a history of adrenal tumor (4 points). Visceral metastases were not detectable (0 point). Bone metastases were isolated (1 point). His total prognostic score was 5 points. So, we chose the surgical strategy of total piecemeal resection. The tumor was excised by total piecemeal resection, pedicle screws, titanium mesh and titanium rods were used to reconstruct the stability; **(G, H)** Postoperative X-ray; **(I–K)** Postoperative sagittal, transverse, and coronal MRI.

SUPPLEMENTARY FIGURE 1
(A–C) Preoperative sagittal, coronal, and transverse MRI images of L1-L2 vertebral body tumors; **(D)** Preoperative transverse CT scan showed L1-L2 vertebral body tumors; **(E)** He had a history of adrenal tumor (4 points). Visceral metastases were not detectable (0 point). Bone metastases were isolated (1 point). His total prognostic score was 5 points. So, we chose the surgical strategy of total en-bloc resection. The tumor was excised by total en-bloc resection, pedicle screws, titanium mesh, bone cement and titanium rods were used to reconstruct the stability; **(F, G)** Postoperative X-ray.

References

1. Ahn CH, Kim JH. Best achievements in pituitary and adrenal diseases in 2020. *Endocrinol Metab (Seoul).* (2021) 36(1):51–6. doi: 10.3803/EnM.2021.108

2. Lee JM, Kim MK, Ko SH, Koh JM, Kim BY, Kim SW, et al. Clinical guidelines for the management of adrenal incidentaloma. *Endocrinol Metab (Seoul).* (2017) 32(2):200–18. doi: 10.3803/EnM.2017.32.2.200

3. Fassnacht M, Assie G, Baudin E, Eisenhofer G, de la Fouchardiere C, Haak HR, et al. Adrenocortical carcinomas and malignant phaeochromocytomas: ESMO-EURACAN clinical practice guidelines for diagnosis, treatment and follow-up. *Ann Oncol* (2020) 31(11):1476–90. doi: 10.1016/j.annonc.2020.08.2099

4. Ebbehoj A, Li D, Kaur RJ, Zhang C, Singh S, Li T, et al. Epidemiology of adrenal tumours in Olmsted county, Minnesota, USA: a population-based cohort study. *Lancet Diabetes Endocrinol* (2020) 8(11):894–902. doi: 10.1016/S2213-8587(20)30314-4

5. Libe R, Borget I, Ronchi CL, Zaggia B, Kroiss M, Kerkhofs T, et al. Prognostic factors in stage III-IV adrenocortical carcinomas (ACC): An European network for the study of adrenal tumor (ENSAT) study. *Ann Oncol* (2015) 26(10):2119–25. doi: 10.1093/annonc/mdv329

6. Berruti A, Libe R, Lagana M, Ettaieb H, Sukkari MA, Bertherat J, et al. Morbidity and mortality of bone metastases in advanced adrenocortical carcinoma: A multicenter retrospective study. *Eur J Endocrinol* (2019) 180(5):311–20. doi: 10.1530/EJE-19-0026

7. Liu S, Zhou X, Huo Z, Yao S, Wang Y, Liu Y. Clinical features and prognosis analysis of metastatic spinal pheochromocytoma: A single center retrospective study. *J Bone Oncol* (2020) 24:100312. doi: 10.1016/j.jbo.2020.100312

8. Ayala-Ramirez M, Palmer JL, Hofmann MC, de la Cruz M, Moon BS, Waguespack SG, et al. Bone metastases and skeletal-related events in patients with malignant pheochromocytoma and sympathetic paraganglioma. *J Clin Endocrinol Metab* (2013) 98(4):1492–7. doi: 10.1210/jc.2012-4231

9. Patchell RA, Tibbs PA, Regine WF, Payne R, Saris S, Kryscio RJ, et al. Direct decompressive surgical resection in the treatment of spinal cord compression caused by metastatic cancer: A randomised trial. *Lancet.* (2005) 366(9486):643–8. doi: 10.1016/S0140-6736(05)66954-1

10. Lee D, Yanamadala V, Shankar GM, Shin JH. Metastatic adrenal cortical carcinoma to T12 vertebrae. *J Clin Neurosci* (2016) 27:166–9. doi: 10.1016/j.jocn.2015.11.009

11. Drane WE, Graham MM, Nelp WB. Imaging of an adrenal cortical carcinoma and its skeletal metastasis. *J Nucl Med* (1983) 24(8):710–2.

12. Ishida K, Inoue Y, Woodhams R, Asano Y, Hara T. Imaging findings of pelvic tumor thrombosis extending from sacral bone metastasis of adrenocortical carcinoma. *Case Rep Radiol* (2012) 2012:919603. doi: 10.1155/2012/919603

13. Kheir E, Pal D, Mohanlal P, Shivane A, Chakrabarty A, Timothy J. Cervical spine metastasis from adrenal pheochromocytoma. *Acta Neurochir (Wien).* (2006) 148 (11):1219–20. doi: 10.1007/s00701-006-0892-4

14. Yurt A, Arda MN, Vardar E. Metastatic pheochromocytoma of the thoracic spinal extradural space. case report and review of the literature. *Kobe J Med Sci* (2005) 51(3-4):49–53.

15. Kaloostian PE, Zadnik PL, Kim JE, Groves ML, Wolinsky JP, Gokaslan ZL, et al. High incidence of morbidity following resection of metastatic pheochromocytoma in the spine. *J Neurosurg Spine.* (2014) 20(6):726–33. doi: 10.3171/2014.3.SPINE13535

16. Mesko S, Deegan BJ, D'Souza NM, Ghia AJ, Chapman BV, Amini B, et al. Spine stereotactic radiosurgery for metastatic pheochromocytoma. *Cureus.* (2019) 11(5):e4742. doi: 10.7759/cureus.4742

17. Liu S, Zhou X, Song A, Li WA, Rastogi R, Wang Y, et al. Successful treatment of malignant pheochromocytoma with sacrum metastases: A case report. *Med (Baltimore).* (2018) 97(35):e12184. doi: 10.1097/MD.0000000000012184

18. Gao X, Wu Z, Wang T, Cao J, Bai G, Xin B, et al. A discussion on the criteria for surgical decision-making in elderly patients with metastatic spinal cord compression. *Global Spine J* (2021) 2192568221991107.

19. Gao X, Zhao C, He S, Fan T, Xu W, Yang C, et al. Treatment and outcomes of 28 patients with spinal metastasis from gynecological cancer. *J Neurooncol.* (2018) 137 (2):387–94. doi: 10.1007/s11060-017-2728-x

20. Ribeiro J, Ribeiro RC, Fletcher BD. Imaging findings in pediatric adrenocortical carcinoma. *Pediatr Radiol* (2000) 30(1):45–51. doi: 10.1007/s002470050013

21. Takano A, Oriuchi N, Tsushima Y, Taketomi-Takahashi A, Nakajima T, Arisaka Y, et al. Detection of metastatic lesions from malignant pheochromocytoma and paraganglioma with diffusion-weighted magnetic resonance imaging: Comparison with 18F-FDG positron emission tomography and 123I-MIBG scintigraphy. *Ann Nucl Med* (2008) 22(5):395–401. doi: 10.1007/s12149-008-0128-1

22. Zhang D, Xu W, Liu T, Yin H, Yang X, Wu Z, et al. Surgery and prognostic factors of patients with epidural spinal cord compression caused by hepatocellular carcinoma metastases: Retrospective study of 36 patients in a single center. *Spine (Phila Pa 1976).* (2013) 38(17):E1090–5. doi: 10.1097/BRS.0b013e3182983bf8

23. Han S, Wang T, Jiang D, Yu Y, Wang Y, Yan W, et al. Surgery and survival outcomes of 30 patients with neurological deficit due to clear cell renal cell carcinoma spinal metastases. *Eur Spine J* (2015) 24(8):1786–91. doi: 10.1007/s00586-015-3912-3

24. Patnaik S, Turner J, Inaparthy P, Kieffer WK. Metastatic spinal cord compression. *Br J Hosp Med (Lond).* (2020) 81(4):1–10. doi: 10.12968/hmed.2019.0399

25. Ibrahim A, Crockard A, Antonietti P, Boriani S, Bunger C, Gasbarrini A, et al. Does spinal surgery improve the quality of life for those with extradural (spinal) osseous metastases? An international multicenter prospective observational study of 223 patients. invited submission from the joint section meeting on disorders of the spine and peripheral nerves, march 2007. *J Neurosurg Spine.* (2008) 8(3):271–8. doi: 10.3171/SPI/2008/8/3/271

26. Steinmetz MP, Mekhail A, Benzel EC. Management of metastatic tumors of the spine: strategies and operative indications. *Neurosurg Focus.* (2001) 11(6):e2. doi: 10.3171/foc.2001.11.6.3

27. Heary RF, Bono CM. Metastatic spinal tumors. *Neurosurg Focus.* (2001) 11(6):e1. doi: 10.3171/foc.2001.11.6.2

28. Almeida MQ, Bezerra-Neto JE, Mendonca BB, Latronico AC, Fragoso M. Primary malignant tumors of the adrenal glands. *Clinics (Sao Paulo).* (2018) 73(suppl 1):e756s. doi: 10.6061/clinics/2018/e756s

29. Pikis S, Itshayek E, Barzilay Y, Hasharoni A, Kaplan L, Gomori M, et al. Preoperative embolization of hypervascular spinal tumors: Current practice and center experience. *Neurol Res* (2014) 36(6):502–9. doi: 10.1179/1743132814Y.0000000361

30. Gunawardane PTK, Grossman A. Phaeochromocytoma and paraganglioma. *Adv Exp Med Biol* (2017) 956:239–59. doi: 10.1007/5584_2016_76

31. Thiex R, Harris MB, Sides C, Bono CM, Frerichs KU. The role of preoperative transarterial embolization in spinal tumors. a large single-center experience. *Spine J* (2013) 13(2):141–9.

32. Cernoch P, Hechelhammer L, von Hessling A, Spross C, Erhardt J, Jost B, et al. Pre-operative embolisation of spinal metastasis: Technique, complication rate and

outcome-clinical experience. *Int Orthop* (2015) 39(7):1399–404. doi: 10.1007/s00264-015-2769-8

33. Gonias S, Goldsby R, Matthay KK, Hawkins R, Price D, Huberty J, et al. Phase II study of high-dose [131I]metaiodobenzylguanidine therapy for patients with metastatic pheochromocytoma and paraganglioma. *J Clin Oncol* (2009) 27(25):4162–8. doi: 10.1200/JCO.2008.21.3496

34. Berruti A, Grisanti S, Pulzer A, Claps M, Daffara F, Loli P, et al. Long-term outcomes of adjuvant mitotane therapy in patients with radically resected adrenocortical carcinoma. *J Clin Endocrinol Metab* (2017) 102(4):1358–65. doi: 10.1210/jc.2016-2894

35. Ayala-Ramirez M, Feng L, Habra MA, Rich T, Dickson PV, Perrier N, et al. Clinical benefits of systemic chemotherapy for patients with metastatic pheochromocytomas or sympathetic extra-adrenal paragangliomas: Insights from the largest single-institutional experience. *Cancer*. (2012) 118(11):2804–12. doi: 10.1002/cncr.26577

36. Postlewait LM, Ethun CG, Tran TB, Prescott JD, Pawlik TM, Wang TS, et al. Outcomes of adjuvant mitotane after resection of adrenocortical carcinoma: A 13-institution study by the US adrenocortical carcinoma group. *J Am Coll Surg* (2016) 222 (4):480–90. doi: 10.1016/j.jamcollsurg.2015.12.013

37. Harari A, Inabnet WB3rd. Malignant pheochromocytoma: A review. *Am J Surg* (2011) 201(5):700–8. doi: 10.1016/j.amjsurg.2010.04.012

38. Meng T, Chen R, Zhong N, Fan T, Li B, Yin H, et al. Factors associated with improved survival following surgical treatment for metastatic prostate cancer in the spine: Retrospective analysis of 29 patients in a single center. *World J Surg Oncol* (2016) 14 (1):200. doi: 10.1186/s12957-016-0961-y

frontiers | Frontiers in Oncology

TYPE Original Research
PUBLISHED 08 February 2023
DOI 10.3389/fonc.2023.1125637

OPEN ACCESS

EDITED BY
Zhidao Xia,
Swansea University, United Kingdom

REVIEWED BY
Fengxia Chen,
Zhongnan Hospital, Wuhan University, China
Zhi Lv,
Second Hospital of Shanxi Medical University, China
Songfeng Chen,
First Affiliated Hospital of Zhengzhou University, China

*CORRESPONDENCE
Songxiang Liu
598628576@qq.com
Zhewei Ye
yezhewei@hust.edu.cn

†These authors have contributed equally to this work and share first authorship

‡These authors have contributed equally to this work and share last authorship

SPECIALTY SECTION
This article was submitted to Surgical Oncology, a section of the journal Frontiers in Oncology

RECEIVED 16 December 2022
ACCEPTED 13 January 2023
PUBLISHED 08 February 2023

CITATION
Huo T, Xie Y, Fang Y, Wang Z, Liu P, Duan Y, Zhang J, Wang H, Xue M, Liu S and Ye Z (2023) Deep learning-based algorithm improves radiologists' performance in lung cancer bone metastases detection on computed tomography.
Front. Oncol. 13:1125637.
doi: 10.3389/fonc.2023.1125637

Deep learning-based algorithm improves radiologists' performance in lung cancer bone metastases detection on computed tomography

Tongtong Huo[1,2†], Yi Xie[1†], Ying Fang[1†], Ziyi Wang[2], Pengran Liu[1], Yuyu Duan[3], Jiayao Zhang[1], Honglin Wang[1], Mingdi Xue[1], Songxiang Liu[1*‡] and Zhewei Ye[1*‡]

[1]Department of Orthopedics, Union Hospital, Tongji Medical College, Huazhong University of Science and Technology, Wuhan, China, [2]Research Institute of Imaging, National Key Laboratory of Multi-Spectral Information Processing Technology, Huazhong University of Science and Technology, Wuhan, China, [3]Department of Radiology, Union Hospital, Tongji Medical College, Huazhong University of Science and Technology, Wuhan, China

Purpose: To develop and assess a deep convolutional neural network (DCNN) model for the automatic detection of bone metastases from lung cancer on computed tomography (CT)

Methods: In this retrospective study, CT scans acquired from a single institution from June 2012 to May 2022 were included. In total, 126 patients were assigned to a training cohort (n = 76), a validation cohort (n = 12), and a testing cohort (n = 38). We trained and developed a DCNN model based on positive scans with bone metastases and negative scans without bone metastases to detect and segment the bone metastases of lung cancer on CT. We evaluated the clinical efficacy of the DCNN model in an observer study with five board-certified radiologists and three junior radiologists. The receiver operator characteristic curve was used to assess the sensitivity and false positives of the detection performance; the intersection-over-union and dice coefficient were used to evaluate the segmentation performance of predicted lung cancer bone metastases.

Results: The DCNN model achieved a detection sensitivity of 0.894, with 5.24 average false positives per case, and a segmentation dice coefficient of 0.856 in the testing cohort. Through the radiologists-DCNN model collaboration, the detection accuracy of the three junior radiologists improved from 0.617 to 0.879 and the sensitivity from 0.680 to 0.902. Furthermore, the mean interpretation time per case of the junior radiologists was reduced by 228 s (p = 0.045).

Conclusions: The proposed DCNN model for automatic lung cancer bone metastases detection can improve diagnostic efficiency and reduce the diagnosis time and workload of junior radiologists.

KEYWORDS

artificial intelligence, deep learning, deep convolutional neural network, lung cancer bone metastases, computer-aided diagnosis

1 Introduction

Lung cancer (LC) is the main cause of cancer-related deaths globally (1). Approximately 1.5 million people are diagnosed with LC every year, with 1.3 million deaths (2). Furthermore, bone is the most common and the initial site of metastases from LC (3). Approximately 30%–70% of bone metastases are associated with LC, and 20%–30% of patients with LC already have bone metastases upon initial diagnosis (4). LC is often asymptomatic at the initial stage. Therefore, patients possibly already have metastases at diagnosis (5, 6). Although bone metastases may progress to pathologic fracture and/or nerve and spinal cord compression; some patients have no painful symptoms at the time of detection (7, 8). Once a tumor metastasizes to the bone, it is practically incurable and has a high mortality rate (9). Therefore, early detection of bone metastasis is important for decreasing morbidity as well as for disease staging, outcome prediction, and treatment planning (10).

Imaging is an important part of the management of bone metastasis (11–13). Computed tomography (CT) has the advantages of good anatomical resolution, soft-tissue contrast, and detailed morphology (14, 15). It also facilitates simultaneous evaluation of the primary and metastatic lesions (12, 16). The most important advantage of CT is the relatively low cost, which is very patient-friendly (17). Thus, in the clinical setting, CT is the most commonly used imaging for the diagnosis of primary cancer and whole-body staging when bone metastases are suspected (17, 18). The measurements of all metastatic lesions are time-consuming, especially, if multiple metastases are present. The heavy workload of image evaluation can be tiresome for radiologists, thus increasing the risk of missing lesions and leading to decreased sensitivity (19). Therefore, automated analysis of CT images is ideal for assisting radiologists in the accurate diagnosis of bone metastasis from LC.

Deep learning has been identified as a key sector in which artificial intelligence could streamline pathways, acting as a triage or screening service, decision aid, or second-reader support for radiologists (20). By now, artificial intelligence with deep convolutional neural network (DCNN) has been exploited to develop automated diagnosis and classification of cancer, including prostate cancer (21, 22), pancreatic cancer (23), gastric cancer (24, 25), breast cancer (26, 27), and LC (28–30). Furthermore, there has been a line of research on DCNN-based automated classification of CT images for the detection of metastasis caused by various primary tumors including gastric cancer (30), breast cancer (31), LC (32), and thyroid cancer (33). There is emerging evidence suggesting that DCNN could also be used to extract information from bone scan images for the automatic detection of LCBM (34, 35).

In this study, we developed a DCNN model that automated detecting LC bone metastases (LCBM) on CT and validated the model internally and externally. We also compared the DCNN model with five radiologists and explored whether it could enhance the diagnostic accuracy of junior radiologists.

Abbreviations: LCBM, Lung cancer bone metastases; AI, Artificial intelligence; DL, Deep learning; DCNN, Deep convolutional neural network; AUC, Area under the receiver operating characteristic curve; PPV, positive predictive value; NPV, Negative predictive value; CT, Computed tomography; ROC, Receiver operating characteristic; ROI, Region of interest; FPs, False positive; IoU, Intersection-over-Union.

2 Materials and methods

2.1 Patients

We collected 102 patients with pathologically confirmed primary LC who were confirmed to have synchronous or metachronous bone metastases and 100 patients who were confirmed to not have bone metastases by CT-guided biopsy pathology from June 2012 to May 2022. After reviewing the clinical and imaging data, we excluded patients who did not undergo CT examination (n = 53); who underwent surgery, chemotherapy, and radiation therapy for bone metastases before CT examination (n = 9); and who had poor CT image quality (n = 14). Finally, the CT images from 126 patients were included for the DCNN model development to detect bone metastases from LC, including a positive sample dataset of patients with biopsy-proven LC and bone metastases (n = 57), and a negative sample dataset of patients with biopsy-proven LC without bone metastases (n = 69). The process of patient enrollment is shown in Figure 1.

We randomly split the whole dataset (n = 126) into three cohorts: training (76 cases, to train the DCNN model), internal validation (12 cases, to fine-tune the hyper-parameters of the DCNN model), and external testing (38 cases, to evaluate the model and radiologists' performance). Furthermore, the patients included in the validation and testing datasets were excluded from the training dataset.

2.2 Imaging preprocessing and annotation

The clinical and imaging information of all patients was obtained through the medical record system and follow-up. To protect patients' privacy, all identifying information, such as name, sex, age, and ID, on CT was anonymized and omitted through image processing when data were first acquired. After image preprocessing in the Digital Imaging and Communications in Medicine (DICOM) format, complete thin-layer CT images were stored (see Supplementary Methods for CT protocols). The manual annotations of bone metastases were performed using LabelMe (36) with an image segmentation software (Mimics; Materialize, Belgium).

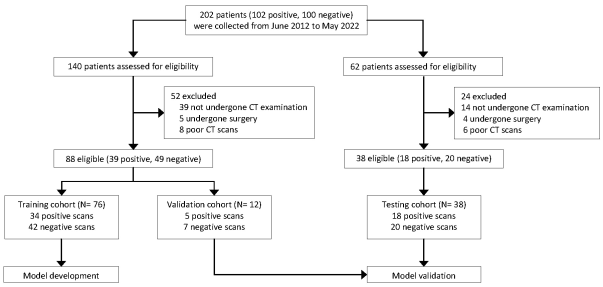

FIGURE 1
Flow chart showing the overall study process. All computed tomography (CT) scans were retrospectively collected from the clinical databases of a single institution.

Two board-certified radiologists (8 and 9 years of experience in CT diagnosis) evaluated all CT examinations and, section by section, manually annotated five locations (spine, pelvis, limb, sternum, and clavicle) on the CT images of patients with LCBM. Two expert radiologists (14 and 20 years of experience in CT diagnosis, respectively) checked and manually delineated the volume of interest of the bone metastatic lesion in a voxel-wise manner on CT images using the diagnosis reports from two board-certified radiologists for establishing the reference standard of bone metastases. Furthermore, both of them repeated the annotations and modifications at least 3 weeks later and used them as ground truth (GT) labels for diagnosis and evaluation.

2.3 Model development

We developed a cascaded three-dimensional (3D) U-Net with 3D spatial SE modules and 3D GAU modules based on 3D U-Net (37), which is a robust state-of-the-art DCNN-based medical image segmentation method (see Supplementary Methods for training protocol). The Cascaded 3D U-Net (38) contains two 3D U-net architectures, wherein the first one is trained on down-sampled images and the second one is trained on full-resolution images. Training on down-sampled images first can enlarge the size of patches concerning the image and also enable the 3D U-Net network to learn more contextual information. Training on full-resolution images next refines the segmentation results predicted from the former 3D U-Net.

The 3D Spatial SE (39) module and 3D GAU (40) module are used more fully as the spatial attention module and the channel attention module to exploit the multiscale and multilevel features, respectively; they guide DCNN to efficiently focus on the targets rather than the background. The flowchart of our DCNN model for segmenting bone metastases is shown in Figure 2. The input of the end-to-end DCNN model is the 3D CT volume, and the output is the segmentation result of the bone metastases margin and the possibility of LCBM.

2.4 Observer study

To scale the proposed deep learning system with human readers, five radiologists (no overlap with the radiologists who labeled and checked the annotations) with 3–8 years of experience in CT diagnosis were required to participate in an independent human-only observer study. These radiologists were randomly shown the testing dataset to independently segment bone metastases and record the localization (corresponding CT layers); they were blinded to the bone metastases results and patient information.

To simulate the real clinical scenario, a radiologists-DCNN model collaboration study was conducted on three junior radiologists with 1–3 years of CT diagnostic experience, besides the independent observer study. These radiologists independently assessed the images to reach the first conclusion (whether bone metastases are present). Readouts of the DCNN model, including lesion labeling and probability of LCBM, were sent to the radiologists for reevaluating the images. The second assessment of radiologists served as the final output. In addition, we scheduled the 8 radiologists to perform the test in different locations to ensure their relative independence.

2.5 Statistical analysis

Our method followed a segmentation methodology to perform a detection task; therefore, both segmentation and detection metrics were important for evaluating the DCNN model performance. The metastases segmentation performance of the network was assessed using the metrics of dice coefficient and Intersection-over-Union (IoU) (41). The dice value indicates the overlapped voxels between the predicted results and GT. Its mathematical definition is as follows:

$$Dice(P, G) = \frac{2|P \cap G|}{|P| + |G|}$$

where denotes the number of labeled voxels, and P and G represent the predicted and GT values, respectively. The larger the

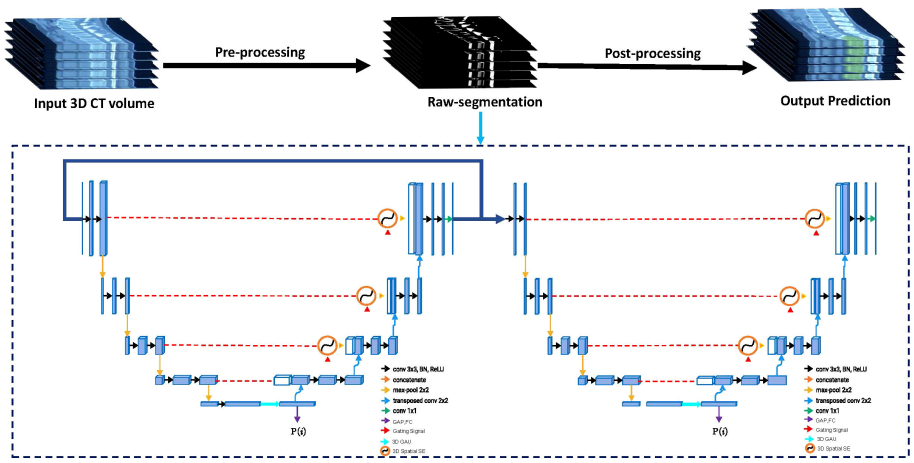

FIGURE 2
The flowchart of the proposed Cascaded 3D-Unet network. The network structure is divided into two parts: encoder and decoder. Between the encoder and decoder, we used the three-dimensional (3D) spatial squeeze and excitation modules (3D Spatial SE) and 3D global attention-up sample modules (3D GAU) to replace the original skip connections used in 3D U-Net.

value of the dice, the higher the degree of overlap between the segmentation prediction and GTs.

The evaluation of detection performance was based on case-based analysis; cases with at least one positive lesion were considered true positive (TP). We compared the model predictions with radiologists with TPs, false negatives (FNs), and false positives (FPs). According to the TP rate (sensitivity) versus the FP rate (1-specificity), we calculated the areas under the receiver operating characteristic (ROC) curve (AUC) and the 95% confidence interval (CI) for the five radiologists (averaged), DCNN model alone, three junior radiologists alone (averaged), and DCNN-assisted three junior radiologists. $P< 0.05$ was considered statistically significant. All statistical analyses were performed using SPSS 22.0 (IBM Corp., Armonk, NY, USA). The interpretation time for each scan was recorded automatically by the viewer and the detection time of the DCNN model was obtained from the computer terminal.

3 Results

No significant difference was noted in age or sex among the monocentric training, validation, and testing cohorts. In total, 34 positive and 42 negative scans were collected for the training dataset. The validation dataset comprised five positive and seven negative scans, and the testing dataset comprised 18 positive and 20 negative scans. The characteristics of the training, validation, and testing cohorts are listed in Table 1.

3.1 Performance of the DCNN model

A threshold of 0.5 (IoU > 0.5) was defined as the detection hit criterion; then, the segmentation metrics were computed with the GT labels generated in the image annotation procedure. At a threshold of

TABLE 1 Characteristics of patients in the three datasets.

Variables	Training Cohort (N=76)	Validation Cohort (N=12)	Testing Cohort (N=38)	Total (N=126)	P value
Age (years), mean ± SD	61.55 ± 13.22	61.48 ± 13.14	61.41 ± 13.45	61.52 ± 13.25	<0.001
Gender					<0.001
Male	44 (57.8%)	7 (58.3%)	22 (57.9%)	73 (57.9%)	
Female	32 (42.2%)	5 (41.7%)	16 (42.1%)	53 (42.1%)	
Positive with bone metastases	33 (43.4%)	5 (41.7%)	19 (50.0%)	57 (45.2%)	
Bone metastasis site					0.417
Spine	14 (42.4%)	2 (40.0%)	8 (42.1%)	24 (42.1%)	
Pelvis	10 (30.3%)	1 (20.0%)	6 (31.6%)	17 (29.8%)	
Limb	5 (15.2%)	1 (20.0%)	3 (15.8%)	9 (15.8%)	
Sternum	3 (9.1%)	1 (20.0%)	2 (10.5%)	6 (10.5%)	
Clavicle	1 (3.0%)	0 (0.0%)	0 (0.0%)	1 (1.8%)	
Negative without bone metastases	43 (56.6%)	7 (58.3%)	19 (50.0%)	69 (54.8%)	
Brain metastases	9 (20.9%)	2 (28.6%)	4 (21.1%)	15 (21.7%)	
Liver metastases	26 (60.5%)	4 (57.1%)	12 (63.2%)	42 (60.9%)	
Lymph nodes metastases	8 (18.6%)	1 (14.3%)	3 (15.8%)	12 (17.4%)	
Primary Subtype					0.034
Small cell lung cancer (SCLC)	63 (82.9%)	10 (83.3%)	32 (84.2%)	105 (83.3%)	
Adenocarcinoma (LUAD)	13 (17.1%)	2 (16.7%)	6 (15.8%)	21 (16.7%)	
Number of tumors					0.002
Single	59 (77.6%)	9 (77.6%)	31 (81.6%)	99 (78.8%)	
Multiple (2)	17 (22.4%)	3 (22.4%)	8 (18.4%)	27 (21.4%)	
Tumor size					0.124
$0 \leq X \leq 3$	16 (20.5%)	2 (16.7%)	8 (21.1%)	26 (20.3%)	
$3 < X \leq 5$	25 (32.9%)	3 (25.0%)	13 (34.2%)	41 (32.5%)	
$5 < X \leq 7$	17 (22.4%)	4 (33.3%)	9 (23.7%)	30 (23.8%)	
>7	18 (23.7%)	3 (25.0%)	8 (21.1%)	29 (23.0%)	
Grade					0.297

(Continued)

TABLE 1 Continued

Variables	Training Cohort (N=76)	Validation Cohort (N=12)	Testing Cohort (N=38)	Total (N=126)	P value
Grade I	4 (5.3%)	3 (25.0%)	9 (23.7%)	31 (24.6%)	
Grade II	19 (25.0%)	8 (66.7%)	23 (60.5%)	75 (59.5%)	
Grade III	44 (57.9%)	1 (8.3%)	4 (10.5%)	14 (11.1%)	
Grade IV	9 (11.8%)	3 (25.0%)	9 (23.7%)	31 (24.6%)	

For patient age, the mean age and standard deviation are presented, with a range of values in parentheses. For other data, the number of patients is presented, with percentages in parentheses.

0.5, the detection sensitivity of our DCNN model was 0.898 with 5.23 average FPs for the validation dataset and 0.894 with 5.24 average FPs for the testing dataset. Besides, our DCNN model achieved an acceptable segmentation performance (dice = 0.859 and 0.856 on the validation and testing datasets, respectively). The overall results of the DCNN model for the validation and testing datasets are shown in Table 2. An illustration of the predicted segmentation by DCNN is shown in Figure 3, where all cases were predicted with highly similar segmentation to GT.

3.2 Comparison with other networks and radiologists

We compared our model with several state-of-the-art deep neural networks in the validation and testing datasets to validate the effectiveness of the proposed DCNN model (Figure 4 and Table 2). As shown in the results, the Cascaded 3D U-Net outperformed the 3D U-NET and 3D FCN (42) by large margins, which verified the effectiveness of network design in the proposed DCNN model. Moreover, the results of the ablation experiments demonstrated the best performance of our 3D U-Net with a 3D GAU module and 3D spatial SE module.

We performed observer studies and compared them with five radiologists using all images in the testing dataset to characterize the diagnostic value of the DCNN model. The DCNN model achieved high performance, outperforming any radiologists for LCBM detection with respect to both the primary metric AUROC (0.875 vs. 0.819 for the best radiologist) and sensitivity (0.894 vs. 0.892) tested in the observer-independent study. As for segmentation performance, our DCNN model outperformed all other networks and five radiologists (Table 2).

TABLE 2 Results of comparison with other networks and five radiologists on the testing cohort.

	AUROC (95% CI)	Accuracy (95% CI)	Sensitivity (95% CI)	Specificity (95% CI)	IoU	Dice	Avg FP
Validation Cohort							
3D FCN	0.775 (0.746–0.803)	0.777 (0.724–0.823)	0.811 (0.792–0.840)	0.741 (0.720–0.766)	0.674 (0.643–0.750)	0.766 (0.736–0.796)	7.64
3D U-NET	0.781 (0.746–0.810)	0.790 (0.738–0.836)	0.810 (0.790–0.843)	0.752 (0.741–0.779)	0.681 (0.686–0.791)	0.785 (0.759–0.819)	7.20
3D GAU U-Net	0.805 (0.798–0.832)	0.807 (0.787–0.821)	0.784 (0.760–0.806)	0.834 (0.809–0.859)	0.693 (0.680–0.722)	0.794 (0.758–0.828)	5.97
3D SSE U-Net	0.853 (0.845–0.881)	0.853 (0.838–0.868)	0.860 (0.795–0.889)	0.850 (0.825–0.873)	0.750 (0.721–0.784)	0.827 (0.781–0.859)	5.65
Cascaded 3D U-Net	0.871 (0.849–0.880)	0.877 (0.821–0.907)	0.893 (0.881–0.905)	0.866 (0.835–0.875)	0.751 (0.701–0.790)	0.843 (0.812–0.888)	5.41
Our network	**0.883 (0.878–0.901)**	**0.886 (0.842–0.922)**	**0.898 (0.881–0.905)**	**0.863 (0.835–0.875)**	**0.782 (0.741–0.810)**	**0.859 (0.826–0.884)**	**5.23**
Testing Cohort							
3D FCN	0.771 (0.749–0.784)	0.773 (0.751–0.794)	0.806 (0.789–0.822)	0.736 (0.710–0.759)	0.677 (0.651–0.754)	0.762 (0.732–0.790)	7.74
3D U-NET	0.775 (0.756–0.796)	0.784 (0.787–0.801)	0.802 (0.785–0.818)	0.748 (0.723–0.770)	0.680 (0.664–0.782)	0.781 (0.750–0.818)	7.50
3D GAU U-Net	0.803 (0.776–0.834)	0.810 (0.799–0.853)	0.778 (0.761–0.818)	0.817 (0.801–0.844)	0.691 (0.674–0.718)	0.791 (0.764–0.823)	6.12
3D SSE U-Net	0.846 (0.828–0.867)	0.847 (0.783–0.897)	0.857 (0.786–0.891)	0.847 (0.819–0.868)	0.749 (0.720–0.798)	0.822 (0.779–0.855)	5.74
Cascaded 3D U-Net	0.868 (0.838–0.872)	0.875 (0.834–0.908)	0.887 (0.881–0.905)	0.854 (0.835–0.867)	0.750 (0.706–0.783)	0.841 (0.810–0.888)	5.58
Our network	**0.875 (0.863–0.883)**	**0.878 (0.867–0.886)**	**0.894 (0.874–0.896)**	**0.857 (0.831–0.885)**	**0.789 (0.733–0.808)**	**0.856 (0.820–0.885)**	**5.24**
Radiologist 1	0.785 (0.759–0.800)	0.771 (0.755–0.798)	0.846 (0.797–0.887)	0.766 (0.737–0.783)	0.642 (0.611–0.688)	0.726 (0.698–0.750)	3.25
Radiologist 2	0.792 (0.776–0.822)	0.793 (0.768–0.802)	0.861 (0.813–0.900)	0.769 (0.733–0.787)	0.668 (0.639–0.690)	0.741 (0.700–0.777)	3.10
Radiologist 3	0.795 (0.779–0.799)	0.799 (0.773–0.813)	0.876 (0.830–0.913)	0.776 (0.753–0.796)	0.679 (0.652–0.721)	0.750 (0.712–0.789)	2.68
Radiologist 4	0.804 (0.791–0.825)	0.810 (0.795–0.827)	0.880 (0.875–0.925)	0.792 (0.770–0.819)	0.691 (0.670–0.744)	0.769 (0.722–0.808)	2.14

(Continued)

TABLE 2 Continued

	AUROC (95% CI)	Accuracy (95% CI)	Sensitivity (95% CI)	Specificity (95% CI)	IoU	Dice	Avg FP
Radiologist 5	0.819 (0.800–0.849)	0.822 (0.801–0.839)	0.892 (0.891–0.929)	0.807 (0.792–0.831)	0.717 (0.700–0.762)	0.798 (0.759–0.841)	1.80
Average of five radiologists	0.799 (0.772–0.821)	0.799 (0.782–0.834)	0.871 (0.841–0.899)	0.782 (0.758–0.800)	0.679 (0.654–0.702)	0.757 (0.730–0.783)	2.59

A comparison of detection and segmentation performance in the testing dataset of our proposed network (Cascaded 3D U-Net with 3D GAU modules and the 3D SSE modules), five other deep neural networks [Cascaded 3D U-Net, 3D FCN, 3D U-net, 3D GAU U-Net (3D U-Net with 3D global attention-up sample modules, and 3D SSE U-Net (3D U-Net with spatial squeeze and excitation modules)]. FP: false positives per scan. IoU: Intersection-over-Union. Dice: dice coefficient The bolded words "Our network" represent our proposed network (Cascaded 3D U-Net with 3D GAU modules and the 3D SSE modules). The bolded words "Validation Cohort" and "Testing Cohort" represent two equal cohorts containing different data.

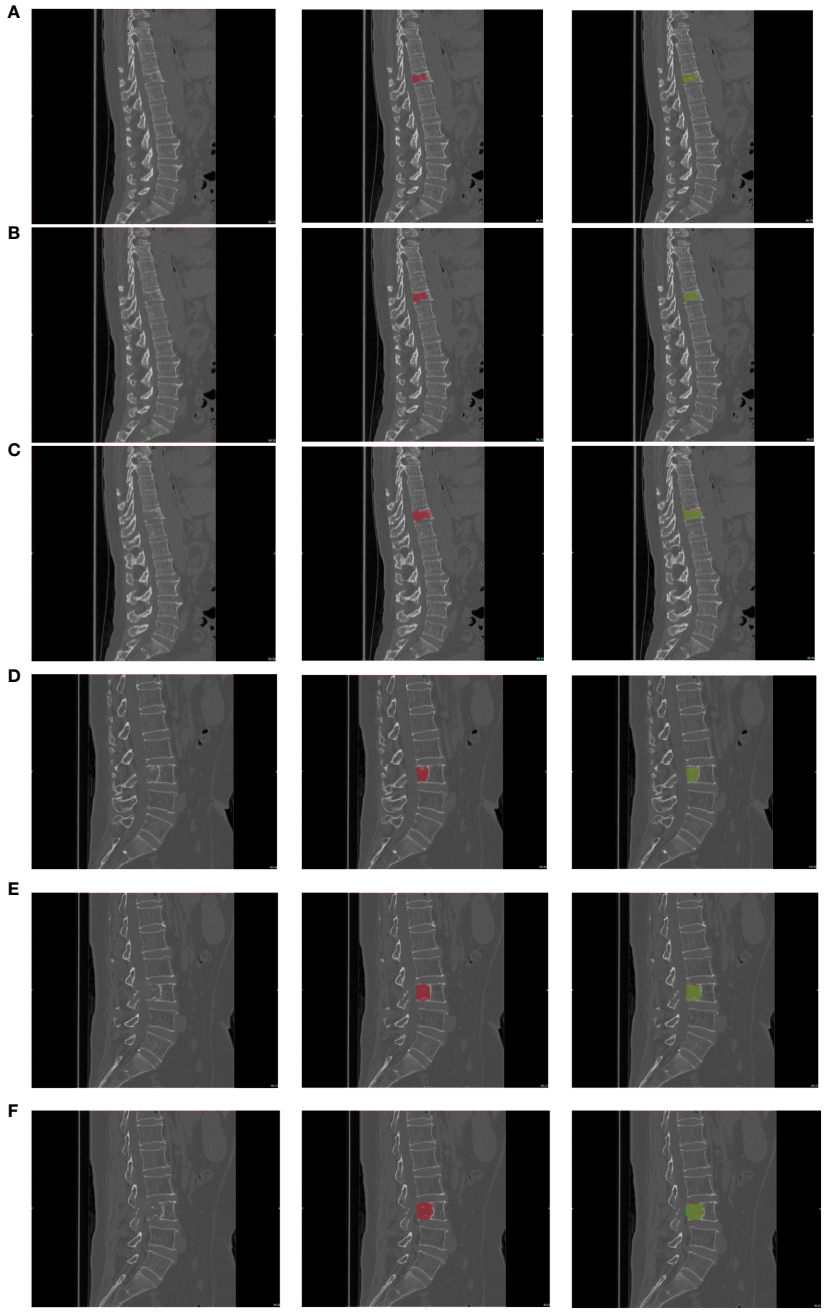

FIGURE 3
The segmentation results. Representative example of a patient with lung cancer bone metastasis with abnormal signals in the 4 lumbar spine **(A–C)** and a patient with lung cancer bone metastasis with abnormal signals in the 11 thoracic spine **(D–F)**, and true-positive lesions with various appearances and locations. From left to right, the three images in a row are the original image, the corresponding GT label (red), and the candidate region output from the deep convolutional neural network (DCNN) (green). Note that the green region on the right image is a candidate region with a threshold of 0.5, and dice was calculated on this region.

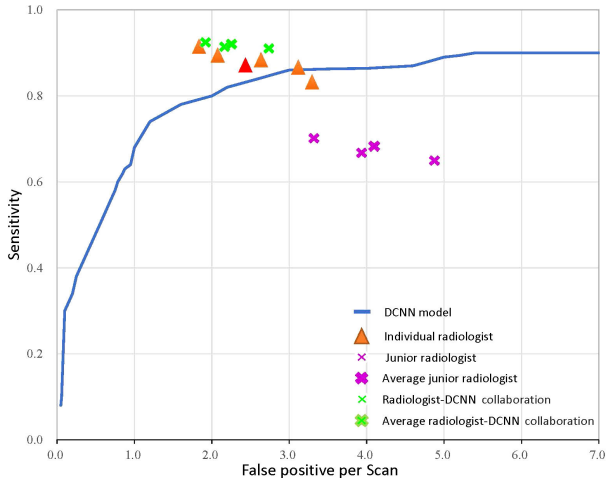

FIGURE 4
The receiver operator characteristic curve for the performance of the deep convolutional neural network (DCNN) model-only, radiologist-only, junior radiologist-only, and junior radiologists-DCNN model collaboration detection performance. Each orange triangle represents the performance of an individual radiologist; each pink fork represents the performance of a junior radiologist without the aid of DCNN; and each green fork represents the performance of a junior radiologist with the aid of DCNN. The red triangle indicates the average value of five radiologists, and the bolded forks indicate the average value of junior radiologists.

TABLE 3 A comparison of the DCNN model and three junior radiologists without and with the DCNN model.

		Age (year)	Experiences (year)	AUROC (95% CI)	Accuracy (95% CI)	Sensitivity (95% CI)	IoU	Dice	Avg Time (s)	Avg FP
DCNN Model		–	–	**0.875 (0.863–0.883)**	**0.878 (0.867–0.886)**	**0.894 (0.874–0.896)**	**0.789 (0.733–0.808)**	**0.856 (0.820–0.885)**	**27**	**5.24**
Junior radiologist only	R6	25	1.5	0.584 (0.567–0.612)	0.597 (0.575–0.614)	0.657 (0.531–0.768)	0.498 (0.480–0.515)	0.589 (0.568–0.610)	412	4.89
	R7	31	2	0.601 (0.588–0.620)	0.609 (0.590–0.632)	0.672 (0.546–0.782)	0.576 (0.534–0.604)	0.663 (0.638–0.686)	312	3.95
	R8	34	3	0.643 (0.611–0.668)	0.645 (0.622–0.671)	0.711 (0.695–0.741)	0.620 (0.586–0.645)	0.708 (0.684–0.733)	387	3.36
	Avg	**30**	**2.17**	**0.609 (0.591–0.634)**	**0.617 (0.602–0.640)**	**0.680 (0.543–0.753)**	**0.565 (0.543–0.598)**	**0.653 (0.637–0.698)**	**370.3**	**4.07**
Junior radiologist with DCNN	R6	25	1.5	0.871 (0.852–0.896)	0.875 (0.860–0.900)	0.898 (0.870–0.922)	0.771 (0.748–0.794)	0.833 (0.800–0.867)	204	2.72
	R7	31	2	0.873 (0.856–0.891)	0.879 (0.875–0.911)	0.901 (0.864–0.924)	0.790 (0.771–0.827)	0.861 (0.811–0.893)	104	2.23
	R8	34	3	0.878 (0.861–0.901)	0.883 (0.869–0.923)	0.907 (0.854–0.924)	0.802 (0.784–0.821)	0.886 (0.844–0.928)	119	1.98
	Avg	**30**	**2.17**	**0.874 (0.857–0.914)**	**0.879 (0.863–0.910)**	**0.902 (0.844–0.921)**	**0.788 (0.764–0.823)**	**0.847 (0.812–0.869)**	**142.3**	**2.31**

FP, false positives per scan. IoU, Intersection-over-Union. Dice, dice coefficient. The bolded words "DCNN Model" represent our proposed network (Cascaded 3D U-Net with 3D GAU modules and the 3D SSE modules). The bolded words "Avg" represent the average of the values in the three cells above.

3.3 Radiologists-DCNN model collaboration

We further validated the radiologists-DCNN model collaboration performance in the testing dataset. As demonstrated, the three junior radiologists (with the assistance of the DCNN model) showed substantial improvement in identifying LCBM (Figure 4 and Table 3).

The DCNN model assisted junior radiologists in diagnosing LCBM with a higher mean AUROC (0.874 [95% CI: 0.807–0.874] vs. 0.609 [95% CI: 0.591–0.634], P< 0.001), mean accuracy (0.879 vs. 0.617, P< 0.001), and mean sensitivity (0.902 vs. 0.680, P = 0.009) compared with those achieved alone. Moreover, the mean interpretation time per case of the junior radiologists was

significantly reduced from 370.3 s to 142.3 s (228 s decrease, P = 0.045) when assisted by the DCNN model.

4 Discussion

Herein, we proposed an improved Cascaded 3D U-Net based on the DCNN model to detect and segment LCBM on CT scans. Radiologists underperformed the DCNN model concerning detection sensitivities, although they achieved much lower average FPs. In the segmentation task, the proposed DCNN model achieved a mean dice of 0.856 and a mean FP of 5.24 in the testing dataset, showing that the proposed model achieved better results than other state-of-the-art networks.

In the radiologists-DCNN model collaboration study, the mean sensitivity of the junior radiologist for LCBM improved from 0.680 to 0.902 with acceptable FPs (2.59). The radiologists-DCNN model collaboration enhanced the detection sensitivity and FPs compared with radiologist-only or DCNN model-only diagnosis, demonstrating the existence of the DCNN model-detected bone metastases that were missed by junior radiologists and vice versa. Moreover, the DCNN model-assisted diagnosis significantly decreased approximately 62% clinical time (142 s vs. 370 s), which had never been evaluated in previous studies.

Prior to our study, two recent studies used deep learning to detect bone metastases from CT images (43, 18). However, both studies focused only on spinal lesions. The spine is the most common site of bone metastases; however, metastases can occur at any site in the entire skeleton (44). Furthermore, both studies formalized the task as two-dimensional detection, whereas our study formalized it as 3D segmentation. Besides, the data and annotation in our study were of a higher standard. In our study, high-quality thin-slice CT scans with a thickness of 1–1.25 mm were used to support the model development. Moreover, we followed a repetitive and retrospective labeling procedure by four radiologists to ensure the high quality of our annotations, thus reducing the risk of overvaluing model performance. Our model achieved significantly higher detection sensitivity and remained consistent across the training, validation, and testing datasets.

Nevertheless, there are still some limitations to this study. First, our study was retrospective and monocentric; therefore, future validations in prospective randomized settings can provide more powerful conclusions. In addition, the sample size was small. We believe that the main reason for such limitation is the somewhat low incidence and prevalence of LCBM (45). Although our results were encouraging, experiments in large multi-center datasets are needed to verify the results in further studies. Second, the training process of the DCNN model depends on the segmentation GT labels of LCBM by radiologists, who also have imperfect reliability. To address this issue, numerous studies have been conducted to train the DCNN model using weak labels (46). Third, the DCNN model was established to detect LCBM so that the patients included in the positive cohort had LC. However, bone metastases may also arise from other solid tumors, such as breast, prostate, colorectal, thyroid, and gynecologic cancers and melanoma (47). Therefore, more generalized DCNN models that can distinguish multiple origins of bone metastases should be followed up. Finally, our DCNN models were designed to deal with a single task of LCBM detection on CT. However, in clinical practice, radiologists may not rely on a single medical file for a final diagnosis, instead, they need to combine other clinical or imaging reports to achieve the diagnosis of LCBM. If the models are built based on a single parameter, their clinical value may be significantly endangered. Therefore, more inclusive models combining various characteristics should be designed and emphasized in the future (48).

In conclusion, our DCNN model collaborated with junior radiologists helped to enhance the diagnostic effectiveness and efficiency in the diagnosis of LCBM on CT, indicating the great potential of DCNN-assisted diagnosis in clinical practice.

Data availability statement

The raw data supporting the conclusions of this article will be made available by the authors, without undue reservation.

Ethics statement

This retrospective study was approved by the hospital ethics committee (Union Hospital, Tongji Medical College, Huazhong University of Science and Technology). The ethics committee waived the requirement of written informed consent for participation.

Author contributions

TH and YX contributed equally to the manuscript. ZY and SZ present the conception of the work; YF and MX acquired the data; SL obtained funding to support the work and built up the research team for joint development; YD and LL labelled the images for further analysis; JZ and HL assisted in collecting data. TH, ZW and PL conducted the statistical analysis; TH drafted the manuscript with critical feedback from all authors. All authors contributed to the article and approved the submitted version.

Funding

This study was supported by the National Natural Science Foundation of China (No. 82172524 and 81974355) and the Artificial Intelligence Major Special Project of Hubei (No. 2021BEA161).

Acknowledgments

We thank Bullet Edits Limited for the linguistic editing and proofreading of the manuscript. We especially thank for the support provided by the Research Institute of Imaging, National Key Laboratory of Multi-Spectral Information Processing Technology, Huazhong University of Science and Technology of China.

Conflict of interest

TH will apply for an International Invention Patent for the DCNN model used in this study pending Union Hospital, Tongji Medical College, Huazhong University of Science and Technology.

The remaining authors declare that the research was conducted in the absence of any commercial or financial relationships that could be construed as a potential conflict of interest.

Publisher's note

All claims expressed in this article are solely those of the authors and do not necessarily represent those of their affiliated organizations, or those of the publisher, the editors and the reviewers. Any product that may be evaluated in this article, or claim that may be made by its manufacturer, is not guaranteed or endorsed by the publisher.

Supplementary material

The Supplementary Material for this article can be found online at: https://www.frontiersin.org/articles/10.3389/fonc.2023.1125637/full#supplementary-material

References

1. Kim ST, Uhm JE, Lee J, Sun JM, Sohn I, Kim SW, et al. Randomized phase II study of gefitinib versus erlotinib in patients with advanced non-small cell lung cancer who failed previous chemotherapy. *Lung Cancer (Amsterdam Netherlands)* (2012) 75(1):82–8. doi: 10.1016/j.lungcan.2011.05.022

2. Torre LA, Bray F, Siegel RL, Ferlay J, Lortet-Tieulent J, Jemal A. Global cancer statistics, 2012. *CA: Cancer J Clin* (2015) 65(2):87–108. doi: 10.3322/caac.21262

3. Ebert W, Muley T, Herb KP, Schmidt-Gayk H. Comparison of bone scintigraphy with bone markers in the diagnosis of bone metastasis in lung carcinoma patients. *Anticancer Res* (2004) 24(5b):3193–201.

4. Katakami N. [Lung cancer with bone metastasis]. *Gan to kagaku ryoho Cancer Chemother* (2006) 33(8):1049–53.

5. Altorki NK, Markowitz GJ, Gao D, Port JL, Saxena A, Stiles B, et al. The lung microenvironment: an important regulator of tumour growth and metastasis. *Nat Rev Cancer* (2019) 19(1):9–31. doi: 10.1038/s41568-018-0081-9

6. Esposito M, Kang Y. Targeting tumor-stromal interactions in bone metastasis. *Pharmacol Ther* (2014) 141(2):222–33. doi: 10.1016/j.pharmthera.2013.10.006

7. Costelloe CM, Rohren EM, Madewell JE, Hamaoka T, Theriault RL, Yu TK, et al. Imaging bone metastases in breast cancer: techniques and recommendations for diagnosis. *Lancet Oncol* (2009) 10(6):606–14. doi: 10.1016/S1470-2045(09)70088-9

8. Hamaoka T, Madewell JE, Podoloff DA, Hortobagyi GN, Ueno NT. Bone imaging in metastatic breast cancer. *J Clin Oncol Off J Am Soc Clin Oncol* (2004) 22(14):2942–53. doi: 10.1200/JCO.2004.08.181

9. Roodman GD. Mechanisms of bone metastasis. *New Engl J Med* (2004) 350 (16):1655–64. doi: 10.1056/NEJMra030831

10. Chang CY, Gill CM, Joseph Simeone F, Taneja AK, Huang AJ, Torriani M, et al. Comparison of the diagnostic accuracy of 99 m-Tc-MDP bone scintigraphy and 18 F-FDG PET/CT for the detection of skeletal metastases. *Acta Radiol (Stockholm Sweden 1987)* (2016) 57(1):58–65. doi: 10.1177/0284185114564438

11. Even-Sapir E. Imaging of malignant bone involvement by morphologic, scintigraphic, and hybrid modalities. *J Nucl Med Off Publication Soc Nucl Med* (2005) 46(8):1356–67.

12. Heindel W, Gübitz R, Vieth V, Weckesser M, Schober O, Schäfers M. The diagnostic imaging of bone metastases. *Deutsches Arzteblatt Int* (2014) 111(44):741–7. doi: 10.3238/arztebl.2014.0741

13. O'Sullivan GJ, Carty FL, Cronin CG. Imaging of bone metastasis: An update. *World J Radiol* (2015) 7(8):202–11. doi: 10.4329/wjr.v7.i8.202

14. Kalogeropoulou C, Karachaliou A, Zampakis P. Radiologic evaluation of skeletal metastases: role of plain radiographs and computed tomography. *Bone Metastases: Springer* (2009) p:119–36. doi: 10.1007/978-1-4020-9819-2_6

15. Yang H-L, Liu T, Wang X-M, Xu Y, Deng S-M. Diagnosis of bone metastases: a meta-analysis comparing 18FDG PET, CT, MRI and bone scintigraphy. *Eur Radiol* (2011) 21(12):2604–17. doi: 10.1007/s00330-011-2221-4

16. Groves AM, Beadsmoore CJ, Cheow HK, Balan KK, Courtney HM, Kaptoge S, et al. Can 16-detector multislice CT exclude skeletal lesions during tumour staging? implications for the cancer patient. *Eur Radiol* (2006) 16(5):1066–73. doi: 10.1007/s00330-005-0042-z

17. Hammon M, Dankerl P, Tsymbal A, Wels M, Kelm M, May M, et al. Automatic detection of lytic and blastic thoracolumbar spine metastases on computed tomography. *Eur Radiol* (2013) 23(7):1862–70. doi: 10.1007/s00330-013-2774-5

18. Chmelik J, Jakubicek R, Walek P, Jan J, Ourednicek P, Lambert L, et al. Deep convolutional neural network-based segmentation and classification of difficult to define metastatic spinal lesions in 3D CT data. *Med Image Anal* (2018) 49:76–88. doi: 10.1016/j.media.2018.07.008

19. Noguchi S, Nishio M, Sakamoto R, Yakami M, Fujimoto K, Emoto Y, et al. Deep learning-based algorithm improved radiologists' performance in bone metastases detection on CT. *Eur Radiol* (2022) 32(11):7976–87. doi: 10.1007/s00330-022-08741-3

20. McKinney SM, Sieniek M, Godbole V, Godwin J, Antropova N, Ashrafian H, et al. International evaluation of an AI system for breast cancer screening. *Nature* (2020) 577 (7788):89–94. doi: 10.1038/s41586-019-1799-6

21. Acar E, Leblebici A, Ellidokuz BE, Başbınar Y, Kaya GÇJTBJOR. Machine learning for differentiating metastatic and completely responded sclerotic bone lesion in prostate cancer: A retrospective radiomics study. *Br Radiol* (2019) 92(1101):20190286. doi: 10.1259/bjr.20190286

22. Kiljunen T, Akram S, Niemelä J, Löyttyniemi E, Seppälä J, Heikkilä J, et al. A deep learning-based automated CT segmentation of prostate cancer anatomy for radiation therapy planning-a retrospective multicenter study. *Diagnost (Basel Switzerland)* (2020) 10(11):959. doi: 10.3390/diagnostics10110959

23. Pelaez-Luna M, Takahashi N, Fletcher JG, Chari ST. Resectability of presymptomatic pancreatic cancer and its relationship to onset of diabetes: a retrospective review of CT scans and fasting glucose values prior to diagnosis. *Am J Gastroenterol* (2007) 102(10):2157–63. doi: 10.1111/j.1572-0241.2007.01480.x

24. Jiang Y, Jin C, Yu H, Wu J, Chen C, Yuan Q, et al. Development and validation of a deep learning CT signature to predict survival and chemotherapy benefit in gastric cancer: A multicenter, retrospective study. *Ann Surg* (2021) 274(6):e1153–e61. doi: 10.1097/SLA.0000000000003778

25. Jiang Y, Zhang Z, Yuan Q, Wang W, Wang H, Li T, et al. Predicting peritoneal recurrence and disease-free survival from CT images in gastric cancer with multitask deep learning: a retrospective study. *Lancet Digital Health* (2022) 4(5):e340–e50. doi: 10.1016/S2589-7500(22)00040-1

26. Rezaeijo SM, Ghorvei M, Mofid B. Predicting breast cancer response to neoadjuvant chemotherapy using ensemble deep transfer learning based on CT images. *J X-ray Sci Technol* (2021) 29(5):835–50. doi: 10.3233/XST-210910

27. Schreier J, Attanasi F, Laaksonen H. A full-image deep segmenter for CT images in breast cancer radiotherapy treatment. frontiers in oncology. *Front Oncol* (2019) 9:677. doi: 10.3389/fonc.2019.00677

28. Ardila D, Kiraly AP, Bharadwaj S, Choi B, Reicher JJ, Peng L, et al. Author correction: End-to-end lung cancer screening with three-dimensional deep learning on low-dose chest computed tomography. *Nat Med* (2019) 25(8):1319. doi: 10.1038/s41591-019-0536-x

29. Alahmari SS, Cherezov D, Goldgof D, Hall L, Gillies RJ, Schabath MB. Delta radiomics improves pulmonary nodule malignancy prediction in lung cancer screening. *IEEE Access Pract Innovations Open Solutions* (2018) 6:77796–806. doi: 10.1109/ACCESS.2018.2884126

30. Cherezov D, Hawkins SH, Goldgof DB, Hall LO, Liu Y, Li Q, et al. Delta radiomic features improve prediction for lung cancer incidence: A nested case-control analysis of the national lung screening trial. *Cancer Med* (2018) 7(12):6340–56. doi: 10.1002/cam4.1852

31. Yang X, Wu L, Ye W, Zhao K, Wang Y, Liu W, et al. Deep learning signature based on staging CT for preoperative prediction of sentinel lymph node metastasis in breast cancer. *Acad Radiol* (2020) 27(9):1226–33. doi: 10.1016/j.acra.2019.11.007

32. Wang YW, Chen CJ, Huang HC, Wang TC, Chen HM, Shih JY, et al. Dual energy CT image prediction on primary tumor of lung cancer for nodal metastasis using deep learning. *Computerized Med Imaging Graphics Off J Computerized Med Imaging Society* (2021) 91:101935. doi: 10.1016/j.compmedimag.2021.101935

33. Lee JH, Ha EJ, Kim JH. Application of deep learning to the diagnosis of cervical lymph node metastasis from thyroid cancer with CT. *Eur Radiol* (2019) 29(10):5452–7. doi: 10.1007/s00330-019-06098-8

34. Zhou X, Wang H, Feng C, Xu R, He Y, Li L, et al. Emerging applications of deep learning in bone tumors: Current advances and challenges. *Front Oncol* (2022) 12:908873. doi: 10.3389/fonc.2022.908873

35. Li T, Lin Q, Guo Y, Zhao S, Zeng X, Man Z, et al. Automated detection of skeletal metastasis of lung cancer with bone scans using convolutional nuclear network. *Phys Med Biol* (2022) 67(1):015004. doi: 10.1088/1361-6560/ac4565

36. Torralba, Antonio, Russell BC, Yuen J. Labelme: Online image annotation and applications. *International Journal of Computer Vision* (2010) 98(8):1467–1484. doi: 10.1007/s11263-007-0090-8

37. Zhong Z, Kim Y, Zhou L, Plichta K, Allen B, Buatti J, et al. (2018). 3D fully convolutional networks for co-segmentation of tumors on PET-CT images, in: *2018 IEEE 15th International Symposium on Biomedical Imaging (ISBI 2018)* Washington, DC, USA, 4-7 April 2018.

38. Isensee F, Jäger PF, Kohl SA, Petersen J, Maier-Hein KH. Automated design of deep learning methods for biomedical image segmentation. *Nature Methods* (2020) 18 (2):203–11. doi: 10.1038/s41592-020-01008-z

39. Roy AG, Navab N, Wachinger C. (2018). Concurrent spatial and channel 'squeeze & excitation'in fully convolutional networks, in: *International conference on medical image computing and computer-assisted intervention Lecture Notes in Computer Science (2018)*, 11070. doi: 10.1007/978-3-030-00928-1_48

40. Li H, Xiong P, An J, Wang LJ. Pyramid attention network for semantic segmentation. *arXiv preprint arXiv:1805.10180* (2018).

41. Zou KH, Warfield SK, Bharatha A, Tempany CM, Kaus MR, Haker SJ, et al. Statistical validation of image segmentation quality based on a spatial overlap index. *Acad Radiol* (2004) 11(2):178–89. doi: 10.1016/S1076-6332(03)00671-8

42. Li L, Zhao X, Lu W, Tan S. Deep learning for variational multimodality tumor segmentation in PET/CT. *Neurocomputing* (2020) 392:277–95. doi: 10.1016/j.neucom.2018.10.099

43. Fan X, Zhang X, Zhang Z, Jiang Y. Deep learning-based identification of spinal metastasis in lung cancer using spectral CT images. *Sci Program* (2021) 2021:2779390. doi: 10.1155/2021/2779390

44. Kakhki VRD, Anvari K, Sadeghi R, Mahmoudian A-S, Torabian-Kakhki MJNMR. Pattern and distribution of bone metastases in common malignant tumors. *Nucl Med Rev Cent East Eur* (2013) 16(2):66–9. doi: 10.5603/NMR.2013.0037

45. Łukaszewski B, Nazar J, Goch M, Łukaszewska M, Stępiński A, Jurczyk MU. Diagnostic methods for detection of bone metastases. *Contemp Oncol (Pozn)* (2017) 21 (2):98–103. doi: 10.5114/wo.2017.68617

46. Wang Y, Lu L, Cheng C-T, Jin D, Harrison AP, Xiao J, et al. Weakly supervised universal fracture detection in pelvic x-rays, in: *Medical Image Computing and Computer Assisted Intervention – MICCAI 2019. MICCAI 2019. Lecture Notes in Computer Science*, (2019) . Springer, Cham. doi: 10.1007/978-3-030-32226-7_51

47. Fornetti J, Welm AL, Stewart SA. Understanding the bone in cancer metastasis. *J Bone Mineral Res Off J Am Soc Bone Mineral Res* (2018) 33(12):2099–113. doi: 10.1002/jbmr.3618

48. Zhou X, Wang H, Feng C, Xu R, He Y, Li L, et al. Emerging applications of deep learning in bone tumors: Current advances and challenges. (2022) 12:908873. doi: 10.3389/fonc.2022.908873

frontiers | Frontiers in Oncology

TYPE Review
PUBLISHED 13 February 2023
DOI 10.3389/fonc.2023.1133828

OPEN ACCESS

EDITED BY
Wenwen Zhang,
Nanjing Medical University, China

REVIEWED BY
Jingfeng Li,
Zhongnan Hospital, Wuhan University, China
Donghua Huang,
Zhejiang University, China
Xiaofeng Zhu,
Jinan University, China

*CORRESPONDENCE
Bo Shuai
bo_shuai@hust.edu.cn

†These authors have contributed equally to this work

SPECIALTY SECTION
This article was submitted to Surgical Oncology, a section of the journal Frontiers in Oncology

RECEIVED 29 December 2022
ACCEPTED 01 February 2023
PUBLISHED 13 February 2023

CITATION
Lu J, Hu D, Zhang Y, Ma C, Shen L and Shuai B (2023) Current comprehensive understanding of denosumab (the RANKL neutralizing antibody) in the treatment of bone metastasis of malignant tumors, including pharmacological mechanism and clinical trials.
Front. Oncol. 13:1133828.
doi: 10.3389/fonc.2023.1133828

Current comprehensive understanding of denosumab (the RANKL neutralizing antibody) in the treatment of bone metastasis of malignant tumors, including pharmacological mechanism and clinical trials

Junjie Lu[1†], Desheng Hu[1†], Yan Zhang[2†], Chen Ma[1†], Lin Shen[1] and Bo Shuai[1*]

[1]Department of Integrated Traditional Chinese and Western Medicine, Union Hospital, Tongji Medical College, Huazhong University of Science and Technology, Wuhan, China, [2]Department of Pain, Union Hospital, Tongji Medical College, Huazhong University of Science and Technology, Wuhan, China

Denosumab, a fully humanized monoclonal neutralizing antibody, inhibits activation of the RANK/RANKL/OPG signaling pathway through competitive binding with RANKL, thereby inhibiting osteoclast-mediated bone resorption. Denosumab inhibits bone loss; therefore, it is used to treat metabolic bone diseases (including postmenopausal osteoporosis, male osteoporosis, and glucocorticoid-induced osteoporosis), in clinical practice. Since then, multiple effects of denosumab have been discovered. A growing body of evidence suggests that denosumab has a variety of pharmacological activities and broad potential in clinical diseases such as osteoarthritis, bone tumors, and other autoimmune diseases. Currently, Denosumab is emerging as a treatment for patients with malignancy bone metastases, and it also shows direct or indirect anti-tumor effects in preclinical models and clinical applications. However, as an innovative drug, its clinical use for bone metastasis of malignant tumors is still insufficient, and its mechanism of action needs to be further investigated. This review systematically summarizes the pharmacological mechanism of action of denosumab and the current understanding and clinical practice of the use of denosumab for bone metastasis of malignant tumors to help clinicians and researchers deepen their understanding of denosumab.

KEYWORDS

denosumab, RANK/RANKL/OPG system, bone metastasis, skeletal-related events, osteoclast

Introduction

The RANK/RANKL/OPG system The Receptor activator of NF-kB/The Receptor activator of NF-kB ligand/ Osteoprotegerin system

The receptor activator of NF-kB ligand (RANKL was originally defined as a new member of the tumor necrosis factor receptor (TNFR) family which is expressed on non-dendritic cells and participates in dendritic cell-mediated T cell proliferation and RANK+T cell activation (1). The discovery of RANKL built a bridge between the bone and the immune system and became an important landmark in the rise of bone immunology (2–4). As the RANKL/RANK (Receptor activator of NF-kB) signaling pathway plays an important role in mediating osteoclast differentiation and function (5), the relationship between RANKL and bone metabolism has been extensively studied.

The differentiation and maturation of osteoblasts is regulated by two systems: the RANK/RANKL system and the macrophage colony-stimulating factor/colony-stimulating factor-1 receptor (M-CSF/c-FMS) system (6). The M-CSF/c-FMS system is responsible for regulating the differentiation of early hematopoietic stem cells (HSCs) into osteoclast precursor cells and the survival of osteoclast precursor cells (7), whereas the RANK/RANKL system is an important trigger for the differentiation of osteoclast precursors into functional osteoclasts. RANKL is a homologous trimeric transmembrane protein which has two receptors: the membrane-binding receptor RANK and the soluble bait receptor OPG (8). In bone, RANKL is expressed in the bone matrix, osteoblast precursor cells, and osteoblasts, and RANK is expressed on the membrane surface of osteoclasts and osteoclast precursors as a membrane-binding receptor (9).

The binding of RANKL to RANK leads to the recruitment of TNF receptor associated factor 6 (TRAF6) as an articulatory molecule, which activates the NF-kB, c-Fos/AP1, MAPK, and other signaling pathways (10), leading to increased activation, amplification, and transcription of the downstream signal nuclear factor of activated T cells (NFATc1) (11), which directly mediates the differentiation of osteoclast precursor cells into osteoclasts (12). NFATc1 is a major regulator of osteogenesis (13). NFATc1 is both a major regulator of osteoclast formation and is involved in the regulation of osteoclast-specific genes (TRAP, Cathepsin K, calcitonin receptor) involved in osteoclast differentiation proliferation and survival (14, 15). The osteeoprotegerin (OPG) inhibits the activation of RANK signaling by competitively binding to RANKL and preventing RANKL from binding to its receptor RANK (16) (Figure 1).

Denosumab is the first and only clinically available RANKL inhibitor that inhibits osteoclast activity by targeting and blocking the binding between RANK and RANKL. While inhibiting the function of mature osteoclasts (17), it also inhibits the maturation of osteoclast precursor cells, reduces bone resorption, and promotes bone reconstruction, thereby delaying bone-related events.

Biology of bone metastasis of malignant tumors

Tumor metastasis is the process by which cancer cells spread from a primary lesion to other sites. Cancer cells metastasize in three major ways: direct invasion, disseminated metastasis, and vascular and lymphatic metastases (18). Tumor metastasis is a complex biological process (19, 20). Tumor cells metastasizing from the primary site to other tissues and organs generally undergo the steps of reducing intercellular adhesion, destructing the epithelial barriers, escaping from immune surveillance, secondary site colonizing, proliferation and growth and lead to skeletal-related event SREs (21) (Figure 2). The three major primary cancers that are most prone to bone metastasis are breast, lung, and prostate cancers (22). Tumor cells colonize the bone microenvironment from the primary site, resulting in bone disease, which is defined as a SREs. Although all are bone metastases, the different origins of the tumors lead to completely opposite characteristics. When osteoblast-mediated bone formation predominates, the bone shows abnormal proliferation and presents with osteosclerotic malignancy; when osteoclast-mediated bone resorption predominates, the bone shows abnormal resorption and presents with osteolytic malignancy (23), and there are also some mixed lesions in which osteosclerosis and osteolysis abnormalities occur simultaneously (24).

Tumor progression or invasion of other tumors leads to the disruption of bone homeostasis, forming a vicious circle between osteoclasts, osteoblasts, immune cells, and tumor cells (25). Malignant tumors release a variety of cytokines that can directly or indirectly activate osteoblasts or osteoclasts. When tumor cells secrete IL-1 (Interleukin-1), IL-6 (Interleukin-6), TNF-α (Tumor Necrosis Factor alpha), and other inflammatory cytokines, they activate osteoclasts in large quantities, leading to enhanced osteolysis activity, which produces inflammatory cytokines in large quantities, forming a vicious circle in the bone microenvironment promoting pro-tumor transformation and tumor cell progression (26). In addition, the alteration of the bone microenvironment and tumor microenvironment will make the immune cells' surveillance and clearance effect on the tumor weaken (27). Tumor cells will block the immune response in many ways, resulting in the weakening of immune cell anti-tumor immunity (28). Physicochemical and environmental factors also play an important role in regulating the progression of tumor metastasis. A hypoxic environment and low pH values are conducive to tumor cell proliferation (29), and this hypoxic acidic environment creates a suitable environment for tumor cell growth, leading to increased levels of tumor cell production, migration, invasion, and proliferation (30).

Bone metastases often lead to serious complications, including fractures, nerve compression, and severe pain, resulting in loss of mobility, a significant increase in medical costs, and a significantly lower quality of life and survival rates (31). Metastases occur in approximately 50% of patients with tumors and are the cause of death in 90% of patients with cancer (32). In the past decades, metastases have been treated using systemic approaches, including

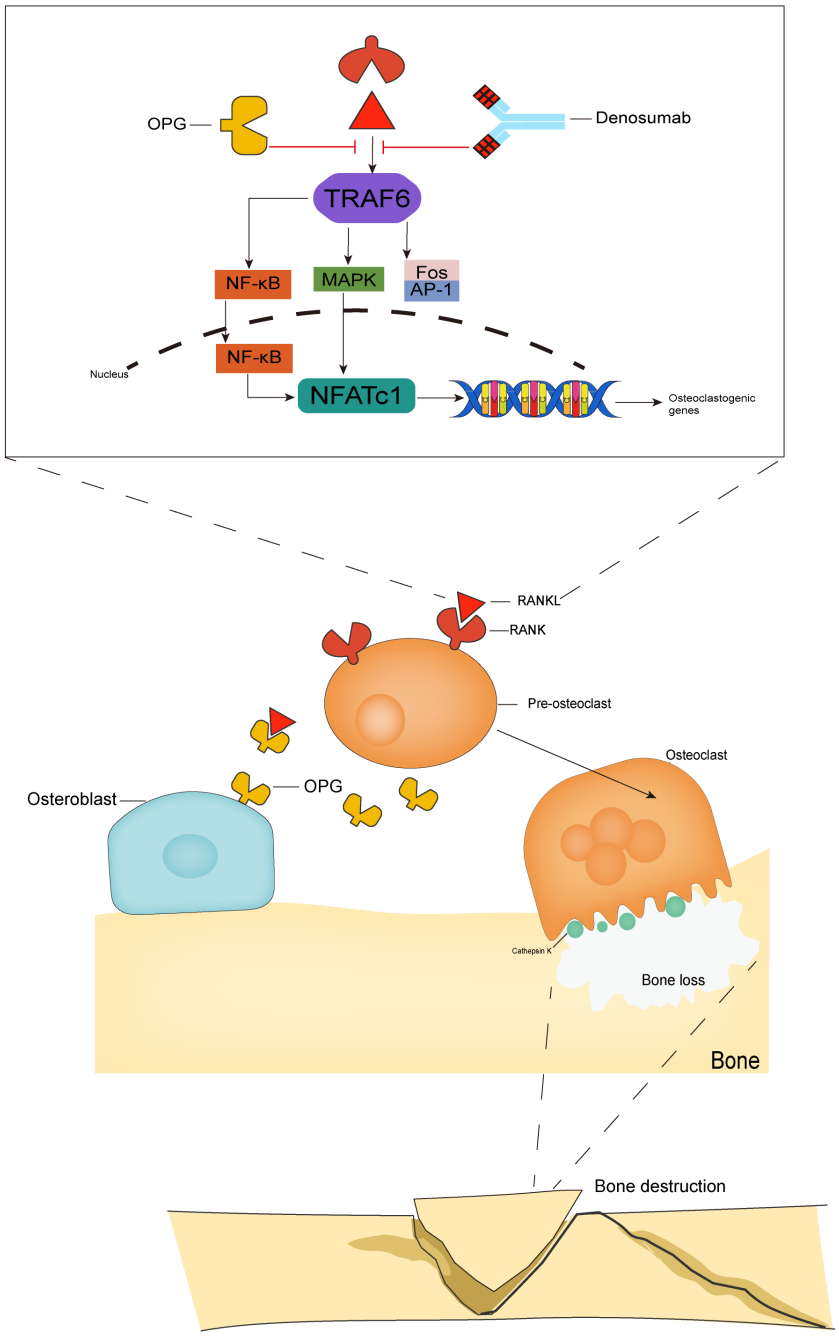

FIGURE 1
The RANK/RANKL/OPG system. The binding of RANKL to RANK leads to TRAF6 recruitment, which activates NF-kB, MAPK and Fos/AP-1 pathways. These activating signals together lead to the activation of NFATc1, a key transcription factor for downstream osteoclast-associated gene activation, which is the hallmark event of osteoclast formation. The OPG competitively binds RANKL and thus inhibits osteoclast activation, while denosumab, which has the same molecular weight as OPG, also binds to RANKL and inhibits osteoclast activation and maturation.

chemotherapy and immunotherapy, but most patients with new or recurrent metastases still die within 5 years of diagnosis (33). This is especially true for the high incidence and high risk of bone metastases, so there is an urgent need to explore in depth the options to prevent and treat bone metastases (34). Bisphosphonates are well documented (35). Recognizing the development of early metastases in women suffering from breast cancer, which usually occur in bone tissue, attempts have been made to use bisphosphonates for early prevention in women with breast cancer as a nonspecific treatment, decreasing the potential impact of SREs and increasing the overall survival benefit (36).

The RANK/RANKL system in tumor metastases to bone

RANKL has been recognized for its role in mediating dendritic cell survival and T cell proliferation, and subsequently for its crucial

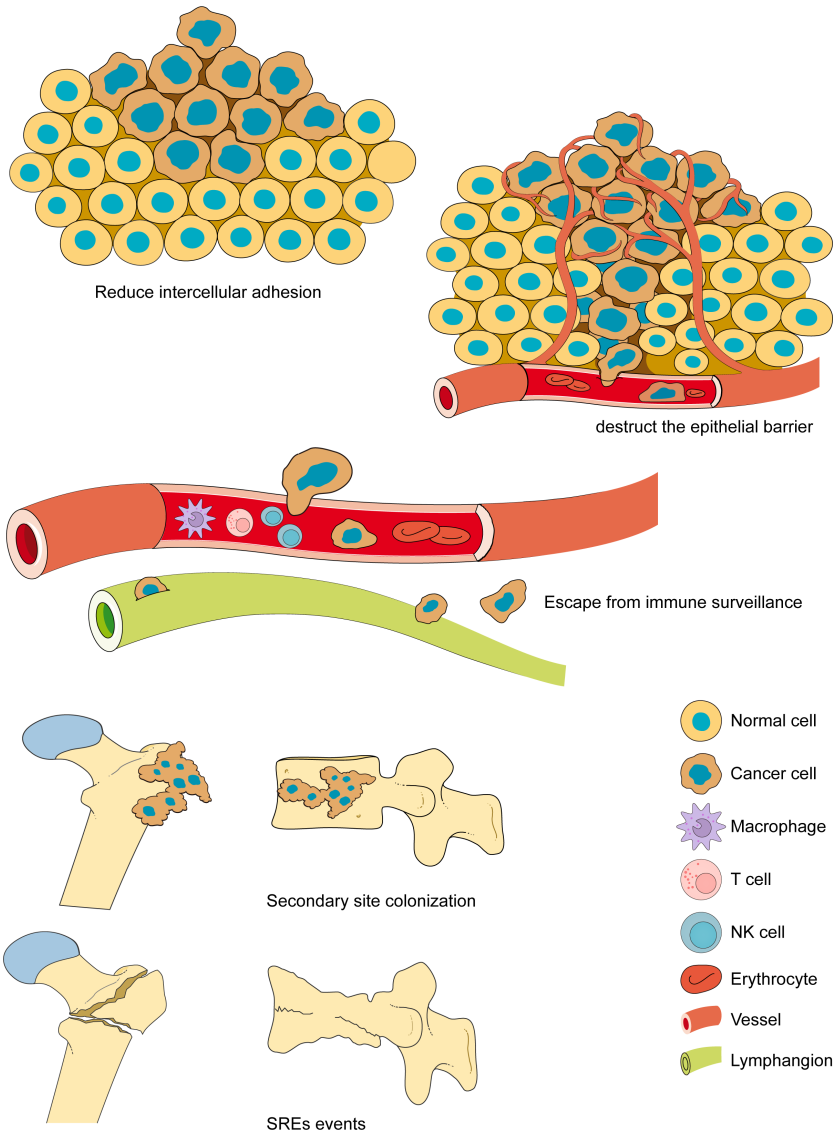

FIGURE 2
The bone metastasis. The bone metastasis is a complex biological process. Tumor cells metastasizing from the primary site to other tissues and organs generally undergo the steps of reducing intercellular adhesion, overcoming barriers, escaping from immunity, colonizing secondary sites, proliferation and growth and lead to SREs. The bone metastases often lead to serious complications, including fractures, nerve compression, and severe pain, resulting in loss of mobility, a significant increase in medical costs, and a significant reduction in quality of life and survival.

roles in mediating osteoclast differentiation and function (37). Thus, it has been intensively studied in the field of bone metabolism, and recently, research has returned to focus on the immune system. Many studies have shown that the RANK/RANKL system plays an essential role in developmental maturation and functional maintenance of the immune system. By genetically engineering RANK- or RANKL-deficient mice, it has been found that RANKL knock out mice show lymph node deficiency and impaired B-cell development (38, 39), and patients with mutations in the TNFRSF11A gene (encoding RANK) show a significant reduction in B-cell numbers (40), which confirms that RANK/RANKL is essential for early T cell and B cell development. In addition, RANK/RANKL intervenes in the interactions between T cells and dendritic cells s, and RANKL enhances dendritic cell formation and function in the absence of co-stimulation and antigen presentation, enhancing the ability of dendritic cells to stimulate the proliferation and differentiation of naive T cells (41). In addition, RANK/RANKL activation triggers intracellular signaling pathways (e.g., MAPK, NF-kB, Fos/AP-1, JNK/ERK/P38), which are involved in tumor proliferation and metabolic activities (42).There are many preclinical studies on the above-mentioned signaling pathways in RANKL activation-induced cancer metastasis. For example, MAPK pathway is involved in RANKL-induced breast cancer cell migration, and inhibition of MAPK pathway activation by specific inhibitors can effectively block RANKL-induced cell migration (43, 44). RANKL induces NF-KB activation leading to enhanced aggressiveness of oral squamous cell carcinoma by suppressing RANKL expression, which inhibits RANKL-induced NF-KB activation thereby suppressing the invasion of oral squamous cell carcinoma into the jawbone (45). However, these intracellular signaling pathways do not exist in isolation, but in crosstalk with each other (46). Until now, evidence on the crosstalk between RANK/RANKL and intracellular signaling

pathways to regulate tumor proliferation and metabolism is still incomplete. and needs further study.

Although it is not clear whether the RANK/RANKL signaling pathway plays a favorable or unfavorable role in tumor proliferation and metabolism, there is no doubt that RANK/RANKL signaling plays a very important role in tumors. RANK/RANKL is expressed in many tumor tissues (39), and many breast cancer patients show abnormally high levels of RANKL expression in primary lesions, and a positive correlation with the incidence of bone metastases (47). RANK/RANKL is directly involved in tumor proliferation and metabolism and regulates the tumor immune microenvironment (48). The activation of dendritic cells releases a large amount of activated cytokines (including IL-1, IL-6, and IL-12) (41), which increase the number of transcriptional factor Foxp3 regulatory T cells (Foxp3+ Tregs) (49), and induce the differentiation of CD4+ T cells into Th1 cells (50), all of which lead to immunosuppression, and allow tumor cells to escape immune surveillance that promotes tumor progression.

The above evidence seems to indicate a negative aspect of the RANK/RANKL system in the progression of tumors and anti-tumor immunity. Because of the effectiveness of osteoclast inhibition in preventing bone metastases, drugs acting on the RANK/RANKL system have been developed and used to treat bone metastases from malignant neoplasm.

The development and pharmacological mechanism of denosumab

OPG was discovered in the 1990s when genomics was developed and used for target identification and Amgen discovered emerging mRNAs through large-scale sequencing and studied the function of these genes *in vivo* by overexpressing them in mouse liver. Mice with OPG transfer gene show a phenotype of increased bone density in the lower limb bones. Following the discovery of the OPG phenotype, subsequent studies began to search for a ligand for OPG. The OPG ligand (OPGL) was screened by fluorescence techniques, and a series of subsequent studies revealed that the OPGL sequence was identical to the RANK ligand RANKL, which was then used as a ligand for OPG. Because of its phenotype of increasing bone density, OPG was used to inhibit bone resorption. Hundreds of variants of OPG were developed and used in preclinical animal models, but all showed poor bioactivity and poor pharmacokinetics, and the subsequent OPG immunoglobulin Fc fusion protein (OPG-Fc) had an extended potency enhancer half-life but presented safety risks in phase I trials. Development of OPG-Fc was discontinued and shifted to RANKL. Amgen reconstituted a fully human monoclonal antibody, denosumab, using a modified Ig2 antibody (the modified Ig2 antibody enhances resistance to papain and thus improves efficacy) with little or no cytotoxicity (antibody-dependent cell-mediated cytotoxicity and complement-dependent cytotoxicity) and improved pharmacokinetics (51).

Denosumab is a fully synthetic monoclonal neutralizing antibody that acts as an IgG2 subclass immunoglobulin, inhibiting osteoclast differentiation, survival, and activity by competitively binding RANKL, thereby blocking RANK binding to RANKL. Denosumab is considered a highly effective inhibitor of osteoclast bone resorption (52). *In vitro* studies have shown that denosumab, similar to OPG, has high affinity for soluble and membrane-bound RANKL (53). Denosumab has good pharmacokinetic properties, and although there are individual metabolic differences, its molecular mass and structural properties allow for rapid absorption and a nonlinear metabolic profile that can be sustained *in vivo* (54). After subcutaneously administration denosumab of 60 mg, maximum serum denosumab concentration was reached on day 10 (range: 2-28 days), with serum levels declining gradually over 3 months (range: 1.5-4.5 months), with a half-life of 26 days (range: 6-52 days). After subcutaneously administration denosumab of 120 mg every 4 weeks, steady-state concentrations were achieved at 6 months. the mean (± standard deviation) serum steady-state trough concentration at 6 months was 20.5 (± 13.5) μg/mL. The mean elimination half-life was 28 days. It can last up to 9 months after a single dose (55). Similar to other monoclonal antibodies, denosumab is likely cleared *in vivo* by the reticuloendothelial system and is not metabolized by the liver or kidneys (56); therefore, no further impairment of renal function or changes in efficacy or pharmacokinetics have been reported with denosumab in clinical trials, including renal replacement therapy in patients with impaired renal function (57). However, pilot studies on the mechanism of clearance of denosumab, and clinical evaluation of hepatic impairment on the efficacy and pharmacokinetics of denosumab have not yet been conducted (Figure 3).

The clinical trials of denosumab on bone metastasis of malignant tumor

The RANKL inhibitor denosumab has entered clinical trials for malignant bone metastases (Figure 4). A prospective double-blind placebo-controlled phase III trial (58) with 3425 subjects showed that denosumab in women with early-stage hormone receptor-positive postmenopausal breast cancer treated with an aromatase inhibitor was effective in reducing bone mineral density and fractures due to aggressive bone resorption, with no significant variation in the incidence of adverse events (58). Another prospective double-blind placebo-controlled phase I trial with 1432 subjects showed that denosumab was effective in preventing bone metastases in non-metastatic castration-resistant prostate cancer, and that denosumab significantly postponed the onset of first bone metastasis in patients with this type of tumor (59). A randomized phase II clinical study showed that in patients experiencing bone metastases associated with malignant tumors, including prostate, breast, or other tumors, who received bisphosphonates by intravenous injection but still had excessive bone resorption (urinary N-terminal peptide uNTx >100 nmol), increased treatment with denosumab was effective in reducing uNTx levels, inhibiting the bone resorption rate, and reducing the incidence of SREs (60). In addition, a double-blind randomized phase III clinical trial showed that treatment with denosumab (120 mg every 4 weeks) prolonged the time to first bone metastasis radiotherapy compared to conventional bisphosphonate anti-bone metastases (61), implying that the time-lapse to bone metastases was delayed in patients receiving denosumab subcutaneous injections, in addition to prolonging the time to the first SREs occurrence and hypercalcemia, reduced pain levels, and improved the well-being of people suffering from bone metastases. In addition, denosumab

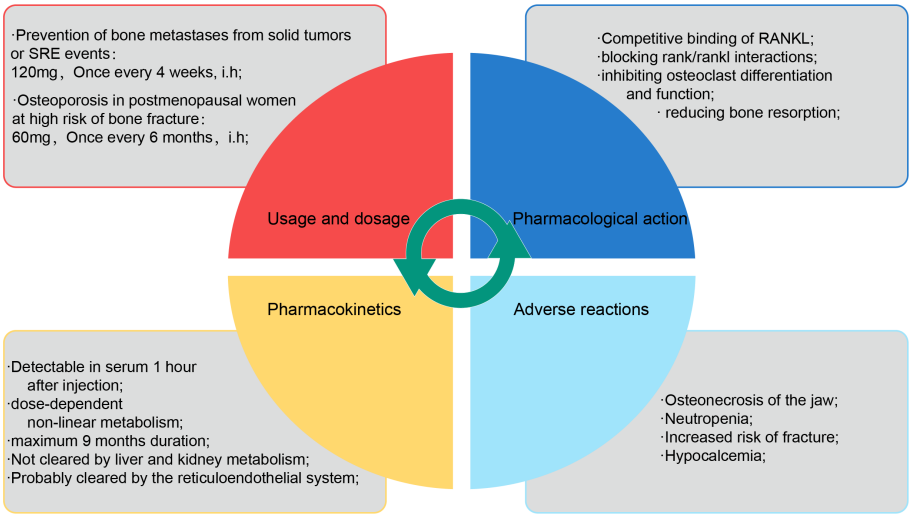

FIGURE 3
The description of denosumab. The properties of denosumab are briefly described in four dimensions: usage and dosage, pharmacological mechanism, pharmacokinetics and adverse reactions.

effectively reduced serum calcium levels in patients with refractory hypercalcemia whose serum calcium could not be controlled with intravenous bisphosphonate therapy (62), achieving an overall remission rate of 64%, delaying the onset of hypercalcemia in patients with advanced bone metastases, achieving a durable therapeutic response in reducing serum calcium, and being used in patients with renal failure (compared to bisphosphonates). Denosumab is neither metabolized nor excreted by the kidneys compared to bisphosphonates), making denosumab a promising second drug to be approved for the treatment of refractory hypercalcemia after zoledronic acid.

The use of denosumab has produced alterations in bone metabolism and therefore its application in some specific skeletal metabolic disorders deserves to be noted. Paget's disease is characterized by local bone metabolism disorder, partial bone overgrowth, disorder of bone reconstruction, abnormal osteoclast metabolism causing bone lysis, compensatory increase of osteoblasts, brittle change of abnormally proliferated bone tissue, bone expansion and loosening, and easy fracture, so some clinical studies abroad use denosumab to intervene in early Paget's disease. In two reported clinical cases (63, 64), patients with Paget's disease treated with bisphosphonates for a long time, who progressed to giant cell tumor of bone, received subcutaneous injections of denosumab (120 mg every 4 weeks), and imaging showed a reduction in tumor size and an improvement in clinical symptoms. Treatment of bone metastases is usually systemic, and radiotherapy and chemotherapy are the conventional means of treatment for bone metastases. Patients with bone metastases have usually undergone systemic treatment prior to the development of bone metastases, does the combination of denosumab and chemotherapy produce a synergistic effect? Does the combination of denosumab and chemotherapy have a synergistic effect? Does it have an effect on effectiveness or does it produce drug resistance? Studies in animal models have shown that inhibition of RANKL improves the efficacy of the chemotherapeutic agent cisplatin, but there are no objective data on the effect of denosumab in combination with chemotherapeutic agents at this time (39).

Based on the above clinical study results, denosumab could be considered for use as a more effective anti-bone metastasis drug than bisphosphonates, because it delays the onset of bone metastases, reduces the frequency of SREs, improves patient life treatment, and can also be used in patients with bone metastases who are allergic to bisphosphonates or have renal failure (65). However, caution should be exercised. The clinical application of drugs is different from preclinical studies, because tumorigenesis is a complex process with differences in the nature of the tumor itself, and tumorigenesis leads to systemic metabolic changes. There are already relevant clinical studies that are skeptical of denosumab for bone metastases from malignant tumors.

A large multicenter prospective randomized clinical trial revealed the effect of adjuvant treatment with denosumab on early-stage female breast cancer patients. A total of 4509 female breast cancer patients were enrolled in the study (66), half of whom received denosumab (120 mg once a month) at the start of chemotherapy for five years, primarily to determine whether denosumab could play an anti-metastatic role. Unfortunately, there was no significant difference between the two groups, and no significant improvement or therapeutic effect on bone metastases, in addition to neutropenia in 15% of patients and osteonecrosis of the jaw in 5% of patients. Another randomized open phase III clinical study showed that adding denosumab to standard first-line platinum-based dual therapy did not improve overall survival in patients with advanced non-small cell lung cancer (NSCLC) (67). These clinical trials showed that the combination of denosumab did not benefit patients and imposed a financial burden on these patients. A large randomized trial showed a 9-fold increase in medical costs for monthly denosumab treatment compared with 3-monthly zoledronic acid treatment, but no significant survival extension or other benefits were observed (68).

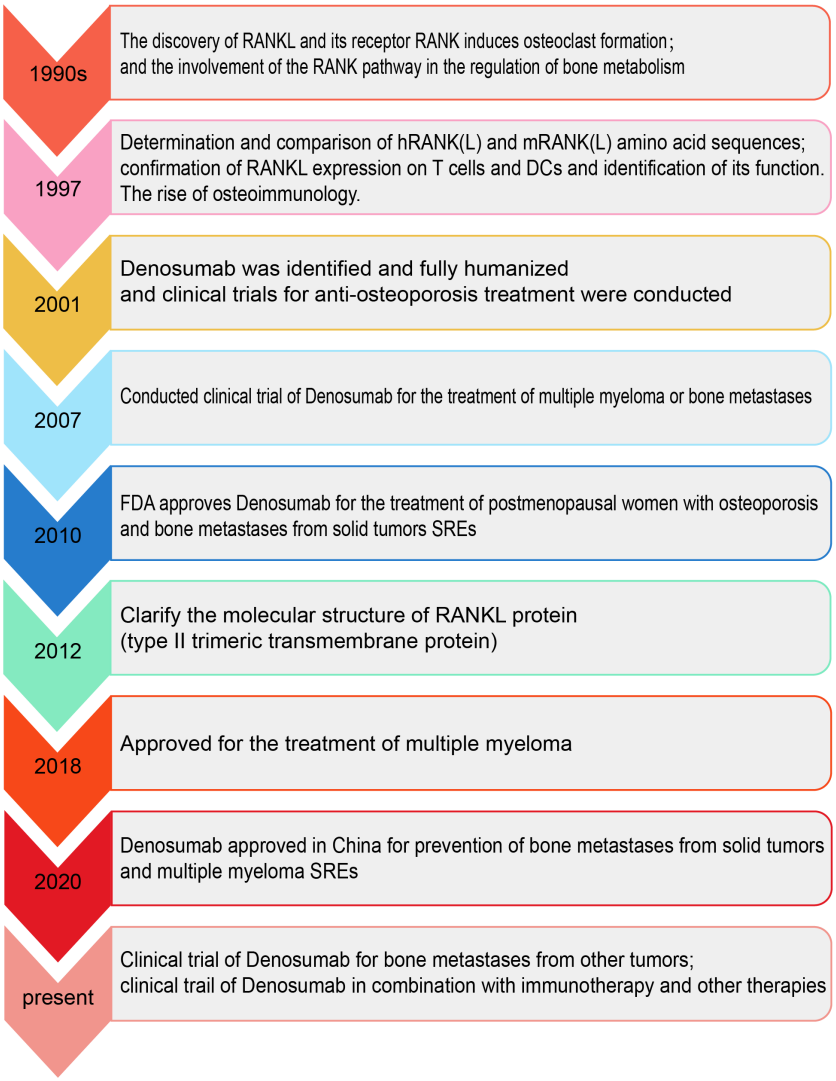

FIGURE 4
The timeline of RANK/RANKL/OPG system and denosumab. The chronological order shows the important events in the process from the discovery of the RANK/RANKL/OPG system and denosumab to its clinical use.

In addition, the increased incidence of adverse events associated with the use of denosumab cannot be ignored, with frequently reported adverse events being osteonecrosis of the jaw, neutropenia, and increased risk of fracture (61, 69).

Based on the above studies, we must carefully evaluate the use of denosumab for the prophylaxis and treatment of bone metastases in malignant tumors. The following questions require careful consideration;

- Whether denosumab is only indicated for certain specific tumor types?
- Whether the use of denosumab brings more clinical benefits and medical cost savings to patients with malignant tumors?
- Whether the combination of denosumab with first-line chemotherapeutic agents may superimpose adverse effects and how to prevent rebound effects after denosumab discontinuation are worthy of prudent evaluation.

Therefore, joint efforts by researchers and clinicians are required.

Conclusion

In 2020, there will be approximately 19.3 million new cancer cases and 10 million cancer deaths worldwide, and with the growing population base and aging population, this number is expected to increase by 47% by 2040, with the global cancer burden reaching 28.4 million cases (70, 71). Approximately 50% of patients with tumors develop metastases, and the majority of patients with tumors die from a variety of complications caused by metastases, rather than from other causes. Bone metastatic disease is most common in some specific cancers, among which the incidence of bone metastasis in breast cancer is approximately 70%, prostate cancer is about 85%, cancer bone metastasis is about 40%, and the incidence of bone metastasis in multiple myeloma is as high as 95% (22). Given the high incidence of these tumors, many bone metastases occur each year, causing great pain and devastation to patients. Most bone metastases occur in the spine, pelvis, ribs, and other important areas (72), causing pain, compression, bone destruction, pathological fractures, and other

serious SREs (73). Approximately 40% of patients with bone metastases experience SREs during antitumor treatment (73).

The evolution of malignant tumor metastasis to the bone is a complex process (74). The metastatic spread of tumor cells includes reducing intercellular adhesion, destructing the epithelial barrier, escaping from immune surveillance, secondary site colonization and SREs events happening (75). However, when tumor cells colonize the bone, it also provides favorable support for the rapid proliferation of tumor cells. The relationship between tumor cells and the bone microenvironment has been compared to the relationship between seeds and soil (76), and the various cells and blood supply in the skeletal system provide a natural breeding ground for tumor cells to colonize and proliferate. However, not all types of tumors develop bone metastasis, and it seems that the characteristics of the seed (i.e., tumor cells) interacting with the soil (i.e., bone microenvironment), play a more important role in the spread of malignant tumor bone metastasis (77), which may explain why some specific primary tumor types (e.g., breast cancer and prostate cancer), are more prone to bone metastasis (78). In addition, differences in the primary foci classify bone metastases into different types, and bone metastases are classified into osteosclerotic malignancies, osteolytic malignancies, and mixed malignancies (79). Osteolytic malignancies are usually primary tumors of breast or lung cancer, whereas osteosclerotic malignancies are usually highly associated with prostate cancer. However, this division is simple and rough, and when bone metastases from malignant tumors occur, skeletal lesions within the bone microenvironment are often complex (80). When bone metastases occur in most solid tumors, there is both an accelerated process of osteolytic destruction and bone formation and reconstruction, and bone metastases in different parts of a single patient's body may be different, i.e. osteolytic bone destruction may occur in one part of the bone and another part of In other words, osteolytic bone destruction may occur in one part of the skeleton, while another part of the skeleton, on the contrary, may develop sclerotic osteogenic lesions or mixed bone metastases. The complexity of bone metastases along with the resistance of neoplastic cells to metastases poses a great challenge for their treatment (81).

The current standard of care for bone metastases from malignant tumors includes bisphosphonates and the RANKL inhibitor, denosumab (82), both drug types which target osteoclast inhibition (83). Bisphosphonates have been used clinically for many years, and a large amount of preclinical evidence fully demonstrates their anti-tumor cell metastatic ability (84, 85). Their action on osteoclasts leads to reduced bone resorption, which may establish a bone microenvironment unfavorable to tumor cell attachment (86). In addition, nitrogen-containing bisphosphonates can inhibit tumor angiogenesis and modulate immunity to exert indirect antitumor activity (87). Due to its good pharmacological activity and cost-effectiveness, zoledronic acid has been the standard of care for the prevention of bone metastases from malignant tumors and other SREs for nearly a decade (88), significantly improving the quality of life and survival of patients with bone metastases (89). However, the pharmacological properties of zoledronic acid have led to adverse effects (mainly acute reactions and renal impairment), making it unavailable to some patients with bone metastases (90), and until the advent of denosumab, these patients had no choice.

Denosumab was approved by the FDA in 2010 for the treatment of bone metastases from solid tumors, and has since become a breakthrough treatment for bone metastases from malignant tumors. Several clinical trials have confirmed that it is as effective as zoledronic acid (91, 92). Several large multicenter prospective double-blind randomized controlled clinical trials have shown that denosumab is effective in delaying the time to first bone metastasis, reducing the incidence of SREs, reducing pain levels in patients with bone metastases, and improving the quality of life in patients with malignancies (93, 94). However, with further clinical studies and the gradual expansion of the included population, the effectiveness of denosumab was gradually questioned (95), and several clinical studies showed that denosumab did not differ from zoledronic acid in terms of overall survival and disease progression (96). In addition, the treatment of bone metastases from malignant tumors is a long-term process, and the cost of the drug is an issue that must be considered. With conflicting clinical data from different institutional centers, more clinical studies and longer follow-up periods are needed to obtain credible evidence about the role of denosumab in malignant bone metastases, its advantages over zoledronic acid, and to analyze the various reported adverse effects from denosumab. The answers are thus both necessary and urgent.

Although clinical studies and conclusions about denosumab are still to be optimized, there is no doubt about its advantages over zoledronic acid. The emergence of denosumab brings hope to patients with bone metastases from malignant tumors combined with renal abnormalities as it is not metabolized and excreted by the kidneys (97). This makes it available for patients with bone metastases from malignant tumors treated with renal replacement therapy. This is particularly important for elderly prostate cancer patients, who are at a high risk of bone metastases. They often suffer from renal insufficiency due to malignant tumor proliferation-induced urinary tract obstruction, for which bisphosphonates are absolutely contraindicated, and who desperately need a drug that can control bone metastases (93). In addition, denosumab reduces the rate of bone resorption by competitively binding to RANKL, resulting in a durable reduction in serum calcium levels. This provides a new approach for the treatment of previously intractable hypercalcemia with bone metastases (98). Denosumab has also been reported to delay pain progression and reduce overall pain levels and analgesic drug use (99), but these reports suffer from inadequate sample sizes and are highly susceptible to subjective evaluations, which are currently unreliable.

Another question that needs to be answered is how does denosumab function in different types of tumors? Although it was approved by the FDA in 2010 for the treatment of bone metastases from solid tumors, it is not yet known whether denosumab is effective for all types of bone metastases from solid tumors (100). Clinical trials in NSCLC have shown that bone metastasis is very common in non-small cell lung cancer; one clinical trial confirmed that 50%-60% of NSCLC tumor tissues express RANKL and RANK, and the trial showed that denosumab can directly block RANKL to inhibit bone metastasis in NSCLC. However, subsequent clinical trials have

indicated the opposite conclusions, since adding denosumab to standard first-line platinum-based dual therapy did not improve overall survival in advanced NSCLC. Data from different studies are conflicting, so there are questions about whether denosumab is effective in NSCLC. A more fundamental issue is that the mechanism of denosumab, which acts on osteoclasts to exert anti-metastatic effects by reducing bone resorption, may be effective in osteolytic bone metastases where osteoclast-mediated bone resorption predominates. However, there is a lack of evidence to demonstrate whether it is effective in sclerotic bone metastases where osteoblast-mediated bone formation predominates.

To minimize the impact of malignant tumor bone metastases on patients and reduce the occurrence of SREs events, the control of bone metastases often requires comprehensive treatment rather than a single therapeutic measure, and the treatment usually includes multiple treatment measures such as radiotherapy, chemotherapy, surgical treatment, immunotherapy, and palliative care. Combination therapy with denosumab is therefore a major clinical issue, most notably denosumab in combination with immunotherapy (101). RANKL, as a bridge between the skeletal and immune systems, will inevitably crosstalk with the immune system; therefore, the outcomes arising from the combination of immunotherapy and denosumab must be seriously considered. Several studies are currently underway to examine the effects of denosumab monotherapy and combination immunotherapy to assess whether the combination has a beneficial effect on progression-free survival and overall survival of patients (102).

In summary, the bone metastasis of malignant tumors has become a major challenge in tumor treatment. The various mechanisms mediating the growth of metastasis and the special skeletal microenvironment bring great challenges to the treatment of bone metastasis, and the emergence of denosumab provides a new path for the treatment of bone metastasis. However, since the understanding of denosumab is not yet perfect, more research is needed in the future to explore the great therapeutic potential of denosumab and provide a more solid and rational basis for clinical use.

Author contributions

BS, JL, CM, and YZ conceived the idea for the study and provided critical revision of the manuscript. LS, DH, and CM collected the information. BS, JL, and DH participated in study design, supervising, writing and drafting of the manuscript. All authors contributed to the article and approved the submitted version.

Funding

This study was partially funded by the National Natural Science Foundation of China (Project Number: 82174182, 81974546, 81974249, and 81901144).

Acknowledgments

The authors would like to thank Editage (www.editage.cn) for English language editing.

Conflict of interest

The authors declare that the research was conducted in the absence of any commercial or financial relationships that could be construed as a potential conflict of interest.

Publisher's note

References

1. Yasuda H. Discovery of the RANKL/RANK/OPG system. *J Bone mineral Metab* (2021) 39(1):2–11. doi: 10.1007/s00774-020-01175-1

2. Nagy V, Penninger JM. The RANKL-RANK story. *Gerontology.* (2015) 61(6):534–42. doi: 10.1159/000371845

3. Ono T, Hayashi M, Sasaki F, Nakashima T. RANKL biology: Bone metabolism, the immune system, and beyond. *Inflammation regeneration.* (2020) 40:2. doi: 10.1186/s41232-019-0111-3

4. Okamoto K, Takayanagi H. Osteoimmunology. *Cold Spring Harbor Perspect Med* (2019) 9(1). doi: 10.1101/cshperspect.a031245

5. Cao X. RANKL-RANK signaling regulates osteoblast differentiation and bone formation. *Bone Res* (2018) 6:35. doi: 10.1038/s41413-018-0040-9

6. Boyce BF. Advances in the regulation of osteoclasts and osteoclast functions. *J Dental Res* (2013) 92(10):860–7. doi: 10.1177/0022034513500306

7. Asagiri M, Takayanagi H. The molecular understanding of osteoclast differentiation. *Bone.* (2007) 40(2):251–64. doi: 10.1016/j.bone.2006.09.023

8. Luan X, Lu Q, Jiang Y, Zhang S, Wang Q, Yuan H, et al. Crystal structure of human RANKL complexed with its decoy receptor osteoprotegerin. *J Immunol (Baltimore Md 1950).* (2012) 189(1):245–52. doi: 10.4049/jimmunol.1103387

9. Eriksen EF. Cellular mechanisms of bone remodeling. *Rev endocrine Metab Disord* (2010) 11(4):219–27. doi: 10.1007/s11154-010-9153-1

10. Chen Y, Chen J, Chen J, Yu H, Zheng Y, Zhao J, et al. Recent advances in seafood bioactive peptides and their potential for managing osteoporosis. *Crit Rev Food Sci Nutr* (2022) 62(5):1187–203. doi: 10.1080/10408398.2020.1836606

11. Lorenzo J. The many ways of osteoclast activation. *J Clin Invest* (2017) 127 (7):2530–2. doi: 10.1172/JCI94606

12. Gohda J, Akiyama T, Koga T, Takayanagi H, Tanaka S, Inoue J. RANK-mediated amplification of TRAF6 signaling leads to NFATc1 induction during osteoclastogenesis. *EMBO J* (2005) 24(4):790–9. doi: 10.1038/sj.emboj.7600564

13. Lu J, Hu D, Ma C , Shuai B. Advances in our understanding of the mechanism of action of drugs (including traditional Chinese medicines) for the intervention and treatment of osteoporosis. *Front Pharmacol* (2022) 13:938447. doi: 10.3389/fphar.2022.938447

14. Zeng XZ, Zhang YY, Yang Q, Wang S, Zou BH, Tan YH, et al. Artesunate attenuates LPS-induced osteoclastogenesis by suppressing TLR4/TRAF6 and PLCγ1-Ca(2+)-NFATc1 signaling pathway. *Acta pharmacologica Sinica.* (2020) 41(2):229–36. doi: 10.1038/s41401-019-0289-6

15. Pang M, Rodríguez-Gonzalez M, Hernandez M, Recinos CC, Seldeen KL, Troen BR. AP-1 and mitf interact with NFATc1 to stimulate cathepsin K promoter activity in osteoclast precursors. *J Cell Biochem* (2019) 120(8):12382–92. doi: 10.1002/jcb.28504

16. Walsh MC, Choi Y. Biology of the RANKL-RANK-OPG system in immunity, bone, and beyond. *Front Immunol* (2014) 5:511. doi: 10.3389/fimmu.2014.00511

17. Polyzos SA, Makras P, Tournis S, Anastasilakis AD. Off-label uses of denosumab in metabolic bone diseases. *Bone.* (2019) 129:115048. doi: 10.1016/j.bone.2019.115048

18. Bergers G, Fendt SM. The metabolism of cancer cells during metastasis. *Nat Rev Cancer.* (2021) 21(3):162–80. doi: 10.1038/s41568-020-00320-2

19. Suhail Y, Cain MP, Vanaja K, Kurywchak PA, Levchenko A, Kalluri R, et al. Systems biology of cancer metastasis. *Cell systems.* (2019) 9(2):109–27. doi: 10.1016/j.cels.2019.07.003

20. Valastyan S, Weinberg RA. Tumor metastasis: Molecular insights and evolving paradigms. *Cell.* (2011) 147(2):275–92. doi: 10.1016/j.cell.2011.09.024

21. Chiang AC, Massagué J. Molecular basis of metastasis. *New Engl J Med* (2008) 359 (26):2814–23. doi: 10.1056/NEJMra0805239

22. Coleman RE, Croucher PI, Padhani AR, Clézardin P, Chow E, Fallon M, et al. Bone metastases. *Nat Rev Dis primers.* (2020) 6(1):83. doi: 10.1016/B978-0-323-47674-4.00056-6

23. Verron E, Schmid-Antomarchi H, Pascal-Mousselard H, Schmid-Alliana A, Scimeca JC, Bouler JM. Therapeutic strategies for treating osteolytic bone metastases. *Drug Discovery Today* (2014) 19(9):1419–26. doi: 10.1016/j.drudis.2014.04.004

24. Clézardin P. Pathophysiology of bone metastases from solid malignancies. *Joint Bone spine.* (2017) 84(6):677–84. doi: 10.1016/j.jbspin.2017.05.006

25. Sethakorn N, Heninger E, Sánchez-de-Diego C, Ding AB, Yada RC, Kerr SC, et al. Advancing treatment of bone metastases through novel translational approaches targeting the bone microenvironment. *Cancers.* (2022) 14(3). doi: 10.3390/cancers14030757

26. Yin JJ, Pollock CB, Kelly K. Mechanisms of cancer metastasis to the bone. *Cell Res* (2005) 15(1):57–62. doi: 10.1038/sj.cr.7290266

27. Mohme M, Riethdorf S, Pantel K. Circulating and disseminated tumour cells - mechanisms of immune surveillance and escape. *Nat Rev Clin Oncol* (2017) 14(3):155–67. doi: 10.1038/nrclinonc.2016.144

28. Santini D, Galluzzo S, Zoccoli A, Pantano F, Fratto ME, Vincenzi B, et al. New molecular targets in bone metastases. *Cancer Treat Rev* (2010) 36 Suppl 3:S6–s10. doi: 10.1016/S0305-7372(10)70013-X

29. Yang C, Tian Y, Zhao F, Chen Z, Su P, Li Y, et al. Bone microenvironment and osteosarcoma metastasis. *Int J Mol Sci* (2020) 21(19). doi: 10.3390/ijms21196985

30. Hiraga T. Hypoxic microenvironment and metastatic bone disease. *Int J Mol Sci* (2018) 19(11). doi: 10.3390/ijms19113523

31. Clézardin P, Coleman R, Puppo M, Ottewell P, Bonnelye E, Paycha F, et al. Bone metastasis: Mechanisms, therapies, and biomarkers. *Physiol Rev* (2021) 101(3):797–855. doi: 10.1152/physrev.00012.2019

32. Ganesh K, Massagué J. Targeting metastatic cancer. *Nat Med* (2021) 27(1):34–44. doi: 10.1038/s41591-020-01195-4

33. Coleman RE. Metastatic bone disease: Clinical features, pathophysiology and treatment strategies. *Cancer Treat Rev* (2001) 27(3):165–76. doi: 10.1053/ctrv.2000.0210

34. Ban J, Fock V, Aryee DNT, Kovar H. Mechanisms, diagnosis and treatment of bone metastases. *Cells.* (2021) 10(11). doi: 10.3390/cells10112944

35. Stresing V, Daubiné F, Benzaid I, Mönkkönen H, Clézardin P. Bisphosphonates in cancer therapy. *Cancer letters.* (2007) 257(1):16–35. doi: 10.1016/j.canlet.2007.07.007

36. Barni S, Mandalà M, Cazzaniga M, Cabiddu M, Cremonesi M. Bisphosphonates and metastatic bone disease. *Ann Oncol Off J Eur Soc Med Oncol* (2006) 17 Suppl 2:ii91–95. doi: 10.1093/annonc/mdj935

37. Walsh MC, Choi Y. Regulation of T cell-associated tissues and T cell activation by RANKL-RANK-OPG. *J Bone mineral Metab* (2021) 39(1):54–63. doi: 10.1007/s00774-020-01178-y

38. Cheng ML, Fong L. Effects of RANKL-targeted therapy in immunity and cancer. *Front Oncol* (2014) 3:329. doi: 10.3389/fonc.2013.00329

39. van Dam PA, Verhoeven Y, Trinh XB. The non-Bone-Related role of RANK/RANKL signaling in cancer. *Adv Exp Med Biol* (2020) 1277:53–62. doi: 10.1007/978-3-030-50224-9_3

40. Rao S, Cronin SJF, Sigl V, Penninger JM. RANKL and RANK: From mammalian physiology to cancer treatment. *Trends Cell Biol* (2018) 28(3):213–23. doi: 10.1016/j.tcb.2017.11.001

41. Anderson DM, Maraskovsky E, Billingsley WL, Dougall WC, Tometsko ME, Roux ER, et al. A homologue of the TNF receptor and its ligand enhance T-cell growth and dendritic-cell function. *Nature.* (1997) 390(6656):175–9. doi: 10.1038/36593

42. Hu J, Hu WX. Targeting signaling pathways in multiple myeloma: Pathogenesis and implication for treatments. *Cancer letters.* (2018) 414:214–21. doi: 10.1016/j.canlet.2017.11.020

43. Zhang L, Teng Y, Zhang Y, Liu J, Xu L, Qu J, et al. Proteasome inhibitor bortezomib (PS-341) enhances RANKL-induced MDA-MB-231 breast cancer cell migration. *Mol Med Rep* (2012) 5(2):580–4. doi: 10.3892/mmr.2011.678

44. Tang ZN, Zhang F, Tang P, Qi XW, Jiang J. RANKL-induced migration of MDA-MB-231 human breast cancer cells *via* src and MAPK activation. *Oncol Rep* (2011) 26 (5):1243–50. doi: 10.3892/or.2011.1368

45. Shin M, Matsuo K, Tada T, Fukushima H, Furuta H, Ozeki S, et al. The inhibition of RANKL/RANK signaling by osteoprotegerin suppresses bone invasion by oral squamous cell carcinoma cells. *Carcinogenesis.* (2011) 32(11):1634–40. doi: 10.1093/carcin/bgr198

46. Renema N, Navet B, Heymann MF, Lezot F, Heymann D. RANK-RANKL signalling in cancer. *Bioscience Rep* (2016) 36(4). doi: 10.1042/BSR20160150

47. Infante M, Fabi A, Cognetti F, Gorini S, Caprio M, Fabbri A. RANKL/RANK/OPG system beyond bone remodeling: Involvement in breast cancer and clinical perspectives. *J Exp Clin Cancer Res CR.* (2019) 38(1):12. doi: 10.1186/s13046-018-1001-2

48. Li B, Wang P, Jiao J, Wei H, Xu W, Zhou P. Roles of the RANKL-RANK axis in immunity-implications for pathogenesis and treatment of bone metastasis. *Front Immunol* (2022) 13:824117. doi: 10.3389/fimmu.2022.824117

49. Francisconi CF, Vieira AE, Azevedo MCS, Tabanez AP, Fonseca AC, Trombone APF, et al. RANKL triggers treg-mediated immunoregulation in inflammatory osteolysis. *J Dental Res* (2018) 97(8):917–27. doi: 10.1177/0022034518759302

50. Vernal R, Díaz-Zúñiga J, Melgar-Rodríguez S, Pujol M, Diaz-Guerra E, Silva A, et al. Activation of RANKL-induced osteoclasts and memory T lymphocytes by porphyromonas gingivalis is serotype dependant. *J Clin periodontology.* (2014) 41 (5):451–9. doi: 10.1111/jcpe.12236

51. Lacey DL, Boyle WJ, Simonet WS, Kostenuik PJ, Dougall WC, Sullivan JK, et al. Bench to bedside: elucidation of the OPG-RANK-RANKL pathway and the development of denosumab. *Nat Rev Drug discovery.* (2012) 11(5):401–19. doi: 10.1038/nrd3705

52. Dougall WC, Holen I, González Suárez E. Targeting RANKL in metastasis. *BoneKEy Rep* (2014) 3:519. doi: 10.1038/bonekey.2014.14

53. Kostenuik PJ, Nguyen HQ, McCabe J, Warmington KS, Kurahara C, Sun N, et al. Denosumab, a fully human monoclonal antibody to RANKL, inhibits bone resorption and increases BMD in knock-in mice that express chimeric (murine/human) RANKL. *J Bone mineral Res Off J Am Soc Bone Mineral Res* (2009) 24(2):182–95. doi: 10.1359/jbmr.081112

54. Keizer RJ, Huitema AD, Damen CW, Schellens JH, Beijnen JH. [The pharmacokinetics of monoclonal antibodies]. *Nederlands tijdschrift voor geneeskunde.* (2007) 151(12):683–8.

55. Gül G, Sendur MA, Aksoy S, Sever AR, Altundag K. A comprehensive review of denosumab for bone metastasis in patients with solid tumors. *Curr Med Res opinion.* (2016) 32(1):133–45. doi: 10.1185/03007995.2015.1105795

56. Wohlrab J. Pharmacokinetic characteristics of therapeutic antibodies. *J der Deutschen Dermatologischen Gesellschaft = J German Soc Dermatol JDDG.* (2015) 13 (6):530–4. doi: 10.1111/ddg.12648

57. Iseri K, Watanabe M, Yoshikawa H, Mitsui H, Endo T, Yamamoto Y, et al. Effects of denosumab and alendronate on bone health and vascular function in hemodialysis patients: A randomized, controlled trial. *J Bone mineral Res Off J Am Soc Bone Mineral Res* (2019) 34(6):1014–24. doi: 10.1002/jbmr.3676

58. Gnant M, Pfeiler G, Dubsky PC, Hubalek M, Greil R, Jakesz R, et al. Adjuvant denosumab in breast cancer (ABCSG-18): a multicentre, randomised, double-blind, placebo-controlled trial. *Lancet (London England)* (2015) 386(9992):433–43. doi: 10.1016/S0140-6736(15)60995-3

59. Smith MR, Saad F, Coleman R, Shore N, Fizazi K, Tombal B, et al. Denosumab and bone-metastasis-free survival in men with castration-resistant prostate cancer: results of a phase 3, randomised, placebo-controlled trial. *Lancet (London England)* (2012) 379 (9810):39–46. doi: 10.1016/S0140-6736(11)61226-9

60. Doshi S, Sutjandra L, Zheng J, Sohn W, Peterson M, Jang G, et al. Denosumab dose selection for patients with bone metastases from solid tumors. *Clin Cancer Res an Off J Am Assoc Cancer Res* (2012) 18(9):2648–57. doi: 10.1158/1078-0432.CCR-11-2944

61. Raje N, Terpos E, Willenbacher W, Shimizu K, García-Sanz R, Durie B, et al. Denosumab versus zoledronic acid in bone disease treatment of newly diagnosed multiple myeloma: An international, double-blind, double-dummy, randomised, controlled, phase 3 study. *Lancet Oncol* (2018) 19(3):370–81. doi: 10.1016/S1470-2045(18)30072-X

62. Hu MI, Glezerman IG, Leboulleux S, Insogna K, Gucalp R, Misiorowski W, et al. Denosumab for treatment of hypercalcemia of malignancy. *J Clin Endocrinol Metab* (2014) 99(9):3144–52. doi: 10.1210/jc.2014-1001

63. Verma V, Puri A, Shah S, Rekhi B, Gulia A. Giant cell tumor developing in paget's disease of bone: A case report with review of literature. *J orthopaedic Case Rep* (2016) 6 (4):103–7. doi: 10.13107/jocr.2250-0685.594

64. Tanaka T, Slavin J, McLachlan SA, Choong P. Anti-osteoclastic agent, denosumab, for a giant cell tumor of the bone with concurrent paget's disease: A case report. *Oncol letters.* (2017) 13(4):2105–8. doi: 10.3892/ol.2017.5693

65. Zhang Z, Pu F, Shao Z. The skeletal-related events of denosumab versus zoledronic acid in patients with bone metastases: A meta-analysis of randomized controlled trials. *J Bone Oncol* (2017) 9:21–4. doi: 10.1016/j.jbo.2017.09.003

66. Coleman R, Finkelstein DM, Barrios C, Martin M, Iwata H, Hegg R, et al. Adjuvant denosumab in early breast cancer (D-CARE): An international, multicentre, randomised, controlled, phase 3 trial. *Lancet Oncol* (2020) 21(1):60–72. doi: 10.1016/S1470-2045(19)30687-4

67. Peters S, Danson S, Hasan B, Dafni U, Reinmuth N, Majem M, et al. A randomized open-label phase III trial evaluating the addition of denosumab to standard first-line treatment in advanced NSCLC: The European thoracic oncology platform (ETOP) and European organisation for research and treatment of cancer (EORTC) SPLENDOUR trial. *J Thorac Oncol Off Publ Int Assoc Study Lung Cancer.* (2020) 15(10):1647–56. doi: 10.1016/j.jtho.2020.06.011

68. Shapiro CL, Moriarty JP, Dusetzina S, Himelstein AL, Foster JC, Grubbs SS, et al. Cost-effectiveness analysis of monthly zoledronic acid, zoledronic acid every 3 months, and monthly denosumab in women with breast cancer and skeletal metastases: CALGB 70604 (Alliance). *J Clin Oncol Off J Am Soc Clin Oncol* (2017) 35(35):3949–55. doi: 10.1200/JCO.2017.73.7437

69. Chen J, Zhou L, Liu X, Wen X, Li H, Li W. Meta-analysis of clinical trials to assess denosumab over zoledronic acid in bone metastasis. *Int J Clin pharmacy.* (2021) 43(1):2–10. doi: 10.1007/s11096-020-01105-1

70. Sung H, Ferlay J, Siegel RL, Laversanne M, Soerjomataram I, Jemal A, et al. Global cancer statistics 2020: GLOBOCAN estimates of incidence and mortality worldwide for 36 cancers in 185 countries. *CA: Cancer J Clin* (2021) 71(3):209–49. doi: 10.3322/caac.21660

71. Morgan E, Soerjomataram I, Rumgay H, Coleman HG, Thrift AP, Vignat J, et al. The global landscape of esophageal squamous cell carcinoma and esophageal adenocarcinoma incidence and mortality in 2020 and projections to 2040: New estimates from GLOBOCAN 2020. *Gastroenterology.* (2022) 163(3):649–658.e642. doi: 10.1053/j.gastro.2022.05.054

72. Demers LM, Costa L, Lipton A. Biochemical markers and skeletal metastases. *Cancer.* (2000) 88(12 Suppl):2919–26. doi: 10.1002/1097-0142(20000615)88:12+<2919::AID-CNCR7>3.0.CO;2-Z

73. Hong S, Youk T, Lee SJ, Kim KM, Vajdic CM. Bone metastasis and skeletal-related events in patients with solid cancer: A Korean nationwide health insurance database study. *PloS One* (2020) 15(7):e0234927. doi: 10.1371/journal.pone.0234927

74. Roodman GD. Mechanisms of bone metastasis. *New Engl J Med* (2004) 350 (16):1655–64. doi: 10.1056/NEJMra030831

75. Fares J, Fares MY, Khachfe HH, Salhab HA, Fares Y. Molecular principles of metastasis: a hallmark of cancer revisited. *Signal transduction targeted Ther* (2020) 5 (1):28. doi: 10.1038/s41392-020-0134-x

76. Liu Q, Zhang H, Jiang X, Qian C, Liu Z, Luo D. Factors involved in cancer metastasis: a better understanding to "seed and soil" hypothesis. *Mol cancer.* (2017) 16 (1):176. doi: 10.1186/s12943-017-0742-4

77. Fidler IJ. The pathogenesis of cancer metastasis: The 'seed and soil' hypothesis revisited. *Nat Rev Cancer.* (2003) 3(6):453–8. doi: 10.1038/nrc1098

78. Fornetti J, Welm AL, Stewart SA. Understanding the bone in cancer metastasis. *J Bone mineral Res Off J Am Soc Bone Mineral Res* (2018) 33(12):2099–113. doi: 10.1002/jbmr.3618

79. Chappard D, Bouvard B, Baslé MF, Legrand E, Audran M. Bone metastasis: Histological changes and pathophysiological mechanisms in osteolytic or osteosclerotic localizations. *A review. Morphologie Bull l'Association Des anatomistes.* (2011) 95 (309):65–75. doi: 10.1016/j.morpho.2011.02.004

80. Ponzetti M, Rucci N. Switching homes: How cancer moves to bone. *Int J Mol Sci* (2020) 21(11). doi: 10.3390/ijms21114124

81. Meads MB, Hazlehurst LA, Dalton WS. The bone marrow microenvironment as a tumor sanctuary and contributor to drug resistance. *Clin Cancer Res an Off J Am Assoc Cancer Res* (2008) 14(9):2519–26. doi: 10.1158/1078-0432.CCR-07-2223

82. Landherr L, Nagykálnai T. [Treatment of bone metastases: Bisphosphonates and denosumab]. *Magyar onkologia.* (2017) 61(2):175–80.

83. Vallet S, Smith MR, Raje N. Novel bone-targeted strategies in oncology. *Clin Cancer Res an Off J Am Assoc Cancer Res* (2010) 16(16):4084–93. doi: 10.1158/1078-0432.CCR-10-0600

84. Wellington K, Goa KL. Zoledronic acid: A review of its use in the management of bone metastases and hypercalcaemia of malignancy. *Drugs.* (2003) 63(4):417–37. doi: 10.2165/00003495-200363040-00009

85. Santini D, Fratto ME, Vincenzi B, Galluzzo S, Tonini G. Zoledronic acid in the management of metastatic bone disease. *Expert Opin Biol Ther* (2006) 6(12):1333–48. doi: 10.1517/14712598.6.12.1333

86. Mundy GR, Yoneda T, Hiraga T. Preclinical studies with zoledronic acid and other bisphosphonates: Impact on the bone microenvironment. *Semin Oncol* (2001) 28(2 Suppl 6):35–44. doi: 10.1016/S0093-7754(01)90263-5

87. Van Acker HH, Anguille S, Willemen Y, Smits EL, Van Tendeloo VF. Bisphosphonates for cancer treatment: Mechanisms of action and lessons from clinical trials. *Pharmacol Ther* (2016) 158:24–40. doi: 10.1016/j.pharmthera.2015.11.008

88. O'Carrigan B, Wong MH, Willson ML, Stockler MR, Pavlakis N, Goodwin A. Bisphosphonates and other bone agents for breast cancer. *Cochrane Database systematic Rev* (2017) 10(10):Cd003474. doi: 10.1002/14651858.CD003474.pub4

89. Saad F. Zoledronic acid: Past, present and future roles in cancer treatment. *Future Oncol (London England).* (2005) 1(2):149–59. doi: 10.1517/14796694.1.2.149

90. Singireesu S, Mondal SK, Yerramsetty S, Misra S. Zoledronic acid induces micronuclei formation, mitochondrial-mediated apoptosis and cytostasis in kidney cells. *Life Sci* (2018) 203:305–14. doi: 10.1016/j.lfs.2018.04.059

91. Peddi P, Lopez-Olivo MA, Pratt GF, Suarez-Almazor ME. Denosumab in patients with cancer and skeletal metastases: A systematic review and meta-analysis. *Cancer Treat Rev* (2013) 39(1):97–104. doi: 10.1016/j.ctrv.2012.07.002

92. Ford JA, Jones R, Elders A, Mulatero C, Royle P, Sharma P, et al. Denosumab for treatment of bone metastases secondary to solid tumours: Systematic review and network meta-analysis. *Eur J Cancer (Oxford Engl 1990).* (2013) 49(2):416–30. doi: 10.1016/j.ejca.2012.07.016

93. Henry DH, Costa L, Goldwasser F, Hirsh V, Hungria V, Prausova J, et al. Randomized, double-blind study of denosumab versus zoledronic acid in the treatment of bone metastases in patients with advanced cancer (excluding breast and prostate cancer) or multiple myeloma. *J Clin Oncol Off J Am Soc Clin Oncol* (2011) 29(9):1125–32. doi: 10.1200/JCO.2010.31.3304

94. Chawla S, Blay JY, Rutkowski P, Le Cesne A, Reichardt P, Gelderblom H, et al. Denosumab in patients with giant-cell tumour of bone: A multicentre, open-label, phase 2 study. *Lancet Oncol* (2019) 20(12):1719–29. doi: 10.1016/S1470-2045(19)30663-1

95. Snedecor SJ, Carter JA, Kaura S, Botteman MF. Denosumab versus zoledronic acid for treatment of bone metastases in men with castration-resistant prostate cancer: A cost-effectiveness analysis. *J Med economics.* (2013) 16(1):19–29. doi: 10.3111/13696998.2012.719054

96. Menshawy A, Mattar O, Abdulkarim A, Kasem S, Nasreldin N, Menshawy E, et al. Denosumab versus bisphosphonates in patients with advanced cancers-related bone metastasis: Systematic review and meta-analysis of randomized controlled trials. *Supportive Care Cancer Off J Multinational Assoc Supportive Care Cancer.* (2018) 26 (4):1029–38. doi: 10.1007/s00520-018-4060-1

97. Chen F, Pu F. Safety of denosumab versus zoledronic acid in patients with bone metastases: A meta-analysis of randomized controlled trials. *Oncol Res Treat* (2016) 39(7-8):453–9. doi: 10.1159/000447372

98. Roukain A, Alwan H, Bongiovanni M, Sykiotis GP, Kopp PA. Denosumab for the treatment of hypercalcemia in a patient with parathyroid carcinoma: A case report. *Front endocrinology.* (2021) 12:794988. doi: 10.3389/fendo.2021.794988

99. Martin M, Bell R, Bourgeois H, Brufsky A, Diel I, Eniu A, et al. Bone-related complications and quality of life in advanced breast cancer: Results from a randomized phase III trial of denosumab versus zoledronic acid. *Clin Cancer Res an Off J Am Assoc Cancer Res* (2012) 18(17):4841–9. doi: 10.1158/1078-0432.CCR-11-3310

100. Kurata T, Nakagawa K. Efficacy and safety of denosumab for the treatment of bone metastases in patients with advanced cancer. *Japanese J Clin Oncol* (2012) 42 (8):663–9. doi: 10.1093/jjco/hys088

101. Li HS, Lei SY, Li JL, Xing PY, Hao XZ, Xu F, et al. Efficacy and safety of concomitant immunotherapy and denosumab in patients with advanced non-small cell lung cancer carrying bone metastases: A retrospective chart review. *Front Immunol* (2022) 13:908436. doi: 10.3389/fimmu.2022.908436

102. Ferrara R, Imbimbo M, Malouf R, Paget-Bailly S, Calais F, Marchal C, et al. Single or combined immune checkpoint inhibitors compared to first-line platinum-based chemotherapy with or without bevacizumab for people with advanced non-small cell lung cancer. *Cochrane Database systematic Rev* (2021) 4(4):Cd013257. doi: 10.1002/14651858.CD013257.pub3

frontiers | Frontiers in Oncology

TYPE Original Research
PUBLISHED 20 February 2023
DOI 10.3389/fonc.2023.1144039

OPEN ACCESS

EDITED BY
Feifei Pu,
Huazhong University of Science and Technology, China

REVIEWED BY
Dandan Zheng,
University of Nebraska Medical Center, United States
Qianlei Zhou,
Sun Yat-sen Memorial Hospital, China
Yuannyu Zhang,
The University of Texas at Dallas, United States

*CORRESPONDENCE
Yong Qin
qinyong0125@126.com
Qianwen Ye
980861223@qq.com
Shengjie Wang
wsjcsusjtu@163.com

SPECIALTY SECTION
This article was submitted to Surgical Oncology, a section of the journal Frontiers in Oncology

RECEIVED 13 January 2023
ACCEPTED 30 January 2023
PUBLISHED 20 February 2023

CITATION
Long Z, Yi M, Qin Y, Ye Q, Che X, Wang S and Lei M (2023) Development and validation of an ensemble machine-learning model for predicting early mortality among patients with bone metastases of hepatocellular carcinoma. *Front. Oncol.* 13:1144039. doi: 10.3389/fonc.2023.1144039

Development and validation of an ensemble machine-learning model for predicting early mortality among patients with bone metastases of hepatocellular carcinoma

Ze Long[1], Min Yi[2], Yong Qin[3]*, Qianwen Ye[4]*, Xiaotong Che[5], Shengjie Wang[6]* and Mingxing Lei[7,8]

[1]Department of Orthopedics, The Second Xiangya Hospital of Central South University, Changsha, China, [2]Institute of Medical Information and Library, Chinese Academy of Medical Sciences and Peking Union Medical College, Beijing, China, [3]Department of Joint and Sports Medicine Surgery, The Second Affiliated Hospital of Harbin Medical University, Harbin, China, [4]Department of Oncology, Hainan Hospital of People's Liberation Army (PLA) General Hospital, Sanya, China, [5]Department of Evaluation Office, Hainan Cancer Hospital, Haikou, China, [6]Department of Orthopaedic Surgery, Shanghai Sixth People's Hospital Affiliated to Shanghai Jiao Tong University, Shanghai, China, [7]Department of Orthopedic Surgery, Hainan Hospital of People's Liberation Army (PLA) General Hospital, Sanya, China, [8]Chinese People's Liberation Army (PLA) Medical School, Beijing, China

Purpose: Using an ensemble machine learning technique that incorporates the results of multiple machine learning algorithms, the study's objective is to build a reliable model to predict the early mortality among hepatocellular carcinoma (HCC) patients with bone metastases.

Methods: We extracted a cohort of 124,770 patients with a diagnosis of hepatocellular carcinoma from the Surveillance, Epidemiology, and End Results (SEER) program and enrolled a cohort of 1897 patients who were diagnosed as having bone metastases. Patients with a survival time of 3 months or less were considered to have had early death. To compare patients with and without early mortality, subgroup analysis was used. Patients were randomly divided into two groups: a training cohort (n = 1509, 80%) and an internal testing cohort (n = 388, 20%). In the training cohort, five machine learning techniques were employed to train and optimize models for predicting early mortality, and an ensemble machine learning technique was used to generate risk probability in a way of soft voting, and it was able to combine the results from the multiply machine learning algorithms. The study employed both internal and external validations, and the key performance indicators included the area under the receiver operating characteristic curve (AUROC), Brier score, and calibration curve. Patients from two tertiary hospitals were chosen as the external testing cohorts (n = 98). Feature importance and reclassification were both operated in the study.

Results: The early mortality was 55.5% (1052/1897). Eleven clinical characteristics were included as input features of machine learning models: sex (p = 0.019), marital status (p = 0.004), tumor stage (p = 0.025), node stage (p = 0.001), fibrosis

score (p = 0.040), AFP level (p = 0.032), tumor size (p = 0.001), lung metastases (p < 0.001), cancer-directed surgery (p < 0.001), radiation (p < 0.001), and chemotherapy (p < 0.001). Application of the ensemble model in the internal testing population yielded an AUROC of 0.779 (95% confidence interval [CI]: 0.727–0.820), which was the largest AUROC among all models. Additionally, the ensemble model (0.191) outperformed the other five machine learning models in terms of Brier score. In terms of decision curves, the ensemble model also showed favorable clinical usefulness. External validation showed similar results; with an AUROC of 0.764 and Brier score of 0.195, the prediction performance was further improved after revision of the model. Feature importance demonstrated that the top three most crucial features were chemotherapy, radiation, and lung metastases based on the ensemble model. Reclassification of patients revealed a substantial difference in the two risk groups' actual probabilities of early mortality (74.38% vs. 31.35%, p < 0.001). Patients in the high-risk group had significantly shorter survival time than patients in the low-risk group (p < 0.001), according to the Kaplan–Meier survival curve.

Conclusions: The ensemble machine learning model exhibits promising prediction performance for early mortality among HCC patients with bone metastases. With the aid of routinely accessible clinical characteristics, this model can be a trustworthy prognostic tool to predict the early death of those patients and facilitate clinical decision-making.

KEYWORDS

bone metastases, machine learning, ensemble model, early mortality, hepatocellular carcinoma

Introduction

Primary liver cancer is the most frequent cause of cancer-related death in most regions of the world, and it is predicted to be the sixth most prevalent cancer worldwide in terms of incidence and mortality in 2020, with up to 906,000 new cases and 830,000 deaths (1). Hepatocellular carcinoma (HCC) is the most common type of liver cancer, and it accounted for 75% to 85% of all cases. Additionally, incidence and mortality are continually rising in many nations (2), and many HCC patients are still at an advanced stage when they are diagnosed (3). Viral hepatitis B and C and cirrhosis, fatty liver disease and diabetes, alcohol, and aflatoxin and aristolochic acid are among the main risk factors for HCC (3). Although the survival prognosis for HCC patients has improved significantly over the past 20 years, thanks to treatments, it is still unsatisfactory, with a median overall survival of only 16.5 to 16.2 months and a median progression-free survival of 5.6 to 5.7 months (4). Additionally, the 5-year survival rate remains less than 20% because of the high recurrence rate (5).

With the improvement of prognosis among HCC patients in recent years due to novel imaging techniques and multidisciplinary therapies, extrahepatic metastases now occur more frequently (6). The bone is a common extrahepatic metastatic site, and the prevalence ranged from 2.0% to 25.0% among patients with HCC (7, 8). Additionally, bone metastasis was responsible for 32.5% to 57.0% of all distant metastasis in HCC patients (9). HCC patients with bone metastases often had expansive soft tissue masses with severe osteolytic bone destruction and this may be explained by the theory of premetastatic niche (10, 11). Regarding prognosis, bone metastasis was a significant risk for survival outcome among HCC patients, and the median survival time was only 2.8–3.3 months among HCC patients with bone metastases (12, 13). The prognosis of those individuals may be improved by tailored therapy, and in order to implement individualized therapy, prediction models for evaluating the survival outcome among HCC patients with bone metastases must be developed.

A number of risk factors, including marital status (14), primary tumor surgery (14), Child-Pugh grade (15, 16), T stage (15), performance status, radiotherapy (17), the presence of ascites at the initial presentation (18), and the number of skeletal metastases (16), have been found to be significantly associated with the survival outcome of HCC patients with bone metastases. The establishment of survival prediction models for HCC patients with bone metastases is facilitated by these risk variables. Nevertheless, confounding factors that offer nonlinear influences and pose issues frequently have an impact on the survival prediction of patients with bone metastases. It should be noted that using machine learning techniques, this issue can be readily solved (19).

Given the poor survival prognosis among those patients, short-term survival forecasting is crucial to create better plans and more appropriate responses. Therefore, this study aims to construct an accurate model to predict the early mortality (three-month mortality) among HCC patients with bone metastases using an ensemble machine learning technique that aggregated the results of multiple machine learning algorithms.

Methods

Data source and eligibility criteria

We extracted data from the Surveillance, Epidemiology, and End Results (SEER) Program. SEER is a large oncologic database which collects information on cancer diagnoses and survival for about 30% of the US population with the effort to reduce the cancer burden. We completed the registration form to obtain SEER*Stat (version 8.4.0.1) after reading and signing the Terms of Use Agreement. This software provides us with interface to access to the SEER database and download corresponding data.

Between January 1, 2000, and December 31, 2019, patients with histologically confirmed HCC were included for the analysis. The exclusive criteria were as follows (1): Patients did not have bone metastases (2); Patients younger than 18 years old (3); Patients did not have the histological diagnosis of adenomas and adenocarcinomas (4); Patients whose causes of death were missing or unknown (5); Patients were alive or dead of other reason (not attributable to liver cancer) with a follow-up interval of only three or less months; and (6) Patients whose survival time was unknown. Complete data were required for stage and liver cancer-specific mortality, and censoring was derived from the vital status recode.

All enrolled patients from the SEER database were divided into two groups: a model training cohort (n = 1509, 80%) and a model testing cohort (n = 388, 20%). The model testing cohort was regarded as the internal testing cohort, and the eligible patients from Hainan Hospital of Chinese PLA General Hospital (Sanya) and Hainan Cancer Hospital (Haikou) were served as the external testing cohort (n = 98). When users access to the SEER database, it is unnecessary to obtain formal ethics approval, since it is covered by its open access policy. This study was approved by the Hainan Hospital of Chinese PLA General Hospital and patients gave informed oral consent prior to data collection.

Variable collection

Age, sex, race, marital status, tumor (T) stage, node (N) stage, fibrosis score, alpha fetoprotein (AFP) level, tumor size, brain metastases, liver metastases, lung metastases, surgery of lymph, cancer-directed surgery, radiation, and chemotherapy were all taken out of the SEER database. Patients having a survival interval of three months or less were considered to have experienced early mortality. Cancer-specific death was recorded and used in the study. In terms of American Joint Committee on Cancer and Extent of Disease classification, T and N stages were used for analysis. Race was divided into black, white, others, and unknown, the others of race included American Indian, AK Native, Asian, and Pacific Islander.

Model training

Selection of model features was determined by subgroup analysis of clinical characteristics in the training group, and significant variables were included as the input features of model building. Five machine learning techniques, including an artificial neural network, gradient boosting decision tree, eXGBoosting machine, decision tree, and support vector machine, were investigated in the study to construct an ensemble machine learning model. Each model received the same input features. These models are widely used for binary classification issues in the field of medicine, and this study chose a wide range of models to reflect this. To further explain, gradient boosting decision tree frequently conducts well with risk classification, but an ensemble was introduced to further improve model robustness in the study. Combining the outputs of the artificial neural network, gradient boosting decision tree, eXGBoosting machine, decision tree, and support vector machine, ensemble machine learning can use models created by numerous machine learning techniques to make predictions. Particularly, ensemble models frequently produce superior predicting performance than individual machine learning models (20, 21). Broad upper and lower bounds were applied to grid and random hyperparameter searches to explore the optimal hyperparameters, and the area under the receiver operating characteristic curve (AUROC) was the primary metric to evaluate the prediction performance after the optimal hyperparameters were finally determined, helping to largely avoid underfitted and overfitted conditions.

Model validation

The AUROC was calculated for model discrimination during model evaluation. The models' capacity for discrimination refers to their power to discern between favorable and unfavorable outcomes. The density probability curve and discrimination slope were used in the analysis as additional indicators showing model discrimination. Brier score and visual examination of calibration plots were used to evaluate model calibration, which reflects the consistency between anticipated and observed outcomes. The predicted risk of an event developing vs. the observed risk were plotted in calibration plots, and the calibration slope and intercept-in-large were derived for each plot. For each machine learning model, a clinical net benefit was also calculated using decision curve analysis; this measure of value was accomplished by making decisions based on model predictions. For each model, other key performance measures included specificity, sensitivity, and accuracy.

Statistical analysis

Using the *t*-test for continuous variables and chi-square test or adjusted continuity chi-square test for proportional variables, the

clinical characteristics between patients in the training and testing groups were compared. In order to interpret feature contributions, in terms of the ensemble machine learning model, Shaley Additive Explanation (SHAP) was utilized. Patients were categorized into two risk groups using the ensemble machine learning model, stratified by the ideal cut-off value (threshold). The chi-square test was used to compare the difference of the actual probability of developing early mortality among patients in the high- and low-risk groups. The Kaplan–Meier method and log-rank test were conducted to create the survival curve among patients stratified by risk groups. The statistical tools used for these analyses included the R statistical software (R Project for Statistical Computing, version 4.1.2) and Python (version 3.9.7). Statistical significance was defined as a two-sided p-value of 0.05.

Results

Process of screening and clinicopathology

The study included 124,770 people with liver cancer in total. A cohort of 1,897 individuals from the SEER database who had been histologically determined to have HCC with bone metastases were included based on the screening criteria (Figure 1). The baseline clinical characteristics of patients are shown in Table 1. The average age of the patients was 65.04 (10.20) years, with the majority of them being men (85.6%), Caucasian (72.6%), and married (46.4%). A large number of tumors were T3 (29.7%) and N0 (62.3%) disease. Up to 62.2% of patients had positive AFP results. In addition to bone metastases, brain metastases, liver metastases, and lung metastases accounted for 3.2%, 7.2%, and 23.0%, respectively, indicating relatively heavy metastatic illness. Only 2.6% of patients received cancer-specific surgery, while 0.6% of patients underwent lymph node surgery. In the entire cohort of patients, 39.7% patients received radiation and 38.7% patients had chemotherapy. There were 55.5% of patients who had events (early mortality from HCC). The median survival time was 3.0 months (range: 0.0–98.0 months).

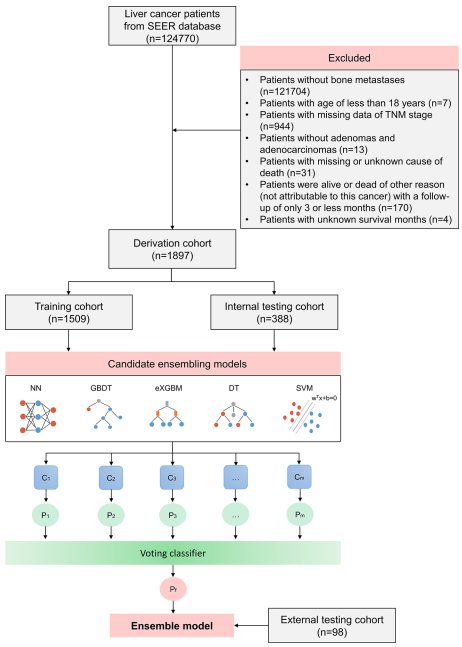

FIGURE 1
Flow chart outlining patient's enrollment, study design, and ensemble machine learning technique.

Development of the ensemble model

A comparison of clinical characteristics was operated between patients in the training and internal testing cohort, and it demonstrated that the two cohorts were comparable because no significant difference was found in the distribution of the clinical characteristics (Table 2). In the training cohort, the study found that early mortality patients in the training cohort were more likely to be men ($p = 0.019$), single ($p = 0.004$), with advanced T ($p = 0.025$) and N ($p = 0.001$) stage, unknown fibrosis score ($p = 0.040$), positive AFP level ($p = 0.032$), larger tumor size ($p = 0.001$), lung metastases ($p < 0.001$), less cancer-directed surgery ($p < 0.001$), less radiation ($p < 0.001$), and less chemotherapy ($p < 0.001$), whereas other clinical characteristics were insignificant (Table 3). Thus, in order to train and improve the models, the aforementioned 11 clinical criteria were used, and the best hyperparameters were found after grid and random hyperparameter searches for each model (Table 4). At last, the ensemble machine learning model was developed in a soft-voting method to combine the results from the five machine learning algorithms in the study, including the artificial neural network, gradient boosting decision tree, eXGBoosting machine, decision tree, and support vector machine.

Validation of the ensemble model

Internal validation of the model was operated in the internal testing cohort, and external validation was performed in the external testing cohort. The baseline characteristics of the external testing cohort are shown in Supplementary Table 1. Application of the ensemble model in the internal testing population yielded an AUROC of 0.779 (95% CI: 0.727–0.820) (Figure 2), which was the largest AUROC among all models, suggesting optimal discrimination in the study. The neural network model had the second-highest AUROC, which was 0.777 (95% CI: 0.730–0.823), and was followed by the eXGBoosting machine model. The external validation showed the AUROC of the ensemble model was 0.764 (95% CI: 0.642–0.886) (Supplementary Figure 1). Each model's probability density curve is shown in Figure 3, which reveals that most models exhibited favorable discrimination with a sizable portion of separation. The similar trend of density curve was also observed in the external validation according to the ensemble model (Supplementary Figure 2). The majority of models displayed positive discrimination, as shown by the calculation of the discrimination slope, which was defined as the mean difference between actual and observed risk probabilities of occurrences (Supplementary Figure 3). External validation elucidated that the discrimination slope was also up to 0.211 in the ensemble model (Supplementary Figure 4). Of note, other machine learning models

10.3389/fonc.2023.1144039

TABLE 1 Baseline clinical characteristics of the entire cohort.

Characteristics	Overall
n	1897
Age (mean (SD))	65.04 (10.20)
Sex	
Female	274 (14.4)
Male	1623 (85.6)
Race (%)	
Black	279 (14.7)
Others	234 (12.3)
Unknown	7 (0.4)
White	1377 (72.6)
Marital status (%)	
Married	881 (46.4)
Others	474 (25.0)
Single	443 (23.4)
Unknown	99 (5.2)
T stage (%)	
T0	20 (1.1)
T1	435 (22.9)
T2	241 (12.7)
T3	564 (29.7)
T4	171 (9.0)
TX	466 (24.6)
N stage (%)	
N0	1181 (62.3)
N1	362 (19.1)
NX	354 (18.7)
Fibrosis score (%)	
Ishak 0–4	59 (3.1)
Ishak 5–6	254 (13.4)
Unknown	1584 (83.5)
AFP level (%)	
Negative	239 (12.6)
Positive	1179 (62.2)
Unknown	479 (25.3)
Tumor size (mm, %)	
Less than 45	105 (5.5)
46–85	143 (7.5)
More than 86	253 (13.3)
Unknown	1396 (73.6)
Brain metastases (%)	
No	1764 (93.0)
Unknown	72 (3.8)
Yes	61 (3.2)
Liver metastases (%)	
No	1690 (89.1)
Unknown	70 (3.7)
Yes	137 (7.2)
Lung metastases (%)	
No	1388 (73.2)
Unknown	72 (3.8)
Yes	437 (23.0)
Surgery of lymph (%)	
Yes	12 (0.6)
None/unknown	1885 (99.4)
Cancer-directed surgery (%)	
Yes	49 (2.6)
None/unknown	1848 (97.4)
Radiation (%)	
Yes	753 (39.7)
None/unknown	1144 (60.3)
Chemotherapy (%)	
Yes	734 (38.7)
None/unknown	1163 (61.3)
Early death (%)	
Yes	1052 (55.5)
No	845 (44.5)

SD, Standard deviation; T, tumor; N, node; AFP, alpha fetoprotein.

produced a higher Brier score than the ensemble machine learning model, indicating a bigger prediction error. Table 5 summarizes additional indicators in greater detail. Calibration plots are displayed in Figures 4, 5 shows the decision curve for each model in the study, showing that models, in particular the ensemble machine learning model, had good clinical usefulness. The calibration plot of the ensemble model in the external validation is shown in Supplementary Figure 5. It showed the calibration curve was not close to the ideal reference line, although the calibration slope was near to 1. To further improve the calibration of the ensemble model, we revised the model *via* subtracting 20.0% in each predicted risk of early mortality. Thus, the new revised calibration plot was provided (Supplementary Figure 6), and it demonstrated that the calibration

10.3389/fonc.2023.1144039

TABLE 2 Clinical characteristics among patients stratified by the splitting group.

Characteristics	Training cohort	Internal testing cohort	p
n	1509	388	
Age [mean (SD)]	64.98 (10.23)	65.28 (10.07)	0.608
Sex (%)			0.681
Female	221 (14.6)	53 (13.7)	
Male	1288 (85.4)	335 (86.3)	
Race (%)			0.978
Black	222 (14.7)	57 (14.7)	
Others	185 (12.3)	49 (12.6)	
Unknown	6 (0.4)	1 (0.3)	
White	1096 (72.6)	281 (72.4)	
Marital status (%)			0.399
Married	694 (46.0)	187 (48.2)	
Others	390 (25.8)	84 (21.6)	
Single	348 (23.1)	95 (24.5)	
Unknown	77 (5.1)	22 (5.7)	
T stage (%)			0.821
T0	15 (1.0)	5 (1.3)	
T1	343 (22.7)	92 (23.7)	
T2	187 (12.4)	54 (13.9)	
T3	456 (30.2)	108 (27.8)	
T4	140 (9.3)	31 (8.0)	
TX	368 (24.4)	98 (25.3)	
N stage (%)			0.435
N0	948 (62.8)	233 (60.1)	
N1	288 (19.1)	74 (19.1)	
NX	273 (18.1)	81 (20.9)	
Fibrosis score (%)			0.184
Ishak 0–4	45 (3.0)	14 (3.6)	
Ishak 5–6	192 (12.7)	62 (16.0)	
Unknown	1272 (84.3)	312 (80.4)	
AFP level (%)			0.353
Negative	189 (12.5)	50 (12.9)	
Positive	928 (61.5)	251 (64.7)	
Unknown	392 (26.0)	87 (22.4)	
Tumor size (mm, %)			0.063
Less than 45	92 (6.1)	13 (3.4)	
46–85	114 (7.6)	29 (7.5)	
More than 86	190 (12.6)	63 (16.2)	
Unknown	1113 (73.8)	283 (72.9)	

(Continued)

TABLE 2 Continued

Characteristics	Training cohort	Internal testing cohort	p
Brain metastases (%)			0.707
No	1400 (92.8)	364 (93.8)	
Unknown	60 (4.0)	12 (3.1)	
Yes	49 (3.2)	12 (3.1)	
Liver metastases (%)			0.563
No	1343 (89.0)	347 (89.4)	
Unknown	59 (3.9)	11 (2.8)	
Yes	107 (7.1)	30 (7.7)	
Lung metastases (%)			0.797
No	1106 (73.3)	282 (72.7)	
Unknown	59 (3.9)	13 (3.4)	
Yes	344 (22.8)	93 (24.0)	
Surgery of lymph (%)			1.000
Yes	10 (0.7)	2 (0.5)	
None/unknown	1499 (99.3)	386 (99.5)	
Cancer-directed surgery (%)			0.206
Yes	43 (2.8)	6 (1.5)	
None/unknown	1466 (97.2)	382 (98.5)	
Radiation (%)			0.863
Yes	597 (39.6)	156 (40.2)	
None/unknown	912 (60.4)	232 (59.8)	
Chemotherapy (%)			0.873
Yes	582 (38.6)	152 (39.2)	
None/unknown	927 (61.4)	236 (60.8)	
Early death (%)			0.516
Yes	843 (55.9)	209 (53.9)	
No	666 (44.1)	179 (46.1)	

SD, Standard deviation; T, tumor; N, node; AFP, alpha fetoprotein.

of the model was further improved. In addition, the AUROC, Baier score, and calibration slope were all improved after the revision of model (Table 5). Based on the above findings, although the decision tree had the poorest prediction performance based on the AUROC, it still had advantages based on the intercept-in-large (-0.065) and specificity (0.810). The intercept-in-large was very near to 0, and the specificity was the highest, among all machine learning models. Thus, the decision tree model was also included to develop the ensemble machine learning model. The study found that the top three important features included chemotherapy, radiation, and lung metastases (Figure 6), according to feature importance analysis using the ensemble machine learning model.

Risk category

Reclassification of patients was conducted using the ensemble machine learning model's threshold of 54.1%. The low-risk group included patients with a forecasted risk probability of 54.1% or less, whereas the high-risk group included patients with a predicted risk probability of more than 54.1%. The actual probability of early mortality was significantly different between the two risk groups ($p < 0.001$, Table 6). The Kaplan–Meier survival curve also showed that patients in the high-risk group had significant shorter survival time in comparison to patients in the low-risk group ($p < 0.001$, log-rank test, Supplementary Figure 7).

10.3389/fonc.2023.1144039

TABLE 3 Clinical characteristics among patients stratified by early death in the training cohort.

Characteristics	Overall	Early death		p
		No	Yes	
n	1509	666	843	
Age [mean (SD)]	64.98 (10.23)	65.07 (10.08)	64.92 (10.35)	0.779
Sex (%)				0.019
Female	221 (14.6)	81 (12.2)	140 (16.6)	
Male	1288 (85.4)	585 (87.8)	703 (83.4)	
Race (%)				0.668
Black	222 (14.7)	98 (14.7)	124 (14.7)	
Others	185 (12.3)	74 (11.1)	111 (13.2)	
Unknown	6 (0.4)	3 (0.5)	3 (0.4)	
White	1096 (72.6)	491 (73.7)	605 (71.8)	
Marital status (%)				0.004
Married	694 (46.0)	340 (51.1)	354 (42.0)	
Others	390 (25.8)	164 (24.6)	226 (26.8)	
Single	348 (23.1)	133 (20.0)	215 (25.5)	
Unknown	77 (5.1)	29 (4.4)	48 (5.7)	
T stage (%)				0.025
T0	15 (1.0)	5 (0.8)	10 (1.2)	
T1	343 (22.7)	175 (26.3)	168 (19.9)	
T2	187 (12.4)	82 (12.3)	105 (12.5)	
T3	456 (30.2)	201 (30.2)	255 (30.2)	
T4	140 (9.3)	49 (7.4)	91 (10.8)	
TX	368 (24.4)	154 (23.1)	214 (25.4)	
N stage (%)				0.001
N0	948 (62.8)	451 (67.7)	497 (59.0)	
N1	288 (19.1)	103 (15.5)	185 (21.9)	
NX	273 (18.1)	112 (16.8)	161 (19.1)	
Fibrosis score (%)				0.040
Ishak 0–4	45 (3.0)	28 (4.2)	17 (2.0)	
Ishak 5–6	192 (12.7)	87 (13.1)	105 (12.5)	
Unknown	1272 (84.3)	551 (82.7)	721 (85.5)	
AFP level (%)				0.032
Negative	189 (12.5)	100 (15.0)	89 (10.6)	
Positive	928 (61.5)	395 (59.3)	533 (63.2)	
Unknown	392 (26.0)	171 (25.7)	221 (26.2)	
Tumor size (mm, %)				0.001
Less than 45	92 (6.1)	50 (7.5)	42 (5.0)	
46–85	114 (7.6)	65 (9.8)	49 (5.8)	
More than 86	190 (12.6)	69 (10.4)	121 (14.4)	

(Continued)

TABLE 3 Continued

Characteristics	Overall	Early death		p
		No	Yes	
Unknown	1113 (73.8)	482 (72.4)	631 (74.9)	
Brain metastases (%)				0.519
No	1400 (92.8)	623 (93.5)	777 (92.2)	
Unknown	60 (4.0)	25 (3.8)	35 (4.2)	
Yes	49 (3.2)	18 (2.7)	31 (3.7)	
Liver metastases (%)				0.071
No	1343 (89.0)	602 (90.4)	741 (87.9)	
Unknown	59 (3.9)	28 (4.2)	31 (3.7)	
Yes	107 (7.1)	36 (5.4)	71 (8.4)	
Lung metastases (%)				<0.001
No	1106 (73.3)	556 (83.5)	550 (65.2)	
Unknown	59 (3.9)	24 (3.6)	35 (4.2)	
Yes	344 (22.8)	86 (12.9)	258 (30.6)	
Surgery of lymph (%)				0.182
Yes	10 (0.7)	7 (1.1)	3 (0.4)	
None/unknown	1499 (99.3)	659 (98.9)	840 (99.6)	
Cancer-directed surgery (%)				<0.001
Yes	43 (2.8)	36 (5.4)	7 (0.8)	
None/unknown	1466 (97.2)	630 (94.6)	836 (99.2)	
Radiation (%)				<0.001
Yes	597 (39.6)	376 (56.5)	221 (26.2)	
None/unknown	912 (60.4)	290 (43.5)	622 (73.8)	
Chemotherapy (%)				<0.001
Yes	582 (38.6)	409 (61.4)	173 (20.5)	
None/unknown	927 (61.4)	257 (38.6)	670 (79.5)	

SD, Standard deviation; T, tumor; N, node; AFP, alpha fetoprotein.

Discussion

This study constructed a model to predict early mortality among HCC patients with bone metastases, and the model was developed using the ensemble machine learning technique that combined the results of multiple machine-learning algorithms, including an artificial neural network, gradient boosting decision tree, eXGBoosting machine, decision tree, and support vector machine. The ensemble model outperformed other algorithms in terms of both discrimination and calibration, as evidenced by its greatest AUROC and lowest Brier score. This model might be a helpful predictive tool to determine the likelihood that these individuals would develop early death and to aid in therapeutic decision-making.

In HCC patients with bone metastases, the early mortality rate was 55.5%, showing a comparatively high rate of early death in these patients. According to current literature, the median survival period was only about 2.8 to 3.3 months among HCC patients with bone metastases (12–14). In the present study, the median survival time was 3.0 months (range: 0.0–98.0 months), and this number was consistent with other studies (12–14). But a retrospective study which was conducted by Hirai et al. (8) reported that the median survival was up to 11.07 months after the diagnosis of bone metastases among HCC patients. In addition, a study with small sample size found that the median survival time was 10.0 months among patients with skeletal metastases due to HCC after surgical treatment (16). After analyzing 37 HCC patients with bone metastases, Kim et al. showed that the median survival was 6.2 months (18). The incidence of early death was 26.5% in the external testing cohort, and this number was significantly lower than that in the cohort from the SEER database. The difference might be that the external testing cohort had a significantly higher rate of cancer

TABLE 4 Models and their hyperparameters.

Models	Hyperparameters
Neural Network	MLPClassifier (alpha=1e-05, hidden_layer_sizes=100, random_state=42)
Gradient Boosting Decision Tree	GradientBoostingClassifier (max_depth=1, max_features='auto', min_samples_leaf=186, min_samples_split=179, n_estimators=102, random_state=42)
eXGBoosting Machine	XGBClassifier (base_score=0.5, booster='gbtree', colsample_bylevel=1, colsample_bynode=1, colsample_bytree=1, enable_categorical=False, gamma=0, gpu_id=-1, importance_type=None, interaction_constraints='', learning_rate=0.125, max_delta_step=0, max_depth=75, min_child_weight=56, missing=nan, monotone_constraints='()', n_estimators=36, n_jobs=8, num_parallel_tree=1, predictor='auto', random_state=42, reg_alpha=0, reg_lambda=1, scale_pos_weight=1, subsample=1, tree_method='exact', use_label_encoder=False, validate_parameters=1, verbosity=None)
Decision Tree	DecisionTreeClassifier (max_depth=24, max_features='auto', min_samples_leaf=100, min_samples_split=173, random_state=42)
Support Vector Machine	SVC (C=0.09837555188414593, gamma=0.11638567021515211, probability=True)

surgery (43.9% vs. 2.6%) and chemotherapy (67.3% vs. 38.7%), as compared to the patients from the SEER cohort. In addition, HCC patients with bone metastases from the SEER database were initially diagnosed, whereas in the external testing cohort HCC patients who later developed bone metastases after initial HCC diagnosis were enrolled for analysis. The aforesaid discrepancy may be explained by the small size of the study sample and the population variability.

Numerous researches have looked into the potential risk and protective factors for determining the likelihood that HCC patients with bone metastases would survive. For instance, Guo et al. (14) revealed that married status was independently associated with better survival outcome among HCC patients with bone metastases at initial diagnosis after analyzing 1567 cases from the SEER database. Japanese researchers showed that age of more than 75 years, hepatitis C-virus etiology, and Child-Pugh class B/C were significantly relevant to a worse survival outcome after enrolling 76 patients, and the study also pointed out that pathological fracture or paralysis had no impact on the survival (8). In addition, Honda et al. (15) also demonstrated that Child-Pugh grade and T stage were correlated with overall survival among 99 HCC patients with bone metastases. In a retrospective study of 42 cases, the number of bone metastases and Child-Pugh class were found as independent prognostic factors. However, In a retrospective study of 37 HCC patients presenting with bone metastases, it showed that the presence of ascites was the sole risk factor for survival, while other variables, such as age, gender, performance status, Child-Pugh class, AFP, and treatment for HCC were insignificant (18). Regarding therapeutic approaches, primary tumor surgery (14),

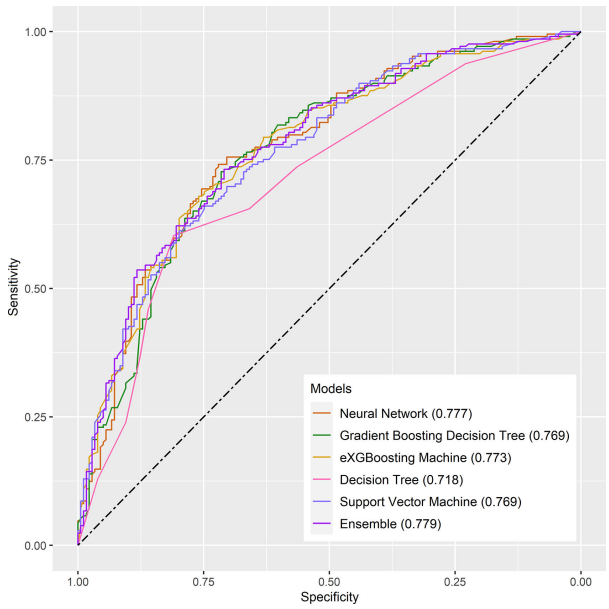

FIGURE 2
The receiver operating characteristic curves for the machine learning models in the internal testing cohort.

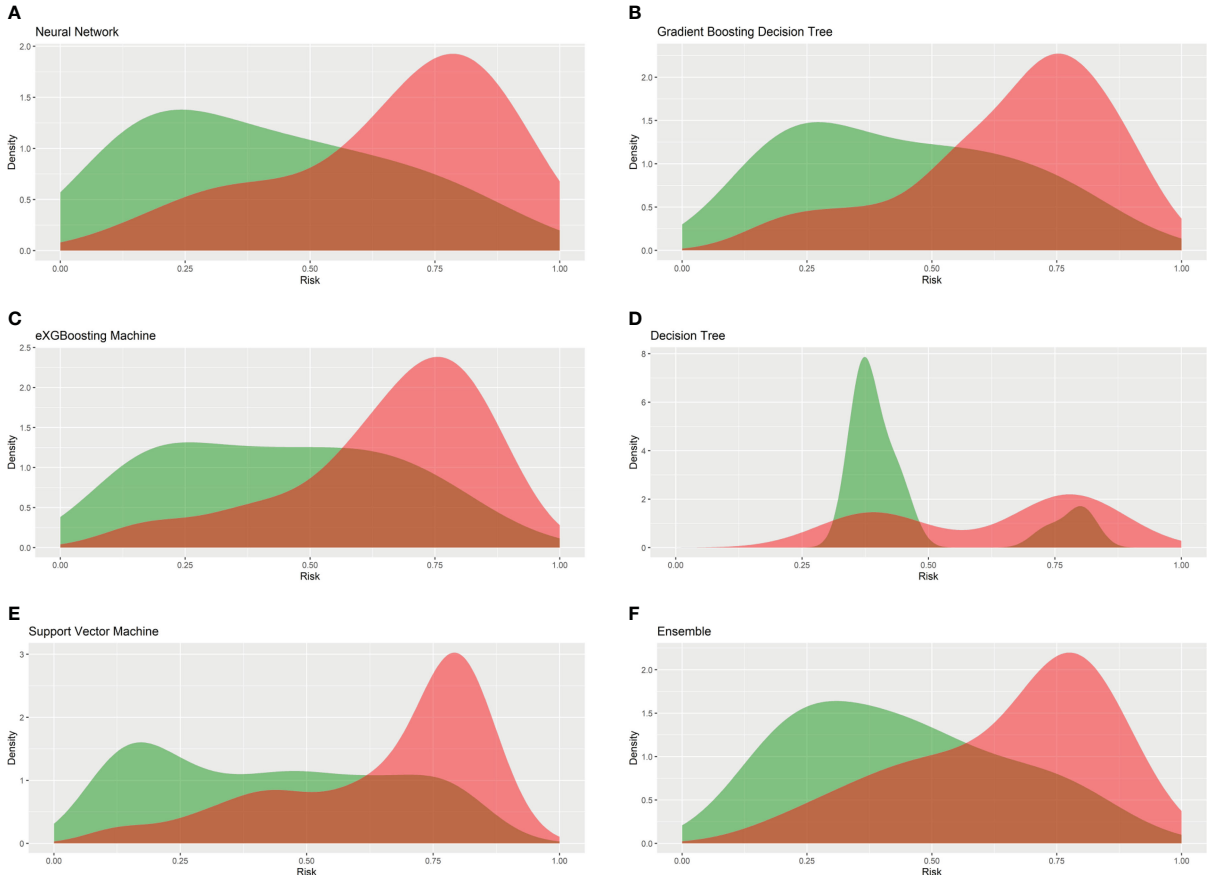

FIGURE 3
Density cures of the machine learning models in the internal testing cohort. **(A)** Neural network; **(B)** gradient boosting decision tree; **(C)** eXGBoosting machine; **(D)** decision tree; **(E)** support vector machine; **(F)** ensemble model.

TABLE 5 Key performance indicators of models.

Models	AUROC	Baier score	Intercept-in-large	Calibration slope	Specificity	Sensitivity	Accuracy	Threshold
Neural Network	0.777 (0.730–0.823)	0.192	-0.019	0.875	0.721	0.742	0.732	0.571
Gradient Boosting Decision Tree	0.769 (0.722–0.817)	0.194	-0.107	1.016	0.715	0.727	0.722	0.578
eXGBoosting Machine	0.773 (0.727–0.820)	0.194	-0.096	1.021	0.760	0.679	0.716	0.624
Decision Tree	0.718 (0.668–0.769)	0.206	-0.065	1.056	0.810	0.603	0.698	0.587
Support Vector Machine	0.769 (0.723–0.816)	0.196	0.918	-0.032	0.799	0.612	0.698	0.669
Ensemble[a]	0.779 (0.733–0.825)	0.191	-0.091	1.104	0.709	0.732	0.722	0.541
Ensemble[b]	0.764 (0.642–0.886)	0.195	-1.022	1.083	0.778	0.692	0.755	0.549
Ensemble[c]	0.778 (0.658–0.887)	0.159	-0.064	0.999	0.778	0.692	0.755	0.349

AUROC, Area under the receiver operating characteristic curve.
[a]indicates internal testing cohort;
[b]indicates external testing cohort;
[c]indicates external testing cohort after model revision.

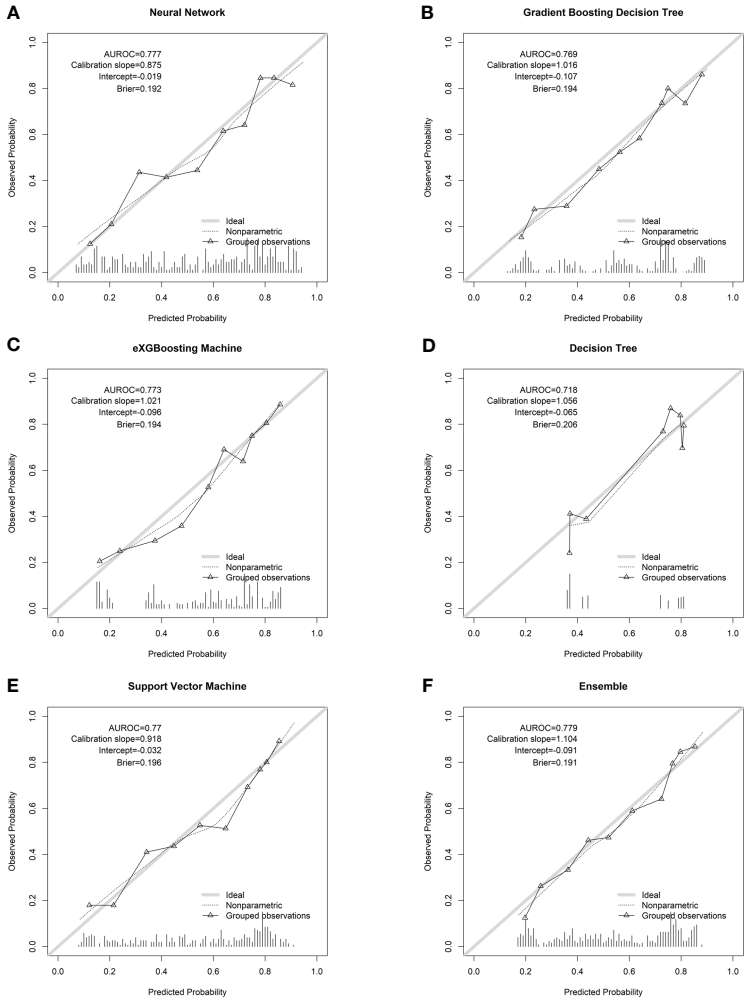

FIGURE 4
Calibration plots of the machine learning models in the internal testing cohort. **(A)** Neural network; **(B)** gradient boosting decision tree; **(C)** eXGBoosting machine; **(D)** decision tree; **(E)** support vector machine; **(F)** ensemble model.

chemotherapy (12), radiation (17), and palliation care (17) were proved to be beneficial for survival outcome among those patients. In the present study, feature importance demonstrated that the top three most important features were chemotherapy, radiation, and lung metastases, and the impact of the three clinical characteristics on survival has been confirmed in previous studies (22). Chemotherapy and radiation were protective factors for early death. In addition, among HCC patients, lung metastases showed a worse prognosis than bone metastases (6), demonstrating that lung metastases had a significant negative impact on survival.

For patients with HCC, a number of survival prediction models have been put forth to forecast the outcome of survival. For example, Liang et al. (23) used the Cancer Genome Atlas cohort to construct a survival prediction model for HCC patients utilizing 10 ferroptosis-related genes, and the International Cancer Genome Consortium cohort to validate the model. The AUROC for estimating 1-year survival was 0.68, 2-year survival was 0.69, and 3-year survival was 0.72. Yan et al. (24) established a survival prediction model after analyzing 3620 patients with early HCC and the model consisted of eight variables including age, race, grade, T stage, surgery, chemotherapy, tumor size, and marital status. The 3- and 5-year AUROC were 0.767 and 0.766, respectively. More recently, after enrolling 2514 HCC patients in a multicenter database, a nomogram prediction model for survival was proposed using eight clinical characteristics for patients with and without adjuvant transcatheter arterial chemoembolization, and validation of the nomogram showed that the C-index was slightly above 0.75 (25). Liu et al. (26) developed a radiomics nomogram to predict the overall survival of HCC patients after hepatectomy. To begin with, this study constructed a radiomics signature in terms of seven overall survival related texture parameters, and then the radiomics signature incorporating with other four clinical characteristics (AFP, platelet-to-lymphocyte ratio, tumor size, and microvascular invasion) was used to develop the radiomics nomogram. The radiomics nomogram had an AUROC value of 0.747 in the training cohort and 0.777 in the validation cohort. However, studies on developing survival prediction specifically among HCC patients with bone metastases were scarce. To our knowledge, this study was the first to construct an accurate model to predict early mortality specifically among HCC patients with bone

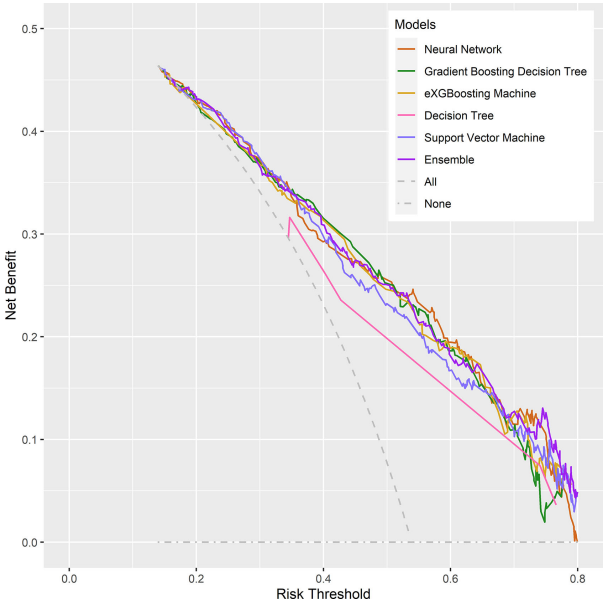

FIGURE 5
Decision curve analysis of the machine learning models in the internal testing cohort.

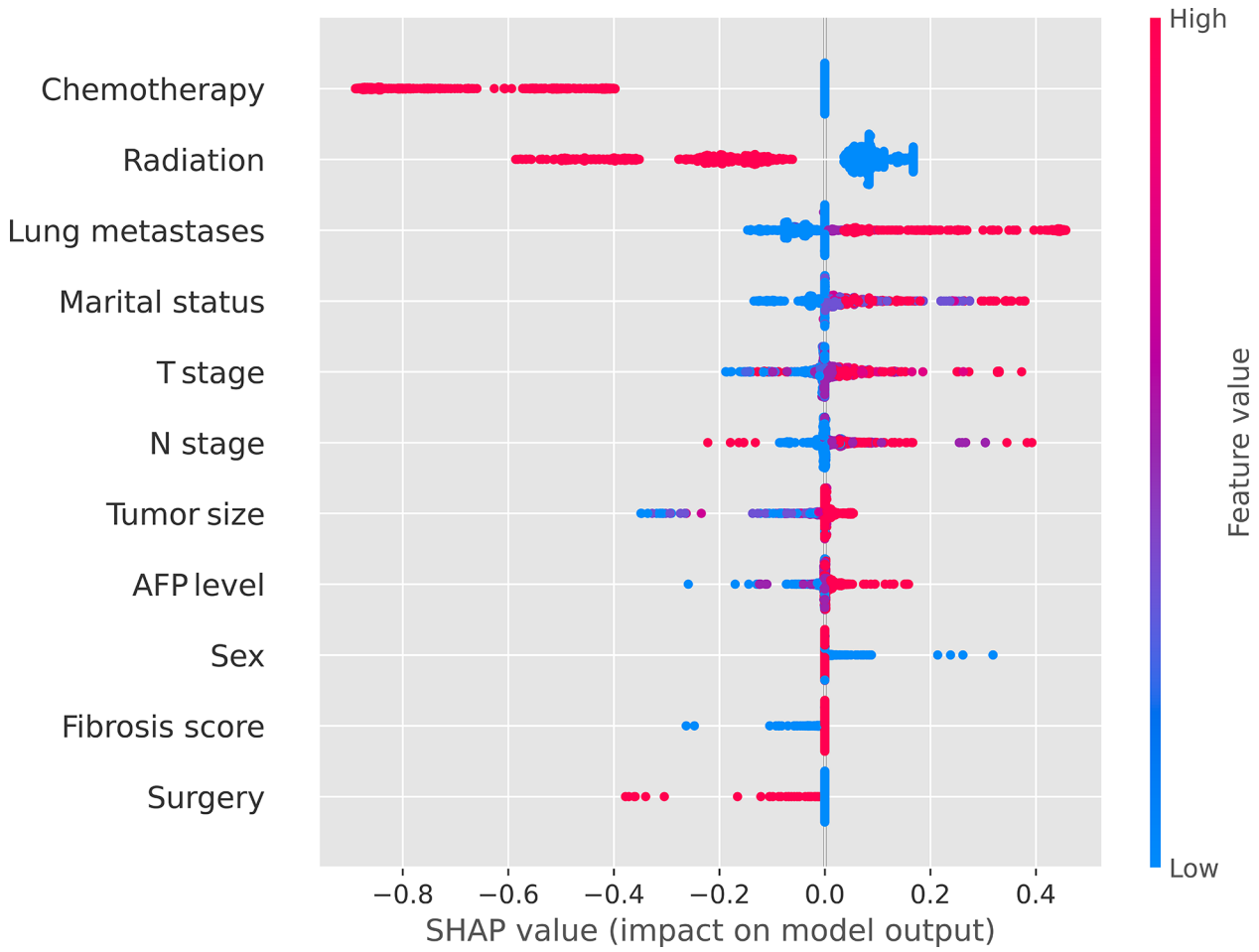

FIGURE 6
Feature importance in terms of the ensemble machine learning model.

TABLE 6 Risk stratification of patients in the internal validation cohort based on the ensemble model.

Risk group	Patients (n = 388)	Predicted risk	Observed risk	p
Low risk (≤0.541)	185	34.52%	31.35%	<0.001
High risk (>0.541)	203	74.11%	74.38%	

metastases using the ensemble machine learning technique, and this technique was able to combine the results of multiple machine-learning algorithms. Of note, the ensemble model had favorable discrimination and calibration in terms of AUROC (0.779) and Brier score (0.191), respectively. Notably, as compared to the AUROC in the above studies, our study had the highest AUROC, suggesting the accuracy of the prediction model was favorable.

Reclassification of patients showed that actual probability of early mortality was significant difference between the two risk groups (74.38% vs. 31.35%, $p < 0.001$). To be specific, patients in the high-risk group were 2.37 times more likely to suffer early death as compared to patients in the low-risk group. The Kaplan–Meier survival curve also demonstrated that patients in the high-risk group had significant shorter survival time in comparison to patients in the low-risk group. Patients in the high-risk group may therefore require greater care. Surgery may not be advised for those individuals because they were at a high danger of passing away within 3 months, would not have enough time to recuperate from surgery, and had slim prospects of ever benefiting from it. In addition, a multidisciplinary cooperation was recommended to manage HCC patients with bone metastases due to its complexity (11), and if there were no specifically targeted drugs, the therapeutic aim of treatments is directed at palliation of symptoms (11).

Limitations

The restrictions of this study are outlined below: (1) Because some clinical criteria, such as Child-Pugh grade, are not available in the SEER database, this study's selection of variables is constrained. (2) The information that was taken from the SEER database was on the condition at the time of the initial diagnosis, suggesting that bone metastases that occur in the later stages may not have been documented. (3) The model showed positive predictive performance in both the internal and external validation, but additional external validation is still needed to increase the model's generalizability.

Conclusions

In conclusion, the ensemble machine learning model shows promising prediction performance for early mortality among HCC patients with bone metastases. This model can be a prognostic tool to predict the survival outcome of those patients and facilitate clinical decision-making. Surgery might not be advised for patients in the high-risk group because they had a high chance of passing away within 3 months. For a subset of patients, chemotherapy, radiation therapy, and the avoidance or treatment of lung metastases are advised due to their positive effects on survival.

Data availability statement

Publicly available datasets were analyzed in this study. Training and internal testing data are available at https://seer.cancer.gov/. External testing data are available under reasonable request to the corresponding authors.

Ethics statement

This study was approved by Hainan Hospital of Chinese PLA General Hospital and patients gave informed written consent prior to data collection. Written informed consent for participation was not required for this study in accordance with the national legislation and the institutional requirements.

Author contributions

All authors conceived and designed the analysis; ZL, SW, XC, and QY oversaw data collection, YQ and ML performed the analysis, and all authors provided clinical interpretation of the findings. MY and ML drafted the manuscript. The corresponding author has full access to all the data in the study and had final responsibility for the decision to submit for publication. All authors contributed to the article and approved the submitted version.

Funding

This study was supported by National Orthopedics and Sports Rehabilitation Clinical Medical Research Center Innovation Fund Project (2021-NCRC-CXJJ-PY-20).

Conflict of interest

The authors declare that the research was conducted in the absence of any commercial or financial relationships that could be construed as a potential conflict of interest.

Publisher's note

All claims expressed in this article are solely those of the authors and do not necessarily represent those of their affiliated organizations, or those of the publisher, the editors and the reviewers. Any product that may be evaluated in this article, or

claim that may be made by its manufacturer, is not guaranteed or endorsed by the publisher.

Supplementary material

The Supplementary Material for this article can be found online at: https://www.frontiersin.org/articles/10.3389/fonc.2023.1144039/full#supplementary-material

SUPPLEMENTARY FIGURE 1
The receiver operating characteristic curve for the ensemble model in the external testing cohort.

SUPPLEMENTARY FIGURE 2
Density cure for the ensemble model in the external testing cohort.

SUPPLEMENTARY FIGURE 3
Discrimination slope of the models in the internal testing cohort. A, Neural network; B, gradient boosting decision tree; C, eXGBoosting machine; D, decision tree; E, support vector machine; F, ensemble model.

SUPPLEMENTARY FIGURE 4
Discrimination slope of the ensemble model in the external testing cohort.

SUPPLEMENTARY FIGURE 5
Calibration plot of the ensemble model in the external testing cohort.

SUPPLEMENTARY FIGURE 6
Calibration plot of the ensemble model in the external testing cohort after model revision.

SUPPLEMENTARY FIGURE 7
Kaplan–Meier survival curve among patients stratified by risk group ($p < 0.0001$, log-rank test).

References

1. Sung H, Ferlay J, Siegel RL, Laversanne M, Soerjomataram I, Jemal A, et al. Global cancer statistics 2020: GLOBOCAN estimates of incidence and mortality worldwide for 36 cancers in 185 countries. *CA Cancer J Clin* (2021) 71:209–49. doi: 10.3322/caac.21660

2. Kulik L, El-Serag HB. Epidemiology and management of hepatocellular carcinoma. *Gastroenterology* (2019) 156:477–91. doi: 10.1053/j.gastro.2018.08.065

3. Yang JD, Hainaut P, Gores GJ, Amadou A, Plymoth A, Roberts LR. A global view of hepatocellular carcinoma: trends, risk, prevention and management. *Nat Rev Gastroenterol Hepatol* (2019) 16:589–604. doi: 10.1038/s41575-019-0186-y

4. Ramdhani K, Smits MLJ, Lam M, Braat A. Combining selective internal radiation therapy with immunotherapy in treating hepatocellular carcinoma and hepatic colorectal metastases: A systematic review. *Cancer Biother Radiopharm* (2023). doi: 10.1089/cbr.2022.0071

5. Allemani C, Weir HK, Carreira H, Harewood R, Spika D, Wang XS, et al. Global surveillance of cancer survival 1995-2009: analysis of individual data for 25,676,887 patients from 279 population-based registries in 67 countries (CONCORD-2). *Lancet* (2015) 385:977–1010. doi: 10.1016/S0140-6736(14)62038-9

6. Zhan H, Zhao X, Lu Z, Yao Y, Zhang X. Correlation and survival analysis of distant metastasis site and prognosis in patients with hepatocellular carcinoma. *Front Oncol* (2021) 11:652768. doi: 10.3389/fonc.2021.652768

7. Seo HJ, Kim GM, Kim JH, Kang WJ, Choi HJ. F-FDG PET/CT in hepatocellular carcinoma: detection of bone metastasis and prediction of prognosis. *Nucl Med Commun* (2015) 36:226–33. doi: 10.1097/MNM.0000000000000246

8. Hirai T, Shinoda Y, Tateishi R, Asaoka Y, Uchino K, Wake T, et al. Early detection of bone metastases of hepatocellular carcinoma reduces bone fracture and paralysis. *Jpn J Clin Oncol* (2019) 49:529–36. doi: 10.1093/jjco/hyz028

9. Chen D, Li Z, Song Q, Qian L, Xie B, Zhu J. Clinicopathological features and differential diagnosis of hepatocellular carcinoma in extrahepatic metastases. *Med (Baltimore)* (2018) 97:e13356. doi: 10.1097/MD.0000000000013356

10. Belli A, Gallo M, Piccirillo M, Izzo F. Bone metastases as initial presentation of hepatocellular carcinoma. *Lancet Oncol* (2019) 20:e549. doi: 10.1016/S1470-2045(19)30417-6

11. Lasagna A, Cuzzocrea F, Maccario G, Mahagna A, Sacchi P, Mondelli MU. Bone metastases and hepatocellular carcinoma: some food for thought. *Future Oncol* (2021) 17:3777–80. doi: 10.2217/fon-2021-0689

12. Bhatia R, Ravulapati S, Befeler A, Dombrowski J, Gadani S, Poddar N. Hepatocellular carcinoma with bone metastases: Incidence, prognostic significance, and management-Single-Center experience. *J Gastrointest Cancer* (2017) 48:321–5. doi: 10.1007/s12029-017-9998-6

13. Schmid RK, Johnstone CA, Robbins JR. Palliative radiation for bone metastases from hepatocellular carcinoma: practice patterns and the amount of remaining life spent receiving treatment. *Ann Palliat Med* (2022) 11:1900–10. doi: 10.21037/apm-21-2657

14. Guo X, Xu Y, Wang X, Lin F, Wu H, Duan J, et al. Advanced hepatocellular carcinoma with bone metastases: Prevalence, associated factors, and survival estimation. *Med Sci Monit* (2019) 25:1105–12. doi: 10.12659/MSM.913470

15. Honda Y, Aikata H, Honda F, Nakano N, Nakamura Y, Hatooka M, et al. Clinical outcome and prognostic factors in hepatocellular carcinoma patients with bone metastases medicated with zoledronic acid. *Hepatol Res* (2017) 47:1053–60. doi: 10.1111/hepr.12844

16. Cho HS, Oh JH, Han I, Kim HS. Survival of patients with skeletal metastases from hepatocellular carcinoma after surgical management. *J Bone Joint Surg Br volume* (2009) 91:1505–12. doi: 10.1302/0301-620X.91B11.21864

17. Sakaguchi M, Maebayashi T, Aizawa T, Ishibashi N, Fukushima S, Saito T. Radiation therapy and palliative care prolongs the survival of hepatocellular carcinoma patients with bone metastases. *Intern Med* (2016) 55(9):1077–83. doi: 10.2169/internalmedicine.55.6003

18. Kim SU, Kim DY, Park JY, Ahn SH, Nah HJ, Chon CY, et al. Hepatocellular carcinoma presenting with bone metastasis: clinical characteristics and prognostic factors. *J Cancer Res Clin Oncol* (2008) 134:1377–84. doi: 10.1007/s00432-008-0410-6

19. Fox R. Directed molecular evolution by machine learning and the influence of nonlinear interactions. *J Theor Biol* (2005) 234:187–99. doi: 10.1016/j.jtbi.2004.11.031

20. Liu J, Guo W, Sakkiah S, Ji Z, Yavas G, Zou W, et al. Machine learning models for predicting liver toxicity. *Methods Mol Biol* (2022) 2425:393–415. doi: 10.1007/978-1-0716-1960-5_15

21. Nanayakkara S, Fogarty S, Tremeer M, Ross K, Richards B, Bergmeir C, et al. Characterising risk of in-hospital mortality following cardiac arrest using machine learning: A retrospective international registry study. *PloS Med* (2018) 15:e1002709. doi: 10.1371/journal.pmed.1002709

22. Hu C, Yang J, Huang Z, Liu C, Lin Y, Tong Y, et al. Diagnostic and prognostic nomograms for bone metastasis in hepatocellular carcinoma. *BMC Cancer* (2020) 20:494. doi: 10.1186/s12885-020-06995-y

23. Liang J, Wang D, Lin H, Chen X, Yang H, Zheng Y, et al. A novel ferroptosis-related gene signature for overall survival prediction in patients with hepatocellular carcinoma [Research paper]. *Int J Biol Sci* (2020) 16:2430–41. doi: 10.7150/ijbs.45050

24. Yan B, Su BB, Bai DS, Qian JJ, Zhang C, Jin SJ, et al. A practical nomogram and risk stratification system predicting the cancer-specific survival for patients with early hepatocellular carcinoma. *Cancer Med* (2021) 10:496–506. doi: 10.1002/cam4.3613

25. Liang L, Li C, Wang MD, Wang H, Zhou YH, Zeng YY, et al. Development and validation of a novel online calculator for estimating survival benefit of adjuvant transcatheter arterial chemoembolization in patients undergoing surgery for hepatocellular carcinoma. *J Hematol Oncol* (2021) 14:165. doi: 10.1186/s13045-021-01180-5

26. Liu Q, Li J, Liu F, Yang W, Ding J, Chen W, et al. A radiomics nomogram for the prediction of overall survival in patients with hepatocellular carcinoma after hepatectomy. *Cancer Imaging* (2020) 20:82. doi: 10.1186/s40644-020-00360-9

frontiers | Frontiers in Oncology

TYPE Original Research
PUBLISHED 22 February 2023
DOI 10.3389/fonc.2023.1138837

OPEN ACCESS

EDITED BY
Feifei Pu,
Huazhong University of Science and Technology, China

REVIEWED BY
Shunbin Xiong,
University of Texas MD Anderson Cancer Center, United States
Yanxin Chang,
Eastern Hepatobiliary Surgery Hospital, China

*CORRESPONDENCE
Xiuxin Han
hanxiuxintjmu@163.com
Guowen Wang
wangguowenhrb@163.com

SPECIALTY SECTION
This article was submitted to Surgical Oncology, a section of the journal Frontiers in Oncology

RECEIVED 06 January 2023
ACCEPTED 08 February 2023
PUBLISHED 22 February 2023

CITATION
Zhang C, Feng J, Liu Y, Zhang Y, Song W, Ma Y, Han X and Wang G (2023) Direct and indirect damage zone of radiofrequency ablation in porcine lumbar vertebra. *Front. Oncol.* 13:1138837. doi: 10.3389/fonc.2023.1138837

Direct and indirect damage zone of radiofrequency ablation in porcine lumbar vertebra

Chao Zhang[1], Jinyan Feng[1], Yongheng Liu[1], Yan Zhang[1], Weijie Song[2], Yulin Ma[1], Xiuxin Han[1*] and Guowen Wang[1*]

[1]Department of Bone and Soft Tissue Tumor, Tianjin Medical University Cancer Institute and Hospital, National Clinical Research Center for Cancer, Key Laboratory of Cancer Prevention and Therapy, Tianjin's Clinical Research Center for Cancer, Tianjin Medical University Cancer Institute and Hospital, Tianjin, China, [2]Department of Animal Laboratory, Tianjin Medical University Cancer Institute and Hospital, National Clinical Research Center for Cancer, Key Laboratory of Cancer Prevention and Therapy, Tianjin's Clinical Research Center for Cancer, Tianjin Medical University Cancer Institute and Hospital, Tianjin, China

Objectives: To explore the direct and indirect heat damage zone of radiofrequency ablation (RFA) in porcine vertebrae and to verify the safety of RFA in a vascularized vertebral tumor model.

Methods: RFA was performed in the porcine lumbar vertebrae. Magnetic resonance (MR) imaging, hematoxylin and eosin (HE), and terminal deoxynucleotidyl transferase dUTP nick end labelling (TUNEL) were used to assess the extent of direct and indirect injuries after RFA. The cavity of lumbar vertebrae was made, and the adjacent muscle flap was used to fill the cavity to make a vertebrae tumor model. RFA was performed in the vascularized vertebral tumor model.

Results: T1-weighted images showed a hypointensive region in the center surrounded by a more hypointensive rim on day 0 and 14. T2-weighted images showed that RFA zone was hypointensive on day 0. On day 7, hypointensity was detected in the center surrounded by a hyperintensive rim. HE showed that the RFA zone could be clearly observed on day 14. Thin bone marrow loss areas were seen around the RFA zone, which was consistent with the hyperintensive rim on the T2-weighted images. TUNEL showed a large number of apoptotic cells in the RFA zone. During RFA in the vertebral tumor model, the temperature of all monitoring positions was less than 45 °C.

Conclusion: Using *in vivo* experiments, the effective zone of RFA was evaluated by MR imaging and pathology, and the direct and indirect damage range were obtained. The safety of RFA was verified by RFA in a vascularized vertebral tumor model.

KEYWORDS

radiofrequency ablation, vertebrae, tumor model, direct damage, indirect damage

Abbreviations: RFA, Radiofrequency ablation; MRI, Magnetic resonance imaging; CT, Computed tomography; L, Lumbar vertebra; HE, Hematoxylin and eosin; TUNEL, Terminal deoxynucleotidyl transferase dUTP nick end labelling; EDTA, Ethylene Diamine Tetraacetic Acid.

Introduction

Bone is the third most common metastasis site in all cancer patients, and the spine is the most common metastasis site. Of patients with a malignant tumor, 10-40% will eventually have spinal metastasis (1–3). Spinal metastasis often leads to neurological dysfunction, sphincter dysfunction, hypercalcemia, pathological fracture, and even paralysis (4). In addition to systemic treatment, the main purpose of spinal metastases treatment is to minimize pain, maintain mechanical stability, and improve the quality of life. Although the main method for the treatment of painful bone metastasis is radiotherapy, the pain relief after radiotherapy may be partial, delayed, and temporary (5). Pain caused by spinal metastases is usually not effectively alleviated by systemic therapy such as chemotherapy, hormone therapy, radiotherapy, and bisphosphonates (6). In the past decade, RFA has developed rapidly in the treatment of spinal metastases, and its efficacy has been recognized (7–9).

RFA has been widely used as a minimally invasive treatment in bone metastases, especially in palliative pain treatment of the spine, pelvis, long bone, etc. (10, 11). The molecular oscillation of charged tissue in the RFA zone produces friction heat, which leads to coagulation necrosis of the tumor (11–13). When the temperature of RFA reaches 45°C, irreversible necrosis can occur within a few hours. When the temperature reaches 50-55°C, irreversible cell damage can occur within 4-6 minutes. When the temperature reaches 60-100°C, protein coagulation necrosis occurs immediately. When the temperature reaches 100-110°C, the tissue will be carbonized and vaporized (14).

RFA can effectively kill tumor cells without damaging the stability of the vertebra, thereby reducing the risk of pathological fracture. Several studies have demonstrated that percutaneous RFA is a safe technique that can be very effective in relieving pain in patients with spinal metastases (15–18). RFA has been widely used in palliative treatment of spinal metastases, but there are corresponding side effects of RFA, including bleeding, infection, skin injury, organ injury, spinal cord, and nerve root injury (19, 20). Several reports evaluated the RFA damage lesion by MR imaging and HE, and evaluated the safety of RFA, which has certain guiding significance for the clinical application of RFA (21, 22). RFA in the treatment of liver tumors, heat injury includes two stages, direct heat injury and indirect heat injury (23). But there was no study to further clarify the indirect heat injury of RFA in vertebral metastases.

Therefore, we need to study the direct and indirect heat damage zone of RFA in the vertebra. In this study, the damage zone of RFA in porcine lumbar vertebrae was studied *in vivo*. The area of coagulation necrosis was evaluated by MR imaging and HE. TUNEL was used to evaluate the apoptosis of vertebral cells. The tumor model of vertebra was constructed to verify the safety of RFA.

Materials and methods

Institutional animal care ethics approval was obtained for the study. Eight Bama miniature pigs, weighing 35-40 kg, were used in this study; six pigs were used for RFA in normal vertebrae, and two pigs were used for RFA in tumor model vertebrae. Tarlov score was used to evaluate the walking function of pigs before and after RFA (24). Tarlov score can be divided into six grades. Grade 0: no activity of hind limbs, no weight bearing. Grade 1: the hind limbs can move occasionally but cannot bear weight. Grade 2: the hind limbs move frequently or forcefully but cannot bear weight. Level 3: the hind limbs can support the body weight and walk 1-2 steps. Grade 4: walkable with only mild impairment. Grade 5: normal walking.

Radiofrequency ablation system

RITA ® The 1500x generator (angiodynamics, Inc., Manchester, Ga., USA) can emit 460khz RF current with a maximum power of 250W. The perfusion pump can continuously infuse normal saline into the probe to increase the range of RFA. Probe(17g): starburst flex (uniblade) unipolar perfusion probe. Continuous saline infusion at the tip of the probe can effectively increase the RFA zone, which has been approved by FDA for the treatment of bone tumors.

Anesthesia

To begin, sedative drugs were delivered through an intramuscular injection of Sumianxin (0.2ml/kg) and 3% phenobarbital (1ml/kg). It took about 5-10 minutes for the pig to fall asleep. The vein channel was established through the ear vein, and the intravenous indwelling needle was inserted. 8-10ml of general anesthesia drug was injected (propofol injection, 2mg/kg, Fentanyl citrate injection, 2ug/kg, Rocuronium injection, 1mg/kg). Endotracheal intubation was performed with an insertion depth of about 28cm. After successful intubation, a ventilator was connected, and anesthetics were given continuously. The vital signs such as respiration, heart rate, and electrocardiogram were observed.

Surgery

The Bama miniature pig was fixed on the operating table in a prone position. The hair of the waist, bilateral thighs, and buttocks were shaved. Two negative plates were applied to the buttocks and thighs of the pig. The surgical zone was disinfected with Iodophor, and sterile operating sheets were laid down. The posterior median incision of the lumbar spine was made with a length of about 20cm. The skin, subcutaneous, and fascia were incised to separate the erector spinae muscle and expose the spinous process, lamina, articular process, and transverse process of l1-l6. Through the right pedicle approach, the RFA channel was made. The needle entry point was the intersection of the superior articular process and transverse process, about the middle line of transverse process, and the inclination angle was approximately 25 to 30 degrees.

RFA in normal vertebrae

Previous literature reported that the number of lumbar vertebrae in pigs was 6-7 (25). The experimental animal in this

study was the Bama miniature pig, and each pig had six lumbar vertebrae. RFA was performed in L1, L2, L3, L4, and L5 vertebrae of six Bama miniature pigs, and L5 vertebra was not ablated as control group. The ablation parameters were set as power 35W, temperature 70 °C, active tip 1cm, and ablation time 20 minutes. Thermocouples were placed in the spinal canal, the pedicle hole, and the anterior edge of the vertebra to monitor the temperature in real time. MR imaging (GE, 3.0T discovery, MR750) was performed on 0, 7, and 14 days after RFA. The scanning sequences were T1-weighted and T2-weighted. In T1-weighted and T2-weighted images, the longest diameter of RFA was measured.

The three groups of pigs were euthanized at three separate time points, and then the lumbar vertebrae were taken out. A high-precision hard tissue slicer was used to cut the vertebrae to obtain a complete cross-section of the vertebral body. The thickness of the section was about 2 mm. The maximum diameter of ablation range of gross specimens was measured. Then the special embedding box was used for embedding, ethylene diamine tetraacetic acid (EDTA) was used for decalcification, and the decalcification of samples was observed regularly. Finally, HE and TUNEL were used to evaluate the range of RFA. According to the effective range of HE staining, the maximum diameter of RFA was measured.

RFA in vertebral tumor model

Two Bama miniature pigs were used to make vertebral tumor models. First, an electric grinding drill was used to grind along L1, L3, and L5 pedicle direction, and a quasi-circular cavity with a diameter of about 1.7cm was ground in the upper 1/3 of the vertebra to ensure the integrity of the surrounding bone. The adjacent erector spinae muscle was separated to form the adjacent muscle flap with blood supply, which was filled in the vertebra to construct the vertebral tumor model. RFA was performed on the vertebral tumor model. The ablation parameters were set as power 35W, temperature 70°C, needle length 1cm, and ablation time 20 minutes. Temperature measurement points were arranged in the spinal canal (posterior cortex of vertebra near spinal cord), nerve root foramen, and anterior edge of vertebral body, and thermocouples were used to monitor the temperature in real time.

Statistical analysis

IBM SPSS 23.0 statistics software was used for statistical analysis. The maximum diameters of the RFA zone in MR imaging, HE, and gross samples were measured. ANOVA was used for comparison between the three groups, α=0.05 was taken as the test level, and $P < 0.05$ showed a statistical difference.

Results

Neurological function

In this study, RFA was performed on the lumbar vertebrae of eight Bama miniature pigs. All Bama miniature pigs were evaluated with Tarlov score before and after the experiment to evaluate the walking function of lower limbs and sphincter function. All pigs could walk normally after RFA. Tarlov score was 5. No pigs had sphincter dysfunction.

Gross specimen

On day 0 after RFA, the transverse plane of the vertebrae showed no significant changes in the RFA zone compared to the normal vertebrae(Figure 1). On day 14 after RFA, the zone of RFA in the vertebra showed gray-white changes, with thin layers of gray-black rim around the center (Figures 1A, B).

MR imaging

The RFA regions were evaluated by coronal plane and axial plane. T1-weighted images (Figures 2C, I) showed hypointensity in the center surrounded by a more hypointensive rim on day 0 and 14. T2-weighted images showed the RFA zone was hypointensive on day 0 (Figures 2A, B). On day 7, the lesion demonstrated hypointensity at the center with hyperintensity at the periphery on coronal and axial T2WI (Figures 2D, E). On day 14, the hyperintensive rim was more obvious (Figures 2G, H), which was consistent with the hypointensive rim in T1-weighted images(Figure 2I). Compared with T1-weighted, T2-weighted images more clearly show the zone of RFA.

HE

On day 0 after RFA, HE showed no significant differences in trabecular structure, osteoblasts, and marrow composition between the RFA zone and the normal vertebra (Figure 3). On the 14th day after RFA, HE showed that the trabecular bone remained intact in the RFA zone. However, compared with normal vertebra, the bone marrow in the trabecula was significantly reduced, and the number of osteoblasts covered by trabecula in the ablation zone was also significantly reduced, especially in the peripheral zone of RFA. It formed a circular bone marrow loss zone (Figures 1A, B), which was consistent with the hyperintensive rim in MR images.

TUNEL

TUNEL was performed on 0 and 14 days after RFA. On day 0, TUNEL showed that a large number of apoptotic cells existed and the nuclei of apoptotic cells were green. Apoptotic cells were mainly distributed around the ablation zone, and were mainly bone marrow tissue (Figure 4).

RFA diameter measurement

The diameter of RFA was measured in gross specimens, HE, and MR images. The average diameter in gross specimens was 18.72 ± 2.69cm, that in HE was 18.28 ± 2.41, and that in MR images was 17.88

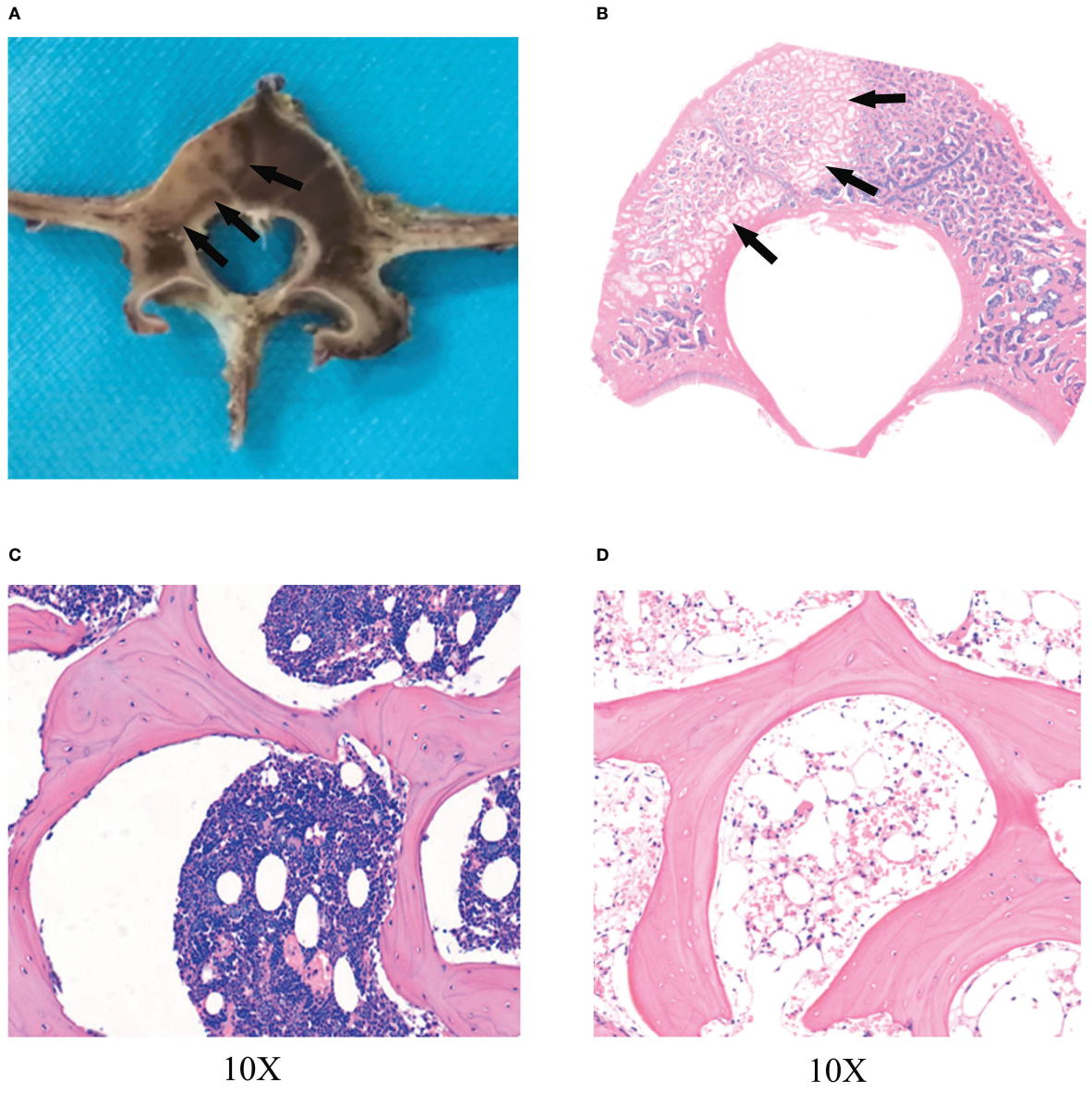

FIGURE 1
The zone of RFA. **(A)** Radiofrequency ablation (RFA) lesion in vertebra by transverse plane. The zone of RFA in the vertebra showed gray-white changes, with thin layers of gray-black rim (black arrows) around the center on day 14. **(B)** Hematoxylin and eosin (HE) showed a clear radiofrequency ablation zone (black arrows) on day 14. A circular bone marrow deletion zone can be seen around radiofrequency ablation lesion. The trabeculae remained intact, but the number of bone marrow cells in the trabeculae and the number of osteoblasts covering the trabeculae were significantly reduced, especially in the surrounding zones (black arrows) of radiofrequency ablation. **(C)** The zone of radiofrequency ablation was observed at 10X. **(D)** Normal vertebra.

± 2.06cm. The three measurement methods were not statistically significant(P=0.86) (Figure 5). The three measurement methods can be used as an effective method to measure the range of RFA.

Safety in vertebral tumor model

According to the previous study, muscle was used to fill the vertebrae to make the vertebral body tumor model (26). In this study, a grinding drill was applied to the L1, L3, and L5 vertebrae through the right pedicle to make the cavity (Figures 6A, B), and the adjacent erector spinae muscle flap was separated, and the vascularized muscle flap was filled into the vertebrae cavity to make the vertebral body tumor model (Figure 6C). RFA was performed in the tumor model to monitor the temperature in the spinal canal, nerve root foramen, and anterior edge of vertebrae (Figure 6D). The temperature of all monitoring points was within the safe range (Figure 7). The safety of RFA in a vertebral tumor model was verified.

Discussion

RFA has been widely used in the clinical treatment of spinal metastases, but the related complications during RFA cannot be ignored. At present, the research on the distribution of a thermal field of RFA in vertebra is very limited. In this study, it was found

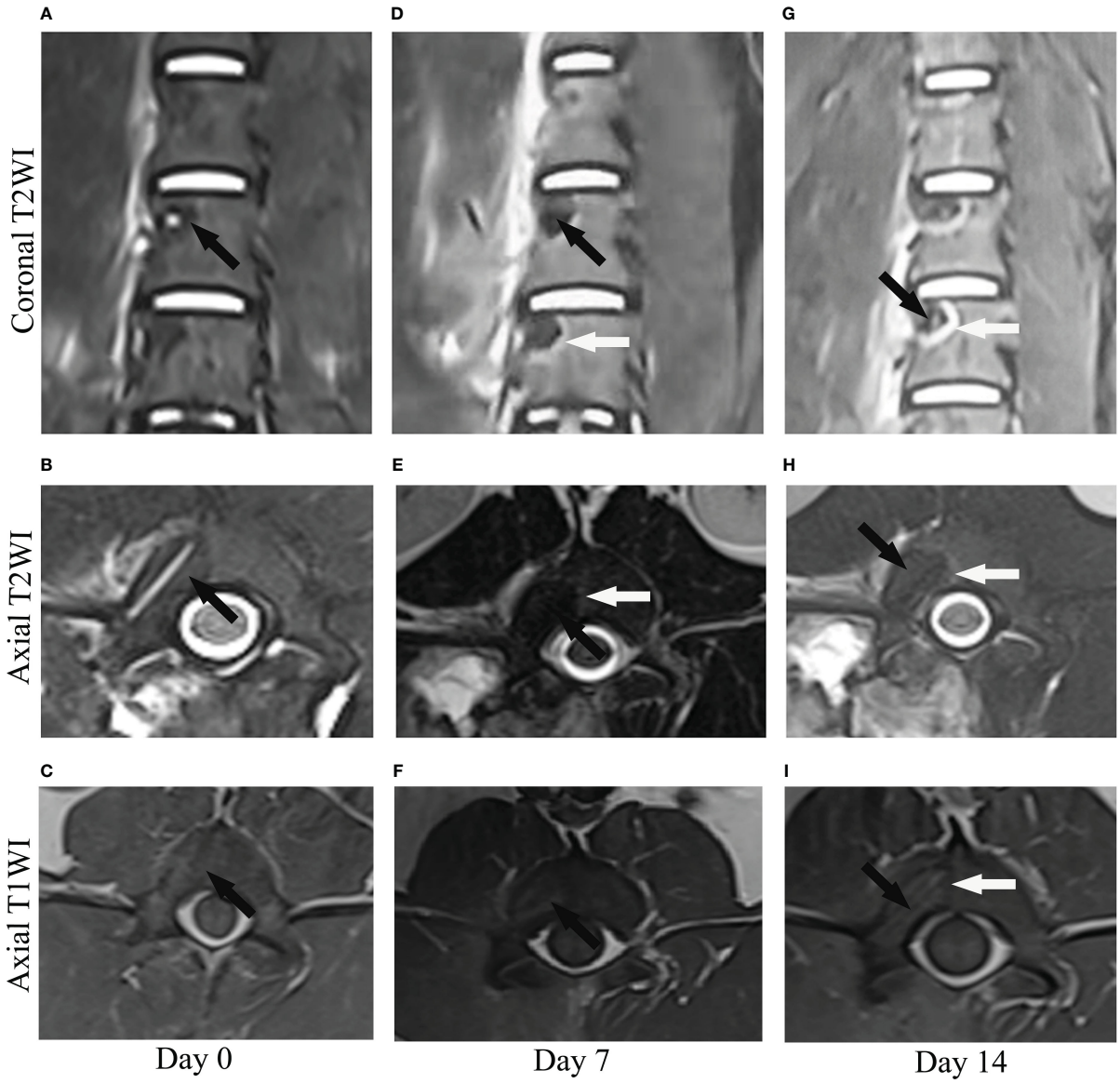

FIGURE 2
The image manifestation of a lesion on coronal and axial T2-weighted images (T2WI) and axial T1-weighted images (T1WI) at different time points (day 0, 7, 14) after radiofrequency ablation. **(A–C)** On day 0, the lesion showed hypointensity (black arrow) on coronal and axial T2WI and isointensity (black arrow) on axial T1WI. **(D–F)** On day 7, the lesion demonstrated hypointensity (Black arrow) at the center with hyperintensity (white arrow) at the periphery on coronal and axial T2WI and heterogenous intensity at the center with slightly hypointensity at the periphery on axial T1WI (Black arrow). **(G–I)** On day 14, the peripheral ring (white arrow) which manifested as hyperintensity on coronal and axial T2WI and hypointensity at the center was clearer than that of day 7.

that the RFA in pig vertebra was safe, and the effective therapeutic range could be obtained by controlling the parameters of RFA, including the action temperature, power, action time, and length of active tip. MR imaging evaluated the zone of RFA in vertebrae. The area of coagulation necrosis (14 days after RFA) can be observed by HE under the microscope. The area of apoptosis in the vertebrae can be observed by TUNEL. The direct and indirect damage range were obtained by MR imaging and HE.

You et al. (27) found that the local temperature around the RFA zone is inversely proportional to the distance when RFA is performed in the vertebra *in vitro*. In general, RFA equipment, relevant parameters, type of electrode, and conductivity of tumor tissue are the factors affecting the size of thermal lesions. The RFA electrode used in this study is a unipolar perfusion electrode, which is approved by the FDA and can be used in the treatment of bone tumors. Continuous drip of normal saline during RFA can increase the conductivity of the tissue around the electrode. Through continuous perfusion of normal saline, heat is dissipated to the tissue far from the electrode to enhance thermal conductivity. Therefore, continuous perfusion during RF ablation can enhance the ablation effect.

You et al. (27) found that there was a significant positive correlation between ablation zone and ablation time within a certain time, meaning a sufficient volume of RF ablation zone can be produced by adjusting the length of ablation time. In this study, the active tip was set at 1cm, the ablation temperature was set at 70°C, and the action time was set at 20min. The radiofrequency ablation in the

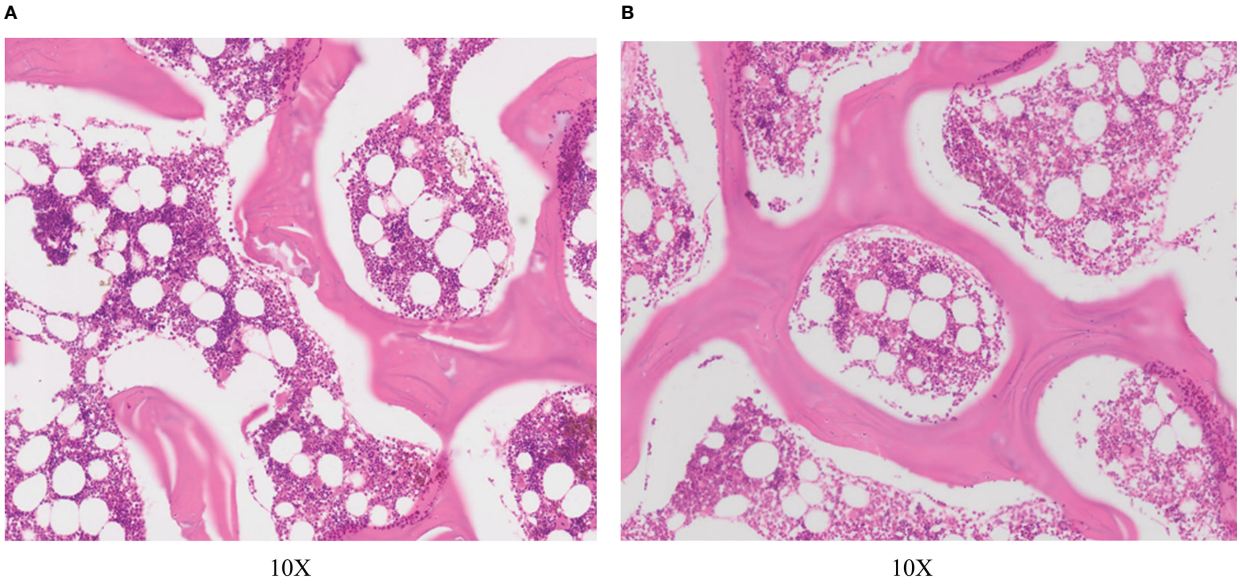

FIGURE 3
HE on day 0. **(A)** Normal vertebra. **(B)** Radiofrequency ablation zone.

vertebra was enough to ensure that the spinal cord, nerve root, and other important tissues would not suffer thermal damage, and the ablation range could be clearly observed through MR imaging.

The zone of ablation was evaluated by means of magnetic resonance imaging, gross specimens, and histopathological sections. The size by three means were consistent (28). In this study, the maximum diameter of pathology can be obtained by thin-layer sections of gross specimens. However, MR imaging has layer thickness. The layer thickness of MR images in this study was 3mm, which made it difficult to ensure that the maximum diameter can be obtained by tomography. Therefore, there will be an error between MR images and the maximum diameter of pathological sections, but this error is not statistically significant through statistical analysis in this study.

In an *in vivo* experiment, Pezeshki et al. (21) performed RFA of porcine vertebra, monitored the temperature around the vertebral body during RFA, and evaluated the neurological function after treatment, proving that RFA was safe. MR imaging assessments were conducted

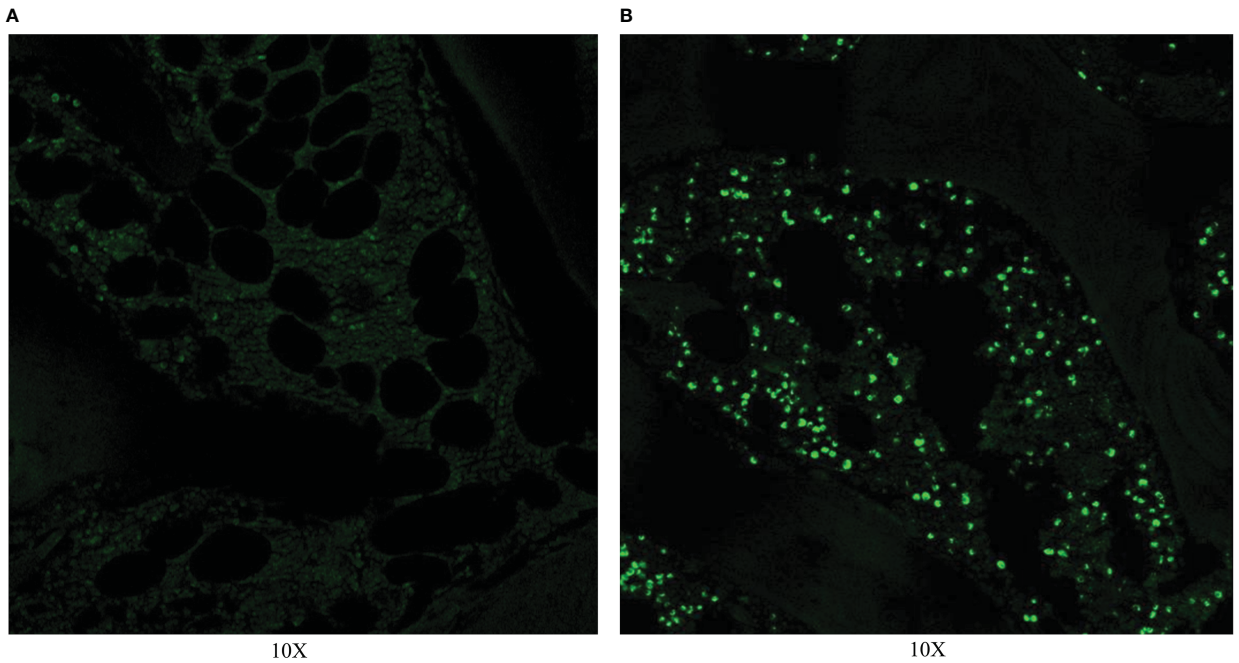

FIGURE 4
TUNEL on day 0. **(A)**TUNEL showed no apoptotic cell in normal vertebra. **(B)** TUNEL showed a large number of apoptotic cells in the ablation zone.

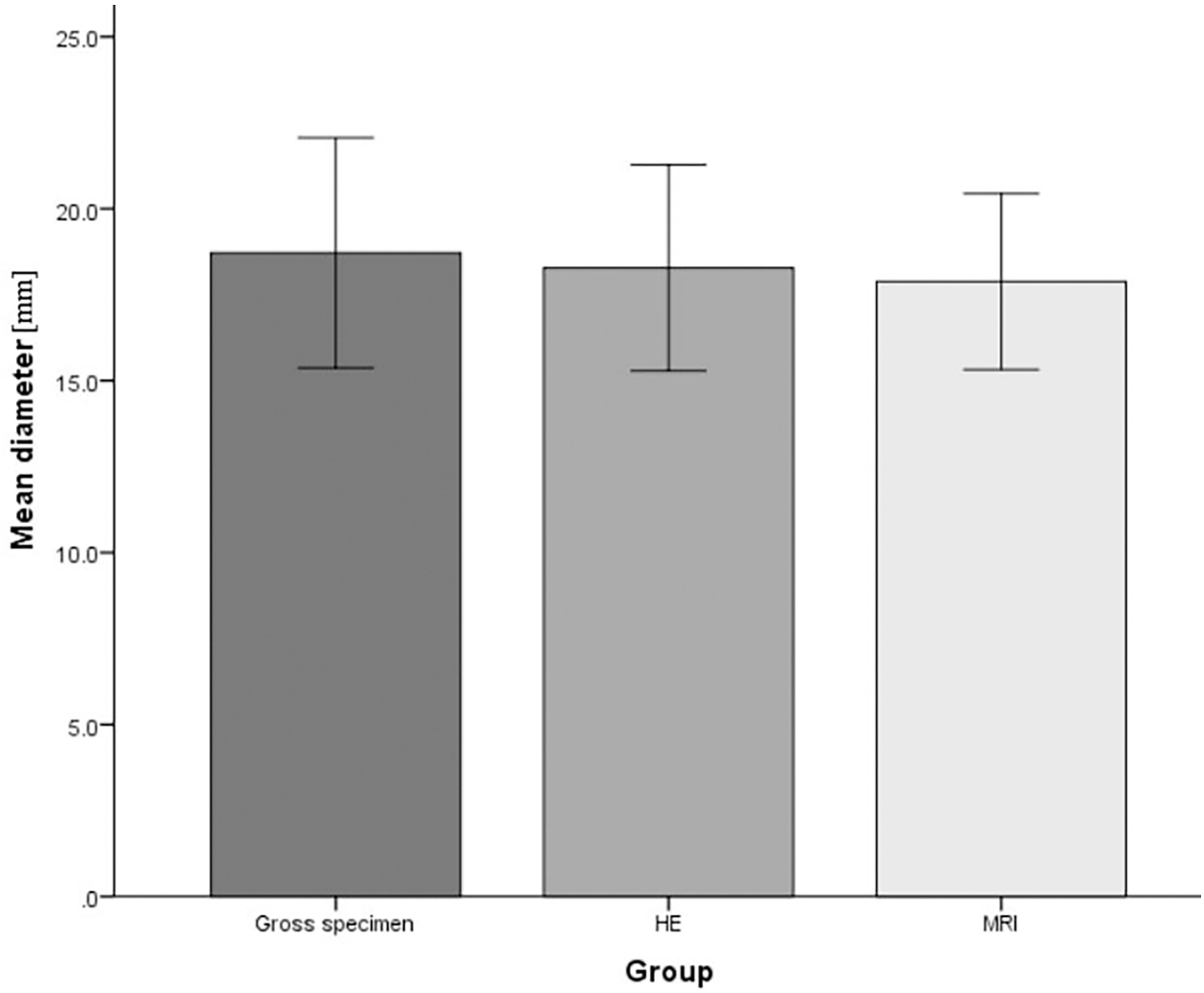

FIGURE 5
The diameter of radiofrequency ablation (RFA) in gross specimens, Hematoxylin and eosin (HE), and magnetic resonance (MR) imaging. The average diameter was 18.72 ± 2.69cm in gross specimens, 18.28 ± 2.41in HE, 17.88 ± 2.06cm in MR images.

pre- and posttreatment. RF lesions were apparent in the T2-weighted sequences, which showed a combination of hypointensive and hyperintensive regions, often demonstrating a hyperintensive peripheral rim on day 14. In this study, RFA was performed on porcine lumbar vertebrae. The effective range of RFA can be clearly observed on days 0, 7, and 14 in T2-weighted images. The range of RFA can be more clearly observed on day 14, and there is a hyperintensive rim, which is consistent with the results of previous literature (21).

Studies have shown that after RFA, in addition to direct damage, the tissue will still suffer indirect damage after ablation is stopped (23). Clinical and experimental data showed that the tissue damage will continue after thermal ablation is stopped (23, 29, 30), but the mechanism of such damage remains to be studied. Related studies have reported that after hyperthermia, RFA should be delayed by 5-7 days to clearly observe the thermal lesion (23). The indirect injury mechanism may also be related to many factors, including cell apoptosis, macrophages, cytokine release, and ischemia-reperfusion injury. The related mechanism of indirect injury in vertebra needs to be further studied (23). In this study, it was found in MR imaging that a hyperintensive rim was observed around coagulation necrosis on the 7th and 14th days after RFA, and was clearer on the 14th day. At the same time, the scope of coagulative necrosis could be clearly observed by HE on 14th day, and a thin layer of bone marrow loss zone could be observed around the outermost periphery of coagulative necrosis, which was close to the hyperintensive rim of MR images. This study considered that this zone may be the indirect injury zone of RFA in the vertebra.

Spinal metastases are divided into osteogenic type, osteolytic type, and mixed type. Different types of bone destruction of spinal metastases have different electrical conductivity in the vertebra. According to previous studies, the temperature field distribution of RFA in vertebrae, and many studies were carried out in normal vertebral bodies (21, 27). Compared with spinal metastases, RFA in normal vertebral bodies has a large error in evaluating the temperature field area and safety. Relevant studies have reported that different vertebral metastasis models were made for RFA research, including

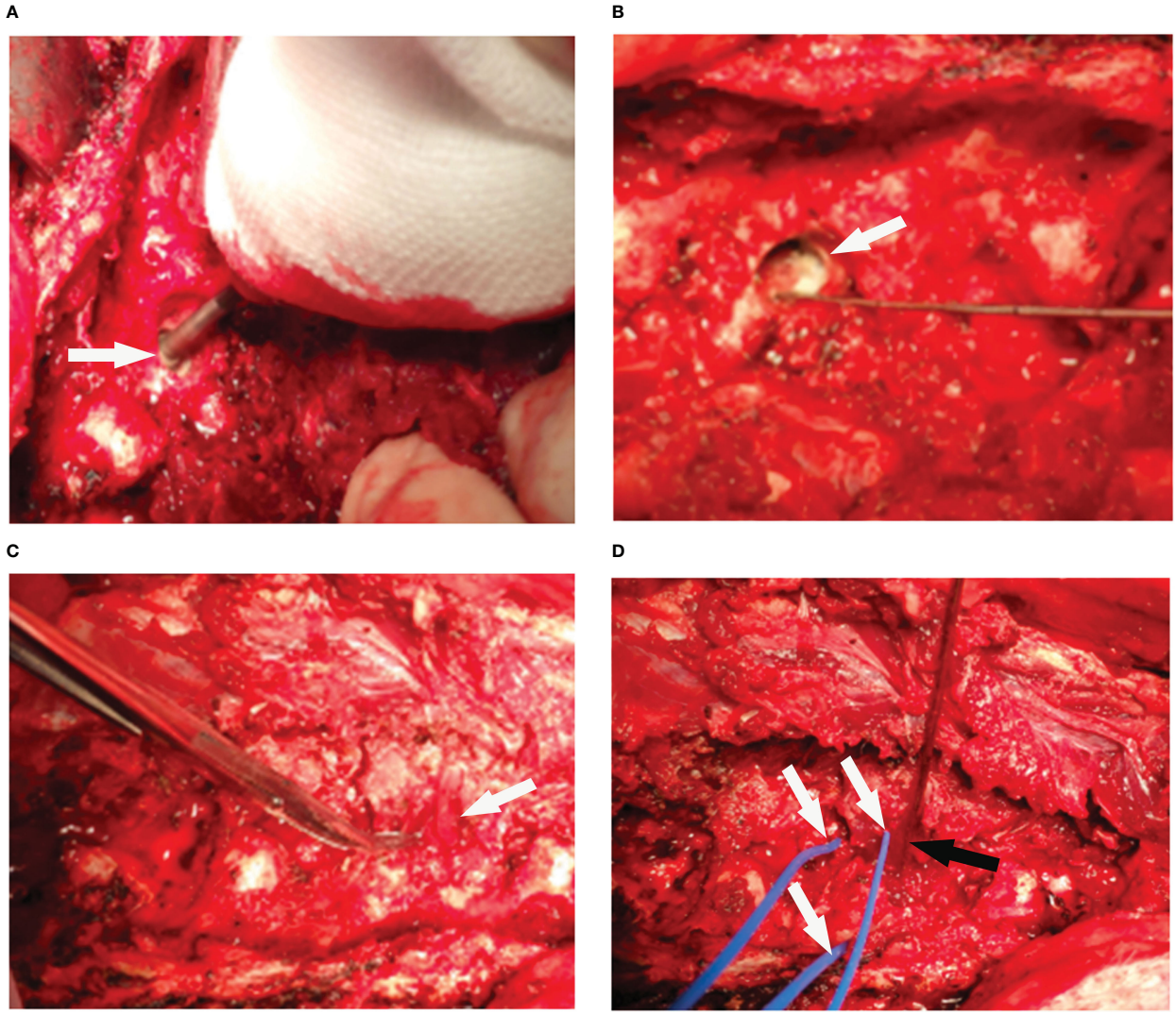

FIGURE 6
The process of making a vertebral tumor model. **(A)** The holes were drilled through the pedicle of vertebral with a grinding drill (arrow). **(B)** The cavity was made in vertebra (arrow). **(C)** The adjacent muscle flap was separated (arrow), and the vascularized muscle flap was used to fill the vertebral cavity. **(D)** Radiofrequency ablation was performed in the vertebral tumor model (black arrow), and the temperature of the peripheral spinal cord, nerve root foramen, and anterior edge of vertebra were monitored (arrows) in real time.

filling muscle tissue to simulate metastasis (26, 31). But the tumor is characterized by rich blood supply, so filling muscle tissue to build a tumor model lacks this important feature of tumors. In this study, the vertebral cavity was made, and the adjacent vascularized muscle flap was separated to fill the cavity to simulate the vertebral tumor. Compared with previous studies, this model had blood supply, and the safety of RFA was verified in this vertebral tumor model.

The experimental animal of this study was pig. Compared with human vertebrae, the vertebrae of pig are smaller. The RFA power and temperature setting explored in this experiment were safe, but the relevant parameters need to be reset for RFA in human vertebral metastases. The experimental results can only be used as a reference. The action time in this study was 20 minutes. The zone of RFA can be better evaluated by MR imaging, but the optimal action time needs more research and further demonstration. Because it was difficult to make a spinal metastasis model in large animals, the zone of RFA in this study was carried out in normal vertebrae. The actual ablation range in vertebral tumors may change due to different tumor tissues.

Conclusion

In this study, RFA was performed on Bama miniature pigs. Thermocouples were used to monitor the temperature in the spinal canal, nerve root foramen, and anterior edge of the vertebral body in real time to verify the safety of RFA. MR imaging and HE methods were used to evaluate the zone of direct and indirect damage of RFA. Whether indirect injury can cause thermal injury to the spinal cord and its mechanism need to be further studied. The model of

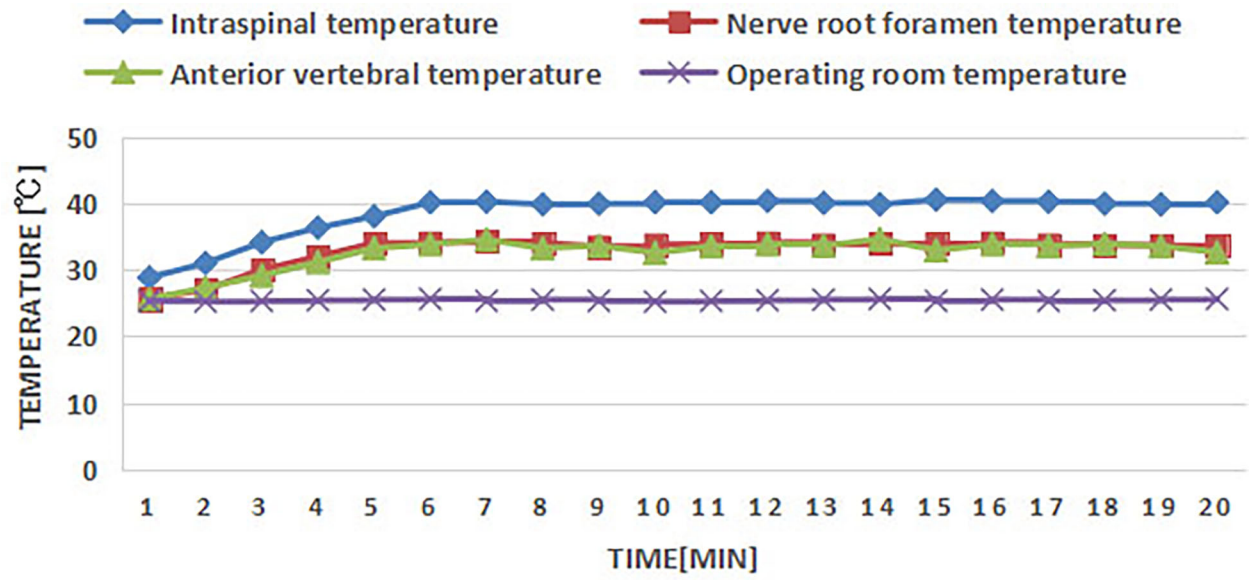

FIGURE 7
Temperature measurement points in spinal canal, nerve root foramen, and anterior edge of vertebrae.

lumbar vertebral tumor was made and RFA of vertebral tumor was performed to verify the safety, which provides a certain theoretical basis for the safe and effective development of perfusion electrode monopole needle in spinal metastasis.

Data availability statement

The original contributions presented in the study are included in the article/supplementary material. Further inquiries can be directed to the corresponding authors.

Ethics statement

The animal study was reviewed and approved by Tianjin Medical University Cancer Institute and Hospital. Written informed consent was obtained from the owners for the participation of their animals in this study.

Author contributions

All authors listed have made a substantial, direct, and intellectual contribution to the work and approved it for publication.

Funding

This work was supported by the Science & Technology Development Fund of Tianjin Education Commission for Higher Education grant number 2021KJ195.

Acknowledgments

The scientific guarantor of this publication is Prof. Yue Zhu.

Conflict of interest

The authors declare that the research was conducted in the absence of any commercial or financial relationships that could be construed as a potential conflict of interest.

Publisher's note

References

1. Greenlee RT, Murray T, Bolden S, Wingo PA. Cancer statistics, 2000. *CA Cancer J Clin* (2000) 50(1):7–33. doi: 10.3322/canjclin.50.1.7

2. Li S, Peng Y, Weinhandl ED, Blaes AH, Cetin K, Chia VM, et al. Estimated number of prevalent cases of metastatic bone disease in the US adult population. *Clin Epidemiol* (2012) 4:87–93. doi: 10.2147/CLEP.S28339

3. Delank KS, Wendtner C, Eich HT, Eysel P. The treatment of spinal metastases. *Dtsch Arztebl Int* (2011) 108(5):71–9. doi: 10.3238/arztebl.2011.0071

4. Joaquim AF, Powers A, Laufer I, Bilsky MH. An update in the management of spinal metastases. *Arq Neuropsiquiatr* (2015) 73(9):795–802. doi: 10.1590/0004-282X20150099

5. Lutz S, Berk L, Chang E, Chow E, Hahn C, Hoskin P, et al. Palliative radiotherapy for bone metastases: an ASTRO evidence-based guideline. *Int J Radiat Oncol Biol Phys* (2011) 79(4):965–76. doi: 10.1016/j.ijrobp.2010.11.026

6. Rosenthal D, Callstrom MR. Critical review and state of the art in interventional oncology: benign and metastatic disease involving bone. *Radiology* (2012) 262(3):765–80. doi: 10.1148/radiol.11101384

7. Ma Y, Wallace AN, Madaelil TP, Jennings JW. Treatment of osseous metastases using the spinal tumor ablation with radiofrequency (STAR) system. *Expert Rev Med Devices* (2016) 13(12):1137–45. doi: 10.1080/17434440.2016.1256772

8. Bagla S, Sayed D, Smirniotopoulos J, Brower J, Neal RJ, Dick B, et al. Multicenter prospective clinical series evaluating radiofrequency ablation in the treatment of painful spine metastases. *Cardiovasc Intervent Radiol* (2016) 39(9):1289–97. doi: 10.1007/s00270-016-1400-8

9. Zhang C, Han X, Li L, Zhang C, Ma Y, Wang G. Posterior decompression surgery and radiofrequency ablation followed by vertebroplasty in spinal metastases from lung cancer. *Med Sci Monit* (2020) 26:e925169. doi: 10.12659/MSM.925169

10. Tomasian A, Gangi A, Wallace AN, Jennings JW. Percutaneous thermal ablation of spinal metastases: Recent advances and review. *AJR Am J Roentgenol* (2018) 210 (1):142–52. doi: 10.2214/AJR.17.18205

11. Buscarini L, Rossi S, Fornari F, Di Stasi M, Buscarini E. Laparoscopic ablation of liver adenoma by radiofrequency electrocauthery. *Gastrointest Endosc* (1995) 41(1):68–70. doi: 10.1016/s0016-5107(95)70279-2

12. Kim YS, Rhim H, Lim HK, Choi D, Lee MW, Park MJ. Coagulation necrosis induced by radiofrequency ablation in the liver: histopathologic and radiologic review of usual to extremely rare changes. *Radiographics* (2011) 31(2):377–90. doi: 10.1148/rg.312105056

13. Rosenthal DI, Springfield DS, Gebhardt MC, Rosenberg AE, Mankin HJ. Osteoid osteoma: percutaneous radio-frequency ablation. *Radiology* (1995) 197 (2):451–4. doi: 10.1148/radiology.197.2.7480692

14. Tatli S, Tapan U, Morrison PR, Silverman SG. Radiofrequency ablation: technique and clinical applications. *Diagn Interv Radiol* (2012) 18(5):508–16. doi: 10.4261/1305-3825.DIR.5168-11.1

15. Cazzato RL, Garnon J, Caudrelier J, Rao PP, Koch G, Gangi A. Percutaneous radiofrequency ablation of painful spinal metastasis: a systematic literature assessment of analgesia and safety. *Int J Hyperthermia* (2018) 34(8):1272–81. doi: 10.1080/02656736.2018.1425918

16. Di Staso M, Gravina GL, Zugaro L, Bonfili P, Gregori L, Franzese P, et al. Treatment of solitary painful osseous metastases with radiotherapy, cryoablation or combined therapy: Propensity matching analysis in 175 patients. *PloS One* (2015) 10 (6):e129021. doi: 10.1371/journal.pone.0129021

17. Di Staso M, Zugaro L, Gravina GL, Bonfili P, Marampon F, Di Nicola L, et al. A feasibility study of percutaneous radiofrequency ablation followed by radiotherapy in the management of painful osteolytic bone metastases. *Eur Radiol* (2011) 21(9):2004–10. doi: 10.1007/s00330-011-2133-3

18. Rosian K, Hawlik K, Piso B. Efficacy assessment of radiofrequency ablation as a palliative pain treatment in patients with painful metastatic spinal lesions: A systematic review. *Pain Physician* (2018) 21(5):E467–76. doi: 10.36076/ppj.2018.5.E467

19. Philip A, Gupta S, Ahrar K, Tam AL. A spectrum of nerve injury after thermal ablation: a report of four cases and review of the literature. *Cardiovasc Intervent Radiol* (2013) 36(5):1427–35. doi: 10.1007/s00270-012-0491-0

20. Nakatsuka A, Yamakado K, Maeda M, Yasuda M, Akeboshi M, Takaki H, et al. Radiofrequency ablation combined with bone cement injection for the treatment of bone malignancies. *J Vasc Interv Radiol* (2004) 15(7):707–12. doi: 10.1097/01.rvi.0000133507.40193.e4

21. Pezeshki PS, Woo J, Akens MK, Davies JE, Gofeld M, Whyne CM, et al. Evaluation of a bipolar-cooled radiofrequency device for ablation of bone metastases: preclinical assessment in porcine vertebrae. *Spine J* (2014) 14(2):361–70. doi: 10.1016/j.spinee.2013.08.041

22. Nour SG, Aschoff AJ, Mitchell IC, Emancipator SN, Duerk JL, Lewin JS. MR imaging-guided radio-frequency thermal ablation of the lumbar vertebrae in porcine models. *Radiology* (2002) 224(2):452–62. doi: 10.1148/radiol.2242011269

23. Nikfarjam M, Muralidharan V, Christophi C. Mechanisms of focal heat destruction of liver tumors. *J Surg Res* (2005) 127(2):208–23. doi: 10.1016/j.jss.2005.02.009

24. Tarlov IM, Klinger H. Spinal cord compression studies. II. time limits for recovery after acute compression in dogs. *AMA Arch Neurol Psychiatry* (1954) 71 (3):271–90.

25. Sheng SR, Wang XY, Xu HZ, Zhu GQ, Zhou YF. Anatomy of large animal spines and its comparison to the human spine: a systematic review. *Eur Spine J* (2010) 19 (1):46–56. doi: 10.1007/s00586-009-1192-5

26. Groetz SF, Birnbaum K, Meyer C, Strunk H, Schild HH, Wilhelm KE. Thermometry during coblation and radiofrequency ablation of vertebral metastases: a cadaver study. *Eur Spine J* (2013) 22(6):1389–93. doi: 10.1007/s00586-012-2647-7

27. You NK, Lee HY, Shin DA, Choi GH, Yi S, Kim KN, et al. Radiofrequency ablation of spine: an experimental study in an ex vivo bovine and *in vivo* swine model for feasibility in spine tumor. *Spine (Phila Pa 1976)* (2013) 38(18):E1121–7. doi: 10.1097/BRS.0b013e31829c2e12

28. Wallace AN, Hillen TJ, Friedman MV, Zohny ZS, Stephens BH, Greco SC, et al. Percutaneous spinal ablation in a sheep model: Protective capacity of an intact cortex, correlation of ablation parameters with ablation zone size, and correlation of postablation MRI and pathologic findings. *AJNR Am J Neuroradiol* (2017) 38 (8):1653–9. doi: 10.3174/ajnr.A5228

29. Wiersinga WJ, Jansen MC, Straatsburg IH, Davids PH, Klaase JM, Gouma DJ, et al. Lesion progression with time and the effect of vascular occlusion following radiofrequency ablation of the liver. *Br J Surg* (2003) 90(3):306–12. doi: 10.1002/bjs.4040

30. Ni Y, Mulier S, Miao Y, Michel L, Marchal G. A review of the general aspects of radiofrequency ablation. *Abdom Imaging* (2005) 30(4):381–400. doi: 10.1007/s00261-004-0253-9

31. Kawai T, Kaminou T, Sugiura K, Hashimoto M, Ohuchi Y, Adachi A, et al. Creation of a tumor-mimic model using a muscle paste for radiofrequency ablation of the lung. *Cardiovasc Intervent Radiol* (2009) 32(2):296–302. doi: 10.1007/s00270-008-9463-9

frontiers | Frontiers in Oncology

TYPE Original Research
PUBLISHED 14 March 2023
DOI 10.3389/fonc.2023.1149342

OPEN ACCESS

EDITED BY
Feifei Pu,
Huazhong University of Science and Technology, China

REVIEWED BY
Yu Xiuchun,
960th Hospital of the PLA, China
Lin Nong,
The Second Affiliated Hospital of Thejiang University, China
Jianxiang Liu,
Huazhong University of Science and Technology, China

*CORRESPONDENCE
Hong Duan
duanhong1970@126.com

SPECIALTY SECTION
This article was submitted to Surgical Oncology, a section of the journal Frontiers in Oncology

RECEIVED 21 January 2023
ACCEPTED 27 February 2023
PUBLISHED 14 March 2023

CITATION
Wu F, Fang X, Yuan D, Xiong Y, Luo Y, Zhang W, Tu C and Duan H (2023) Preserving the rectus femoris and improving limb function after total femoral prosthesis replacement following resection of femoral malignant tumors. *Front. Oncol.* 13:1149342. doi: 10.3389/fonc.2023.1149342

Preserving the rectus femoris and improving limb function after total femoral prosthesis replacement following resection of femoral malignant tumors

Fan Wu[1,2], Xiang Fang[1], Dechao Yuan[1], Yan Xiong[1], Yi Luo[1], Wenli Zhang[1], Chongqi Tu[1] and Hong Duan[1]*

[1]Department of Orthopedics, West China School of Medicine/West China Hospital, Sichuan University, Chengdu, China, [2]Department of Orthopedics, Zigong Fourth People's Hospital, Zigong, China

Background: Current research is focused on the factors that influence the maintenance of limb function after total femoral replacement. This retrospective study investigated the difference in functional outcomes in patients with invasion of the rectus femoris *vs*. an intact rectus femoris that underwent total femoral replacement with a modular total femur prosthesis.

Methods: The medical records of patients who underwent total femoral replacement with a modular total femur prosthesis between July 2010 and March 2017 at our institute were retrospectively reviewed. The patients were divided into two groups: group A had invasion of the rectus femoris and group B had an intact rectus femoris. Functional status was assessed using the Musculoskeletal Tumor Society Rating Scale (MSTS) and the Harris Hip Score (HHS). Complications were assessed using the International Society of Limb Salvage classification that was published in 2011 and modified in 2014.

Results: The mean total MSTS score (23.0 $\pm$ 4.8 *vs*. 17.6 $\pm$ 3.1; $P = 0.02$) and the mean total HHS score (80.17 $\pm$ 6.24 *vs*. 55.38 $\pm$ 13.30; $P = 0.001$) were significantly higher in patients with intact rectus femoris compared with patients with invasion of the rectus femoris. Patients with an intact rectus femoris achieved significantly better limb function (support and gait) and active range of motion ($P < 0.05$). The overall complication rate was 35.7%.

Conclusions: Functional outcomes after total femoral replacement were significantly better in patients with an intact rectus femoris compared with patients with invasion of the rectus femoris, possibly because more muscle mass can be preserved around the femur in patients with an intact rectus femoris.

KEYWORDS

femur, tumor, total femoral prosthesis replacement, limb-salvage, rectus femoris invasion

1 Introduction

The femur is commonly affected by primary and secondary malignant bone tumors that require radical surgical excision in the lower extremities (1). The primary purpose of the treatment is to save the patient's life. A patient with a femur malignant tumor has a very poor prognosis, and until 1972, the survival rates ranged from 5% to 20% (2), and before the 1980s, amputation was the only treatment. Furthermore, the survival rate of the patients is not improved by amputation (3), the limb function is not good, and the psychological trauma is profound. With the advancement of surgical techniques, implant designs, diagnostic imaging systems, and chemotherapy methods, not only has the survival rate increased significantly but also limb salvage after tumor resection has become a standard approach and flourished. To date, the 5-year survival rate of osteosarcoma has been reported to be between 65% and 86% (4).

When tumors have extensive involvement and have multiple or skip lesions and when previous distal or proximal replacement failed, the treatment is quite difficult, and in such instances, total femur replacement (TFR) is recommended (5). Hip disarticulation, turnabout procedure (6), and tibial turn-up procedure (7) are alternative surgical approaches. The prosthesis includes a metallic system procedure (8) and a total femoral allograft (9). Considering its mature use and accessibility, a metallic system prosthesis is most commonly used in the clinic. TFR can restore the integrity of the femur and allow the patients to resume ambulation pain-free, and the function of TFR was much better than hip dislocation (2) and turnabout and turn-up procedures (7, 10). In addition, limb salvage is the expectation of most patients.

TFR requires a great sacrifice for the affected muscles. The extent of quadriceps removal has been reported to influence the long-term functional efficiency of a patient's gait, and the function of patients who have had reserved the rectus femoris after total knee replacement for treating the distal femoral tumors is better than the function of those who had not reserved the rectus femoris (11). Theoretically, the rectus femoris is the only muscle in the quadriceps that spans from the hip to the knee joint, and the function is to bend the hip and extend the knee; preserving the rectus femoris in total femur replacement had a better hip and knee function similar to total knee replacement.

To counteract or prevent the factors that contribute to the limitation of the hip and knee functions after TFR, it may prove valuable to reserve the rectus femoris to increase hip and knee function. We performed a retrospective cohort study to determine whether there are differences between a TFR with and without the rectus femoris invasion. We sought to conclude 1) the effect of total femur replacement and 2) whether patients without invasion of the rectus femoris had a better hip and knee range of motion (ROM) or a better function.

2 Materials and methods

We retrospectively reviewed 14 patients with total femoral prosthesis replacement between July 2010 and March 2017 at our institute. There were eight men and six women, with ages ranging from 16 to 75 years (average age of 44.8 years). There were 11 cases of primary tumors and 3 cases of metastatic tumors. The origin of the primary cases was as follows: three involved the diaphysis, two the distal third of the femur, four the long segment of the shaft, and two the proximal third of the femur; three metastases involved the long segment of the femur (one caused pathological fracture) which were secondary to lung cancer. All patients had more than one segment of the femur involved, which required a total femur replacement, as retaining any part of the femur for proximal, shaft, or distal prostheses would have been inappropriate and unstable. The most common diagnosis in these cases was osteosarcoma (eight cases). The patients were divided into two groups: group A had invasion of the rectus femoris (eight cases), and group B had an intact rectus femoris (six cases) (Table 1). This study cohort was approved by the Ethics Committee of West China Hospital of Sichuan University, and all the participants were informed about the surgical approaches.

2.1 Surgical procedures

Preoperative systematic evaluations and examinations, including clinical evaluations, plain radiographs, single-photon emission computerized tomography (SPECT) scans, chest radiographs, and computed tomography (CT) scans, were performed to assess local lesions and metastases. Magnetic resonance imaging (MRI) was used to determine the extent of tumor invasion, including the involvement of soft tissue, especially neurovascular tissue.

All the patients with osteosarcoma received preoperative and postoperative chemotherapies with high-dose methotrexate, doxorubicin, cisplatin, and ifosfamide. The patients with femur pathological fractures following metastasis tumor received targeted drugs and comprehensive treatment for the primary tumor.

The patients received a modular total femur prosthesis (Chunlizhengda Co. Ltd., Beijing, China), which contains a bipolar femoral head component and a fixed hinge, cemented, and constrained total knee system.

Surgery was performed using the long lateral approach to the femur (Figure 1E) and involved three steps. After a long incision was made on the lateral side from 10 cm proximal to the greater trochanter to the anterolateral aspect of the patellar tendon and tibial tuberosity, en-bloc excision of the entire femur was performed. At the proximal thigh, the gluteus medius, gluteus minimus, and deep external rotators were detached depending on the surgical margin (5, 12). The gluteus maximus tendon was separated, and the sciatic nerve and vascular bundles were exposed and well protected. The hip capsule was dissected around the femoral neck, and the femoral head was dislocated. At the distal thigh, the patella was turned to the medial dislocation; the neurovascular bundles were separated from the tumor, exposed, and protected well; the adductor muscles were separated and the muscles attached to the linea aspera were removed; the capsule at the knee was divided; and then the total femur was removed. The tumor is resected according to the principles (13), endeavoring to

TABLE 1 Clinical characteristics of the included patients.

Number	Age (years)/gender	Diagnosis	Rectus femoris invasion	MSTS	HHS	Follow-up time (months)
1	75/M	Metastatic tumor	No	22	75	Alive, 17
2	54/M	Metastatic tumor	No	18	76	Alive, 14
3	47/F	Osteosarcoma	Yes	23	76	Dead, 12
4	28/F	Osteosarcoma	Yes	15	44	Dead, 16
5	25/F	Osteosarcoma	Yes	18	52	Dead, 13
6	62/M	Osteosarcoma	Yes	16	36	Dead, 11
7	68/M	Chondrosarcoma	No	28	81	Alive, 58
8	73/M	Osteosarcoma	No	21	74	Alive, 18
9	16/F	Osteosarcoma	No	29	90	Alive, 27
10	32/F	Chondrosarcoma	No	20	83	Alive, 32
11	17/M	Osteosarcoma	Yes	16	51	Alive, 18
12	19/M	Osteosarcoma	No	21	69	Alive, 43
13	42/F	Chondrosarcoma	Yes	18	64	Alive, 12
14	72/M	Metastatic tumor	Yes	14	51	Dead, 15

HSS, Harris Hip Score; MSTS, Musculoskeletal Tumor Society Rating Scale.

FIGURE 1
Total femoral prosthesis replacement. A 15-year old girl with left femur osteosarcoma. **(A)** X-ray before operation, **(B–D)** CT, MRI and SPECT image showing massive involvement, **(E)** Surgical incision, **(F)** Total femur prosthesis in operation, **(G)** X-ray post-operation, **(H–J)** Functional outcome at 33 months.

achieve a satisfactory resection margin while the lesion was completely removed. A transverse osteotomy was performed 10 mm below the tibial joint line to allow the cementation of the tibial component. The second main step was the reconstruction of the defect with a prosthesis. The proximal tibia was osteotomized and the tibia component was inserted and then the cement was fixed. The femoral components were assembled, and the stability and tension were tested. Finally, in the third main step, the tissue was reconstructed. The remaining hip capsule was fixed around the neck of the prosthesis, and the external rotation muscles were sutured to the repaired capsule to strengthen. The remaining psoas muscle was rotated forward and was sutured on the capsule. The remaining abductor muscles will be placed on the proximal side of the prosthesis and reattached to the metal ring or the remaining greater trochanter, an artificial ligament was needed if these structures were not sufficient. The concept of the principle of the tumor-free technique was very important. Careful hemostasis was crucial, and dead space was eliminated as much as possible. When the wound was sutured, the prosthesis was covered with the rest of the muscles, and the wound was sutured in layers, with an indwelling drainage tube. If necessary, the vascularized gastrocnemius muscle flap blood vessels were used to cover the wound. All patients used an abduction brace after surgery. All patients received intravenous broad-spectrum antibiotics before and after the surgery.

Patients with total femoral replacement can gain full independence through a comprehensive and adequate rehabilitation program. Physical therapy techniques such as muscle contraction, passive and active exercises, and isometric exercises were very useful during early rehabilitation. Certain exercises, such as active hip abduction or knee flexion, were permitted 3-4 weeks later to protect the muscles which have been reattached to the prosthesis. Partial weight-bearing was allowed 6 weeks later. After 8~12 weeks, patients were advised to practice walking with a single crutch to determine whether their walking gait has normalized or not.

Patients were followed up every month in the first 3 months, every 3 months for the first year, and then every 6 months. A chest CT scan was performed every 3 months during the first year and then every 6 months for patients with osteosarcoma. A SPECT bone scan was performed every 6 months in the first year, then once a year, until the last follow-up.

2.2 Outcome measures

Functional status was assessed using the Musculoskeletal Tumor Society Rating Scale (MSTS) (14) and the Harris Hip Score (HHS) at the last follow-up. The MSTS constitutes six items (pain, function, emotional acceptance, use of an external support, walking ability, gait alteration) scored on a scale of 0 to 5 to a maximum of 30, with higher scores indicating better function. The HHS constitutes 10 items in domains that include pain, function, absence of deformity, and ROM, scored to a maximum of 100 with higher scores indicating better function. Complications were assessed using the International Society of Limb Salvage classification that was published in 2011 (15) and modified in 2014 (16). Type I is soft tissue failure, type II is aseptic loosening with clinical and radiographic signs of loosening, type III is structural failure, type IV is periprosthetic infection requiring removal and subsequent reimplantation of the implant, and type V is tumor progression (16).

2.3 Statistical analyses

Statistical analyses were performed with the SPSS software package version 24.0 (SPSS Inc., Chicago, IL, USA). Groups were compared using independent *t*-tests and the chi-square test for the continuous and categorical variables, respectively. A *P*-value <0.05 was considered significant.

3 Results

The demographic and clinical characteristics of the included patients stratified by invasion of the rectus femoris (group A) or an intact rectus femoris (group B) are summarized in Table 2. There were no significant differences in age ($P = 0.27$), gender ($P = 0.569$), diagnosis ($P = 0.486$), operative time ($P = 0.759$), blood loss ($P = 0.59$), or follow-up period ($P = 0.182$) between the two groups.

The functional results of patients with invasion of the rectus femoris (group A) and an intact rectus femoris (group B) are summarized in Table 3. The mean total MSTS score was 66.4% (19.93/30). The mean total MSTS score was significantly higher in patients with an intact rectus femoris (23.0 ± 4.8) compared with patients with invasion of the rectus femoris (17.6 ± 3.1) ($P = 0.02$). Specifically, patients with an intact rectus femoris scored significantly better on the function ($P = 0.04$), support ($P = 0.003$), and gait ($P = 0.016$) items of the MSTS, but there were no significant differences in the pain ($P = 0.20$), emotional acceptance ($P = 0.802$), or walking ($P = 0.178$) items between the two groups. The mean total HHS score was significantly higher in patients with an intact rectus femoris (80.17 ± 6.24) compared with patients with invasion of the rectus femoris (55.38 ± 13.30) ($P = 0.001$). Specifically, patients with an intact rectus femoris scored significantly better in the pain ($P = 0.003$), function ($P = 0.001$), and ROM ($P = 0.026$) domains of the HHS, but there was no significant difference in the deformity domain between the two groups ($P = 0.433$).

3.1 Complications

In general, the complication rate was 35.7% (5/14). Four patients suffered tumor progression (type V failure), three patients had pulmonary metastases, and one patient had local recurrence and amputation 8 months later. One patient experienced deep venous thrombosis that was resolved with antithrombotic therapy. There was no incidence of superficial or deep infection, sciatic paralysis, hip dislocation, or aseptic loosening.

TABLE 2 Demographic and clinical characteristics of the included patients stratified by invasion of the rectus femoris or an intact rectus femoris.

	Invasion of the rectus femoris	Intact rectus femoris	*P*-value	95% CI
Age	39.0 ± 20.3	52.7 ± 23.9	0.270	−12.10, 39.44
Gender			0.569	−0.79, 0.45
Male	4	4		
Female	4	2		
Follow-up (months)	17.5 ± 10.6	27.7 ± 16.3	0.182	−5.46, 25.79
Operative time (min)	235.0 ± 40.1	240.8 ± 24.2	0.759	−34.60, 46.27
Blood loss (ml)	1225.0 ± 710	1008.3 ± 743.2	0.590	−1,069.06, 635.73
Diagnosis			0.486	
Osteosarcoma	5	3		
Chondrosarcoma	2	1		
Metastatic tumor	1	2		

TABLE 3 Functional outcomes of the included patients stratified by invasion of the rectus femoris or an intact rectus femoris.

	Invasion of the rectus femoris	Intact rectus femoris	*P*-value	95% CI
MSTS				
Total score	17.6 ± 3.1	23.0 ± 4.8	0.02	1.00, 9.75
Pain	3.38 ± 0.52	3.83 ± 0.75	0.20	−0.28, 1.20
Function	2.75 ± 0.71	3.67 ± 0.82	0.04	0.03, 1.81
Emotional acceptance	3.75 ± 0.46	3.83 ± 0.75	0.802	−0.62, 0.79
Supporting	2.38 ± 0.74	4.00 ± 0.89	0.003	0.67, 2.58
Walking	2.63 ± 1.06	3.50 ± 1.2	0.178	−0.46, 2.21
Gait	2.63 ± 1.06	4.00 ± 0.63	0.016	0.31, 2.44
HHS				
Total score	55.38 ± 13.30	80.17 ± 6.24	0.001	11.92, 37.66
Pain	30.50 ± 6.48	40.67 ± 1.63	0.003	4.21, 16.12
Function	17.50 ± 6.68	32.50 ± 5.89	0.001	7.52, 22.49
Deformity	3.63 ± 0.52	3.83 ± 0.41	0.433	−0.35, 0.77
ROM	2.50 ± 0.54	3.17 ± 0.41	0.026	0.10, 1.24

HHS, Harris Hip Score; MSTS, Musculoskeletal Tumor Society Rating Scale; ROM, range of motion.

4 Discussion

Total femoral prosthesis replacement is a procedure rarely done, and the indications are not well defined (3). From the first total femur prosthesis reported in 1965, the indications focused mainly on oncology diseases, and many authors applied them to malignant femur tumors (1–3, 17). A high-grade malignant tumor that affected the femur widely or totally, or skip lesions, has been the indication for this procedure, including osteosarcoma, Ewing's sarcoma, chondrosarcoma (18), undifferentiated sarcoma, huge soft tissue tumor, metastatic tumor, and local recurrent osteosarcoma. Moreover, the applications were developed gradually for non-oncology diseases, which can affect the integrity of the femur and could repeatedly cause pathological fractures, such as Paget's disease, osteogenesis imperfecta (19), fibrous dysplasia with massive idiopathic osteolysis, massive femoral hemophilic pseudotumor (20), and hydatid disease (21). Here, we summarized the main large case series of femoral prosthesis replacement for oncology in the current literature in Table 4. Hip and knee arthroplasty revisions with severe bone defects using conventional methods are difficult procedures, and in severe

TABLE 4 Main large case series of total femur replacement for oncology in the current literature.

Ref.	Publication	*N*	Age	Indications	Follow-up (months)	Patients living at the time of publication	Survivorship	All-cause revision rate	Complications
Ahmed (12)	Arch Orthop Trauma Surg	9	47 (10-74)	Oncology	51 (8-200)	4/9	No failures	0%	Infection (2), tibial component loosening (1)
Mankin et al. (22)	Clin Orthop Relat Res	15	52 ± 1 (16-82)	Oncology (14), non-oncology (1)	54 (12-192)	7/15	NA	33.3%	Infection (1), prosthesis failure (4)
Nerubay et al. (23)	Clin Orthop Relat Res	19	20	Oncology	18-96	7/19	NA	–	Wound-healing problems (10), infection (1), popliteal vein injury (1), prosthesis failure (1)
Steinbrink et al. (24)	J Bone Joint Surg Br	32 (28 patients)	56 (21-81)	Oncology (6), non-oncology (22)	6-84	23/28	NA	9.4%	Infection (2), hip dislocation (1), prosthesis failure (1), patellar pain (1)
Ward et al. (25)	Clin Orthop Relat Res	21	44.6 (11-91)	Oncology (17), non-oncology (4)	31 (1-125)	11/21	NA	2.4%	Infection (3), hip dislocation (2), patellar pain (1)
Sevelda et al. (26)	Clin Orthop Relat Res	11	64 (41-78)	Metastatic carcinoma	5 (1-31)	8/11 died after 6 months	NA	–	Hip dislocation (1), infection (1), local recurrence (1)
Liu et al. (27)	World Journal of Surgical Oncology	21	21.8	Osteosarcoma	71.2	72.5% last follow-up	66.7% at 5 years	–	Superficial infection (2), deep infection (1), patella fracture (1), local recurrence (1), pulmonary metastases (9), tibial stem loosening (3)
Puri et al. (28)	Indian J Orthop	8	32	Osteosarcoma (5), Ewing's sarcoma (1), chondrosarcoma (2)	33 (9-72)	5/8 (24-72months)	5/8	–	Infection (1), metastasis (1), 3 cm shortening (1)
Jones et al. (29)	J Surg Oncol	54	40.6 ± 19.9	Primary sarcoma (40), metastatic sarcoma (1), metastatic carcinoma (12), lymphoma (1)	48 (1-252)	28/40	28/40	–	Hip dislocation (5), femoral malrotation (1), infection (4)
Muratori (30)	Journal of Orthopaedics	32	54.2 (13-82)	Oncology (23), non-oncology (9)	60	NA	NA	–	Superficial infection (2), deep infection (1), dislocation (2)

NA, not available.
The symbol "-" means that column was not mentioned in the article.

periprosthetic fractures (31), a second-stage arthroplasty approach to prevent infection is required (32). TFR provides patients with a functional limb and enables patients to remain pain-free for the rest of their lives (3).

The mean MSTS score and ROM of the 14 patients were 66.4% (19.93/30) and 65.9°, and the mean HHS score of the hip was 66 (44-90). Similar to the results of Sewell et al. (1), the mean MSTS score was 67% and the mean HHS was 70%. However, in contrast to the study of Sewell et al. (1), we did not compare the difference between the primary and the secondary TFRs because our sample size was too small. This function score is generally lower than TKR and THR, but it is acceptable to those tumor patients. Our typical case function is provided in the supplement video (Figure 1, Supplement 1).

The function after TFR was good for pathological fractures following metastasis. In our three cases with pathological fractures, the function was good (the mean MSTS score was 18). Similar to the report of Mankin et al. (22), involving a total of 15 patients with 2

found to have metastatic carcinomas, the function and quality of life of the survivors were good. Total femoral prosthesis arthroplasty can recover early functional weight-bearing walking and exercise and effectively guarantee improvement in the quality of life of the survivor. However, the resection of the entire femur requires wide exposure and a prolonged procedure time. As the amount of intraoperative blood as well as surgical trauma is large, surgeons must dynamically assess the patient's heart–lung capability and degree of tolerance. In the study of Sevelda et al. (26), the authors summarized that of the 11 patients with metastatic carcinoma of the femur, 8 of them died 6 months after the operation, so they believe that TFR does not warrant greater life expectancy, and patients with extensive metastatic disease to the femur should be offered palliative care rather than major reconstruction. Thus, an increase in the sample size for TFR for pathological fractures is needed. In Table 4, we summarized the main functional outcomes and follow-up results of TFR in the literature.

The rectus femoris is very important in the function of patients with TFR. In our cases, we found that patients without rectus femoris invasion had better limb function (including supporting, walking, and gait) and a greater range of active hip movement than those with rectus femoris invasion. The rectus femoris is the only muscle in the quadriceps that spans from the hip to the knee joint, and its anatomical location is superficial in the quadriceps. Once the rectus femoris of a patient is invaded, then he will have a wider resection to obtain enough surgical boundaries, and fewer muscles around the femur could be preserved. Benedetti et al. (11) reported similar results for total knee arthroplasty in the distal femoral tumor that preserves the rectus femoris. Similar to our findings, Morris et al. (5) proposed that a lack of hip abductors or knee extensor procedures resulted in a poor functional outcome as the patient cannot control the limb. Nakayama et al. (33) reported that the most influential factor in the functional outcomes after TFR was whether the rectus femoris was preserved or not. Du et al. (34) found that the use of an artificial ligament to reconstruct soft tissue can improve limb function after TFR, but this was indirectly confirmed. The mean MSTS function score was 66.4% (19.93/30), similar to the reports by Ahmed (12), Kalra et al. (3), and Du et al. (34). The mean HHS score of the hip was 66 (44-90), similar to the report by Sewell et al. (1), and the overall mean HHS score was 70 (51-86). TFR provides most of the patients with a functional limb, which can be weight-bearing and make walking pain-free.

The reported complication rates vary (35, 36), and we summarized the main complications of TFR in the literature in Table 4. In our cases, the complication rate was 35.7% (5/14). Common complications included infection, aseptic failure, hip dislocation, and vascular and sciatic nerve injury. The most frequent complications were dislocation and infection (37, 38). Our cases have no infection mainly because we use an impulse-type flusher and plenty of saline water to wash the wounds. In the report by Kalra et al. (3), the deep infection rate was 7%, which was similar to the report by Mankin et al. (22). While in the report by Natarajan (17), the deep infection rate was 11.8%. Friesecke et al. (38) published the largest known series of total femur prostheses, involving 100 consecutive patients, and the infection rate was 13%. The dislocation rate reported by Friesecke et al. (38) was 6%; however, our cases and the report by Sevelda et al. (39) do not have dislocations. The reason why we had no dislocation was mainly due to the good reconstruction of the hip abductor, and we used artificial ligaments for large defects. Du et al. (34) found that the use of an artificial ligament can decrease the dislocation rate. The greater trochanter and the accompanying outriggers are essential to maintain the stability of the prosthesis, so it is very important to refix these outsoles to the prosthesis.

The current data from a series of patients suggest that TFR plays a role in treating malignant or even severely damaged benign femoral lesions. The death and complication rates are high, which might be due to the degree of malignancy, size, and vascularity of the lesion, but the functional outcome of the survivors is reasonable and better than hip dislocation or hemisection. In metastatic femoral metastases with pathological fractures, the quality of life can be improved within a limited lifetime.

Our study has some limitations. First, the number of cases is small, due to the rare indication for this procedure, although our data cover a span of 8 years. Second, it has a retrospective design, which had some selection bias from the inclusion of non-randomized patients. Third, our cases had different types of tumors, which received an individualized general prognosis because of the rare indications for TFR.

5 Conclusion

We believe that our report provides the expected results for patients with femoral tumors who require total femoral replacement. This form of reconstruction provides predictable results after the removal of the femoral tumor. TFR is a good and reliable method for the salvage of the femoral tumor limb.

Data availability statement

The original contributions presented in the study are included in the article/Supplementary Material. Further inquiries can be directed to the corresponding author.

Ethics statement

The studies involving human participants were reviewed and approved by Ethics Committee of West China Hospital of Sichuan University. Written informed consent to participate in this study was provided by the participants' legal guardian/next of kin. Written informed consent was obtained from the individual(s) for the publication of any identifiable images or data included in this article.

Author contributions

FW contributed to the conception and execution of the research and the writing of the manuscript. XF, DY, WZ, CT and HD were responsible for the integrity and analysis of the data. YX and YL contributed to the conception and execution of the research. All

authors contributed to the article and approved the submitted version.

Acknowledgments

The authors would like to thank all the participating patients, as well as the study nurses, co-investigators, and colleagues who made this trial possible.

Conflict of interest

The authors declare that the research was conducted in the absence of any commercial or financial relationships that could be construed as a potential conflict of interest.

Publisher's note

Supplementary material

The Supplementary Material for this article can be found online at: https://www.frontiersin.org/articles/10.3389/fonc.2023.1149342/full#supplementary-material

References

1. Sewell MD, Spiegelberg BG, Hanna SA, Aston WJ, Bartlett W, Blunn GW, et al. Total femoral endoprosthetic replacement following excision of bone tumours. *J Bone Joint Surg Br* (2009) 91(11):1513–20. doi: 10.1302/0301-620X.91B11.21996

2. Katznelson A, Nerubay J. Total femur replacement in sarcoma of the distal end of the femur. *Acta Orthop Scand* (1980) 51(5):845–51. doi: 10.3109/17453678008990883

3. Kalra S, Abudu A, Murata H, Grimer RJ, Tillman RM, Carter SR. Total femur replacement: primary procedure for treatment of malignant tumours of the femur. *Eur J Surg Oncol* (2010) 36(4):378–83. doi: 10.1016/j.ejso.2009.11.002

4. Morris CD, Wustrack RL, Levin AS. Limb-salvage options in growing children with malignant bone tumors of the lower extremity: A critical analysis review. *JBJS Rev* (2017) 5(7):e7. doi: 10.2106/JBJS.RVW.16.00026

5. Morris HG, Capanna R, Campanacci D, Del Ben M, Gasbarrini A. Modular endoprosthetic replacement after total resection of the femur for malignant tumour [Research support, non-U.S. *Gov't Review]. Int Orthop* (1994) 18(2):90–5. doi: 10.1007/BF02484417

6. Cammisa FPJr., Glasser DB, Otis JC, Kroll MA, Lane JM, Healey JH. The van nes tibial rotationplasty. a functionally viable reconstructive procedure in children who have a tumor of the distal end of the femur [Comparative study research support, non-U.S. gov't]. *J Bone Joint Surg Am vol* (1990) 72(10):1541–7.

7. McDonald DJ, Scott SM, Eckardt JJ. Tibial turn-up for long distal femoral bone loss. *Clin orthop related Res* (2001) 383):214–20. doi: 10.1097/00003086-200102000-00025

8. Pan K, Chan W, Shanmugam P, Ong G, Kamaruddin F, Tan S. Large Volume osteosarcomas of the femur treated with total femoral replacement. *Malays Orthop J* (2014) 8(1):32–6. doi: 10.5704/MOJ.1403.015

9. Urch SE, Moskal JT. Simultaneous ipsilateral revision total hip arthroplasty and revision total knee arthroplasty with entire femoral allograft [Case reports]. *J Arthroplasty* (1998) 13(7):833–6. doi: 10.1016/S0883-5403(98)90040-7

10. Otsuka T, Okuda T, Sekiya I, Tsuji H, Matsui N, Nishi G. Rotation plasty for osteosarcoma of the femur [Case reports]. *J Reconstr Microsurg* (1998) 14(8):545–9. doi: 10.1055/s-2008-1040773

11. Benedetti MG, Catani F, Donati D, Simoncini L, Giannini S. Muscle performance about the knee joint in patients who had distal femoral replacement after resection of a bone tumor. an objective study with use of gait analysis. *J Bone Joint Surg Am vol* (2000) 82(11):1619–25. doi: 10.2106/00004623-200011000-00016

12. Ahmed AR. Total femur replacement. *Arch Orthop Trauma Surg* (2010) 130 (2):171–6. doi: 10.1007/s00402-009-0945-2

13. Enneking WF, Spanier SS, Goodman MA. A system for the surgical staging of musculoskeletal sarcoma. *Clin orthop related Res* (1980) 153):106–20. doi: 10.1097/00003086-198011000-00013

14. Enneking WF, Dunham W, Gebhardt MC, Malawar M, Pritchard DJ. A system for the functional evaluation of reconstructive procedures after surgical treatment of tumors of the musculoskeletal system. *Clin orthop related Res* (1993) 286):241–6. doi: 10.1097/00003086-199301000-00035

15. Henderson ER, Groundland JS, Pala E, Dennis JA, Wooten R, Cheong D, et al. Failure mode classification for tumor endoprostheses: retrospective review of five institutions and a literature review [Review]. *J Bone Joint Surg Am vol* (2011) 93 (5):418–29. doi: 10.2106/JBJS.J.00834

16. Henderson ER, O'Connor MI, Ruggieri P, Windhager R, Funovics PT, Gibbons CL, et al. Classification of failure of limb salvage after reconstructive surgery for bone tumours a modified system including biological and expandable reconstructions. *J Bone Joint Surg Am vol* (2014) 96:1436–40. doi: 10.1302/0301-620x.96b11

17. Natarajan MV, Balasubramanian N, Jayasankar V, Sameer M. Endoprosthetic reconstruction using total femoral custom mega prosthesis in malignant bone tumours. *Int Orthop* (2009) 33(5):1359–63. doi: 10.1007/s00264-009-0737-x

18. Zheng K , Yu X-c, Xu S-F, Wang L. Total femur replacement for treatment of chondrosarcoma involving the entire femur. *Orthop Surgery*. (2015) 7(3):286–7. doi: 10.1111/os.12191

19. Sanz-Ruiz P, Villanueva-Martinez M, Calvo-Haro JA, Carbo-Laso E, Vaquero-Martin J. Total femur arthroplasty for revision hip failure in osteogenesis imperfecta: limits of biology. *Arthroplast Today* (2017) 3(3):154–9. doi: 10.1016/j.artd.2017.01.001

20. Buchowski JM, Cascio BM, Streiff MB, Frassica FJ. Resection and reconstruction of a massive femoral hemophilic pseudotumor [Case reports]. *Clin orthop related Res* (2005) 430):237–42. doi: 10.1097/01.blo.0000137545.37824.b0

21. Moore D, Baker KC, Les K. Hydatid disease of the femur treated with a total femoral replacement. *JBJS Case Connect* (2015) 5(1):e7. doi: 10.2106/jbjs.cc.m.00279

22. Mankin HJ, Hornicek FJ, Harris M. Total femur replacement procedures in tumor treatment [Comparative study]. *Clin orthop related Res* (2005), 438:60–4. doi: 10.1097/00003086-200509000-00012

23. Nerubay J, Katznelson A, Tichler T, Rubinstein Z, Morag B, Bubis JJ. Total femoral replacement. *Clin orthop related Res* (1988) 229):143–8. doi: 10.1097/00003086-198804000-00018

24. Steinbrink K, Engelbrecht E, Fenelon GC. The total femoral prosthesis. a preliminary report. *J Bone Joint Surg Br vol* (1982) 64(3):305–12. doi: 10.1302/0301-620x.64b3.7096396

25. Ward WG, Dorey F, Eckardt JJ. Total femoral endoprosthetic reconstruction. *Clin orthop related Res* (1995) 316):195–206. doi: 10.1097/00003086-199507000-00027

26. Sevelda F, Waldstein W, Panotopoulos J, Kaider A, Funovics PT, Windhager R. Is total femur replacement a reliable treatment option for patients with metastatic carcinoma of the femur? *Clin Orthop Relat Res* (2018) 476(5):977–83. doi: 10.1007/s11999.0000000000000125

27. Liu T, Zhang X, Zhang Q, Guo X. Total femoral reconstruction with custom prosthesis for osteosarcoma. *World J Surg Oncol* (2016) 14:93. doi: 10.1186/s12957-016-0852-2

28. Puri A, Gulia A, Chan WH. Functional and oncologic outcomes after excision of the total femur in primary bone tumors: Results with a low cost total femur prosthesis. *Indian J Orthop* (2012) 46(4):470–4. doi: 10.4103/0019-5413.98834

29. Jones KB, Griffin AM, Chandrasekar CR, Biau D, Babinet A, Deheshi B, et al. Patient-oriented functional results of total femoral endoprosthetic reconstruction following oncologic resection [Multicenter study research support, N.I.H., extramural]. *J Surg Oncol* (2011) 104(6):561–5. doi: 10.1002/jso.22003

30. Muratori F, Mondanelli N, Prifti X, Scoccianti G, Roselli G, Frenos F, et al. Total femur prosthesis in oncological and not oncological series. *Survival failures J Orthop* (2020) 17:215–20. doi: 10.1016/j.jor.2019.11.009

31. Lombardi AVJr., Berend KR. The shattered femur: radical solution options [Research support, non-U.S. *Gov't]. J Arthroplasty* (2006) 21(4 Suppl 1):107–11. doi: 10.1016/j.arth.2006.01.007

32. Sherman SL, Cunneen KP, Walcott-Sapp S, Brause B, Westrich GH. Custom total femur spacer and second-stage total femur arthroplasty as a novel approach to infection and periprosthetic fracture [Case reports]. *J Arthroplasty* (2008) 23(5):781–6. doi: 10.1016/j.arth.2007.05.027

33. Nakayama T, Matsumoto S, Shimoji T, Ae K, Tanizawa T, Gokita T. The significance of rectus femoris for the favorable functional outcome after total femur replacement. *Plast Reconstr Surg Glob Open* (2016) 4(3):e630. doi: 10.1097/GOX.0000000000000610

34. Du Z, Tang S, Yang R, Tang X, Ji T, Guo W. Use of an artificial ligament decreases hip dislocation and improves limb function after total femoral prosthetic replacement following femoral tumor resection. *J Arthroplasty* (2017) 33(5):1507–14 doi: 10.1016/j.arth.2017.12.017

35. Yoshida Y, Kojima T, Taniguchia M, Tokuhashia Y. Experiences with total femur replacement for malignant bone and soft tissue tumors. *Asian Biomed* (2012) 6 (1):123–7. doi: 10.5372/1905-7415.0601.137

36. Amanatullah DF, Trousdale RT, Hanssen AD, Lewallen DG, Taunton MJ. Non-oncologic total femoral arthroplasty: retrospective review. *J Arthroplasty* (2014) 29 (10):2013–5. doi: 10.1016/j.arth.2014.05.012

37. Toepfer A, Harrasser N, Petzschner I, Pohlig F, Lenze U, Gerdesmeyer L, et al. Is total femoral replacement for non-oncologic and oncologic indications a safe procedure in limb preservation surgery? a single center experience of 22 cases. *Eur J Med Res* (2018) 23(1):5. doi: 10.1186/s40001-018-0302-4

38. Friesecke C, Plutat J, Block A. Revision arthroplasty with use of a total femur prosthesis. *J Bone Joint Surg Am* (2005) 87(12):2693–701. doi: 10.2106/JBJS.D.02770

39. Sevelda F, Schuh R, Hofstaetter JG, Schinhan M, Windhager R, Funovics PT. Total femur replacement after tumor resection: Limb salvage usually achieved but complications and failures are common. *Clin orthop related Res* (2015) 473(6):2079–87. doi: 10.1007/s11999-015-4282-1

frontiers | Frontiers in Oncology

TYPE Review
PUBLISHED 16 March 2023
DOI 10.3389/fonc.2023.1156618

OPEN ACCESS

EDITED BY
Feifei Pu,
Huazhong University of Science and Technology, China

REVIEWED BY
Zhongmeng Lai,
Fujian Medical University Union Hospital, China
Han Wu,
Wuhan University, China
Songfeng Chen,
First Affiliated Hospital of Zhengzhou University, China

*CORRESPONDENCE
Bin Zhao
zzbb3737@126.com
Xiaofeng Zhao
ff860808@126.com

†These authors have contributed equally to this work

SPECIALTY SECTION
This article was submitted to Surgical Oncology, a section of the journal Frontiers in Oncology

RECEIVED 01 February 2023
ACCEPTED 02 March 2023
PUBLISHED 16 March 2023

CITATION
Jing D, Zhao Q, Zhao Y, Lu X, Feng Y, Zhao B and Zhao X (2023) Management of pain in patients with bone metastases. *Front. Oncol.* 13:1156618. doi: 10.3389/fonc.2023.1156618

Management of pain in patients with bone metastases

Doudou Jing[1†], Qian Zhao[2†], Yibo Zhao[1], Xiangdong Lu[1], Yi Feng[1], Bin Zhao[1*] and Xiaofeng Zhao[1*]

[1]Department of Orthopaedics, The Second Hospital of Shanxi Medical University, Taiyuan, China, [2]Department of Endocrine, The Second Hospital of Shanxi Medical University, Taiyuan, China

Cancer-induced bone pain (CIBP) has a considerable impact on patients' quality of life as well as physical and mental health. At present, patients with CIBP are managed according to the three-step analgesic therapy algorithm proposed by the World Health Organization. Opioids are commonly used as the first-line treatment for moderate-to-severe cancer pain but are limited due to addiction, nausea, vomiting and other gastrointestinal side effects. Moreover, opioids have a limited analgesic effect in some patients. In order to optimize the management of CIBP, we must first identify the underlying mechanisms. In some patients, surgery, or surgery combined with radiotherapy or radiofrequency ablation is the first step in the management of CIBP. Various clinical studies have shown that anti-nerve growth factor (NGF) antibodies, bisphosphonates, or RANKL inhibitors can reduce the incidence and improve the management of cancer pain. Herein, we review the mechanisms of cancer pain and potential therapeutic strategies to provide insights for optimizing the management of CIBP.

KEYWORDS

cancer-induced bone pain, pain management, surgery, conservative therapy, traditional Chinese medicine

Introduction

The skeleton is one of the most common metastatic sites in patients with solid tumors such as breast cancer, prostate cancer, kidney cancer and lung cancer (1, 2). The incidence of bone metastasis is associated with considerable economic burden and profound impacts on both physical and mental health. Moreover, patients with bone metastases have

Abbreviations: CIBP, Cancer-induced bone pain; NGF, Nerve growth factor; SREs, Skeletal related events; VEGF, Vascular endothelial growth factor; IL-1, Interleukin-1; IL-6, Interleukin-6; IL-8, Interleukin-8; IL-11, Interleukin-11; TNF-α, Tumor necrosis factor-α; PTHrP, Parathyroid hormone related peptide; OPG, Osteoprotegerin; MCP-1, Monocyte chemoattractant protein-1; MIP-1a, Macrophage inflammatory protein-1a; ATP, Adenosine triphosphate; ETAR, Endothelin receptor; PG, Prostaglandin; TRPV1, Transient receptor potential channel, vanillin subfamily member 1; ASIC3, Acid sensing ion channel 3; P2X3, Purinergic receptor; PGE2, Prostaglandin E2; TME, Tumor microenvironment; CGRP, Calcitonin gene related peptide; IL-18, Interleukin 18; HDACs, Deacetylase; EGFR, Epidermal growth factor receptor; PAG, Periaqueductal gray matter; PVP, Percutaneous vertebroplasty; PKP, Percutaneous kyphoplasty.

significantly lower survival compared with patients without bone metastases (3). With the continuous progress being made in radiotherapy, chemotherapy and surgical treatment, survival time in patients with bone metastases has increased in recent years. However, cancer-induced bone pain (CIBP) is associated with reduced quality of life and negative effects on mental health. Management of CIBP is considered one of most important issues in the treatment of patients with bone metastases. Currently, the recommended strategy is the three-step analgesic therapy pathway proposed by the World Health Organization. Importantly, the effectiveness of this strategy is limited by multiple adverse effects including addiction, nausea, vomiting and other gastrointestinal reactions (4). In addition, some patients experience sub-optimal efficacy. Therefore, how to optimize the management of CIBP has become a hot topic in cancer research.

Mechanism of bone metastasis

Bone plays a number of complex roles in the body including but not limited to exercise, support and protection of vital organs. Various cells, such as osteoblasts, osteoclasts, adipocytes, and macrophages maintain homeostasis and ensure the basic function of bone (1). Under physiological conditions, the rate of bone resorption and bone formation is finely balanced through the complex interactions between various hormones and cytokines secreted by different types of cell. Menopause and senescence can break balance of bone homeostasis, leading to a series of skeletal related events (SREs). The number of patients experiencing SREs has increased in recent years due to prolonged survival in patients with cancer, in particular breast cancer, lung cancer, prostate cancer, kidney cancer and thyroid cancer (5). Once bone metastasis occurs, tumor cells change the balance of bone absorption and bone reconstruction leading to the formation of metastatic tumors (6). The most likely sites for bone metastasis are regions with a highly active bone marrow microenvironment that promotes cell growth, such as vertebrae (87%), ribs (77%), pelvis (63%), and proximal humerus and femur (3). Bone metastases can be divided into osteolytic lesions, osteogenic lesions, or mixed lesions. However, regardless of the type of lesion, osteoclasts and osteoblasts are both active participants (7).

Stephen Paget proposed the hypothesis of "seed and soil" to explain how bone remodeling induces tumor re-implantation and development during bone metastasis. Metastasis from a primary tumor site is a multi-step and multifactorial process, including primary site erosion, breakthrough of basement membrane, escape of nesting apoptosis, and adhesion, colonization and invasion in distant organs (showed in Figure 1). Once in the bone, tumor cells promote the secretion of various cytokines such as RANKL, Vascular endothelial growth factor (VEGF), Interleukin-1 (IL-1), Interleukin-6 (IL-6), Interleukin-8 (IL-8), Interleukin-11 (IL-11) and Tumor necrosis factor-α (TNF-α) directly or indirectly, which induces the formation and maturation of osteoclasts resulting in massive bone absorption, which provides favorable conditions for tumor cell colonization (8). In fact, different tumors have different ways to change the balance of local bone metabolism. For example, breast cancer cells secrete parathyroid hormone related peptide (PTHrP) to activate osteoblasts to secrete RANKL and inhibit the expression of osteoprotegerin(OPG), which ultimately leads to increased osteoclast activity and the occurrence of bone

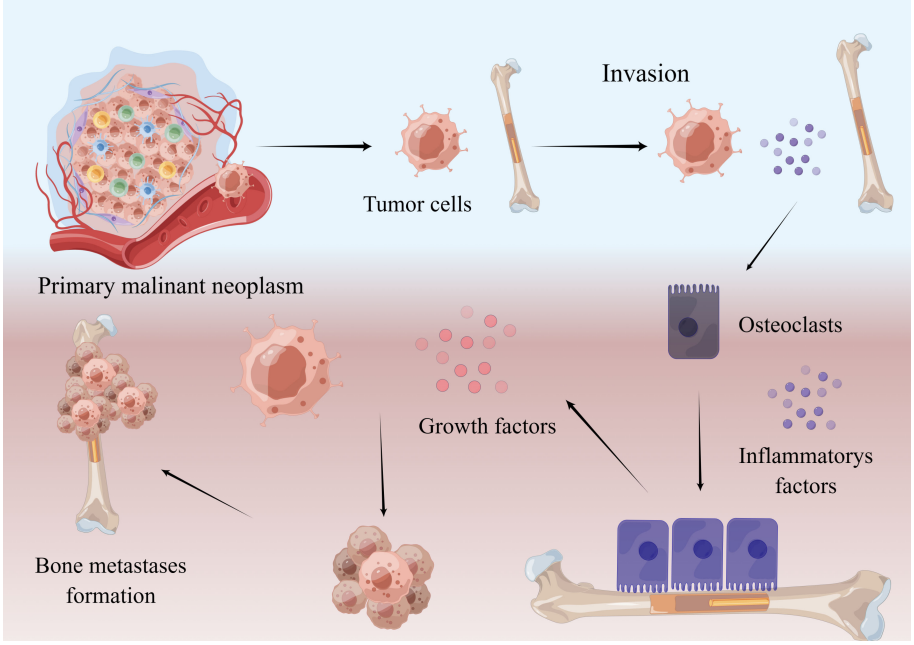

FIGURE 1
Mechanism of bone metastasis. Malignant neoplasm cells break away from the primary focus and enter the bone. By interacting with other cells, tumor cells secrete RANKL and some inflammatory factors, which promote the maturation of osteoclasts. Osteoclasts absorb bone and release growth factors in bone, which promote tumor growth and bone metastases formation. This figure is designed by Figdraw.

metastasis (9). It is also worth noting that activation of bone absorption leads to the release of a large number of growth factors. As a result, these growth factors stimulate the growth of tumor cells, leading to positive feedback to promote tumor growth (10, 11).

Mechanism of CIBP

CIBP occurs at all stages of bone metastasis and becomes more difficult to control as the degree of tumor growth increases. Research shows that 64% of patients with bone metastasis suffered CIBP, and of those, 75–90% experience severe CIBP (12). CIBP includes background pain, spontaneous pain and occasional (induced) pain. Background pain, aggravated by disease progression, is a continuous dull pain that can usually be controlled by traditional analgesic strategies. Breakthrough cancer pain is extreme pain that is associated with an incidence of 40–81% (13). Breakthrough pain is intermittent, often occurs quickly, and lasts for a short time. Opioids do not adequately control spontaneous pain, and subsequent overuse may be associated with side effects such as nausea, vomiting and respiratory depression (14).

The underlying mechanisms of CIBP may involve inflammatory, ischemic, compressive or injurious neuropathological processes (15) (showed in Figure 2). We know that there is a rich distribution of sensory nerves in bone, and most of the nerve fibers are distributed in the periosteum, A-delta and peptic C fibers (TrkA+). There are fewer nerve fibers distributed in the bone marrow and the bone cortex. Once tumor cells coloize bone, they recruit and activate osteoclasts and osteoblasts. Combined with highly active bone resorption and bone formation, bone metastases grow and proliferate. During this process, the imbalance of bone homeostasis induced by tumor cells leads to the occurrence of micro fractures. Micro fractures activate nociceptors, which leads to pain. The malignant growth of tumor tissue is associated with compression, which can also stimulate nociceptive sensory neurons (16). Additionally, with malignant growth of bone metastasis, various immune cells are recruited into the tumor including macrophages, T cells, and NK cells. Massive inflammatory factors or mediators, including prostaglandin E2 (PGE2), Nerve growth factor (NGF), bradykinin and proinflammatory cytokines (TNF-α, IL-1β, IL-6, IL-8, IL-15), chemokines (CCL5), monocyte chemoattractant protein-1 (MCP-1), macrophage inflammatory protein-1a (MIP-1a), and extracellular adenosine triphosphate (ATP), are secreted by various immune cells following interaction with tumor cells. Research shows that inflammatory factors can directly activate receptors located in sensory nerve fibers, including the endothelin receptor (ETAR), prostaglandin (PG) receptor, TrkA receptor, bradykinin receptor, cytokine receptor, chemokine receptor, transient receptor potential channel, vanillin subfamily member 1(TRPV1), acid sensing ion channel 3 (ASIC3) and purinergic receptor (P2X3), resulting in CIBP (17).

Tumor cells also induce nerve sprouting and promote the growth of sensory nerves and sympathetic nerves into tumor tissue, resulting in CIBP. NGF is an essential neurotrophic factor that induces the growth of sensory and sympathetic nerves, which is highly expressed in tumor cells and various immune cells in the tumor microenvironment (TME). NGF is commonly identified in

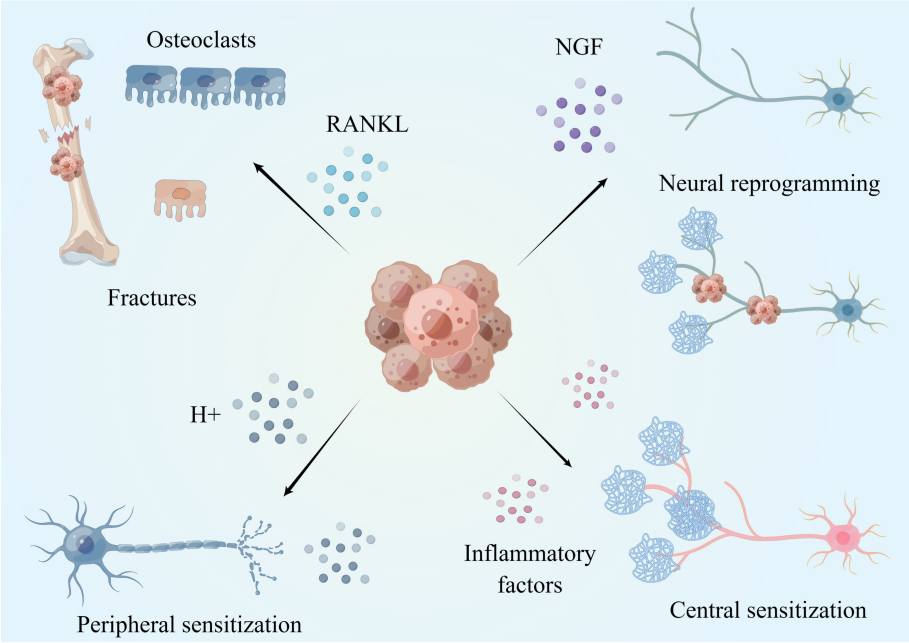

FIGURE 2
Mechanism of CIBP. Tumor can promote osteoclast maturation and bone resorption by secreting a large amount of RANKL, leading to micro-fracture and pain occurrence. The acidic microenvironment formed by tumor cells can induce peripheral nerve sensitization and promote the occurrence of cancer pain. Tumors induce nerve reprogramming and cancer pain by secreting NGF. Long-term peripheral stimulation and inflammatory factors cause changes in neurons, central sensitization and pain. This figure is designed by Figdraw.

prostate cancer, gastric cancer, and breast cancer (18, 19). Recently, a study showed that high expression of NGF is closely related to CIBP (20). Exogenous NGF application, overexpression of NGF, and inhibition of NGF degradation can induce mechanical pain and thermal hyperalgesia in animal models of pain. Inhibition of NGF and its receptors can significantly inhibit the development of tumors and related spontaneous and induced pain behaviors (21–25). It also has been shown that NGF can activate nociceptors and ion channels (such as P2X3, TRPV1, ASIC-3) by up-regulating the expression of a variety of proteins such as substance P, calcitonin gene related peptide (CGRP), and bradykinin, resulting in CIBP (17). More importantly, NGF can induce neural remodeling. In normal tissues, the sensory and sympathetic nerves are separated. However, tumor cells induce and drive the generation and growth of axons and nerves by secreting high levels of NGF. As a result, by increasing the density of nerve fibers, NGF also stimulates sensory nerve fibers and sympathetic nerve fibers to produce connections and form a neuroma-like structure in the tumor, known as Neural reprogramming (26). It is clear that the formation of neuroma-like structures in tumor tissues is closely related to CIBP (27–29). In the prostate bone metastatic tumor model, multiple nerve fibers were observed, mixing with prostate cancer cells and related stromal cells, to form a beaded neuroma-like structure (30). Anti-NGF treatment significantly reduced the density of nerve fibers, the formation of neuroma-like structures, the frequency of CIBP, and the generation of tumor-induced nociceptive behavior. It has been reported that anti-NFG treatment can also reduce bone damage caused by sarcoma (31, 32). In addition to NGF, tumors also secrete other neurotrophic substances such as brain derived neurotrophic factor (BDNF), which is closely related to cancer pain (33–35).

In addition to directly activating peripheral nociceptors, the low pH and hyperinflammatory state of the TME will lead to the remodeling of nociceptors in tumor tissue. Long-term stimulation with H+ ions and sustained inflammatory factors continuously activates nociceptors, leading to increased sensitivity of nociceptive neurons and amplification of their afferent nerve signals, which called as peripheral sensitization. Once peripheral sensitization occurs, as a result, even if the stimulation is not enough to trigger nociceptive signal transduction, this can still result in pain signal transduction in patients with cancer (36). Continuous activation of peripheral nociceptors can also lead to central sensitization.

The complex microenvironment in tumor tissue is associated with long-term and high-intensity activation of peripheral high-density nociceptors and induce changes in the central nervous system through a variety of mechanisms, which is manifested in the increased responsiveness to peripheral stimuli, thus generating central sensitization(Central sensitization refers to the abnormal increase of excitability or enhancement of synaptic transmission of pain-related neurons in the spinal cord and above, including the increase of spontaneous discharge activity of neurons, the expansion of sensory domain, the reduction of threshold to external stimuli, the enhancement of response to suprathreshold stimuli and other pathological changes, thus amplifying the transmission of pain signals. Its corresponding clinical manifestations include spontaneous pain, hyperalgesia and allodynia.) and inducing cancer pain. Studies have shown that under stimulation by tumor tissue, glial cells in the spinal cord are activated, especially spinal microglia and astrocytes. The overactive state of spinal microglia and astrocytes is one of the key factors that activates central sensitization and leads to CIBP (2, 37–40). Glial cells also promote CIBP by secreting interleukin 1 (IL-1) and interleukin 18 (IL-18) (41, 42). Multiple targets and signal pathways in spinal cord glial cells, such as protein deacetylase (HDACs) (39), epidermal growth factor receptor (EGFR) and MCP-1 (43), have been shown to be involved in the formation of CIBP through central sensitization. Glial cells located near the periaqueductal gray matter (PAG) of the midbrain are also activated in tumor-bearing mice, and a several cytokines such as IL-1 and IL-6 are secreted to activate the PI3K-AKT pathway in PAG, leading to central sensitization and cancer pain. Blocking this signal pathway can reduce mechanical and thermal hyperalgesia in rats with bone cancer (44).

It is estimated that 20–85% of patients who receive neurotoxic chemotherapy will experience peripheral neuropathy (15, 45–47). The usage of platinum-based antineoplastic agents, vinca alkaloids, epothilones (ixabepilone), taxanes, proteasome inhibitors (bortezomib) and immunomodulatory drugs (thalidomide) often results in the development of peripheral neuropathy, which may be accompanied by changes in motor and autonomic nerve function (48). The mechanism of peripheral neuropathy may involve mitochondrial dysfunction and oxidative stress, the release of inflammatory mediators (cytokines and chemical factors), ion channel dysfunction and intracellular signal transduction. However, the mechanisms remain to be fully elucidated (49).

Overall, the mechanisms underlying the occurrence and deterioration of CIBP are complex and involve tumor implantation, bone metabolism, enhancement of mechanical stimulation, activation and alteration of peripheral nerves, peripheral nerve remodeling, and activation/adaptive changes in the central nervous system. It will be vital to understand these mechanisms to facilitate the optimal management of CIBP in practice.

Pain management of bone metastases

Management of CIBP in patients with bone metastasis is an important issue, and the strategy of analgesia accompanies the life of patients, which is involved the three-ladder model of analgesia proposed by the World Health Organization

Nonopioids, such as nonsteroidal anti-inflammatory drugs (NSAIDs) are often the first-line therapy for CIBP. They are effective against mild-to-moderate pain; however, there is little evidence for the effectiveness of NSAIDs in patients with CIBP (50). While NSAIDs may inhibit cancer-related pain in some patients, they are unlikely to provide gain additional benefits in patients with moderate-to-severe CIBP who have already been treated with strong opioids. Furthermore, the long-term use of NSAIDs has been associated with cardiovascular and gastrointestinal risks (51). Some studies have shown that NSAIDs may have limited anti-tumor effects; however, there is a lack of robust clinical data to support these conclusions (52).

Weak opioids, such as tramadol and codeine, are not commonly used to manage CIBP because there is limited evidence for their effectiveness. Low-dose morphine is associated with more rapid and effective analgesic effects than opioids (53, 54).

For severe CIBP, strong oral and percutaneous opioids are the first choice for patients. Studies have shown that buprenorphine, oxycodone, fentanyl and morphine have similar analgesic effects and gradually achieve complete analgesia with adequate drug supply. Morphine is the first-line treatment for breakthrough pain and is associated with effective pain control (55). However, research shows that prolonged use of strong opioids is associated with side effects such as nausea, lethargy, vomiting and constipation (56). Detrimental effects of opioids on the liver and kidney compound the side effect of opioids. Epidural intrathecal injection of opioids can significantly relieve cancer pain; however, this type of pain management requires administration by healthcare professional and may be expensive.

Methadone is an effective substitute for morphine, oxycodone, fentanyl and other opioid drugs, which shows incomplete cross tolerance with other opioid receptors. However, due to significant inter-individual differences in the plasma half-life of methadone, it should be used only under the supervision of professional doctors. Although morphine and methadone show similar analgesic effects after single dose administration, it is recommended to reduce the anodynia dose by one quarter to one twelfth when switching from another opioid to methadone to prevent side effects such as respiratory depression (57).

Surgery

In patients with a long-life expectancy and no important organ metastasis, surgical resection is the first choice for patients with bone metastases with only one site metastasis.

For other metastatic spine tumors, patients with unstable spine, spinal cord compression or nerve function injury, tumor resection and reconstruction surgery are also should be chose firstly, for reducing compression on the spinal cord, which can relieve local pain by improving neural function (58). Various scoring systems such as the revised Tokuhashi scoring system and Tomita scoring system indicate estimated prognosis and appropriate treatment strategies in different patients (59). The evaluation indicators of these systems include patients' general condition, the number of bone metastases outside the spine, the number of vertebral bodies involved, and whether the metastases in key organs are resectable. Based on these comprehensive scoring systems, surgeons can predict each patient's survival period and determine the optimal treatment method. In fact, timely surgical intervention can fully relieve CIBP. Encouragingly, scoring systems are constantly improving. There is also the possibility that algorithms could be developed for specific tumor types to further improve the accuracy of scoring. VEGF, EGFR and other molecular markers in tumor tissue can also be included in scoring systems to provide more accurate estimations of survival time and therapeutic effect (60, 61).

Spinal separation surgery is an option for patients with bone metastases who cannot tolerate total spine resection. After surgery, radiotherapy should be administered for maximum anti-tumor effects (62). For patients with bone metastasis without spinal cord compression and spinal instability, minimally invasive spinal surgery (Percutaneous vertebroplasty, PVP or Percutaneous kyphoplasty, PKP) may be considered. The heat released by bone cement during surgery can kill local nerves and tumor tissue and effectively relieve the pain associated with thoracolumbar metastatic tumors. Post-operative adjuvant radiotherapy can also be effective in these patients (63, 64).

For long-bone metastasis, the Mirels predictive score is widely used in clinical practice (65). Based on this score, the optimal treatment strategy is identified according to metastasis location, the severity of pain, X-ray findings, and the invasion rate of lesions. In keeping with the tumor-free principle, biological reconstruction is the main goal of this surgery and pain can be significantly relieved using this method (66). Three-dimensional printing technology may be a new choice for reconstruction after resection. It can be used to print complex structures that are difficult to fabricate using traditional processes and overcome the problems of stress shielding and low biological activity of conventional prostheses (67).

For pelvis metastasis, there is no widely recognized scoring system. Because the pelvic anatomy is complex and adjacent to important organs and blood vessels, the resection and reconstruction of pelvic metastasis must be performed by experienced surgeons. While this surgery can help to relieve CIBP, the effects of such a complex surgery can be associated with additional pain.

Radiotherapy

Radiotherapy is a safe and effective strategy to relieve CIBP who are not suitable or cannot tolerate surgical treatment. Radiotherapy can significantly relieve CIBP. Studies have shown that 60% of patients with bone metastases experience significant pain relief after radiotherapy. Intraoperative radiotherapy is associated with particularly effective control of pain; however, it is worth noting that radiotherapy may lead to the occurrence of fracture or nerve injury in the spinal cord (68). Compared with ordinary radiotherapy, stereotactic body radiotherapy (SBRT) can deliver high-dose radiation to tumors while protecting adjacent normal tissues. Research shows that the local control rate of SBRT can reach 90%, and the probability of vertebral fracture and nerve injury after radiotherapy can be significantly reduced (69, 70). Evidence shows that more than 80% of patients can achieve significant remission of CIBP in a few days. Importantly, the safety of spinal SBRT depends on the tolerance of adjacent organs, especially the spinal cord. On the premise of ensuring the safety of the spinal cord, the radiation dose can be appropriately increased to avoid recurrence at the outer edge of the tumor target area. In clinical application, the strategy that radiotherapy combined with other therapies is common in manage CIBP in bone metastasis. Compared with radiotherapy alone, those strategy has a higher pain relief rate (71, 72).

Radiofrequency ablation

Radiofrequency ablation (RFA) includes microwave ablation and low-temperature ablation. RFA can be combined with radiotherapy and surgery. Research shows that RFA is associated with effective local pain control in around 64–77% of cases, which can relieve 70–100% of the pain related to bone metastases. After RFA treatment, PVP or PKP can prevent fracture and stabilize the surgical effect (73). However, the application of RFA must be carefully considered particularly in cases where structures such as the spinal cord, main nerves and blood vessels are within 1 cm of the tumor.

Bone-targeted therapy

Bisphosphonates are pyrophosphate analogues that combine with hydroxyapatite on the bone surface, directly inhibiting the attachment, differentiation and maturation of osteoclasts, which reduces the rate of bone absorption. Bisphosphonates have become the standard of care for bone metastases and have been shown to reduce the incidence of hypercalcemia and the rate of SREs. Studies have shown that regardless of whether radiotherapy and chemotherapy are combined, bisphosphonate treatment reduces the occurrence of CIBP (74). However, it is worth noting that bisphosphonates do not have a significant inhibitory effect on acute pain.

The RANKL/RANK signal pathway is a central to the regulation of osteoclast differentiation and activation. RANKL activates RANK binding on the surface of osteoclast precursor cells, and promotes osteoclast maturation. Denosumab, the most widely used RANKL inhibitor, prevents RANKL from combining with RANK, thus inhibiting the formation and activation of osteoclasts, result in reduced bone absorption and increased bone mass. Treatment with denosumab has been shown to inhibit tumor metastasis (75–77).

It is worth mentioning that many studies have found that compared with bisphosphonates, Denosumab have more advantages in reducing SREs and alleviating pain (76, 78, 79).

NGF inhibitor

Many humanized anti-NGF antibodies have shown encouraging results in clinical trials. Moreover, anti-NGF antibodies has a significant inhibitory effect on CIBP, especially neural cancer pain. Additionally, experiments in mice show that NGF antibody treatment reduces bone damage caused by tumors, delays fracture time, and prolongs the use of tumor-carrying limbs, although the underlying mechanisms of these effects are unknown (32). Both exercise and weight bearing can promote bone health. However, there are no studies on the ability of NGF to promote the recovery of patients' motor function. Once bone metastases are diagnosed, some patients decline surgery since the chance of removing all tumor cells is very slim. As a result, NSAIDs and weak opioids are commonly used as first-line treatment according to the principles of three steps of cancer medication. After cancer pain develops to a certain extent, strong opioids are often used to control the pain. Since the growth of nerves and the formation of peripheral sensitization may be implicated in the early stages of bone metastasis formation, there is limited potential for successful treatment with anti-NGF therapy. At present, we could not identify any studies evaluating the effectiveness of anti-NGF therapy for the prevention of CIBP.

Anticonvulsants and antidepressants

Neuropathic pain is an important component of CIBP. Therefore, in recent years, pregabalin has been increasingly used in the treatment of CIBP and is particularly effective especially for medium- and short-term CIBP (80, 81). The efficacy of gabapentin in the treatment of CIBP is limited.

Antidepressants including amitriptyline and duloxetine can also be used for the treatment of neuropathic pain. Data show that both of these drugs can help to improve quality of life in patients with CIBP (12).

Traditional Chinese medicine

Traditional Chinese medicine can be used to treat pain, including CIBP. The advantages of traditional Chinese medicine include rich dosage forms, light toxicity and side effects, and improved tolerability compared with more established methods. For these reasons, it has gained traction as a treatment option for patients with CIBP. Studies have shown that astragalus, psoralen, scutellaria barbata, atractylodes macrocephala, and corydalis can significantly inhibit CIBP in patients with cancer (82–85). Insect drugs, such as scorpion and Huchansu have also been shown to be effective for the management of CIBP (86–88).

Acupuncture is effective for alleviating pain and can help to reduce the need for opioids (89). Electrical stimulation with acupuncture combined with opioids has potential to reduce the side effects associated with opioids and improve quality of life in patients with CIBP (90–92). Research shows that acupuncture activates sympathetic nerve fibers to increase endogenous opioids at inflammatory sites to inhibit pain. Various inflammatory factors such as β- Endorphin and 5-HT are implicated in the relief of pain through acupuncture, both at the peripheral and central level (93). Injection of acupoints can also reduce the frequency of cancer pain (94).

Although the mechanisms of treating cancer pain with traditional Chinese medicine are not yet fully elucidated, it is clear that this form of medicine has unique advantages for treating cancer pain compared with more commonly used

methods. Going forward, it will be important to understand the mechanisms by which Chinese medicine is able to reduce CIBP, and to standardize usage and dosage to allow more widespread use.

Other therapy

Injection of a TNF-α antagonist can partly block the mechanical hyperalgesia in oral cancer (95, 96). In addition, recent studies show that the application of some immune agents, such as anti-PD-L1 monoclonal antibodies, Sting inhibitors, and *in vitro* immune cell adoptive therapy can also relieve the pain caused by primary tumors and bone metastases (97–100).

Conclusions

The management of CIBP is a complex issue for patients and physicians. Active pain management, such as early surgical intervention for eligible patients. Radiotherapy and microwave therapy can be combined with surgical intervention to obtain a higher pain relief rate and promote the patient to recover the patient's nerve and activity function as soon as possible. Early intervention with RANKL inhibitors, bisphosphonates or anti-NGF antibodies in patients who are not candidates for surgery may improve quality of life. Traditional Chinese medicine and acupuncture also have the potential to become important options for CIBP management. Overall, there is no single solution for managing CIBP in all patients. Only by fully elucidating the underlying mechanisms of cancer pain will it be possible to optimize the management of CIBP in real-world practice.

Author contributions

DJ and ZQ conceived the manuscript and drafted the manuscript. YBZ and XDL contributed to data collection. YF, BZ, and XFZ reviewed the manuscript. All authors contributed to the article and approved the submitted version.

Conflict of interest

The authors declare that the research was conducted in the absence of any commercial or financial relationships that could be construed as a potential conflict of interest.

Publisher's note

References

1. Fornetti J, Welm AL, Stewart SA. Understanding the bone in cancer metastasis. *J Bone Miner Res* (2018) 33:2099–113. doi: 10.1002/jbmr.3618

2. Chen SP, Sun J, Zhou YQ, Cao F, Braun C, Luo F, et al. Sinomenine attenuates cancer-induced bone pain *via* suppressing microglial JAK2/STAT3 and neuronal CAMKII/CREB cascades in rat models. *Mol Pain* (2018) 14:1744806918793232. doi: 10.1177/1744806918793232

3. Coleman RE, Croucher PI, Padhani AR, Clezardin P, Chow E, Fallon M, et al. Bone metastases. *Nat Rev Dis Primers* (2020) 6:83. doi: 10.1038/s41572-020-00216-3

4. Zajaczkowska R, Kocot-Kepska M, Leppert W, Wordliczek J. Bone pain in cancer patients: Mechanisms and current treatment. *Int J Mol Sci* (2019) 20(23):6047. doi: 10.3390/ijms20236047

5. Li B, Wang P, Jiao J, Wei H, Xu W, Zhou P. Roles of the RANKL-RANK axis in immunity-implications for pathogenesis and treatment of bone metastasis. *Front Immunol* (2022) 13:824117. doi: 10.3389/fimmu.2022.824117

6. Clezardin P, Coleman R, Puppo M, Ottewell P, Bonnelye E, Paycha F, et al. Bone metastasis: mechanisms, therapies, and biomarkers. *Physiol Rev* (2021) 101:797–855. doi: 10.1152/physrev.00012.2019

7. Yang M, Liu C, Yu X. Skeletal-related adverse events during bone metastasis of breast cancer: current status. *Discov Med* (2019) 27:211–20.

8. Gdowski AS, Ranjan A, Vishwanatha JK. Current concepts in bone metastasis, contemporary therapeutic strategies and ongoing clinical trials. *J Exp Clin Cancer Res* (2017) 36:108. doi: 10.1186/s13046-017-0578-1

9. Othman A, Winogradzki M, Lee L, Tandon M, Blank A, Pratap J. Bone metastatic breast cancer: Advances in cell signaling and autophagy related mechanisms. *Cancers (Basel)* (2021) 13(17):4310. doi: 10.3390/cancers13174310

10. Norregaard KS, Jurgensen HJ, Gardsvoll H, Engelholm LH, Behrendt N, Soe K. Osteosarcoma and metastasis associated bone degradation-a tale of osteoclast and malignant cell cooperativity. *Int J Mol Sci* (2021) 22(13):6865. doi: 10.3390/ijms22136865

11. Hiraga T. Bone metastasis: Interaction between cancer cells and bone microenvironment. *J Oral Biosci* (2019) 61:95–8. doi: 10.1016/j.job.2019.02.002

12. Scarborough BM, Smith CB. Optimal pain management for patients with cancer in the modern era. *CA Cancer J Clin* (2018) 68:182–96. doi: 10.3322/caac.21453

13. Lohre ET, Thronaes M, Klepstad P. Breakthrough cancer pain in 2020. *Curr Opin Support Palliat Care* (2020) 14:94–9. doi: 10.1097/SPC.0000000000000494

14. Davies AN. Breakthrough cancer pain. *Curr Pain Headache Rep* (2014) 18:420. doi: 10.1007/s11916-014-0420-9

15. Feller L, Khammissa RAG, Bouckaert M, Ballyram R, Jadwat Y, Lemmer J. Pain: Persistent postsurgery and bone cancer-related pain. *J Int Med Res* (2019) 47:528–43. doi: 10.1177/0300060518818296

16. Bortolin A, Neto E, Lamghari M. Calcium signalling in breast cancer associated bone pain. *Int J Mol Sci* (2022) 23(3):1902. doi: 10.3390/ijms23031902

17. Hirose M, Kuroda Y, Murata E. NGF/TrkA signaling as a therapeutic target for pain. *Pain Pract* (2016) 16:175–82. doi: 10.1111/papr.12342

18. Pundavela J, Roselli S, Faulkner S, Attia J, Scott RJ, Thorne RF, et al. Nerve fibers infiltrate the tumor microenvironment and are associated with nerve growth factor production and lymph node invasion in breast cancer. *Mol Oncol* (2015) 9:1626–35. doi: 10.1016/j.molonc.2015.05.001

19. Griffin N, Faulkner S, Jobling P, Hondermarck H. Targeting neurotrophin signaling in cancer: The renaissance. *Pharmacol Res* (2018) 135:12–7. doi: 10.1016/j.phrs.2018.07.019

20. Yoneda T, Hiasa M, Okui T, Hata K. Sensory nerves: A driver of the vicious cycle in bone metastasis? *J Bone Oncol* (2021) 30:100387. doi: 10.1016/j.jbo.2021.100387

21. Slatkin N, Zaki N, Wang S, Louie J, Sanga P, Kelly KM, et al. Fulranumab as adjunctive therapy for cancer-related pain: A phase 2, randomized, double-blind, placebo-controlled, multicenter study. *J Pain* (2019) 20:440–52. doi: 10.1016/j.jpain.2018.09.014

22. Kumar V, Mahal BA. NGF - the TrkA to successful pain treatment. *J Pain Res* (2012) 5:279–87. doi: 10.2147/JPR.S33408

23. Bimonte S, Cascella M, Forte CA, Esposito G, Cuomo A. The role of anti-nerve growth factor monoclonal antibodies in the control of chronic cancer and non-cancer pain. *J Pain Res* (2021) 14:1959–67. doi: 10.2147/JPR.S302004

24. Han L, Jiang J, Xue M, Qin T, Xiao Y, Wu E, et al. Sonic hedgehog signaling pathway promotes pancreatic cancer pain *via* nerve growth factor. *Reg Anesth Pain Med* (2020) 45:137–44. doi: 10.1136/rapm-2019-100991

25. Guedon JG, Longo G, Majuta LA, Thomspon ML, Fealk MN, Mantyh PW. Dissociation between the relief of skeletal pain behaviors and skin hypersensitivity in a model of bone cancer pain. *Pain* (2016) 157:1239–47. doi: 10.1097/j.pain.0000000000000514

26. Buehlmann D, Ielacqua GD, Xandry J, Rudin M. Prospective administration of anti-nerve growth factor treatment effectively suppresses functional connectivity alterations after cancer-induced bone pain in mice. *Pain* (2019) 160:151–9. doi: 10.1097/j.pain.0000000000001388

27. Lucchesi M, Lanzetta G, Antonuzzo A, Rozzi A, Sardi I, Favre C, et al. Developing drugs in cancer-related bone pain. *Crit Rev Oncol Hematol* (2017) 119:66–74. doi: 10.1016/j.critrevonc.2017.08.005

28. Park SH, Eber MR, Fonseca MM, Patel CM, Cunnane KA, Ding H, et al. Usefulness of the measurement of neurite outgrowth of primary sensory neurons to study cancer-related painful complications. *Biochem Pharmacol* (2021) 188:114520. doi: 10.1016/j.bcp.2021.114520

29. Silverman DA, Martinez VK, Dougherty PM, Myers JN, Calin GA, Amit M. Cancer-associated neurogenesis and nerve-cancer cross-talk. *Cancer Res* (2021) 81:1431–40. doi: 10.1158/0008-5472.CAN-20-2793

30. Jimenez-Andrade JM, Ghilardi JR, Castaneda-Corral G, Kuskowski MA, Mantyh PW. Preventive or late administration of anti-NGF therapy attenuates tumor-induced nerve sprouting, neuroma formation, and cancer pain. *Pain* (2011) 152:2564–74. doi: 10.1016/j.pain.2011.07.020

31. Bloom AP, Jimenez-Andrade JM, Taylor RN, Castaneda-Corral G, Kaczmarska MJ, Freeman KT, et al. Breast cancer-induced bone remodeling, skeletal pain, and sprouting of sensory nerve fibers. *J Pain* (2011) 12:698–711. doi: 10.1016/j.jpain.2010.12.016

32. McCaffrey G, Thompson ML, Majuta L, Fealk MN, Chartier S, Longo G, et al. NGF blockade at early times during bone cancer development attenuates bone destruction and increases limb use. *Cancer Res* (2014) 74:7014–23. doi: 10.1158/0008-5472.CAN-14-1220

33. Ostrow KL, Donaldson KJ, Caterina MJ, Belzberg A, Hoke A. The secretomes of painful versus nonpainful human schwannomatosis tumor cells differentially influence sensory neuron gene expression and sensitivity. *Sci Rep* (2019) 9:13098. doi: 10.1038/s41598-019-49705-w

34. Grayson M, Arris D, Wu P, Merlo J, Ibrahim T, Fang-Mei C, et al. Oral squamous cell carcinoma-released brain-derived neurotrophic factor contributes to oral cancer pain by peripheral tropomyosin receptor kinase b activation. *Pain* (2022) 163:496–507. doi: 10.1097/j.pain.0000000000002382

35. Zhang Y, Lin C, Wang X, Ji T. Calcitonin gene-related peptide: A promising bridge between cancer development and cancer-associated pain in oral squamous cell carcinoma. *Oncol Lett* (2020) 20:253. doi: 10.3892/ol.2020.12116

36. Duitama M, Moreno Y, Santander SP, Casas Z, Sutachan JJ, Torres YP, et al. TRP channels as molecular targets to relieve cancer pain. *Biomolecules* (2021) 12(1):1. doi: 10.3390/biom12010001

37. Chen YL, Feng XL, Cheung CW, Liu JA. Mode of action of astrocytes in pain: From the spinal cord to the brain. *Prog Neurobiol* (2022) 219:102365. doi: 10.1016/j.pneurobio.2022.102365

38. Midavaine E, Cote J, Marchand S, Sarret P. Glial and neuroimmune cell choreography in sexually dimorphic pain signaling. *Neurosci Biobehav Rev* (2021) 125:168–92. doi: 10.1016/j.neubiorev.2021.01.023

39. He XT, Hu XF, Zhu C, Zhou KX, Zhao WJ, Zhang C, et al. Suppression of histone deacetylases by SAHA relieves bone cancer pain in rats *via* inhibiting activation of glial cells in spinal dorsal horn and dorsal root ganglia. *J Neuroinflamm* (2020) 17:125. doi: 10.1186/s12974-020-01740-5

40. Meng W, Hao MM, Yu N, Li MY, Ding JQ, Wang BH, et al. 2-bromopalmitate attenuates bone cancer pain *via* reversing mitochondrial fusion and fission imbalance in spinal astrocytes. *Mol Pain* (2019) 15:1744806919871813. doi: 10.1177/1744806919871813

41. Huo W, Zhang Y, Liu Y, Lei Y, Sun R, Zhang W, et al. Dehydrocorydaline attenuates bone cancer pain by shifting microglial M1/M2 polarization toward the M2 phenotype. *Mol Pain* (2018) 14:1744806918781733. doi: 10.1177/1744806918781733

42. Liu S, Liu YP, Lv Y, Yao JL, Yue DM, Zhang MY, et al. IL-18 contributes to bone cancer pain by regulating glia cells and neuron interaction. *J Pain* (2018) 19:186–95. doi: 10.1016/j.jpain.2017.10.003

43. Zheng XQ, Wu YH, Huang JF, Wu AM. Neurophysiological mechanisms of cancer-induced bone pain. *J Adv Res* (2022) 35:117–27. doi: 10.1016/j.jare.2021.06.006

44. Li Y, Bao Y, Zheng H, Qin Y, Hua B. The nonreceptor protein tyrosine kinase src participates in every step of cancer-induced bone pain. *BioMed Pharmacother* (2021) 141:111822. doi: 10.1016/j.biopha.2021.111822

45. Velasco R, Navarro X, Gil-Gil M, Herrando-Grabulosa M, Calls A, Bruna J. Neuropathic pain and nerve growth factor in chemotherapy-induced peripheral neuropathy: Prospective clinical-pathological study. *J Pain Symptom Manage* (2017) 54:815–25. doi: 10.1016/j.jpainsymman.2017.04.021

46. Khasabova IA, Seybold VS, Simone DA. The role of PPARgamma in chemotherapy-evoked pain. *Neurosci Lett* (2021) 753:135845. doi: 10.1016/j.neulet.2021.135845

47. Sarezky J, Sachs G, Elinzano H, Stavros K. Cancer and peripheral nerve disease. *Clin Geriatr Med* (2021) 37:289–300. doi: 10.1016/j.cger.2021.01.003

48. Zajaczkowska R, Kocot-Kepska M, Leppert W, Wrzosek A, Mika J, Wordliczek J. Mechanisms of chemotherapy-induced peripheral neuropathy. *Int J Mol Sci 20* (2019) 20(6):1451. doi: 10.3390/ijms20061451

49. Shim HS, Bae C, Wang J, Lee KH, Hankerd KM, Kim HK, et al. Peripheral and central oxidative stress in chemotherapy-induced neuropathic pain. *Mol Pain* (2019) 15:1744806919840098. doi: 10.1177/1744806919840098

50. Strawson J. Nonsteroidal anti-inflammatory drugs and cancer pain. *Curr Opin Support Palliat Care* (2018) 12:102–7. doi: 10.1097/SPC.0000000000000332

51. Thiruchenthooran V, Sanchez-Lopez E, Gliszczynska A. Perspectives of the application of non-steroidal anti-inflammatory drugs in cancer therapy: Attempts to overcome their unfavorable side effects. *Cancers (Basel)* (2023) 15(2):475. doi: 10.3390/cancers15020475

52. Mercadante S, Casuccio A, Agnello A, Pumo S, Kargar J, Garofalo S. Analgesic effects of nonsteroidal anti-inflammatory drugs in cancer pain due to somatic or visceral mechanisms. *J Pain Symptom Manage* (1999) 17:351–6. doi: 10.1016/S0885-3924(98)00141-9

53. Chapman EJ, Edwards Z, Boland JW, Maddocks M, Fettes L, Malia C, et al. Practice review: Evidence-based and effective management of pain in patients with advanced cancer. *Palliat Med* (2020) 34:444–53. doi: 10.1177/0269216319896955

54. Wiffen PJ, Derry S, Moore RA. Tramadol with or without paracetamol (acetaminophen) for cancer pain. *Cochrane Database Syst Rev* (2017) 5:CD012508. doi: 10.1002/14651858.CD012508

55. Alarcon MDL, Estevez FV, Cabezon-Gutierrez L, Padros MC, Martin-Arroyo JMT, Rebollo MA, et al. Expert consensus on the management of breakthrough cancer pain in older patients. *A Delphi study. J Geriatr Oncol* (2019) 10:643–52. doi: 10.1016/j.jgo.2019.03.012

56. Nosek K, Leppert W, Nosek H, Wordliczek J, Onichimowski D. A comparison of oral controlled-release morphine and oxycodone with transdermal formulations of buprenorphine and fentanyl in the treatment of severe pain in cancer patients. *Drug Des Devel Ther* (2017) 11:2409–19. doi: 10.2147/DDDT.S141007

57. Fallon M, Giusti R, Aielli F, Hoskin P, Rolke R, Sharma M, et al. Management of cancer pain in adult patients: ESMO clinical practice guidelines. *Ann Oncol* (2018) 29:iv166–91. doi: 10.1093/annonc/mdy152

58. Stewart CL, Warner S, Ito K, Raoof M, Wu GX, Kessler J, et al. Cytoreduction for colorectal metastases: liver, lung, peritoneum, lymph nodes, bone, brain. when does it palliate, prolong survival, and potentially cure? *Curr Probl Surg* (2018) 55:330–79. doi: 10.1067/j.cpsurg.2018.08.004

59. Tokuhashi Y, Uei H, Oshima M. Classification and scoring systems for metastatic spine tumors: a literature review. *Spine Surg Relat Res* (2017) 1:44–55. doi: 10.22603/ssrr.1.2016-0021

60. Gregory TM, Coriat R, Mir O. Prognostic scoring systems for spinal metastases in the era of anti-VEGF therapies. *Spine (Phila Pa 1976)* (2013) 38:965–6. doi: 10.1097/BRS.0b013e3182609d38

61. Yang M, Xu W, Liu T, Yang X, Wang P, Wu S, et al. Development and validation of a novel survival prediction model in patients with spinal metastasis from non-small cell lung cancer. *Spine (Phila Pa 1976)* (2019) 44:246–57. doi: 10.1097/BRS.0000000000002816

62. Di Perna G, Cofano F, Mantovani C, Badellino S, Marengo N, Ajello M, et al. Separation surgery for metastatic epidural spinal cord compression: A qualitative review. *J Bone Oncol* (2020) 25:100320. doi: 10.1016/j.jbo.2020.100320

63. Pezeshki PS, Davidson S, Murphy K, McCann C, Slodkowska E, Sherar M, et al. Comparison of the effect of two different bone-targeted radiofrequency ablation (RFA) systems alone and in combination with percutaneous vertebroplasty (PVP) on the biomechanical stability of the metastatic spine. *Eur Spine J* (2016) 25:3990–6. doi: 10.1007/s00586-015-4057-0

64. Wu W, Zhang X, Li X, Liu H, Xu L, Liu T, et al. Comparison of the clinical outcomes of percutaneous kyphoplasty for the management of osteolytic and osteoblastic-related metastatic vertebral lesions. *J Neurointerv Surg* (2022) 14:938–41. doi: 10.1136/neurintsurg-2021-018007

65. Crenn V, Carlier C, Gouin F, Sailhan F, Bonnevialle Pmembers of the So.F.C.O.T. High rate of fracture in long-bone metastasis: Proposal for an improved mirels predictive score. *Orthop Traumatol Surg Res* (2020) 106:1005–11. doi: 10.1016/j.otsr.2020.03.034

66. Pu F, Zhang Z, Wang B, Liu J, Shao Z. En bloc resection and intercalary prosthesis implantation for the treatment of humeral diaphyseal bone metastases. *Int Orthop* (2021) 45:281–8. doi: 10.1007/s00264-020-04845-x

67. Pu F, Wu W, Jing D, Yu Y, Peng Y, Liu J, et al. Three-dimensional-printed titanium prostheses with bone trabeculae enable mechanical-biological reconstruction after resection of bone tumours. *Biomater Transl* (2022) 3:134–41. doi: 10.12336/biomatertransl.2022.02.005

68. Tsukamoto S, Kido A, Tanaka Y, Facchini G, Peta G, Rossi G, et al. Current overview of treatment for metastatic bone disease. *Curr Oncol* (2021) 28:3347–72. doi: 10.3390/curroncol28050290

69. De la Pinta C. SBRT in non-spine bone metastases: a literature review. *Med Oncol* (2020) 37:119. doi: 10.1007/s12032-020-01442-1

70. Zeng KL, Tseng CL, Soliman H, Weiss Y, Sahgal A, Myrehaug S. Stereotactic body radiotherapy (SBRT) for oligometastatic spine metastases: An overview. *Front Oncol* (2019) 9:337. doi: 10.3389/fonc.2019.00337

71. Yamada K, Kaise H, Taguchi T, Horiguchi J, Takao S, Suzuki M, et al. Strontium-89 plus zoledronic acid versus zoledronic acid for patients with painful bone metastatic breast cancer. *J Bone Miner Metab* (2022) 40:998–1006. doi: 10.1007/s00774-022-01366-y

72. Lu CW, Shao J, Wu YG, Wang C, Wu JH, Lv RX, et al. Which combination treatment is better for spinal metastasis: Percutaneous vertebroplasty with radiofrequency ablation, 125I seed, zoledronic acid, or radiotherapy? *Am J Ther* (2019) 26:e38–44. doi: 10.1097/MJT.0000000000000449

73. Yevich S, Chen S, Metwalli Z, Kuban J, Lee S, Habibollahi P, et al. Radiofrequency ablation of spine metastases: A clinical and technical approach. *Semin Musculoskelet Radiol* (2021) 25:795–804. doi: 10.1055/s-0041-1740351

74. He F, Matsumoto Y. Basic and clinical associations between bone and cancer. *Immunol Med* (2020) 43:103–6. doi: 10.1080/25785826.2020.1754084

75. Cleeland CS, Body JJ, Stopeck A, von Moos R, Fallowfield L, Mathias SD, et al. Pain outcomes in patients with advanced breast cancer and bone metastases: results from a randomized, double-blind study of denosumab and zoledronic acid. *Cancer-Am Cancer Soc* (2013) 119:832–8. doi: 10.1002/cncr.27789

76. Smith MR, Coleman RE, Klotz L, Pittman K, Milecki P, Ng S, et al. Denosumab for the prevention of skeletal complications in metastatic castration-resistant prostate cancer: comparison of skeletal-related events and symptomatic skeletal events. *Ann Oncol* (2015) 26:368–74. doi: 10.1093/annonc/mdu519

77. Dorff TB, Agarwal N. Bone-targeted therapies to reduce skeletal morbidity in prostate cancer. *Asian J Androl* (2018) 20:215–20. doi: 10.4103/aja.aja_12_18

78. Chen F, Pu F. Safety of denosumab versus zoledronic acid in patients with bone metastases: A meta-analysis of randomized controlled trials. *Oncol Res Treat* (2016) 39:453–9. doi: 10.1159/000447372

79. Zhang Z, Pu F, Shao Z. The skeletal-related events of denosumab versus zoledronic acid in patients with bone metastases: A meta-analysis of randomized controlled trials. *J Bone Oncol* (2017) 9:21–4. doi: 10.1016/j.jbo.2017.09.003

80. Gul SK, Tepetam H, Gul HL. Duloxetine and pregabalin in neuropathic pain of lung cancer patients. *Brain Behav* (2020) 10:e01527. doi: 10.1002/brb3.1527

81. Fallon MT. Neuropathic pain in cancer. *Br J Anaesth* (2013) 111:105–11. doi: 10.1093/bja/aet208

82. Su P, Leng Y, Liu J, Yu Y, Wang Z, Dang H. Comparative analysis of the efficacy and safety of different traditional Chinese medicine injections in the treatment of cancer-related pain: A Bayesian network meta-analysis. *Front Pharmacol* (2021) 12:803676. doi: 10.3389/fphar.2021.803676

83. Luo Y, Wang CZ, Sawadogo R, Tan T, Yuan CS. Effects of herbal medicines on pain management. *Am J Chin Med* (2020) 48:1–16. doi: 10.1142/S0192415X20500019

84. Perez AT, Arun B, Tripathy D, Tagliaferri MA, Shaw HS, Kimmick GG, et al. A phase 1B dose escalation trial of scutellaria barbata (BZL101) for patients with metastatic breast cancer. *Breast Cancer Res Treat* (2010) 120:111–8. doi: 10.1007/s10549-009-0678-5

85. Chen Y, Cheng CS, Tan HY, Tam CW, Wang N, Feng Y. Efficacy of herbal medicines intervention for colorectal cancer patients with chemotherapy-induced gastrointestinal toxicity - a systematic review and meta-analysis. *Front Oncol* (2021) 11:629132. doi: 10.3389/fonc.2021.629132

86. Richard SA, Kampo S, Sackey M, Hechavarria ME, Buunaaim ADB. The pivotal potentials of scorpion buthus martensii karsch-Analgesic-Antitumor peptide in pain management and cancer. *Evid Based Complement Alternat Med* (2020) 2020:4234273. doi: 10.1155/2020/4234273

87. Yu J, Luo Y, Jin H, Lv J, Zhou T, Yabasin IB, et al. Scorpion alleviates bone cancer pain through inhibition of bone destruction and glia activation. *Mol Pain* (2020) 16:1744806920909993. doi: 10.1177/1744806920909993

88. Xu J, Qian SS, Chen YG, Li DY, Yan Q. [Systematic review and meta-analysis of efficacy and safety of huachansu in treating cancer-related pain]. *Zhongguo Zhong Yao Za Zhi* (2019) 44:2627–36. doi: 10.19540/j.cnki.cjcmm.20190304.003

89. He Y, Guo X, May BH, Zhang AL, Liu Y, Lu C, et al. Clinical evidence for association of acupuncture and acupressure with improved cancer pain: A systematic review and meta-analysis. *JAMA Oncol* (2020) 6:271–8. doi: 10.1001/jamaoncol.2019.5233

90. Liang Y, Bao G, Gong L, Zhou J, Kong X, Ran R, et al. Evaluating the analgesic effect and advantage of transcutaneous electrical acupoint stimulation combined with opioid drugs for moderate to severe cancer-related pain: a study protocol for a randomized controlled trial. *Trials* (2019) 20:40. doi: 10.1186/s13063-018-3145-y

91. Dai L, Liu Y, Ji G, Xu Y. Acupuncture and derived therapies for pain in palliative cancer management: Systematic review and meta-analysis based on single-arm and controlled trials. *J Palliat Med* (2021) 24:1078–99. doi: 10.1089/jpm.2020.0405

92. He L, Tan K, Lin X, Yi H, Wang X, Zhang J, et al. Multicenter, randomized, double-blind, controlled trial of transcutaneous electrical nerve stimulation for pancreatic cancer related pain. *Med (Baltimore)* (2021) 100:e23748. doi: 10.1097/MD.0000000000023748

93. Zhang R, Lao L, Ren K, Berman BM. Mechanisms of acupuncture-electroacupuncture on persistent pain. *Anesthesiology* (2014) 120:482–503. doi: 10.1097/ALN.0000000000000101

94. Cheon S, Zhang X, Lee IS, Cho SH, Chae Y, Lee H. Pharmacopuncture for cancer care: a systematic review. *Evid Based Complement Alternat Med* (2014) 2014:804746. doi: 10.1155/2014/804746

95. Scheff NN, Ye Y, Bhattacharya A, MacRae J, Hickman DN, Sharma AK, et al. Tumor necrosis factor alpha secreted from oral squamous cell carcinoma contributes to cancer pain and associated inflammation. *Pain* (2017) 158:2396–409. doi: 10.1097/j.pain.0000000000001044

96. Salvo E, Tu NH, Scheff NN, Dubeykovskaya ZA, Chavan SA, Aouizerat BE, et al. TNFalpha promotes oral cancer growth, pain, and schwann cell activation. *Sci Rep* (2021) 11:1840. doi: 10.1038/s41598-021-81500-4

97. Wang K, Gu Y, Liao Y, Bang S, Donnelly CR, Chen O, et al. PD-1 blockade inhibits osteoclast formation and murine bone cancer pain. *J Clin Invest* (2020) 130:3603–20. doi: 10.1172/JCI133334

98. Wang K, Donnelly CR, Jiang C, Liao Y, Luo X, Tao X, et al. STING suppresses bone cancer pain *via* immune and neuronal modulation. *Nat Commun* (2021) 12:4558. doi: 10.1038/s41467-021-24867-2

99. Zhou X, Qiao G, Ren J, Wang X, Wang S, Zhu S, et al. Adoptive immunotherapy with autologous T-cell infusions reduces opioid requirements in advanced cancer patients. *Pain* (2020) 161:127–34. doi: 10.1097/j.pain.0000000000001702

100. Ji RR, Chamessian A, Zhang YQ. Pain regulation by non-neuronal cells and inflammation. *Science* (2016) 354:572–7. doi: 10.1126/science.aaf8924

frontiers | Frontiers in Oncology

TYPE Review
PUBLISHED 05 April 2023
DOI 10.3389/fonc.2023.1165380

OPEN ACCESS

EDITED BY
Wenwen Zhang,
Nanjing Medical University, China

REVIEWED BY
Qiuyu Liu,
Henan Provincial People's Hospital, China
Yanping Yang,
Shanghai University of Traditional Chinese Medicine, China

*CORRESPONDENCE
Fengxia Chen
fengxiachen@whu.edu.cn
Zengwu Shao
1985XH0536@hust.edu.cn
Zhicai Zhang
zhicaizhang@126.com

†These authors have contributed equally to this work

SPECIALTY SECTION
This article was submitted to Surgical Oncology, a section of the journal Frontiers in Oncology

RECEIVED 14 February 2023
ACCEPTED 10 March 2023
PUBLISHED 05 April 2023

CITATION
Yu Y, Li K, Peng Y, Wu W, Chen F, Shao Z and Zhang Z (2023) Animal models of cancer metastasis to the bone. *Front. Oncol.* 13:1165380. doi: 10.3389/fonc.2023.1165380

Animal models of cancer metastasis to the bone

Yihan Yu[1†], Kanglu Li[1†], Yizhong Peng[1†], Wei Wu[1], Fengxia Chen[2*], Zengwu Shao[1*] and Zhicai Zhang[1*]

[1]Department of Orthopedics, Union Hospital, Tongji Medical College, Huazhong University of Science and Technology, Wuhan, Hubei, China, [2]Department of Radiation and Medical Oncology, Zhongnan Hospital, Wuhan University, Wuhan, Hubei, China

Cancer metastasis is a major cause of mortality from several tumors, including those of the breast, prostate, and the thyroid gland. Since bone tissue is one of the most common sites of metastasis, the treatment of bone metastases is crucial for the cure of cancer. Hence, disease models must be developed to understand the process of bone metastasis in order to devise therapies for it. Several translational models of different bone metastatic tumors have been developed, including animal models, cell line injection models, bone implant models, and patient-derived xenograft models. However, a compendium on different bone metastatic cancers is currently not available. Here, we have compiled several animal models derived from current experiments on bone metastasis, mostly involving breast and prostate cancer, to improve the development of preclinical models and promote the treatment of bone metastasis.

KEYWORDS

bone metastases, animal models, breast cancer, prostate cancer, cell lines

1 Introduction

Metastasis is a frequent malignant manifestation of cancer in the mid to late stages of tumor progression. Metastasis to the bone, one of the most common sites, occurs when cancer cells migrate from the original site and invade bone tissue. It indicates adverse prognosis, and can cause severe pain, fractures, impaired mobility, and death. The invasion of cancer cells into target sites involves several stages. Initially, they invade the surroundings of the original site, breaching the vasculature and entering the circulation. Then, depending on molecular signals on cell membranes or in their microenvironment, they invade a particular target organ along their path of circulation (1, 2). Although the precise process has not been elucidated yet, the invasion appears to last many months if not years (3). Once a bulk of invasive cancer cells agglomerate into a mass, metastasis begins. Cancer cells modify the surrounding tissues and vasculature to favor their growth. Cancer treatment often involves a combination of radiation, chemotherapy, and medications to reduce the pain and inflammation.

Breast cancer, one of the most prevalent malignant tumors, exhibits a 40% likelihood to eventually develop bone metastases (4, 5). Bone tissue is the most common target site of breast

cancer. Bone metastasis reflects potential skeletal-related events and poor clinical results. To improve the current therapies for bone-metastasized breast cancer, animal models that mimic the human tumor microenvironment have been used in preclinical experiments (6). Prostate cancer is the second most frequently occurring cancer in men. It preferentially metastasizes to the bone, and presents a worse prognosis at the metastatic stage. Rarely lethal when restricted to its primary site, the 5-year-survival rate of prostate cancer decreases by 29.8% when it metastasizes to the bone, explaining its rank as the fifth leading cause of tumor-related mortality in males (7). Antimetastatic agents need to be urgently developed and the prognosis following bone metastasis must be improved.

Multiple animal models have been used in clinical research to explore the mechanisms and prognosis of tumor metastasis. Translational models have been used to study the advanced stages of tumor metastases, reveal potential protein targets, and develop metastasis-related treatments. However, fully reproducing human bone metastases in animal models is difficult. Nevertheless, by selecting different cell lines, animal strains, and tumor transplantation methods, animal models can be constructed to answer various questions.

In this review, we have discussed the animal models of bone metastasis most commonly used in preclinical experiments and their underlying mechanisms. No single model can represent all the genetic mechanisms of bone metastasis, which requires whole-body organisms. Here, we have compiled a selection of animal models to assist in future studies (Figure 1).

2 Commonly used animals in building animal models

Basing animal models of bone metastasis on general disease models is unreliable. Because the etiology of bone metastasis of human and animal cancers is different, different cancers have different metastatic targets. For example, mouse breast cancer may preferentially metastasize to the lung, while human breast cancer mainly metastasizes to the bone (2). Lung tumors may specifically metastasize to the vertebral column (8, 9). Hence, researchers are required to modify the animal models based on their experiments. The mouse is the most common animal of choice to construct bone metastasis models.

2.1 Breast cancer

Animal models based on human breast cancer cells are commonly constructed using rodents, such as mice or rats, and used in preclinical experiments (10). Both immunodeficient and immunocompetent animals are used. Nude mice of the Balb/c background are frequently used because they are susceptible to both human and rodent breast cancer cell lines (2). Due to the lack of a thymus, immune responses are hardly generated in most of these mice following the injection of cancer cells, which significantly improves the success rate of model construction. Non-obese diabetic/severe combined immunodeficiency (NOD/SCID) mice are immunodeficient mice commonly used in xenograft experiments. Disabilities in the immune system of NOD/SCID mice affect the growth of lymph cells as well as immune signaling. Yin's team used NOD/SCID mice paired with the MDA-MB-231 cell line to investigate how runt-related transcription factor 2, an osteogenesis-related factor, promotes breast cancer and bone metastasis (11).

The demand for crossbred or genetically engineered mice has also increased to better meet experimental needs (12–16). Mice that have been crossed and repeatedly backcrossed can offer an *in vivo* environment better suited to investigate the mechanism of breast cancer bone metastasis (13). In Laura's experiment, Col1a-Krm2

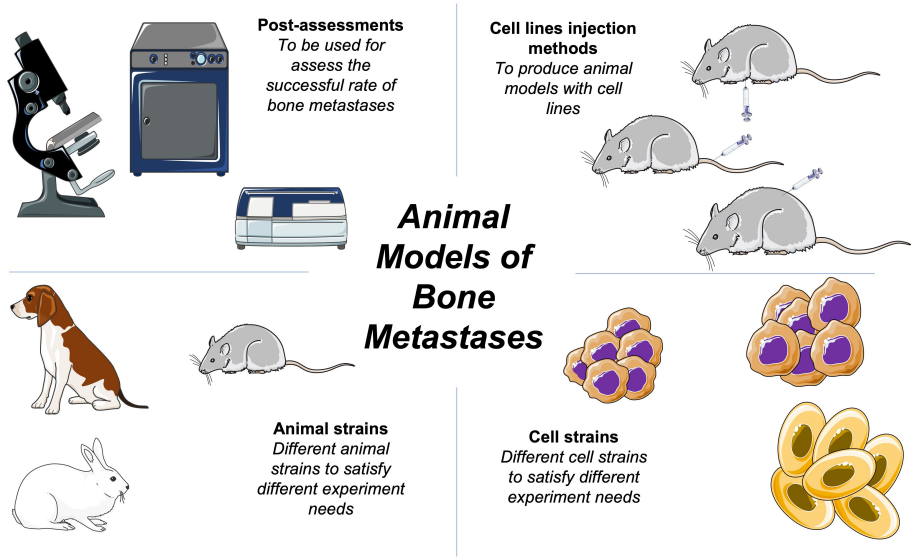

FIGURE 1
Schematic of basic bone metastases animal models methods.

mice were backcrossed with NOD/SCID/IL2rγ^{null} (NSG) mice for 10 generations to introduce an immunocompromised background (13). They found that cancer metastasis to other organs like the spine may be prevented in rather young animals. By modifying the animal model into adult mice and backcrossing over 10 generations, they could focus on the early stages of human breast cancer metastasis. Devignes' team also backcrossed Floxed mice bred in previous experiments with FVB/n wild-type mice for 10 generations to achieve genetic reconstitution consistent with their experimental requirements. Based on whether the *HIF* gene was expressed, mice were divided into two groups to verify whether the HIF signaling pathway in osteoblasts could promote breast cancer cell invasion and bone metastasis (14).

Unlike these experiments, Mercatali's team used zebrafish as a special model to study bone metastasis (17). Visualizing zebrafish embryos and easy genetic manipulation provide researchers with a new method of studying cancer progression.

2.2 Prostate cancer

The first model of prostate cancer – the Dunning rat – exhibits a spontaneous development of the disease (7). However, this model did not show a tendency for bone metastasis, and R-3327 cells derived from the Dunning rat can only metastasize to the lymph nodes. Dogs are also listed as candidate animal models, but they rarely develop prostate cancer due to the lack of androgen receptors on their cell membranes (7). The internal organization of mice femur includes a high-woven bone structure that is less fibrolamellar in nature, providing conditions amenable for bone metastasis (10, 18).

Transgenic mouse models have the advantage of lacking immune responses to injected cells or xenografts (19). Transgenic adenocarcinoma of the mouse prostate (TRAMP) is one of the most famous transgenic models, exhibiting metastases to the lung and lymph nodes rather than the bone (19, 20). The promoters expressed in neuroendocrine cells, such as the probasin promoter in TRAMP, drive transgenic oncogene expression. NOD/SCID mouse is one of the most used immunodeficient animal models in prostate cancer bone metastasis experiments (21–25). Landgraf created a new model for studying prostate cancer bone metastasis by modifying NSG mice with a humanized tissue-engineered bone construct (hTEBC), which facilitates cancer cell growth (23). Ganguly's team injected PC3 cells into the tibia of 6-week-old NSG mice to explore whether NOTCH3 induces tumor-specific elevation and secretion *via* MMP-3 (21).

However, the existing models are still limited to some of the detectable cancer-related factors, and cannot provide a comprehensive or linear picture of bone metastasis.

3 Cancer cell lines

Both patient-derived cancer tissues and immortalized cancer cell lines are used for transplantation. Patient-derived cancer tissues show genetic concordance between the clinic and the animal models, and help to establish consistent animal models specific to particular cancer cell lines. However, these models may face obstacles in the form of ethics and tissue availability. Cell lines, after several passages, can generate stable primary or secondary cancer sites. Moreover, researchers can genetically edit cell lines by using luciferase genes or knocking out certain genes (26–28).

3.1 Breast cancer

Immortalized human breast cancer cell lines, such as MDA-MB-231, 4T1, and MCF-7, are more easily available than patient-derived tissues. They possess obvious breast cancer target characteristics, and can also exhibit a tendency for bone metastasis after multiple passages (Table 1) (2, 5, 11, 51). They can help restore human bone metastasis in animal models. The bone-homing capabilities of MDA-MB-231 sub-lines can be enhanced *via* generation injections, and up to 90% of MDA-MB-231-bone cells can form neoplasms (52–54). Using 5–8-week-old mice is vital to achieve bone metastasis *via* intracardiac, intra-arterial, or intravenous injections. Farhoodi injected 4T1 cells into the mammary fat pad of Balb/c mice, and then examined their legs for bone metastases. Once its incidence was confirmed, the mice were sacrificed to collect the metastatic tumor cells from the leg bones. These cells were cultivated to purify tumor cells with bone-metastatic tendencies (51). They purified their experimental cells to improve the success rate.

Different pairs of cell lines can also be combined to test certain concepts. Yin's team compared MCF-7 and HCC1954 to validate whether KRT13, a protein from the keratin family, promotes stemness, metastasis, and cellular invasiveness (55). Han's group estimated the metastatic rate of different cell lines (56). They found that the proliferation of MDA-MB-453, UACC-893, and HCC-202 cells increased in the eighth week, while MDA-MB-361, UACC-812, BT-474, and ZR-75-1 cells exhibited moderate proliferation but obvious migration. Using HCC-2218 and HCC1419 cells, tumors did not form, suggesting that both lack the ability to metastasize to the bone. The tumors formed by HCC-202 and MDA-MB-361 cells decreased in size after the sixth week, indicating that these two cell lines may not survive long-term metastasis (56). Eckhardt et al. also tested several cell lines, and NSG mice were used in xenograft studies involving MDA-MB-231 and SUM159 cells (37).

3.2 Prostate cancer

Like other cancer cell lines, those of prostate cancer also originate from both humans and animals (Table 1). R-3327, derived from the Dunning rat, has been used to investigate human prostate cancer due to its spontaneous neoplasm development (57). Other animal-derived cell lines, such as PA-III or AT6-1, naturally form osteolytic and osteoblastic lesions similar to human bone metastases in animal models (57–59). RM1, derived from the mouse prostate, is a highly metastatic cell line, but does not metastasize to the bone (60). Although it can induce consistent bone lesions in mouse models, it is a transformed cell line, not a natural one.

TABLE 1 Common cancer cell lines in bone metastases.

Cancer	Cell Lines	Origin	Model System	Metastases Preference
BCa	MDA-MB-231	Human mammary adenocarcinoma from a 51-year-old Caucasian female	Balb/c nude, MF1 nude, NSG	Mouse long bones, spine and jaw (29–34)
	MCF-7	Human mammary adenocarcinoma from a 69-year-old Caucasian female	Balb/c nude, NOD/SCID	Mouse long bones (32–34)
	T47D	Human mammary ductal carcinoma isolated from a pleural effusion	Balb/c nude, NOD/SCID	Mouse long bones (35, 36)
	4T1	Stage IV mammary tumor from a female Balb/c cfC3H mouse	Balb/c cfC3H	Mouse long bones, Spine, jaw, lungs, and spleen (37–40)
PCa	PC3	Bone metastases from a 62-year-old white man	Balb/c nude, NOD/SCID, NSG	Mouse long bones, spine (33, 41–45)
	LNCaP	Supraclavicular lymph node from a 50-year-old white man	Balb/c nude, SCID	Mouse long bones, spine (29, 46–48)
	DU145	Brain metastases from a 69-year-old white man	Balb/c nude, Ncr nu/nu, NOD	Mouse long bones (25, 45, 47, 49, 50)

BCa, breast cancer; PCa, prostate cancer.

PC3, DU145, and LNCaP are patient-derived cell lines commonly used in prostate cancer animal models. They are easily available and possess the basic prostate cancer cell targets. PC3, derived from the bone metastases of a 62-year-old white man, was selected by isolating highly invasive cells from bone metastatic lesions. Landgraf implanted an hTEBC structure based on the bone-homing properties of PC3 cells, followed by an intracardiac injection of Luc-transfected cancer cells, facilitating the construction of models for transferring the human osteoblast line PC3 to hTEBC and the murine femur (23). Studies on LNCaP, PC3, and DU145 cells, all of which differ in their sensitivity to androgens, showed that prostate cancer-secreted growth differentiation factor 15 modulates the potential for bone remodeling in metastatic bone lesions (49, 61). Lang's team grouped five common prostate cancer cell lines to verify whether PCAT7, a bone metastasis-related long non-coding RNA, activates the transforming growth factor-β/suppressor of mothers against decapentaplegic signaling pathway by upregulating transforming growth factor-β receptor 1. Its negative correlation with miR-324-5p was also investigated (62). Sohn's team tried to intracardiacally inject LNCaP cell lines grouped with $CD133^+$. The overexpression of $CD133^+$ in LNCaP cells enhanced their cancer stem cell-like characteristics in terms of colony formation, migration, etc. The $CD133^+$ group exhibited a bone metastasis rate of 80%, compared with 20% in the Vec group. Moreover, the $CD133^+$ group showed a significant violation of the diffuse osteolytic characteristics of the spinal cord and the vertebral bodies (29).

4 Preparation of cell lines for transplantation

4.1 Orthotopic inoculation of cells

In situ injection of cancer cells best reproduces the process of cancer metastasis in the human body. Injected into mouse mammary fat pads, tumor cells can be seeded through the vasculature towards the target organs – a method that achieves 40–60% of bone metastases in breast cancer animal models (63). To study the function of TIE2, a tyrosine kinase receptor, in osteolytic bone metastasis, Drescher's team administered both bilateral mammary fat pad injections and left ventricular injections to the grouped mice. The correlation between carcinoma *in situ* and bone metastasis was evaluated to determine whether TIE2 inhibition stimulates the dormant breast cancer cells and promotes bone metastasis (34). Likewise, Spadazzi's team injected MCF-7 cells into the left ventricle and mammary fat pads of NSG mice to investigate whether trefoil factor-1 could exert estrogen-induced effects (64).

However, this method suffers from a considerable variation in metastatic tumor growth, besides the comorbidity caused by development of the tumor (Table 2) (73). In addition, it poses the problem of small bone metastases while the primary tumor has grown beyond an ethically reasonable size (5), which seriously compromises the detection of stimulated bone metastases.

Some scientists have also suggested subcutaneous allografts to model bone metastasis. Peiffer's team provided a detailed protocol of resecting subcutaneous prostate cancer allografts from immunocompetent mice (65). Bone metastases, abdominal cavity metastases, and local invasion all occurred in eight mice. This study demonstrated that resection of subcutaneous allografts from mice can lead to the development of metastasis; however, the duration of the experiment was extended by the removal of the prostate gland and precise operations.

4.2 Intravascular injection

Intravascular injection is a way of inoculating cells into the blood circulation. Unlike in orthotopic or ectopic inoculation, tumor cells injected *via* this method can localize to the target site through the intravascular circulation (Table 2) (66). Intra-arterial injections are usually administered to the left ventricle, limiting the clearance of cells that occurs when they pass through the lung

TABLE 2 Implantation methods for bone metastases models.

Cell Injection Methods	Module of metastases studied	Advantages	Disadvantages
Orthotopic Inoculation	Primary tumor and invasively distant metastases	Study of tumor growth *in situ* and distant metastases	Unstable bone metastasis success rate (65–67)
Intracardiac	Circulation and metastases	Easily producing metastases	Requiring sophisticated skills (68–70)
Caudal Vessels	Circulation and metastases	More visualization of circulation inoculation	Potential lung metastases (7, 24, 51)
Intraosseous	Bone metastases	Most convenient and successful method for bone metastases models	Not reflecting the complete course of tumor metastasis (71)
Allografts/Xenografts	Depend on location	Reflecting natural heritability and cellular heterogeneity	Usually requiring immunodeficient mice and high maintenance (23, 72)

capillaries (10, 53, 67). Tail vein injection, which is the more common intravenous injection today, effectively increases the rate of bone metastasis while also increasing the rate of mortality in mice (51).

Animal models currently rely on intracardiac injections to realize the process of bone metastasis. Tumor cells are injected into the circulation through the left ventricle of mice, after which they go through the processes of adhesion, degradation, and migration to finally cause metastases in different organs, thereby simulating the process of bloodway metastasis of tumors. Using intracardiac injections to probe the role of cancer-associated factors in the regulation of tumor bone metastasis has become the preferred modeling approach (44–46). Zheng et al. used this method to prove that osteoblastic Niche-derived Jagged1 sensitizes bone metastases (15). Wang's team showed that the bone sialoprotein–αvβ3 integrin axis functioned significantly more efficiently in cancer cell bone metastasis when integrin was overexpressed. For comparison, stained specimens of the brain, lung, tibia, and femur were collected after left ventricular injection in nude mice (52). Although the postoperative mortality is relatively high, the survival rate can still exceed 90% with practice.

Caudal vessel injection can produce a higher rate of metastasis to the leg bone than to other vital organs. This method offers better accuracy than intracardiac injection because the visibility of tail vessels enables researchers to observe the flow of cancer cell fluids within (74). Caudal vascular injections can either be intravenous or arterial. Injecting through the tail artery will reduce the elimination of tumor cells in pulmonary capillaries and improve the success rate of colonization to the bone, while tail vein injection will promote tumor metastasis to the lung (2, 51, 74). In Farhoodi's experiments, the 4T1 cell model tail artery injection mice showed a significant number of tumor cells localized to the subinguinal fat pad and the leg bone (51). Tumor cells were found in the leg bones of all 32 mice injected through the tail artery, and the rate of bone metastasis following complete tail veil injection was greater than 90% as well. Metastases were also detected in 70% of other target locations 2 weeks post-injection. Hamaidi et al. determined the effect of Lim1 on the adhesion, epithelial–mesenchymal transition, invasion, and metastatic progression of cancer cell surface targets after injection of the renal carcinoma cell line Caki2/786 through the lateral caudal vein of nude mice (75). However, caudal vein injection also resulted in metastatic foci in the lungs of mice.

Multiple factors affect the success of experiments involving vascular injection. Operator skill gaps, standard cell operation procedures, and pressure within the caudal vessels can all influence the growth rate and success of tumor bone metastasis (51). Dilation of the caudal vessels prior to injection or the use of fluorescein to reveal vessel flow can improve the effectiveness of the injection. Non-directed intracardiac injection is still associated with a risk of thrombosis due to the procoagulant activity of tumor cells after accurate completion. The mortality of post-inoculation animal models may be reduced by injecting low-molecular weight heparin into the tail vein 10 minutes before inoculation (76).

4.3 Intraosseous injection

Metastatic tumors can bypass the pre-metastatic process if they are directly ectopically implanted into the bone. The growth of tumor cells inside the bone depends on their interaction with bone cells and the bone microenvironment (Table 2) (77, 78). Therefore, while intraosseous injection can help examine local tumor behavior within the bone microenvironment, it cannot be used to study the early stages of bone metastasis (79). Researchers typically inject 50,000–100,000 cancer cells directly into the tibia or femurs of mice, avoiding the possible comorbidity of the animals' primary tumor (80, 81). Chen et al. observed that Brachyury, one gene affects tail length in mice, was expressed at a low level in the highly metastatic MDA-MB-231 cell line while it was highly expressed in the poorly metastatic T47D cell line when breast cancer cells were injected into the top anterior condylar region of the right tibia of mice. Nude mice showed significant swelling at the injection site 4 weeks post-injection, and X-ray revealed tumor-induced osteolytic lesions (35). After injecting prostate cancer cells into the left tibia of Balb/c nude mice, Thulin's team performed bone tumor development status assays using peripheral quantitative computed tomography (CT) and microCT to investigate the effect of signal transducer and activator of transcription 3 (STAT3) inhibitors on STAT3-regulated

prostate cancer bone metastasis. The STAT3 inhibitor treatment resulted in an intact tibial bone microenvironment with no tumor formation or sclerotic response in mice, whereas the VCaP group showed sclerotic bone tumor response up to 85% (48).

4.4 Allograft and xenograft models

Transplanting allogeneic or xenogeneic tissues into animal models is a common way of modeling bone metastasis (Table 2). Since animals with different genetic backgrounds respond to allogeneic tissues differently, selecting the appropriate tissue source is especially important. In the case of xenografts, patient-derived tumor tissues can better reflect the biological characteristics of tumor bone metastasis in humans (82). Patient-derived xenografts aim to directly transplant human tumor tissue into immunodeficient mice, which represents natural heritability and cellular heterogeneity in human cancer better than simple cell-transplantation models (83). Among animal models, xenografts can only be performed in immunocompromised or immunodeficient animals. Aoki et al. first grew tumor tissue from bone metastases by intraperitoneally injecting it into male thymus-free nu/nu nude mice (42). The tumors were surgically processed to 1-mm^3 fragments to be implanted into the proximal left tibia of the nude mice when they reached 10 mm in diameter. They observed tumor growth in all eight mice. Landgraf's hTEBC model is likewise based on the low immune response of NSG mice to xenografts, while adding humanized components to mimic human tumor bone metastasis as satisfyingly as possible in mice (23).

5 Assessment of animal models of bone metastasis

After injecting cancer cells into mice, bone lesions develop quickly, necessitating researchers to detect physiological conditions, bone changes, and tumor lesions in a timely manner.

Establishing bone metastasis models using luciferase or fluorescent protein-labeled cell lines allows researchers to monitor tumor development in the bones of living animals (15, 39–41). Oliemuller et al. studied the effects of SOX11 on cell invasion and bone metastasis using DCIS-Luc cells, generated by transducing the cells with luciferase 2 lentiviral particles (84). Arriaga's team bred NPK^{EYFP} mice by crossing NPK mice with the Rosa-CAG-LSL-EYFP-WPRE reporter allele, facilitating *in vivo* fluorescence visualization and quantification of YFP-positive prostate tumors and metastases (85).

In turn, instrumentation such as the IVIS system can provide more accurate quantitative indicators through fluorescent or bioluminescent readings obtained from tumors (76–78). Typically, tumor growth in the bone is measured once or twice a week. The area of osteolytic lesions and abnormal bone remodeling can be assessed visually by X-ray or *in vivo* microCT (45–47, 85). Hinz's team then used the IVIS system. After injecting MDA-MB-231 cells into the left ventricle of NSG mice, they performed IVIS bioluminescence assays weekly to assess osteolytic lesions caused by bone metastasis from triple-negative breast cancer. The inoculation of AKT3-knockout 231-BO cells into NSG mice resulted in enhanced bone metastases (86). Another team validated the effect of intracardiacally injecting MDA-MB-231-derived osteotropic cells into nude mice by examining osteolytic lesions in their hind tibia and femurs by microCT. MicroCT images showed that NKX2-8-silenced cell lines were more likely to produce earlier bone metastases, while its overexpression delayed the appearance of metastases, inhibited osteoclast activity, and reduced bone metastatic lesions (87).

At the end of the animal test, the mice should be examined simultaneously for extraosseous metastases. All relevant organs and metastases are fixed in 10% formalin for analysis. For histological studies, samples are fixed in paraformaldehyde for 24–48 hours and then decalcified in paraformaldehyde/ethylenediaminetetraacetic acid solution for 2 weeks. The decalcified paraffin-embedded bone should be sectioned for hematoxylin and eosin staining and evaluated using image analysis software. Bone conversion-related growth factors in the serum can also be assayed (88, 89). Metastases from the lung, liver, and brain tissue can likewise be analyzed and studies investigating the correlation between the area and the number of bone metastases can be performed (90).

6 Conclusion

Bone metastasis is a common manifestation of cancer deterioration in the mid and late stages of the disease. Much research has been done on the invasion of cancer cells, from migration to the bone tissue and beyond; however, much needs to be understood yet. Animal models are vital tools in preclinical metastatic experiments that can help identify the key steps in bone metastasis. Here, we have summarized the experimental animals, cell lines, cell implantation techniques, and evaluation methods used while studying common breast and prostate cancer bone metastases. For preclinical animal testing, immunodeficient animals are used to achieve xenograft growth without eliciting a host immune response. In preclinical studies, many investigators have successfully improved the success of tumor cell colonization to the bone by backcrossing cell lines and transgenic mice. More importantly, most animal tests related to cancer bone metastasis have been performed using cancer cell line injection models. Although the early stages of bone metastasis cannot be studied, these models are effective for studying the interaction between cancer cells and the bone microenvironment.

However, using mice to study human tumor immunity has its limitations. The differences in bone metastasis pathways between humans and animal models can explain why the success of preclinical treatments is not perfectly reproduced in humans. The

inability to present a complete and comprehensive picture of the whole process of bone metastasis is also a problem that needs to be addressed while engineering animal models today.

Author contributions

All authors contributed equally to this work. All authors contributed to the article and approved the submitted version.

Funding

National Natural Science Foundation of China.

Conflict of interest

The authors declare that the research was conducted in the absence of any commercial or financial relationships that could be construed as a potential conflict of interest.

Publisher's note

All claims expressed in this article are solely those of the authors and do not necessarily represent those of their affiliated organizations, or those of the publisher, the editors and the reviewers. Any product that may be evaluated in this article, or claim that may be made by its manufacturer, is not guaranteed or endorsed by the publisher.

References

1. Zhang L, Gaskins K, Yu Z, Xiong Y, Merino MJ, Kebebew E. An *in vivo* mouse model of metastatic human thyroid cancer. *Thyroid Off J Am Thyroid Assoc* (2014) 24 (4):695–704. doi: 10.1089/thy.2013.0149

2. Tulotta C, Groenewoud A, Snaar-Jagalska BE, Ottewell P. Animal models of breast cancer bone metastasis. *Methods Mol Biol Clifton NJ* (2019) 1914:309–30. doi: 10.1007/978-1-4939-8997-3_17

3. Gawrzak S, Rinaldi L, Gregorio S, Arenas EJ, Salvador F, Urosevic J, et al. MSK1 regulates luminal cell differentiation and metastatic dormancy in ER+ breast cancer. *Nat Cell Biol* (2018) 20(2):211–21. doi: 10.1038/s41556-017-0021-z

4. Zhang L, Qu J, Qi Y, Duan Y, Huang YW, Zhou Z, et al. EZH2 engages TGFβ signaling to promote breast cancer bone metastasis *via* integrin β1-FAK activation. *Nat Commun* (2022) 13(1):2543. doi: 10.1038/s41467-022-30105-0

5. Horas K, Zheng Y, Zhou H, Seibel MJ. Animal models for breast cancer metastasis to bone: Opportunities and limitations. *Cancer Invest.* (2015) 33(9):459–68. doi: 10.3109/07357907.2015.1065500

6. Deasy SK, Erez N. A glitch in the matrix: Organ-specific matrisomes in metastatic niches. *Trends Cell Biol* (2022) 32(2):110–23. doi: 10.1016/j.tcb.2021.08.001

7. Berish RB, Ali AN, Telmer PG, Ronald JA, Leong HS. Translational models of prostate cancer bone metastasis. *Nat Rev Urol.* (2018) 15(7):403–21. doi: 10.1038/s41585-018-0020-2

8. Liang H, Zhou L, Hu Z, Ge Y, Zhang T, Chen Q, et al. Siglec15 checkpoint blockade for simultaneous immunochemotherapy and osteolysis inhibition in lung adenocarcinoma spinal metastasis *via* a hollow nanoplatform. *Small Weinh Bergstr Ger* (2022) 18(29):e2107787. doi: 10.1002/smll.202107787

9. Wang K, Jiang L, Hu A, Sun C, Zhou L, Huang Y, et al. Vertebral-specific activation of the CX3CL1/ICAM-1 signaling network mediates non-small-cell lung cancer spinal metastasis by engaging tumor cell-vertebral bone marrow endothelial cell interactions. *Theranostics* (2021) 11(10):4770–89. doi: 10.7150/thno.54235

10. Haq M, Goltzman D, Tremblay G, Brodt P. Rat prostate adenocarcinoma cells disseminate to bone and adhere preferentially to bone marrow-derived endothelial cells. *Cancer Res* (1992) 52(17):4613–9. doi: 10.1038/s41467-022-30105-0

11. Yin X, Teng X, Ma T, Yang T, Zhang J, Huo M, et al. RUNX2 recruits the NuRD (MTA1)/CRL4B complex to promote breast cancer progression and bone metastasis. *Cell Death Differ* (2022) 29(11):2203–17. doi: 10.1038/s41418-022-01010-2

12. Zuo H, Yang D, Wan Y. Fam20C regulates bone resorption and breast cancer bone metastasis through osteopontin and BMP4. *Cancer Res* (2021) 81(20):5242–54. doi: 10.1158/0008-5472.CAN-20-3328

13. Brylka L, Jähn-Rickert K, Baranowsky A, Neven M, Horn M, Yorgan T, et al. Spine metastases in immunocompromised mice after intracardiac injection of MDA-MB-231-SCP2 breast cancer cells. *Cancers* (2022) 14(3):556. doi: 10.3390/cancers14030556

14. Devignes CS, Aslan Y, Brenot A, Devillers A, Schepers K, Fabre S, et al. HIF signaling in osteoblast-lineage cells promotes systemic breast cancer growth and metastasis in mice. *Proc Natl Acad Sci USA* (2018) 115(5):E992–1001. doi: 10.1073/pnas.1718009115

15. Zheng H, Bae Y, Kasimir-Bauer S, Tang R, Chen J, Ren G, et al. Therapeutic antibody targeting tumor- and osteoblastic niche-derived Jagged1 sensitizes bone metastasis to chemotherapy. *Cancer Cell* (2017) 32(6):731–747.e6. doi: 10.1016/j.ccell.2017.11.002

16. Ouarné M, Bouvard C, Boneva G, Mallet C, Ribeiro J, Desroches-Castan A, et al. BMP9, but not BMP10, acts as a quiescence factor on tumor growth, vessel normalization and metastasis in a mouse model of breast cancer. *J Exp Clin Cancer Res CR.* (2018) 37:209. doi: 10.1186/s13046-018-0885-1

17. Mercatali L, La Manna F, Groenewoud A, Casadei R, Recine F, Miserocchi G, et al. Development of a patient-derived xenograft (PDX) of breast cancer bone metastasis in a zebrafish model. *Int J Mol Sci* (2016) 17(8):1375. doi: 10.3390/ijms17081375

18. Kerschnitzki M, Wagermaier W, Roschger P, Seto J, Shahar R, Duda GN, et al. The organization of the osteocyte network mirrors the extracellular matrix orientation in bone. *J Struct Biol* (2011) 173(2):303–11. doi: 10.1016/j.jsb.2010.11.014

19. Kang J, La Manna F, Bonollo F, Sampson N, Alberts IL, Mingels C, et al. Tumor microenvironment mechanisms and bone metastatic disease progression of prostate cancer. *Cancer Lett* (2022) 530:156–69. doi: 10.1016/j.canlet.2022.01.015

20. Gingrich JR, Barrios RJ, Morton RA, Boyce BF, DeMayo FJ, Finegold MJ, et al. Metastatic prostate cancer in a transgenic mouse. *Cancer Res* (1996) 56(18):4096–102.

21. Ganguly SS, Hostetter G, Tang L, Frank SB, Saboda K, Mehra R, et al. Notch3 promotes prostate cancer-induced bone lesion development *via* MMP-3. *Oncogene* (2020) 39(1):204–18. doi: 10.1038/s41388-019-0977-1

22. Polavaram NS, Dutta S, Islam R, Bag AK, Roy S, Poitz D, et al. Tumor- and osteoclast-derived NRP2 in prostate cancer bone metastases. *Bone Res* (2021) 9(1):24. doi: 10.1038/s41413-021-00136-2

23. Landgraf M, Lahr CA, Sanchez-Herrero A, Meinert C, Shokoohmand A, Pollock PM, et al. Humanized bone facilitates prostate cancer metastasis and recapitulates therapeutic effects of zoledronic acid in vivo. *Bone Res* (2019) 7:31. doi: 10.1038/s41413-019-0072-9

24. Hu CY, Chen J, Qin XH, You P, Ma J, Zhang J, et al. Long non-coding RNA NORAD promotes the prostate cancer cell extracellular vesicle release *via* microRNA-541-3p-regulated PKM2 to induce bone metastasis of prostate cancer. *J Exp Clin Cancer Res CR.* (2021) 40(1):98. doi: 10.1186/s13046-021-01891-0

25. Li L, Ameri AH, Wang S, Jansson KH, Casey OM, Yang Q, et al. EGR1 regulates angiogenic and osteoclastogenic factors in prostate cancer and promotes metastasis. *Oncogene* (2019) 38(35):6241–55. doi: 10.1038/s41388-019-0873-8

26. Luo A, Xu Y, Li S, Bao J, Lü J, Ding N, et al. Cancer stem cell property and gene signature in bone-metastatic breast cancer cells. *Int J Biol Sci* (2020) 16(14):2580–94. doi: 10.7150/ijbs.45693

27. Jenkins DE, Hornig YS, Oei Y, Dusich J, Purchio T. Bioluminescent human breast cancer cell lines that permit rapid and sensitive *in vivo* detection of mammary tumors and multiple metastases in immune deficient mice. *Breast Cancer Res BCR* (2005) 7(4):R444–454. doi: 10.1186/bcr1026

28. Sawada Y, Kikugawa T, Iio H, Sakakibara I, Yoshida S, Ikedo A, et al. GPRC5A facilitates cell proliferation through cell cycle regulation and correlates with bone metastasis in prostate cancer. *Int J Cancer* (2020) 146(5):1369–82. doi: 10.1002/ijc.32554

29. Sohn HM, Kim B, Park M, Ko YJ, Moon YH, Sun JM, et al. Effect of CD133 overexpression on bone metastasis in prostate cancer cell line LNCaP. *Oncol Lett* (2019) 18(2):1189–98. doi: 10.3892/ol.2019.10443

30. Sung NJ, Kim NH, Surh YJ, Park SA. Gremlin-1 promotes metastasis of breast cancer cells by activating STAT3-MMP13 signaling pathway. *Int J Mol Sci* (2020) 21 (23):9227. doi: 10.3390/ijms21239227

31. Marino S, de Ridder D, Bishop RT, Renema N, Ponzetti M, Sophocleous A, et al. Paradoxical effects of JZL184, an inhibitor of monoacylglycerol lipase, on bone

remodelling in healthy and cancer-bearing mice. *EBioMedicine* (2019) 44:452–66. doi: 10.1016/j.ebiom.2019.05.048

32. Zhang Z, Xu Q, Song C, Mi B, Zhang H, Kang H, et al. Serum- and glucocorticoid-inducible kinase 1 is essential for osteoclastogenesis and promotes breast cancer bone metastasis. *Mol Cancer Ther* (2020) 19(2):650–60. doi: 10.1158/1535-7163.MCT-18-0783

33. Kim B, Kim H, Jung S, Moon A, Noh DY, Lee ZH, et al. A CTGF-RUNX2-RANKL axis in breast and prostate cancer cells promotes tumor progression in bone. *J Bone Miner Res* (2020) 35(1):155–66. doi: 10.1002/jbmr.3869

34. Drescher F, Juárez P, Arellano DL, Serafín-Higuera N, Olvera-Rodriguez F, Jiménez S, et al. TIE2 induces breast cancer cell dormancy and inhibits the development of osteolytic bone metastases. *Cancers* (2020) 12(4):868. doi: 10.3390/cancers12040868

35. Chen M, Zou S, He C, Zhou J, Li S, Shen M, et al. Transactivation of SOX5 by brachyury promotes breast cancer bone metastasis. *Carcinogenesis* (2020) 41(5):551–60. doi: 10.1093/carcin/bgz142

36. Zhao C, Cai X, Wang Y, Wang D, Wang T, Gong H, et al. NAT1 promotes osteolytic metastasis in luminal breast cancer by regulating the bone metastatic niche *via* NF-κB/IL-1B signaling pathway. *Am J Cancer Res* (2020) 10(8):2464–79.

37. Eckhardt BL, Cao Y, Redfern AD, Chi LH, Burrows AD, Roslan S, et al. Activation of canonical BMP4-SMAD7 signaling suppresses breast cancer metastasis. *Cancer Res* (2020) 80(6):1304–15. doi: 10.1158/0008-5472.CAN-19-0743

38. Zhang D, Iwabuchi S, Baba T, Hashimoto S, Mukaida N, Sasaki S. Involvement of a transcription factor, Nfe2, in breast cancer metastasis to bone. *Cancers* (2020) 12 (10):3003. doi: 10.3390/cancers12103003

39. Sasaki S, Zhang D, Iwabuchi S, Tanabe Y, Hashimoto S, Yamauchi A, et al. Crucial contribution of GPR56/ADGRG1, expressed by breast cancer cells, to bone metastasis formation. *Cancer Sci* (2021) 112(12):4883–93. doi: 10.1111/cas.15150

40. Sun J, Huang J, Lan J, Zhou K, Gao Y, Song Z, et al. Overexpression of CENPF correlates with poor prognosis and tumor bone metastasis in breast cancer. *Cancer Cell Int* (2019) 19:264. doi: 10.1186/s12935-019-0986-8

41. Connelly ZM, Jin R, Zhang J, Yang S, Cheng S, Shi M, et al. FOXA2 promotes prostate cancer growth in the bone. *Am J Transl Res* (2020) 12(9):5619–29. doi: 10.1038/s41413-021-00178-6

42. Aoki Y, Masaki N, Tome Y, Kubota Y, Aoki Y, Bouvet M, et al. Non-invasively imageable tibia-tumor-fragment implantation experimental-bone-metastasis mouse model of GFP-expressing prostate cancer. *Vivo Athens Greece* (2022) 36(4):1647–50. doi: 10.21873/invivo.12876

43. Shin SH, Kim I, Lee JE, Lee M, Park JW. Loss of EGR3 is an independent risk factor for metastatic progression in prostate cancer. *Oncogene* (2020) 39(36):5839–54. doi: 10.1038/s41388-020-01418-5

44. Huang S, Wa Q, Pan J, Peng X, Ren D, Li Q, et al. Transcriptional downregulation of miR-133b by REST promotes prostate cancer metastasis to bone *via* activating TGF-β signaling. *Cell Death Dis* (2018) 9(7):779. doi: 10.1038/s41419-018-0807-3

45. Meng X, Vander Ark A, Daft P, Woodford E, Wang J, Madaj Z, et al. Loss of TGF-β signaling in osteoblasts increases basic-FGF and promotes prostate cancer bone metastasis. *Cancer Lett* (2018) 418:109–18. doi: 10.1016/j.canlet.2018.01.018

46. Li Q, Wang M, Hu Y, Zhao E, Li J, Ren L, et al. MYBL2 disrupts the hippo-YAP pathway and confers castration resistance and metastatic potential in prostate cancer. *Theranostics* (2021) 11(12):5794–812. doi: 10.7150/thno.56604

47. Zhao Z, Li E, Luo L, Zhao S, Liu L, Wang J, et al. A PSCA/PGRN-NF-κB-Integrin-α4 axis promotes prostate cancer cell adhesion to bone marrow endothelium and enhances metastatic potential. *Mol Cancer Res MCR* (2020) 18(3):501–13. doi: 10.1158/1541-7786.MCR-19-0278

48. Thulin MH, Määttä J, Linder A, Sterbova S, Ohlsson C, Damber JE, et al. Inhibition of STAT3 prevents bone metastatic progression of prostate cancer *in vivo*. *Prostate* (2021) 81(8):452–62. doi: 10.1002/pros.24125

49. Siddiqui JA, Seshacharyulu P, Muniyan S, Pothuraju R, Khan P, Vengoji R, et al. GDF15 promotes prostate cancer bone metastasis and colonization through osteoblastic CCL2 and RANKL activation. *Bone Res* (2022) 10(1):6. doi: 10.1038/s41413-021-00178-6

50. Zhang B, Li Y, Wu Q, Xie L, Barwick B, Fu C, et al. Acetylation of KLF5 maintains EMT and tumorigenicity to cause chemoresistant bone metastasis in prostate cancer. *Nat Commun* (2021) 12(1):1714. doi: 10.1038/s41467-021-21976-w

51. Farhoodi HP, Segaliny AI, Wagoner ZW, Cheng JL, Liu L, Zhao W. Optimization of a syngeneic murine model of bone metastasis. *J Bone Oncol* (2020) 23:100298. doi: 10.1016/j.jbo.2020.100298

52. Wang L, Song L, Li J, Wang Y, Yang C, Kou X, et al. Bone sialoprotein-αvβ3 integrin axis promotes breast cancer metastasis to the bone. *Cancer Sci* (2019) 110 (10):3157–72. doi: 10.1111/cas.14172

53. Wetterwald A, van der Pluijm G, Que I, Sijmons B, Buijs J, Karperien M, et al. Optical imaging of cancer metastasis to bone marrow: A mouse model of minimal residual disease. *Am J Pathol* (2002) 160(3):1143–53. doi: 10.1016/S0002-9440(10)64934-6

54. Nutter F, Holen I, Brown HK, Cross SS, Evans CA, Walker M, et al. Different molecular profiles are associated with breast cancer cell homing compared with colonisation of bone: Evidence using a novel bone-seeking cell line. *Endocr Relat Cancer* (2014) 21(2):327–41. doi: 10.1530/ERC-13-0158

55. Yin L, Li Q, Mrdenovic S, Chu GCY, Wu BJ, Bu H, et al. KRT13 promotes stemness and drives metastasis in breast cancer through a plakoglobin/c-myc signaling pathway. *Breast Cancer Res BCR* (2022) 24(1):7. doi: 10.1186/s13058-022-01502-6

56. Han Y, Azuma K, Watanabe S, Semba K, Nakayama J. Metastatic profiling of HER2-positive breast cancer cell lines in xenograft models. *Clin Exp Metastasis* (2022) 39(3):467–77. doi: 10.1007/s10585-022-10150-1

57. Liepe K, Geidel H, Haase M, Hakenberg OW, Runge R, Kotzerke J. New model for the induction of osteoblastic bone metastases in rat. *Anticancer Res* (2005) 25 (2A):1067–73.

58. Blouin S, Baslé MF, Chappard D. Rat models of bone metastases. *Clin Exp Metastasis* (2005) 22(8):605–14. doi: 10.1007/s10585-006-9002-5

59. Lamoureux F, Ory B, Battaglia S, Pilet P, Heymann MF, Gouin F, et al. Relevance of a new rat model of osteoblastic metastases from prostate carcinoma for preclinical studies using zoledronic acid. *Int J Cancer* (2008) 122(4):751–60. doi: 10.1002/ijc.23187

60. Power CA, Pwint H, Chan J, Cho J, Yu Y, Walsh W, et al. A novel model of bone-metastatic prostate cancer in immunocompetent mice. *Prostate* (2009) 69 (15):1613–23. doi: 10.1002/pros.21010

61. Wang W, Yang X, Dai J, Lu Y, Zhang J, Keller ET. Prostate cancer promotes a vicious cycle of bone metastasis progression through inducing osteocytes to secrete GDF15 that stimulates prostate cancer growth and invasion. *Oncogene* (2019) 38 (23):4540–59. doi: 10.1038/s41388-019-0736-3

62. Lang C, Dai Y, Wu Z, Yang Q, He S, Zhang X, et al. SMAD3/SP1 complex-mediated constitutive active loop between lncRNA PCAT7 and TGF-β signaling promotes prostate cancer bone metastasis. *Mol Oncol* (2020) 14(4):808–28. doi: 10.1002/1878-0261.12634

63. Lee JH, Kim B, Jin WJ, Kim JW, Kim HH, Ha H, et al. Trolox inhibits osteolytic bone metastasis of breast cancer through both PGE2-dependent and independent mechanisms. *Biochem Pharmacol* (2014) 91(1):51–60. doi: 10.1016/j.bcp.2014.06.005

64. Spadazzi C, Mercatali L, Esposito M, Wei Y, Liverani C, De Vita A, et al. Trefoil factor-1 upregulation in estrogen-receptor positive breast cancer correlates with an increased risk of bone metastasis. *Bone* (2021) 144:115775. doi: 10.1016/j.bone.2020.115775

65. Peiffer LB, Hicks J, Sosa RY, De Marzo AM, Sfanos KS, Maynard JP. Modeling human prostate cancer metastasis in mice *via* resection of subcutaneous allografts. *Front Oncol* (2022) 12:877536. doi: 10.3389/fonc.2022.877536

66. Yip RKH, Rimes JS, Capaldo BD, Vaillant F, Mouchemore KA, Pal B, et al. Mammary tumour cells remodel the bone marrow vascular microenvironment to support metastasis. *Nat Commun* (2021) 12(1):6920. doi: 10.1038/s41467-021-26556-6

67. Chang J, Sun X, Ma X, Zhao P, Shi B, Wang Y, et al. Intra-cardiac injection of human prostate cancer cells to create a bone metastasis xenograft mouse model. *J Vis Exp JoVE* (2022) 189). doi: 10.3791/64589

68. Chen M, Wu C, Fu Z, Liu S. ICAM1 promotes bone metastasis *via* integrin-mediated TGF-β/EMT signaling in triple-negative breast cancer. *Cancer Sci* (2022) 113 (11):3751–65. doi: 10.1111/cas.15532

69. Labanca E, Yang J, Shepherd PDA, Wan X, Starbuck MW, Guerra LD, et al. Fibroblast growth factor receptor 1 drives the metastatic progression of prostate cancer. *Eur Urol Oncol* (2022) 5(2):164–75. doi: 10.1016/j.euo.2021.10.001

70. Capietto AH, Lee S, Clever D, Eul E, Ellis H, Ma CX, et al. Effective treatment of established bone metastases can be achieved by combinatorial osteoclast blockade and depletion of granulocytic subsets. *Cancer Immunol Res* (2021) 9(12):1400–12. doi: 10.1158/2326-6066.CIR-21-0232

71. Engelmann J, Zarrer J, Gensch V, Riecken K, Berenbrok N, Luu TV, et al. Regulation of bone homeostasis by MERTK and TYRO3. *Nat Commun* (2022) 13 (1):7689. doi: 10.1038/s41467-022-33938-x

72. Boudreau MW, Duraki D, Wang L, Mao C, Kim JE, Henn MA, et al. A small-molecule activator of the unfolded protein response eradicates human breast tumors in mice. *Sci Transl Med* (2021) 13(603):eabf1383. doi: 10.1126/scitranslmed.abf1383

73. Bibby MC. Orthotopic models of cancer for preclinical drug evaluation: Advantages and disadvantages. *Eur J Cancer Oxf Engl 1990* (2004) 40(6):852–7. doi: 10.1186/s13046-018-0813-4

74. Kuchimaru T, Kataoka N, Nakagawa K, Isozaki T, Miyabara H, Minegishi M, et al. A reliable murine model of bone metastasis by injecting cancer cells through caudal arteries. *Nat Commun* (2018) 9:2981. doi: 10.1038/s41467-018-05366-3

75. Hamaidi I, Coquard C, Danilin S, Dormoy V, Béraud C, Rothhut S, et al. The Lim1 oncogene as a new therapeutic target for metastatic human renal cell carcinoma. *Oncogene* (2019) 38(1):60–72. doi: 10.1038/s41388-018-0413-y

76. Stocking KL, Jones JC, Everds NE, Buetow BS, Roudier MP, Miller RE. Use of low-molecular-weight heparin to decrease mortality in mice after intracardiac injection of tumor cells. *Comp Med* (2009) 59(1):37–45.

77. Robinson BD, Sica GL, Liu YF, Rohan TE, Gertler FB, Condeelis JS, et al. Tumor microenvironment of metastasis in human breast carcinoma: A potential prognostic marker linked to hematogenous dissemination. *Clin Cancer Res Off J Am Assoc Cancer Res* (2009) 15(7):2433–41. doi: 10.1158/1078-0432.CCR-08-2179

78. Coleman RE, Gregory W, Marshall H, Wilson C, Holen I. The metastatic microenvironment of breast cancer: Clinical implications. *Breast Edinb Scotl* (2013) 22 Suppl 2:S50–56. doi: 10.1016/j.breast.2013.07.010

79. Halpern J, Lynch CC, Fleming J, Hamming D, Martin MD, Schwartz HS, et al. The application of a murine bone bioreactor as a model of tumor: bone interaction. *Clin Exp Metastasis* (2006) 23(7–8):345–56. doi: 10.1007/s10585-006-9044-8

80. Zhu W, Sheng D, Shao Y, Zhang Q, Peng Y. Neuronal calcitonin gene-related peptide promotes prostate tumor growth in the bone microenvironment. *Peptides* (2021) 135:170423. doi: 10.1016/j.peptides.2020.170423

81. Zheng Y, Seibel MJ, Zhou H. Methods in bone biology: Cancer and bone. In: Duque G, Watanabe K, editors. *Osteoporosis Res: Animal models*. London: Springer London (2011). p. 83–91. doi: 10.1007/978-0-85729-293-3_7

82. Holzapfel BM, Thibaudeau L, Hesami P, Taubenberger A, Holzapfel NP, Mayer-Wagner S, et al. Humanised xenograft models of bone metastasis revisited: Novel insights into species-specific mechanisms of cancer cell osteotropism. *Cancer Metastasis Rev* (2013) 32(1–2):129–45. doi: 10.1007/s10555-013-9437-5

83. Lin D, Xue H, Wang Y, Wu R, Watahiki A, Dong X, et al. Next generation patient-derived prostate cancer xenograft models. *Asian J Androl.* (2014) 16(3):407–12. doi: 10.4103/1008-682X.125394

84. Oliemuller E, Newman R, Tsang SM, Foo S, Muirhead G, Noor F, et al. SOX11 promotes epithelial/mesenchymal hybrid state and alters tropism of invasive breast cancer cells. *eLife* (2020) 9. doi: 10.7554/eLife.58374

85. Arriaga JM, Panja S, Alshalalfa M, Zhao J, Zou M, Giacobbe A, et al. A MYC and RAS co-activation signature in localized prostate cancer drives bone metastasis and castration resistance. *Nat Cancer* (2020) 11):1082–96. doi: 10.1038/s43018-020-00125-0

86. Hinz N, Baranowsky A, Horn M, Kriegs M, Sibbertsen F, Smit DJ, et al. Knockdown of AKT3 activates HER2 and DDR kinases in bone-seeking breast cancer cells, promotes metastasis *In vivo* and attenuates the TGFβ/CTGF axis. *Cells* (2021) 10 (2):430. doi: 10.3390/cells10020430

87. Abudourousuli A, Chen S, Hu Y, Qian W, Liao X, Xu Y, et al. NKX2-8/PTHrP axis-mediated osteoclastogenesis and bone metastasis in breast cancer. *Front Oncol* (2022) 12:907000. doi: 10.3389/fonc.2022.907000

88. Maimon A, Levi-Yahid V, Ben-Meir K, Halpern A, Talmi Z, Priya S, et al. Myeloid cell-derived PROS1 inhibits tumor metastasis by regulating inflammatory and immune responses *via* IL-10. *J Clin Invest* (2021) 131(10):e126089. doi: 10.1172/JCI126089

89. Cai WL, Huang WD, Li B, Chen TR, Li ZX, Zhao CL, et al. microRNA-124 inhibits bone metastasis of breast cancer by repressing interleukin-11. *Mol Cancer* (2018) 17(1):9. doi: 10.1186/s12943-017-0746-0

90. He Y, Luo W, Liu Y, Wang Y, Ma C, Wu Q, et al. IL-20RB mediates tumoral response to osteoclastic niches and promotes bone metastasis of lung cancer. *J Clin Invest* (2022) 132(20):e157917. doi: 10.1172/JCI157917

frontiers | Frontiers in Oncology

TYPE Original Research
PUBLISHED 06 April 2023
DOI 10.3389/fonc.2023.1115898

OPEN ACCESS

Hong Duan,
Sichuan University, China

REVIEWED BY
Zhiwen Luo,
Chinese Academy of Medical Sciences and Peking Union Medical College, China
Junyi Liao,
The First Affiliated Hospital of Chongqing Medical University, China

*CORRESPONDENCE
Jing Feng
fengjingwhyyy@163.com
Fengxia Chen
fengxiachen@whu.edu.cn
Zhicai Zhang
zhicaizhang@hust.edu.cn

†These authors have contributed equally to this work

SPECIALTY SECTION
This article was submitted to Surgical Oncology, a section of the journal Frontiers in Oncology

RECEIVED 04 December 2022
ACCEPTED 17 March 2023
PUBLISHED 06 April 2023

CITATION
Pu F, Yu Y, Shao Z, Wu W, Feng J, Chen F and Zhang Z (2023) Clinical efficacy of customized modular prosthesis in the treatment of femoral shaft metastases. *Front. Oncol.* 13:1115898. doi: 10.3389/fonc.2023.1115898

Clinical efficacy of customized modular prosthesis in the treatment of femoral shaft metastases

Feifei Pu[1,2†], Yihan Yu[2†], Zengwu Shao[2], Wei Wu[2], Jing Feng[1*], Fengxia Chen[3*] and Zhicai Zhang[2*]

[1]Department of Orthopedics, Wuhan Hospital of Traditional Chinese and Western Medicine (Wuhan No.1 Hospital), Tongji Medical College, Huazhong University of Science and Technology, Wuhan, Hubei, China, [2]Departments of Orthopedics, Union Hospital, Tongji Medical College, Huazhong University of Science and Technology, Wuhan, Hubei, China, [3]Department of Radiation and Medical Oncology, Zhongnan Hospital, Wuhan University, Wuhan, Hubei, China

Purpose: To examine clinical outcomes of a specialized modular prosthesis used to fill a bone deficiency following removal of femoral shaft metastases.

Methods: Eighteen patients with femoral shaft metastases who underwent en bloc resection and implantation of a personalized modular prosthesis between December 2014 and December 2019 were retrospectively analyzed. Pain, limb function, and quality of life were evaluated using the visual analog scale (VAS), Musculoskeletal Tumor Society (MSTS) scale, International Society of Limb Salvage (ISOLS) scoring system, Karnofsky Performance Status (KPS) scale, and Nottingham Health Profile (NHP) scale. The Kaplan–Meier technique was used to analyze patient survival.

Results: The operation duration was 90–150 min (mean, 115 min), and the osteotomy length was 9–16 cm (mean, 11.72 cm). The patients were followed for 12–62 months (mean, 25.28 months). The VAS and NHP ratings were lower at 3, 6, and 12 months after surgery than before surgery, while the MSTS, ISOLS, and KPS scores were higher after surgery than they had been before. These differences were statistically significant ($P<0.05$). The survival period was between 7 and 62 months (mean, 20.89 months), and the rates of survival at 1-year and 2-year were 72.22% and 27.78%, respectively. Except for two patients with aseptic prosthesis loosening during the follow-up period, there were no problems.

Conclusion: En bloc excision and implantation of a personalized modular prosthesis can reduce pain and improve the ability of patients with femoral shaft metastases to perform daily activities, thereby improving their quality of life.

KEYWORDS

femoral shaft, bone metastases, en bloc resection, customized modular prosthesis, surgical treatment

1 Introduction

The long bones of the limbs are frequently affected by bone metastases, and the femoral shaft is the most frequently affected site, accounting for 25% to 71% of long bone metastases, 25% of which lead to pathological fracture (1). Metastases in the femoral shaft can result in excruciating pain, limb impairment, and lower quality of life (2). Bone metastases weaken bones and cause pathological fractures, both of which are significant risk factors for death (3). The best treatment plan must be chosen to prevent and treat pathological fractures in patients with bone metastases (4).

There is a broad agreement that limb salvage surgery enhances the quality of life of patients with limb shaft metastases owing to recent advancements in radiotherapy, chemotherapy, surgical techniques, targeted therapy, and immunotherapy for comprehensive cancer treatment (5). Following the removal of a bone tumor, several reconstruction techniques can be used, each with advantages and disadvantages. These techniques include biological reconstruction, artificial articulation-allograft reconstruction, intramedullary needle fixation, plate screw fixation, and tumor prosthesis replacement (6, 7). The most popular reconstruction technique in limb salvage surgery is prosthesis replacement because it can quickly relieve pain and restore limb function, while having a low incidence of post-operative complications (8–10).

Because of their positive clinical outcomes, personalized modular prostheses have recently gained recognition as a new treatment option for femoral shaft metastases (11–13). Intercalary prosthesis implantation provides the advantages of no delayed end healing and no autogenous or allogeneic bone fractures (14–16). Early post-operative functional exercise is possible because the prosthesis has good strength and can bear significant stress, provided that the post-operative limb force line is normal. Additionally, because the prosthesis may be customized, the osteotomy plane can precisely reach the area that needs to be excised, thereby reducing the chance of local recurrence. En bloc resection and intercalary prosthesis insertion take less time during surgery when the diaphysis is being repaired following large-segment osteotomy.

However, the surgical impact, functional success, and consequences of the treatment of femoral shaft metastases are not entirely obvious owing to the short duration of clinical use. This study sought to provide 18 patients with femoral shaft metastases with an effective surgical alternative by summarizing the results of en bloc resection and installation of tailored modular prostheses.

2 Materials and methods

2.1 Ethical approval and consent to participate

This retrospective study adhered to the Declaration of Helsinki and was authorized by our school's Ethics Committee. Our ethics committee approved the process and data collection.

2.2 Inclusion and exclusion criteria

The inclusion criteria were as follows: femoral shaft metastases, an expected survival time of >3 months, an effective fixation length of the remaining bone marrow cavity at both ends after osteotomy of >5 cm, pathological fractures or a Mirels score of >9, and complete data with a follow-up period of >3 months. Patients with poor general health who could not handle anesthesia or surgery were excluded.

2.3 Patients

In Wuhan Hospital of Traditional Chinese and Western Medicine (Wuhan No. 1 Hospital) and Union Hospital, Tongji Medical College, Huazhong University of Science and Technology, 18 patients (of which five had pathological fractures) with femoral shaft metastases were treated between December 2014 and December 2019 by employing en bloc excision and implantation of a personalized modular prosthesis. There were 11 men and seven women aged 46–79 years (median, 65.94 years) in this group. All patients' lower limb pain and activity restrictions led them to visit the hospital. The central segment of the femoral shaft was the location of the tumor lesions in all cases. The primary tumor types were lung cancer (n = 7), kidney cancer (n = 4), breast cancer (n = 2), thyroid cancer (n = 2), cervical cancer (n = 1), colon cancer (n = 1), and stomach cancer (n = 1).

2.4 Prosthetic design

Magnetic resonance imaging and preoperative radiography were performed to customize the modular prosthesis, which was created and produced by Beijing Lidak Technology Co., Ltd. (Beijing, China). The distal and proximal prosthesis stems, as well as the intermediate screws, were the main parts of the prosthesis, which were made of a titanium alloy (Ti6A14V). The distal and proximal prosthesis stems were grooved, and a two-fold taper connected the implanted prosthesis to the bone (Figures 1A, B).

2.5 Surgical procedure

The lateral thigh approach was used in patients who were positioned in the supine position. The length of the incision was chosen based on the degree of tumor involvement revealed on preoperative magnetic resonance imaging. Following skin and deep fascia incisions, the tumor location of the femoral shaft metastases was visible between the vastus lateralis and vastus posteris. The degree of intramedullary invasion revealed by magnetic resonance imaging was used to calculate osteotomy length and plane. The periosteum was removed at the osteotomy plane, and periosteum strippers were positioned on either side to safeguard nearby soft tissue. To complete en bloc resection, a chainsaw was used to chop the diseased bone fragment (Figures 2A, B).

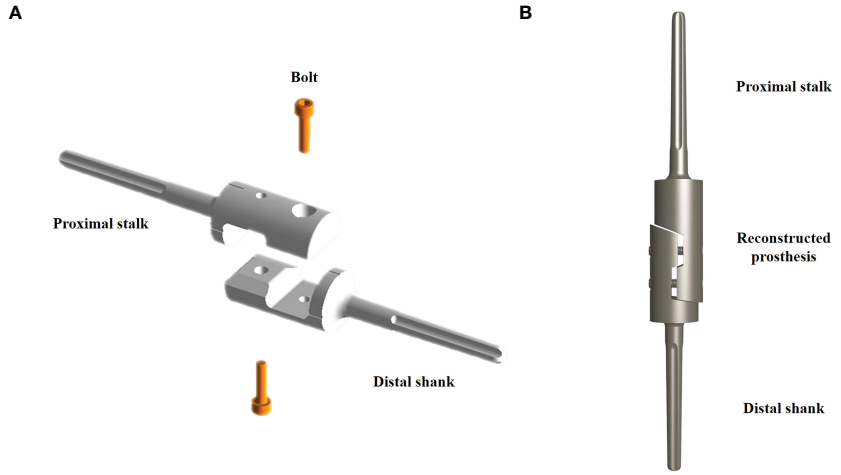

FIGURE 1
Schematic diagram of the customized modular prosthesis. **(A)** The decomposition components include the distal prosthesis stem, proximal prosthesis stem, and two intermediate screws. **(B)** Schematic diagram of the assembled intercalary prosthesis.

The medullary cavity was completely enlarged (Figure 2C), and the prosthesis was placed (Figure 2D). The bone marrow cavity was filled with bone cement and reset according to the designated normal limb force line. The prosthesis stalk in the fixed region of the medulla was at least 5 cm long. To position the prosthesis correctly, the medullary cavity was filled with a prosthesis stem coated with bone cement (Figure 2E). Once the bone cement cooled and dried, the connecting piece was secured with two screws, and the segmental prosthesis was then attached (Figure 2F). The extracted bone was submitted to a pathologist for analysis. A negative pressure drainage tube was inserted after full hemostasis, and the surgical incision was stitched together layer-by-layer. In Figures 3, 4, two typical instances of femoral shaft metastases after en bloc excision and implantation of a specially designed modular prosthesis are shown.

2.6 Post-operative treatment

A negative pressure drainage tube was typically installed for 48 h and withdrawn when the daily discharge dropped below 50 mL. Analgesia, anticoagulant treatment, and postoperative infection control were frequently administered. A variety of post-operative systemic therapies, including radiotherapy, chemotherapy, hormone therapy, biotherapy, and immunotherapy, were used, depending on the systemic health of the patient and the features

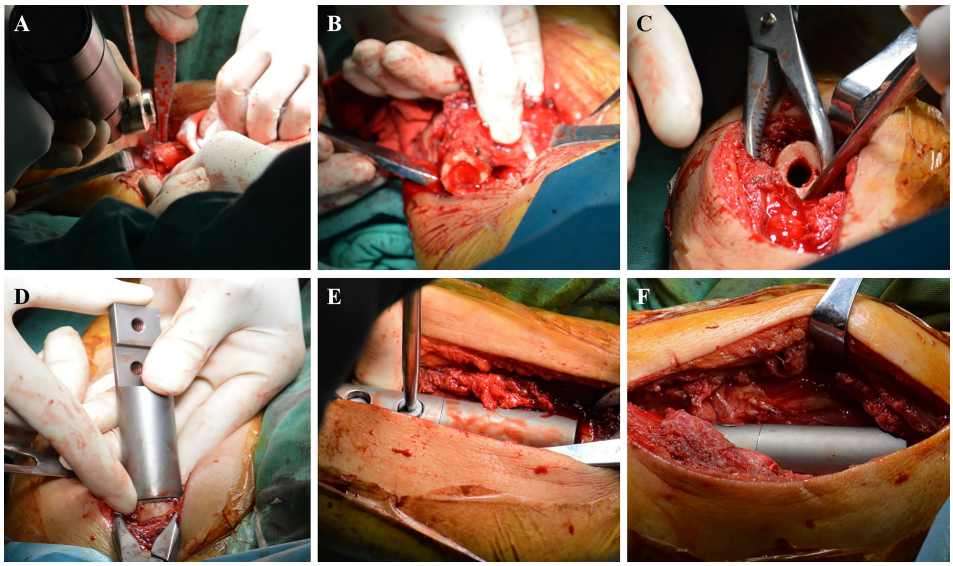

FIGURE 2
Surgical procedure. **(A)** The distal diseased bone is cut by a chainsaw. **(B)** The diseased bone is removed. **(C)** The medullary cavity is expanded. **(D)** Simulated prosthesis is installed. **(E)** The prosthesis is locked with screws. **(F)** Intercalary prosthesis is assembled.

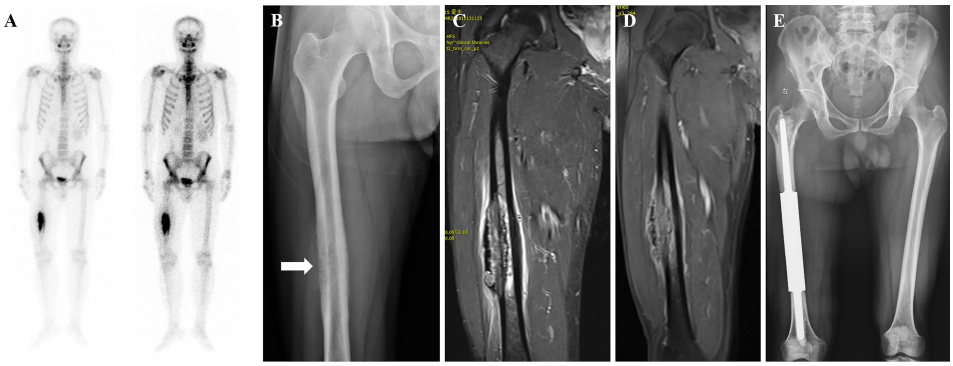

FIGURE 3
A patient with isolated metastasis of the right femoral shaft. **(A)** Emission Computed Tomography showing an isolated metastatic lesion in the right femoral shaft with active metabolism. **(B)** Radiograph showing osteolytic destruction of the right femoral shaft. **(C, D)** Magnetic resonance image showing decreased T1-weighted image signal and increased T2-weighted image signal, consistent with the diagnosis of osteolytic bone metastases. **(E)** Post-operative radiograph of customized modular prosthesis implantation.

of the underlying metastatic tumor. Bisphosphonates or denosumab were administered for the management of bone pain and prevention of skeletal-related events.

2.7 Outcome assessment

The amount of intraoperative blood loss, surgery time, wound healing time, postoperative infection, internal fixation loosening or fracture, and re-fracture were recorded. After surgery, distant metastasis and local recurrence in the affected limb were routinely monitored.

Pre and post surgery (at 3, 6, and 12 months), the severity of pain was assessed using the visual analog scale (VAS), with a high score denoting severe discomfort (17). Lower limb function was assessed using the Musculoskeletal Tumor Society (MSTS) functional score, with a total score of 30; a high score indicates good function of the affected limb (18). A high score implies good limb function in the International Society of Limb Salvage (ISOLS) rating system (19). The Karnofsky Performance Status (KPS) scale was used to evaluate functional status; a high score indicates good functional health (20). The Nottingham Health Profile (NHP) scale was used to measure quality of life; a low score suggests minimal functional impairment and a good quality of life (21).

2.8 Statistical analysis

SPSS (version 21.0; IBM Corp., Armonk, NY, USA) was used for the statistical analysis. Using the paired sample t-test, the VAS pain, functional, and quality of life scores were compared. Statistical significance was set at $P<0.05$.

3 Results

Table 1 lists the traits of the study participants. Each patient underwent an effective surgery and had stable vital signs throughout the procedure. Following surgery, post-operative pathology findings revealed bone metastases despite total removal of all tumors. The

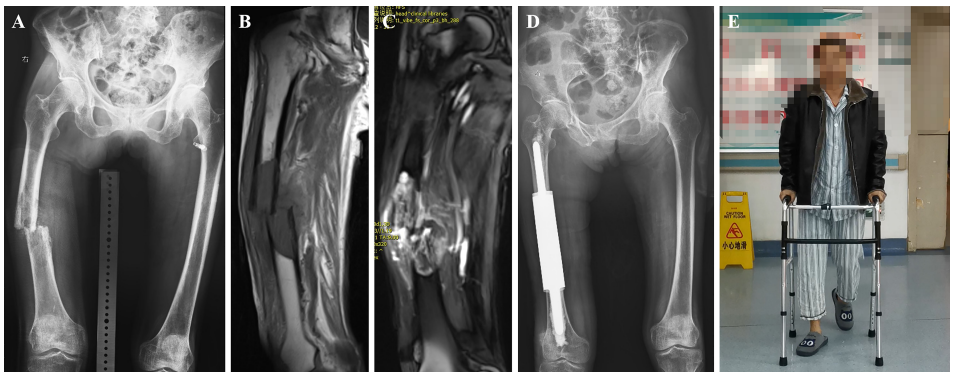

FIGURE 4
A case of metastatic lesion of the right femoral shaft with pathological fracture. **(A)** Radiograph showing osteolytic destruction of the right femoral shaft. **(B, C)** Long T1 and T2 signal shadows in the medullary cavity, local nodular changes, swelling of the surrounding muscle group, and increased signal. **(D)** Post-operative radiograph of customized modular prosthesis implantation. **(E)** Functional photo of the patient on the third postoperative day.

TABLE 1 Clinical characteristics of patients.

Case no.	Sex	Age, years	Pathological fracture	Follow-up time, month	Primary site of metastases	Surgical duration, min	Osteotomy length, cm	First time of postoperative ambulation, days	Local recurrence	Survival time, month
1	Female	63	No	32	lung cancer	120	10	4	No	32
2	Male	54	No	28	breast cancer	100	12	3	No	21
3	Male	68	No	45	lung cancer	110	15	5	No	38
4	Female	63	Yes	37	kidney cancer	120	11	4	No	26
5	Male	72	No	12	thyroid cancer	90	10	6	No	9
6	Female	56	Yes	18	breast cancer	110	9	5	No	18
7	Male	69	No	15	lung cancer	140	10	4	No	15
8	Male	64	No	26	kidney cancer	100	12	4	No	10
9	Male	71	No	18	lung cancer	120	14	5	No	7
10	Female	62	Yes	16	kidney cancer	130	10	3	No	11
11	Male	79	No	22	stomach cancer	115	16	6	No	19
12	Female	72	No	17	thyroid cancer	150	11	5	No	17
13	Male	58	Yes	62	lung cancer	125	14	4	No	62
14	Female	61	No	25	cervical cancer	105	12	5	No	25
15	Male	66	No	18	lung cancer	100	13	7	No	18
16	Male	75	No	26	lung cancer	120	10	3	No	17
17	Female	71	Yes	15	colon cancer	110	12	5	No	8
18	Male	63	No	23	kidney cancer	105	10	4	No	23

osteotomies ranged in length from 9 to 16 cm (mean, 11.72 cm), and the surgical duration ranged from 90 to 150 min (mean, 115.00 min). Patients were monitored for 12–62 months (mean, 25.28 months). No issues emerged during the observation period, except for two patients' aseptic prostheses becoming looser.

The VAS and NHP scores decreased at 3, 6, and 12 months after surgery; however, the MSTS, ISOLS, and KPS scores increased, and the changes were statistically significant ($P<0.05$) (Table 2). The survival period was between 7 and 62 months (mean, 20.89 months), and the 1-year and 2-year survival rates were 72.22% and 27.78%, respectively (Figure 5).

4 Discussion

Patients with local tumor control, close pathological fractures, or failure of preventive internal fixation are candidates for whole-segment excision of primary or metastatic long-shaft malignancies (10, 22). Following a major resection of a diaphysis tumor, reconstructive techniques include the placement of massive allografts or autografts, replantation of inactive tumor bone, distraction osteogenesis, and insertion of segmental prostheses (23–27). Large allograft segments are immobilized during allograft implantation using intramedullary nails or steel plates

TABLE 2 Comparison of preoperative and postoperative pain, functional status, and quality of life.

Item	Preoperative*	Postoperative third month	Postoperative sixth month**	Postoperative twelfth month***
Pain degree				
VAS score	8.54 ± 1.02	4.38 ± 0.57	2.38 ± 0.52	2.45 ± 0.22
Limb function				
MSTS score	22.17 ± 1.75	27.56 ± 1.98	28.28 ± 1.56	28.75 ± 2.13
ISOLS score	21.36 ± 1.06	25.69 ± 1.32	27.91 ± 1.31	28.19 ± 1.72
Life quality				
KPS score	61.83 ± 5.38	75.98 ± 5.40	77.58 ± 2.91	78.87 ± 1.72
NHP score	290.48 ± 28.56	226.42 ± 18.57	195.76 ± 23.18	195.26 ± 17.93

VAS, visual analogue scale; MSTS, musculoskeletal tumor society system; ISOLS, international society of limb salvage; KPS, karnofsky perfor mance status; NHP, nottingham health profile. *: the postoperative third, sixth, and twelfth months compared to the preoperative, P<0.05; **: compared to postoperative third month, P>0.05; ***: compared to postoperative sixth month, P>0.05.

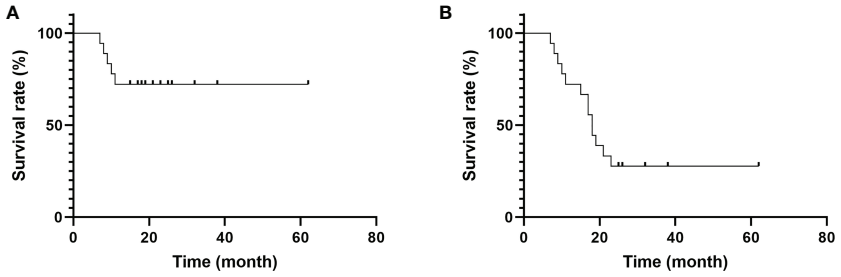

FIGURE 5
Survival time of patients. **(A)** The 1-year survival rate was 72.22%. **(B)** The 2-year survival rate was 27.78%.

(28). If the transplant is successful, no future revision surgery is required because the bone may permanently fuse with the allograft. Additionally, the transplanted allograft bone may cling to the repaired soft tissue, improving the post-operative stability (29). However, allografts have several major disadvantages, including allograft or residual bone fracture, graft rejection, non-union or poor matching between the allograft and autologous bone, and allograft non-union (30, 31). Additionally, even without a rejection reaction, the transplanted autologous bone may be unable to support weight for a considerable amount of time following the procedure, severely impairing the quality of life and reducing the function of the damaged limb (32). This approach cannot be used to reconstruct a significant backbone defect and carries the risk of graft breakage (33). After receiving inactivation treatment, the tumor tissue from the bone that constitutes the tumor segment is removed and replanted in its original location, restoring the continuity of the limb (34). However, it has drawbacks such as wound non-union, infection, fracture non-union, and replanted bone fracture, which have resulted in this kind of surgical method to be gradually abandoned (35). Distraction osteogenesis is a lengthy treatment that does not promote functional recovery or post-operative radiotherapy, carries the potential risk of needle tract infection, and is inappropriate for patients with metastatic disease (36).

The broad resection and repair of diaphysis tumors have recently used intercalary prosthesis implantation owing to the rapid development of biomaterials, biomechanics, iconography, internal fixation technology, and other procedures (10, 37, 38). Intercalary prosthesis implantation is clearly superior to intramedullary needle fixation, allogeneic bone transplantation, external fixation, and other techniques in terms of resisting extrusion, bending, and twisting (6). In a previous investigation, intercalary prosthesis implantation did not cause graft fracture or fracture healing after autologous and allogeneic bone transplantation (39). Functional exercise can be guaranteed in the early post-operative period, and normal function of the affected limb can be restored relatively sooner as the prosthesis has enough strength to bear stress similar to normal bone tissue, provided that the post-operative anatomical force line of the limb is normal (6). The osteotomy plane can precisely reach the area that needs to be excised because of the prosthesis's ability to be customized, thereby lowering the local recurrence rate (40). In the case of diaphysis repair after large-segment osteotomy, the duration of the intercalary prosthesis implantation procedure is similarly reduced. These are well-known advantages of using an intercalary prosthesis over other types of restorations. These findings show that installing a tailored modular prosthesis has the added benefits of less trauma and less procedure time.

After intercalary prosthesis implantation, problems include prosthesis loosening, prosthesis wear, and prosthesis fracture, with prosthesis loosening being the most significant (41). Deviation of the limb force line is caused by loosening of the prosthesis, which can negatively impact the quality of life and necessitate reoperation. When the residual diaphysis or prosthesis cavity stalk becomes shorter following osteotomy, resulting in uneven tension on the prosthesis, prosthesis loosening may develop. Otherwise, it would be impossible to use bone cement to secure the prosthesis (42). In the case of a short prosthesis cavity stalk, some researchers have inserted an external cortical plate for better fixation to prevent prosthesis loosening; however, its long-term effects are yet to be determined (10). Despite the high prevalence of prosthesis loosening following surgery, few patients require reoperation for this complication (16, 43). Huang et al. described 16 cases of femoral metastatic tumors with pathological fractures treated with intercalary prosthesis implantation, one of which developed aseptic loosening 7 months following surgery (10). Sewell et al. reported 18 cases of tibial cancer treated with intercalary prosthesis implantation, four of which exhibited aseptic loosening. The authors considered that a stronger rotational force, larger medullary void in the metaphysis, and problematic distribution of bone cement contributed to easy loosening of the prosthesis (42). In our investigation, no complications occurred throughout the follow-up period, except for aseptic prosthesis loosening in two patients; however, revision surgery was not performed because the patients' function was satisfactory.

In determining the success or failure of a surgery, post-operative function is an essential factor. Several biomechanical investigations (11) have proven that intercalary prostheses perform better than conventional fastening systems under various types of loading (four-point bending, torsion, and compression). Intercalary

prosthetic repair is advantageous for patients with metastatic diaphyseal malignancies because of the advantages of instant stability, preservation of surrounding joints, and early return of function, according to research employing intercalary prostheses (9, 12, 16, 37, 40, 41). The MSTS score is used to evaluate the functional status of the musculoskeletal system of the skeleton after tumor removal and repair. Obtaining an adequate knowledge of surgical efficacy requires both subjective and objective post-operative evaluations. Ahlmann et al. retrospectively evaluated the clinical efficacy of intercalary prosthesis implantation in six patients with diaphyseal bone tumors, with a mean follow-up period of 21.6 months, and reported an average MTST score of 27 points, indicating that 90% of the functional status was restored (40). Abudu et al. reported the clinical outcomes in 13 cases of tibial and femoral diaphyseal tumors treated with intercalary prosthesis implantation; at the most recent follow-up, 84% of the patients' function had been restored (44). The average post-operative MSTS score after intercalary prosthesis implantation for humeral malignancies, as reported by McGrath et al. (43), suggested 77% restoration of the patients' functional status. In our study, the MSTS scores at 3, 6, and 12 months post-operatively were, 27.56 ± 1.98, 28.28 ± 1.56, and 28.75 ± 2.13, respectively. The three-dimensional printed prosthesis has a stronger bone integration effect and is worth looking forward to. The host bone is closely embedded with the prosthesis to achieve immediate stability, the microporous layer on the surface of the prosthesis is fused with the host bone, enabling long-term stability of the prosthesis (8, 9).

In the treatment of bone metastases, multimodal therapy is emphasized to prevent the progression of pain and skeletal-related events, and individualized treatment has become the direction of future development (45, 46). A multidisciplinary team of professionals in the diagnosis and treatment of bone tumors should select the most appropriate treatment strategy based on the patient's unique condition, pathological type, metastasis, life expectancy, and family financial standing (47). In our study, the median survival time was 20.89 months, while the rate of complications was only 11.11%; the lower complication rate is more appropriate for patients with bone metastases who have a limited survival time.

5 Conclusion

For the treatment of femoral shaft metastases, en bloc resection and customized modular prosthesis implantation can reduce pain, improve limb function, and improve the quality of life. However, owing to the lack of a control group and the small sample size in our study, their efficacy should be tested further. Additionally, owing to the great variation in patients and primary tumors, it is difficult to generalize accurate and reliable universal principles and conclusions.

Data availability statement

The original contributions presented in the study are included in the article/supplementary material. Further inquiries can be directed to the corresponding authors.

Ethics statement

The studies involving human participants were reviewed and approved by the institutional review board of our hospital. The patients/participants provided their written informed consent to participate in this study. Written informed consent was obtained from the individual(s) for the publication of any potentially identifiable images or data included in this article.

Author contributions

FP and ZZ performed the study and wrote the manuscript. FP and ZZ made substantial contributions to conception and design of the study. ZS and YY were responsible for the design of the study. YY and WW analyzed the study data. JF and FC assisted with the statistical analysis. YY and FC critically revised the manuscript, provided final approval of the version to be published and made substantial contributions to conception and design. All authors contributed to the article and approved the submitted version.

Funding

This work was supported by The National Natural Science Foundation of China (grant no. 82274559, 81904231).

Conflict of interest

The authors declare that the research was conducted in the absence of any commercial or financial relationships that could be construed as a potential conflict of interest.

Publisher's note

References

1. Trompeter A. Management of metastatic bone disease (MBD). *Injury* (2022) 53 (12):3869–71. doi: 10.1016/j.injury.2022.09.054

2. Kask G, Nieminen J, Parry MC, van Iterson V, Pakarinen TK, Ratasvuori M, et al. Revision rate of reconstructions in surgically treated diaphyseal metastases of bone. *Eur J Surg Oncol* (2019) 45(12):2424–30. doi: 10.1016/j.ejso.2019.05.021

3. Casadei R, Drago G, Di Pressa F, Donati D. Humeral metastasis of renal cancer: Surgical options and review of literature. *Orthop Traumatol Surg Res* (2018) 104 (4):533–8. doi: 10.1016/j.otsr.2018.03.009

4. Wedin R, Hansen BH, Laitinen M, Trovik C, Zaikova O, Bergh P, et al. Complications and survival after surgical treatment of 214 metastatic lesions of the humerus. *J Shoulder Elbow Surg* (2012) 21(8):1049–55. doi: 10.1016/j.jse.2011.06.019

5. Ricard MM, Stavropoulos NA, Nooh A, Ste-Marie N, Goulding K, Turcotte R. Intramedullary nailing versus plate osteosynthesis for humeral shaft metastatic lesions. *Cureus* (2021) 13(3):e13788. doi: 10.7759/cureus.13788

6. Zhao LM, Tian DM, Wei Y, Zhang JH, Di ZL, He ZY, et al. Biomechanical analysis of a novel intercalary prosthesis for humeral diaphyseal segmental defect reconstruction. *Orthop Surg* (2018) 10(1):23–31. doi: 10.1111/os.12368

7. Sakellariou VI, Mavrogenis AF, Babis GC, Soucacos PN, Magnissalis EA, Papagelopoulos PJ. Comparison of four reconstructive methods for diaphyseal defects of the humerus after tumor resection. *J Appl Biomech* (2012) 28(5):568–78. doi: 10.1123/jab.28.5.568

8. Pu F, Wu W, Jing D, Yu Y, Peng Y, Liu J, et al. Three-dimensional-printed titanium prostheses with bone trabeculae enable mechanical-biological reconstruction after resection of bone tumours. *Biomater Transl* (2022) 3(2):134–41. doi: 10.12336/biomatertransl.2022.02.005

9. Pu F, Zhang Z, Wang B, Liu J, Shao Z. En bloc resection and intercalary prosthesis implantation for the treatment of humeral diaphyseal bone metastases. *Int Orthop* (2021) 45(1):281–8. doi: 10.1007/s00264-020-04845-x

10. Huang HC, Hu YC, Lun DX, Miao J, Wang F, Yang XG, et al. Outcomes of intercalary prosthetic reconstruction for pathological diaphyseal femoral fractures secondary to metastatic tumors. *Orthop Surg* (2017) 9(2):221–8. doi: 10.1111/os.12327

11. McLynn RP, Ondeck NT, Grauer JN, Lindskog DM. What is the adverse event profile after prophylactic treatment of femoral shaft or distal femur metastases? *Clin Orthop Relat Res* (2018) 476(12):2381–8. doi: 10.1097/CORR.0000000000000489

12. Windhager R. CORR insights(®): Outcomes of a modular intercalary endoprosthesis as treatment for segmental defects of the femur, tibia, and humerus. *Clin Orthop Relat Res* (2016) 474(2):549–50. doi: 10.1007/s11999-015-4635-9

13. Lun DX, Hu YC, Yang XG, Wang F, Xu ZW. Short-term outcomes of reconstruction subsequent to intercalary resection of femoral diaphyseal metastatic tumor with pathological fracture: Comparison between segmental allograft and intercalary prosthesis. *Oncol Lett* (2018) 15(3):3508–17. doi: 10.3892/ol.2018.7804

14. Pitera T, Guzik G, Biega P, Tarczyńska M, Gawęda K. Assessment of physical performance and early treatment outcomes after implantation of modular prostheses of femoral and tibial shaft. *Ortop Traumatol Rehabil* (2019) 21(5):349–58. doi: 10.5604/01.3001.0013.5783

15. Benevenia J, Kirchner R, Patterson F, Beebe K, Wirtz DC, Rivero S, et al. Outcomes of a modular intercalary endoprosthesis as treatment for segmental defects of the femur, tibia, and humerus. *Clin Orthop Relat Res* (2016) 474(2):539–48. doi: 10.1007/s11999-015-4588-z

16. Ruggieri P, Mavrogenis AF, Bianchi G, Sakellariou VI, Mercuri M, Papagelopoulos PJ. Outcome of the intramedullary diaphyseal segmental defect fixation system for bone tumors. *J Surg Oncol* (2011) 104(1):83–90. doi: 10.1002/jso.21893

17. Sung YT, Wu JS. The visual analogue scale for rating, ranking and paired-comparison (VAS-RRP): A new technique for psychological measurement. *Behav Res Methods* (2018) 50(4):1694–715. doi: 10.3758/s13428-018-1041-8

18. Xu L, Li X, Wang Z, Xiong J, Wang S. Functional evaluation for patients with lower extremity sarcoma: application of the Chinese version of musculoskeletal tumor society scoring system. *Health Qual Life Outcomes* (2017) 15(1):107. doi: 10.1186/s12955-017-0685-x

19. Jones CW, Shatrov J, Jagiello JM, Millington S, Hong A, Boyle R, et al. Clinical, functional and radiological outcomes of extracorporeal irradiation in limb salvage surgery for bone tumours. *Bone Joint J* (2017) 99-B(12):1681–8. doi: 10.1302/0301-620X.99B12.BJJ-2016-0462.R2

20. Schag CC, Heinrich RL, Ganz PA. Karnofsky performance status revisited: reliability, validity, and guidelines. *J Clin Oncol* (1984) 2(3):187–93. doi: 10.1200/JCO.1984.2.3.187

21. Chung YL, Mitchell HL, Houssien DA, Al-Mahrouki H, Carr AJ, Scott DL. A comparative study of outcome in myositis and other musculoskeletal disorders assessed using the Nottingham health profile. *Clin Exp Rheumatol* (2001) 19(4):447–50.

22. Szczerba P, Guzik G, Bohatyrewicz A, Kotrych D. Bone diaphysis metastases, the ways and results of surgical treatment saving the joints. *Ortop Traumatol Rehabil* (2019) 21(2):107–15. doi: 10.5604/01.3001.0013.1914

23. Aponte-Tinao L, Farfalli GL, Ritacco LE, Ayerza MA, Muscolo DL. Intercalary femur allografts are an acceptable alternative after tumor resection. *Clin Orthop Relat Res* (2012) 470(3):728–34. doi: 10.1007/s11999-011-1952-5

24. Li J, Wang Z, Guo Z, Chen GJ, Fu J, Pei GX. The use of allograft shell with intramedullary vascularized fibula graft for intercalary reconstruction after diaphyseal resection for lower extremity bony malignancy. *J Surg Oncol* (2010) 102(5):368–74. doi: 10.1002/jso.21620

25. Vijayan S, Bartlett W, Lee R, Ostler P, Blunn GW, Cannon SR, et al. Use of irradiated autologous bone in joint sparing endoprosthetic femoral replacement tumor surgery. *Indian J Orthop* (2011) 45(2):161–7. doi: 10.4103/0019-5413.77137

26. Puri A, Byregowda S, Gulia A, Patil V, Crasto S, Laskar S. Reconstructing diaphyseal tumors using radiated (50 Gy) autogenous tumor bone graft. *J Surg Oncol* (2018) 118(1):138–43. doi: 10.1002/jso.25092

27. Lesensky J, Prince DE. Distraction osteogenesis reconstruction of large segmental bone defects after primary tumor resection: pitfalls and benefits. *Eur J Orthop Surg Traumatol* (2017) 27(6):715–27. doi: 10.1007/s00590-017-1998-5

28. Zekry KM, Yamamoto N, Hayashi K, Takeuchi A, Alkhooly AZA, Abd-Elfattah AS, et al. Reconstruction of intercalary bone defect after resection of malignant bone tumor. *J Orthop Surg (Hong Kong)* (2019) 27(1):2309499019832970. doi: 10.1177/2309499019832970

29. Weichman KE, Dec W, Morris CD, Mehrara BJ, Disa JJ. Lower extremity osseous oncologic reconstruction with composite microsurgical free fibula inside massive bony allograft. *Plast Reconstr Surg* (2015) 136(2):396–403. doi: 10.1097/PRS.0000000000001463

30. Pesenti S, Peltier E, Pomero V, Authier G, Roscigni L, Viehweger E, et al. Knee function after limb salvage surgery for malignant bone tumor: Comparison of megaprosthesis and distal femur allograft with epiphysis sparing. *Int Orthop* (2018) 42(2):427–36. doi: 10.1007/s00264-017-3608-x

31. Aurégan JC, Pietton R, Bégué T, Anract P, Biau D. Effect of anatomic site and irradiation on the rates of revision and infection of allograft-prosthesis composites after resection of a primary bone tumor: A meta-analysis. *Arch Orthop Trauma Surg* (2016) 136(10):1371–80. doi: 10.1007/s00402-016-2549-y

32. Yi C, Zheng J, Li R, Lan Y, He M, Lai J, et al. Preliminary proposal: A classification system for reconstruction with autologous femoral head after periacetabular tumors resection. *J Orthop Surg Res* (2021) 16(1):119. doi: 10.1186/s13018-021-02275-y

33. Lawal YZ, Garba ES, Ogirima MO, Dahiru IL, Maitama MI, Abubakar K, et al. Use of non-vascularized autologous fibula strut graft in the treatment of segmental bone loss. *Ann Afr Med* (20181) 10(1):25–8. doi: 10.4103/1596-3519.76571

34. Li Y, Yang Y, Huang Z, Shan H, Xu H, Niu X. Bone defect reconstruction with autologous bone inactivated with liquid nitrogen after resection of primary limb malignant tumors: An observational study. *Med (Baltimore)* (2020) 99(24):e20442. doi: 10.1097/MD.0000000000020442

35. Yu XC, Xu SF, Xu M, Liu XP, Song RX, Fu ZH. Alcohol-inactivated autograft replantation with joint preservation in the management of osteosarcoma of the distal femur: A preliminary study. *Oncol Res Treat* (2014) 37(10):554–60. doi: 10.1159/000367799

36. Verdiyev V, Verdiyev F. Application of distraction osteogenesis in managing bone cysts. *J Orthop Traumatol* (2014) 15(2):103–9. doi: 10.1007/s10195-013-0272-9

37. Zhao J, Yu XC, Xu M, Zheng K, Hu YC, Wang F, et al. Intercalary prosthetic reconstruction for pathologic diaphyseal humeral fractures due to metastatic tumors: Outcomes and improvements. *J Shoulder Elbow Surg* (2018) 27(11):2013–20. doi: 10.1016/j.jse.2018.03.027

38. Zheng K, Yu XC, Hu YC, Shao ZW, Xu M, Wang BC, et al. Outcome of segmental prosthesis reconstruction for diaphyseal bone tumors: A multi-center retrospective study. *BMC Cancer* (2019) 19(1):638. doi: 10.1186/s12885-019-5865-0

39. Ma XL, Wang DB, Ma JX, Wang Y, Sun L, Lu B, et al. Custom-made prosthesis for reconstruction after radical resection for chondrosarcoma of manubrium. *Orthop Surg* (2018) 10(3):272–5. doi: 10.1111/os.12388

40. Ahlmann ER, Menendez LR. Intercalary endoprosthetic reconstruction for diaphyseal bone tumours. *J Bone Joint Surg Br* (2006) 88(11):1487–91. doi: 10.1302/0301-620X.88B11.18038

41. Damron TA, Leerapun T, Hugate RR, Shives TC, Sim FH. Does the second-generation intercalary humeral spacer improve on the first? *Clin Orthop Relat Res* (2008) 466(6):1309–17. doi: 10.1007/s11999-008-0246-z

42. Sewell MD, Hanna SA, McGrath A, Aston WJ, Blunn GW, Pollock RC, et al. Intercalary diaphyseal endoprosthetic reconstruction for malignant tibial bone tumours. *J Bone Joint Surg Br* (2011) 93(8):1111–7. doi: 10.1302/0301-620X.93B8.25750

43. McGrath A, Sewell MD, Hanna SA, et al. Custom endoprosthetic reconstruction for malignant bone disease in the humeral diaphysis. *Acta Orthop Belg* (2011) 77(2):171–9.

44. Abudu A, Carter SR, Grimer RJ. The outcome and functional results of diaphyseal endoprostheses after tumour excision. *J Bone Joint Surg Br* (1996) 78 (4):652–7. doi: 10.1302/0301-620X.78B4.0780652

45. Chen F, Pu F. Safety of denosumab versus zoledronic acid in patients with bone metastases: A meta-analysis of randomized controlled trials. *Oncol Res Treat* (2016) 39(7-8):453–9. doi: 10.1159/000447372

46. Zhang Z, Pu F, Shao Z. The skeletal-related events of denosumab versus zoledronic acid in patients with bone metastases: A meta-analysis of randomized controlled trials. *J Bone Oncol* (2017) 9:21–4. doi: 10.1016/j.jbo.2017.09.003

47. Kimura T. Multidisciplinary approach for bone metastasis: A review. *Cancers (Basel)* (2018) 10(6):156. doi: 10.3390/cancers10060156

frontiers | Frontiers in Oncology

TYPE Original Research
PUBLISHED 05 May 2023
DOI 10.3389/fonc.2023.1129658

OPEN ACCESS

EDITED BY
Wenwen Zhang,
Nanjing First Hospital, Nanjing Medical University, China

REVIEWED BY
Kunal Bharat Gala,
Tata Memorial Hospital, India
Teresa Somma,
Federico II University Hospital, Italy

*CORRESPONDENCE
Shengji Yu
zlyygk@163.com

RECEIVED 22 December 2022
ACCEPTED 24 April 2023
PUBLISHED 05 May 2023

CITATION
Wang L, Lu M, Zhang X, Zhao Z, Li X, Liu T, Xu L and Yu S (2023) Risk factors for pulmonary cement embolism after percutaneous vertebroplasty and radiofrequency ablation for spinal metastases.
Front. Oncol. 13:1129658.
doi: 10.3389/fonc.2023.1129658

Risk factors for pulmonary cement embolism after percutaneous vertebroplasty and radiofrequency ablation for spinal metastases

Luqiang Wang[1], Ming Lu[2], Xinxin Zhang[1], Zhenguo Zhao[1], Xiaoyang Li[1], Ting Liu[1], Libin Xu[1] and Shengji Yu[1]*

[1]Department of Orthopedics, National Cancer Center/National Clinical Research Center for Cancer/Cancer Hospital, Chinese Academy of Medical Sciences and Peking Union Medical College, Beijing, China, [2]Department of Endocrinology, Beijing Tongren Hospital, Capital Medical University, Beijing, China

Objective: Pulmonary cement embolism is a rare but underestimated complication of vertebroplasty due to the relative lack of study and examination. This study aims to investigate the incidence of pulmonary cement embolism in patients with spinal metastasis who undergo PVP with RFA and to analyze the relative risk factors.

Methods: A total of 47 patients were retrospectively included and classified into pulmonary cement embolism (PCE) group and non-pulmonary cement embolism (NPCE) group by comparing pre- and postoperative pulmonary CT scan images. The demographic and clinical information of the patients was obtained. Demographic data in the two groups were compared using the chi-square test for qualitative data and the unpaired t test for quantitative data. Multiple logistic regression analysis was used to identify risk factors related to pulmonary cement embolism.

Results: Pulmonary cement embolism was detected in 11 patients (23.4%), and all patients were asymptomatic and followed up regularly. Risk analysis showed that multiple segments (≥3, p=0.022), thoracic vertebrae (p=0.0008), and unipedicular puncture approach (p=0.0059) were risk factors for pulmonary cement embolism. There was a high incidence of pulmonary cement embolism if bone cement leaked into the para vertebral venous plexus in the thoracic vertebra (p<0.0001). Vein leakage of cement was related to the integrity of the vertebral cortex.

Conclusion: The number of involved vertebrae, lesion location, and puncture approach are independent risk factors for pulmonary cement embolism. There was a high incidence of pulmonary cement embolism if bone cement leaked into the para vertebral venous plexus in the thoracic vertebra. Surgeons should consider these factors when formulating therapeutic strategies.

KEYWORDS

spinal metastases, pulmonary cement embolism, PVP, RFA - radiofrequency ablation, cement vein leakage

Introduction

The spine is the third common site of metastasis, following the lung and the liver (1). It has been reported that approximately 60–70% of patients with systemic cancer will have spinal metastasis (2). Spinal metastases can cause spinal instability, pathological fractures and spinal cord compression, all of which severely affect the quality of life of patients, shortening their lifespans (3). With advancements in cancer treatment, including radiotherapy, molecular targeted therapy, and immunotherapy, the survival rate of cancer patients has greatly improved, which amplifies the problems caused by spinal metastases (4).

Minimally invasive techniques have shown great advantages in the treatment of spinal metastases without causing severe neurological deficits (5). Among these techniques, percutaneous vertebroplasty (PVP) is most commonly used. It involves the percutaneous injection of an acrylic cement, polymethylmethacrylate (PMMA), into the vertebrae under image guidance (6). Vertebroplasty can relieve pain by stabilizing the compromised vertebrae, and the pain alleviation rate has been reported to be up to 70-94% (7–9). However, vertebroplasty has a very limited effect on the control of tumor progression (10).

Radiofrequency ablation (RFA) is another minimally invasive treatment for spinal metastases. It focuses a high-frequency alternating current through a needle electrode into surrounding tissues under image guidance, resulting in friction heating and tissue necrosis (11). RFA was first applied in the musculoskeletal system to treat osteoid osteoma in 1992 (12), and now it has been widely used to treat spinal metastases (13). The combined use of vertebroplasty and RFA has been proven to be safe and effective in treating spinal metastases for stabilisation and pain relief (14, 15).

Pulmonary cement embolism (PCE) is a rare complication of vertebroplasty. The incidence is reported to vary from 0.3% to 28.6% in patients with osteoporosis fracture who have undergone PVP or PKP (16–21). RFA is thought to decrease the risk of PCE (15, 22, 23). It cause thrombosis of the venous plexus, which may prevent embolization events during cement injection (22, 24, 25). An animal study found that a layer of dense cord can be formed at the edge of the tumor after RFA, and this biomembrane barrier can prevent bone cement leakage into the spinal canal during PVP (26). However, there is no related research on PCE in spinal metastatic patients following PVP and RFA.

In this study, we report our experience with vertebroplasty and RFA in the treatment of spinal metastases and analyze the risk factors for PCE following the operation, aiming to help develop therapeutic strategies and prevent this complication.

Materials and methods

Basic information

Spinal metastatic patients treated in the Department of Orthopedics of the Cancer Hospital of the Chinese Academy of Medical Science between February 2021 and February 2022 were retrospectively enrolled, and 47 patients were included in this analysis. All patients gave written informed consent, and the study was approved by the ethics board committee of the hospital.

The demographic and clinical information of patients were obtained from electronic medical records, including age, sex, diagnosis, and involved vertebrae. The visual analog scale (VAS) score (0 = no pain, 10 = severe pain) was recorded to evaluate pain intensity. The Spinal Instability Neoplastic Score (SINS) was calculated per published guidelines (27). Plain radiographs and CT scans of the corresponding vertebrae were obtained before and after the operation. If patients received systemic treatment (chemotherapy, targeted therapy, immunotherapy, endocrinotherapy, bone-protecting agents, and so on) or radiation before surgery was also recorded.

Inclusion criteria and contraindications

The enrollment criteria included the following: i) diagnosis of metastatic cancer; ii) clinical and imaging evidence (MRI or CT) of vertebral metastases in the cervical, thoracic, lumbar or sacral segments; iii) pulmonary CT before and after the operation; iv) expected survival time >3 months; and v) PVP combined with RFA.

Contraindications for the procedure included: i) clinical signs of spinal cord compression or cauda equina syndrome; ii) fractures with epidural involvement and contact with spinal cord or nerve roots; iii) the lesions close to the vital structures such as nerves, spinal cord, blood vessels; and iv) local infection at the puncture site or septicemia. Relative contraindications included vertebral body height reduced more than 75%, and transient chemotherapy –induced hematologic anomalies, including leukopenia ($<2.5\times10^9$/L), thrombocytopenia ($<100.0\times10^9$/L) and elevated international normalized ratio >1.5.

Operative procedures

The patients were placed in the prone position with conscious sedation. A puncture trocar (Zhongshan Shiyitang Medical Equipment Co., Ltd, China) was inserted from the vertebral pedicle to the anterior one-third of the vertebral body under the guidance of C-arm fluoroscopy (Siemens Healthcare, Munich, Germany). The trocar was removed, and a biopsy device (STERYLAB, Italy) was placed to obtain the bone fragments for pathology. Then, a monopole RFA electrode (17G) (MedSphere Shanghai, China) was inserted through the cannula. RFA was conducted for 10 min at a temperature ranging from 80°C to 100°C. The electrode was removed, and prepared high-viscosity polymethyl methacrylate (PMMA) bone cement (Weigao Medical GmbH, China) was injected into the vertebral body under intermittent fluoroscopic examination from the lateral plane. Injection was stopped when substantial resistance was met, or when the PMMA cement reached the posterior margin of the vertebral body, or cement extravasation was identified through fluoroscopy (Supplementary Figure 1). For multi-level cases,

single cement kit was used for each level. 40mg methylprednisolone was given before radiofrequency ablation.

Postoperative management

The patients were sent back to the ward after the operation and made to lie in bed for 6 hours, then could move freely, but a spinal brace was advised. Vital signs as well as sensory motor functions of the lower limbs were closely monitored. Plain radiographs and CT scans were performed before discharge.

The patients were followed up every 3 months for at least 9 months. Pulmonary CT scans were not necessary unless the patient complained of pulmonary-related symptoms. However, patients with spinal metastasis are always hospitalized several times for radiotherapy, chemotherapy, or other treatments, and pulmonary CT scans are essential for hospitalization. PCE was confirmed by comparing pre- and postoperative pulmonary images.

Statistical analysis

Statistical analysis was performed with Prism 8 software (GraphPad Software, San Diego, CA, USA). All measurement data are described as the mean and standard deviation (SD). Demographic data in both groups were compared using the chi-square test for qualitative data and the unpaired t test for quantitative data. Multiple logistic regression analysis was carried out to identify risk factors that were significantly related to PCE resulting from cement leakage. A p value < 0.05 was considered statistically significant.

Results

Baseline characteristics of the patients

PVP and RFA were performed for 47 patients with a total of 84 segments, including 34 thoracic vertebrae and 50 lumbar vertebrae (Table 1). The patients were 19 males and 28 females with a mean age of 59.9 ± 1.6 years (range 34 to 81 years). The preoperative VAS score was 5.1 ± 0.3, and the preoperative SINS score was 9.6 ± 0.4. Among the 47 patients, 42 patients showed osteolytic lesions, and 5 patients exhibited osteoblastic lesions. Operations were performed on one segment in 27 patients, two segments in 11 patients, three segments in 7 patients, four segments in 1 patient, five segments in 2 patients, and six segments in 1 patient. 28 patients received systemic treatment before surgery, and 14 vertebral levels in 8 patients got pre-operative radiation treatment. Among the 84 vertebrae, pathologic compression fracture was found in 35 segments, and the other 49 segments had no compression fracture with obvious imaging abnormalities. The amount of cement injected per lesion ranged from 1.5 to 12 ml with a mean volume of 6.1 ± 0.2 ml. The postoperative pathological diagnoses of the spinal tumors confirmed that they were all metastatic tumors: 12 from lung cancer, 12 from breast cancer, 5 from kidney cancer, 4 from prostate cancer, 2 from bile duct cancer, 2 from thyroid cancer, 2 from gastric cancer, 1 from liver cancer, 1 from ovarian cancer, 1 from cervical cancer, 1 from esophageal cancer, 1 from soft tissue Ewing's sarcoma and 3 from unknown malignancies (Table 2).

TABLE 1 Baseline characteristics of the patients.

	n (%)
Number of patients	47
Age (years)	59.9 ± 1.6
Sex	
Male	19 (40.4)
Female	28 (59.6)
VAS	5.1 ± 0.3
SINS	9.6 ± 0.4
Systermic treatment	
Yes	28 (59.6)
No	19 (40.4)
Preoperative radiation	
Yes	8 (17.0)
No	39 (83.0)
Spine lesion type	
Osteolytic	42 (89.4)
Osteoblastic	5 (10.6)
Segment number	
Single	27 (57.4)
Two	11 (23.4)
Three	5 (10.6)
Four	1 (2.1)
Five	2 (4.3)
Xix	1 (2.1)
Total number of vertebrae affected	84
Thoracic vertebra	34 (40.5)
Lumbar vertebra	50 (59.5)
Vertebrae with pathological fracture	
Yes	35 (41.7)
No	49 (58.3)
PMMA volume per level (ml)	6.1 ± 0.2

Analysis of the risk factors for pulmonary cement embolism

According to the detection of postoperative pulmonary CT scans, the patients were divided into pulmonary cement embolism group (PCE group) and non-pulmonary cement

TABLE 2 Pathologic diagnosis of 47 patients.

Primary tumor	n (%)
lung cancer	12 (25.5)
breast cancer	12 (25.5)
kidney cancer	5 (10.6)
prostate cancer	4 (8.5)
bile duct cancer	2 (4.3)
thyroid cancer	2 (4.3)
gastric cancer	2 (4.3)
liver cancer	1 (2.1)
cervical cancer	1 (2.1)
ovarian cancer	1 (2.1)
esophageal cancer	1 (2.1)
Ewing's sarcoma	1 (2.1)
unclear	3 (6.4)
Total	47

embolism group (NPCE group). The presence of cement in the pulmonary arteries was identified in 11 patients (incidence rate 23.4%), including 5 males and 6 females, with a mean age of 55.7 ± 3.9 years. There were 36 patients in the NPCE group, including 14 males and 22 females, with a mean age of 60.5 ± 1.6 years (Table 3).

All the patients in the PCE group were asymptomatic. No dyspnea, chest pain, cough, tachycardia, or hypoxia was observed. The patients were followed up regularly. There were no critical patients who needed surgical treatment or died. In all 11 patients, pulmonary emboli were located in the subsegmental or peripheral arteries, and no central pulmonary artery embolism was found (Figure 1).

No significant differences were found in age, sex, preoperative VAS scores, SINS scores, or if got systemic treatment between the patients in the NPCE group and PCE group (Table 3). Among the 11 PCE patients, 9 patients showed osteolytic destruction, and the other 2 patients showed osteoblastic lesions, which was not significantly different from the NPCE group. However, 4 patients (36.4%) had multiple segments (≥3) involved in the PCE group, while only 8.3% of patients (3 patients) had multiple segment involvement in the NPCE group, which was a significant difference (p=0.022).

We then set the individual vertebrae as the study object. Lesion location, cortex integrity, compression fracture, preoperative radiation, vein leakage, and PMMA injection volume in vertebrae of the two groups were analyzed (Table 4). The 11 PCE patients had 25 segments involved in total, including 17 thoracic vertebrae and 8 lumbar vertebrae. The NPCE patients had 59 segments in total, including 17 thoracic vertebrae and 42 lumbar vertebrae. The results revealed that patients with thoracic vertebrae treated had a greater chance of developing pulmonary cement embolism (p=0.0008). Patients who had cement vein leakage during surgery also had a significantly increased risk compared with those who did not (p=0.017), especially when leakage occurred in the thoracic vertebrae (p<0.001). The two groups did not show significant differences in cortex integrity, compression fracture, of if got preoperative radiation.

TABLE 3 Comparison of risk factors for PCE between patients of two groups.

	NPCE	PCE	p
Number of patients	36	11	
Age (years)	60.5 ± 1.6	55.7 ± 3.9	0.203
Sex			0.698
Male	14	5	
Female	22	6	
VAS	5.1 ± 0.3	5.1 ± 0.6	0.994
SINS	9.7 ± 0.5	9.1 ± 1.0	0.542
Systermic treatment			0.698
Yes	22	6	
No	14	5	
Spine lesion type			0.354
Osteolytic	33	9	
Osteoblastic	3	2	
Segment number			0.022
≥3	3	4	
≤2	33	7	

Parameters related to technical characteristics

The incidence of complications was closely related to the operators' skills. The parameters related to technical characteristics including operative approach, PMMA volume per level, and operating time were analyzed. Among the 25 segments of PCE group, 80% were treated through unipedicular approach, while the proportion is 47.5% in NPCE group (p=0.006) (Table 5). As the volume of thoracic vertebrae was smaller than lumbar vertebrae, we separated volume on injection reporting between thoracic and lumbar vertebrae. However there were no significant difference between NPCE and PCE groups. There was no difference as to operating time of two groups either.

Relationship of vertebral cortex disruption to vein leakage of cement

Previous data showed that there was a high incidence of PCE if bone cement leaked into the paravertebral venous plexus. We next analyzed the risk factors related to vein leakage of cement. Among

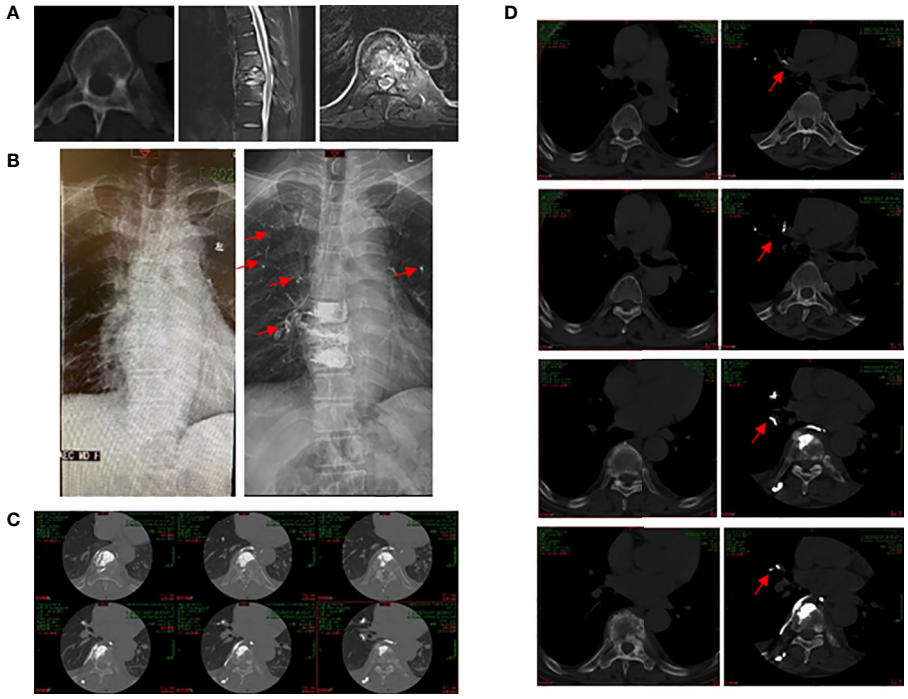

FIGURE 1
51 years old male patient with spinal metastasis from lung cancer underwent PKP and RFA. **(A)** Pre-operative radiographs showed an obvious lesion of eighth thoracic vertebral body. **(B)** Pre-operative (left) and post-operative (right) X-ray images of the chest. Cement pulmonary embolus (red arrows) were found in both lungs after operation. **(C)** Post-operative CT scan illustrated that the cement embolus leaked into the perivertebral venous system. **(D)** Pre-operative (left) and post-operative (right) CT scan images. Red arrows showed the cement embolus.

the 47 patients with 84 vertebrae, 37 vertebrae had vein leakage of bone cement (leakage group, 44%), and the other 47 segments did not have leakage (nonleakage group, 56%). Vertebra integrity, compression fracture, lesion type, location, and PMMA volume were analyzed (Table 6). The results showed no significant differences in lesion type, location, or PMMA volume between the two groups. However, 75.7% of segments (28) in the leakage group showed a disrupted cortex, and only 46.8% of segments (22) in the nonleakage group showed a significant difference (p=0.008).

Discussion

Pulmonary cement embolism is a rare complication of cement augmentation, first reported by Padovani et al. (28) in 1999. Several retrospective studies reported that the incidence of PCE on osteoporosis patients varied from 0.3% to 28.6% (16–21). Spinal tumors are another surgical indication for vertebroplasty, especially spinal metastasis. The risk of PCE in patients with spinal metastasis is thought to be increased (29). Asem analyzed 78 cancer patients with malignant vertebral fractures who underwent vertebroplasty, PCE was detected in 10 (12.8%) patients (30). To my knowledge, we first reported the incidence of PCE in patients with spinal metastasis who undergo PVP with RFA. In our study, we analyzed 84 segments in 47 spinal tumor patients who underwent treatment. The incidence of PCE was 23.4% (11/47), which is higher than Asem's study.

Risk factor analysis can help to reduce the incidence of PCE. Previous studies showed that number of treated vertebral levels, fracture location and operation timing, amount of PMMA injected were thought to be associated with PCE (20, 31). Asem's study showed that multiple myeloma is associated with the highest risk, and no difference in incidence was observed between patients with osteoporotic or malignant vertebral fractures (30).

Our analysis revealed that involvement of a larger number of vertebrae was a factor and that thoracic vertebrae were associated with PCE, which is consistent with previous study. This is readily comprehensible. Thoracic vertebrae are closer to the heart and lung. Operating on a larger number of involved vertebrae will take more time and more PMMA cement will need to be injected, which is challenging not only for the patients but also for the surgeons. Therefore, operating on more than three segments at a time is not recommended (20). We also found the unipedicular approach has a high rate of PCE. However, a previous meta-analysis showed the incidences of cement leakage were similar between the bilateral PVA and unilateral PVA groups (32), which is contrary to our results. In our experience, in order to get the same stabilization effect, we usually injected more volume of bone cement through unipedicular approach compared to the cement volume of each side through bipedicular approach. The injection pressure of each puncture channel may also be high, which could induce cement

TABLE 4 Risk factors for PCE in terms of individual vertebra.

	NPCE	PCE	p
Total number of vertebrae	59	25	
Lesion location			0.0008
Thoracic vertebra	17	17	
Lumbar vertebra	42	8	
Cortex integrity			0.586
Disrupted	34	16	
Intact	25	9	
Compression fracture			0.098
Yes	28	7	
No	31	18	
Preoperative radiation			0.24
Yes	8	6	
No	51	19	
Vein leakage			0.017
Yes	21	16	
No	38	9	
Vein leakage location			<0.0001
Thoracic vertebra	0	15	
Lumbar vertebra	21	1	

TABLE 5 Parameters related to technical characteristics.

	NPCE	PCE	p
Operative approach			0.006
Unipedicular	28	20	
Bipedicular	31	5	
PMMA volume per level (ml)			
Thoracic vertebra	5.2 ± 0.7	5.2 ± 0.4	0.999
Lumbar vertebra	6.6 ± 0.3	6.9 ± 0.6	0.682
Operating time per level (min)	77.1 ± 3.0	71.3 ± 3.2	0.256

leakage. Definitely this result was related to the operators' experience, and the explanation was just a hypothesis. We need to identify it in the future.

Our results also revealed that there was a high incidence of PCE if bone cement leaked into the paravertebral venous plexus, especially when occurred in the thoracic vertebrae. Risk factors for vein leakage of cement have been well studied, including involved segments and surgical skills (33–36). Our data indicated that vertebral cortex integrity is related to vein leakage of cement. If the bone cortex is disrupted, it is easier for the cement to pass through the cortex or into the paravertebral venous plexus.

TABLE 6 Analysis of the risk factors for vein leakage of cement.

	Nonleakage	Leakage	p
Total number of vertebrae	47	37	
Cortex integrity			0.008
Disrupted	22	28	
Intact	25	9	
Spine lesion type			
Osteolytic	41	27	0.098
Osteoblastic	6	10	
PMMA volume per level (ml)	7.8 ± 0.3	6.4 ± 0.3	0.2
Lesion location			0.183
Thoracic vertebra	22	12	
Lumbar vertebra	25	25	

All patients were followed up for at least 9 months, and no patients developed severe pulmonary embolism. Pulmonary CT scans showed that the emboli were stable and did not enlarge. For PCE, there are still no standard treatment guidelines (37). Asymptomatic patients may need close clinical monitoring (38). Some scholars have suggested that anticoagulation should be used to prevent progressive pulmonary artery occlusion; however, there is no consensus on the specific timing anticoagulant treatment (39, 40). For PCE patients with severe symptoms, surgical removal of the embolus and anticoagulant therapy are recommended (41–43).

There are several limitations to this study. The primary limitation is that this was a single-center, retrospective study, including a certain selection bias. Some patients did not undergo postoperative pulmonary CT, which may have led to the underestimation of asymptomatic patients. A secondary limitation is that all operations were performed by the surgical team, operators' skills play a pivotal role in the development of PCE, we did not analyze the different operators or their operative habits.

Conclusion

Our results showed that the number of involved vertebrae, lesion location, and puncture approach are independent risk factors for PCE. There was a high incidence of PCE if bone cement leaked into the para vertebral venous plexus in the thoracic vertebra. The relative risk factors should be fully considered when implementing therapeutic strategies to prevent the occurrence of PCE.

Data availability statement

The raw data supporting the conclusions of this article will be made available by the authors, without undue reservation.

Ethics statement

The studies involving human participants were reviewed and approved by National Cancer Center/National Clinical Research Center for Cancer/Cancer Hospital, Chinese Academy of Medical Sciences and Peking Union Medical College. The patients/participants provided their written informed consent to participate in this study. Written informed consent was obtained from the individual(s) for the publication of any potentially identifiable images or data included in this article.

Author contributions

The authors' contributions to this study were as follows: SY and LW contributed to the study design. LW, ML contributed to the data collection. LW, XZ, ZZ, XL, TL and LX contributed to the statistical analysis. LW and ML played the main role in writing the manuscript. All authors contributed to the article and approved the submitted version.

Funding

This work was supported by the National Natural Science Foundation of China [No. 82003397, No. 82100829, No. 82272964]; the CAMS Innovation Fund for Medical Sciences (CIFMS) [2021-I2MI2 MC&T-B-054].

Conflict of interest

The authors declare that the research was conducted in the absence of any commercial or financial relationships that could be construed as a potential conflict of interest.

Publisher's note

All claims expressed in this article are solely those of the authors and do not necessarily represent those of their affiliated organizations, or those of the publisher, the editors and the reviewers. Any product that may be evaluated in this article, or claim that may be made by its manufacturer, is not guaranteed or endorsed by the publisher.

Supplementary material

The Supplementary Material for this article can be found online at: https://www.frontiersin.org/articles/10.3389/fonc.2023.1129658/full#supplementary-material

References

1. Witham TF, Khavkin YA, Gallia GL, Wolinsky JP, Gokaslan ZL. Surgery insight: current management of epidural spinal cord compression from metastatic spine disease. *Nat Clin Pract Neurol* (2006) 2(2):87–94. doi: 10.1038/ncpneuro0116

2. Shah LM, Salzman KL. Imaging of spinal metastatic disease. *Int J Surg Oncol* (2011) 2011:769753. doi: 10.1155/2011/769753

3. Benhabib H, Meirovich H, David E. Evolving role of minimally invasive techniques in the management of symptomatic bone metastases. *Curr Opin Support Palliat Care* (2021) 15(2):91–8. doi: 10.1097/SPC.0000000000000548

4. Jaipanya P, Chanplakorn P. Spinal metastasis: narrative reviews of the current evidence and treatment modalities. *J Int Med Res* (2022) 50(4):3000605221091665. doi: 10.1177/03000605221091665

5. Flynn SC, Eli IM, Ghogawala Z, Yew AY. Minimally invasive surgery for spinal metastasis: a review. *World Neurosurg* (2022) 159:e32–e9. doi: 10.1016/j.wneu.2021.11.097

6. Georgy BA. Metastatic spinal lesions: state-of-the-Art treatment options and future trends. *AJNR Am J Neuroradiol* (2008) 29(9):1605–11. doi: 10.3174/ajnr.A1137

7. Kobayashi T, Arai Y, Takeuchi Y, Nakajima Y, Shioyama Y, Sone M, et al. Phase I/Ii clinical study of percutaneous vertebroplasty (Pvp) as palliation for painful malignant vertebral compression fractures (Pmvcf): jivrosg-0202. *Ann Oncol* (2009) 20(12):1943–7. doi: 10.1093/annonc/mdp242

8. Lee B, Franklin I, Lewis JS, Coombes RC, Leonard R, Gishen P, et al. The efficacy of percutaneous vertebroplasty for vertebral metastases associated with solid malignancies. *Eur J Cancer* (2009) 45(9):1597–602. doi: 10.1016/j.ejca.2009.01.021

9. Chen G, Luo ZP, Zhang H, Nalajala B, Yang H. Percutaneous kyphoplasty in the treatment of painful osteoblastic metastatic spinal lesions. *J Clin Neurosci* (2013) 20(7):948–50. doi: 10.1016/j.jocn.2012.08.010

10. Wang F, Gu J, Xu C, Li G, Lv P. The combination of radiofrequency ablation and vertebroplasty shows advantages over single vertebroplasty in treating vertebral neoplastic lesions. *Skeletal Radiol* (2022) 51(3):565–71. doi: 10.1007/s00256-021-03788-7

11. Lencioni R, Della Pina C, Bartolozzi C. Percutaneous image-guided radiofrequency ablation in the therapeutic management of hepatocellular carcinoma. *Abdom Imaging* (2005) 30(4):401–8. doi: 10.1007/s00261-004-0254-8

12. Rosenthal DI, Alexander A, Rosenberg AE, Springfield D. Ablation of osteoid osteomas with a percutaneously placed electrode: a new procedure. *Radiology* (1992) 183(1):29–33. doi: 10.1148/radiology.183.1.1549690

13. Filippiadis D, Kelekis A. Percutaneous bipolar radiofrequency ablation for spine metastatic lesions. *Eur J Orthop Surg Traumatol* (2021) 31(8):1603–10. doi: 10.1007/s00590-021-02947-9

14. Zhao W, Wang H, Hu JH, Peng ZH, Chen JZ, Huang JQ, et al. Palliative pain relief and safety of percutaneous radiofrequency ablation combined with cement injection for bone metastasis. *Jpn J Clin Oncol* (2018) 48(8):753–9. doi: 10.1093/jjco/hyy090

15. Reyes M, Georgy M, Brook L, Ortiz O, Brook A, Agarwal V, et al. Multicenter clinical and imaging evaluation of targeted radiofrequency ablation (T-rfa) and cement augmentation of neoplastic vertebral lesions. *J neurointerv Surg* (2018) 10(2):176–82. doi: 10.1136/neurintsurg-2016-012908

16. Venmans A, Klazen CA, Lohle PN, van Rooij WJ, Verhaar HJ, de Vries J, et al. Percutaneous vertebroplasty and pulmonary cement embolism: results from vertos ii. *AJNR Am J Neuroradiol* (2010) 31(8):1451–3. doi: 10.3174/ajnr.A2127

17. Groen RJ, du Toit DF, Phillips FM, Hoogland PV, Kuizenga K, Coppes MH, et al. Anatomical and pathological considerations in percutaneous vertebroplasty and kyphoplasty: a reappraisal of the vertebral venous system. *Spine (Phila Pa 1976)* (2004) 29(13):1465–71. doi: 10.1097/01.brs.0000128758.64381.75

18. El Saman A, Kelm A, Meier S, Sander AL, Eichler K, Marzi I, et al. Intraoperative peep-ventilation during pmma-injection for augmented pedicle screws: improvement of leakage rate in spinal surgery. *Eur J Trauma Emerg Surg* (2013) 39(5):461–8. doi: 10.1007/s00068-013-0319-x

19. Hsieh MK, Kao FC, Chiu PY, Chen LH, Yu CW, Niu CC, et al. Risk factors of neurological deficit and pulmonary cement embolism after percutaneous vertebroplasty. *J Orthop Surg Res* (2019) 14(1):406. doi: 10.1186/s13018-019-1459-4

20. Zou D, Dong S, Du W, Sun B, Wu X. Risk factor analysis of pulmonary cement embolism during percutaneous vertebroplasty or kyphoplasty for osteoporotic vertebral compression fractures. *J Orthop Surg Res* (2021) 16(1):312. doi: 10.1186/s13018-021-02472-9

21. Guo H, Huang H, Shao Y, Qin Q, Liang D, Zhang S, et al. Risk factors for pulmonary cement embolism (Pce) after polymethylmethacrylate augmentation: analysis of 32 pce cases. *Neurospine* (2021) 18(4):806–15. doi: 10.14245/ns.2142616.308

22. David E, Kaduri S, Yee A, Chow E, Sahgal A, Chan S, et al. Initial single center experience: radiofrequency ablation assisted vertebroplasty and osteoplasty using a bipolar device in the palliation of bone metastases. *Ann Palliat Med* (2017) 6(2):118–24. doi: 10.21037/apm.2016.12.02

23. Georgy BA, Wong W. Plasma-mediated radiofrequency ablation assisted percutaneous cement injection for treating advanced malignant vertebral compression fractures. *AJNR Am J Neuroradiol* (2007) 28(4):700–5.

24. Munk PL, Rashid F, Heran MK, Papirny M, Liu DM, Malfair D, et al. Combined cementoplasty and radiofrequency ablation in the treatment of painful neoplastic lesions of bone. *J Vasc Interv Radiol* (2009) 20(7):903–11. doi: 10.1016/j.jvir.2009.03.035

25. Halpin RJ, Bendok BR, Sato KT, Liu JC, Patel JD, Rosen ST. Combination treatment of vertebral metastases using image-guided percutaneous radiofrequency ablation and vertebroplasty: a case report. *Surg Neurol* (2005) 63(5):469–74. doi: 10.1016/j.surneu.2004.04.025

26. Yu Z, Tian S, Wang W, Li Y, Wang Y. Biomembrane formation after radiofrequency ablation prevents bone cement extravasation during percutaneous vertebroplasty for treating vertebral metastases with posterior margin destruction: an animal study. *J Cancer Res Ther* (2020) 16(5):1082–7. doi: 10.4103/jcrt.JCRT_177_20

27. Fisher CG, DiPaola CP, Ryken TC, Bilsky MH, Shaffrey CI, Berven SH, et al. A novel classification system for spinal instability in neoplastic disease: an evidence-based approach and expert consensus from the spine oncology study group. *Spine (Phila Pa 1976)* (2010) 35(22):E1221–9. doi: 10.1097/BRS.0b013e3181e16ae2

28. Padovani B, Kasriel O, Brunner P, Peretti-Viton P. Pulmonary embolism caused by acrylic cement: a rare complication of percutaneous vertebroplasty. *AJNR Am J Neuroradiol* (1999) 20(3):375–7.

29. Geraci G, Lo Iacono G, Lo Nigro C, Cannizzaro F, Cajozzo M, Modica G. Asymptomatic bone cement pulmonary embolism after vertebroplasty: case report and literature review. *Case Rep Surg* (2013) 2013:591432. doi: 10.1155/2013/591432

30. Mansour A, Abdel-Razeq N, Abuali H, Makoseh M, Shaikh-Salem N, Abushalha K, et al. Cement pulmonary embolism as a complication of percutaneous vertebroplasty in cancer patients. *Cancer Imaging* (2018) 18(1):5. doi: 10.1186/s40644-018-0138-8

31. Bopparaju S, Varon J, Surani S. Pulmonary embolism with vertebral augmentation procedures. *Case Rep Pulmonol* (2013) 2013:785307. doi: 10.1155/2013/785307

32. Ma X, Sun H, Liu S, Sang L, Wang K, Dong Y, et al. Cement leakage in vertebral compression fractures between unilateral and bilateral percutaneous vertebral augmentation: a meta-analysis. *Turk Neurosurg* (2022). doi: 10.5137/1019-5149.JTN.37319-21.4

33. Lv B, Ji P, Fan X, Yuan J, Xu T, Yao X, et al. Clinical efficacy of different bone cement distribution patterns in percutaneous kyphoplasty: a retrospective study. *Pain Physician* (2020) 23(4):E409–E16.

34. Takahashi S, Sohgawa E, Suzuki A, Yamamoto A, Sasaki R, Tanaka K, et al. Percutaneous endovascular retrieval of Large cement leakage into the right atrium following cement-augmented pedicle screw instrumentation. *Spine Surg Relat Res* (2021) 5(6):446–9. doi: 10.22603/ssrr.2021-0011

35. Mueller JU, Baldauf J, Marx S, Kirsch M, Schroeder HW, Pillich DT. Cement leakage in pedicle screw augmentation: a prospective analysis of 98 patients and 474 augmented pedicle screws. *J Neurosurg Spine* (2016) 25(1):103–9. doi: 10.3171/2015.10.SPINE15511

36. Kim YJ, Lee JW, Park KW, Yeom JS, Jeong HS, Park JM, et al. Pulmonary cement embolism after percutaneous vertebroplasty in osteoporotic vertebral compression fractures: incidence, characteristics, and risk factors. *Radiology* (2009) 251(1):250–9. doi: 10.1148/radiol.2511080854

37. Schummer W, Schlonski O, Breuer M. Bone cement embolism attached to central venous catheter. *Br J Anaesth* (2014) 112(4):672–4. doi: 10.1093/bja/aet413

38. Krueger A, Bliemel C, Zettl R, Ruchholtz S. Management of pulmonary cement embolism after percutaneous vertebroplasty and kyphoplasty: a systematic review of the literature. *Eur Spine J* (2009) 18(9):1257–65. doi: 10.1007/s00586-009-1073-y

39. Tozzi P, Abdelmoumene Y, Corno AF, Gersbach PA, Hoogewoud HM, von Segesser LK. Management of pulmonary embolism during acrylic vertebroplasty. *Ann Thorac Surg* (2002) 74(5):1706–8. doi: 10.1016/s0003-4975(02)03962-0

40. Janssen I, Ryang YM, Gempt J, Bette S, Gerhardt J, Kirschke JS, et al. Risk of cement leakage and pulmonary embolism by bone cement-augmented pedicle screw fixation of the thoracolumbar spine. *Spine J* (2017) 17(6):837–44. doi: 10.1016/j.spinee.2017.01.009

41. Rothermich MA, Buchowski JM, Bumpass DB, Patterson GA. Pulmonary cement embolization after vertebroplasty requiring pulmonary wedge resection. *Clin Orthop Relat Res* (2014) 472(5):1652–7. doi: 10.1007/s11999-014-3506-0

42. Mills S, Pizones J, Merino Rueda LR, Talavera G, Sanchez-Marquez JM, Fernandez-Baillo N. Cardiac cement embolism after thoracic kyphoplasty: successful conservative treatment with 4-year follow-up. *Int J Spine Surg* (2022) 16(1):27–32. doi: 10.14444/8173

43. Bonardel G, Pouit B, Gontier E, Dutertre G, Mantzarides M, Goasguen O, et al. Pulmonary cement embolism after percutaneous vertebroplasty: a rare and nonthrombotic cause of pulmonary embolism. *Clin Nucl Med* (2007) 32(8):603–6. doi: 10.1097/RLU.0b013e3180a1ad5a

frontiers | Frontiers in Oncology

TYPE Original Research
PUBLISHED 05 May 2023
DOI 10.3389/fonc.2023.1145001

OPEN ACCESS

EDITED BY
Akshara Raghavendra,
University of Texas MD Anderson Cancer Center, United States

REVIEWED BY
K. Shilo,
The Ohio State University, United States
Lorenzo Belluomini,
University of Verona, Italy

*CORRESPONDENCE
Anne-Marie C. Dingemans
a.dingemans@erasmusmc.nl

RECEIVED 15 January 2023
ACCEPTED 21 April 2023
PUBLISHED 05 May 2023

CITATION
Brouns AJWM, Hendriks LEL, Robbesom-van den Berge IJ, Driessen AJHM, Roemen GMJM, van Herpen BLJ, Dekkers Z, Heitzer B, Leunissen DJG, Moonen L, Lunde R, Westenend M, van Driel M, Speel E-JM and Dingemans A-MC (2023) Association of RANKL and EGFR gene expression with bone metastases in patients with metastatic non-small cell lung cancer. *Front. Oncol.* 13:1145001. doi: 10.3389/fonc.2023.1145001

Association of RANKL and EGFR gene expression with bone metastases in patients with metastatic non-small cell lung cancer

Anita J.W.M. Brouns[1,2,3], Lizza E.L. Hendriks[2,3], Iris J. Robbesom-van den Berge[4], Annemariek J.H.M. Driessen[5], Guido M.J.M. Roemen[6], Britt L.J. van Herpen[6], Zoë Dekkers[6], Bas Heitzer[6], Daphne J.G. Leunissen[6], Laura Moonen[6], Ragnar Lunde[7], Marcel Westenend[8], Marjolein van Driel[4], Ernst-Jan M. Speel[6] and Anne-Marie C. Dingemans[2,3,9]*

[1]Department of Respiratory Medicine, Zuyderland, Geleen, Netherlands, [2]Department of Respiratory Medicine, Maastricht University Medical Center+, Maastricht, Netherlands, [3]Department of Pulmonary Diseases, GROW - School for Oncology and Reproduction, Maastricht University Medical Center, Maastricht, Netherlands, [4]Department of Internal Medicine, Erasmus MC, Rotterdam, Netherlands, [5]Department of Clinical Pharmacy and Toxicology, Maastricht University Medical Center+, Maastricht, Netherlands, [6]Department of Pathology, GROW-School for Oncology and Reproduction, Maastricht University Medical Center+, Maastricht, Netherlands, [7]Department of Respiratory Medicine, Laurentius Hospital, Roermond, Netherlands, [8]Department of Respiratory Medicine, Viecuri Medical Center, Venlo, Netherlands, [9]Department of Respiratory Medicine, Erasmus MC Cancer Institute, University Medical Center, Rotterdam, Netherlands

Introduction: Bone metastases are frequent in patients with non-small cell lung cancer (NSCLC). The receptor activator of Nuclear Factor κB (RANK)/RANK ligand (RANKL)/osteoprotegerin (OPG) pathway is important in bone metastases development. Furthermore, epidermal growth factor receptor (EGFR) signaling promotes osteoclast formation and stimulation. The understanding of the biological mechanism of bone metastases development might have implications for treatment strategies. Therefore, we studied whether there is an association between EGFR, RANKL, RANK and OPG gene expression in the tumor and presence of bone metastases in patients with NSCLC.

Methods: From an updated multicenter study, including patients with *EGFR* mutated (*EGFR+*), Kirsten rat sarcoma *(KRAS+)* and *EGFR/KRAS* wildtype metastatic NSCLC, all patients with available formalin-fixed paraffin-embedded (FFPE) tumor samples were selected. Ribonucleic Acid (RNA) was isolated from these samples and gene expressions of EGFR, RANKL, OPG and RANKL were determined *via* quantitative Polymerase Chain Reaction (qPCR). Data on demographics, histology and molecular subtyping, sample origin, presence of bone metastasis, SREs and bone progression were collected. Primary endpoint was relation between EGFR, RANK, RANKL, OPG gene expression, RANKL: OPG ratio and bone metastases.

Results: In 73/335 (32% *EGFR+*, 49% *KRAS+*, 19% *EGFR/KRAS* wildtype) samples from unique patients, gene expression analysis could be performed. Of these 73 patients, 46 (63%) had bone metastases at diagnosis or developed bone metastases during the disease course. No association was found between EGFR expression and presence of bone metastases. Patients with bone metastases had a significantly higher RANKL expression and RANKL: OPG ratio compared to those without. An increased RANKL: OPG ratio resulted in a 1.65x increased risk to develop bone metastases, especially in the first 450 days after diagnosis of metastatic NSCLC.

Conclusion: Increased RANKL gene expression and RANKL: OPG ratio, but not EGFR expression, was associated with presence of bone metastases. Additionally, an increased RANKL: OPG gene ratio was associated with a higher incidence of bone metastases development.

KEYWORDS

bone metastases, receptor activator of nuclear factor κb ligand, epidermal growth factor expression, osteoprotegerin, lung adenocarcinoma, epidermal growth factor mutation

1 Introduction

The skeleton is a common site for tumor metastases of several malignancies. For example, 30-60% of patients with metastatic lung cancer develop bone metastases (1, 2). In patients with bone metastases, bone turnover is disturbed. Normal bone remodeling requires a perfect balance between osteoblasts, osteoclasts and numerous signaling pathways, growth factors and control mechanisms. An important role is reserved for the Receptor activator of Nuclear Factor κB (RANK)/RANK ligand (RANKL)/ osteoprotegerin (OPG, the decoy receptor and antagonist of RANKL) pathway in bone development (3). By binding of RANKL to RANK, an ongoing cascade is set in motion, in which cancer cells stimulate osteoclasts, which in turn degrade the bone. During osteoclastogenic bone resorption different growth factors and cytokines are released from the bone, which stimulate the cancer cells to expansive growth (4).

Epidermal growth factor receptor (EGFR) signaling is involved in the proliferation of osteoclast precursors. Signaling *via* EGFR promotes osteoclast formation and stimulation by inhibition of OPG expression and by increasing monocyte chemoattractant protein 1 (MCP1; which induces osteoclast fusion and activity), macrophage colony-stimulating factor (MSCF) and RANKL expression (5, 6). An *in vitro* study showed that the addition of EGFR-tyrosine kinase inhibitors (EGFR-TKIs) completely blocked RANKL-dependent osteoclast formation and led to apoptosis in matured osteoclasts. These observations suggest an essential role for EGFR signaling in RANKL-mediated osteoclast differentiation and survival (7).

EGFR protein expression, determined by immunohistochemistry, in non-small cell lung cancer (NSCLC) is up-regulated in 40-80% of the tumors (8, 9). Conflicting results exist regarding the association of EGFR protein expression and *EGFR* mutations in NSCLC: some studies showed a higher EGFR protein expression in tumor samples (n=133-970) of patients with *EGFR* mutated (*EGFR*+) NSCLC (10, 11), while others (n=102-159) showed no association (12, 13). The up-regulated EGFR protein expression in the tumor (which possibly results in increased EGFR signaling) that was observed in some studies evaluating *EGFR*+ NSCLC, could be an explanation for our previously reported higher incidence of bone metastases in *EGFR*+ NSCLC compared with Kirsten rat sarcoma (*KRAS*+) and *EGFR/KRAS* wildtype NSCLC (14).

To the best of our knowledge, it has never been studied in a clinical setting whether there is an association between EGFR, RANKL, RANK and OPG gene expression in the tumor and presence of bone metastases in patients with NSCLC. In this study, we tried answering this question since understanding the biological mechanism of bone metastases development might have implications for adequate bone metastasis screening and (prophylactic) treatment decisions.

2 Materials and methods

Data from a study of patients with metastatic NSCLC were used (1). In this case-control study, for every patient with *EGFR*+ NSCLC (i.e., exon 19 deletion or exon 21 point mutation), the consecutive patients with a *KRAS*+ and *EGFR/KRAS* wildtype NSCLC were included as a case-control group. Wildtype was defined as *EGFR* and *KRAS* mutation negative NSCLC, as extensive molecular testing was not standard of care at that time. The established database covered the period from 01-10-2008 to 01-08-2012 and was updated (additional patients as well as updated data) till 01-09-2017 (1). For the current study all patients with available formalin-

fixed paraffin-embedded (FFPE) tissue samples were selected. This study was approved by the ethics committee of Maastricht UMC+ (METC 2017-0318) and the need for informed consent was waived.

2.1 Data collection

The in-and outpatient medical records of all patients were retrieved. Eligible patients were patients with metastatic NSCLC, with data regarding molecular analysis and follow-up and sufficient FFPE tumor tissue available. The following data were collected: demographics, date of diagnosis of metastatic NSCLC, smoking status, histology, mutation status, site of biopsy 1 (e.g. pathology obtained from bone, lung, lymph node, adrenal lesion), baseline bone metastasis, development of bone metastases during treatment, treatment, skeletal related events (SREs) and time of death. SREs were defined as pathological fracture, spinal cord compression, necessity for radiation to bone (for pain or impending fracture) or surgery to bone (15).

2.2 Measurement of EGFR, RANKL, RANK and OPG gene expression

EGFR, RANKL, RANK and OPG expression was measured by reverse transcriptase quantitative real time Polymerase Chain Reaction (RT-qPCR) on ribonucleic acid (RNA) extracted from FFPE tissue. Data were presented as relative mRNA levels calculated by the equation $2^{-\text{delta cycling time (Ct)}}$. Delta CT is CT of target gene minus CT of housekeeping gene. Data were expressed on a logarithmic scale. See Supplementary Material for a more detailed explanation of the measurement of gene expression.

2.3 Statistics

Statistical analysis was conducted with SPSS (v20; SPSS Inc., Chicago, IL) and SAS 9.4. Descriptive statistics of demographic and clinical variables were obtained. Categorical variables were compared using chi-square tests and continuous variables were compared using the Mann-Whitney U Test or the Kruskal-Wallis test. Reverse Kaplan-Meier was used for calculating median follow-up time. Due to small sample sizes, bone metastases at baseline or development of bone metastases during disease were grouped together and classified as “bone metastases present”. EGFR gene expression was represented in quartiles, as there is no standard cut-off for high or low EGFR gene expression.

Competing risk analysis was used for the association between RANKL: OPG ratio and time to development of bone metastases for patients without bone metastases. The proportional hazards assumption was tested using time-dependent Cox regression analyses with interaction between RANKL: OPG ratio and time. Due to violation of this assumption the analysis was separated in two time intervals and the -2LogLikelihood was compared between models with different time-cut-off points to identify the best cut-off (i.e., the model with the lowest -2LogLikelihood).

The relation of EGFR, RANK, RANKL, OPG gene expression, RANKL: OPG ratio and bone metastases was the primary endpoint of this study. Secondary endpoints were 1) Association between sample origin (primary site, non-bone metastasis, metastasis in general except bone, bone) and expression of EGFR, RANK, RANKL and OPG and RANKL: OPG ratio, 2) Expression of EGFR, RANK, RANKL and OPG and RANKL: OPG ratio in different molecular subgroups (*EGFR*+, *KRAS*+, *EGFR*/*KRAS* wildtype) in relation to bone metastases.

3 Results

3.1 Patient characteristics

From 169 patients (50%) of the total group of 335 patients, FFPE tumor samples were available. Ultimately, sufficient RNA could be extracted from 73 samples (Flowchart in Figure 1). In 52 out of 73 patients (81%), the pathology samples were obtained at diagnosis of metastatic disease. The other 21 patients were primarily diagnosed with early-stage NSCLC and had a median time to detection of metastatic disease of 550 days (range 87-2196 days). Patient characteristics are shown in Table 1. Median follow-up from diagnosis of metastatic NSCLC was 58.5 months (95% confidence interval (CI): 34.8-82.2 months).

3.2 EGFR, RANKL, RANK, OPG gene expression

EGFR, RANKL, RANK and OPG gene expressions were non-normally distributed (data not shown). The median EGFR expression was 0.84 (interquartile range (IQR) 1.67), the median RANKL expression was 0.02 (IQR 0.05), the median OPG expression was 0.09 (IQR 0.10) and the median RANK expression was 0.02 (IQR 0.03) (Figure 2).

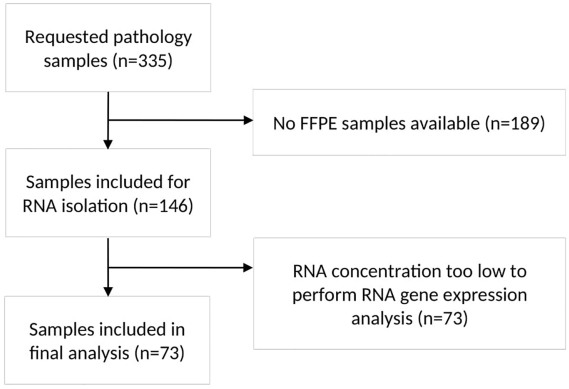

FIGURE 1
Flowchart of pathology sample selection. The flowchart showed the process of sample selection and reasons for exclusion of samples. n, number; FFPE, formalin-fixed paraffin-embedded; RNA, Ribonucleic acid.

TABLE 1 Patient characteristics.

Characteristics	Total n=73
Female n (%)	46 (63)
Never smoker n (%)	8 (11)
Mean age at diagnosis metastatic NSCLC, years (range)	62.8 (32-84)
Molecular subgroup n (%)	
EGFR+ *KRAS*+ *EGFR*/*KRAS* wildtype	23 (32) 36 (49) 14 (19)
Tumor origin n (%)	
Lung (primary tumor) Bone Other metastasis	29 (40) 9 (12) 35 (48)
Metastatic disease at diagnosis n (%)	47 (64)
Bone metastases at diagnosis stage IV n (%)	27 (37)
Bone metastases at diagnosis or during course of disease n (%)	46 (63)
SRE n (%)*	26 (57)
Type of SRE n (%)#	
Radiotherapy Pathologic fracture Surgery Spinal cord compression	25 (96) 4 (15) 6 (23) 2 (8)
BTA use in all patients n (%)$ Denosumab Bisphosphonate	9 (12) 1 (1) 8 (11)

n, number; EGFR+, Epidermal Growth Factor Receptor mutation; KRAS+, Kirsten rat sarcoma mutation; SRE, skeletal related event; BTA, bone targeted agent.
*Percentages were calculated by group of patients with bone metastases.
#Percentages were calculated by subgroup of all pts with SREs (n=26). Some patients experienced more than one SRE.
$Denosumab was used in one patient without bone metastases, all patients who used bisphosphonates had bone metastases.

3.3 Association between EGFR gene expression and RANKL, RANK and OPG gene expression or RANKL: OPG ratio and presence of bone metastases

EGFR expression was similar for patients with and without bone metastases (p=0.479). The percentage of patients with and without bone metastases was comparable between all EGFR quartiles (p=0.174, Figure 3A). Patients with bone metastases had an increased tumor RANKL expression and increased RANKL: OPG ratio, compared to those without bone metastases (p=0.002 and p=0.026 respectively).

Subdividing patients based on EGFR quartiles showed that RANKL gene expression was numerically higher in all EGFR quartiles for patients with bone metastases and statistically higher in the second and third EGFR quartile (Figure 3C). In the different EGFR quartiles, no significant differences for OPG, RANK gene expressions and RANKL: OPG ratio and presence of bone metastases were observed (Figures 3B, D, E).

3.4 EGFR, RANKL, RANK and OPG gene expression or RANKL: OPG ratio in primary tumors and metastases

The obtained tumor samples were subdivided based on site of origin: primary tumor (n=29), non-bone metastases (e.g., lymph node, liver, adrenal grand, parietal pleura, brain, other; n=35) and bone metastases (n=9). No difference was found for the percentage of tumor cells in the pathology sample and RANKL gene expression (data not shown). For the whole population of patients with and without bone metastases, significantly higher RANKL gene expression was observed in bone samples than in samples derived from the primary tumor (p=0.025). Pathology samples of both non-bone as well as bone metastases had a significant higher RANKL: OPG ratio in comparison to samples of the primary tumor (p=0.004 and p=0.028). The OPG gene expression was significantly lower in samples of bone metastases compared to non-bone metastases (p=0.043). RANK gene expression was significantly higher in samples of non-bone metastases in comparison to the primary

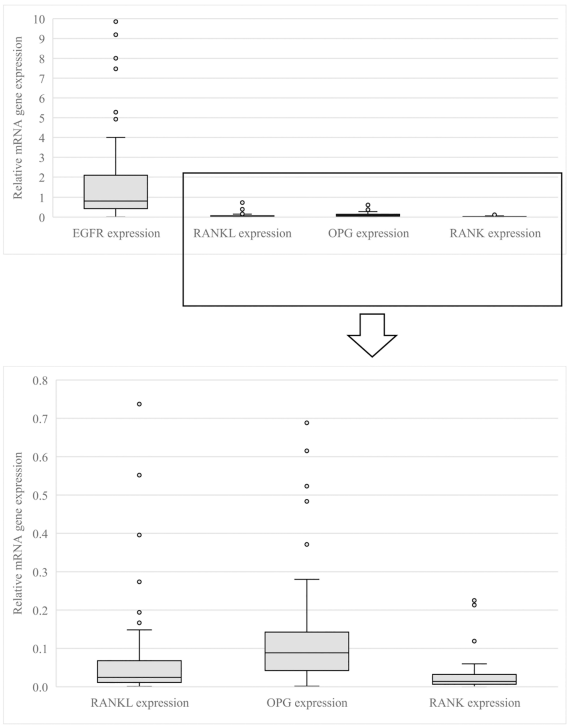

FIGURE 2
EGFR, RANKL, OPG, RANK gene expression in all patients. This figure shows the relative EGFR, RANKL, OPG and RANK gene expression measured on pathology samples of all patients. EGFR, Epidermal Growth Factor Receptor; RANKL, Receptor Activator of Nuclear Factor κB ligand; OPG, osteoprotegerin; RANK, Receptor Activator of Nuclear Factor κB.

tumor (p=0.047). Figure 4 shows the different gene expression of the pathology samples. In the group of patients with bone metastases, no significant differences were observed between the various sample origins, only a trend to significance for OPG gene expression and RANKL: OPG ratio (p=0.072, p=0.079).

3.5 Gene expression of EGFR, RANKL, RANK and OPG or RANKL: OPG ratio in different NSCLC molecular subgroups in relation to bone metastases

Independent of the presence of bone metastases, patients with an *EGFR* mutation had a significantly higher EGFR expression, compared to patients with a *KRAS*+ or *EGFR/KRAS* wildtype NSCLC (p<0.001) (Supplementary Material, Figure 1A).

Patients with *KRAS*+ NSCLC and bone metastases had a significantly higher RANKL expression and higher RANKL: OPG ratio (p=0.002) compared to patients with *KRAS*+ NSCLC without bone metastases (p=0.017). This was not found for the other molecular subgroups. The OPG expression was significantly higher for patients with bone metastases in the subgroup of patients with *EGFR*+ and *EGFR/KRAS* wildtype NSCLC (p=0.021 and p=0.028) (Supplementary Material, Figures 1B-E). No significant difference was observed between the different expression levels and presence of SREs in patients with bone metastases (data not shown).

3.6 Association between RANKL: OPG ratio and time to development of bone metastases

The RANKL: OPG ratio in relation to bone metastases development violated the proportional hazards assumption, therefore an early and late effect was determined. The hazard ratio (HR) of the RANKL: OPG ratio in the first 450 days after diagnosis of metastatic NSCLC was 1.65 (95% CI: 0.66-4.12) and decreased to 0.17 (95% CI: 0.03-0.95) thereafter.

4 Discussion

Previously, we showed that bone metastases were more frequent in patients with *EGFR*+ metastatic NSCLC than in patients with *KRAS*+ or *EGFR/KRAS* wildtype NSCLC, and that post bone metastases survival was significantly longer in patients with *EGFR* + NSCLC (1, 14). Based on preclinical data, showing that EGFR expression inhibits OPG expression and increases RANKL expression (5, 6), we hypothesized that the earlier observed increased EGFR gene expression in *EGFR*+ NSCLC (8, 9) may lead to an altered shift of RANKL expression or RANKL: OPG ratio and thereby promote bone metastases in *EGFR*+ NSCLC. In the current study, we indeed found that *EGFR*+ NSCLC had a significantly higher EGFR gene expression as compared to *KRAS*+ or *EGFR/KRAS* wildtype NSCLC. We could not demonstrate any association between EGFR gene expression level and the presence of bone metastases. However, patients with bone metastases had a significantly higher RANKL expression and RANKL: OPG ratio compared to those without bone metastases; possibly because the bone microenvironment in those with bone metastases released cytokines or growth factors which induced RANKL expression also in the tumor. This increased RANKL and RANKL: OPG ratio is in line with observations in an *in vitro* study in three human NSCLC cell lines and in 127 NSCLC tumor samples (52 primary tumors and 75 bone metastasis samples) in which the expression of RANKL, RANK and OPG was estimated by RT-PCR in cell lines and by immunohistochemistry (IHC) on tumor tissue (16). In addition, both *in vitro* and *in vivo* an increased RANKL expression and elevated RANKL: OPG ratio was associated with an enhanced potential of NSCLC to metastasize to the bone (16). Our data confirmed that patients with NSCLC with a higher RANKL: OPG ratio more often developed bone metastases, primarily in the first 450 days after diagnosis of metastatic NSCLC. Various studies have been performed to investigate biomarkers related to bone metastases or skeletal related event development. Examples are bone specific alkaline phosphatase in serum, urine N-terminal telopeptide in urine and C-X-C- Motif Chemokine Receptor 4 on the tumor (17). However, most of these are not used in daily practice as there is no recognized standard because of inconsistent study results. We showed an increased RANKL expression

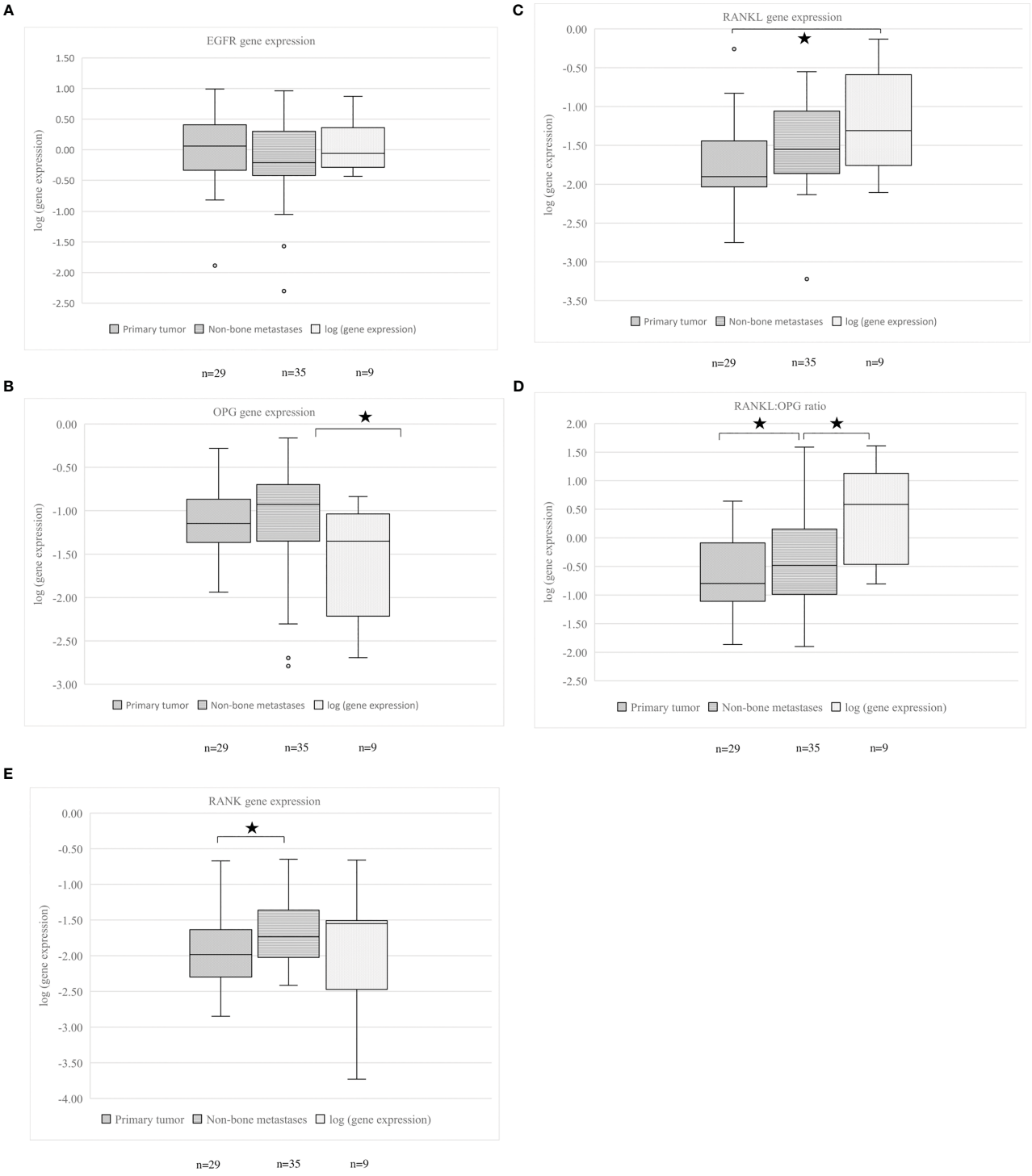

FIGURE 3
(A–E) EGFR, OPG, RANKL gene expression, RANKL: OPG ratio and RANK gene expression in relation to presence of bone metastases. Patients were subdivided in groups by EGFR expression. The first quartile is the lowest and the fourth quartile is the highest EGFR gene expression. **(A)** EGFR gene expression, **(B)** OPG gene expression, **(C)** RANKL gene expression, **(D)** RANKL: OPG ratio, **(E)** RANK gene expression. An asterisk denotes a significant difference between groups. EGFR, Epidermal Growth Factor Receptor; OPG, osteoprotegerin; RANKL, Receptor Activator of Nuclear Factor κB ligand; RANK, Receptor Activator of Nuclear Factor κB.

especially in patients with *KRAS*+ NSCLC and bone metastases. As far as we know, no data about RANKL expression in this subgroup exists. Human lung adenocarcinoma data sets only showed that RANKL expression was significantly higher in *KRAS*+ lung adenocarcinoma compared to *KRAS* wildtype lung adenocarcinoma (18).

As previously reported in breast or renal cell carcinoma, RANKL triggers the migration and metastasis of RANK

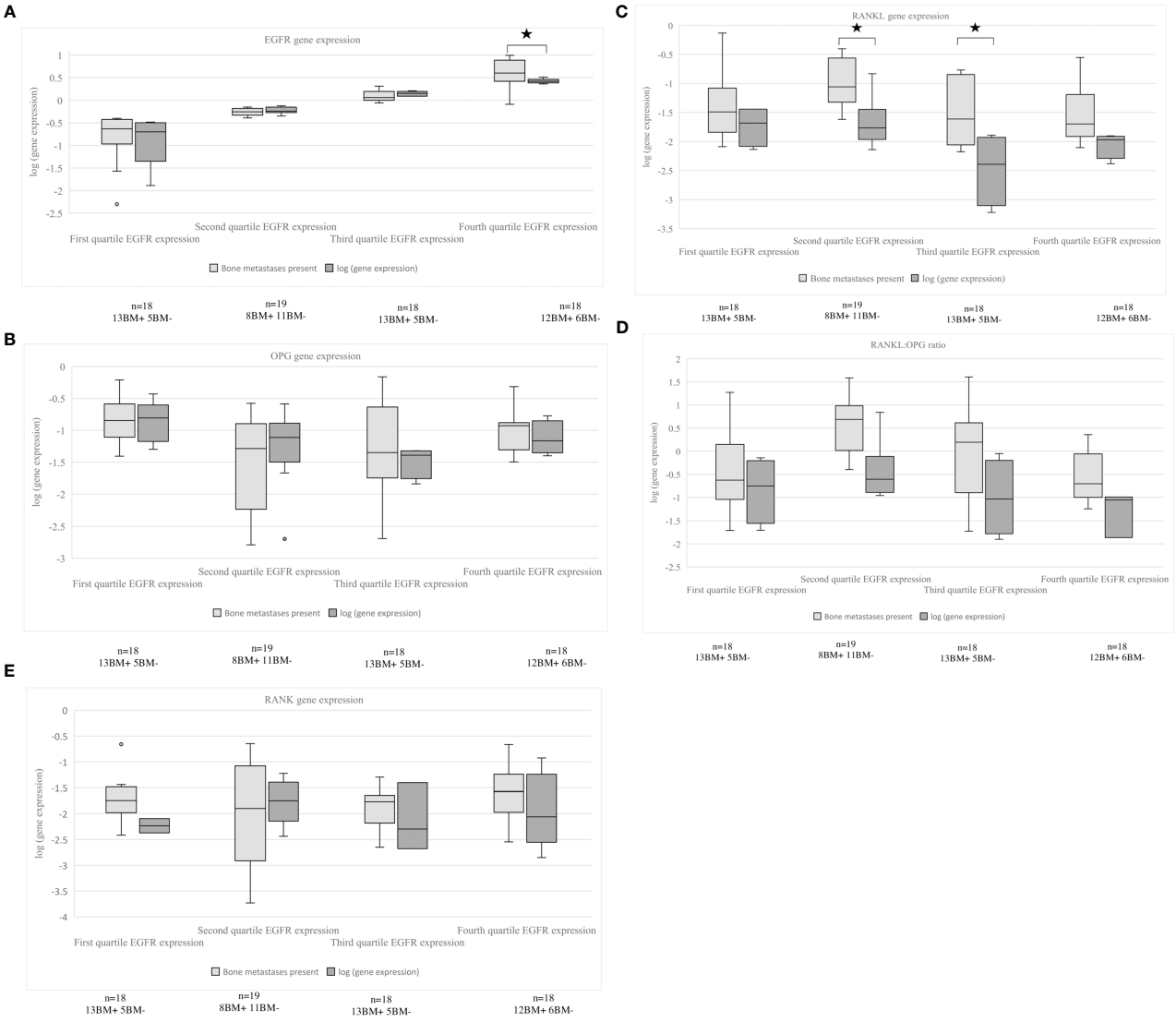

FIGURE 4
(A–E) EGFR, RANKL, OPG gene expression, RANKL: OPG ratio and RANK gene expression in relation to site of tumor biopsy. **(A)** EGFR expression, **(B)** OPG expression, **(C)** RANKL expression, **(D)** RANKL: OPG ratio, **(E)** RANK expression, all expressions are shown in primary tumor, non-bone metastases and bone metastases. An asterisk denotes a significant difference between groups. EGFR, Epidermal Growth Factor Receptor; OPG, osteoprotegerin; RANKL, Receptor Activator of Nuclear Factor κB ligand; RANK, Receptor Activator of Nuclear Factor κB.

expressing cancer cells (19, 20). A retrospective analysis in patients with non-metastatic breast cancer (n=509) showed a positive association between higher RANKL serum levels (measured by enzyme linked immune sorbent assay [ELISA]) and presence of disseminated tumor cells in the bone marrow and also with the development of bone metastases (21). Moreover, patients within the highest quartile of RANKL had a 4.6 increased risk for developing bone metastases compared to those within the lowest quartile (21). This is in line with our observation that patients with bone metastases had higher RANKL expression, especially in *KRAS* +NSCLC. It is not known whether the effect of RANKL inhibition (e.g., denosumab) on bone metastases related outcomes in patients with high versus low RANKL expression is different. In the Splendour trial no survival benefit was found when denosumab was added to first-line chemotherapy in patients with metastatic NSCLC (2). However, these patients were unselected for the presence of bone metastases and bone related outcomes were not reported. It would be of interest to explore the outcomes in patients with bone metastases and evaluate whether there is a relation between bone metastases related outcomes and RANKL expression (tumor or serum) as well as RANKL/OPG ratio (2).

In the current study, we could not find an explanation for our previously observed higher incidence of bone metastases in patients with *EGFR*+ NSCLC (14). Although EGFR gene expression was higher, no association with a higher RANKL gene expression or RANKL: OPG ratio in tumor samples was observed. It could be that the tumor tissue is not the correct place to measure these values. Nowadays, more and more studies point on the role of extracellular vesicles (EVs) in bone metastases development in multiple types of cancer (22–24). An *in vitro* study

showed that CRL-2868 NSCLC cells containing an *EGFR* 19 deletion, secrete exosomes containing EGFR ligand and Amphiregulin. These EVs were able to induce *in vitro* osteoclast differentiation of murine RAW264.7 cells by activation of EGFR phosphorylation and induction of matrix metalloproteinase-9 and tartrate-resistant acid phosphatase expression. These results were confirmed *ex vivo* by the finding that patient derived EVs were able to modulate osteoclastogenesis in human osteoclast precursors (23). Therefore, future studies should also focus on EVs in patients with (*EGFR*+) NSCLC to unravel the biological mechanism of bone metastases formation.

This study has its limitations. First, due to unavailability of tumor samples or impossibility to perform the gene expression analysis, the sample size was not large enough to have sufficient power for subgroup analysis. A second limitation is the different origin of the pathological samples, which could create bias in expression analysis as, by nature, RANKL expression in bone is higher than in lung tissue (25). However, as we had only nine bone samples in our analysis, we think this did not significantly affected our results. Third, not all patients underwent a 2-deoxy-2-[fluorine-18] fluoro-D-glucose positron emission tomography-computer tomography scan (FDG-PET-CT scan) or bone scintigraphy, therefore it could be that presence of bone metastases is underestimated as not all asymptomatic bone metastases will have been diagnosed by regular computed tomography of the chest and upper abdomen. Finally, patients with bone metastases and development of bone metastases during disease were grouped together and in doing so, one can ask whether the biological behavior of the tumor is the same in both groups. However, when analyzing both groups separately, the results remained similar (data not shown).

In conclusion, our study showed no association between EGFR gene expression and presence of bone metastases in patients with NSCLC; however, patients with bone metastases had a higher RANKL gene expression and RANKL: OPG ratio. An elevated RANKL: OPG ratio was associated with a higher incidence of bone metastases development, especially in the first year after diagnosis of metastatic NSCLC.

Data availability statement

The raw data supporting the conclusions of this article will be made available by the authors, without undue reservation.

Ethics statement

The studies involving human participants were reviewed and approved by Medisch-ethische toetsingscommissie Maastricht. Written informed consent for participation was not required for this study in accordance with the national legislation and the institutional requirements.

Author contributions

AB: conceptualization, methodology, validation, formal analysis, investigation, writing-original draft, writing - review & editing, visualization, funding acquisition. LH: conceptualization, methodology, writing - review & editing, supervision, funding acquisition. IR-VB: conceptualization, methodology, validation, formal analysis, investigation, writing - review & editing. AD: formal analysis, writing - review & editing. GR: conceptualization, methodology, resources, writing - review & editing. BLJH: investigation, methodology, writing - review & editing. ZD: investigation, writing - review & editing. BH: investigation, methodology, writing - review & editing. DL: methodology, writing - review & editing. LM: methodology, writing - review & editing. RL: resources, writing - review & editing. MW: recourses, writing - review & editing. MD: conceptualization, methodology, validation, writing - review & editing, supervision. E-JS: conceptualization, writing - review & editing. A-MD: conceptualization, writing - review & editing, supervision, funding acquisition. All authors contributed to the article and approved the submitted version.

Funding

This study was funded by a grant (no number) from the Five4Five Foundation, Cancer Research Fund Limburg (2018). Data were presented at ELCC 2023 as a poster (number 72p).

Conflict of interest

There are no conflicts of interest related to this manuscript. Outside this manuscript: Author AB: participation on advisory board of Jansen. Author LH: research funding Roche Genentech. AstraZeneca, Boehringer Ingelheim, Takeda, Beigene under negotiation all payments were paid to the institution. Speaker's fee from MSD, Lilly. Fees for educational webinars: Benecke, Medtalks, VJOncology self, high5oncology institution. Support for attending meetings and/or travel: Roche Genentech. Advisory board BMS, Eli Lilly, Roche Genentech, Pfizer, Takeda, MSD, Merck, Novartis, Boehringer Ingelheim, Amgen, Janssen. Mentorship program with key opinion leaders: funded by AstraZeneca. Interview sessions funded by Roche Genentech, Bayer, Lilly. Local PI of clinical trials: AstraZeneca, Novartis, BMS, MSD/Merck, GSK, Takeda, Blueprint Medicines, Roche Genentech, Janssen Pharmaceuticals, Mirati, Abbvie, Gilead. Author A-MD: Roche: Advisory Board, Steering Committee Eli Lilly: Honorarium Boehringer Ingelheim: Advisory Board Astra Zeneca: Honorarium, Advisory Board Jansen: Honorarium industry sponsored symposium Chiesi: Honorarium Amgen: Advisory Board, research support Pfizer: Honorarium Bayer: Advisory Board Takeda: Honorarium Pharmamar: Advisory Board Sanofi: Advisory Boar.

The remaining authors declare that the research was conducted in the absence of any commercial or financial relationships that could be construed as a potential conflict of interest.

Publisher's note

All claims expressed in this article are solely those of the authors and do not necessarily represent those of their affiliated organizations, or those of the publisher, the editors and the reviewers. Any product that may be evaluated in this article, or claim that may be made by its manufacturer, is not guaranteed or endorsed by the publisher.

Supplementary material

The Supplementary Material for this article can be found online at: https://www.frontiersin.org/articles/10.3389/fonc.2023.1145001/full#supplementary-material

References

1. Hendriks LE, Smit EF, Vosse BA, Mellema WW, Heideman DA, Bootsma GP, et al. EGFR mutated non-small cell lung cancer patients: more prone to development of bone and brain metastases? *Lung Cancer* (2014) 84(1):86–91. doi: 10.1016/j.lungcan.2014.01.006

2. Peters S, Danson S, Hasan B, Dafni U, Reinmuth N, Majem M, et al. A randomized open-label phase III trial evaluating the addition of denosumab to standard first-line treatment in advanced NSCLC: the European thoracic oncology platform (ETOP) and European organisation for research and treatment of cancer (EORTC) SPLENDOUR trial. *J Thorac Oncol* (2020) 10:1647–56. doi: 10.1016/j.jtho.2020.06.011

3. Weilbaecher KN, Guise TA, McCauley LK. Cancer to bone: a fatal attraction. *Nat Rev Cancer* (2011) 11(6):411–25. doi: 10.1038/nrc3055

4. Pantano F, Clezardin P, Santini D. RANK/RANKL pathway in cancer: biological activity beyond bone? *J Bone Oncol* (2012) 1(3):67–8. doi: 10.1016/j.jbo.2012.11.001

5. Schneider MR, Sibilia M, Erben RG. The EGFR network in bone biology and pathology. *Trends Endocrinol Metab* (2009) 20(10):517–24. doi: 10.1016/j.tem.2009.06.008

6. Kang Y. Dissecting tumor-stromal interactions in breast cancer bone metastasis. *Endocrinol Metab (Seoul)* (2016) 31(2):206–12. doi: 10.3803/EnM.2016.31.2.206

7. Yi T, Lee HL, Cha JH, Ko SI, Kim HJ, Shin HI, et al. Epidermal growth factor receptor regulates osteoclast differentiation and survival through cross-talking with RANK signaling. *J Cell Physiol* (2008) 217(2):409–22. doi: 10.1002/jcp.21511

8. Hirsch FR, Varella-Garcia M, Cappuzzo F. Predictive value of EGFR and HER2 overexpression in advanced non-small-cell lung cancer. *Oncogene* (2009) 28 Suppl 1: S32–7. doi: 10.1038/onc.2009.199

9. Hirsch FR, Varella-Garcia M, Bunn PAJr., Di Maria MV, Veve R, Bremmes RM, et al. Epidermal growth factor receptor in non-small-cell lung carcinomas: correlation between gene copy number and protein expression and impact on prognosis. *J Clin Oncol* (2003) 21(20):3798–807. doi: 10.1200/JCO.2003.11.069

10. Douillard JY, Pirker R, O'Byrne KJ, Kerr KM, Storkel S, von Heydebreck A, et al. Relationship between EGFR expression, EGFR mutation status, and the efficacy of chemotherapy plus cetuximab in FLEX study patients with advanced non-small-cell lung cancer. *J Thorac Oncol* (2014) 9(5):717–24. doi: 10.1097/JTO.0000000000000141

11. Liang Z, Zhang J, Zeng X, Gao J, Wu S, Liu T. Relationship between EGFR expression, copy number and mutation in lung adenocarcinomas. *BMC Cancer* (2010) 10:376. doi: 10.1186/1471-2407-10-376

12. Cappuzzo F, Hirsch FR, Rossi E, Bartolini S, Ceresoli GL, Bemis L, et al. Epidermal growth factor receptor gene and protein and gefitinib sensitivity in non-small-cell lung cancer. *J Natl Cancer Inst* (2005) 97(9):643–55. doi: 10.1093/jnci/dji112

13. Tsao AS, Tang XM, Sabloff B, Xiao L, Shigematsu H, Roth J, et al. Clinicopathologic characteristics of the EGFR gene mutation in non-small cell lung cancer. *J Thorac Oncol* (2006) 1(3):231–9. doi: 10.1016/S1556-0864(15)31573-2

14. Kuijpers C, Hendriks LEL, Derks JL, Dingemans AC, van Lindert ASR, van den Heuvel MM, et al. Association of molecular status and metastatic organs at diagnosis in patients with stage IV non-squamous non-small cell lung cancer. *Lung Cancer* (2018) 121:76–81. doi: 10.1016/j.lungcan.2018.05.006

15. Kuchuk M, Addison CL, Clemons M, Kuchuk I, Wheatley-Price P. Incidence and consequences of bone metastases in lung cancer patients. *J Bone Oncol* (2013) 2(1):22–9. doi: 10.1016/j.jbo.2012.12.004

16. Peng X, Guo W, Ren T, Lou Z, Lu X, Zhang S, et al. Differential expression of the RANKL/RANK/OPG system is associated with bone metastasis in human non-small cell lung cancer. *PloS One* (2013) 8(3):e58361. doi: 10.1371/journal.pone.0058361

17. Chai X, Yinwang E, Wang Z, Wang Z, Xue Y, Li B, et al. Predictive and prognostic biomarkers for lung cancer bone metastasis and their therapeutic value. *Front Oncol* (2021) 11:692788. doi: 10.3389/fonc.2021.692788

18. Faget J, Contat C, Zangger N, Peters S, Meylan E. RANKL signaling sustains primary tumor growth in genetically engineered mouse models of lung adenocarcinoma. *J Thorac Oncol* (2018) 13(3):387–98. doi: 10.1016/j.jtho.2017.11.121

19. Jones DH, Nakashima T, Sanchez OH, Kozieradzki I, Komarova SV, Sarosi I, et al. Regulation of cancer cell migration and bone metastasis by RANKL. *Nature* (2006) 440(7084):692–6. doi: 10.1038/nature04524

20. Mikami S, Katsube K, Oya M, Ishida M, Kosaka T, Mizuno R, et al. Increased RANKL expression is related to tumour migration and metastasis of renal cell carcinomas. *J Pathol* (2009) 218(4):530–9. doi: 10.1002/path.2567

21. Rachner TD, Kasimir-Bauer S, Gobel A, Erdmann K, Hoffmann O, Browne A, et al. Prognostic value of RANKL/OPG serum levels and disseminated tumor cells in nonmetastatic breast cancer. *Clin Cancer Res* (2019) 25(4):1369–78. doi: 10.1158/1078-0432.CCR-18-2482

22. Rossi M, Battafarano G, D'Agostini M, Del Fattore A. The role of extracellular vesicles in bone metastasis. *Int J Mol Sci* (2018) 19(4):1136–48. doi: 10.3390/ijms19041136

23. Taverna S, Pucci M, Giallombardo M, Di Bella MA, Santarpia M, Reclusa P, et al. Amphiregulin contained in NSCLC-exosomes induces osteoclast differentiation through the activation of EGFR pathway. *Sci Rep* (2017) 7(1):3170. doi: 10.1038/s41598-017-03460-y

24. Urabe F, Patil K, Ramm GA, Ochiya T, Soekmadji C. Extracellular vesicles in the development of organ-specific metastasis. *J Extracell Vesicles* (2021) 10(9): e12125. doi: 10.1002/jev2.12125

25. Renema N, Navet B, Heymann MF, Lezot F, Heymann D. RANK-RANKL signalling in cancer. *Biosci Rep* (2016) 36(4):36–52. doi: 10.1042/BSR20160150

frontiers | Frontiers in Oncology

TYPE Review
PUBLISHED 19 June 2023
DOI 10.3389/fonc.2023.1188357

OPEN ACCESS

EDITED BY
Feifei Pu,
Huazhong University of Science and Technology, China

REVIEWED BY
Junfei Guo,
Third Hospital of Hebei Medical University, China
Yanxia Chen,
Second Affiliated Hospital of Nanchang University, China
Jing Chen,
Nanjing University of Chinese Medicine, China

*CORRESPONDENCE
Jitian Li
jitianlee@hotmail.com
Hongjian Liu
hongjianmd@126.com

†These authors have contributed equally to this work and share first authorship

RECEIVED 17 March 2023
ACCEPTED 01 June 2023
PUBLISHED 19 June 2023

CITATION
Hao Y, Zhang F, Ma Y, Luo Y, Zhang Y, Yang N, Liu M, Liu H and Li J (2023) Potential biomarkers for the early detection of bone metastases. *Front. Oncol.* 13:1188357. doi: 10.3389/fonc.2023.1188357

Potential biomarkers for the early detection of bone metastases

Yang Hao[1,2†], Feifan Zhang[1,3†], Yan Ma[1], Yage Luo[1], Yongyong Zhang[1], Ning Yang[1], Man Liu[1], Hongjian Liu[4*] and Jitian Li[1,2,3*]

[1]Laboratory of Molecular Biology, Henan Luoyang Orthopedic Hospital (Henan Provincial Orthopedic Hospital), Zhengzhou, China, [2]Henan University of Chinese Medicine, Zhengzhou, China, [3]Hunan University of Chinese Medicine, Changsha, China, [4]Department of Orthopaedics, the First Affiliated Hospital of Zhengzhou University, Zhengzhou, China

The clinical manifestations of bone metastases are diversified while many sites remain asymptomatic at early stage. As the early diagnosis method is not perfect and the early symptoms of tumor bone metastasis are not typical, bone metastasis is not easy to be detected. Therefore, the search for bone metastasis-related markers is effective for timely detection of tumor bone metastases and the development of drugs to inhibit bone metastases. As a result, bone metastases can only be diagnosed when symptoms are found, increasing the risk of developing skeletal-related event (SREs), which significantly impairs the patient's quality of life. Therefore, the early diagnosis of bone metastases is of great importance for the treatment and prognosis of cancer patients. Changes of bone metabolism indexes appear earlier in bone metastases, but the traditional biochemical indexes of bone metabolism lack of specificity and could be interfered by many factors, which limits their application in the study of bone metastases. Some new biomarkers of bone metastases have good diagnostic value, such as proteins, ncRNAs, circulating tumor cells (CTCs). Therefore, this study mainly reviewed the initial diagnostic biomarkers of bone metastases which were expected to provide references for the early detection of bone metastases.

KEYWORDS

bone metastases, biomarkers, ncRNAs, circulating tumor cells, exosome

1 Introduction

Bone metastasis occurs when tumor cells spread to the bones. When people suffering from cancer, with the progression of the disease, the cancer cells invade the blood vessels. As the blood flows, the cancer cells may travel to the bone marrow and continue to rise, forming bone metastases (1). Distant metastases are a typical characteristic of malignant tumor, as well as one of the main reasons leading to treatment failure of tumor patients (2). On average, 1 out of every 5 patients will suffer from bone metastases. Theoretically, almost all types of cancers may metastasize to bone, among which lung cancer, breast cancer and prostate

cancer are the most frequent (3). Digestive tract tumors such as stomach cancer, bowel cancer, pancreatic cancer, etc., can also appear, relatively low risk. There are three types of bone metastases: osteolytic, osteoblastic and mixed (4, 5). Only clear diagnosis and symptomatic treatment will have beneficial clinical effect (6). Osteogenic bone metastases are widespread in prostate cancer, accounting for about 10% of bone metastases. Lytic bone metastases account for 70%, which are atypical lung and breast cancer (4).

The early diagnosis of malignant tumors is very critical to the recovery. In clinical practice, some of cancer patients showed symptoms such as waist and leg pain or anemia (especially those who had a history of this, such as rheumatic inflammation, lumbar disc herniation, etc.), but they did not pay enough attention (7). In fact, it is highly likely that this is a precursor of tumor bone metastases. If the bone lesions and complications of bone metastases cannot be treated reasonably, it will do great harm, such as pathological fractures, which often paralyze patients in bed, as well as the severe pain will seriously affect the quality of life of patients (8, 9).

Early diagnosis of bone metastases is of major importance. The main symptom of bone metastases is persistent pain with continuously aggravated, which may also cause mobility impairment. The commonly used imaging methods for the diagnosis of bone metastases have different characteristics. As for X-ray, specificity is high but sensitivity is low. The positive rate of bone ECT imaging is high, but there exist false positive and false negative problems (5, 10). CT and MRI have high specificity and accuracy, but are not appropriate for general examination. positron emission computed tomography PET has a high positive rate, but it doesn't applicable to simple bone lesions, and the price is relatively high, which limited its application in clinic (11, 12). Theoretically, the changes of biochemical indexes of bone metabolism during bone metastases are earlier than those in imaging (13, 14). However, traditional biochemical indexes of bone metabolism with low specificity limits their application in the study of bone metastases (15, 16).

Some new biomarkers of bone metastases have good diagnostic value, such as proteins, ncRNAs, biomarkers in liquid biopsy and other biochemical indicators. These new types of biomarkers have demonstrated great potential in the initial diagnosis of bone metastases. In the study we searched relevant researches for bone metastases biomarkers, which mainly provides reference for early diagnosis of bone metastases, as shown in Figure 1.

2 Application of commonly used protein biomarkers in bone metastases

Protein biomarkers are most commonly used in the clinical diagnosis and prognosis of bone metastases. It indicates proteins in the blood whose presence or abnormal expression is often associated with certain types of tumors. These proteins can be detected in tumor cells, surrounding tissues, and blood, these biomarkers can be employed to monitor patient responsiveness and effectiveness during treatment. However, it is important to emphasize that a single blood biomarker is not enough to detect the tumor. It is usually used in conjunction with other tests, imaging and clinical symptoms to determine the status of the tumor. The presence of digestive system tumors and the occurrence of bone metastases may lead to increasing carbohydrate resistance, such as the indexes of alpha-fetoprotein (AFP), carcinoembryonic antigen (CEA), prostate specific antigen (PSA), CA199, CA724, CA50, and CA242.

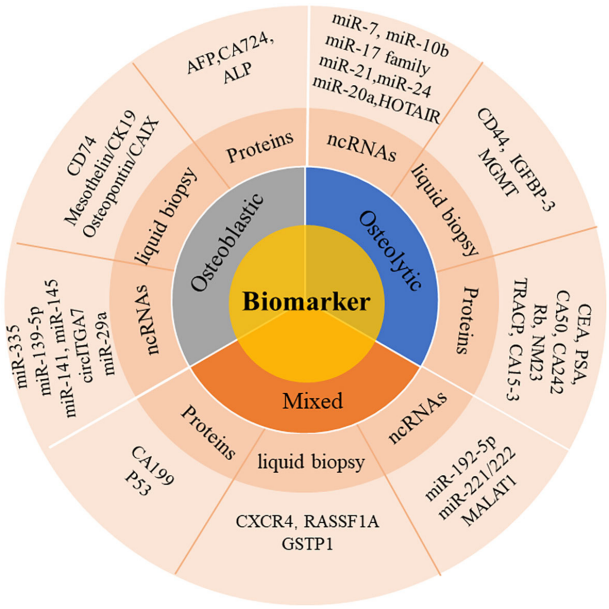

FIGURE 1
The role of partial biomarkers in bone metastase.

Except that most commonly used for bone metastases tumor biomarkers include bone specific alkaline phosphatase (BALP), tartrate-resistant acid phosphatase (TRACP), tumor necrosis factor (TNF), carbohydrate antigen 15-3 (CA15-3). The exact contents were shown in Table 1. The diagnostic performance of each biomarker was presented shown in Table 2.

2.1 AFP

AFP, known as hepatoembryonic antigen, is a biomarker for the identification of bone metastases (43). It plays a major role in embryonic and early embryonic development, but the adult owned the low level of AFP. AFP is commonly used as the diagnostic biomarker for liver, testicular, and ovarian carcinoma. Moreover, AFP can be used to predict bone metastases, which is a manifestation of antigen movement in a specific direction (43, 44). Studies showed that the serum level of AFP in patients with non-small cell lung cancer can be utilized to predict location-based tumor susceptibility and duration of location-based tumor treatment (45, 46). Another study showed that higher serum AFP level in the patients of cancer indicated the risk of bone metastases and thus to infer more effective cancer treatment options (44, 47). High level of serum AFP has been shown to help to diagnose patients with bone metastases with diagnostic accuracy of 75% as well as to predict tumor size, location, risk of metastases, and duration of treatment (40, 48). Recent studies have found that it can be utilized to assess location-based tumor susceptibility, as well as tumor size, location, and duration of treatment. To sum up, AFP is a significant biomarker for the detection of bone metastases.

2.2 CEA

CEA is a common antigenic factor that plays an important role in a variety of cancers, such as Colon cancer, stomach cancer, pancreatic cancer, small intestinal adenocarcinoma, lung cancer, liver cancer, breast cancer (49). CEA is a biomarker widely used in colorectal cancer screening and monitoring treatment response. However, its low sensitivity and specificity in bone tumors limit its application in bone metastasis. CEA is of particular importance in bone metastases. At present, CEA is used primarily to detect the occurrence and development of bone metastases, especially in breast cancer, lung cancer and gastrointestinal tumors (50, 51). CEA has excellent sensitivity and specificity, which can be used to assess the existence of bone metastases. The sensitivity and specificity of serum CEA were 19.0%-56.1% and 50%-92%, in the gastrointestinal tumors (39). At present, more and more studies have pointed out that CEA can help accurately diagnose bone metastases and improve the curative effect. Clinical trials have shown that increased CEA levels were linked to reduced efficacy in patients with breast cancer bone metastases (52, 53). In addition, CEA also has significant application value for clarifying tumor manifestations, namely the range of bone metastases and bone changes, so as to provide objective guidance for clinical treatment planning.

TABLE 1 Application of commonly used biomarkers of bone metastases.

Biobiomarker	Bone transition stage	Clinical application	Deregulation
AFP	Osteoblastic	Detect the occurrence and development of bone metastases, especially in breast cancer, lung cancer and colon cancer.	Low-expression
CEA	Osteolytic	Provide objective guidance for clinical treatment planning and treatment.	Over-expression
PSA	Osteolytic	Screening, diagnosis and efficacy evaluation of prostate cancer.	Over-expression
CA199	Mixed	Predict the malignant transformation and prognosis of liver cancer.	Over-expression
CA724	Osteoblastic	Clinical diagnosis and prognosis of found guilty of an important tumor biomarker in breast cancer.	Over-expression
CA50	Osteolytic	Detect bone metastases of liver cancer.	Low-expression
CA242	Osteolytic	An epigenetic specific antigen used to detect bone metastases in gastric cancer	Over-expression
Rb	Osteolytic	Rb plays an important role in the regulation of bone metastases suppressor genes such as Osteoprotegerin.	Low-expression
P53	Mixed	Patients with bone metastases expressing p53 have a poor prognosis.	Over-expression
NM23	Osteolytic	NM23 is associated with cell proliferation, invasion, and metastases of bone metastases, and is generally associated with poor treatment response and prognosis.	Low-expression
ALP	Osteoblastic	Reflecting bone metastases lesions, and is regarded as a biomarker of early differentiation of osteoblast precursor cells.	Over-expression
BALP	Osteolytic	BALP level is a key predictor of treatment response and prognosis of bone metastases.	Over-expression
TRACP	Osteolytic	A decline in TRACP levels is usually associated with a better prognosis for treatment. In addition, monitoring TRACP levels can also help determine the timing and regimen of treatment and possible problems with bone metabolism.	Over-expression
CA15-3	Osteolytic	CA15-3 levels are often elevated in breast cancer patients with bone metastases.	Over-expression

TABLE 2 Diagnostic performance of commonly used biomarkers of bone metastases in single study.

biomarkers	primary cancer types	Study population characteristics		Diagnostic performance				Ref.
		cases group	Controls group	Research method	Se. (%)	Sp. (%)	AUC	
AFP/AFP-L3	HCC	50	484	uTASWako i30	63.30	90.00	/	Tayob N et al. (2022) (17)
AFP	HCC	79	77	Microchip capillary electrophoresis	68.35	81.82	0.683-0.818	Park SJ et al. (18)
AFP	HCC	104	336	Retrospective analysis	71.00	91.00	/	Zhu AX et al. (19)
AFP	HCC	36	31	LC-MS	88.90	82.90	0.892	Luo et al. (20)
AFP	HCC	135	302	Genome-wide discovery	71.00	90.00	0.92	Chalasani NP et al. (21)
AFP	HCC	90	60	Immunohistochemical	82.60	96.20	/	Chen D et al. (22)
AFP	GCT	41	35	Retrospective analysis	71.00	80.00	/	Calaminus G et al. (23)
ALP	RCC	111	261	Histopathologic analysis	57.90	83.50	0.749	Chen XY et al. (24)
Calcium	RCC	111	261	Histopathologic analysis	36.80	95.20	0.633	Chen XY et al. (24)
HB	RCC	111	261	Histopathologic analysis	71.10	65.30	0.665	Chen XY et al. (24)
HB+ALP	RCC	111	261	Histopathologic analysis	47.40	91.00	/	Chen XY et al. (24)
HB+CA	RCC	111	261	Histopathologic analysis	34.20	97.60	/	Chen XY et al. (24)
ALP+CA	RCC	111	261	Histopathologic analysis	28.90	97.90	/	Chen XY et al. (24)
HB+CA+ALP	RCC	111	261	Histopathologic analysis	28.90	98.20	/	Chen XY et al. (24)
uNTX	NSCLC	100	50	Osteomark, Princeton, NJ	48.00	86.00	0.74	Tamiya et al. (25)
sNTX	NSCLC	100	50	Osteomark, Princeton, NJ	40.00	87.00	0.71	Tamiya et al. (25)
CTX	NSCLC	16	18	ELISA, RIA	73.70	86.70	0.68	Lumachi et al. (26)
ICTP	LC	47	44	Radioimmunoassay, immunoassay	71.40	87.90	/	Aruga et al. (27)
fDPD	LC	47	44	Radioimmunoassay, immunoassay	61.00	93.00	/	Aruga et al. (27)
PICP	LC	47	44	Radioimmunoassay, immunoassay	28.60	87.90	/	Aruga et al. (27)
BGP	LC	47	44	Radioimmunoassay, immunoassay	12.30	81.80	/	Aruga et al. (27)
ALP	LC	47	44	Radioimmunoassay, immunoassay	55.60	79.50	/	Aruga et al. (27)
BALP	LC	47	44	Radioimmunoassay, immunoassay	44.40	93.20	/	Aruga et al. (27)
ICTP	LC	140	50	Double-antibody Radioimmunoassay	92.00	70.00	0.816	Horiguchi et al. (28)
CEA	LC	140	50	Double-antibody Radioimmunoassay	60.00	55.00	0.571	Horiguchi et al. (28)
CYFRA 21-1	LC	140	50	Double-antibody Radioimmunoassay	60.00	45.00	0.538	Horiguchi et al. (28)
ProGRP	LC	140	50	Double-antibody Radioimmunoassay	42.00	65.00	0.557	Horiguchi et al. (28)
ALP	LC	140	50	Double-antibody Radioimmunoassay	22.50	92.00	0.654	Horiguchi et al. (28)

(Continued)

TABLE 2 Continued

biomarkers	primary cancer types	Study population characteristics		Diagnostic performance				Ref.
		cases group	Controls group	Research method	Se. (%)	Sp. (%)	AUC	
Ca	LC	140	50	Double-antibody Radioimmunoassay	0.070	100.00	0.321	Horiguchi et al. (28)
ALP	LC	30	152	Hitachi747 autoanalyzer	26.70	97.30	0.857	Min et al. (29)
ICTP	LC	130	135	ELISA	63.10	90.40	0.835	Tang et al. (30)
BAP	LC	130	135	ELISA	63.10	77.00	0.760	Tang et al. (30)
TRACP 5b	LC	130	135	ELISA	58.50	80.70	0.753	Tang et al. (30)
CTX	NSCLC	16	18	Automated Immunometric assay	73.30	86.70	0.794	Lumachi et al. (26)
CEA	NSCLC	16	18	ELISA	55.50	62.50	0.588	Lumachi et al. (26)
CYFRA	NSCLC	16	18	Immunochemiluminescent assay	65.00	78.60	0.706	Lumachi et al. (26)
TRAP5b	NSCLC	16	18	ELISA	30.40	76.20	0.676	Lumachi et al. (26)
PINP	NSCLC	16	18	RIA	72.20	81.20	0.765	Lumachi et al. (26)
ICTP	LC	21	65	ELISA	86.40	84.60	0.87	Yokoyama et al. (31)
TRACP5b	NSCLC	72	69	Immunoassay	63.90	76.80	0.749	Yao et al. (32)
PSA	PC	771	13	ELISA-PSA	91.30	98.70	/	Modoni et al. (33)
BSP	PC	42	41	ELISA	80.95	72.80	/	Wei et al. (34)
PSA	PC	42	41	ELISA	57.14	64.80	/	Wei et al. (34)
ICTP	PC	42	41	ELISA	69.05	76.80	/	Wei et al. (34)
ALP	PC	42	41	ELISA	71.43	88.80	/	Wei et al. (34)
PSA	PC	87	99	ELISA	46.77	53.33	/	Szot et al. (35)
PICP	BC	92	53	ELISA	28.10	83.90		Zissimopoulos et al. (36)
ICTP	BC	92	53	ELISA	48.60	94.00		Zissimopoulos et al. (36)
CEA	BC	92	53	ELISA	42.00	65.00		Zissimopoulos et al. (36)
CA15-3	BC	92	53	ELISA	78.00	86.00		Zissimopoulos et al. (36)
ICTP+CEA +CA15-3	BC	92	53	ELISA	82.00	96.00		Zissimopoulos et al. (36)
PICP+PSA	PC	68	61	ELISA	78.00	96.00	0.970	Zissimopoulos et al. (36)
PICP	PC	42	6	RIA	54.00	93.00	0.840	Zissimopoulos et al. (37)
PSA	PC	42	6	RIA	68.00	91.00	0.880	Zissimopoulos et al. (37)
ICTP	BC	25	12	ELISA	56.00	93.00	/	Tähtelä et al. (38)
PICP	BC	25	12	ELISA	24.00	100.00	/	Tähtelä et al. (38)
PINP	BC	25	12	ELISA	30.00	98.00	/	Tähtelä et al. (38)
CEA	BC	164	200	ELISA+ TECAN	56.70	92.00	/	Wang et al. (39)

(Continued)

TABLE 2 Continued

biomarkers	primary cancer types	Study population characteristics		Diagnostic performance				Ref.
		cases group	Controls group	Research method	Se. (%)	Sp. (%)	AUC	
CA19-9	BC	164	200	ELISA+ TECAN	36.00	82.50	/	Wang et al. (39)
CA125	BC	164	200	ELISA+ TECAN	25.60	97.00	/	Wang et al. (39)
CA15-3	BC	164	200	ELISA+ TECAN	44.50	84.50	/	Wang et al. (39)
TPS	BC	164	200	ELISA+ TECAN	50.00	89.50	/	Wang et al. (39)
CEA+ CA19-9	BC	164	200	ELISA+ TECAN	67.10	78.00	/	Wang et al. (39)
CEA+ CA125	BC	164	200	ELISA+ TECAN	66.50	89.00	/	Wang et al. (39)
CEA+ CA15-3	BC	164	200	ELISA+ TECAN	68.90	88.00	/	Wang et al. (39)
CEA+ TPS	BC	164	200	ELISA+ TECAN	78.70	82.00	/	Wang et al. (39)
CA19-9+CA125	BC	164	200	ELISA+ TECAN	50.00	80.50	/	Wang et al. (39)
CA19-9+CA15-3	BC	164	200	ELISA+ TECAN	60.40	79.50	/	Wang et al. (39)
CA19-9+TPS	BC	164	200	ELISA+ TECAN	64.60	73.50	/	Wang et al. (39)
CA125+ CA15-3	BC	164	200	ELISA+ TECAN	52.40	91.50	/	Wang et al. (39)
CA125+ TPS	BC	164	200	ELISA+ TECAN	56.70	86.50	/	Wang et al. (39)
CA15-3+ TPS	BC	164	200	ELISA+ TECAN	63.40	85.00	/	Wang et al. (39)
Ferritin	NENpts	62	40	EIA	100.00	73.00	0.88	Rosiek et al. (40)
BMG	NENpts	62	40	EIA	100.00	46.00	0.74	Rosiek et al. (40)
CA125	NENpts	62	40	EIA	100.00	39.00	0.66	Rosiek et al. (40)
CEA	NENpts	62	40	EIA	50.00	98.00	0.70	Rosiek et al. (40)
AFP	NENpts	62	40	EIA	50.00	66.00	0.55	Rosiek et al. (40)
CA19-9	NENpts	62	40	EIA	67.00	59.00	0.52	Rosiek et al. (40)
CEA	lung cancer	133	562	Histopathology	76.77	86.33	0.67	Jiang et al. (41)
CA50	lung cancer	133	562	Histopathology	70.00	82.81	0.623	Jiang et al. (41)
CA125	lung cancer	133	562	Histopathology	87.72	72.97	0.748	Jiang et al. (41)
NSE	lung cancer	133	562	Histopathology	82.70	73.00	0.7	Jiang et al. (41)
Ferritin	lung cancer	133	562	Histopathology	92.20	75.40	0.619	Jiang et al. (41)
CYFRA21-1	lung cancer	133	562	Histopathology	54.70	73.70	0.697	Jiang et al. (41)
CEA	BC	54	49	qPCR	48.90	97.10	0.915	Mercatali et al. (42)
CA15-3	BC	54	49	qPCR	64.40	94.40	0.886	Mercatali et al. (42)
OPG	BC	54	49	qPCR	74.10	87.70	0.825	Mercatali et al. (42)
OPG+CEA	BC	54	49	qPCR	84.40	79.50	0.938	Mercatali et al. (42)
OPG+CA15-3	BC	54	49	qPCR	86.70	72.90	0.922	Mercatali et al. (42)
RANK-L	BC	54	49	qPCR	57.40	67.40	0.692	Mercatali et al. (42)
RANK-L+CEA	BC	54	49	qPCR	73.30	50.00	0.907	Mercatali et al. (42)
RANKL+CA15-3	BC	54	49	qPCR	75.6	47.20	0.894	Mercatali et al. (42)
RANK-L/OPG	BC	54	49	qPCR	40.70	77.50	0.70	Mercatali et al. (42)

2.3 ALP and PSA

ALP and PSA are widely used to predict bone metastases of prostate cancer, but their accuracy and reliability in the diagnosis of bone metastases are inconsistent (54). Serum ALP is derived from osteoblasts with isoenzyme activities, which can hydrolyze phosphate esters. Moreover, serum ALP, can be used to indicate the specificity of reflecting bone metastases lesions, regarded as a biomarker of early differentiation of osteoblast precursor cells. ALP is specific biomarkers of bone tissue and widely utilized in bone tumors. The expression level of ALP can be used to estimate the balance between bone reconstruction and destruction. (55). Salter et al. found that ALP was oleophilic, which was an important biomarker reflecting osteoblast activity and tumor progression (56). Rao et al. suggested that ALP was a serum biomarker in predicting bone metastases of prostate cancer (57). Serum PSA, a serine protease, is commonly used in screening, diagnosis and efficacy evaluation of prostate cancer (58). In patients of prostate cancer with bone metastases, due to the proliferation of prostate cancer cells, a large amount of PSA was produced and secreted into the blood, resulting in elevated serum PSA (59, 60). PSA is a good indicator of bone metastases of prostate cancer. The higher the PSA, the greater the risk of bone metastases. When PSA < 20ng/ml, the risk of bone metastases was relatively small, while when PSA > 100ng/ml, the risk of bone metastases was higher than 80%. Therefore, further testing and prophylaxis were recommended when PSA > 20ng/ml (61). Although bone metastases are common sites of prostate cancer, the use of PSA in the diagnosis of bone metastases is limited.

2.4 CA and Rb

CA is used more frequently for the detection of breast and bowel cancer. CA199 is an important biomarker and apparent specific antigen for the detection of bone metastases of liver cancer. Studies have shown that the expression level of CA199 was related to the metastases of liver cancer, with the excellent ability to predict the malignant transformation and prognosis of liver cancer (39, 62). CA724 used for clinical diagnosis and prognosis of found guilty of an important tumor biomarker in breast cancer. Studies have shown that increased level of CA724 may represent increased bone metastases potential of breast cancer, which was more accurate for symptomatic radiotherapy (63, 64). CA50 is an apparent exclusive cancer biomarker used to detect bone metastases of liver cancer. The experimental results indicated that the level of CA50 can serve as a biomarker to predict the potential of bone metastases of liver cancer (65, 66). CA242 is an epigenetic specific antigen used to detect bone metastases in gastric cancer. Studies have indicated that increased level of CA242 can be used to predict bone metastases in gastric cancer, and can effectively help to improve the treatment efficiency and anti-cancer therapeutic effect of tumors (67, 68).

Rb is widely used in the diagnosis of bone-derived tumors, whose reduced expression indicates an increased risk of bone metastasis. (69). P53 is a tumor suppressor gene protein that is abnormally expressed in a variety of tumors. NM23 is an RNA-binding protein that is abnormally expressed in non-small cell lung cancer and some other cancers, whose application in bone tumors is restricted.

In conclusion, the current researches on protein biomarkers of bone metastases are still in the primary stage. Despite the fact that some biomarkers have been proved to have certain application value, more biomarkers need to be explored and applied in the accurate diagnosis of bone metastases and the formulation of treatment plans.

3 Application of ncRNA as biomarkers in bone metastases

With the development of high-throughput sequencing technology and bioinformatics, a large number of ncRNA, such as miRNA, lncRNA and circRNA, have been found to be involved in gene expression regulation, cell differentiation, etc (70, 71). In addition, they are closely related to the occurrence and development of tumors.

3.1 miRNA

miRNA in mammalian serum and plasma have high stability and can be stable under repeated freeze-thaw and different pH conditions (70, 72–74).

miRNA plays an important role in the diagnosis of bone metastases, which can help doctors to identify cancer metastases to bone in order to provide timely treatment (70, 71). Currently, many studies have shown that the expression level of miRNA from samples can be used to identify the presence of bone partially implanted cancer cells (70, 72, 75–77). Some miRNA such as let-7 (78, 79), miR-125b (80, 81), and miR-21 were significantly expressed in experimental tumor migration into the mouse bone, contributing to the identification and diagnosis of bone metastatic cancer (82–84). miRNA plays an important role in tumor therapy, and it has attracted more and more attention as new therapeutic biomarkers (85, 86). Targeting miRNA therapy can reduce drug toxicity and achieve higher efficacy by accurately identifying and treating bone metastases. Contemporary studies have shown that miRNAs-based therapy has a significant promoting effect on inhibiting the growth, invasion and immune resistance of bone metastases (7, 87). Currently, miRNAs that have been considered as biomarkers of bone metastases include miR-21, miR-141, miR-221/222, miR-24, miR-20a, miR-145, miR-29a, miR-26a, miR-22, miR-125b, miR-15b, miR-193b, miR-196a, and miR-101 et al., which were shown in Table 3.

3.1.1 miR-21

miR-21 has been extensively studied as a key biomarker for various types of cancer, including breast, lung, prostate, ovarian, and colorectal cancers (82–84). One study found that miR-21 was significantly up regulated in bone metastases tissue samples,

TABLE 3 Application of ncRNA biomarkers of bone metastases.

Biobiomarker	Bone transition stage	Primary cancer types	Study population characteristics		Clinical application	Deregulation	Ref.
			Cases group	Controls group			
miR-192-5p	Mixed	LC	68	78	Early diagnosis and prediction of bone metastases.	Low-expression	Zou P et al. (88)
miR-335	Osteoblastic	SCLC	10	5	Diagnosis of bone metastases in prostate cancer, miR-335 might target cytokines linked to osteoclast induction and bone turnover.	Over-expression	Gong et al. (89)
miR-139-5p	Osteoblastic	NSCLC	25	30	As a biobiomarker and treatment target in monitoring and controlling bone metastases.	Down-regulated	Xu et al. (90)
miR-139-5p	Mixed	EWS	19	/	Down-regulation of miR-139-5p is associated with disease progression in EWS and may serve as a risk assessment biobiomarker.	Down-regulated	Roberto et al. (91)
miR-124-3p	Mixed	EWS	19	/	Down-regulation of miR-124-3p is associated with disease progression in EWS and may serve as a risk assessment biobiomarker.	Down-regulated	Roberto et al. (91)
miR-584-5p	Mixed	EWS	19	/	Down-regulation of miR-584-5p is associated with disease progression in EWS and may serve as a riskassessment biobiomarker.	Down-regulated	Roberto et al. (91)
miR-7	Osteolytic	BC	51	4	Promoting cancer cell progress and consequently results in NSCLC growth. miR-7 may become promising molecular therapies in NSCLC treatment.	Down-regulated	Vimalraj et al. (92)
let-7c	Mixed	LAC	/	/	Low levels of let-7c expression and metastases, venous invasion, advanced TNM stages and poor survival of NSCLC patients.	Down-regulated	Zhao et al. (79)
miR-10b	Osteolytic	BC	122	59	An independent prognostic factor in NSCLC patients.	Up-regulated	Zhao et al. (93)
miR-17 family	Osteolytic	OS	75	/	Not only decrease cisplatin-resistant but also reduce migration by inhibiting EMT in A549/DDP cells.	Over-expression	Arabi et al. (94)
miR-21	Osteolytic	OS	65	/	Regulate the biological characteristics of tumor cells and the ability of bone metastases.	Low-expression	Yuan et al.(82)
miR-16/miR-15a	Osteoblastic	PC	99	5	miR-15/miR-16 control organ-confined and distant invasion of prostate cancer cells.	Over-expression	Bonci et al.(83)
miR-141	Osteoblastic	PC	52	89	Inhibit the growth of osteoclasts by inhibiting the synthesis of bone morph regulatory factors.	Down-expression	Huang et al. (69)
miR-221/222	Mixed	PC	18	3	Actively involved in bone metastases of cancers such as prostate cancer and breast cancer.	Low-expression	Xu et al. (95)
miR-24	Osteolytic	OS	/	/	Affect the onset, development and subsequent therapeutic effect of bone metastases.	Over-expression	Liu et al. (2017) (96)
miR-20a	Osteolytic	OS	10	8	Enhance immune function, reduce inflammatory response and promote the body's immune response to tumors.	Over-expression	Koshkina et al. (97)
miR-145	Osteoblastic	ESCC	19	19	Affecting the migration and reproduction of cancer cells in bone marrow, and helping to inhibit the occurrence of bone metastatic tumors.	Over-expression	Cui et al. (98)
miR-29a	Osteoblastic	SCLC	10	/	Inhibit the mechanism of cancer cells, and inhibit the migration and reproduction of cancer cells in bone marrow, thus inhibiting the occurrence of bone metastatic tumors.	Over-expression	Gong et al. (89)
HOTAIR	Mix	BC	/	/	HOTAIR affects and blocks the growth, metastasis and apoptosis of breast cancer cells through the miR-20a-5p/HMGA2 axis	Down-expression	Zhao et al. (99)
circITGA7	Mix	OS	/	/	circITGA7 may be involved in the occurrence and development of bone metastases	Down-expression	Fang et al. (100)

compared to primary tumor tissue samples from patients with breast cancer (9). Furthermore, they observed that serum levels of miR-21 were significantly higher in breast cancer patients with bone metastases. They suggested that miR-21 could be used as a non-invasive biomarker to detect bone metastases in breast cancer patients. Similarly, another study found that miR-21 was over expressed in bone metastases tissue samples from patients with prostate cancer. They observed that miR-21 expression was positively correlated with bone metastases, suggesting that miR-21 could be used as a prognostic biomarker to predict the progression of bone metastases in prostate cancer patients (101). One study analyzed miR-21 expression in serum samples from patients with breast cancer and bone metastases, as well as healthy controls, drawing a conclusion that serum levels of miR-21 were significantly higher in breast cancer patients with bone metastases, compared to healthy controls. (102). Overall, the above studies suggested that miR-21 was a promising biomarker in the detecting and monitoring of bone metastases in various types of cancer. Its potential use as a therapeutic target warrants further investigation in preclinical and clinical studies.

3.1.2 miR-141

miR-141 has been a top priority in the study of bone metastases in recent years (103, 104). miR-141 can inhibit adenovirus transcription factors, immune response and apoptosis-mediated response, and exert a huge effect on inhibiting tumor growth to promote factor expression and inhibit gene expression regulation (105, 106). Studies have shown that miR-141 is paramount in preventing the development of bone metastases (106). In previous studies, miR-141 can prohibit the growth of osteoclasts by inhibiting the synthesis of bone morph regulatory factors, thus delaying the metastases process (107, 108). Meanwhile, miR-141 interdicted the migration and invasion of bone metastases. In addition, miR-141 can also induce tumor cell apoptosis, thus playing a momentous role in the process of bone metastases (109, 110). In conclusion, miR-141 is instrumental in inhibiting the development of bone metastatic tumors and may be essential in clinical diagnosis and treatment of bone metastatic tumors in the future.

3.2 lncRNA and circRNA

lncRNA and circRNA are a class of emerging ncRNA, playing important roles in the occurrence and development of human diseases. In recent years, more and more studies have shown that lncRNA and circRNA may also be strong candidates for tumor biomarkers of bone metastasis. There are some studies have found that lncRNA is crucical in bone metastasis. For example, one research has shown that metastasis-associated lung adenocarcinoma transcript 1 (MALAT1) can promote tumor cell invasion and migration, whose expression level was elevated in patients with bone metastasis (111). Other lncRNAs such as HOX antigens intergenic RNA (HOTAIR) and taurine unregulated gene 1 (TUG1) have also been found to be closely associated with the occurrence and development of bone metastases. HOTAIR affected and blocked the growth, metastasis, and apoptosis of breast cancer cells through the miR-20a-5p/HMGA2 axis. In the past few years, studies have found that lncRNA-SOX2OT may have clinical diagnostic value and can be employed as an *in vitro* diagnostic biomarker for bone metastases (110). It was found that the level of lncRNA-SOX2OT in serum in patients with bone metastases were significantly higher than those in the control group (112). Besides, studies had found that lncRNA-SOX2OT might regulate the phenotype of bone metastatic tumor cells. It was also found that lncRNA-SOX2OT inhibited the expression of MMP-13, which explained why lncRNA -Sox2OT may be associated with the regulation of bone metastases (113). Moreover, by combining multiple gene factors, we found that HIF-1, Hypoxia, and LCC-Sox2OT gene regulatory networks may present in bone metastases. What' more, the researchers suggested that the expression of LCC-Sox2OT may be related to cell status, which can be used to identify biomarkers *in vitro*, and to identify and forecast the incidence of bone metastatic tumors *in vivo* (54, 112, 114, 115).

In contrast, circRNA has been relatively poorly studied in bone metastasis (99). What's more, some studies have shown that circRNA may also be a biomarker of bone metastases. For instance, there reported a study showing that circITGA7 (circular RNA-integrin subunit alpha 7) may be involved in the occurrence and development of bone metastases. This circular transcription can inhibit apoptosis of a variety of cells, whose expression level was significantly increased in patients with bone metastasis (100). Of course, studies on tumor biomarkers for bone metastases in lncRNA and circRNA are still in the preliminary stage, and their potential mechanisms and clinical application value need to be further verified and explored.

4 Bone metastasis biomarkers in liquid biopsy

Compared with traditional tissue sample biopsies, liquid biopsy-based markers have the following advantages:1. Non-invasive: Liquid sample collection is relatively simple, such as blood, urine, etc., without tissue excision or puncture, which can reduce patients' pain and risk. 2. Systemic: Liquid samples can reflect the situation of the whole body, avoiding local errors in the collection of tissue samples, making them more representative and comprehensive. 3. High sensitivity: the concentration of markers in liquid samples is relatively stable and is not affected by tissue heterogeneity, making the detection results more accurate and reliable. 4. Good repeatability: liquid sample collection is relatively simple and non-invasive, which can be collected multiple times to monitor tumor growth and metastasis. 5. Forward-looking: in the detection and monitoring of early tumors, liquid biopsy can provide a more flexible and sensitive detection method, and improve the rate of early diagnosis and treatment of tumors. For tumor biomarkers of bone metastasis in liquid biopsy, molecular indicators related to bone metastasis, such as ctDNA, exosomes and circulating tumor cells (CTCs), were mainly screened from biological fluids such as blood or urine.

TABLE 4 Bone metastasis tumor biomarkers in liquid biopsy.

Biobiomarker	Bone transition stage	Primary cancer types	Clinical application	Deregulation	Ref.
CD44	Osteolytic	SCLC	An important role as an early diagnostic biomarker and prognostic indicator of bone metastases.	Over-expression	Zhao et al. (116)
CXCR4	Mixed	LC	Associated with metastases of tumor cells to bone tissue and can be used as an essential biomarker of bone metastatic tumors.	Over-expression	Chai et al. (54)
CD74	Osteoblastic	NSCLC	Predict the pathological changes of tumors and the prognosis of tumor patients after treatment.	Up-regulated	Loreth et al. (2021) (117)
Mesothelin /CK19	Osteoblastic	ESCC	Diagnose and predict the development of tumors.	Over-expression	Zhang et al. (2010) (118)
Osteopontin /CAIX	Osteoblastic	BC	Assess the risk of tumor invasiveness and metastases.	Low-expression	Jiwa et al. (2014) (119)
CXCR4	Mixed	Gastrointestinal malignancies	Associated with metastases of tumor cells to bone tissue and can be used as an essential biomarker of bone metastatic tumors.	Over-expression	Roberto et al. (91)

These indicators have the advantages of high sensitivity, non-trauma and dynamic monitoring, which can be utilized to achieve early detection, monitor and prediction of bone metastasis. Corresponding contents were shown in Table 4.

4.1 ctDNA

ctDNA is a piece of DNA which was released into the blood by cancer cells with certain specificity and sensitivity. ctDNA is a piece of DNA that is released into the bloodstream when cancer cells die or die. Unlike normal plasma DNA, ctDNA contains specific variations from tumor cells. Therefore, ctDNA can be used as a non-invasive "liquid biopsy" method, which can be widely used in the early diagnosis, treatment monitoring and prognosis assessment of tumors. ctDNA has the following advantages: 1. Non-invasive: ctDNA sampling is simple and non-invasive, requiring no painful tissue removal or cancer cell culture. 2. High sensitivity: The proportion of ctDNA in the blood is very low, so it can be detected even in the mild disease, especially in the primary tumor detection has a better application prospect. 3. High specificity: ctDNA contains specific variations from tumor cells, which can distinguish different subtypes and tumors at different stages of synchronization. 4. Real-time dynamic monitoring can be realized: ctDNA can reflect real-time treatment progress, drug resistance and relapse, which can provide doctors with better treatment strategies. To sum up, ctDNA as a tumor marker has great advantages and has gradually become a hot spot in cancer research.

In the detection of bone metastases, studies on ctDNA as a kind of biomarker in bone metastases mainly focus on the following aspects. ctDNA tests based on gene mutations. Firstly, some mutations associated with bone metastases, such as the fatty acid acylase gene (ACSL5) and the fusion gene TMPRSS2-ERG, had been shown to have high sensitivity and specificity when ctDNA was detected in the blood. These mutations were valuable for the detection of bone metastases (120). For example, one study found that ctDNA, which detected a deletion of the *PTEN* and mutation of the *TP53*, had high sensitivity and specificity in the plasma of prostate cancer patients. Secondly, the detection of ctDNA is based on epigenetic changes. Bone metastasis is also closely associated with epigenetic changes in DNA methylation and histone modification. Studies had shown that some epigenetic biomarkers such as *RASSF1A* (121), *IGFBP-3* (74), *MGMT* and ctDNA of *GSTP1* can be detected in patients with bone metastases. These biomarkers provided an accurate value for the early detection and evaluation of bone metastases. Finally, the detection of ctDNA based on microsatellite instability (MSI), which is usually caused by the depletion of mismatch repair systems *in vivo* and is a hallmark of many familial non-multiple systemic tumors. It has been noted that the appearance of MSI in cancer cells is closely related to the occurrence and development of bone metastasis. There was a study showed that the detection of MSI in ctDNA could be used to evaluate the prognosis of bone metastases in intestinal cancer, providing a reference for the selection of treatment (122). In conclusion, the research and application of ctDNA as tumor biomarkers in bone metastases are developing and improving all the time. Although it still faces some technical and methodological bottlenecks, future studies will continuously improve its application prospect and clinical value. It is expected to become an important indicator in the timely detection, prognosis assessment and treatment monitoring of bone metastases.

4.2 CTCs

CTCs are cells shed from tumors and enter the peripheral blood of the body, which are the highest manifestation of the spread of malignant tumors. The genetic characteristics or antigens of CTCs are identical to those of primary tumor cells, but the method of obtaining CTCS is less invasive and highly reproducible (123).

Systematic monitoring of CTCS through liquid biopsies enables monitoring of disease processes, detecting emerging resistance genes, and identifying new molecular targets (124). Relevant studies had shown that CTCs were highly invasive and malignant, and could evade immune surveillance of the body. CTCs can reflect the characteristics of tumor metastases and disease changes in patients with malignant tumors, playing crucial part in the curative effect and recurrence prediction of malignant tumors, so as to provide a reference for the early diagnosis and treatment of diseases (125). Detection of CTCs is a prerequisite for distant metastases of solid tumors (126). The specific contents were shown in Table 4.

Taking CD44 for example. CD44 is a protein, which is deemed to be a pathological indicator. It is generically known as CD44 receptor, also known as adhesion molecule, which is a variety of tumor cell adhesion molecule genes, associated with signal activation and cell cross-coupling of cell molecules (127, 128). Clinical studies had shown that CD44 was a diagnostic biomarker and prognostic indicator in a variety of tumors, including liver cancer, stomach cancer, esophageal cancer, ovarian cancer, prostate cancer, etc. It can be found in blood, cellular mediators, tissue biopsy specimens, tumor cells, and normal cells (129, 130). Studies had shown that the expression of CD44 was related to the expression of late genes such as *PD-L1*. Its expression may also matter in the early detection of tumors and later forms of metastases. Laboratory studies have demonstrated that CD44 can form binding with chemical factors of mitogen and cell surface, improve cell binding to other cell surface molecules and thus increase the risk of bone metastases (127, 131).

4.3 Exosomes

Extracellular vehicles (EVs) include apoptotic bodies (ABs), microvesicles (MVs), and exosomes, encapsulate tumor-specific content, and transmit them into environmental cells and circulation. Exosomes as molecular biomarkers, play major roles in diagnostic decisions and treatment selection in the detection of cancer bone metastases (132). Exosomes have relatively stable components that confer biological effects on adjacent or distal cells. Exosomes are also nanoparticles secreted by all cell types (133, 134). Due to their nature as nanovesicles, exosomes can be transferred proximal and distal across different biological barriers. Exosomes have been used as transport carriers for a variety of molecules including proteins and different RNA (135).

Therefore, exosomes can be used not only as reaction markers of different diseases and physiological states, but also as tools of *in vitro* genetic engineering for the treatment of different diseases and organs. This shows that exosomes, as communication mediators between cells, have infinite potential as biomarkers. From the perspective of exosome functioned as molecular biomarkers, exosomes function importantly in the molecular linkage of bone metastases tumor, accurate detection and quantification of bone metastases tumor biomarkers, which are extremely important (136). On the one hand, the studies of exosome molecular biomarker will provide useful information that can help clinicians more accurately in diagnosing bone metastases. Exosomes can be detected diagnostic cancer biomarkers in body fluids, such as prostate specific nucleic acid expression (PNA), gastrointestinal specific protein expression (GIP), and respiratory specific nucleic acid expression (RNA) (137, 138), which can identify cancer cells faster and more accurately, providing more detailed and reliable molecular information of cancer cells, so as to better predict the trend of cancer cell metastases and provide more accurate treatment guidance.

miR-375 and miR-141, which from exosomes, are the main biomarkers of bone metastases, which are mainly involved in regulating the respiration and proliferation of cancer cells (7, 57). The increased expression of miR-375 can promote the malignant proliferation of cancer cells. On the contrary, miR-141 will promote and inhibit the proliferation of cancer cells, reduce the damage to sensitive cancer cells, and decrease the resistance to drug-resistant cancer cells (139). In addition, TM256, LAMTOR1 and VATL were tumor biomarkers associated with miR-141 and miR-375. TM256 can recognize the increased expression of miR-141 and promote the proliferation and growth of cancer cells (103). LAMTOR1 can recognize the increased expression of miR-141 and miR-375 and inhibit the proliferation and growth of cancer cells (69). VATL can recognize the increased expression of miR-375 and promote malignant proliferation of cancer cells. ADIRF was a specific tumor biomarker that can detect and recognize increased expression of miR-375 and miR-141, thereby contributing to the growth and proliferation of cancer cells (104, 140).

5 Application of other kinds of biomarkers in bone metastases

DNA methylation is a joint biological modification that affects gene expression by introducing methyl groups into DNA molecules through methylase. In tumor cells, the change of DNA methylation degree is closely linked to tumor growth, cell proliferation and development. Currently, there are many biomarkers of bone metastases based on DNA methylation, which include many different types. Glutathione S transferase P1 (GSTP1) is an antioxidant enzyme whose DNA methylation leaded to decreased expression levels, which had been demonstrated in many tumor cases, including bone metastases (141). SEPT9 was often considered a biomarker of DNA methylation. Recent studies had shown that exon 8 methylation of SEPT9 was a valid biomarker for blood samples (both venous and serum) from lung cancer patients (141, 142). The HOXB gene family is a member of the HOX gene superfamily, and HOXB7 may acted as a proto-oncogene in a variety of malignancies (143). DNA methylation of HOXB7 gene played an essential role in bone metastasis of prostate cancer cells (144). That is to say, DNA methylation of bone metastases tumor biomarkers provides a novel idea and means for the diagnosis, monitor and treatment of bone metastases. However, more studies are required to confirm their clinical application prospects as well as their sensitivity, specificity and stability.

Histone methylation is a key epigenetic modification, which plays a balancing and regulating role in gene transcription and expression. Tumor markers of bone metastases targeted at histone

methylation mainly include the following aspects. H3K9me3 is the triumphalist form of the 9th lysine of histone H3 and is a silencing marker for many genes. The loss or reduction of H3K9me3 in bone metastases may be related to its enhanced ability to metastasize and the difference in prognosis (145). H3K27me3 is the triumphalist form of the 27th lysine of histone H3, which plays an important role in cell growth and differentiation. Reduction of H3K27me3 in bone metastasis may lead to inhibition of apoptosis and the growth and metastasis of cancer cells (146). H3K4me3 is the triumphalist form of lysine at the fourth position of histone H3, which is a marker of enrichment in genes with high transcriptional activity. During the treatment of patients with bone metastases, prominent expression of H3K4me3 was associated with the prognosis and progression of bone metastases (147). In conclusion, the study of histone methylation tumor markers of bone metastasis provides a novel idea and means for the early detection and treatment of bone metastasis. Although there are still some challenges in the application, they are expected to be one of the principal markers of bone metastasis in the future.

6 Perspectives and future opportunities

This paper mainly introduces the commonly used clinical protein biomarkers, ncRNA, and liquid biopsy biomarkers. Each type has its specific advantages, limitations in the clinical application. Protein-based tumor biomarkers have been extensively studied and have a wide range of applications, including diagnosis, disease surveillance and therapeutic strategies. Numerous protein measurement techniques and automated methods have been rapidly developed, making high-throughput identification and measurement easy and fast. Proteins can be interfered with by external factors (such as diet and preparations), and in some cases of proteins may be non-specific, which can lead to false positives. So, the interpretation of the results does not necessarily reflect accurate. Compared with proteins, the structure and function of ncRNAs are still being studied, so understanding the role of ncRNAs and their detection techniques are limited. Some ncRNAs may be raised at similar levels in multiple tumor types and non-tumor diseases, so there may be some limitations in the differential diagnosis process. To sum up, these types of biomarkers have their peculiar advantages and disadvantages, and the future development will be different depending on the specific application. Among them, miRNA, as an emerging method, may be the future direction while further understanding its biological role and mechanism. Due to the wide variety of biomarkers, this study mainly elaborated protein, ncRNAs, liquid biopsy biomarkers and other studied biomarkers, which were mainly derived from serum plasma and tissue. Our team will conduct a more comprehensive and detailed description of such biomarkers in subsequent studies, so as to provide reference for the clinical application of biomarkers of bone metastases and the early diagnosis of diseases.

Future research on how to find new methods of screening and detecting biomarkers, and the set of cut-off value, etc., not only for detection but also for prognosis is needed. Firstly, large-scale prospective clinical studies are required. More large-scale prospective clinical studies are needed to confirm the sensitivity, specificity, and stability of different markers, as well as their feasibility for early detection, classification, and treatment of bone metastases. Secondly, combinations of multiple biomarkers can be studied. Combined with biomarkers of different types of bone metastases, a more accurate diagnosis and prediction model was established. In the process of integration, it is necessary to investigate the interaction, influence and cooperation among different biomarkers, and establish the corresponding bioinformatics model and algorithm combined with bioinformatics. Finally, multidisciplinary cooperation and communication is important. There is necessary to have closer collaboration among clinicians, basic scientists, bioinformatics specialists and engineers to leverage their expertise and skills to better support the research and application of markers for bone metastases.

In conclusion, in the future, the study of bone metastases tumor markers will gradually develop from a single biomarker study to a systematic and integrated research model, so as to more accurately and comprehensively understand the biological characteristics and clinical manifestations of bone metastases, promoting more significant progress in the diagnosis and treatment of bone metastases.

Author contributions

JL and HL conceived the research. YH and FZ conducted the study and drafted the manuscript, and they contributed equally to this work. YM, YL, YZ, NY, ML contributed to the acquisition, or interpretation of data and critically reviewed and revised the article for important intellectual content. All authors contributed to the article and approved the submitted version.

Funding

This work was supported by the National Natural Science Foundation of China (82004397), the Innovation Fund of National Clinical Research Center for Orthopedics, Sports Medicine & Rehabilitation (2021-NCRC-CXJJ-PY-13), Young Elite Scientists Sponsorship Program by CAST (2021-QNRC2-A06), and the Major Project of TCM research in Henan Province (2023ZY2136).

Conflict of interest

The authors declare that the research was conducted in the absence of any commercial or financial relationships that could be construed as a potential conflict of interest.

Publisher's note

References

1. Yin JJ, Pollock CB, Kelly K. Mechanisms of cancer metastases to the bone. *Cell Res* (2005) 15:57–62. doi: 10.1038/sj.cr.7290266

2. Jimenez-Andrade JM, Mantyh WG, Bloom AP, Ferng AS, Geffre CP, Mantyh PW. Bone cancer pain. *Ann N Y Acad Sci* (2010) 1198:173–81. doi: 10.1111/j.1749-6632.2009.05429.x

3. Coleman RE, Croucher PI, Padhani AR, Clézardin P, Chow E, Fallon M, et al. Bone metastases. *Nat Rev Dis Primers* (2020) 6:83. doi: 10.1038/s41572-020-00216-3

4. Alfranca A, Martinez-Cruzado L, Tornin J, Abarrategi A, Amaral T, de Alava E, et al. Bone microenvironment signals in osteosarcoma development. *Cell Mol Life Sci* (2015) 72:3097–113. doi: 10.1007/s00018-015-1918-y

5. Yip RKH, Rimes JS, Capaldo BD, Vaillant F, Mouchemore KA, Pal B, et al. Mammary tumour cells remodel the bone marrow vascular microenvironment to support metastases. *Nat Commun* (2021) 12:6920. doi: 10.1038/s41467-021-26556-6

6. Kruger TE, Miller AH, Godwin AK, Wang J. Bone sialoprotein and osteopontin in bone metastases of osteotropic cancers. *Crit Rev Oncol Hematol* (2014) 89:330–41. doi: 10.1016/j.critrevonc.2013.08.013

7. Li Z, Li LX, Diao YJ, Wang J, Ye Y, Hao XK. Identification of urinary exosomal miRNAs for the non-invasive diagnosis of prostate cancer. *Cancer Manag Res* (2021) 13:25–35. doi: 10.2147/cmar.S272140

8. Hirai T, Shinoda Y, Tateishi R, Asaoka Y, Uchino K, Wake T, et al. Early detection of bone metastases of hepatocellular carcinoma reduces bone fracture and paralysis. *Jpn J Clin Oncol* (2019) 49:529–36. doi: 10.1093/jjco/hyz028

9. Wang Y, Ding Y, Guo N, Wang S. MDSCs: key criminals of tumor pre-metastatic niche formation. *Front Immunol* (2019) 10:172. doi: 10.3389/fimmu.2019.00172

10. Shackleton M, Yuen K, Little AF, Schlicht S, McLachlan SA. Reliability of X-rays and bone scans for the assessment of changes in skeletal metastases from breast cancer. *Intern Med J* (2004) 34:615–20. doi: 10.1111/j.1445-5994.2004.00637.x

11. Wei Y, Xiao J, Zou L. Masticator space: CT and MRI of secondary tumor spread. *AJR Am J Roentgenol* (2007) 189:488–97. doi: 10.2214/ajr.07.2212

12. Rong J, Wang S, Ding Q, Yun M, Zheng Z, Ye S. Comparison of 18 FDG PET-CT and bone scintigraphy for detection of bone metastases in breast cancer patients. a meta-analysis. *Surg Oncol* (2013) 22:86–91. doi: 10.1016/j.suronc.2013.01.002

13. Dyrberg E, Hendel HW, Huynh THV, Klausen TW, Løgager VB, Madsen C, et al. (68) Ga-PSMA-PET/CT in comparison with (18)F-fluoride-PET/CT and whole-body MRI for the detection of bone metastases in patients with prostate cancer: a prospective diagnostic accuracy study. *Eur Radiol* (2019) 29:1221–30. doi: 10.1007/s00330-018-5682-x

14. Donners R, Figueiredo I, Tunariu N, Blackledge M, Koh DM, de la Maza M, et al. Multiparametric bone MRI can improve CT-guided bone biopsy target selection in cancer patients and increase diagnostic yield and feasibility of next-generation tumour sequencing. *Eur Radiol* (2022) 32:4647–56. doi: 10.1007/s00330-022-08536-6

15. Aryal A, Kumar VS, Shamim SA, Gamanagatti S, Khan SA. What is the comparative ability of 18F-FDG PET/CT, 99mTc-MDP skeletal scintigraphy, and whole-body MRI as a staging investigation to detect skeletal metastases in patients with osteosarcoma and Ewing sarcoma? *Clin Orthop Relat Res* (2021) 479:1768–79. doi: 10.1097/corr.0000000000001681

16. Ottosson F, Baco E, Lauritzen PM, Rud E. The prevalence and locations of bone metastases using whole-body MRI in treatment-naïve intermediate- and high-risk prostate cancer. *Eur Radiol* (2021) 31:2747–53. doi: 10.1007/s00330-020-07363-x

17. Tayob N, Kanwal F, Alsarraj A, Hernaez R, El-Serag HB. The performance of AFP, AFP-3, DCP as biomarkers for detection of hepatocellular carcinoma (HCC): a phase 3 biobiomarker study in the united states. *Clin Gastroenterol Hepatol* (2023) 21 (2):415–23. doi: 10.1016/j.cgh.2022.01.047

18. Park SJ, Jang JY, Jeong SW, Cho YK, Lee SH, Kim SG, et al. Usefulness of AFP, AFP-L3, and PIVKA-II, and their combinations in diagnosing hepatocellular carcinoma. *Med (Baltimore)* (2017) 96(11):e5811. doi: 10.1097/MD.0000000000005811

19. Zhu AX, Dayyani F, Yen CJ, Ren Z, Bai Y, Meng Z, et al. Alpha-fetoprotein as a potential surrogate biobiomarker for atezolizumab + bevacizumab treatment of hepatocellular carcinoma. *Clin Cancer Res* (2022) 28(16):3537–45. doi: 10.1158/1078-0432.CCR-21-3275

20. Luo P, Yin P, Hua R, Tan Y, Li Z, Qiu G, et al. Multicenter serum metabolite biobiomarker identification study for the early detection of hepatocellular carcinoma. *Hepatology* (2018) 67(2):662–75. doi: 10.1002/hep.29561

21. Chalasani NP, Ramasubramanian TS, Bhattacharya A, Olson MC, Edwards V DK, Roberts LR, et al. A novel blood-based panel of methylated DNA and protein biomarkers for detection of early-stage hepatocellular carcinoma. *Clin Gastroenterol Hepatol* (2021) 19(12):2597–2605.e4. doi: 10.1016/j.cgh.2020.08.065

22. Chen D, Li Z, Song Q, Qian L, Xie B, Zhu J. Clinicopathological features and differential diagnosis of hepatocellular carcinoma in extrahepatic metastases. *Med (Baltimore).* (2018) 97(50):e13356. doi: 10.1097/MD.0000000000013356

23. Calaminus G, Schneider DT, Bökkerink JP, Gadner H, Harms D, Willers R, et al. Prognostic value of tumor size, metastases, extension into bone, and increased tumor biomarker in children with malignant sacrococcygeal germ cell tumors: a prospective evaluation of 71 patients treated in the German cooperative protocols maligne keimzelltumoren (MAKEI) 83/86 and MAKEI 89. *J Clin Oncol* (2003) 21(5):781–6. doi: 10.1200/JCO.2003.03.125

24. Chen XY, Lan M, Zhou Y, Chen WZ, Hu D, Liu JM, et al. Risk factors for bone metastasis from renal cell cancer. *J Bone Oncol* (2017) 9:29–33. doi: 10.1016/j.jbo.2017.10.004

25. Tamiya M, Tokunaga S, Okada H, Suzuki H, Kobayashi M, Sasada S, et al. Prospective study of urinary and serum cross-linked n-telopeptide of type I collagen (NTx) for diagnosis of bone metastasis in patients with lung cancer. *Clin Lung Cancer.* (2013) 14(4):364–9. doi: 10.1016/j.cllc.2012.11.006

26. Lumachi F, Santeufemia DA, Del Conte A, Mazza F, Tozzoli R, Chiara GB, et al. Carboxy-terminal telopeptide (CTX) and amino-terminal propeptide (PINP) of type I collagen as biomarkers of bone metastases in patients with non-small cell lung cancer. *Anticancer Res* (2013) 33(6):2593–6.

27. Aruga A, Koizumi M, Hotta R, Takahashi S, Ogata E. Usefulness of bone metabolic biomarkers in the diagnosis and follow-up of bone metastasis from lung cancer. *Br J Cancer* (1997) 76(6):760–4. doi: 10.1038/bjc.(1997).458

28. Horiguchi T, Tachikawa S, Kondo R, Hirose M, Teruya S, Ishibashi A, et al. Usefulness of serum carboxy-terminal telopeptide of type I collagen (ICTP) as a biomarker of bone metastasis from lung cancer. *Jpn J Clin Oncol* (2000) 30(4):174–9. doi: 10.1093/jjco/hyd043

29. Min JW, Um SW, Yim JJ, Yoo CG, Han SK, Shim YS, et al. The role of whole-body FDG PET/CT, Tc 99m MDP bone scintigraphy, and serum alkaline phosphatase in detecting bone metastasis in patients with newly diagnosed lung cancer. *J Korean Med Sci* (2009) 24(2):275–80. doi: 10.3346/jkms.2009.24.2.275

30. Tang C, Liu Y, Qin H, Li X, Guo W, Li J, et al. Clinical significance of serum BAP, TRACP 5b and ICTP as bone metabolic biomarkers for bone metastasis screening in lung cancer patients. *Clin Chim Acta* (2013) 426:102–7. doi: 10.1016/j.cca.2013.09.011

31. Yokoyama T, Yamamoto M, Shima K, Suzuki K, Sako C, Ito G, et al. Clinical usefulness of serum pyridinoline cross-linked carboxyterminal telopeptide of type I collagen for diagnosis of bone metastases in patients with primary lung cancer. *Respirology* (2005) 10:300–304. doi: 10.1111/j.1440-1843.2005.00713.x

32. Yao NS, Wu YY, Janckila AJ, Ku CH, Hsieh AT, Ho CL, et al. Serum tartrate-resistant acid phosphatase 5b (TRACP5b) activity as a biobiomarker for bone metastasis in non-small cell lung cancer patients. *Clin Chim Acta* (2011) 412(1-2):181–5. doi: 10.1016/j.cca.2010.09.038

33. Modoni S, Calò E, Nardella G, Ritrovato G, Frusciante V. PSA and bone scintigraphy. *Int J Biol biomarkers.* (1997) 12(4):158–61. doi: 10.1177/172460089701200404

34. Wei RJ, Li TY, Yang XC, Jia N, Yang XL, Song HB. Serum levels of PSA, ALP, ICTP, and BSP in prostate cancer patients and the significance of ROC curve in the diagnosis of prostate cancer bone metastases. *Genet Mol Res* (2016) 15(2):gmr7707. doi: 10.4238/gmr.15027707

35. Szot W, Kostkiewicz M, Zając J, Owoc A, Bojar I. Prostate cancer in patients from rural and suburban areas–PSA value, Gleason score and presence of metastases in bone scan. *Ann Agric Environ Med* (2014) 21(4):888–92. doi: 10.5604/12321966.1129953

36. Zissimopoulos A, Stellos K, Matthaios D, Petrakis G, Parmenopoulou V, Babatsikou F, et al. Type I collagen biomarkers in the diagnosis of bone metastases in breast cancer, lung cancer, urinary bladder cancer and prostate cancer. comparison to CEA, CA 15-3, PSA and bone scintigraphy. *J BUON.* (2009) 14(3):463–72.

37. Zissimopoulos A, Stellos C, Petrakis G, Baziotis N. In process citation correlation of procollagen (I) with prostate specific antigen and bone scan for the diagnosis of bone metastases in patients with prostate carcinoma. *Hell J Nucl Med* (2004) 7(3):162–7.

38. Tähtelä R, Thölix E. Serum concentrations of type I collagen carboxyterminal telopeptide (ICTP) and type I procollagen carboxy-and aminoterminal propeptides (PICP, PINP) as biomarkers of metastatic bone disease in breast cancer. *Anticancer Res* (1996) 16(4B):2289–93.

39. Wang W, Xu X, Tian B, Wang Y, Du L, Sun T, et al. The diagnostic value of serum tumor biomarkers CEA, CA19-9, CA125, CA15-3, and TPS in metastatic breast cancer. *Clin Chim Acta* (2017) 470:51–5. doi: 10.1016/j.cca.2017.04.023

40. Rosiek V, Wójcik-Giertuga M, Kos-Kudła B. Serum tumor biomarkers for detection of bone metastases in patients with lung neuroendocrine neoplasms". *Cancer Treat Res Commun* (2022) 31:100533. doi: 10.1016/j.ctarc.2022.100533

41. Jiang M, Chen P, Zhang X, Guo X, Gao Q, Ma L, et al. Metabolic phenotypes, serum tumor biomarkers, and histopathological subtypes in predicting bone metastasis: analysis of 695 patients with lung cancer in China. *Quant Imaging Med Surg* (2023) 13 (3):1642–54. doi: 10.21037/qims-22-741

42. Mercatali L, Ibrahim T, Sacanna E, Flamini E, Scarpi E, Calistri D, et al. Bone metastases detection by circulating biomarkers: OPG and RANK-l. *Int J Oncol* (2011) 39(1):255–61. doi: 10.3892/ijo.2011.1001

43. Galle PR, Foerster F, Kudo M, Chan SL, Llovet JM, Qin S, et al. Biology and significance of alpha-fetoprotein in hepatocellular carcinoma. *Liver Int* (2019) 39:2214–29. doi: 10.1111/liv.14223

44. Evdokimova VN, Butterfield LH. Alpha-fetoprotein and other tumour-associated antigens for immunotherapy of hepatocellular cancer. *Expert Opin Biol Ther* (2008) 8:325–36. doi: 10.1517/14712598.8.3.325

45. Okunaka T, Kato H, Konaka C, Yamamoto H, Furukawa K. Primary lung cancer producing alpha-fetoprotein. *Ann Thorac Surg* (1992) 53:151–2. doi: 10.1016/0003-4975(92)90778-3

46. Xiong S, Tang K, Luo F. An extensive surgical resection in stage T4 small cell lung cancer with cardiac invasion: a case report and literature review. *Ann Med Surg (Lond)* (2022) 81:104448. doi: 10.1016/j.amsu.2022.104448

47. Tonyali O, Gonullu O, Ozturk MA, Kosif A, Civi OG. Hepatoid adenocarcinoma of the lung and the review of the literature. *J Oncol Pharm Pract* (2020) 26:1505–10. doi: 10.1177/1078155220903360

48. Aass N, Klepp O, Cavallin-Stahl E, Dahl O, Wicklund H, Unsgaard B, et al. Prognostic factors in unselected patients with nonseminomatous metastatic testicular cancer: a multicenter experience. *J Clin Oncol* (1991) 9:818–26. doi: 10.1200/jco.1991.9.5.818

49. Beauchemin N, Arabzadeh A. Carcinoembryonic antigen-related cell adhesion molecules (CEACAMs) in cancer progression and metastases. *Cancer Metastases Rev* (2013) 32:643–71. doi: 10.1007/s10555-013-9444-6

50. Shibata C, Nakano T, Yasumoto A, Mitamura A, Sawada K, Ogawa H, et al. Comparison of CEA and CA19-9 as a predictive factor for recurrence after curative gastrectomy in gastric cancer. *BMC Surg* (2022) 22:213. doi: 10.1186/s12893-022-01667-z

51. Teijeira A, Migueliz I, Garasa S, Karanikas V, Luri C, Cirella A, et al. Three-dimensional colon cancer organoids model the response to CEA-CD3 T-cell engagers. *Theranostics* (2022) 12:1373–87. doi: 10.7150/thno.63359

52. Ayan AK, Erdemci B, Orsal E, Bayraktutan Z, Akpinar E, Topcu A, et al. Is there any correlation between levels of serum ostepontin, CEA, and FDG uptake in lung cancer patients with bone metastases? *Rev Esp Med Nucl Imagen Mol* (2016) 35:102–6. doi: 10.1016/j.remn.2015.09.002

53. Numata T, Endo T, Yanai H, Ota K, Yamamoto Y, Shimizu K, et al. Serum CEA and CYFRA levels in ALK-rearranged NSCLC patients: correlation with distant metastases. *In Vivo* (2020) 34:2095–100. doi: 10.21873/invivo.12013

54. Chai X, Yinwang E, Wang Z, Wang Z, Xue Y, Li B, et al. Predictive and prognostic biomarkers for lung cancer bone metastases and their therapeutic value. *Front Oncol* (2021) 11:692788. doi: 10.3389/fonc.2021.692788

55. Ge YW, Liu XL, Yu DG, Zhu ZA, Ke QF, Mao YQ, et al. Graphene-modified CePO4 nanorods effectively treat breast cancer-induced bone metastases and regulate macrophage polarization to improve osteo-inductive ability. *J Nanobiotechnology* (2021) 19:11. doi: 10.1186/s12951-020-00753-9

56. Salter RS, Fitchen J. Evaluation of a chemiluminescence method for measuring alkaline phosphatase activity in whole milk of multiple species and bovine dairy drinks: interlaboratory study. *J AOAC Int* (2006) 89:1061–70. doi: 10.1093/jaoac/89.4.1061

57. Liu Z, Dong N, Hui H, Wang Y, Liu F, Xu L, et al. Endothelial cell-derived tetrahydrobiopterin prevents aortic valve calcification. *Eur Heart J* (2022) 43:1652–64. doi: 10.1093/eurheartj/ehac037

58. Oketch-Rabah HA, Roe AL, Rider CV, Bonkovsky HL, Giancaspro GI, Navarro V, et al. United states pharmacopeia (USP) comprehensive review of the hepatotoxicity of green tea extracts. *Toxicol Rep* (2020) 7:386–402. doi: 10.1016/j.toxrep.2020.02.008

59. Barry MJ, Simmons LH. Prevention of prostate cancer morbidity and mortality: primary prevention and early detection. *Med Clin North Am* (2017) 101:787–806. doi: 10.1016/j.mcna.2017.03.009

60. Maestroni U, Cavalieri DM, Campobasso D, Guarino G, Ziglioli F. PSA-IgM and iXip in the diagnosis and management of prostate cancer: clinical relevance and future potential. a review. *Acta BioMed* (2022) 92:e2021344. doi: 10.23750/abm.v92i6.12058

61. Conteduca V, Oromendia C, Eng KW, Bareja R, Sigouros M, Molina A, et al. Clinical features of neuroendocrine prostate cancer. *Eur J Cancer.* (2019) 121:7–18. doi: 10.1016/j.ejca.2019.08.011

62. Ren W, Hou J, Yang C, Wang H, Wu S, Wu Y, et al. Extracellular vesicles secreted by hypoxia pre-challenged mesenchymal stem cells promote non-small cell lung cancer cell growth and mobility as well as macrophage M2 polarization *via* miR-21-5p delivery. *J Exp Clin Cancer Res* (2019) 38:62. doi: 10.1186/s13046-019-1027-0

63. Xu Y, Zhang P, Zhang K, Huang C. The application of CA72-4 in the diagnosis, prognosis, and treatment of gastric cancer. *Biochim Biophys Acta Rev Cancer* (2021) 1876:188634. doi: 10.1016/j.bbcan.2021.188634

64. Healthcare Engineering JO. Retracted: effect of apatinib combined with seggio on the expression of serum AFP and CA724 and long-term survival rate in patients with advanced gastric cancer undergoing comfortable nursing intervention. *J Healthc Eng* (2022) 2022:9756408. doi: 10.1155/2022/9756408

65. Pan Q, Law COK, Yung MMH, Han KC, Pon YL, Lau TCK. Novel RNA aptamers targeting gastrointestinal cancer biomarkers CEA, CA50 and CA72-4 with superior affinity and specificity. *PloS One* (2018) 13:e0198980. doi: 10.1371/journal.pone.0198980

66. Huang H, Yu X, Han X, Hao J, Zhao J, Bebek G, et al. Piwil1 regulates glioma stem cell maintenance and glioblastoma progression. *Cell Rep* (2021) 34:108522. doi: 10.1016/j.celrep.2020.108522

67. Zhang Y, Yang J, Li H, Wu Y, Zhang H, Chen W. Tumor biomarkers CA19-9, CA242 and CEA in the diagnosis of pancreatic cancer: a meta-analysis. *Int J Clin Exp Med* (2015) 8:11683–91. doi: 10.1136/bmjopen-2017-018175

68. Dou H, Sun G, Zhang L. CA242 as a biobiomarker for pancreatic cancer and other diseases. *Prog Mol Biol Transl Sci* (2019) 162:229–39. doi: 10.1016/bs.pmbts.2018.12.007

69. Huang P, Chen A, He W, Li Z, Zhang G, Liu Z, et al. BMP-2 induces EMT and breast cancer stemness through Rb and CD44. *Cell Death Discovery* (2017) 3:17039. doi: 10.1038/cddiscovery.2017.39

70. Iaquinta MR, Lanzillotti C, Mazziotta C, Bononi I, Frontini F, Mazzoni E, et al. The role of microRNAs in the osteogenic and chondrogenic differentiation of mesenchymal stem cells and bone pathologies. *Theranostics* (2021) 11:6573–91. doi: 10.7150/thno.55664

71. Puppo M, Taipaleenmäki H, Hesse E, Clézardin P. Non-coding RNAs in bone remodelling and bone metastases: mechanisms of action and translational relevance. *Br J Pharmacol* (2021) 178:1936–54. doi: 10.1111/bph.14836

72. Croset M, Santini D, Iuliani M, Fioramonti M, Zoccoli A, Vincenzi B, et al. MicroRNAs and bone metastases: a new challenge. *Molecules* (2014) 19:10115–28. doi: 10.3390/molecules190710115

73. Nugent M. MicroRNA function and dysregulation in bone tumors: the evidence to date. *Cancer Manag Res* (2014) 6:15–25. doi: 10.2147/cmar.S53928

74. Lang J, Zhao Q, He Y, Yu X. Bone turnover biomarkers and novel biomarkers in lung cancer bone metastases. *biomarkers* (2018) 23:518–26. doi: 10.1080/1354750x.2018.1463566

75. Zhao Q, Li P, Ma J, Yu X. MicroRNAs in lung cancer and lung cancer bone metastases: biomarkers for early diagnosis and targets for treatment. *Recent Pat Anticancer Drug Discovery* (2015) 10:182–200. doi: 10.2174/1574892810666150120163617

76. Croset M, Pantano F, Kan CWS, Bonnelye E, Descotes F, Alix-Panabières C, et al. miRNA-30 family members inhibit breast cancer invasion, osteomimicry, and bone destruction by directly targeting multiple bone metastases-associated genes. *Cancer Res* (2018) 78:5259–73. doi: 10.1158/0008-5472.Can-17-3058

77. Puppo M, Valluru MK, Clézardin P. MicroRNAs and their roles in breast cancer bone metastases. *Curr Osteoporos Rep* (2021) 19:256–63. doi: 10.1007/s11914-021-00677-9

78. Zhang YK, Zhu WY, He JY, Chen DD, Huang YY, Le HB, et al. miRNAs expression profiling to distinguish lung squamous-cell carcinoma from adenocarcinoma subtypes. *J Cancer Res Clin Oncol* (2012) 138:1641–50. doi: 10.1007/s00432-012-1240-0

79. Zhao B, Han H, Chen J, Zhang Z, Li S, Fang F, et al. MicroRNA let-7c inhibits migration and invasion of human non-small cell lung cancer by targeting ITGB3 and MAP4K3. *Cancer Lett* (2014) 342:43–51. doi: 10.1016/j.canlet.2013.08.030

80. Bao X, Ren T, Huang Y, Wang S, Zhang F, Liu K, et al. Induction of the mesenchymal to epithelial transition by demethylation-activated microRNA-125b is involved in the anti-migration/invasion effects of arsenic trioxide on human chondrosarcoma. *J Exp Clin Cancer Res* (2016) 35:129. doi: 10.1186/s13046-016-0407-y

81. Maroni P, Bendinelli P, Matteucci E, Desiderio MA. The therapeutic effect of miR-125b is enhanced by the prostaglandin endoperoxide synthase 2/cyclooxygenase 2 blockade and hampers ETS1 in the context of the microenvironment of bone metastases. *Cell Death Dis* (2018) 9:472. doi: 10.1038/s41419-018-0499-8

82. Yuan J, Chen L, Chen X, Sun W, Zhou X. Identification of serum microRNA-21 as a biobiomarker for chemosensitivity and prognosis in human osteosarcoma. *J Int Med Res* (2012) 40:2090–7. doi: 10.1177/030006051204000606

83. Bonci D, Coppola V, Patrizii M, Addario A, Cannistraci A, Francescangeli F, et al. A microRNA code for prostate cancer metastases. *Oncogene* (2016) 35:1180–92. doi: 10.1038/onc.2015.176

84. Ren X, Shen Y, Zheng S, Liu J, Jiang X. miR-21 predicts poor prognosis in patients with osteosarcoma. *Br J BioMed Sci* (2016) 73:158–62. doi: 10.1080/09674845.2016.1220710

85. He B, Zhao Z, Cai Q, Zhang Y, Zhang P, Shi S, et al. miRNA-based biomarkers, therapies, and resistance in cancer. *Int J Biol Sci* (2020) 16:2628–47. doi: 10.7150/ijbs.47203

86. Kara G, Calin GA, Ozpolat B. RNAi-based therapeutics and tumor targeted delivery in cancer. *Adv Drug Delivery Rev* (2022) 182:114113. doi: 10.1016/j.addr.2022.114113

87. Mishra S, Yadav T, Rani V. Exploring miRNA-based approaches in cancer diagnostics and therapeutics. *Crit Rev Oncol Hematol* (2016) 98:12–23. doi: 10.1016/j.critrevonc.2015.10.003

88. Zou P, Zhu M, Lian C, Wang J, Chen Z, Zhang X, et al. miR-192-5p suppresses the progression of lung cancer bone metastasis by targeting TRIM44. *Sci Rep* (2019) 9 (1):19619. doi: 10.1038/s41598-019-56018-5

89. Gong M, Ma J, Guillemette R, Zhou M, Yang Y, Yang Y, et al. miR-335 inhibits small cell lung cancer bone metastases *via* IGF-IR and RANKL pathways. *Mol Cancer Res* (2014) 12(1):101–10. doi: 10.1158/1541-7786.MCR-13-0136

90. Xu S, Yang F, Liu R, Li X, Fan H, Liu J, et al. Serum microRNA-139-5p is downregulated in lung cancer patients with lytic bone metastasis. *Oncol Rep* (2018) 39 (5):2376–84. doi: 10.3892/or.2018.6316

91. Roberto GM, Delsin LEA, Vieira GM, Silva MO, Hakime RG, Gava NF, et al. ROCK1-PredictedmicroRNAs dysregulation contributes to tumor progression in Ewing sarcoma. *Pathol Oncol Res* (2020) 26(1):133–9. doi: 10.1007/s12253-017-0374-4

92. Vimalraj S, Miranda PJ, Ramyakrishna B, Selvamurugan N. Regulation of breast cancer and bone metastasis by microRNAs. *Dis biomarkers.* (2013) 35(5):369–87. doi: 10.1155/2013/451248

93. Zhao FL, Hu GD, Wang XF, Zhang XH, Zhang YK, Yu ZS. Serum overexpression of microRNA-10b in patients with bone metastatic primary breast cancer. *J Int Med Res* (2012) 40(3):859–66. doi: 10.1177/147323001204000304

94. Arabi L, Gsponer JR, Smida J, Nathrath M, Perrina V, Jundt G, et al. Upregulation of the miR-17-92 cluster and its two paraloga in osteosarcoma - reasons and consequences. *Genes Cancer.* (2014) 5(1-2):56–63. doi: 10.18632/genesandcancer.6

95. Xu Q, Li P, Chen X, Zong L, Jiang Z, Nan L, et al. miR-221/222 induces pancreatic cancer progression through the regulation of matrix metalloproteinases. *Oncotarget* (2015) 6:14153–64. doi: 10.18632/oncotarget.3686

96. Liu Z., Liu Z., Zhang Y., Li Y., Liu B., Zhang K. miR-24 represses metastasis of human osteosarcoma cells by targeting Ack1 via AKT/MMPs pathway. *Biochem Biophys Res Commun* (2017) 486(2):211–7. doi: 10.1016/j.bbrc.2017.02.045

97. Koshkina N, Yang Y, Kleinerman ES. The Fas/FasL signaling pathway: its role in the metastatic process and as a target for treating osteosarcoma lung metastases. *Adv Exp Med Biol* (2020) 1258:177–87. doi: 10.1007/978-3-030-43085-6_12

98. Cui XB, Li S, Li TT, Peng H, Jin TT, Zhang SM, et al. Targeting oncogenic PLCE1 by miR-145 impairs tumor proliferation and metastases of esophageal squamous cell carcinoma. *Oncotarget* (2016) 7:1777–95. doi: 10.18632/oncotarget.6499

99. Zhao W, Geng D, Li S, Chen Z, Sun M. LncRNA HOTAIR influences cell growth, migration, invasion, and apoptosis *via* the miR-20a-5p/HMGA2 axis in breast cancer. *Cancer Med* (2018) 7(3):842–55. doi: 10.1002/cam4.1353

100. Fang C, Wang X, Guo D, Fang R, Zhu T. Circular RNA CircITGA7 promotes tumorigenesis of osteosarcoma *via* miR-370/PIM1 axis. *Comput Math Methods Med* (2020) 2020:1367576. doi: 10.1155/2020/1367576

101. Li F, Li H, Hou Y. Identification and analysis of survival-associated ceRNA triplets in prostate adenocarcinoma. *Oncol Lett* (2019) 18(4):4040–7. doi: 10.3892/ol.2019.10752

102. Liu M., Mo F., Song X., He Y., Yuan Y., Yan J., et al. Exosomal hsa-miR-21-5p is a biomarker for breast cancer diagnosis. *PeerJ* (2021) 9:e12147. doi: 10.7717/peerj.12147

103. Zhang HL, Qin XJ, Cao DL, Zhu Y, Yao XD, Zhang SL, et al. An elevated serum miR-141 level in patients with bone-metastatic prostate cancer is correlated with more bone lesions. *Asian J Androl* (2013) 15:231–5. doi: 10.1038/aja.2012.116

104. Ye Y, Li SL, Ma YY, Diao YJ, Yang L, Su MQ, et al. Exosomal miR-141-3p regulates osteoblast activity to promote the osteoblastic metastases of prostate cancer. *Oncotarget* (2017) 8:94834–49. doi: 10.18632/oncotarget.22014

105. Guo X, Han T, Hu P, Guo X, Zhu C, Wang Y, et al. Five microRNAs in serum as potential biomarkers for prostate cancer risk assessment and therapeutic intervention. *Int Urol Nephrol* (2018) 50:2193–200. doi: 10.1007/s11255-018-2009-4

106. Yang G, Lu Z, Meng F, Wan Y, Zhang L, Xu Q, et al. Circulating miR-141 as a potential biobiomarker for diagnosis, prognosis and therapeutic targets in gallbladder cancer. *Sci Rep* (2022) 12:10072. doi: 10.1038/s41598-022-13430-8

107. Yang S, Zhang W, Cai M, Zhang Y, Jin F, Yan S, et al. Suppression of bone resorption by miR-141 in aged rhesus monkeys. *J Bone Miner Res* (2018) 33:1799–812. doi: 10.1002/jbmr.3479

108. Tian L, Sun S, Li W, Yuan L, Wang X. Down-regulated microRNA-141 facilitates osteoblast activity and inhibits osteoclast activity to ameliorate osteonecrosis of the femoral head *via* up-regulating TGF-β2. *Cell Cycle* (2020) 19:772–86. doi: 10.1080/15384101.2020.1731053

109. Wang CY, Li SY, Xiao YX, Zhen L, Wei XG, Tang XB, et al. miR-141-3p affects β-catenin signaling and apoptosis by targeting Ubtd2 in rats with anorectal malformations. *Ann N Y Acad Sci* (2022) 1518:315–27. doi: 10.1111/nyas.14924

110. Ni Z, Shen Y, Wang W, Cheng X, Fu Y. miR-141-5p affects the cell proliferation and apoptosis by targeting BTG1 in cervical cancer. *Cancer Biother Radiopharm* (2021). doi: 10.1089/cbr.2021.0227

111. Liu M, Sun W, Liu Y, Dong X. The role of lncRNA MALAT1 in bone metastasis in patients with non-small cell lung cancer. *Oncol Rep* (2016) 36(3):1679–85. doi: 10.3892/or.2016.4909

112. Chang X, Zhang H, Yang Q, Pang L. LncRNA SOX2OT affects cervical cancer cell growth, migration and invasion by regulating SOX2. *Cell Cycle* (2020) 19:1391–403. doi: 10.1080/15384101.2020.1750812

113. Chen K, Yu B, Liao J. LncRNA SOX2OT alleviates mesangial cell proliferation and fibrosis in diabetic nephropathy *via* Akt/mTOR-mediated autophagy. *Mol Med* (2021) 27:71. doi: 10.1186/s10020-021-00310-6

114. Stewart CL, Warner S, Ito K, Raoof M, Wu GX, Kessler J, et al. Cytoreduction for colorectal metastases: liver, lung, peritoneum, lymph nodes, bone, brain. when does it palliate, prolong survival, and potentially cure? *Curr Probl Surg* (2018) 55:330–79. doi: 10.1067/j.cpsurg.2018.08.004

115. Wang N, Liu F, Xi W, Jiang J, Xu Y, Guan B, et al. Development and validation of risk and prognostic nomograms for bone metastases in Chinese advanced colorectal cancer patients. *Ann Transl Med* (2021) 9:875. doi: 10.21037/atm-21-2550

116. Zhao C, Zhang Z, Hu X, Zhang L, Liu Y, Wang Y, et al. Hyaluronic acid correlates with bone metastasis and predicts poor prognosis in small-cell lung cancer patients. *Front Endocrinol (Lausanne).* (2022) 12:785192. doi: 10.3389/fendo.2021.785192

117. Loreth D., Schuette M., Zinke J., Mohme M., Piffko A., Schneegans S., et al. CD74 and CD44 Expression on CTCs in Cancer Patients with Brain Metastasis. *Int. J. Mol. Sci* (2021) 22(13):6993. doi: 10.3390/ijms22136993

118. Zhang X., Chen S.B., Chen J.X., Wen J., Yang H., Xie M.R., et al. CK19 mRNA expression in the bone marrow of patients with esophageal squamous cell carcinoma and its clinical significance. *Dis Esophagus* (2010) 22(13):6993. doi: 10.3390/ijms22136993.x

119. Jiwa L. S., van Diest P. J., Hoefnagel L. D., Wesseling J., Wesseling P., Moelans C. B. Upregulation of Claudin-4, CAIX and GLUT-1 in distant breast cancer metastases. *BMC Cancer* (2014) 14:864. doi: 10.1186/1471-2407-14-864

120. Ma W, Li T, Wu S, Li J, Wang X, Li H. LOX and ACSL5 as potential relapse biomarkers for pancreatic cancer patients. *Cancer Biol Ther* (2019) 20(6):787–98. doi: 10.1080/15384047.2018.1564565

121. Mehrotra J, Vali M, McVeigh M, Kominsky SL, Fackler MJ, Lahti-Domenici J, et al. Very high frequency of hypermethylated genes in breast cancer metastasis to the bone, brain, and lung. *Clin Cancer Res* (2004) 10(9):3104–9. doi: 10.1158/1078-0432.ccr-03-0118

122. Barata P, Agarwal N, Nussenzveig R, Gerendash B, Jaeger E, Hatton W, et al. Clinical activity of pembrolizumab in metastatic prostate cancer with microsatellite instability high (MSI-h) detected by circulating tumor DNA. *J Immunother Cancer.* (2020) 8(2):e001065. doi: 10.1136/jitc-2020-001065

123. Mohme M, Riethdorf S, Pantel K. Circulating and disseminated tumour cells - mechanisms of immune surveillance and escape. *Nat Rev Clin Oncol* (2017) 14:155–67. doi: 10.1038/nrclinonc.2016.144

124. Garcés JJ, Cedena MT, Puig N, Burgos L, Perez JJ, Cordon L, et al. Circulating tumor cells for the staging of patients with newly diagnosed transplant-eligible multiple myeloma. *J Clin Oncol* (2022) 40:3151–61. doi: 10.1200/jco.21.01365

125. Iuliani M, Simonetti S, Ribelli G, Napolitano A, Pantano F, Vincenzi B, et al. Current and emerging biomarkers predicting bone metastases development. *Front Oncol* (2020) 10:789. doi: 10.3389/fonc.2020.00789

126. Leblanc R, Peyruchaud O. Metastases: new functional implications of platelets and megakaryocytes. *Blood* (2016) 128:24–31. doi: 10.1182/blood-2016-01-636399

127. Feng S, Wu ZX, Zhao Z, Liu J, Sun K, Guo C, et al. Engineering of bone- and CD44-Dual-Targeting redox-sensitive liposomes for the treatment of orthotopic osteosarcoma. *ACS Appl Mater Interfaces* (2019) 11:7357–68. doi: 10.1021/acsami.8b18820

128. Sun X, Li K, Hase M, Zha R, Feng Y, Li BY, et al. Suppression of breast cancer-associated bone loss with osteoblast proteomes *via* Hsp90ab1/moesin-mediated inhibition of TGFβ/FN1/CD44 signaling. *Theranostics* (2022) 12:929–43. doi: 10.7150/thno.66148

129. Pang X, Gong K, Zhang X, Wu S, Cui Y, Qian BZ. Osteopontin as a multifaceted driver of bone metastases and drug resistance. *Pharmacol Res* (2019) 144:235–44. doi: 10.1016/j.phrs.2019.04.030

130. Niu Y, Yang H, Yu Z, Gao C, Ji S, Yan J, et al. Intervention with the bone-associated tumor vicious cycle through dual-protein therapeutics for treatment of skeletal-related events and bone metastases. *ACS Nano* (2022) 16:2209–23. doi: 10.1021/acsnano.1c08269

131. Liu L, Zhang C, Wang J, Liu X, Qu H, Zhang G, et al. A high level of lncFGD5-AS1 inhibits epithelial-to-Mesenchymal transition by regulating the miR-196a-5p/SMAD6/BMP axis in gastric cancer. *BMC Cancer* (2021) 21:453. doi: 10.1186/s12885-021-08192-x

132. Yu L, Sui B, Fan W, Lei L, Zhou L, Yang L, et al. Exosomes derived from osteogenic tumor activate osteoclast differentiation and concurrently inhibit osteogenesis by transferring COL1A1-targeting miRNA-92a-1-5p. *J Extracell Vesicles* (2021) 10:e12056. doi: 10.1002/jev2.12056

133. Doyle LM, Wang MZ. Overview of extracellular vesicles, their origin, composition, purpose, and methods for exosome isolation and analysis. *Cells* (2019) 8(7):727. doi: 10.3390/cells8070727

134. Kalluri R, LeBleu VS. The biology, function, and biomedical applications of exosomes. *Science* (2020) 367(6478):eaau6977. doi: 10.1126/science.aau6977

135. O'Brien K, Breyne K, Ughetto S, Laurent LC, Breakefield XO. RNA Delivery by extracellular vesicles in mammalian cells and its applications. *Nat Rev Mol Cell Biol* (2020) 21(10):585–606. doi: 10.1038/s41580-020-0251-y

136. Wu K, Feng J, Lyu F, Xing F, Sharma S, Liu Y, et al. Exosomal miR-19a and IBSP cooperate to induce osteolytic bone metastases of estrogen receptor-positive breast cancer. *Nat Commun* (2021) 12:5196. doi: 10.1038/s41467-021-25473-y

137. Medeiros B, Allan AL. Molecular mechanisms of breast cancer metastases to the lung: clinical and experimental perspectives. *Int J Mol Sci* (2019) 20(9):2272. doi: 10.3390/ijms20092272

138. Akoto T, Saini S. Role of exosomes in prostate cancer metastases. *Int J Mol Sci* (2021) 22(7):3528. doi: 10.3390/ijms22073528

139. Colletti M, Tomao L, Galardi A, Paolini A, Di Paolo V, De Stefanis C, et al. Neuroblastoma-secreted exosomes carrying miR-375 promote osteogenic differentiation of bone-marrow mesenchymal stromal cells. *J Extracell Vesicles* (2020) 9:1774144. doi: 10.1080/20013078.2020.1774144

140. Ge J, Liu M, Zhang Y, Xie L, Shi Z, Wang G. SNHG10/miR-141-3p/WTAP axis promotes osteosarcoma proliferation and migration. *J Biochem Mol Toxicol* (2022) 36: e23031. doi: 10.1002/jbt.23031

141. Warton K, Samimi G. Methylation of cell-free circulating DNA in the diagnosis of cancer. *Front Mol Biosci* (2015) 2:13. doi: 10.3389/fmolb.2015.00013

142. Palanca-Ballester C, Rodriguez-Casanova A, Torres S, Calabuig-Fariñas S, Exposito F, Serrano D, et al. Cancer epigenetic biomarkers in liquid biopsy for high incidence malignancies. *Cancers (Basel).* (2021) 13(12):3016. doi: 10.3390/cancers13123016

143. Jiang W, Kai J, Li D, Wei Z, Wang Y, Wang W. lncRNA HOXB-AS3 exacerbates proliferation, migration, and invasion of lung cancer *via* activating the PI3K-AKT pathway. *J Cell Physiol* (2020) 235(10):7194–203. doi: 10.1002/jcp.29618

144. Shi Z, Zhang H, Jie S, Yang X, Huang Q, Mao Y, et al. Long non-coding RNA SNHG8 promotes prostate cancer progression through repressing miR-384 and up-regulating HOXB7. *J Gene Med* (2021) 23(3):e3309. doi: 10.1002/jgm.3309

145. Chen M, Jiang Y, Sun Y. KDM4A-mediated histone demethylation of SLC7A11 inhibits cell ferroptosis in osteosarcoma. *Biochem Biophys Res Commun* (2021) 550:77–83. doi: 10.1016/j.bbrc.2021.02.137

146. Deligezer U, Yaman F, Darendeliler E, Dizdar Y, Holdenrieder S, Kovancilar M, et al. Post-treatment circulating plasma BMP6 mRNA and H3K27 methylation levels discriminate metastatic prostate cancer from localized disease. *Clin Chim Acta* (2010) 411(19-20):1452–6. doi: 10.1016/j.cca.2010.05.040

147. Shu J, Li L, Sarver AE, Pope EA, Varshney J, Thayanithy V, et al. Imprinting defects at human 14q32 locus alters gene expression and is associated with the pathobiology of osteosarcoma. *Oncotarget* (2016) 7(16):21298–314. doi: 10.18632/oncotarget.6965

Frontiers in Oncology

Advances knowledge of carcinogenesis and tumor progression for better treatment and management

The third most-cited oncology journal, which highlights research in carcinogenesis and tumor progression, bridging the gap between basic research and applications to imrpove diagnosis, therapeutics and management strategies.

Discover the latest Research Topics

See more →

Frontiers

Avenue du Tribunal-Fédéral 34
1005 Lausanne, Switzerland
frontiersin.org

Contact us

+41 (0)21 510 17 00
frontiersin.org/about/contact